

# Imidazolidinones in Amine Catalysis

Julian H. Rowley

2014

Supervised by Professor Nicholas C. O. Tomkinson

Department of Pure and Applied Chemistry

*A thesis submitted to the University of Strathclyde in part fulfilment of regulations  
for the degree of Doctor of Philosophy in Chemistry.*



## Abstract

Iminium ion activation is a rapidly expanding and contemporary area of synthetic chemistry in which a number of enantio- and diastereoselective transformations have been developed. Despite the substantial attributes of the area, high catalyst loadings, aldehyde substrate specificity and incomplete understanding of the catalytic process detracts from iminium ion activation being fully competitive with metal-based alternatives. Within this Thesis a series of investigations are presented to address some of these perceived shortcomings.

In *Chapter 2*, a novel imidazolidinone containing an  $\alpha$ -electron withdrawing group is evaluated as an asymmetric catalyst for Diels-Alder cycloaddition reactions. A substrate and reaction scope is presented and the conformational preference of the imidazolidinone is probed to rationalise the origins of enantioselectivity.

In *Chapter 3*, further understanding of the conformational preference of the MacMillan first generation imidazolidinone is gained using chiral optical spectroscopic measurements. For the first time each proposed intermediate in the full catalytic cycle is observed using mass spectrometry.

In *Chapter 4*, a hybrid secondary amine is designed based upon the diarylprolinol ether and imidazolidinone scaffold.

In *Chapter 5*, the 3-position of the imidazolidinone ring is investigated as a potential site to install electron withdrawing groups to influence the catalytic cycle.

In *Chapter 6*, efforts are made to tackle  $\alpha,\beta$ -unsaturated aldehyde substrate specificity through the design of  $C_2$  symmetric amines suitable for use in iminium activation of  $\alpha,\beta$ -unsaturated ketones.

*Chapter 7* and *Chapter 8* are both outside the immediate subject area of this thesis. In *Chapter 7* a novel amino acid amide dimer architecture is revealed. Investigations into substrate scope, stability and conformational rigidity are presented. In *Chapter 8* a mechanistic investigation into the malonyl peroxide mediated alkene dioxygenation reaction is made. DFT calculations and a mechanistic probe substrate are used to define the nature of the interaction between the peroxide and alkene.

*Chapter 9* summarises the work contained within *Chapters 2–8* and suggests some avenues along which research could be continued.



## **Acknowledgements**

Firstly I would like to thank Nick for his drive, wisdom, and supervision throughout my PhD. Nick's enthusiasm towards research, dedication to his group and devotion to teaching has allowed me to develop on a scientific and personal level for which I will be eternally grateful.

I would like to thank Jamie Platts for his tuition on the computational aspects of my work and Tell Tuttle for the use of his computer cluster. Also, I would like to thank my collaborators: Christian Johannessen, Ewan Blanch, Steven Christie and Colin Creaser for their willingness to engage in an unfamiliar area of research.

My thanks are extended to past and present members of the Tomkinson group. In particular Leo Samulis, Mike Rawling, John Brazier, Jacky Yau, Sylvain Picon, James Tellam, Tomasz Kubczyk, Justyna Wojno, Andrei Dragan, Lola Beltran-Molina, Camille Indey, Stuart Davidson and many ERASMUS and project students, with whom I have shared laughs, beers and discussions over the past few years. I would like to give special thanks to Mike for his ability to always raise a smile, artistic drawings and for the occasional sensible scientific discussion! I would also like to thank the many additional friends and colleagues at both Cardiff University and The University of Strathclyde who have contributed in many ways throughout the last 3 years.

I would also like to thank my partner Kate for her love, support, encouragement and persistence through what ended up being a rather long-distance relationship. I would also like to thank EasyJet, FlyBE and Virgin Trains for providing affordable and (reasonably) reliable modes of transport which enabled us to regularly see each other.

Finally, I would like to thank my Mum for her love, nurturing and support throughout everything I have chosen to do. Without her I would never have made it to the privileged position I am in today.

Thank you all.

---

**Table of Contents**

<b>Declaration</b> .....	<b>i</b>
<b>Abstract</b> .....	<b>ii</b>
<b>Acknowledgements</b> .....	<b>iv</b>
<b>Table of Contents</b> .....	<b>v</b>
<b>Abbreviations</b> .....	<b>xi</b>
<b>1 Secondary Amine Organocatalysis</b> .....	<b>2</b>
1.1 Preface.....	2
1.2 Organocatalysis .....	2
1.2.1 A Historical Perspective.....	2
1.2.2 Modes of Organocatalysis.....	4
1.2.3 MacMillan Group Reaction Development .....	6
1.3 Iminium Ion Activation.....	10
1.3.1 Preface.....	10
1.3.2 The Beginnings of Iminium Activation .....	10
1.4 Iminium Activation in the Group.....	15
1.4.1 Mechanistic Insight .....	15
1.4.2 Catalyst Development .....	16
1.4.3 DFT Calculations .....	20
1.5 Project Aims.....	24
<b>2 Evaluation of a Novel Imidazolidinone</b> .....	<b>26</b>
2.1 Introduction .....	26
2.2 Diels-Alder Cycloaddition Reactions .....	26
2.2.1 Synthesis of Imidazolidinone 38.....	26
2.2.2 Catalyst Performance .....	28
2.2.3 Dienophile Substrate Scope .....	30

---

2.2.4 Competition Reactions .....	35
2.2.5 Asymmetric Catalyst Efficiency .....	37
2.3 Rationalising Enantioselectivity.....	39
2.3.1 DFT Calculations .....	39
2.3.2 Isolation of Iminium Ion Intermediates.....	40
2.3.3 Analysing Conformation Using VT NMR Spectroscopy .....	48
2.4 Reaction Scope.....	49
2.4.1 Friedel Crafts Alkylation .....	49
2.4.2 $\alpha$ -Oxybenzoylation.....	52
2.4.3 Conjugate Addition of Pyrrole .....	53
2.5 Conclusions .....	56
<b>3 Observing Iminium Ion Intermediates .....</b>	<b>60</b>
3.1 Attribution .....	60
3.2 Introduction .....	60
3.3 Iminium Ion Conformation .....	62
3.3.1 Literature Observations .....	62
3.3.2 Chiral Optical Spectroscopy .....	65
3.3.3 Iminium Ion Conformation Using Chiral Optical Spectroscopy .....	69
3.3.4 Iminium Ion Conformation Using ROA .....	69
3.3.5 Iminium Ion Conformation Using VCD .....	78
3.4 Conclusions .....	82
3.5 Observing the Catalytic Cycle .....	83
3.5.1 Isolation of 24 and 25.....	83
3.5.2 Detection of 24 and 25 .....	85
3.5.3 Characterisation of Ions .....	88
3.6 Conclusions .....	90

---

<b>4 A Hybrid Imidazolidinone Catalyst .....</b>	<b>93</b>
4.1 Introduction .....	93
4.2 Results and Discussion.....	94
4.2.1 Computational Evaluation.....	94
4.2.2 Synthesis of 1,2-Unsubstituted Imidazolidinones.....	97
4.2.3 Synthesis of the Hybrid Imidazolidinone.....	102
4.2.4 Evaluation of 123 as a Catalyst.....	106
4.3 Conclusions .....	107
<b>5 Electron Withdrawing Groups on Imidazolidinones.....</b>	<b>110</b>
5.1 Introduction .....	110
5.2 Results and Discussion.....	111
5.2.1 Non-Electron Withdrawing Substituents .....	111
5.2.2 Electron Withdrawing Substituents.....	113
5.3 Conclusions .....	118
<b>6 C<sub>2</sub> Symmetric Catalyst Design .....</b>	<b>120</b>
6.1 Introduction .....	120
6.2 Results and Discussion.....	122
6.2.1 C <sub>2</sub> Symmetric Amine Modelling.....	122
6.2.2 Pseudo C <sub>2</sub> Symmetric Amine Modelling .....	126
6.2.3 Pseudo C <sub>2</sub> Symmetric Amine Synthesis .....	128
6.2.4 Modelling Pseudo C <sub>2</sub> Symmetric Amine 200.....	134
6.2.5 Synthetic Evaluation of 200.....	135
6.3 Conclusions .....	138
<b>7 Chiral at Nitrogen Amino Acid Dimers .....</b>	<b>140</b>
7.1 Introduction .....	140
7.2 Results and Discussion.....	141

---

7.2.1 Amino Acid Substrate Scope .....	141
7.2.2 Altering the Amide.....	147
7.2.3 Modification of the Methylene Bridge.....	149
7.2.4 Conformational Rigidity .....	153
7.3 Conclusions .....	155
<b>8 Alkene Dihydroxylation using Malonoyl Peroxides: A Mechanistic Study... 158</b>	
8.1 Preface.....	158
8.2 Introduction .....	158
8.3 Plausible Mechanistic Pathways .....	160
8.4 Computational Evidence for Mechanistic Pathways .....	163
8.4.1 A Step-Wise Ionic Pathway .....	164
8.4.2 A $\beta$ -Lactone Intermediate .....	167
8.4.3 A Radical Pathway .....	169
8.4.4 SET Interaction .....	169
8.5 Experimental Evidence for Mechanistic Pathway .....	171
8.5.1 Radical Clocks .....	171
8.5.2 Synthesis of Radical Clock Alkene.....	172
8.5.3 Synthesis of Peroxide 231 .....	174
8.5.4 Reaction of Radical Clock 250 with Peroxide 231 .....	174
8.6 Conclusions .....	178
<b>9 Conclusions and Future Work..... 180</b>	
9.1 Overview .....	180
9.2 Imidazolidinone Comparison .....	181
9.3 Imidazolidinone Stability .....	182
9.4 The Catalytic Cycle.....	183
9.5 Amino Acid Amide Dimerisation .....	184

---

9.6 Alkene Dihydroxylation Using Malonoyl Peroxide .....	185
9.7 Future Work .....	187
9.7.1 Catalyst Reactivity .....	187
9.7.2 Chiral Optical Spectroscopy .....	187
9.7.3 Observing the Catalytic Cycle .....	188
9.7.4 Amino Acid Dimers .....	188
9.7.5 Alkene Dihydroxylation.....	189
<b>10 Experimental .....</b>	<b>192</b>
10.1 Generic Methods .....	192
10.2 Reaction Monitoring and General Procedures .....	193
10.2.1 Reaction Monitoring .....	193
10.2.2 General Procedure for Cinnamaldehyde Screening .....	196
10.3 Compounds .....	200
10.4 General Method for Detecting Intermediates by ESI-MS.....	254
10.5 HPLC .....	254
10.5.1 Preparation of Racemates for Separation.....	254
10.5.2 Derivatisations.....	255
10.5.3 HPLC Separation Conditions.....	255
10.6 DFT Calculations .....	258
<b>11 Appendices .....</b>	<b>260</b>
11.1 Appendix A: X-Ray Crystallography Parameters.....	260
11.2 Appendix B: <sup>1</sup> H NMR Spectra for Radical Clock Reaction .....	352
11.3 Appendix C: NOESY NMR Spectrum for 200.....	354
11.4 Appendix D: Crude Data from Reaction Monitoring .....	355
11.4.1 Data from Chapter 2.....	355
11.4.2 Data from Chapter 5.....	357

11.4.3 Data from Chapter 8.....	357
11.5 Appendix E: Example HPLC Traces .....	358
11.6 Appendix F: Publications from Work Contained within this Thesis To Date .....	365
<b>12 References .....</b>	<b>367</b>

## Abbreviations

Many abbreviations have been used throughout this thesis and are detailed below:

Å	Angstroms ( $1 \times 10^{-10}$ metres)
Abs	absorption
Ac	acetyl
ACE	Asymmetric Catalyst Efficiency
ACES	Asymmetric Catalyst Efficiency Speed
AD	asymmetric dihydroxylation
app.	apparent
APT	Atomic Polar Tensor
ATR	Attenuated Total Reflectance
B3LYP	Becke, 3 parameter, Lee-Yang-Parr functional
BHandH	Becke's half and a half functional
Bn	benzyl
Boc	<i>tert</i> -butoxycarbonyl
br.	broad
Bu	butyl
Bz	benzoyl
c	concentration ( $\text{g } 100 \text{ mL}^{-1}$ )
C	Celsius
cal	calories
CCS	Collision Cross Section
CD	Circular Dichroism
CI	chemical ionisation
CPCM	Conductor-like Polarizable Continuum Model
d	doublet
DBU	1,8-diazabicyclo[5.4.0]undec-7-ene
DCC	dicyclohexylcarbodiimide
DCM	dichloromethane
decomp.	decomposition



---

DFT	Density Functional Theory
DMF	dimethylformamide
E	generic electrophile
ECD	Electronic Circular Dichroism
ee	enantiomeric excess
$E_{\text{HOMO}}$	energy of the HOMO
EI	electron impact
$E_{\text{LUMO}}$	energy of the LUMO
eq	equivalent
ES	electrospray
ESI	electrospray ionisation
Et	ethyl
EWG	Electron Withdrawing Group
g	gram(s)
GC	gas-liquid chromatography
h	hour(s)
hept	heptet
HOMO	Highest Occupied Molecular Orbital
HPLC	High-Performance Liquid Chromatography
HRMS	High-Resolution Mass Spectrometry
Hz	hertz
IMS	Ion Mobility Spectrometry
<i>i</i> Pr	<i>iso</i> -propyl
IR	infrared
<i>J</i>	coupling constant
J	joules
K	degrees kelvin
kJ	kilojoules
LA	generic Lewis acid
LC	<i>see HPLC</i>
LUMO	Lowest Unoccupied Molecular Orbital
<i>m</i>	mass

---

M	molar (mol dm <sup>-3</sup> )
m	multiplet
MALDI	Matrix Assisted Laser Desorption Ionisation
Me	methyl
mg	milligram(s)
MHz	megahertz
min	minute(s)
mL	millilitre(s)
MM3	molecular mechanics
mmol	millimole(s)
mol	mole(s)
mol%	molar percentage
mp	melting point
MS	Mass Spectrometry
Ms	methanesulfonyl
MsOH	methanesulfonic acid
M <sub>wt</sub>	molecular weight
NMR	Nuclear Magnetic Resonance
Nu	generic nucleophile
<i>p</i>	<i>para</i>
PCM	Polarisable Continuum Model
PEM	photoelastic modulator
Ph	phenyl
ppm	parts per million
<i>p</i> -TSA	<i>para</i> -Toluenesulfonic acid
q	quartet
quant.	quantitative
ROA	Raman Optical Activity
RSC	Royal Society of Chemistry
rt	room/ambient temperature
s	singlet
SET	Single Electron Transfer

---

SOMO	Singularly Occupied Molecular Orbital
t	triplet
<sup>t</sup> Bu	<i>tertiary</i> -butyl
TES	triethylsilyl
Tf	trifluoromethanesulfonyl
TFA	trifluoroacetic acid
THF	tetrahydrofuran
TLC	Thin Layer Chromatography
TMS	trimethylsilyl
TS	Transition State
UV	ultraviolet
VCD	Vibrational Circular Dichroism
VROA	Vibrational Raman Optical Activity
VT	Variable Temperature
wt.	weight
z	charge
Δ	heat under reflux
μL	microlitre(s)

# **Chapter 1: Introduction**

## 1 Secondary Amine Organocatalysis

### 1.1 Preface

Secondary amine catalysis, specifically mechanistic understanding and catalyst development, has been a long-standing and fruitful research theme within the group. To build upon existing knowledge and address shortfalls associated with iminium ion activation, a research project was undertaken to further understand the catalytic cycle and to design and evaluate novel catalyst architectures.

### 1.2 Organocatalysis

#### 1.2.1 A Historical Perspective

Organocatalysis, “the acceleration of chemical reactions with a substoichiometric amount of organic compound”, arguably had a fairly slow beginning.<sup>1</sup> The concept was first documented in 1898 when Knoevenagel discovered that piperidine facilitated a condensation reaction between benzaldehydes and malonates.<sup>2</sup> However, only small developments were made in the area for around 100 years.<sup>3</sup> The lack of precedent caused Seebach to overlook the idea when he suggested “new synthetic methods are most likely to be encountered in the fields of biological and organometallic chemistry” in his 1990 review on the future of organic synthesis.<sup>4</sup> However, upon defining the concept of Organocatalysis in 2000 MacMillan unwittingly gave the overlooked idea a renaissance in synthetic chemistry.<sup>1</sup>

In recent decades, the field of Organocatalysis has captured the imagination of the synthetic community. This has been highlighted by the dramatic increase in the number of publications dedicated to the concept (Figure 1.1).

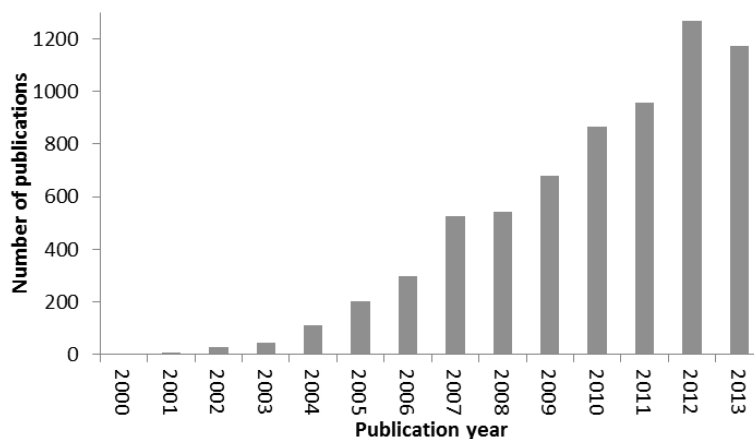


Figure 1.1 Number of Publications Containing the Concept of “Organocatalysis” (SciFinder January 2014)

The popularity of Organocatalysis has been driven by the ever increasing demand for catalytic asymmetric methodologies. This is in part due to the lucrative single enantiomer pharmaceutical compound market which is worth annually over 1 trillion US dollars.<sup>5</sup> Organocatalysis has also benefitted from the emergence of the idea of “Green Chemistry”. Driven by social and economic pressure, the field of Green Chemistry has emerged to encompass methodologies which are seen to be more environmentally benign than traditional approaches. Green Chemistry has a significant backing with a dedicated RSC journal and an ever-increasing level of publication (Figure 1.2).<sup>6</sup>

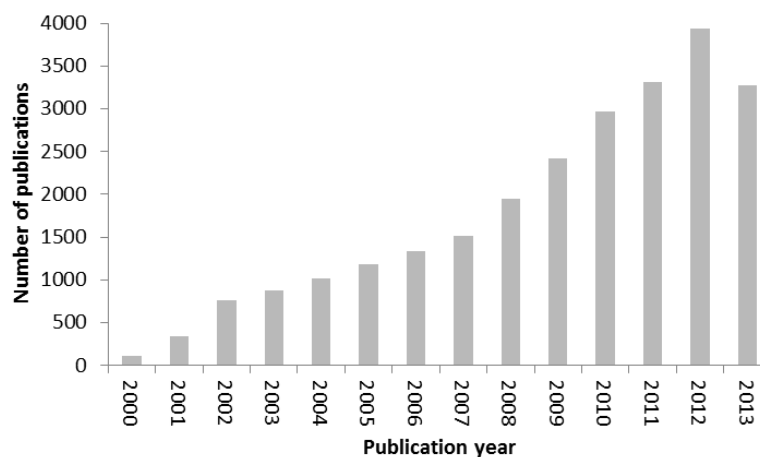


Figure 1.2 Number of Publications Containing the Concept of “Green Chemistry” (SciFinder January 2014)

The combination of demand for new and improved catalytic asymmetric methodologies, drive towards Green Chemistry and ever increasing scepticism towards heavy metals has embedded the concept of Organocatalysis as a fundamental part of modern synthetic chemistry.

### 1.2.2 Modes of Organocatalysis

Organocatalysis can be defined by 5 different methods of activation; iminium catalysis, enamine catalysis, hydrogen-bonding catalysis, counterion catalysis and SOMO catalysis.<sup>7</sup> All of these are now recognised as generic methods of substrate activation and are used widely within synthetic chemistry. Each method can be grouped into LUMO, HOMO or SOMO modes of activation.

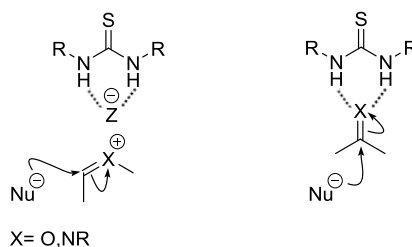


Figure 1.3 Counterion and Hydrogen-Bonding Catalysis

LUMO Activation incorporates hydrogen-bonding catalysis,<sup>8</sup> counterion catalysis (Figure 1.3)<sup>9</sup> and iminium catalysis (Figure 1.4).<sup>3</sup> These methods withdraw electron density from the  $\pi$ -system of the substrate which lowers the energy level of the LUMO ( $E_{\text{LUMO}}$ ) and promotes reaction.<sup>7</sup>

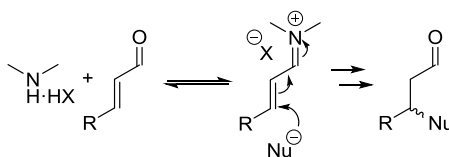


Figure 1.4 Iminium Catalysis

HOMO Activation includes enamine catalysis which is used to  $\alpha$ -functionalise aldehydes.<sup>10</sup> Dienamine catalysis can also be performed to  $\gamma$ -functionalise  $\alpha,\beta$ -unsaturated aldehydes (Figure 1.5).<sup>11</sup> Enamine catalysis renders the  $\alpha$ - or  $\gamma$ -position nucleophilic by transforming the substrate into a reactive species with a raised energy level of the HOMO ( $E_{\text{HOMO}}$ ).<sup>7</sup>

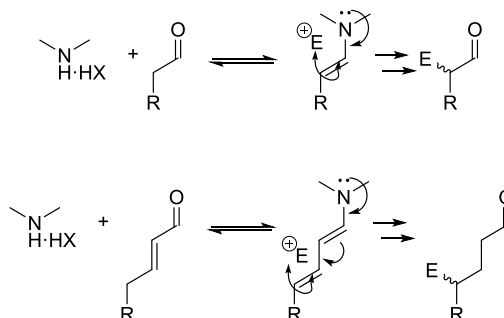


Figure 1.5 Enamine and Dienamine Catalysis

SOMO Activation also  $\alpha$ -functionalises aldehydes.<sup>12</sup> To form the SOMO species, an enamine is reacted with a single electron oxidant to form a radical cation which is then reactive towards weakly nucleophilic “SOMOphiles” (Figure 1.6).<sup>7</sup> This mode of activation can be seen as complimentary to enamine catalysis. However, the requirement for rigorous exclusion of oxygen renders SOMO activation less attractive to synthetic chemists.



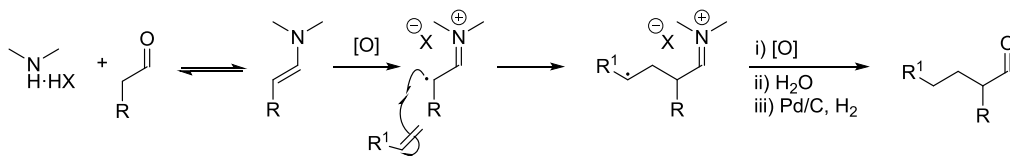
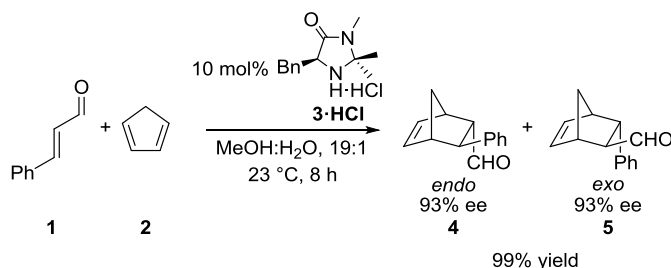


Figure 1.6 Outline of SOMO Catalysis

Hydrogen bond donors and amines have emerged as key architectures in Organocatalysis. Amine catalysts, in particular imidazolidinones, have been shown to be highly versatile and can be used in all three modes of organocatalytic activation. The power of the imidazolidinone was first recognised by MacMillan in his seminal paper in 2000.<sup>1</sup> A Diels-Alder cycloaddition reaction between cinnamaldehyde (**1**) and cyclopentadiene (**2**) catalysed by 10 mol% of imidazolidinone **3**·HCl was described (Scheme 1.1). In just 8 hours at ambient temperature in the presence of air and water *endo* (**4**) and *exo* (**5**) products were furnished with an overall yield of 99% in a 1:1.3 ratio. In addition, **4** and **5** were both produced in 93% enantiomeric excess.



Scheme 1.1 Imidazolidinone Catalysed Diels-Alder Reaction

### 1.2.3 MacMillan Group Reaction Development

After reporting the first asymmetric organocatalytic Diels-Alder reaction, the MacMillan group continued to utilise the imidazolidinone scaffold. Methodologies using iminium catalysis to conduct Diels-Alder cycloadditions,<sup>1,13</sup> [3+2] cycloadditions,<sup>14</sup> Friedel-Crafts alkylations,<sup>15</sup> conjugate additions,<sup>16</sup> heteroaromatic alkylations<sup>17</sup> and conjugate reductions<sup>18</sup> have all been developed and reported (Figure 1.7).

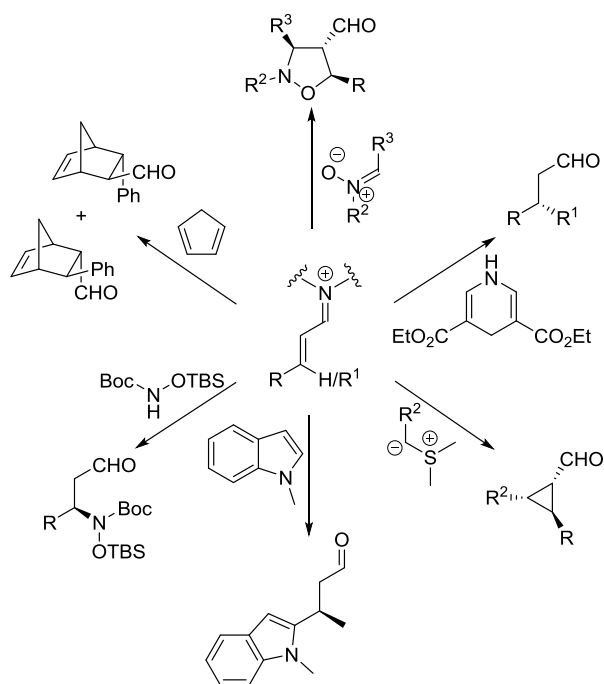


Figure 1.7 Iminium Catalysed Transformations

It should be noted that imidazolidinones are not suitable for all transformations. One example is the sulfur ylide mediated cyclopropanation (Figure 1.7) which operates using proline inspired catalyst **7**.<sup>19</sup>

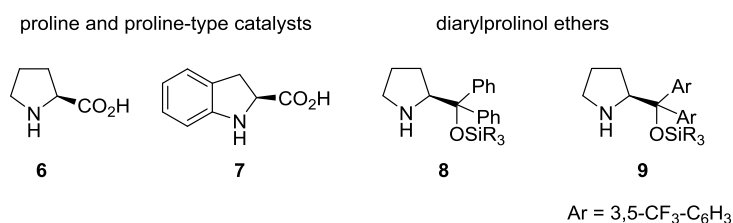


Figure 1.8 Alternative Catalysts to Imidazolidinones

Diarylprolinol ethers (Figure 1.8) have emerged as another class of amine catalyst.<sup>20</sup> They have been found to form highly reactive enamines<sup>21</sup> and a variety of transformations have been developed which exploit this reactivity.<sup>20</sup> The scaffold has also been used in iminium activation, however, it has been observed to offer low catalytic rates compared to imidazolidinones.<sup>22</sup>

Unlike diarylprolinol ethers, imidazolidinones have seldom been used for enamine catalysis. This is likely to be due to the electron-withdrawing nature of the imidazolidinone which results in enamines with reduced nucleophilicity.<sup>21</sup> Despite this, MacMillan has demonstrated that imidazolidinones can be used for some enamine catalysed transformations and has used the scaffold to catalyse the  $\alpha$ -halogenation of aldehydes (Figure 1.9).<sup>23,24</sup>

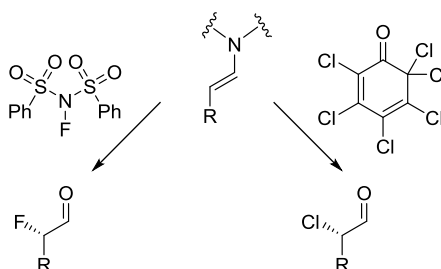


Figure 1.9 Imidazolidinone Catalysed  $\alpha$ -Halogenation of Aldehydes

MacMillan's insight into the field of Organocatalysis was further exemplified when he pioneered SOMO catalysis.<sup>12</sup> The SOMO activation method uses imidazolidinone catalysts and a variety of transformations have now been developed including;  $\alpha$ -vinylation,<sup>25</sup>  $\alpha$ -enolation,<sup>12</sup> carbo-oxidation,<sup>26</sup>  $\alpha$ -heteroarylation<sup>27</sup> and  $\alpha$ -allylation of aldehydes or ketones (Figure 1.10).<sup>27,28</sup>

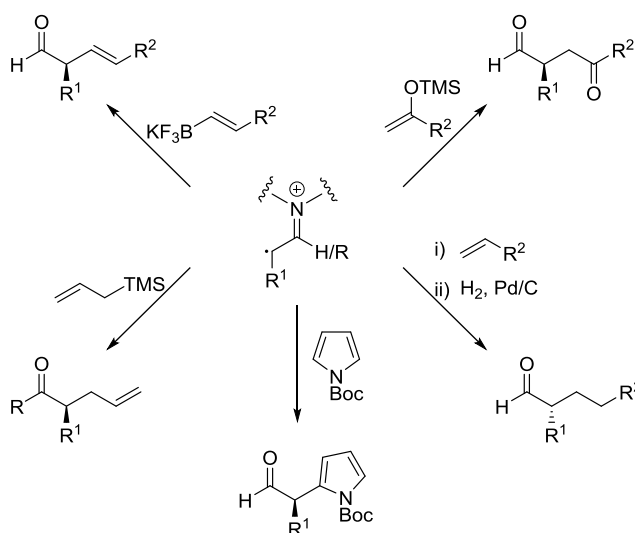


Figure 1.10 SOMO Transformations

More recently, the group has combined Organocatalysis with other methods of activation to give synergistic catalytic methodology. An example of this is the twinning of enamine catalysis with copper activation of iodonium triflate salts to  $\alpha$ -vinylate and  $\alpha$ -arylate aldehydes (Figure 1.11).<sup>29,30</sup>

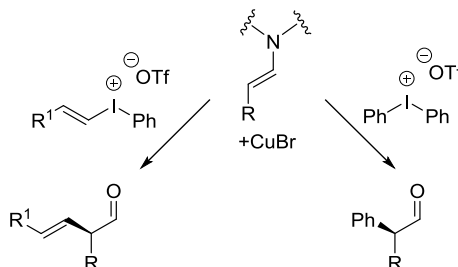


Figure 1.11 Synergistic Transformations

Work by MacMillan elegantly highlights the versatility of amine-based catalysis and demonstrates that novel catalyst architectures can be applied to many transformations and activation methods. Therefore, when designing novel catalysts it is important to remember they could be used outside their initial design scope.

## 1.3 Iminium Ion Activation

### 1.3.1 Preface

The field of iminium activation has become well known in synthetic chemistry and research in the area is headed by many different principal researchers across the globe. The diverse array of contributions to the field have been thoroughly documented elsewhere,<sup>3,31-34</sup> therefore, within this thesis only directly applicable literature will be discussed.

### 1.3.2 The Beginnings of Iminium Activation

Iminium ion activation was developed as a metal-free alternative to Lewis acid catalysis. It was envisaged as “a carbogenic system that exists as a rapid equilibrium between an electron-deficient and an electron-rich state”.<sup>1</sup>

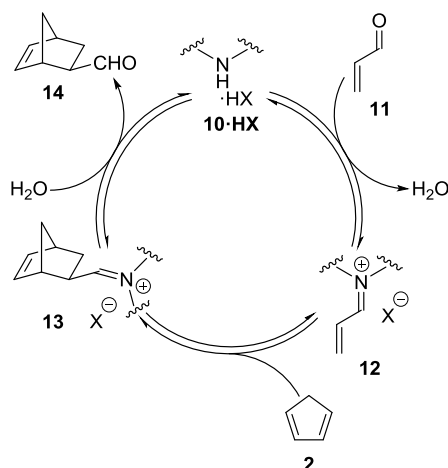
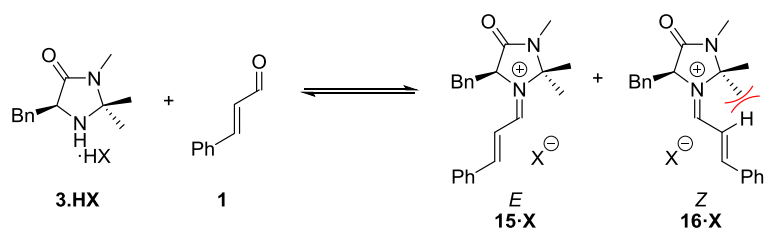


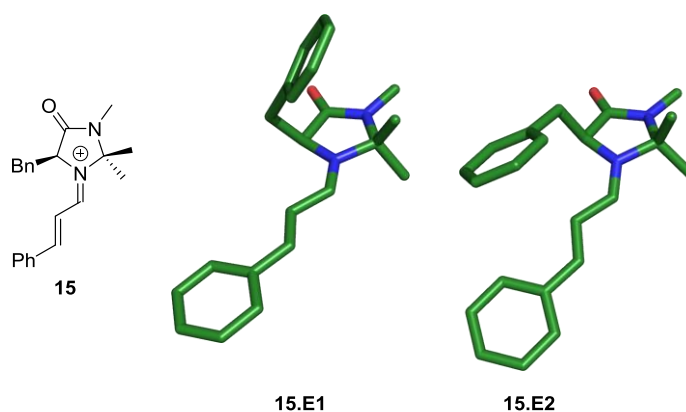
Figure 1.12 Proposed Catalytic Cycle for Iminium Catalysed Diels-Alder Reactions

The concept of iminium activation centres around condensation between an  $\alpha,\beta$ -unsaturated carbonyl compound (**11**) and a secondary amine salt (**10·HX**) to form an iminium ion (**12**). The iminium ion (**12**) possesses an electron-deficient  $\pi$ -system and hence has a lower  $E_{\text{LUMO}}$  compared to **11** which promotes reaction with nucleophilic species such as dienes (**2**). The iminium ion of the product (**13**) then undergoes hydrolysis to give the product aldehyde (**14**) and regenerate **10·HX**.



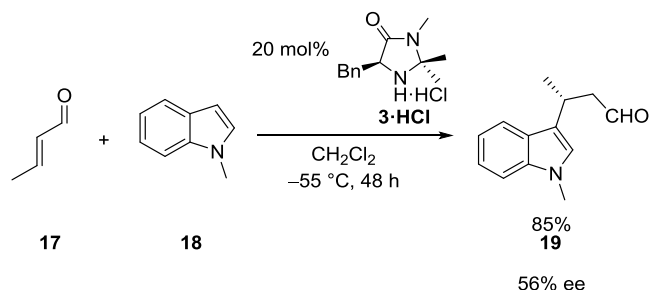
Scheme 1.2 Iminium Ion Isomer Formation

The concept of iminium activation was first used by MacMillan to catalyse a Diels-Alder reaction between **1** and **2** (Scheme 1.1).<sup>1</sup> The reaction attained high yields and furnished products with high levels of enantiomeric excess. MacMillan proposed that the reaction followed the postulate of iminium catalysis and that no competing pathways were occurring. Due to non-bonding interactions between the geminal methyl groups and the  $\alpha$ -proton disfavoured formation of the *Z*-isomer **16·X** only the *E*-iminium ion intermediate **15·X** was thought to be present for reaction (Scheme 1.2).

Figure 1.13 Conformations of Iminium Ion **15**

Asymmetry was reported to be directed by the benzyl group on the imidazolidinone ring.<sup>1</sup> MM3 calculations on the iminium ion intermediate (**15**) suggested that upon iminium ion formation the benzyl group of the catalyst extended over the  $\pi$ -system which prevented the diene from approaching the top *Re*-face (**15.E2**, Figure 1.13). Hence, cycloaddition occurred predominantly at the bottom *Si*-face which rendered the transformation asymmetric. However, this rationale became questionable when it was found that reactions which occur *via* open transition states were found to result

in products with poor levels of enantiomeric excess. For example, the reaction of crotonaldehyde (**17**) with *N*-methyl indole (**18**) catalysed by 20 mol% **3**·HCl gave the product (**19**) in a good yield (85%) but poor ee (56%) (Scheme 1.3).<sup>17</sup>



Scheme 1.3 *N*-Methyl Indole Conjugate Addition

The lack of asymmetry in reactions with open transition states rendered the reported low energy conformation of **15** (**15.E2**) questionable. If **15.E2** was the preferred conformation then high levels of asymmetry would be anticipated for both open and closed transition state reactions. This is because the benzyl group would shield the *Re*-face of the  $\alpha$ - and  $\beta$ - carbons of the iminium  $\pi$ -system which would lead to reaction occurring only at the *Si*-face for both reaction types (Figure 1.14).

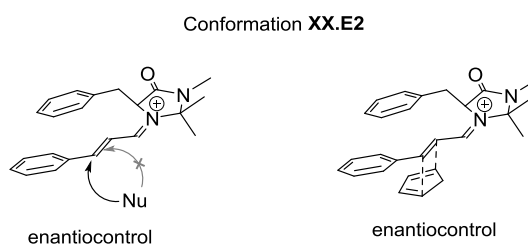


Figure 1.14 Enantiocontrol in Open and Closed Transition State Reactions with Conformation **15.E2**

Some researchers were unconvinced by MacMillan's rationale, higher level DFT calculations were conducted by Houk<sup>35</sup> and also within our group<sup>36</sup> which revealed that **15.E1** was the preferred conformation of iminium ion **15**. This was further reinforced by variable temperature <sup>1</sup>H NMR spectroscopy studies and single crystal X-ray crystallographic analysis. The newly proposed low-energy conformation **15.E1** correlated with experimental results. In **15.E1** the benzyl group offers no steric

shielding to either face of the  $\beta$ -carbon (Figure 1.15), hence, conjugate addition reactions which proceed *via* open transition states such as the alkylation of indole (Scheme 1.3) furnish products with poor ee. Reactions which proceed *via* closed transition states, for example the Diels-Alder reaction (Scheme 1.1), furnish products with high ee as the benzyl group shields the *Re*-face of the  $\alpha$ -carbon, hence, the diene can only approach from the *Si*-face (Figure 1.15).

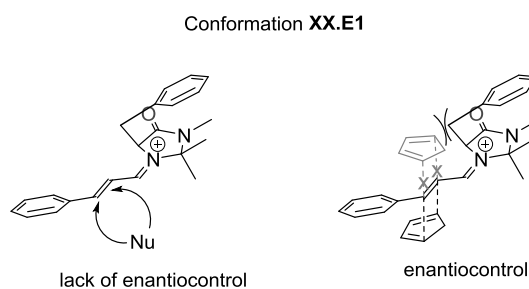


Figure 1.15 Enantiocontrol in Open and Closed Transition State Reactions with  
Conformation **15.E1**

To overcome the lack of success with reactions proceeding through open transition states a new imidazolidinone (**20·HCl**) was designed.<sup>17</sup>

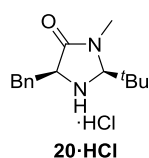


Figure 1.16 Imidazolidinone Suitable for Open Transition State Reactions

The addition of a *t*butyl group prevented the benzyl group from adopting a low energy conformation over the imidazolidinone ring and encouraged it to reside over the iminium  $\pi$ -system. This offered shielding to the  $\beta$ -carbon and hence reactions proceeded with high levels of asymmetry (Figure 1.17). However, a drawback of this new catalyst was that low reaction temperatures were required to obtain high levels of selectivity. A possible explanation for this was reported by Seebach. He showed that **20** suffers from poor control of iminium ion geometry (9:1, **21:22**) at ambient



temperatures<sup>37</sup> and this may be responsible for the poor selectivity observed at ambient temperature (Figure 1.17).

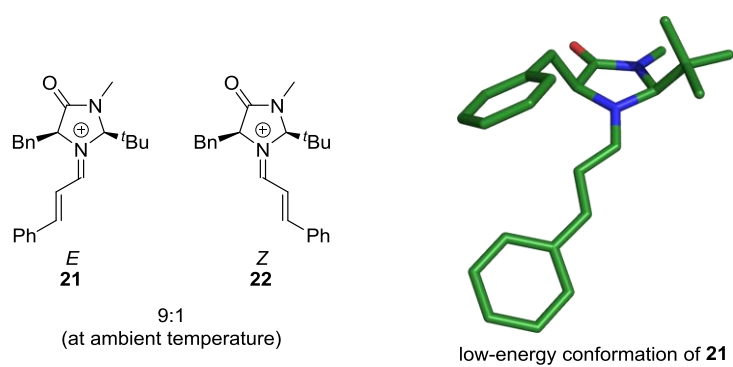


Figure 1.17 Iminium Ion Geometry and Conformation

## 1.4 Iminium Activation in the Group

### 1.4.1 Mechanistic Insight

Understanding and rationalising mechanism, reactivity and selectivity before attempting to improve methodology is core to the group's research ethos. This has driven extensive investigations into the secondary amine catalysed Diels-Alder reaction.

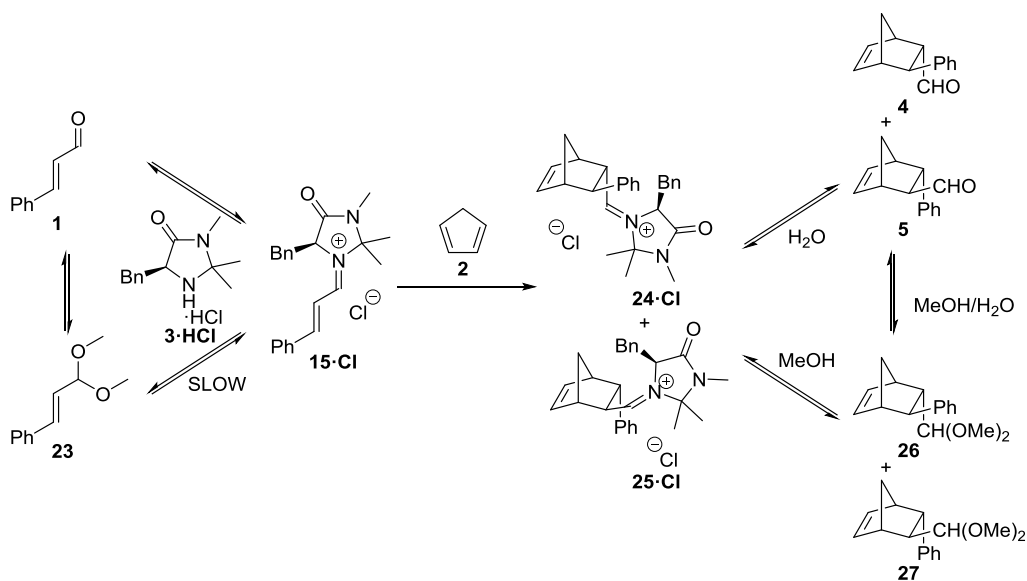


Figure 1.18 Overall Catalytic Process Incorporating Solvent Effects

The originally proposed catalytic cycle (Figure 1.12) was found to be somewhat more complicated (Figure 1.18).<sup>38</sup> The use of a methanol-based solvent system leads to each aldehyde being in equilibrium with the corresponding acetal and these additional species were observed to influence the overall reaction.

Formation of **15·Cl** directly from acetal **23** was observed to be slow compared to formation from aldehyde **1**. Cycloaddition between **15·Cl** and **2** was seen to be rapid and restricted by the formation of **15·Cl**. **24·Cl** and **25·Cl** were not observed and assumed to be short-lived. Hence, iminium ion formation was deemed to be rate determining. Addition of water to the system was seen to perturb the equilibrium between **1** and **23** and increase the effective concentration of **1**. Therefore, water was

observed to increase the overall rate of the catalytic process by increasing the availability of **1** which can condense with **3·HCl** to form **15·HCl**.

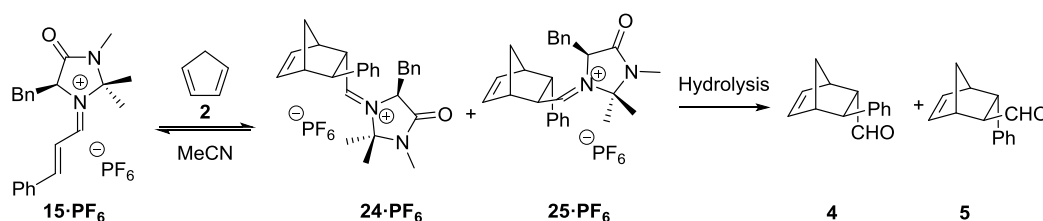


Figure 1.19 Cycloaddition Reversibility

The subtleties of the methanol/water solvent system were investigated further when it was discovered that **15·PF<sub>6</sub>**, a stable crystalline hexafluorophosphate salt, could be isolated. **15·PF<sub>6</sub>** was added to **2** in anhydrous acetonitrile and cycloaddition was observed to occur. However, under the anhydrous reaction conditions, the enantiomeric excesses of **4** and **5** (obtained after hydrolysis of an aliquot of reaction mixture) were observed to erode over time which indicated that the cycloaddition step was reversible. Under normal reaction conditions **4** and **5** would be intercepted by water or methanol at a faster rate than the retro Diels-Alder reaction. Therefore, products with high enantiomeric excess are obtained.

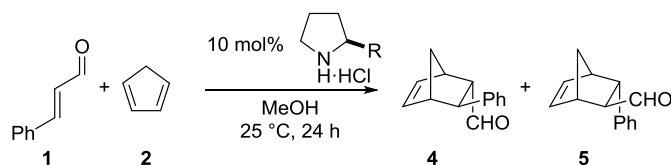
Overall the methanol/water solvent system was observed to influence reactivity and selectivity. This highlighted that choice of solvent was important for iminium ion catalysed reactions.

### 1.4.2 Catalyst Development

The reaction between cinnamaldehyde (**1**) and cyclopentadiene (**2**) catalysed by the MacMillan imidazolidinone (**3·HCl**) is used as the literature benchmark (Scheme 1.1). The readily obtainable reagents, high levels of conversion and excellent selectivities have rendered it an ideal reaction with which to screen novel catalysts.

Insight into catalyst development was made when amines possessing an  $\alpha$ -electron withdrawing group were found to offer enhanced catalytic rates. This was first observed in a series of substituted pyrrolidines (Table 1.1). The level of conversion

in the reaction between **1** and **2** in methanol was observed to correlate with the strength of the electron withdrawing group (EWG). **30·HCl** possessed the strongest EWG ( $\text{CF}_3$ ) and gave a high reaction conversion (93%) whereas **29·HCl** possessed a weaker EWG ( $\text{CO}_2\text{Et}$ ) and gave an average reaction conversion (62%) and pyrrolidine **28·HCl** with no EWG gave a very low reaction conversion.<sup>39</sup>



Amine	R	Conversion
<b>28·HCl</b>	H	<5%
<b>29·HCl</b>	$\text{CO}_2\text{Et}$	62%
<b>30·HCl</b>	$\text{CF}_3$	93%

Table **1.1** Influence of EWG's on Reaction Conversion

The relationship between the presence of an EWG and catalytic rate can be rationalised by considering the subtleties of iminium ion formation (Figure **1.20**). During formation of iminium ions from carbonyl compounds and amines, many equilibria are in operation (Figure **1.20**), each of which can be influenced by the electronics of the amine. To drive Equilibrium 1 and Equilibrium 3 forward an amine with reduced basicity is required. However, to positively influence Equilibrium 2 the amine must be nucleophilic. As nucleophilicity is linked to basicity, the electronics of the amine need to be balanced. Hence, it is logical that addition of an EWG influences catalytic rate by influencing Equilibrium 1 and Equilibrium 3, but the positive relationship between rate and strength of EWG will be finite due to Equilibrium 2.

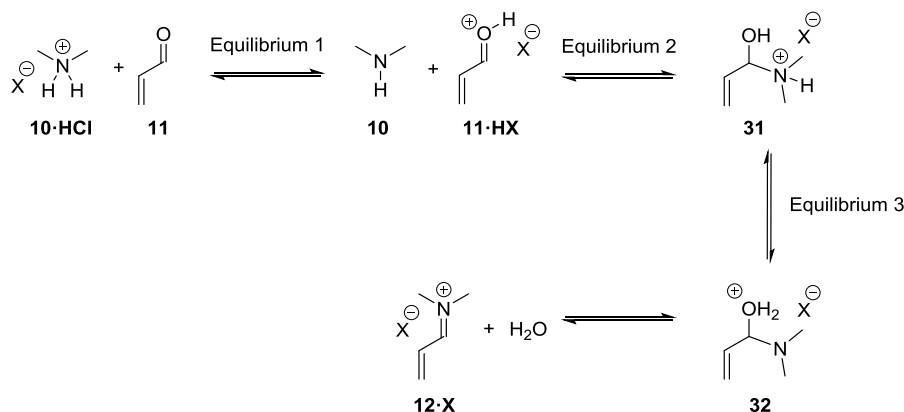


Figure 1.20 Subtleties of Iminium Ion Formation

Seeking to furnish high-performance catalysts which offer high levels of enantioselectivity, the chiral imidazolidinone scaffold was investigated. A series of imidazolidinones possessing electron-withdrawing groups were targeted for synthesis (Figure 1.21)

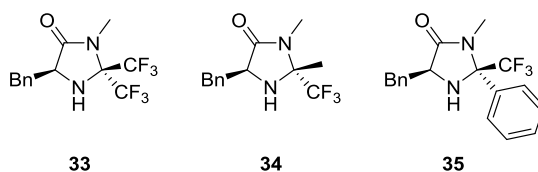
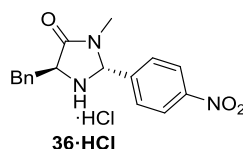
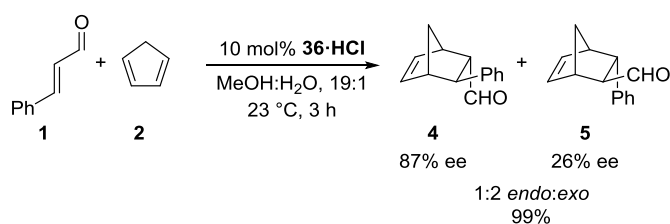


Figure 1.21 Imidazolidinones Possessing Electron-Withdrawing Groups

Imidazolidinone **33**, possessing two  $\alpha\text{-CF}_3$  groups, was considered to be the key target. However, despite significant efforts to prepare and isolate **33** none were successful.<sup>40</sup> Preparation of imidazolidinones **34** and **35** was, however, possible. It was discovered that **35** could not be transformed into its corresponding hydrochloride salt which indicated that the phenyl ring and trifluoromethyl group significantly diminished the basicity of the nitrogen. This was also reflected in its lack of capacity as a catalyst. Unlike **35**, **34** was amenable to hydrochloride salt formation; however, it was observed to evolve hydrogen chloride under reduced pressure and was also observed to be catalytically inactive. Both **34** and **35** demonstrated the finite nature of the relationship between strength of EWG and catalytic activity.

Figure 1.22 Imidazolidinone Containing an  $\alpha$ -EWG

Attempts at finding a catalytically active imidazolidinone possessing an  $\alpha$ -EWG had failed. However, the idea was pursued further and led to imidazolidinone **36·HCl**. The 4-nitrophenyl group was found to be an EWG with appropriate strength to positively influence catalytic activity. **36·HCl** provided 99% conversion in the benchmark reaction over 3 h at 10 mol% catalyst loading (Scheme 1.4).<sup>41</sup> This was a marked improvement over the MacMillan imidazolidinone (**3·HCl**) which was reported to take 8 h to furnish the same conversion under identical reaction conditions.

Scheme 1.4 Diels-Alder Reaction Catalysed by **36·HCl**

Despite its improved catalytic rate, **36·HCl** was limited by the low levels of ee observed. The *endo*-isomer (**4**) was furnished in a reasonable ee of 87%, however, the *exo*-isomer (**5**) was formed in a poor ee of just 26%. To overcome this, rational design was used whereby the imidazolidinone (**36**) was redesigned to incorporate both the benzyl group and the *cis*-methyl group from the literature benchmark **3** (Figure 1.23). It was thought that this would render the origins of enantioselectivity identical to those of **3** which would lead to products with high levels of enantiomeric excess. Combination of this design rationale and the 4-nitrophenyl EWG led to the development of **38**.

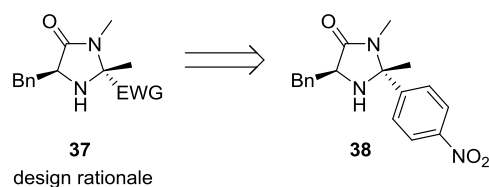
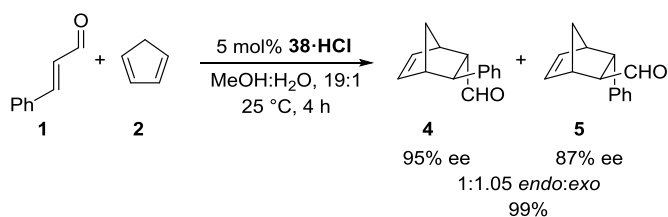


Figure 1.23 Imidazolidinone Rational Design

Akin to **36·HCl**, **38·HCl** offered enhanced levels of catalytic turnover compared to **3·HCl** and achieved complete conversion in 4 h at 5 mol% loading. In addition, as designed, products with high levels of enantiomeric excess were obtained (Scheme 1.5).<sup>40</sup> The *endo*-isomer (**4**) was found to have an ee of 95%, 2% higher than the literature benchmark. However, the excellent selectivity was not replicated in the *exo*-isomer (**5**) which was found to have an ee of 87%, 6% lower than the benchmark.

Scheme 1.5 Benchmark Reaction Catalysed by **38·HCl**

The discovery of **38** provided an ideal opening into the realms of low-catalyst loadings. However, its application was only investigated in the benchmark reaction and, hence, its full capabilities remained unknown. For example, it was unknown if **38·HCl** could be used to accelerate reactions other than the Diels-Alder cycloaddition.

### 1.4.3 DFT Calculations

Conformational analysis using DFT calculations on intermediates (such as **15**) has enabled enantioselectivity to be rationalised<sup>36</sup> and has been used to predict diastereofacial shielding for novel amine catalysts.<sup>40</sup> In addition, proton affinity calculations, a measure of amine basicity,<sup>42</sup> have been seen to have an inverse correlation with catalytic rate for the literature catalysts (Figure 1.24).<sup>22,40</sup> For

example, diarylprolinol ether **39** and imidazolidinone **3** were found to have proton affinities of 998 kJ mol<sup>-1</sup> and 943 kJ mol<sup>-1</sup> respectively, a difference which was reflected in their performance in the benchmark reaction. Imidazolidinone **3** was observed to offer higher catalytic rates compared to **39**. This relationship also correlates with an  $\alpha$ -EWG increasing catalytic rate as an EWG will reduce the basicity of the amine and, hence, lower the proton affinity which leads to increased levels of reactivity.

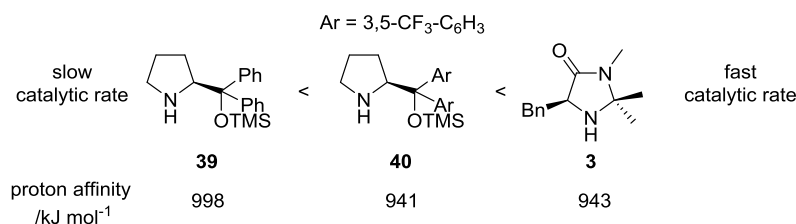


Figure 1.24 Literature Catalysts with Rate Compared to Proton Affinity

Alongside proton affinity, isomeric excesses of iminium ion intermediates have been calculated. The idea of isomeric excess was derived from the concept of enantiomeric excess and provides an indication of iminium ion selectivity. It can be calculated by finding low-energy conformations of *E*- and *Z*- iminium ions and using their energies in a Boltzmann distribution to determine an iminium ion ratio. The ratio is then converted to isomeric excess using the equation shown in Figure 1.25.

$$\text{Isomeric Excess (IE)} = \frac{N_E - N_Z}{N_E + N_Z} \times 100$$

Example:  
 an *E/Z* iminium ion ratio of 9:1  $\text{IE} = \frac{9 - 1}{9 + 1} \times 100 = 80\%$

Figure 1.25 Isomeric Excess Calculation

If it is assumed that each iminium ion isomer shares equal reactivity, a single iminium ion isomer must form to furnish products with high levels of enantiomeric excess. For example, if **41** and **42** formed in a 1:1 ratio and both experienced steric shielding from the unhindered-face, each isomer would have a different face available for reaction (Figure 1.26). Iminium ion **41** has an exposed *Si*-face and **42**



has an exposed *Re*-face, therefore, if reaction occurred at the unshielded face of each isomer at an equal rate a racemic product would be obtained. Hence, isomeric excess is an important value which can be linked to enantioselectivity.

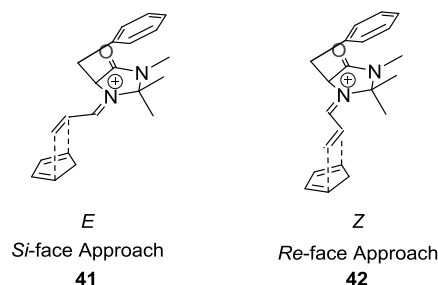


Figure 1.26 Attack on different Iminium Ion Isomers

In addition to being calculated using DFT methods, enantiomeric excess can also be determined experimentally. Equilibria can be setup by mixing amine salts and  $\alpha,\beta$ -unsaturated aldehydes. These mixtures can then be analysed by  $^1\text{H}$  NMR spectroscopy and the relative integrals of resonances corresponding to each isomer can be transformed into an isomeric excess value. Calculated isomeric excesses have been shown to correlate strongly with experimentally determined isomeric excess values (19:1  $\text{CD}_3\text{OD}/\text{D}_2\text{O}$ , 0.1 M amine hydrochloride, 0.5 M cinnamaldehyde). This is important as it indicates that the predicted values are a good indication of iminium ion distribution in solution (Figure 1.27).<sup>40</sup>

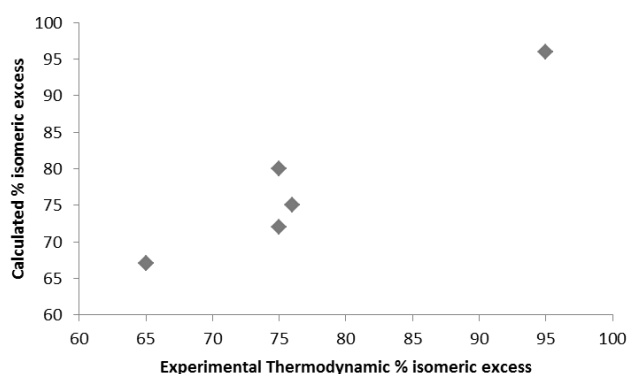


Figure 1.27 Calculated Isomeric Excess Compared to Experimental Isomeric Excess

Calculated isomeric excess values have been seen to correlate with enantiomeric excesses of *exo* Diels-Alder adducts (Figure 1.28). Hence, as designed, isomeric excess can be used as a predictive model for catalyst performance.<sup>40</sup> For example, the MacMillan catalyst (**3**) has a calculated isomeric excess of 95%, experimental isomeric excess of 96% and furnishes the *exo* adduct in 93% ee.

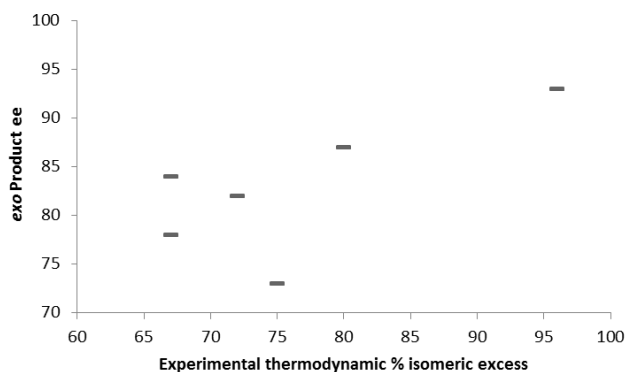


Figure 1.28 Correlation between Isomeric Excess and Product ee from the Benchmark Reaction (Scheme 1.1)

Proton affinity and isomeric excess calculations have been seen to correlate with experimental observations, hence, they could be used to predict catalytic performance. However, it should be noted that the predictive parameters are not entirely robust. For example, proton affinity values suggest that diarylprolinol **40** (PA = 941 kJ mol<sup>-1</sup>) should offer a comparable catalytic rate to the MacMillan imidazolidinone **3** (PA = 943 kJ mol<sup>-1</sup>). However, in the benchmark reaction **40** is a significantly slower catalyst compared to **3**. Isomeric excess has also been seen to sometimes incorrectly predict performance. For example, imidazolidinone **36** has a calculated isomeric excess of 94%. However, in the benchmark reaction it furnishes the *exo* adduct with an ee of only 26%. This suggests that isomeric excess should only be applied to imidazolidinones possessing a methyl group *cis* to the benzyl group. Therefore, despite these predictive parameters showing promise, they do have a few limitations and need to be used with care.

## **1.5 Project Aims**

The principle aims of this research were to build upon existing roots of knowledge and feed into tackling some of the perceived shortcomings of iminium ion activation, which are:

- High catalyst loadings
- Lack of transformations using  $\alpha,\beta$ -unsaturated ketone substrates
- Incomplete understanding of the origins of enantioselectivity

To address these shortcomings, projects were designed to reduce catalyst loading, rationalise and tackle the redundancy of enone substrates, increase understanding of the catalytic cycle and further define origins of asymmetric induction. These series of projects are presented herein.

## **Chapter 2: Evaluation of a Novel Imidazolidinone**

## 2 Evaluation of a Novel Imidazolidinone

### 2.1 Introduction

A long-term goal within the group was to develop an imidazolidinone which offers higher catalyst turnover than the literature benchmark in Diels-Alder reactions. Creating a catalyst that performs better than the MacMillan imidazolidinone (**3**·HCl) was no easy task.<sup>1</sup> The discovery that addition of an  $\alpha$ -EWG to the amine scaffold increases catalytic rate led to imidazolidinone **38**·HCl which offered a faster catalytic rate and comparable enantioselectivity to the MacMillan imidazolidinone (**3**·HCl) in the benchmark Diels-Alder cycloaddition reaction between cinnamaldehyde (**1**) and cyclopentadiene (**2**).

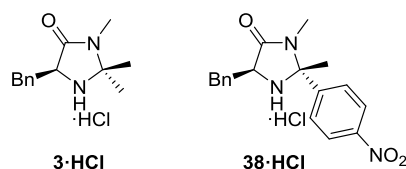


Figure 2.1 Literature Benchmark

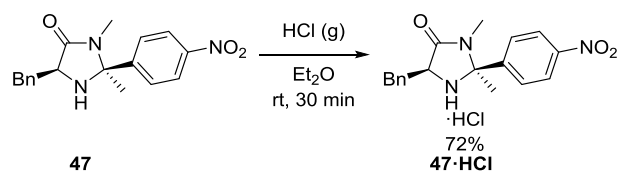
Imidazolidinone **38** was not evaluated beyond the benchmark reaction and this rendered its scope unknown. Within this chapter, dienophile substrate and reaction limitations are investigated and compared to the MacMillan imidazolidinone (**3**). In addition, the iminium ion intermediate (**77**) is probed to rationalise the origins of enantioselectivity.

## 2.2 Diels-Alder Cycloaddition Reactions

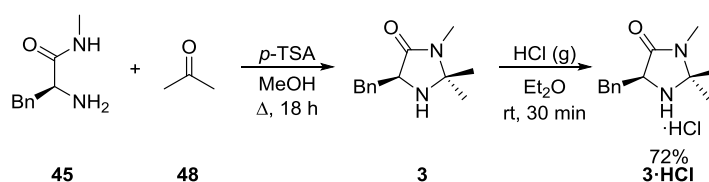
### 2.2.1 Synthesis of Imidazolidinone **38**

Preparation of imidazolidinones **3** and **38** was required before assessment of catalytic performance could commence. Precursor amino amide **45** was synthesised in a good yield of 75% from commercially available ester **43**·HCl and ethanolic methylamine (**44**) (Scheme 2.1).



Scheme 2.4 Formation of Hydrochloride Salt **47·HCl**

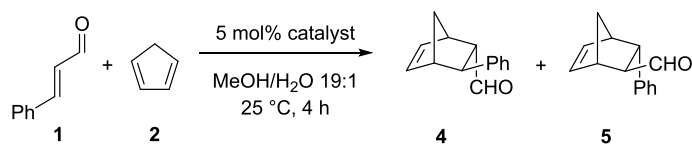
Despite commercial availability of the MacMillan first generation imidazolidinone (**3·HCl**), it was prepared in-house at a significantly reduced cost. Amino amide **45** was condensed with acetone (**48**) in the presence of *p*-TSA to give imidazolidinone **3**. Treatment of an ethereal solution of the crude reaction mixture with anhydrous hydrogen chloride furnished **3·HCl** in 72% yield (Scheme 2.5). In a similar manner to **38**, the freebase imidazolidinone (**3**) was subjected to HPLC on a chiral stationary phase and found to have an ee >98%.



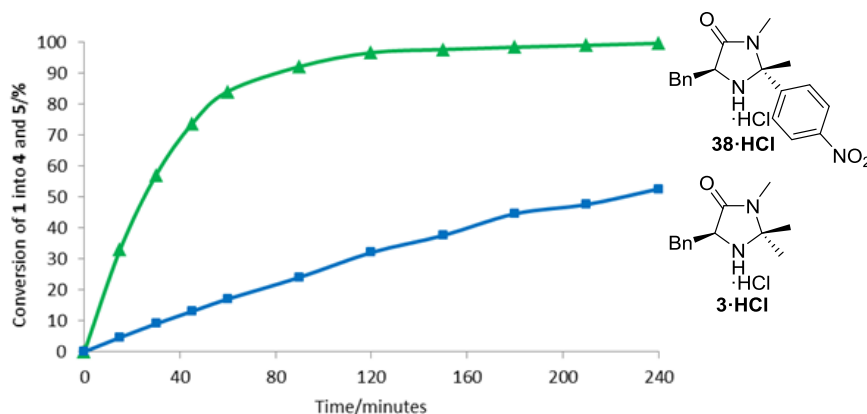
Scheme 2.5 Synthesis of MacMillan First Generation Imidazolidinone

### 2.2.2 Catalyst Performance

Upon its discovery, the catalytic performance of **38** had only been assessed using the benchmark Diels-Alder reaction between cinnamaldehyde (**1**) and cyclopentadiene (**2**) (Scheme 2.6). Reaffirming this result was deemed to be a good starting point from which to further explore the potential of **38**. Reactions were carried out using 5 mol% catalyst loading (hydrochloride salt), 1 equivalent of cinnamaldehyde (**1**) and 2.5 equivalents of cyclopentadiene (**2**) as a 1 M solution in methanol/water (19:1). Aliquots were systematically taken and quenched by the removal of volatile **2** under reduced pressure. Subjection to acidic hydrolysis converted dimethyl acetals of **2**, **4** and **5** to their parent aldehydes. Reaction conversion of **1** into **4** and **5** was then determined using  $^1\text{H}$  NMR spectroscopy (see Chapter 10 for full details). Catalysts **3** and **38** were examined under identical reaction conditions to enable direct comparison of the reaction rates.



Scheme 2.6 Benchmark Reaction used for Monitoring

Figure 2.2 Kinetic Comparison between Imidazolidinones **3·HCl** and **38·HCl** in the Benchmark Reaction

Imidazolidinone **38·HCl** was observed to be approximately six times quicker than the literature benchmark **3·HCl** which agreed with previous observations (Figure 2.2).<sup>40</sup> To allow full comparison between **38·HCl** and **3·HCl**, the ee's of the products were determined. Due to their poor chromophore, **4** and **5** were converted to their corresponding 2,4-dinitrophenyl hydrazones. The hydrazones were then analysed by HPLC on a chiral stationary phase (Table 2.1).<sup>43</sup>

Catalyst	<i>endo:exo</i> ( <b>4:5</b> )	<b>4</b> ee	<b>5</b> ee
<b>3·HCl</b>	1:1.33	93%	93%
<b>38·HCl</b>	1:1.05	95%	87%

Table 2.1 Benchmark Product ee's Obtained Using **3** and **38**

Imidazolidinone **3** furnished an *endo/exo* (**4/5**) ratio of 1:1.33 and both adducts were found to have an ee of 93% which was consistent with literature performance.<sup>1</sup> Imidazolidinone **38·HCl** was observed to have virtually no selectivity between isomers and produced **4** and **5** in a 1:1.05 ratio. **4** was found to have a superior ee of



95% compared to the 93% ee obtained with the benchmark catalyst. Unfortunately this was not replicated in **5** which was found to have an ee 6% lower (87%) than the literature benchmark. Despite a decrease in enantioselectivity for the *exo* adduct, **38·HCl** offered remarkably better performance compared to **3·HCl**.

### 2.2.3 Dienophile Substrate Scope

Having observed excellent performance with cinnamaldehyde (**1**) as the dienophile attention was focused on other substrates. To gain an idea of substrate tolerance three aliphatic aldehydes were selected (Figure 2.3). Aldehyde **49** was chosen as a general aliphatic substrate with minimal steric demands, aldehyde **50** was selected to probe increased steric effects about the  $\gamma$ -position and aldehyde **11** was chosen as it is unsubstituted at the  $\gamma$ -position.

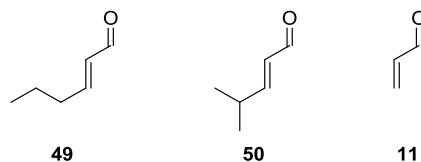
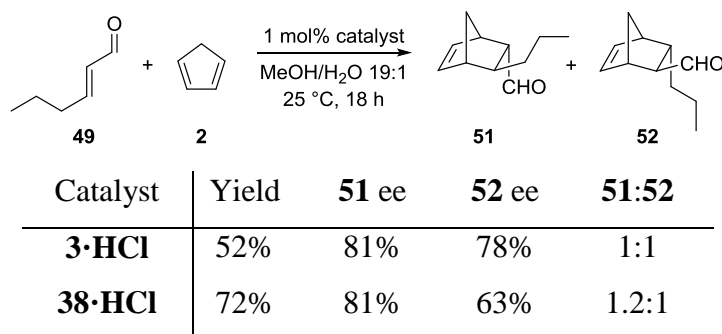
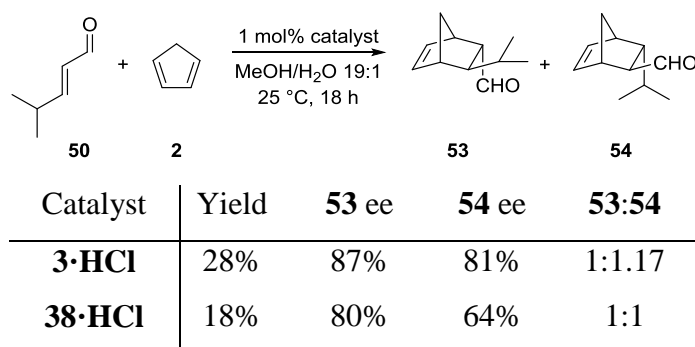


Figure 2.3 Aliphatic Dienophile Substrates

Aldehydes **49**, **50** and **11** are volatile and hence reaction monitoring would be challenging. As an alternative, catalyst loading was lowered to 1 mol% and reactions were run for 18 hours. Product yields were then used to compare the performance of **3·HCl** and **38·HCl**. After isolation, the Diels-Alder adducts were converted to the corresponding 2,4-dinitrophenyl hydrazones and their ee's were determined by HPLC on a chiral stationary phase.

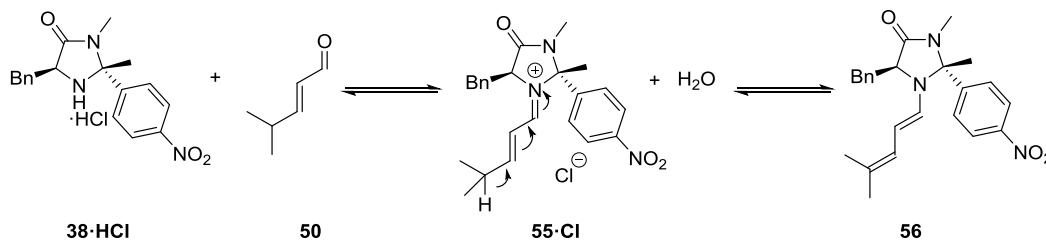
Table 2.2 Comparison of **3·HCl** and **38·HCl** with Aliphatic Substrate **49**

Imidazolidinone **38·HCl** was found to offer enhanced performance with aldehyde **49** and gave a 20% increase in yield over imidazolidinone **3·HCl** (Table 2.2). Both imidazolidinones were observed to furnish the *endo* adduct with identical enantiomeric excesses of 81%. However, as observed with cinnamaldehyde (**1**), imidazolidinone **38·HCl** produced the *exo* adduct with an inferior ee (63%) compared to the MacMillan imidazolidinone (**3·HCl**) (78%).

Table 2.3 Comparison of **3·HCl** and **38·HCl** with Substrate **50**

Substrate **50** found a limitation of imidazolidinone **38·HCl**. A yield of 18% was obtained, lower than that of **3·HCl** (28%). In addition, the enantiomeric excesses of **53** and **54** were 7% and 17% lower than those obtained using **3·HCl** (Table 2.3). A lower yield combined with inferior enantiomeric excesses rendered **3·HCl** superior to **38·HCl**. A combination of an electron-withdrawing imidazolidinone and the increased substitution at the  $\gamma$ -position of **50** were thought to potentially encourage dienamine formation (Scheme 2.7). Efforts were made to observe dienamine **56**, however, mixtures of **38·HCl** and **50** were found to produce a multitude of products over time and a dienamine was not identifiable by  $^1\text{H}$  NMR spectroscopy. Despite

not having observed **56**, the degradation of **50** in the presence of **38·HCl** did suggest that dienamine formation followed by reaction with **50** was a plausible idea which could lead to a reduction in the formation of **53** and **54**.



Scheme 2.7 Proposed Dienamine Formation

To reduce product volatility, substrate **11** was evaluated using cyclohexadiene (**57**). Like cyclopentadiene (**2**), cyclohexadiene (**57**) is a conformationally fixed *s-cis* diene; therefore, the change was thought to have minimal influence on reactivity. In addition to a different diene, the solvent system was changed as methanol was found to rapidly react with **11** under acidic reaction conditions. Therefore, acetonitrile was used in place of methanol to maintain a monophasic solvent system (Table 2.4).

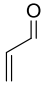
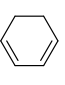
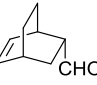
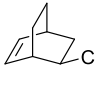
		$\xrightarrow[25\text{ }^\circ\text{C, 18 h}]{1\text{ mol\% catalyst, MeCN/H}_2\text{O 19:1}}$				
<b>11</b>	<b>57</b>	<b>58</b>	<b>59</b>			
Catalyst	Yield	<b>58</b> ee	<b>59</b> ee	<b>58:59</b>		
<b>3·HCl</b>	44%	91%	33%	15:1		
<b>38·HCl</b>	45%	81%	4%	11.3:1		

Table 2.4 Comparison of **3·HCl** and **38·HCl** with Substrate **11**

Equal product yields were obtained using catalysts **3·HCl** and **38·HCl** with aldehyde **11**. Disappointingly, **38·HCl** provided products **58** and **59** with enantiomeric excesses of 81% and 4% respectively, lower than those obtained with **3·HCl** (91% and 33% respectively). This rendered **3·HCl** a better catalyst for this substrate under the reaction conditions examined.

Overall, imidazolidinone **38·HCl** was seen to offer enhanced rates of reaction with cinnamaldehyde (**1**) and linear alkyl  $\alpha,\beta$ -unsaturated aldehyde **49** compared to **3·HCl**. However, high levels of enantiomeric excess were only obtained using **1**. To explore the successful cinnamaldehyde substrate, a range of *p*-substituted cinnamaldehydes were screened. **60** and **61** were chosen as electron-rich substrates and **62** and **63** were selected as electron poor substrates (Figure 2.4).

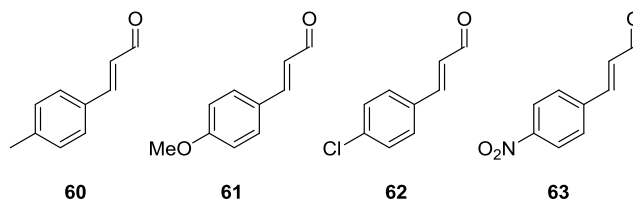
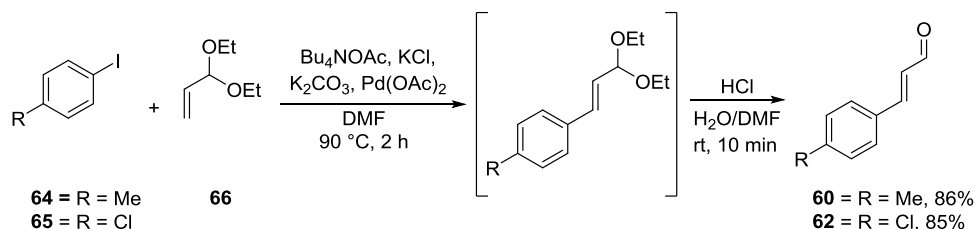


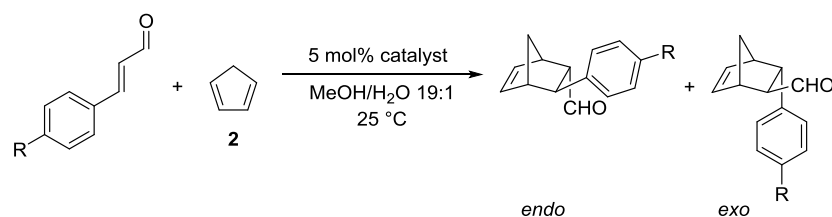
Figure 2.4 Cinnamaldehyde Substrates

Scheme 2.8 Synthesis of Cinnamaldehydes *via* Heck Reaction

Cinnamaldehydes **61** and **63** were commercially available. **60** and **62** were prepared using a Heck cross coupling between the corresponding aryl iodide (**64** or **65**) and acrolein diethyl acetal (**66**) followed by an acidic deprotection (Scheme 2.8).<sup>44</sup> **60** and **62** were obtained in good yields of 86% and 85% respectively.

To provide comparable results, each cinnamaldehyde was used in conjunction with **3·HCl** and **38·HCl**. A 5 mol% catalyst loading and cyclopentadiene (**2**) were used and both reactions were quenched (by removal of volatile **2**) when complete consumption of the aldehyde was observed by TLC (Table 2.5). A biphasic acidic hydrolysis was then performed using a TFA, chloroform and water mixture to convert any dimethyl acetals to their parent aldehydes. Products were then isolated by flash column chromatography. After reduction of the product aldehydes using

sodium borohydride, enantiomeric excesses were determined by HPLC on a chiral stationary phase.



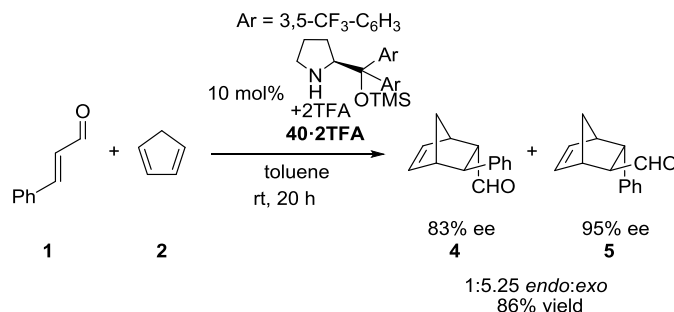
Catalyst	R	Reaction	Isolated	<i>(endo adduct)</i>		<i>(exo adduct)</i>	<i>endo:exo</i>
		Time	Yield	ee	ee		
<b>3•HCl</b>	H	4 h	53%	<b>(4)</b> 93%	<b>(5)</b> 93%	1:1.33	
<b>38•HCl</b>	H	4 h	99%	<b>(4)</b> 95%	<b>(5)</b> 87%	1:1.05	
<b>3•HCl</b>	OMe	20 h	34%	<b>(67)</b> 91%	<b>(68)</b> 91%	1:1.37	
<b>38•HCl</b>	OMe	20 h	95%	<b>(67)</b> 96%	<b>(68)</b> 87%	1:1.06	
<b>3•HCl</b>	NO <sub>2</sub>	5.5 h	27%	<b>(69)</b> 83%	<b>(70)</b> 83%	1:1.29	
<b>38•HCl</b>	NO <sub>2</sub>	5.5 h	94%	<b>(69)</b> 95%	<b>(70)</b> 84%	1.11:1	
<b>3•HCl</b>	Cl	4.5 h	45%	<b>(71)</b> 92%	<b>(72)</b> 89%	1:1.33	
<b>38•HCl</b>	Cl	4.5 h	95%	<b>(71)</b> 96%	<b>(72)</b> 84%	1.07:1	
<b>3•HCl</b>	Me	5 h	24%	<b>(73)</b> 92%	<b>(74)</b> 92%	1:1.34	
<b>38•HCl</b>	Me	5 h	75%	<b>(73)</b> 94%	<b>(74)</b> 86%	1:1	

Table 2.5 Screening of Cinnamaldehydes

In each case **38•HCl** outperformed **3•HCl** and provided higher yields for electron-rich, electron-neutral and electron-poor cinnamaldehydes. In addition, **38•HCl** produced *endo* adducts with higher levels of enantiomeric excess compared to **3•HCl**. Of particular note was 4-nitrocinnamaldehyde (**63**) whereby, along with a significant rate advantage, **38•HCl** furnished the *endo* (**69**) and *exo* (**70**) adducts in higher ee (95% and 84% respectively) compared to **3•HCl**. Product ratios were unnoteworthy at around 1:1 *endo:exo* using imidazolidinone **38•HCl** compared to the MacMillan imidazolidinone (**3•HCl**) whereby the *exo* adduct was slightly favoured in each case.

### 2.2.4 Competition Reactions

The MacMillan imidazolidinone (**3·HCl**) is not the only catalyst to have been used in the reaction between cinnamaldehyde (**1**) and cyclopentadiene (**2**).



Scheme 2.9 Diarylprolinol Ether Catalysed Diels-Alder Reaction

Diarylprolinol ether **40·2TFA** has also been used to catalyse this reaction. **40·2TFA** furnishes **4** and **5** in 83% and 95% ee respectively and the products are obtained in a 1:5.25 ratio in favour of the *exo* adduct (**5**) (Scheme 2.9).<sup>45</sup> Like **3·HCl**, **40·2TFA** requires high catalyst loadings and long reaction times.

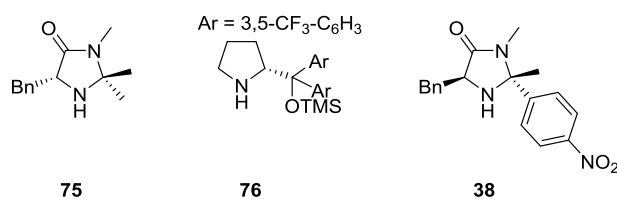
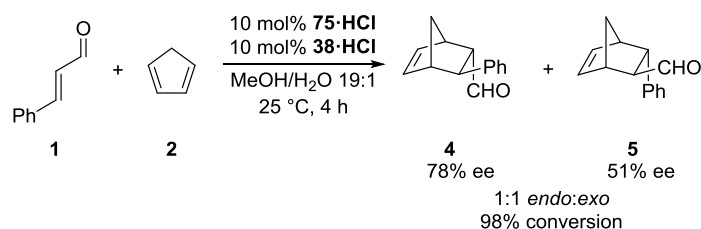


Figure 2.5 Literature Benchmark Catalysts for Competition Reactions

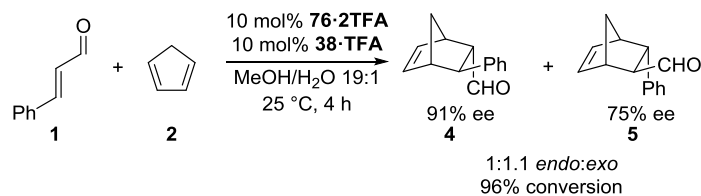
To highlight the performance advantage of **38** over the literature benchmarks, competition reactions were envisaged. Using secondary amines **75·HCl** and **76·2TFA** would furnish products of the opposite enantiomer compared to imidazolidinone **38**. Therefore, using mixtures of catalysts that produce products of opposite enantiomer in a reaction would provide a competitive environment in which both enantiomers of product can be formed. However, as **38** offers significantly faster catalytic rates than **75** (and presumably **76**<sup>22</sup>), it would be anticipated that enantioenriched products resulting from the reaction being catalysed by **38** would be obtained.

In the competition reactions, imidazolidinone **75** and diarylprolinol **76** were used as reported in the literature; **75** was used as the hydrochloride salt (**75·HCl**) whereas **76** was used in conjunction with two equivalents of TFA (**76·2TFA**). **38** was used as either the hydrochloride salt (**38·HCl**) or with one equivalent of TFA (**38·TFA**). Each reaction was allowed to run for 4 hours to ensure sufficient conversion of **1** to products **4** and **5**.



Scheme 2.10 Competition Reaction One

In the first competition reaction 10 mol% MacMillan imidazolidinone (**75·HCl**) and 10 mol% imidazolidinone **38·HCl** were used. After a 4 hour reaction time, a conversion of 98% was obtained and products **4** and **5** were obtained in a 1:1 ratio (Scheme 2.10). As anticipated, **4** and **5** were enantioenriched and had enantiomeric excesses of 78% and 51% respectively. Importantly, the major enantiomer was from the reaction being catalysed by **38·HCl**. The ee of the *exo*-adduct was degraded more than that of the *endo*-adduct. This was thought to arise as **75·HCl** favours formation of the *exo*-adduct (**5**), therefore, **75·HCl** produces more of the minor enantiomer of **5** compared to **4** during the reaction. However, this theory was not reflected in the dr of the reaction.



Scheme 2.11 Competition Reaction Two

In the second competition reaction, 10 mol% **76·2TFA** and 10 mol% **38·TFA** were used. A good conversion of 96% was obtained after a 4 hour reaction time. The products **4** and **5** were furnished in a 1:1.1 ratio with 91% and 75% ee respectively (Scheme 2.11). Similarly to the first competition reaction, the major enantiomer was from the reaction being catalysed by **38·TFA**. The diarylprolinol ether (**76·2TFA**) is known to produce **4** and **5** in a 1:5.25 ratio (Scheme 2.9). This caused the ee of **5** to be reduced more than the ee of **4** and the product ratio to be slightly in favour of **5** in the reaction.

Each competition reaction showcased the ability of **38** to offer higher catalytic rates than the literature benchmarks.

### 2.2.5 Asymmetric Catalyst Efficiency

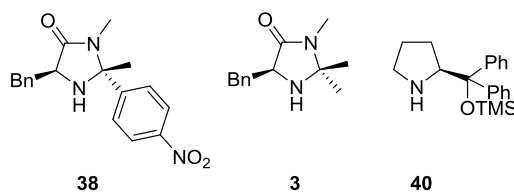
Comparing asymmetric catalysts is a significant challenge. Focus is often centralised on individual components of the reaction rather than the overall picture. To overcome this problem, a catalyst “Asymmetric Catalyst Efficiency” (ACE) factor has been proposed (Figure 2.6).<sup>46</sup> The ACE factor appeared to be a suitable tool to compare **38** with the literature benchmarks (**3** and **40**).

$$\text{ACE} = \frac{\text{Product } M_{\text{wt}}}{\text{Catalyst } M_{\text{wt}}} \times \frac{1}{\text{Catalyst Loading}} \times \frac{\text{ee}}{100} \times \text{Yield}$$

Figure 2.6 Equation to Determine ACE

To remove any bias from the calculation of ACE factors, all reaction details were taken from the literature<sup>1,45</sup> and for consistency, data from reactions between cinnamaldehyde (**1**) and cyclopentadiene (**2**) were used. As two products are formed (**4** and **5**) in differing ee and ratio depending on the catalyst, a weighted ee was calculated. In addition, although the catalyst system can be said to be a combination of amine and co-acid, for simplicity only the molecular weight of the amine was considered.





Catalyst	Product M <sub>wt</sub>	Catalyst M <sub>wt</sub>	Catalyst loading	Yield	Weighted ee	RXN Time	ACE
<b>38</b>	198	325.4	5 mol%	99%	91	4 h	11.0
<b>3</b>	198	218.3	5 mol%	99%	93	21 h	16.8
<b>40</b>	198	597.5	10 mol%	86%	93	20 h	2.7

Table 2.6 Calculation of ACE Factors

Omission of reaction time was observed to be an oversight of the ACE factor (Table 2.6). Literature benchmark **3** had a better ACE factor than **38** even though **38**, a significantly faster catalyst, was reacted at the same catalyst loading and furnished products with a comparable weighted ee. To overcome this limitation, an Asymmetric Catalyst Efficiency Speed (ACES) defined as ACE/RXN time was calculated.<sup>46</sup> In addition, ‘turnover’ was also determined (yield / (catalyst loading × RXN time)) and used as another comparison factor (Table 2.7).

Catalyst	ACE	ACES /h <sup>-1</sup>	Turnover /h <sup>-1</sup>
<b>38</b>	11.0	2.75	4.95
<b>3</b>	16.8	0.8	0.94
<b>40</b>	2.7	0.135	0.43

Table 2.7 Catalyst Performance Measures

Incorporation of reaction time into the ACE factors gave ACES values which correlated as anticipated. **40** had the lowest ACES value of 0.135, followed by **3** (0.8) and **38** (2.75). The ‘turnover’ number offered a similar trend to ACES. Overall, the ACES calculation suggested **38** was 3.4 times more efficient than **3** and 20 times more efficient than **40** in the Diels-Alder reaction between cinnamaldehyde (**1**) and cyclopentadiene (**2**). The turnover numbers indicated **38** outperformed **3** by a factor of 5.2 and **40** by a factor of 10.

### 2.3 Rationalising Enantioselectivity

The design of imidazolidinone **38** incorporated a methyl group *cis* to the benzyl group rendering the *Re*-face identical to that of the MacMillan imidazolidinone. This was thought to cause the benzyl groups on **15**·PF<sub>6</sub> and **77**·PF<sub>6</sub> (Figure 2.7) to behave in a similar fashion and hence cause **3** to have similar origins of enantioselectivity to **36**. However, this design principle had been assumed and not verified.

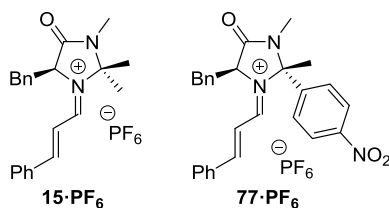


Figure 2.7 Iminium Ion Intermediates

#### 2.3.1 DFT Calculations

Before examining the conformational preferences of **77** experimentally, Density Functional Theory (DFT) calculations were performed (BHandH, 6-31+G\*\*, Acetonitrile PCM). Similarly to iminium ion **15** (see Chapter 3), the conformation of the benzyl group was probed to find low-energy conformers. For the two possible iminium ions (**77.E** and **78.Z**) three conformations of the benzyl arm were found (Figure 2.8) giving a total of six structures.

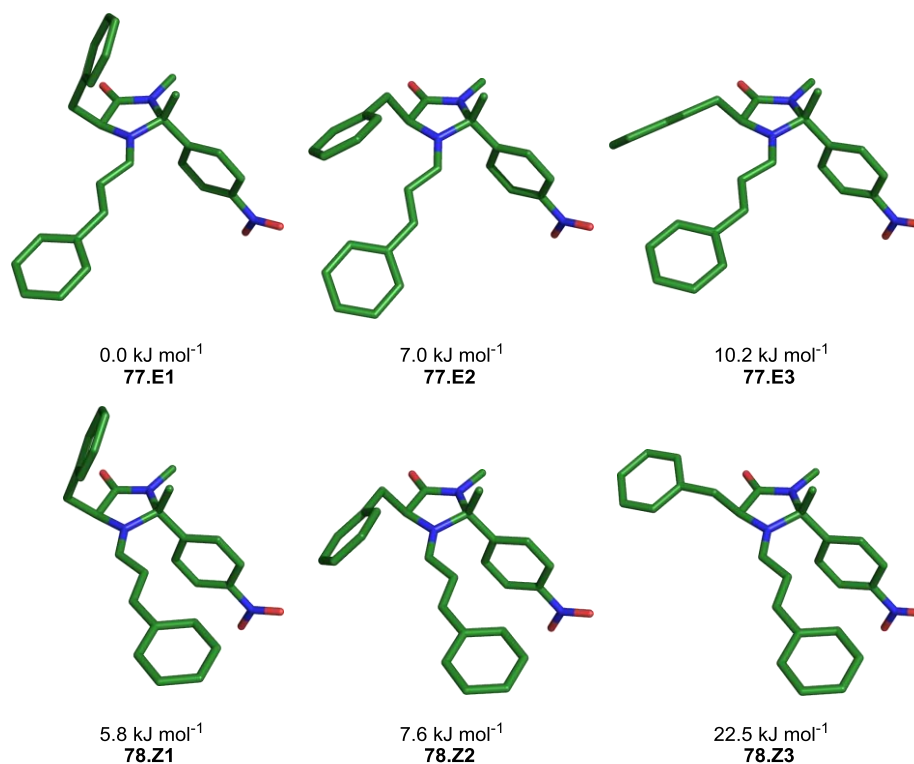


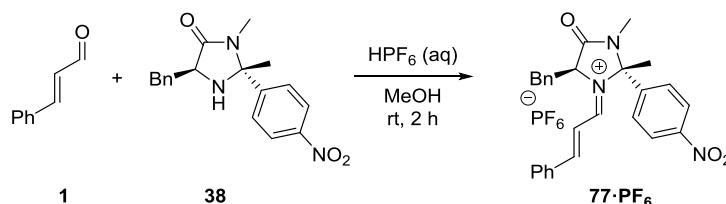
Figure 2.8 DFT Calculated Low-Energy Conformers of **78**

In a similar manner to **15**, iminium ion **77** possessed a low-energy conformation whereby the benzyl group resides over the top of the imidazolidinone ring (**77.E1**, 0 kJ mol<sup>-1</sup>). Another two conformers of the benzyl group were found for the *E*-iminium ion, however, both of these were higher in energy (**77.E2**, 7.0 kJ mol<sup>-1</sup>, **77.E3**, 10.2 kJ mol<sup>-1</sup>). This was encouraging evidence that **38** had the capacity to mimic **3**. In addition, the DFT calculations eluded that the *Z* isomer would be accessible (**78.Z1**, 5.8 kJ mol<sup>-1</sup>) and an *E/Z* iminium ion ratio of 7.5:1 was predicted.

### 2.3.2 Isolation of Iminium Ion Intermediates

Having observed that conformations of **77** are likely to be similar to those of **15**, further evidence was sought to reaffirm the similarities experimentally. Isolation of the iminium ion (**77**·**PF**<sub>6</sub>) was therefore targeted which would allow for variable temperature NMR spectroscopy and single-crystal X-ray analysis to be performed to allow further comparison.

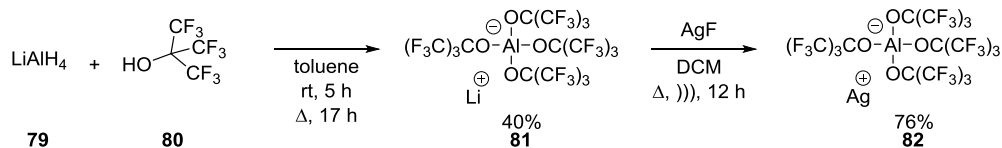
Preparation and isolation of **77**·**PF<sub>6</sub>** turned out to be a non-trivial task. Using methodology (methanol, 1 eq. aqueous hexafluorophosphoric acid) which had previously been used to isolate iminium ions derived from **1** and **3** (**15**) yielded amorphous gums which contained a mixture of **77**·**PF<sub>6</sub>**, **38** and **1** (Scheme 2.12). Attempts to purify by washing or crystallisation all returned mixtures.



Scheme 2.12 Attempted Formation of **77**·**PF<sub>6</sub>**

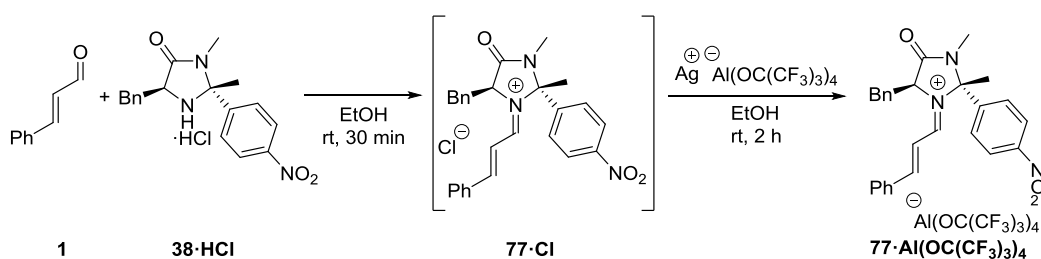
The counterion had previously been seen to influence solubility of the iminium ion but not the behaviour in solution or solid-state.<sup>36</sup> Having failed to isolate the hexafluorophosphate salt **77**·**PF<sub>6</sub>**, screening non-coordinating anions seemed to be the next logical step. Hexafluorophosphoric acid was substituted with perchloric acid (HClO<sub>4</sub>), tetrafluoroboric acid (HBF<sub>4</sub>) and fluoroantimonic acid (HSbF<sub>6</sub>). All of which had the potential to provide non-coordinating anions suitable for iminium ion isolation. Unfortunately, all co-acids rendered amorphous gums containing a mixture of compounds which were not amenable to purification attempts.

Convinced that the issue surrounding unsuccessful isolation was due to the counterion, further alternatives were sought. Seebach had documented a case whereby iminium ion isolation and crystallisation had been troublesome.<sup>47</sup> However, the problem had been overcome using a very large aluminate anion. Despite no commercial availability, the straight forward preparation of the required silver salt (**82**) rendered it worth examining. Perfluoro-*tert*-butanol (**80**) was added to a suspension of lithium aluminium hydride in toluene to give lithium salt **81** (40%) which was then treated with silver fluoride in DCM and subjected to reflux and sonication to give **82** in 76% yield (Scheme 2.13).



Scheme 2.13 Synthesis of Non-Coordinating Aluminate Anion

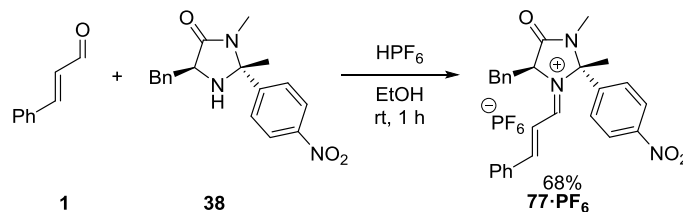
No reports of a protonated derivative of **82** are present within the literature. Therefore, hydrochloride salt **38·HCl** was added to a solution of cinnamaldehyde (**1**) in ethanol followed by the addition of **82**. It was thought that the silver cation would trap the chloride anion to give silver chloride which would allow the aluminate ion to act as a counterion to the iminium ion. After filtration and trituration with ether a solid was obtained containing **77·Al(OC(CF<sub>3</sub>)<sub>3</sub>)<sub>4</sub>**, **38** and **1**. Attempts isolate **77·Al(OC(CF<sub>3</sub>)<sub>3</sub>)<sub>4</sub>** from the mixture by crystallisation resulted in recovery of an imidazolidinone salt (**38·Al(OC(CF<sub>3</sub>)<sub>3</sub>)<sub>4</sub>**) or an oil with a similar composition to the crude reaction mixture.



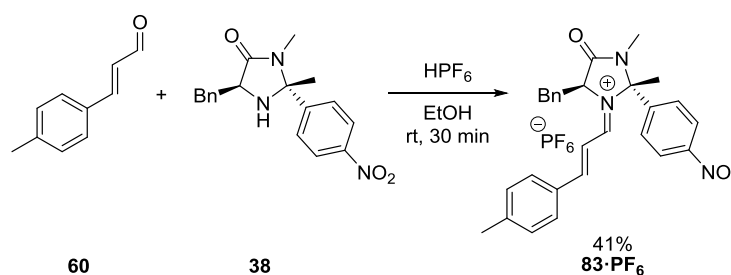
Scheme 2.14 Formation of Iminium Ion with Aluminate Counterion

Having observed that changing the counterion produced gums containing a mixture of compounds, focus was returned to the hexafluorophosphate counterion. As with other ‘super acids’, hexafluorophosphoric acid can only be purchased as a hydrate in solution. Therefore, the addition of hexafluorophosphoric acid also introduces water into the reaction mixture, something which was considered to be potentially problematic when attempting to isolate an iminium ion. Despite no literature reports of an anhydrous hexafluorophosphoric acid it was thought that instead of being stabilised by hydration, the acid may be stable in an anhydrous ethanolic environment. Aqueous hexafluorophosphoric acid was added to ethanol along with activated 3 Å molecular sieves (1 g per mL of acid). The solution was left for 24 h

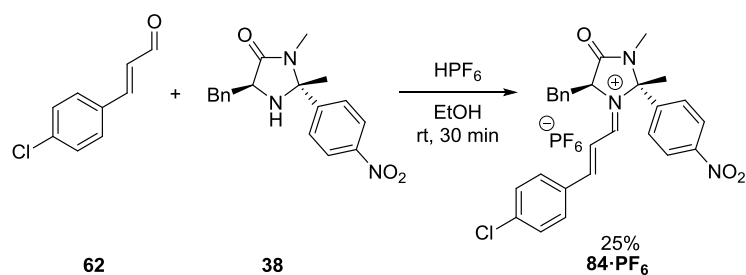
before being added to a mixture of imidazolidinone (**38**) and cinnamaldehyde (**1**). It was noticed, however, that after 72 h a white precipitate forms in the solution. Hence, ethanolic solutions of hexafluorophosphoric acid were only kept for 48 h.

Scheme 2.15 Isolation of **77·PF<sub>6</sub>**

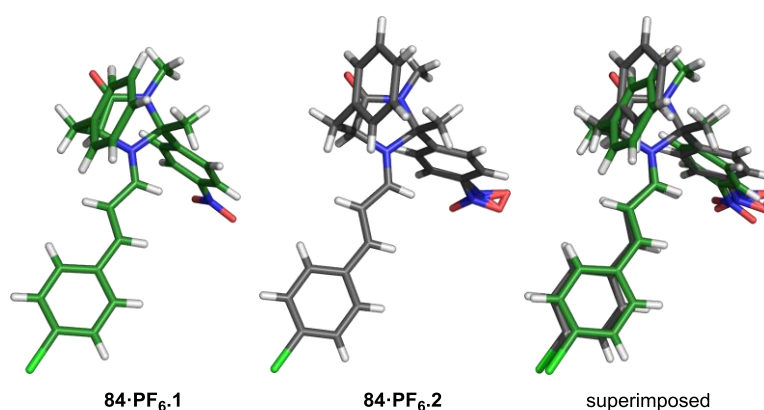
Encouragingly, upon addition of ethanolic hexafluorophosphoric acid to an ethanolic solution of **1** and **38**, a yellow precipitate formed (Scheme 2.15). After removal of the supernatant and careful washing with ethanol followed by ether, **77·PF<sub>6</sub>** was obtained as a yellow powder with minimal contaminants (68%). Unfortunately, it was not possible to crystallise **77·PF<sub>6</sub>**, therefore, obtaining an X-ray structure of an iminium ion derived from **38** was beginning to look unlikely. However, having successfully developed methodology whereby iminium ions derived from **38** could be isolated, altering the aldehyde substrate appeared to be a logical next step in the pursuit of a crystalline iminium ion.

Scheme 2.16 Isolation of Iminium Ion Derived from *p*-Methylcinnamaldehyde

*p*-Methylcinnamaldehyde (**60**) was subjected to the same reaction conditions as described above and the corresponding iminium ion (**83·PF<sub>6</sub>**) was isolated (41%, Scheme 2.16). Disappointingly, like **77·PF<sub>6</sub>**, **83·PF<sub>6</sub>** resisted crystallisation.

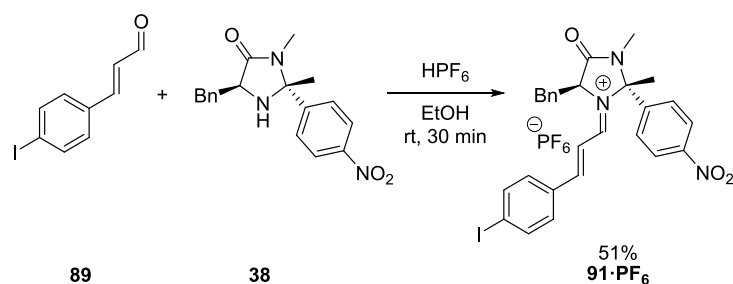
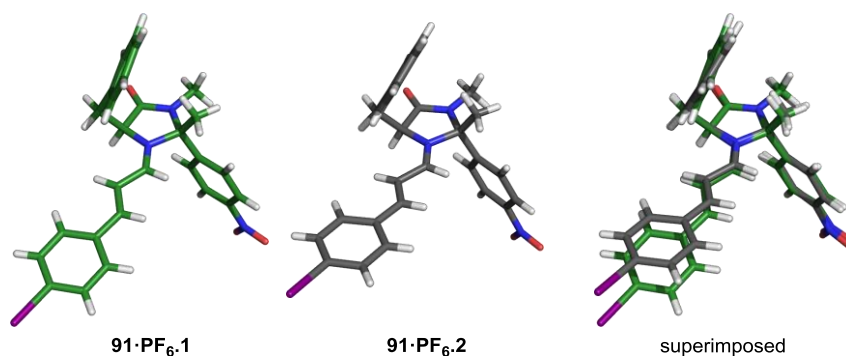
Scheme 2.17 Isolation of Iminium Ion Derived from *p*-Chlorocinnamaldehyde

An iminium ion (**84**·**PF<sub>6</sub>**) derived from *p*-chlorocinnamaldehyde (**62**) was also isolated (25%) in the same manner (Scheme 2.17). **84**·**PF<sub>6</sub>** appeared to be slightly more amenable to crystallisation compared to **77**·**PF<sub>6</sub>** and **83**·**PF<sub>6</sub>** and after many crystallisation attempts a single crystal suitable for X-ray crystallographic analysis was obtained. Unfortunately, despite best efforts, the crystal quality was rather poor and one anion (removed for clarity) and one nitro group (in **84**·**PF<sub>6</sub>**.**2**) had to be modelled as disordered. Two conformers were present within the crystal. One conformer, **84**·**PF<sub>6</sub>**.**2** possessed the previously seen CH– $\pi$  interaction whereby the benzyl arm resides over the *cis*-methyl group. The other conformer, **84**·**PF<sub>6</sub>**.**1** seemingly possessed a previously unseen cation– $\pi$  interaction whereby the aromatic ring of the benzyl group resided directly over the nitrogen atom of the iminium ion. The cation– $\pi$  interaction could not be replicated using DFT calculations and therefore it was unclear if this was present due to crystal packing or if it was a true phenomenon.

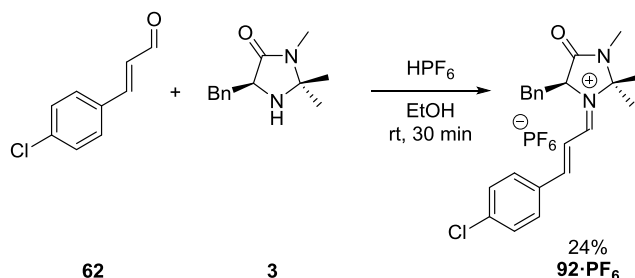
Figure 2.9 Single Crystal X-ray Structures of **84**·**PF<sub>6</sub>** (anions removed for clarity)





Scheme 2.20 Isolation of Iminium Ion Derived from *p*-IodocinnamaldehydeFigure 2.10 Single Crystal X-ray Structures of  $91 \cdot \text{PF}_6$  (anions removed for clarity)

The two solid-state conformers ( $91 \cdot \text{PF}_6\text{-1}$  and  $91 \cdot \text{PF}_6\text{-2}$ ) both featured CH- $\pi$  interactions and no indication of a cation- $\pi$  interaction was present (Figure 2.10). It seemed rational to assume that the previously seen cation- $\pi$  interaction in  $84 \cdot \text{PF}_6$  was due to the crystal packing. However, to further probe the unusual conformer ( $84 \cdot \text{PF}_6\text{-1}$ ) an iminium ion derived from **3** and *p*-chlorocinnamaldehyde (**62**) was prepared ( $92 \cdot \text{PF}_6$ , 24%, Scheme 2.21) to see if the conformation of the benzyl group could be replicated using a different imidazolidinone.

Scheme 2.21 Isolation of Iminium Ion Derived from *p*-Chlorocinnamaldehyde and **3**

Crystals of **92**·PF<sub>6</sub> suitable for X-ray analysis were prepared and an X-ray structure was obtained (Figure 2.11). Similarly to the other iminium ions derived from *p*-halogenated cinnamaldehydes (**84**·PF<sub>6</sub> and **91**·PF<sub>6</sub>), two conformers were present in the crystal (Figure 2.11). However, the intriguing cation- $\pi$  interaction observed in the X-ray structure of **84**·PF<sub>6</sub> was not present in **92**·PF<sub>6.1 or **92**·PF<sub>6.2 which further suggested that the observation was an isolated occurrence solely associated with **84**·PF<sub>6</sub>.</sub></sub>

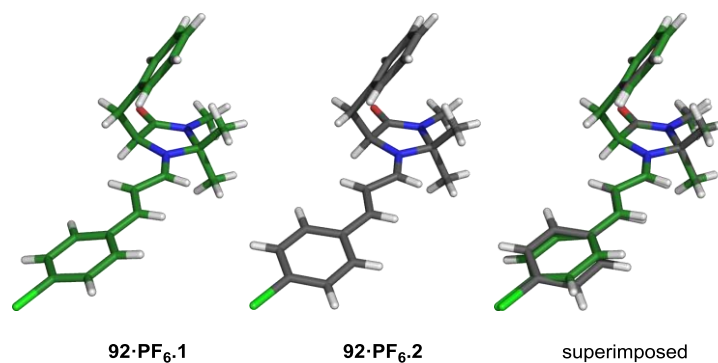


Figure 2.11 Single Crystal X-ray Structures of **92**·PF<sub>6</sub> (anions removed for clarity)

Although independent from solution phase conformation, the X-ray structures supported the DFT calculations and provided further evidence that iminium ions derived from **38** were conformationally similar to those derived from **3**.

### 2.3.3 Analysing Conformation Using VT NMR Spectroscopy

The conformation of iminium ion **15**·PF<sub>6</sub> in solution had previously been analysed using VT <sup>1</sup>H NMR spectroscopy (See Chapter 3 for further information).<sup>36</sup> Therefore, to continue comparison of **3** with **38** <sup>1</sup>H NMR experiments on **77**·PF<sub>6</sub> were performed at 242, 294 and 343 Kelvin (Figure 2.12).

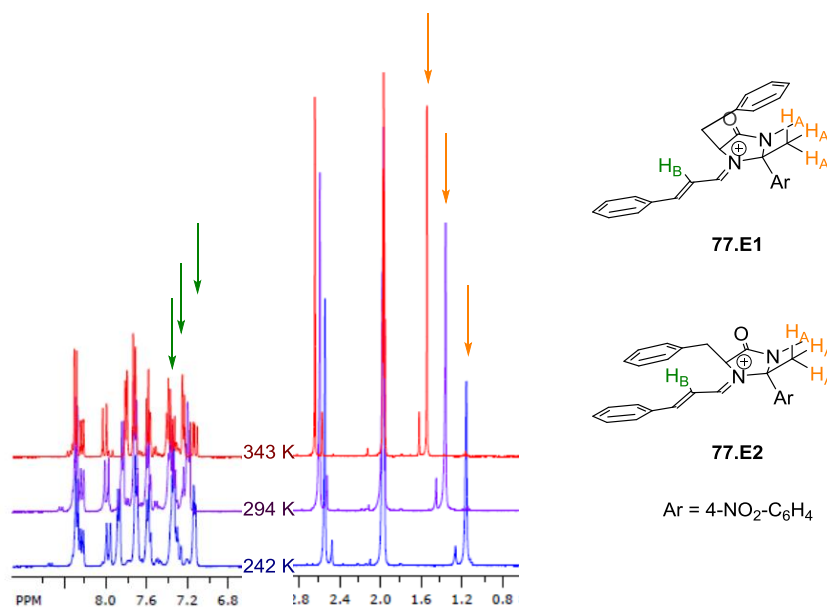


Figure 2.12 VT <sup>1</sup>H NMR Analysis of **77**·PF<sub>6</sub>

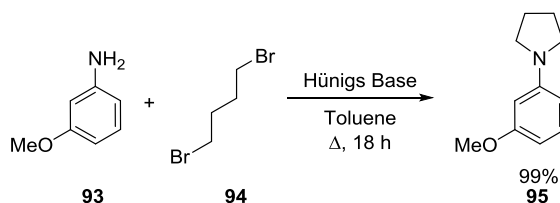
Analysis of the VT <sup>1</sup>H NMR spectroscopy experiments showed that the chemical shift of H<sub>A</sub> and H<sub>B</sub> on **77**·PF<sub>6</sub> were temperature dependent. H<sub>A</sub> experienced greater electronic shielding as the temperature was decreased. This was characteristic of the benzyl group spending more time over the imidazolidinone ring at lower temperatures. Further evidence towards the conformational preference of the benzyl group was obtained from the resonance arising from H<sub>B</sub>. At lower temperatures H<sub>B</sub> experienced less shielding which indicated that the benzyl group resides over H<sub>B</sub> for shorter periods of time. Both of these changes in chemical shift provided evidence towards **77.E1** being the lowest energy conformer in solution. In addition, this was in full agreement with the VT <sup>1</sup>H NMR spectroscopy studies performed on **15**·PF<sub>6</sub>.<sup>36</sup>

## 2.4 Reaction Scope

Imidazolidinone **38** had been seen to be an excellent catalyst for Diels-Alder cycloaddition reactions with cinnamaldehydes. Attention was next focused on other iminium ion catalysed reactions in which cinnamaldehyde featured as a substrate.

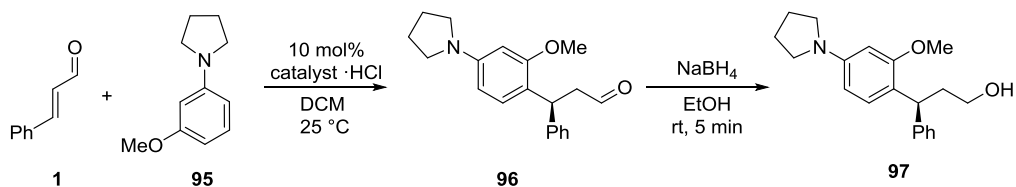
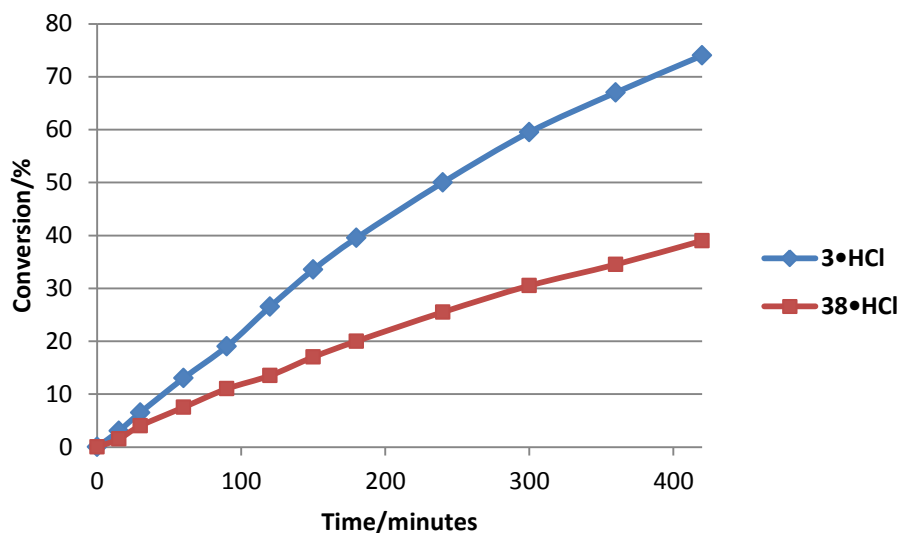
### 2.4.1 Friedel Crafts Alkylation

A conjugate addition reaction which proceeded through an open transition state was deemed to be a good contrast to a Diels-Alder cycloaddition reaction. The conjugate addition reaction between electron-rich amino anisole **95** and cinnamaldehyde **1**, reported by MacMillan, was selected (Scheme 2.23).<sup>49</sup> The use of cinnamaldehyde (**1**) and straightforward preparation of **95** from *m*-anisidine (**93**) and dibromobutane (**94**) (99%, Scheme 2.22) rendered the transformation attractive.



Scheme 2.22 Synthesis of Electron-rich Amino Anisole **95**

A method of monitoring the reaction between **1** and **95** was sought. For ease it was desirable to use <sup>1</sup>H NMR spectroscopy. Removal of aliquots from the reaction mixture followed by dilution with CDCl<sub>3</sub> was found not to quench the reaction and depending on access to NMR spectrometers this could have posed a problem. Reducing the aldehydes present using sodium borohydride was found to be an effective method of quenching the reaction. Aliquots of reaction mixture were added to sodium borohydride in ethanol and after aqueous workup were analysed by <sup>1</sup>H NMR spectroscopy. Resonances arising from the two protons adjacent to the hydroxyl group on cinnamyl alcohol (resulting from the reduction of **1**) and the proton between the two aromatic groups on **97** were found to be suitable to determine reaction conversion.

Scheme 2.23 Conjugate Addition of **95** to Cinnamaldehyde **1**Figure 2.13 Comparison of Imidazolidinones **3·HCl** and **38·HCl** in the reaction between **1** and **95**

Imidazolidinone **38·HCl** showed an inferior rate compared to **3·HCl**. It was known that **38·HCl** resulted in faster rates of iminium ion formation with cinnamaldehyde (**1**) compared to **3·HCl**, hence, iminium ion formation did not appear to be rate determining in this reaction. The electron-withdrawing nature of **38** would be anticipated to give an iminium  $\pi$ -system with a lower  $E_{\text{LUMO}}$  compared to **3** which renders the iminium ion more reactive. Therefore, if nucleophilic attack was rate determining it would be anticipated that **38·HCl** would be a faster catalyst. With this in mind it seemed likely that another part of the catalytic cycle aside from iminium ion formation and nucleophilic attack was influencing catalytic rate.

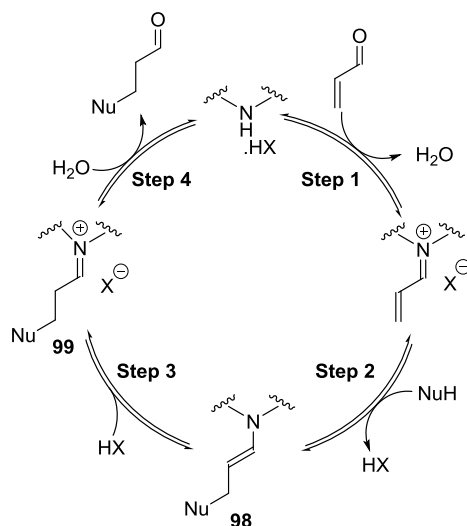


Figure 2.14 Plausible Catalytic Cycle for Secondary Amine Catalyzed Conjugate Addition Reactions

Unlike cycloaddition reactions, conjugate addition reactions proceed *via* enamine intermediates (Figure 2.14, **98**, Step 3). Mayr reported that enamines derived from imidazolidinones are significantly less reactive than enamines derived from amines which are less electron withdrawing.<sup>21</sup> Hence, Step 3 of the catalytic cycle is likely to be directly impacted by the nature of substituents on the imidazolidinone. **38** possesses an electron withdrawing group which was thought to result in an enamine intermediate (**101**) with inferior nucleophilicity compared to an enamine derived from **3** (**100**) (Figure 2.15). This would lead to slower formation of the iminium ion of the product (Figure 2.14, **99**, Step 4) and hence reduce catalyst turnover. Although we had no direct evidence for this possibility, it provided a potential explanation to our experimental observations.

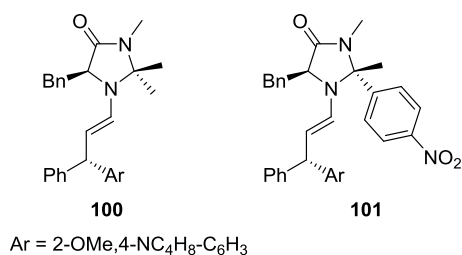
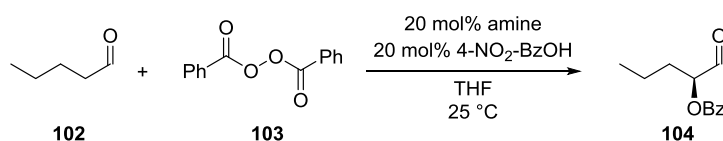


Figure 2.15 Proposed Enamine Intermediates

### 2.4.2 $\alpha$ -Oxybenzoylation

To gain further evidence for **38** forming less reactive enamines compared to **3**, a reaction which uses enamine activation was sought. The  $\alpha$ -oxybenzoylation of valeraldehyde (**102**) using benzoyl peroxide (**103**), an amine catalyst and 4-nitrobenzoic acid had previously been developed within the group (Scheme 2.24).<sup>50</sup> The transformation is operationally simple, uses commercially available reagents and proceeds well with imidazolidinones which rendered it ideal to probe our hypothesis.



Scheme 2.24  $\alpha$ -Oxybenzoylation of Aldehydes

Dilution of the reaction mixture (containing **102**, **103**, **104**, amine and co-acid) into CDCl<sub>3</sub> was found to quench the reaction. Therefore, to obtain data, aliquots were removed, quenched by dilution and then analysed by <sup>1</sup>H NMR spectroscopy. The resonances arising from the aldehyde protons of **102** and **104** were used to determine reaction conversion.

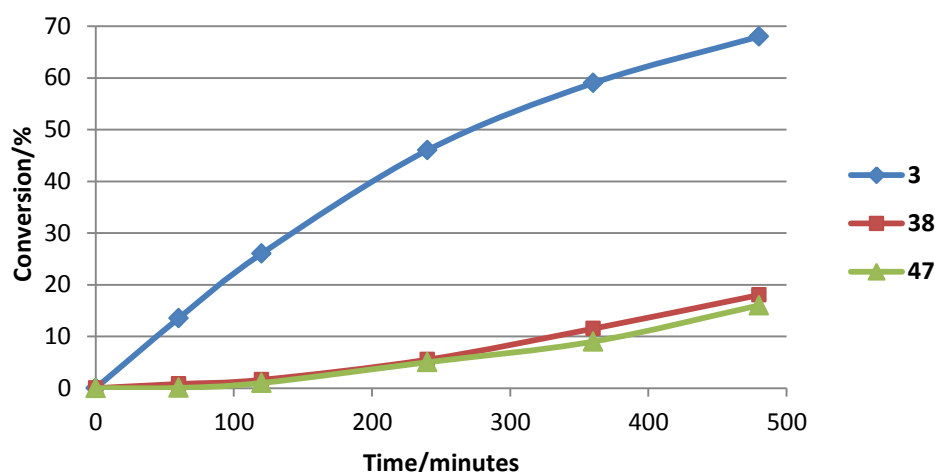


Figure 2.16 Catalytic Performance of **3**, **38** and **47** in the  $\alpha$ -Oxybenzoylation of **102**

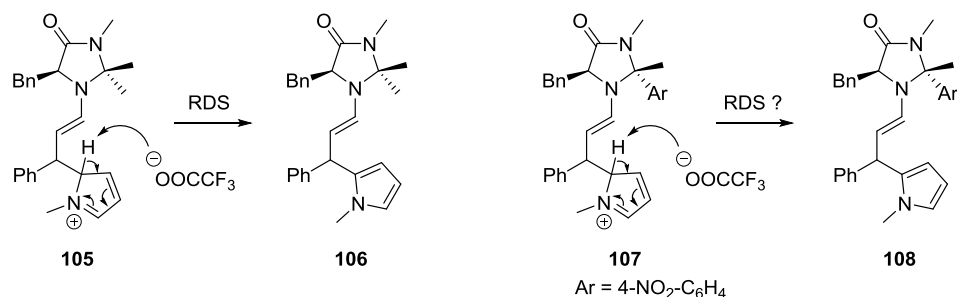
As anticipated, imidazolidinone **38** performed significantly slower than the MacMillan imidazolidinone (**3**). However, the additional aromatic ring on **38** could render the enamine intermediate more sterically hindered. To evaluate this the *cis*-derivative of **38** (**47**) was screened in the reaction. **47** was found to offer a very similar catalytic rate to **38** which, due to the reduced sterics on the reactive *si*-face of the enamine intermediate, suggested that reduced nucleophilicity of the enamine was responsible for the lower catalytic rates experienced with **38** rather than increased sterics.

### 2.4.3 Conjugate Addition of Pyrrole

Imidazolidinone **38** had been seen to offer excellent catalytic rates where iminium ion formation is rate determining. However, in cases featuring enamine intermediates **38** was less effective as a catalyst when compared to **3**. The conjugate addition of *N*-methylpyrrole to cinnamaldehyde proceeds through an enamine intermediate. However, the rate determining step of this reaction has been determined to be deprotonation of the pyrrolium intermediate.<sup>51</sup> Therefore, assuming the rate determining step does not change, **38** would be anticipated to offer equal rates of reaction compared with **3**. This is because deprotonation of intermediates **105** and

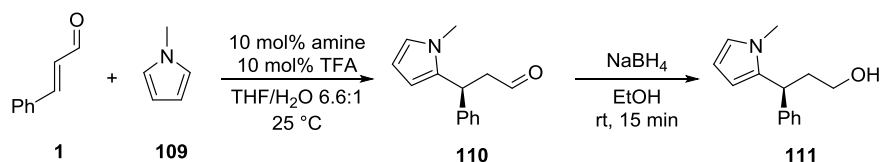


**107** should be independent of the imidazolidinone structure and only rely upon the counterion (Figure 2.25).



Scheme 2.25 Intermediates from the Conjugate Addition of *N*-Methylpyrrole

Imidazolidinones **3** and **38** were used in conjunction with 1 equivalent of TFA. The reaction between cinnamaldehyde (**1**) and *N*-methyl pyrrole (**109**) was monitored by removing aliquots of reaction mixture over time and quenched by addition of each aliquot to sodium borohydride in ethanol. The conversion was then determined by <sup>1</sup>H NMR spectroscopy using the integrals of the resonances arising from the two protons adjacent to the hydroxyl group on cinnamyl alcohol (derived from unreacted **1**) and the proton between the two aromatic rings on **111**.



Scheme 2.26 Conjugate Addition of *N*-Methylpyrrole

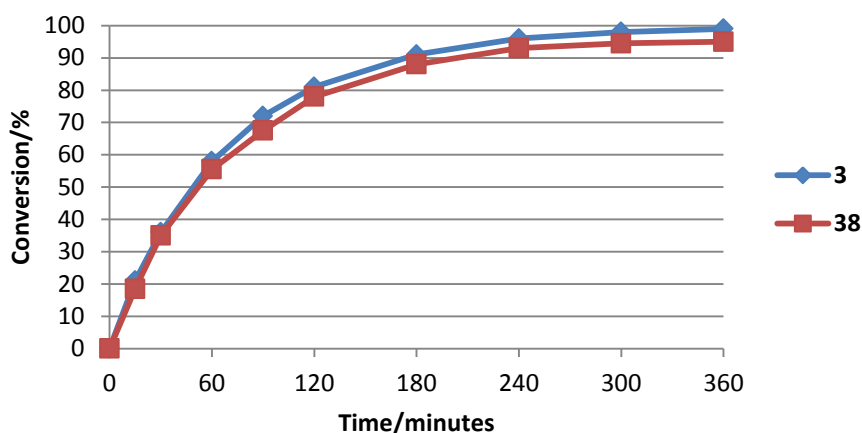
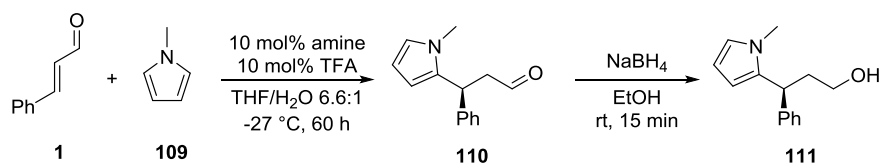


Figure 2.17 Catalytic Performance of **3** and **38** in the Conjugate Addition of *N*-Methylpyrrole

Consistent with our hypothesis, imidazolidinones **3** and **38** proceeded with very similar catalytic rates. This reaffirmed that **38** can only offer superior rates of reaction in cases where iminium ion formation is rate determining.

The conjugate addition of pyrrole has been reported to go *via* a concerted transition state. In particular, the *exo* trajectory has been shown to be favoured using DFT calculations.<sup>35</sup> When using imidazolidinone **38**, *exo* products from Diels-Alder cycloaddition reactions have been observed to have lower enantiomeric excesses compared to *endo* products. Therefore, whilst offering comparable catalytic rates it would be anticipated that **38** would give products with a lower enantiomeric excess compared to **3**.



Scheme 2.27 Conjugate Addition of *N*-Methylpyrrole at Low Temperature

The reactions were repeated at  $-27\text{ }^{\circ}\text{C}$  for 60 hours to mimic literature conditions (Scheme 2.27).<sup>15</sup> After a 60 hour reaction time the complete reaction mixture was quenched using sodium borohydride in ethanol and **111** was isolated using flash column chromatography. The enantiomeric excesses of **111** were then determined using HPLC on a chiral stationary phase (Table 2.8).

Imidazolidinone	Yield	ee of <b>111</b>
<b>3</b>	68%	89%
<b>38</b>	66%	79%

Table 2.8 Summary of Results from *N*-Methylpyrrole Conjugate Addition

Imidazolidinones **3** and **38** gave **111** in near equal isolated yield which reaffirmed that **3** and **38** possessed similar reactivity under these conditions. The major product enantiomer was the same for each catalyst which indicated that similar transition state assemblies were in operation and as anticipated, **38** furnished **11** with a slightly lower ee (79%) compared to **3** (89%) which was in agreement with the *exo* trajectory being favoured.

## 2.5 Conclusions

Work within this chapter set out to compare and contrast imidazolidinone **38** with the literature benchmark **3**. Assessments of reactivity and substrate scope in Diels-Alder reactions were made, the origins of enantioselectivity were probed and a reaction scope was investigated.

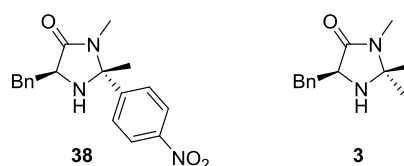


Figure 2.18 Novel Imidazolidinone **38** and Literature Benchmark **3**

**38·HCl** was found to offer catalytic rates approximately 6 times faster than **3·HCl** in Diels-Alder cycloaddition reactions. In addition, high levels of asymmetric induction were observed. However, the outstanding performance was limited to cinnamaldehyde substrates. Asymmetric induction with aliphatic substrates was observed to be poor and for  $\gamma$ -disubstituted  $\alpha,\beta$ -unsaturated aldehydes a 35% reduction in product yield was obtained. The performance of imidazolidinone **38·HCl** in Diels-Alder reactions using cinnamaldehyde substrates was showcased using competition reactions between **38** and the (*R*)-enantiomer of the MacMillan imidazolidinone (**75**) and the (*R*)-enantiomer of the Hayashi diarylprolinol ether (**76**). Despite having a competitive environment, products were obtained with good levels of asymmetry resulting from catalysis by **38**. Asymmetric Catalyst Efficiency Speed (ACES)<sup>46</sup> calculations which convert reaction time, enantioselectivity, catalyst molecular weight, catalyst loading and product yield to a single numerical value were used to quantitatively compare **38** against the literature benchmarks (**3** and **40**). **38** was found to be 3.4 times more efficient than **3** and 20 times more efficient than **40**.

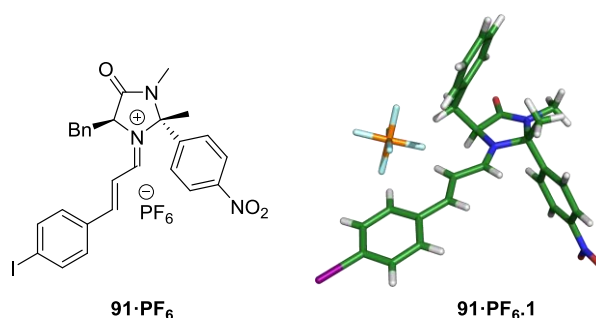


Figure 2.19 Isolated Iminium Ion and Single Crystal X-ray Structure

To probe the origins of enantioselectivity, methodology to isolate iminium ions derived from cinnamaldehydes and **38** was developed. Conformational studies on the isolated iminium ions were performed using X-ray crystallography and VT <sup>1</sup>H NMR spectroscopy. Combined with DFT calculations, iminium ions derived from **38** were found to possess a similar low-energy conformation in solution and solid state (for example **77.E1**) compared to iminium ions derived from **3** (**15.E1**). This suggested that the major reaction pathways responsible for producing products in high enantiomeric excess are similar for **3** and **38**.

Finally, **38** was found to only offer enhanced rates of reaction where iminium ion formation is rate determining and was observed to afford products in reduced rates compared to **3** in reactions which proceed *via* enamine intermediates. This was rationalised based upon the electron withdrawing nature of the substituents on **38** which results in formation of enamines with reduced nucleophilicity. In cases where the rate determining step is independent of the amine catalyst, such as the secondary amine catalysed conjugate addition of pyrroles to cinnamaldehydes, **38** was observed to offer comparable rates of reaction to **3**, albeit with slightly lower levels of asymmetric induction.

# **Chapter 3: Observing Iminium Ion Intermediates**

## 3 Observing Iminium Ion Intermediates

### 3.1 Attribution

Work contained within this chapter was, in part, performed alongside collaborators. Chiral optical spectroscopic measurements were initially attempted at Cardiff University, UK, by myself and Anwen Clementson, a masters student working under my direct supervision. Spectra were subsequently obtained at the University of Manchester, UK, by Dr Ewan Blanch and at the University of Antwerp, Belgium, by Prof. Christian Johannessen and myself.

Ion mobility and collision cross section measurements were performed by Victoria Wright under the supervision of Prof. Colin Creaser and Dr Steven Christie at Loughborough University, UK. Collision cross section calculations were performed by Fernando Castro under the supervision of Prof. Carles Bo at The Institute of Chemical Research of Catalonia, Spain.

### 3.2 Introduction

Mechanism can be used to explain substrate reactivity and reaction products, hence, it is seen to be the fundamental underpinning of synthetic chemistry. Based upon the proposed catalytic cycle (Figure 3.1), a number of mechanistic studies have been performed on the imidazolidinone catalysed Diels-Alder reaction.<sup>1</sup> Investigations have been made using both experimental and computational techniques.<sup>36-39,52-54</sup>

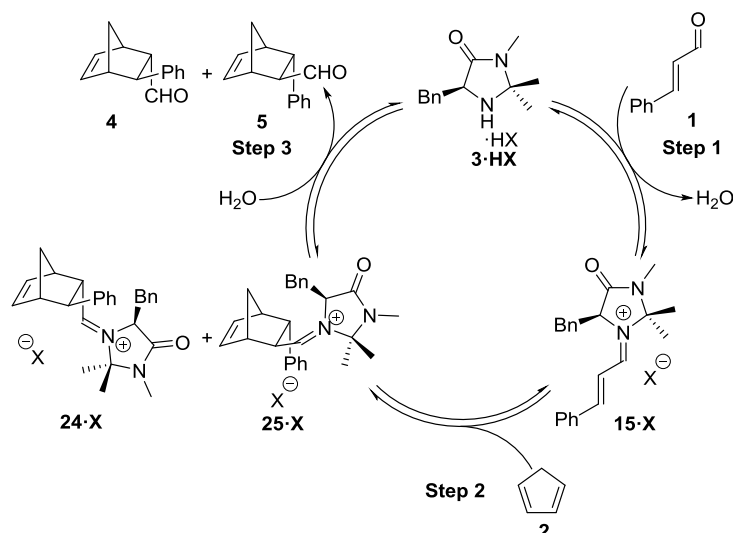


Figure 3.1 Proposed Catalytic Cycle for Imidazolidinone Catalysed Diels-Alder Reaction between Cinnamaldehyde (**1**) and Cyclopentadiene (**2**)

Despite numerous investigations, a few aspects of the catalytic cycle (Figure 3.1) are still somewhat mysterious. The conformation of **15·X** is responsible for installing asymmetry in the products. However, investigations into conformational flexibility have not all been conducted under conditions relevant to the reaction. Therefore, the exact mode of asymmetric induction is unknown. Another, rather surprising, uncertainty lies with iminium ions **24·X** and **25·X**. Despite being central to the proposed catalytic cycle, **24·X** and **25·X** have never been directly observed.

Within this chapter, endeavours are made to quantify the potential conformations of **15·X** experimentally under reaction relevant conditions to gain further insight into the origins of asymmetric induction. In addition, to complete the catalytic cycle, efforts to observe and characterise **24·X** and **25·X** are made.

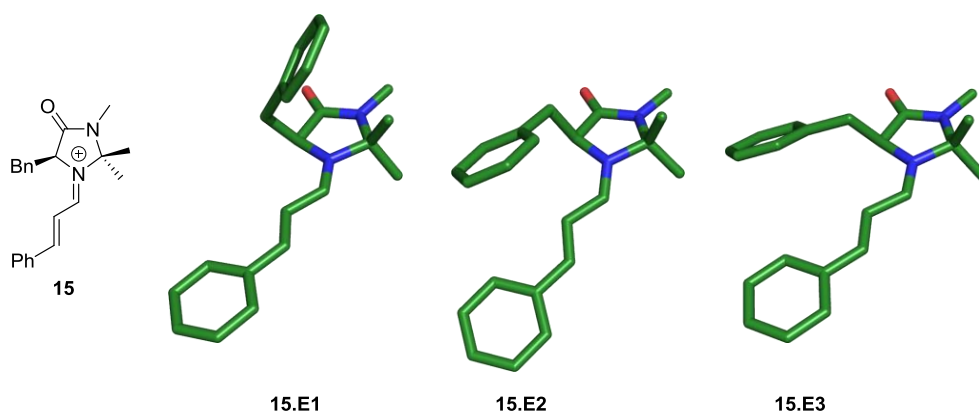


### 3.3 Iminium Ion Conformation

#### 3.3.1 Literature Observations

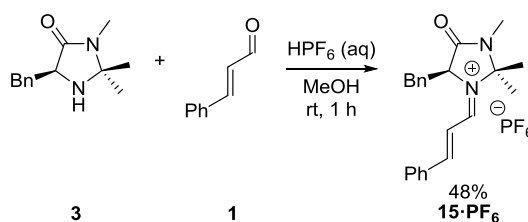
The conformational flexibility of iminium ion **15** has previously been examined in the group.<sup>36</sup> Although the observations are well documented, they were revisited to reignite the drive to further understand **15**.

DFT calculations (BHandH/6-31+G\*\*), previously reported in the gas phase, were repeated.<sup>35,36</sup> In addition, calculations were performed using acetonitrile solvation. In agreement with literature reports, three conformations of **15** were identified. In both the gas and solution phase **15.E1** (where the benzyl group sits over the imidazolidinone ring) was determined to be the lowest energy conformer and was anticipated to have a majority population at 298 K (Table 3.1). The next lowest-energy conformation was where the benzyl group sits over the reactive  $\pi$ -system (6.2 kJ mol<sup>-1</sup>, **15.E2**). Significantly higher in energy to this conformation was **15.E3** (13.6 kJ mol<sup>-1</sup>) whereby the benzyl group lies towards the carbonyl.



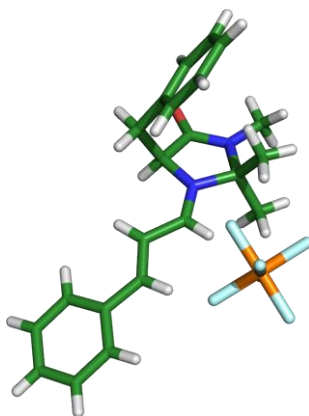
Calculation	<b>15.E1</b>	<b>15.E2</b>	<b>15.E3</b>
BHandH/6-31+G** Gas Phase	0.0 kJ mol <sup>-1</sup> (94.4%)	7.3 kJ mol <sup>-1</sup> (5.1%)	13.0 kJ mol <sup>-1</sup> 0.5%
BHandH/6-31+G** PCM Acetonitrile	0.0 kJ mol <sup>-1</sup> (92.2%)	6.2 kJ mol <sup>-1</sup> (7.4%)	13.6 kJ mol <sup>-1</sup> (0.4%)

Table 3.1 Relative Energies of Calculated Conformations.  
(Boltzmann Occupation at 298 K Given in Parenthesis)

Scheme 3.1 Preparation of Iminium Ion **15**·PF<sub>6</sub>

To experimentally evaluate **15**, it was prepared as the hexafluorophosphate salt from **1**, **3** and hexafluorophosphoric acid (Scheme 3.1). Purification of the crude by crystallisation from isopropanol and acetonitrile gave **15**·PF<sub>6</sub> as bright yellow crystals (48%). Despite the reactivity of **15**·PF<sub>6</sub>, once isolated it was observed to be bench stable for a number of years in a sealed vial.

Firstly, **15**·PF<sub>6</sub> was analysed by single crystal X-ray crystallography. The conformation of **15**·PF<sub>6</sub> in the solid state was seen to be in agreement with low-energy conformer **15.E1** (Figure 3.2) which was consistent with literature findings.<sup>36</sup>

Figure 3.2 Single Crystal X-ray Structure of **15**·PF<sub>6</sub>

To replicate the reported <sup>1</sup>H NMR spectroscopy studies, a 0.9 M solution of **15**·PF<sub>6</sub> in d<sub>3</sub>-acetonitrile was prepared.<sup>36</sup> <sup>1</sup>H NMR experiments were performed at 343, 294, 242 and 233 Kelvin. As anticipated, certain resonances were particularly affected by variations in temperature. As the temperature was reduced, the population of the lowest energy conformer **15.E1** increased. This was reflected by the increased

shielding experienced by  $H_A$  arising from the benzyl group residing over the imidazolidinone ring for longer periods of time (Figure 3.3). In contrast,  $H_B$  became less shielded as the benzyl group spent less time in the vicinity of  $H_B$  at reduced temperatures. These findings were consistent with previous observations.<sup>36</sup>

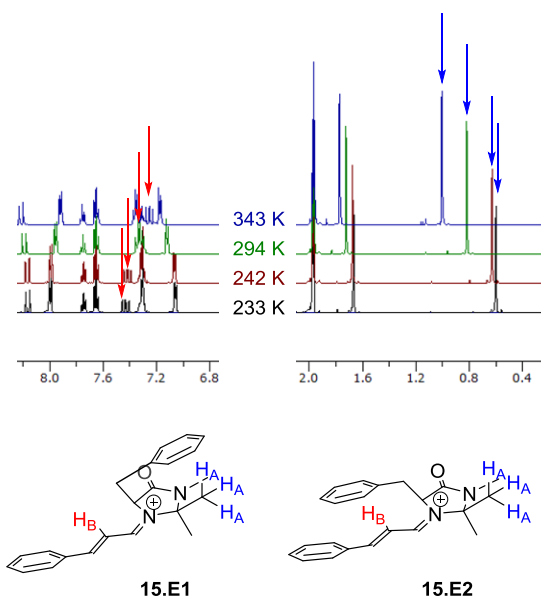


Figure 3.3 Selected Portions of Variable Temperature  $^1\text{H}$  NMR Spectra

Neither the X-ray crystallography nor  $^1\text{H}$  NMR experiments explicitly quantify the precise location of the benzyl group in solution. X-ray crystallography is a solid-state technique which, combined with the possibility of high-energy conformers forming crystals, renders it somewhat irrelevant. Variable temperature  $^1\text{H}$  NMR spectroscopy shows conformational averages and whilst it gave evidence that **15.E1** was the lowest energy conformer, it did not provide any indication of the population distribution in solution.

The Curtin-Hammett principle states that low-energy species are not necessarily the reactive species which can cause difficulties when relating ground-state phenomena to kinetics. It was thought that the Curtin-Hammett principle could play a role when relating the conformational preference of **15** to reactivity and performance of imidazolidinone **3** as a catalyst. However, comparing the performance of **3** in reactions which proceed *via* open transition states with the performance of **3** in

reactions which proceed *via* closed transition states suggests that the low-energy conformation of the iminium ion intermediate (**15.E1**) is a reactive conformation. In addition, DFT calculations have shown that transition states associated with **15.E1** are lower in energy compared to transition states associated with **15.E2** and **15.E3**.<sup>35,55</sup> Due to the experimental observations and DFT calculations, **15.E1** was deemed to be a low-energy and reactive conformation which meant that investigations into the conformational preference of **15** would avoid problems associated with the Curtin-Hammett principle. Hence, to expand the understanding of **3** a technique to quantify conformers of **15** in solution was sought.

### 3.3.2 Chiral Optical Spectroscopy

Chiral compounds are optically active and synthetic chemists generally measure this phenomenon by passing plane polarised 589 nm (sodium D line) light through a sample of known concentration and pathlength. A detector is then used to measure the angle between the incident and transmitted polarised light (Figure 3.4). The result is transformed into a specific rotation value, also known as an  $[\alpha]_D$ . Beyond comparison with literature values to confirm absolute configuration, specific rotation measurements are often viewed merely as another piece of analytical data. However, the optical activity of chiral molecules can be exploited beyond specific rotation measurements.

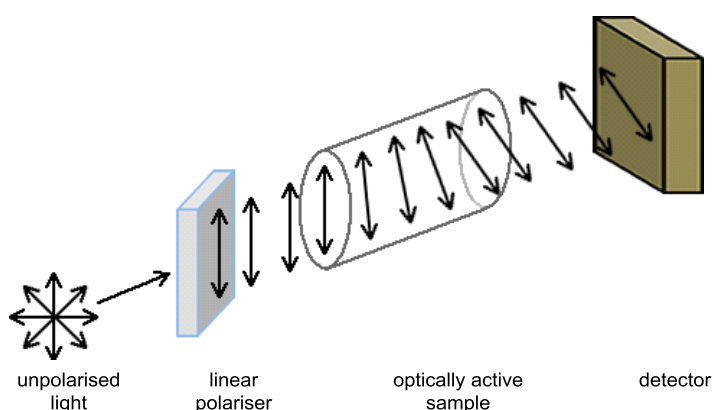


Figure 3.4 Schematic Diagram of a Polarimeter

In addition to rotating plane polarised light, optically active molecules differentially absorb left and right handed circularly polarised light. One enantiomer will preferentially absorb one direction and *vice versa*. This is known as circular dichroism (CD) (Figure 3.5).<sup>56</sup> CD can be used over the entire electromagnetic spectrum which has enabled the phenomenon to be exploited in the UV-visible range (200–800 nm) to give electronic circular dichroism (ECD) and in the infra-red region ( $\sim 4000\text{--}600\text{ cm}^{-1}$ ) to give vibrational circular dichroism (VCD).<sup>57</sup>

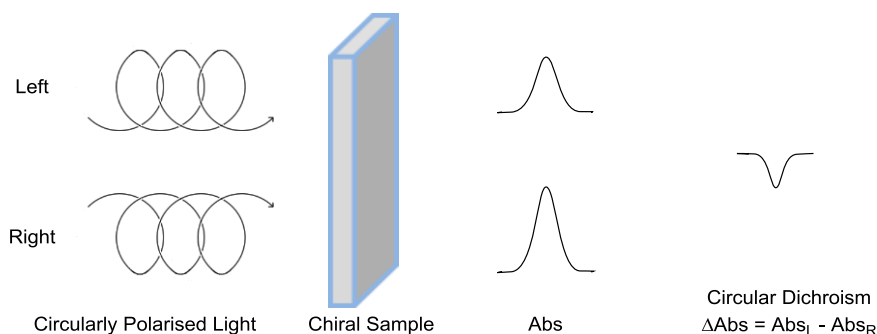


Figure 3.5 Principle of Circular Dichroism

Both ECD and VCD can be used to determine absolute configuration. In addition, the two techniques are sensitive to molecular conformation which has led to their use in solution-phase protein folding studies.<sup>56,58,59</sup> A number of accessible electronic transitions need to be present to determine detailed conformational information by ECD. Therefore, VCD is often a more appropriate technique for probing conformation of small molecules.

Despite being a division of IR spectroscopy, aside from the laser, a VCD spectrometer is significantly more complex than an IR spectrometer (Figure 3.6). Polychromatic IR laser light is passed through a Michelson interferometer. The resultant single frequency light is linearly polarised using a filter and then circularly polarised using a photoelastic modulator (PEM). The circularly polarised light is then passed through the sample. At this point, due to extensive manipulation and loss through the sample, the light intensity is very low, hence, lenses are used to re-focus the light before it enters a highly-sensitive liquid nitrogen cooled detector. Electronic manipulation and Fourier transform allows VCD and IR data to be obtained.<sup>57</sup>

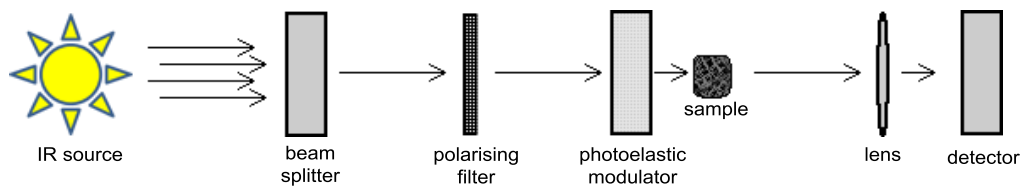


Figure 3.6 Simplified Schematic Diagram of a VCD Instrument

Despite the complex instrumentation, since the advent of commercially available VCD spectrometers, performing a VCD experiment is now as simple as recording an IR spectrum. An IR cell with BaF<sub>2</sub> windows containing the analyte in solution is inserted into the instrument and under full automation VCD can be recorded at the click of a button. In a similar manner to IR, it is possible to measure solid state VCD. However, samples must be completely uniform with minimal imperfections and custom made cells are also required. Hence, solid state VCD is relatively uncommon.

Another form of chiral optical spectroscopy is Vibrational Raman Optical Activity (VROA, also known as ROA). ROA is a division of Raman spectroscopy and observes vibrational and rotational properties of molecules. Hence, ROA can be seen as being complimentary to VCD. Unlike VCD and ECD, whereby the absorption of light eludes to stereochemical information, in ROA the stereochemical information is contained in circularly polarized Raman scattered photons.<sup>57</sup> Similarly to VCD, ROA is a highly sensitive technique and suitable for analysing conformations of small molecules.<sup>60</sup>

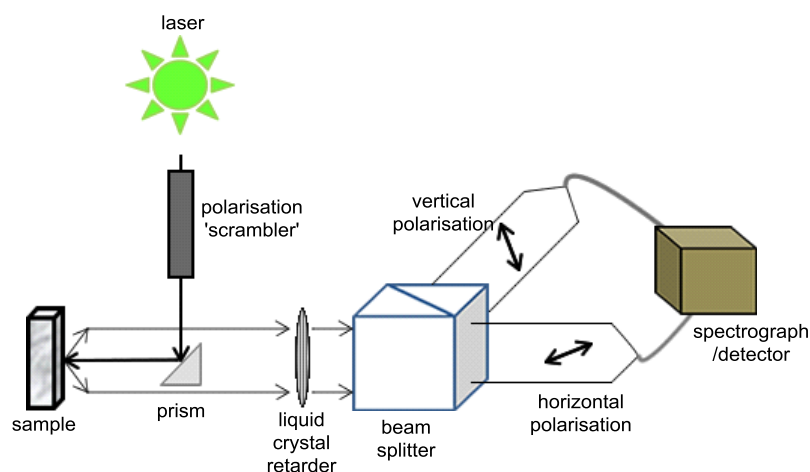


Figure 3.7 Simplified Schematic Diagram of an ROA Spectrometer

Like VCD, ROA has become more accessible due to commercial interest which has led to automation. The commercially available ChiralRAMAN (BioTools, Inc) ROA spectrometers use a somewhat similar setup to a Raman spectrometer.<sup>60</sup> However, the incident and scattered light require significant manipulation to obtain ROA (Figure 3.7).<sup>57,60</sup> Single wavelength laser light is passed through a polarisation scrambler to remove any inherent polarisation. A prism is then used to deflect the laser beam into the sample. Like Raman spectroscopy; some light passes through the sample, some is absorbed and some is backscattered. The backscattered light passes through a liquid crystal retarder which converts any circular polarisation into linear polarisation. A beam splitter then separates polarised light into horizontal and vertical components before fibre optic cables transmit the beams to a detector. After some processing, an ROA spectrum can be obtained.

Importantly, in addition to relatively simple acquisition, VCD and ROA spectra can be predicted using DFT calculations. Although, due to simpler underlying theory, VCD calculations are somewhat more reliable than ROA calculations.<sup>61,62</sup> In the literature, calculated spectra are often used to verify experimental observations and good correlation between theory and experiment has been observed for small molecules.<sup>63,64</sup> In addition, conformational studies using experimental and calculated spectra have been performed.<sup>64-67</sup>

### 3.3.3 Iminium Ion Conformation Using Chiral Optical Spectroscopy

VCD and ROA appeared to be potential methods to probe **15**·PF<sub>6</sub> in solution and determine a population distribution of conformers. However, it became apparent that there was a lack of operational university-based VCD spectrometers in the United Kingdom. Therefore, despite the possibility of poor computational prediction, the investigation was pursued using ROA.

### 3.3.4 Iminium Ion Conformation Using ROA

To determine if each conformer (Figure 3.8) could be distinguished by its ROA spectrum, DFT calculations were performed on **15.E1**, **15.E2** and **15.E3** using the Gaussian09 suite of programmes. In accordance with literature,<sup>63,67</sup> a high level of theory (B3LYP/6-311++G\*\*) was used including CPCM acetonitrile solvation.<sup>53,57</sup> Three fairly different spectra were obtained (Figure 3.9).

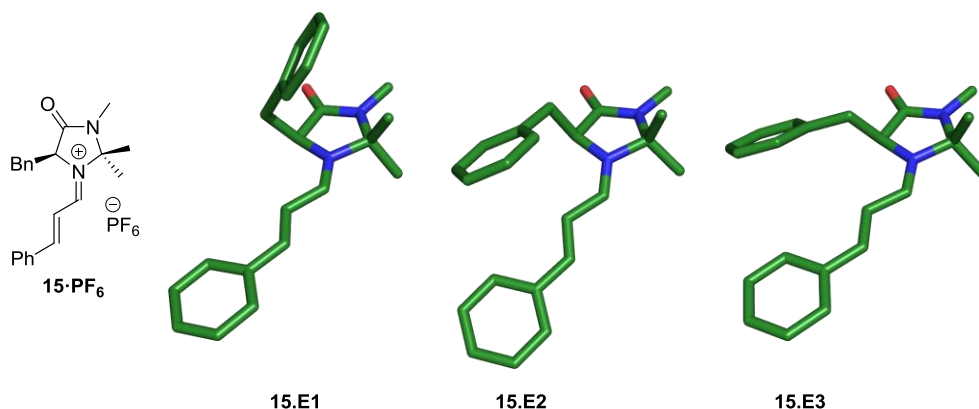


Figure 3.8 Low-Energy Conformations of **15**



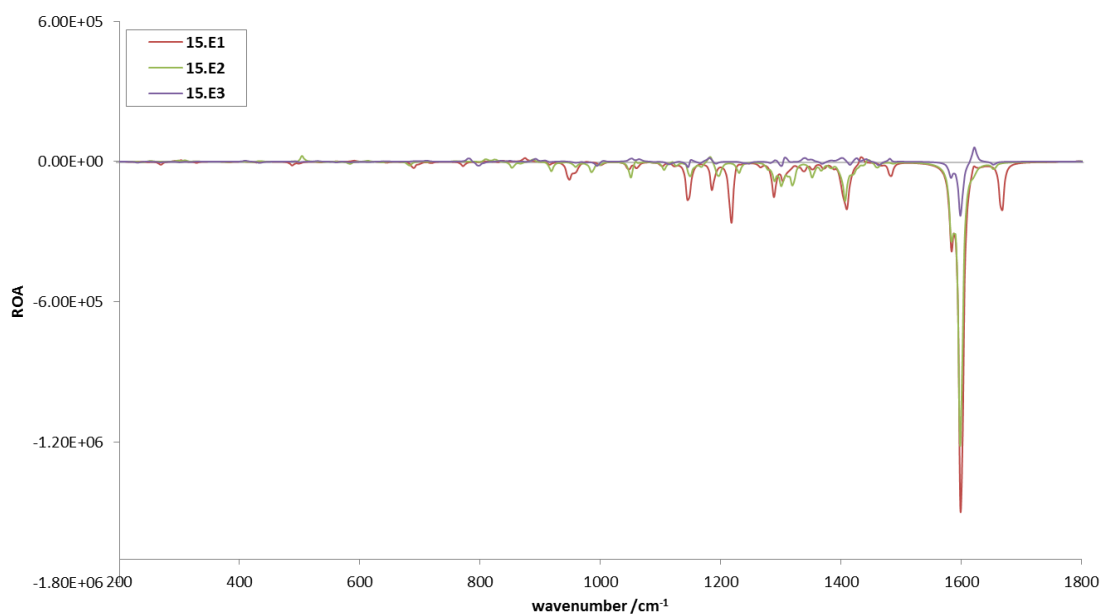


Figure 3.9 Calculated ROA for Low-Energy Conformations of **15**

The ROA spectrum for **15.E3** was significantly different from the other two. It was not monosignate and contained virtually no peaks between 200 and 1500  $\text{cm}^{-1}$ . In addition, the peak at 1600  $\text{cm}^{-1}$  was significantly smaller compared to the predicted spectra for **15.E1** and **15.E2**. Therefore, it appeared that it would be easy to identify **15.E3**. However, if **15.E3** was present alongside the other conformers its signals would likely be buried and hence it may not be visible. Distinguishing between **15.E1** and **15.E2** was more of a challenge. Only subtle differences between the calculated spectra were present. The three peaks between 1100 and 1250  $\text{cm}^{-1}$  and the single peak at 1680  $\text{cm}^{-1}$  were only present in the spectrum for **15.E1**. These few, somewhat subtle, differences appeared to be the only handles to distinguish **15.E1** and **15.E2**.

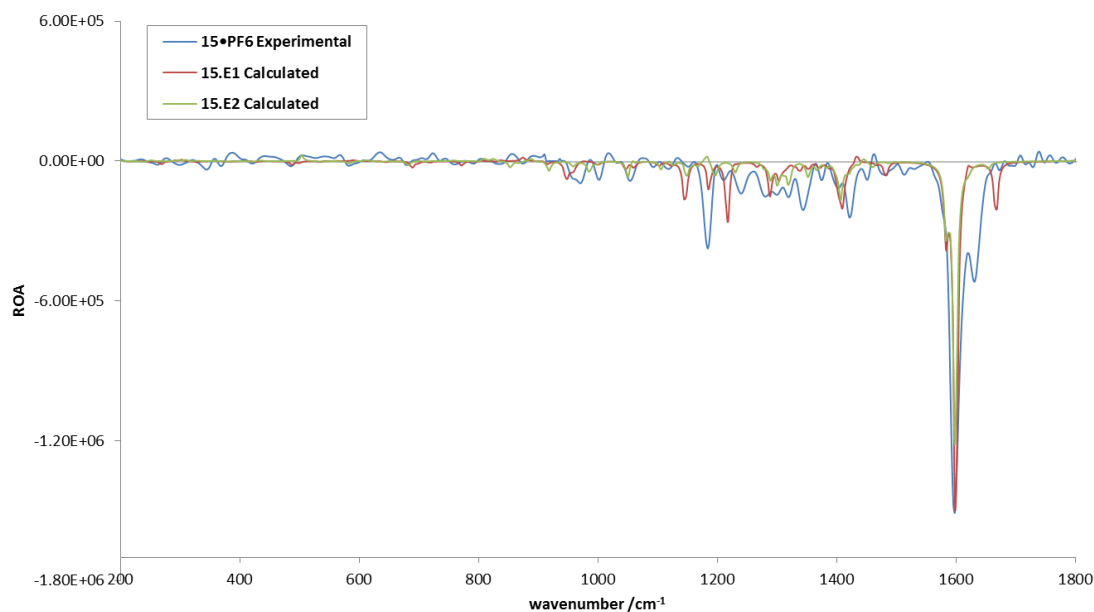
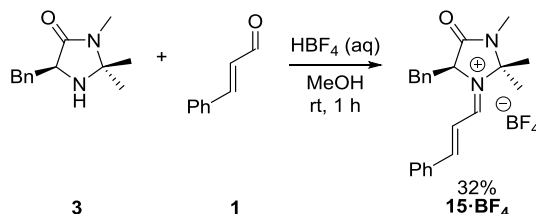


Figure 3.10 Calculated and Experimental ROA Spectra for **15•PF<sub>6</sub>**

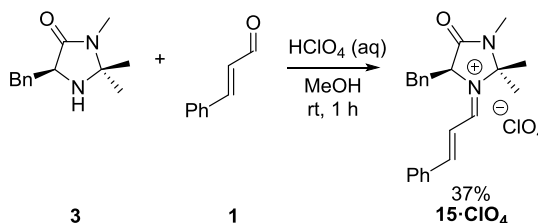
Despite the calculations suggesting **15.E1** and **15.E2** would furnish similar ROA spectra, a 7 mg mL<sup>-1</sup> solution of **15•PF<sub>6</sub>** in acetonitrile was prepared and the ROA spectrum was recorded. The experimental spectrum somewhat resembled the calculated spectra for both **15.E1** and **15.E2** (Figure 3.10). However, neither were absolute matches. The presence of ROA activity between 900 and 1350 cm<sup>-1</sup> seemed to relate more to **15.E1** than **15.E2**. However, the peak in **15.E1**, resulting from the carbonyl, predicted to be at 1680 cm<sup>-1</sup> was either at a lower frequency (~1620 cm<sup>-1</sup>) or was absent from the experimental spectrum. Overall, evidence loosely suggested that **15.E1** was the majority conformer in solution; however, the desired conformation distribution could not be determined.

Although the original question seemingly could not be answered by ROA, a good quality spectrum had been obtained. Combined with willing collaborators, it was a good opportunity to investigate if the choice of counterion influences iminium ion conformation in solution. Although any observed changes in the ROA spectrum would have been unquantifiable, any evidence of the anion playing a role was of interest.

To probe whether the counterion influenced iminium ion conformation, **15·BF<sub>4</sub>** and **15·ClO<sub>4</sub>** were prepared from **1** and **3** (Scheme 3.2 and Scheme 3.3). After purification by crystallisation **15·BF<sub>4</sub>** and **15·ClO<sub>4</sub>** were isolated in 32% and 37% yield respectively. 7 mg mL<sup>-1</sup> acetonitrile solutions of both **15·BF<sub>4</sub>** and **15·ClO<sub>4</sub>** were made and their ROA spectra were measured (Figure 3.11).



Scheme 3.2 Synthesis of Tetrafluoroborate Iminium Salt



Scheme 3.3 Synthesis of Perchlorate Iminium Salt

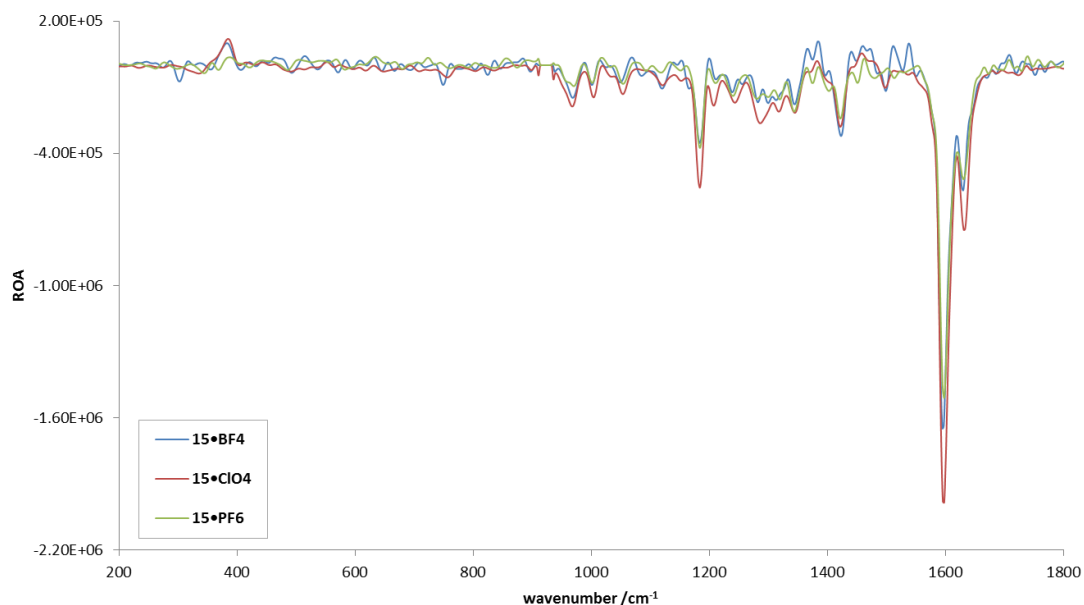
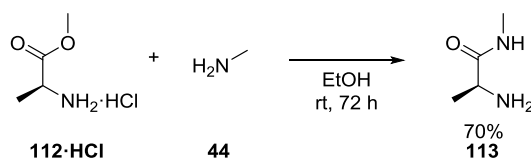


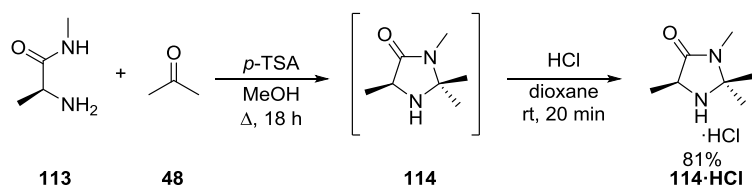
Figure 3.11 Effect of Counterion on Iminium Ion Conformation

Near identical ROA spectra were obtained for **15**•PF<sub>6</sub>, **15**•BF<sub>4</sub> and **15**•ClO<sub>4</sub> (the minor discrepancies between them are likely to arise from slight variations in concentration). This important observation suggested that the conformation of the reactive iminium ion is not influenced by the counterion in solution. Therefore, should any alterations in selectivity be observed upon variation of the co-acid, they should not be attributed to changes in iminium ion conformation.

So far, ROA had not quantified conformers of **15** in solution and correlations between calculated and experimental spectra were weak. However, it was not known if an average of many different conformers was being observed or if the computationally calculated ROA spectra were incorrect. A rigid system was envisaged as a potential probe to see if conformational flexibility was causing the disagreement. Switching the amino acid residue from phenylalanine to alanine appeared to be a solution as this would significantly reduce conformational flexibility but retain chirality.

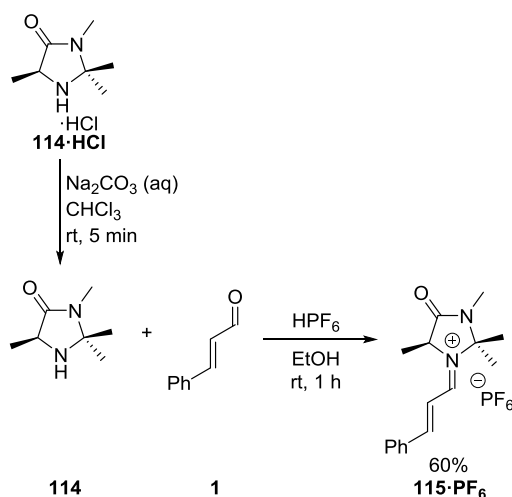
Scheme 3.4 Synthesis of Amide **113**

Amino amide **113** was prepared from commercially available ester (**112·HCl**) and ethanolic methylamine **44** (70%, Scheme 3.4). **113** was then cyclised with acetone (**48**) in the presence of *p*-TSA to give **114**. Although not required as the hydrochloride salt, treatment of crude **114** in dioxane with hydrogen chloride afforded **114·HCl** in high purity and good yield (81%) without the need for purification (Scheme 3.5).



Scheme 3.5 Synthesis of Alanine Derived Imidazolidinone

Before attempting to form **115·PF<sub>6</sub>**, hydrochloride salt **114·HCl** was freebased analysed by HPLC on a chiral stationary phase to check enantiopurity. The ee was found to be >98% which rendered the amine suitable for use in the next step. Ethanolic hexafluorophosphoric acid was added to **114** followed by excess cinnamaldehyde (**1**). Iminium ion **115·PF<sub>6</sub>** was obtained as a yellow precipitate (60%, Scheme 3.6). **115·PF<sub>6</sub>** was found not to be amenable to crystallisation. Hence, the crude was washed with ethanol and diethyl ether to obtain **115·PF<sub>6</sub>** in a suitable purity.

Scheme 3.6 Synthesis of Conformationally Inflexible Iminium Ion **115**

A  $7 \text{ mg mL}^{-1}$  acetonitrile solution of **115·PF<sub>6</sub>** was made and an ROA spectrum was recorded. A very noisy signal was obtained. The concentration was increased 10 fold and the ROA was re-recorded. An ROA spectrum was obtained but still appeared significantly noisier than the spectrum obtained for **15·PF<sub>6</sub>**. Therefore, in order to confirm if it was a true ROA signal, the opposite enantiomer (**D-115·PF<sub>6</sub>**) was prepared and its ROA spectrum was recorded. As anticipated, a fairly equal and opposite ROA spectrum was obtained indicating that below  $1400 \text{ cm}^{-1}$  ROA was being observed and not just background noise (Figure 3.12).

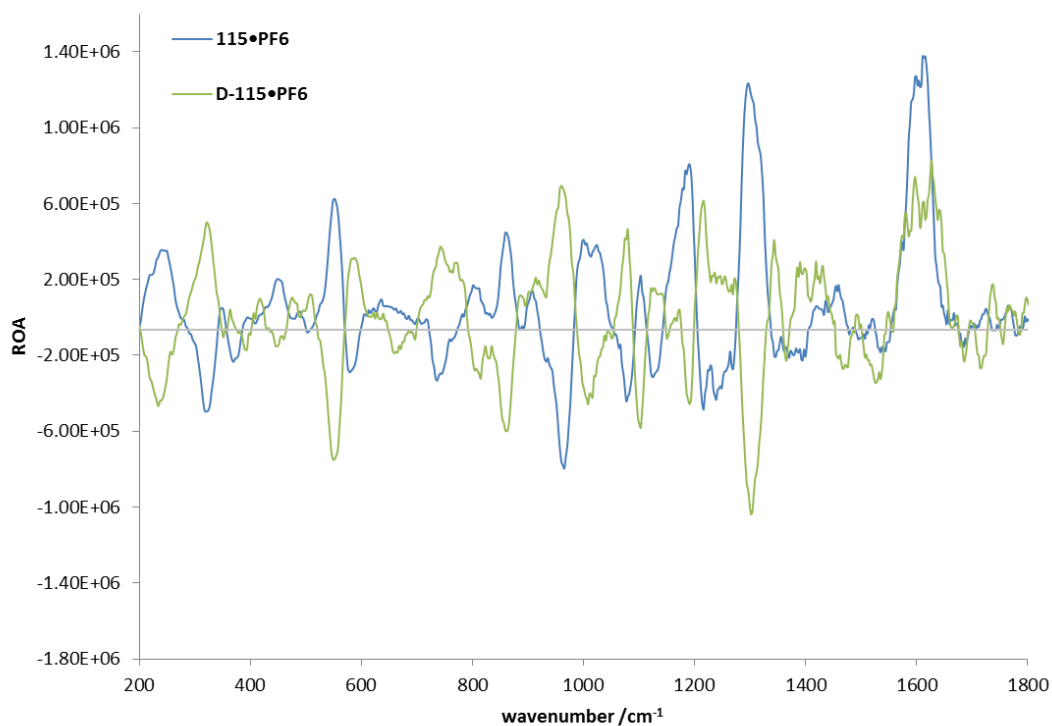


Figure 3.12 ROA Spectra of **115**•PF<sub>6</sub> and its Enantiomer

An ROA spectrum for **115** was calculated. As the peak at 1600 cm<sup>-1</sup> appeared to be either an artefact or noise (Figure 3.12), comparison between the experimental and calculated spectra was made between 200 and 1400 cm<sup>-1</sup> (Figure 3.13).

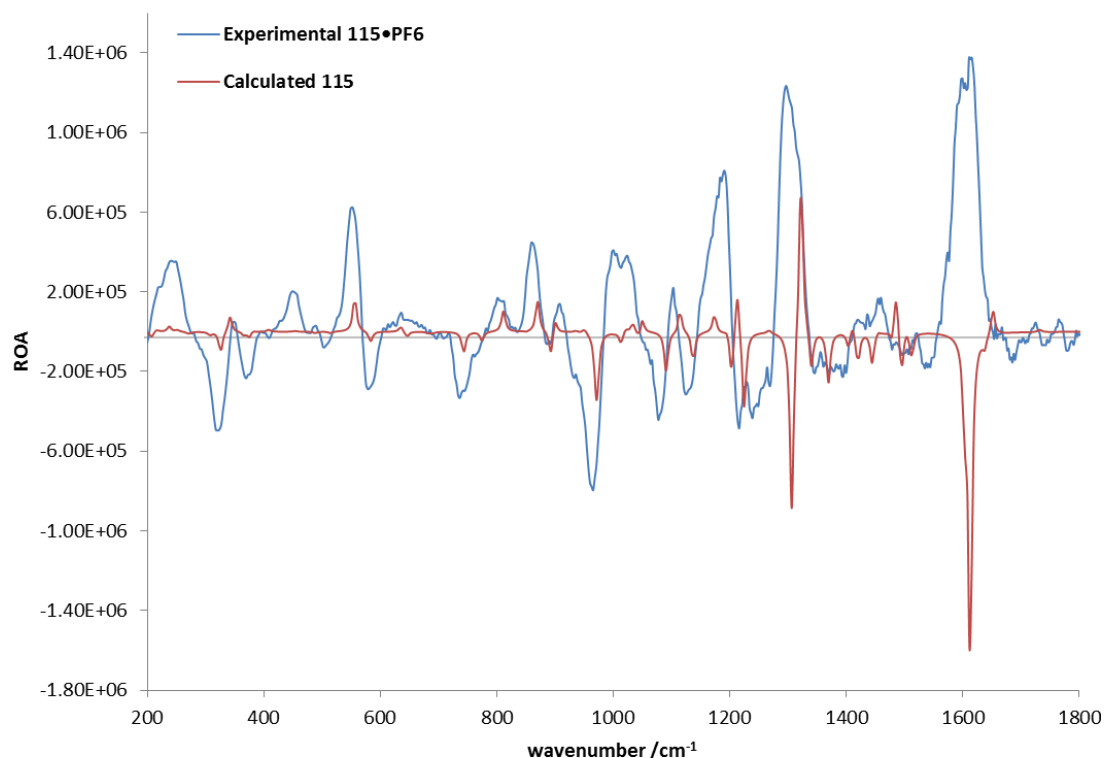


Figure 3.13 Comparison of Calculated and Experimental ROA Spectra of **115•PF<sub>6</sub>**

A reasonable correlation between the experimental and calculated ROA was observed. In particular, the region between 200 and 1000  $\text{cm}^{-1}$  appeared to be comparable (although the magnitude of the signals was different). This suggested that for a conformationally rigid iminium ion, reasonable agreement between calculated and experimental spectra could be obtained. However, it seemed plausible that if a less than perfect correlation was obtained for a conformationally rigid system, it is likely to be difficult to obtain a good correlation for a flexible system. This was a sticking point and suggested ROA would not be able to answer our question and provide quantitative values for conformations of **15•PF<sub>6</sub>** in solution.



### 3.3.5 Iminium Ion Conformation Using VCD

As ROA had not been able to solve our conundrum, the search for time on a VCD spectrometer was reignited. Thankfully the search was short lived, relocation of a collaborator opened up access to a VCD spectrometer which enabled the project to continue.

When recording a VCD spectrum the choice of solvent is important. A solvent with minimal IR activity in the window of interest ( $1100\text{--}1900\text{ cm}^{-1}$ ) must be used. Due to solubility, and to keep close to reaction conditions, using acetonitrile as the solvent was preferential. However, an IR spectrum of acetonitrile contains a CH-bend at  $\sim 1500\text{ cm}^{-1}$  rendering it unsuitable for VCD/IR measurements. To circumvent this problem, deuterated acetonitrile can be used as the CD-bend resides at  $\sim 1000\text{ cm}^{-1}$  which is outside the range of interest.

To begin the study using VCD, conformationally rigid **115** $\cdot\text{PF}_6$  was analysed to see the level of correlation between an experimentally measured and a computationally calculated VCD spectrum of an iminium ion. A  $35\text{ mg mL}^{-1}$  solution of **115** $\cdot\text{PF}_6$  was prepared using  $\text{d}^3$ -acetonitrile and a VCD spectrum was recorded. In addition, using the same level of theory as for ROA, the VCD spectrum for **115** was calculated (Figure 3.15).

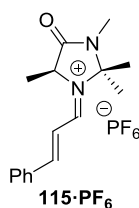


Figure 3.14 Conformationally Rigid Iminium Ion **115** $\cdot\text{PF}_6$

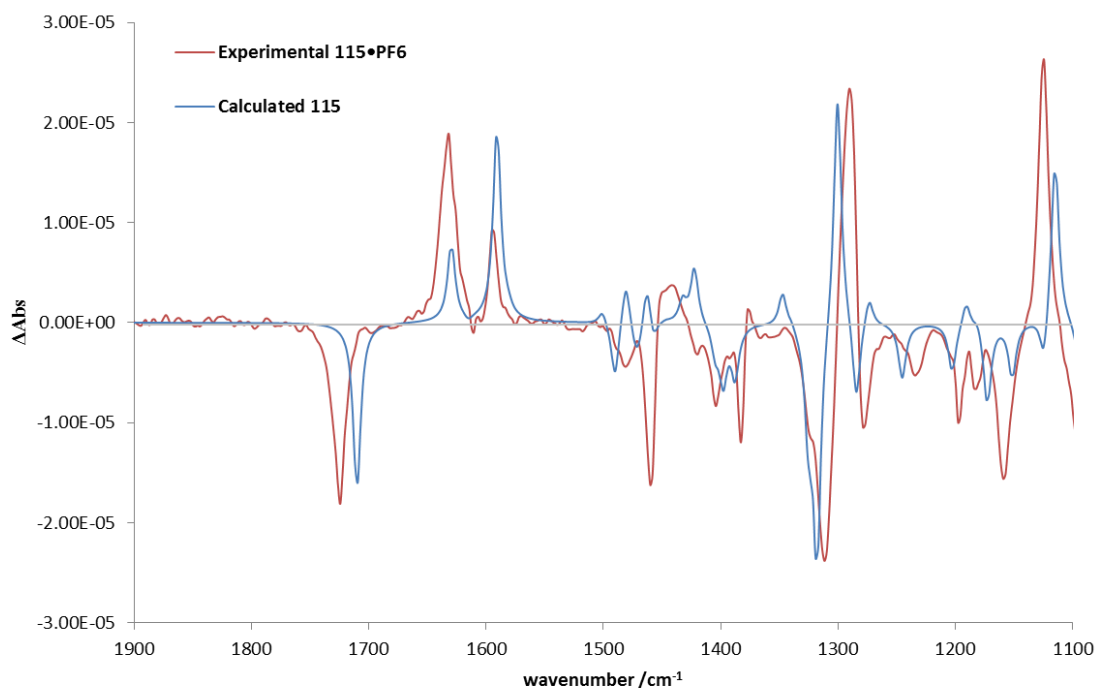
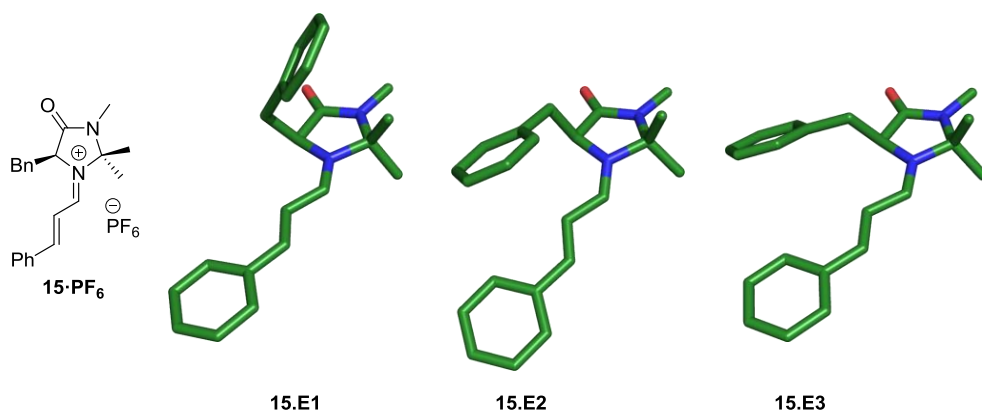
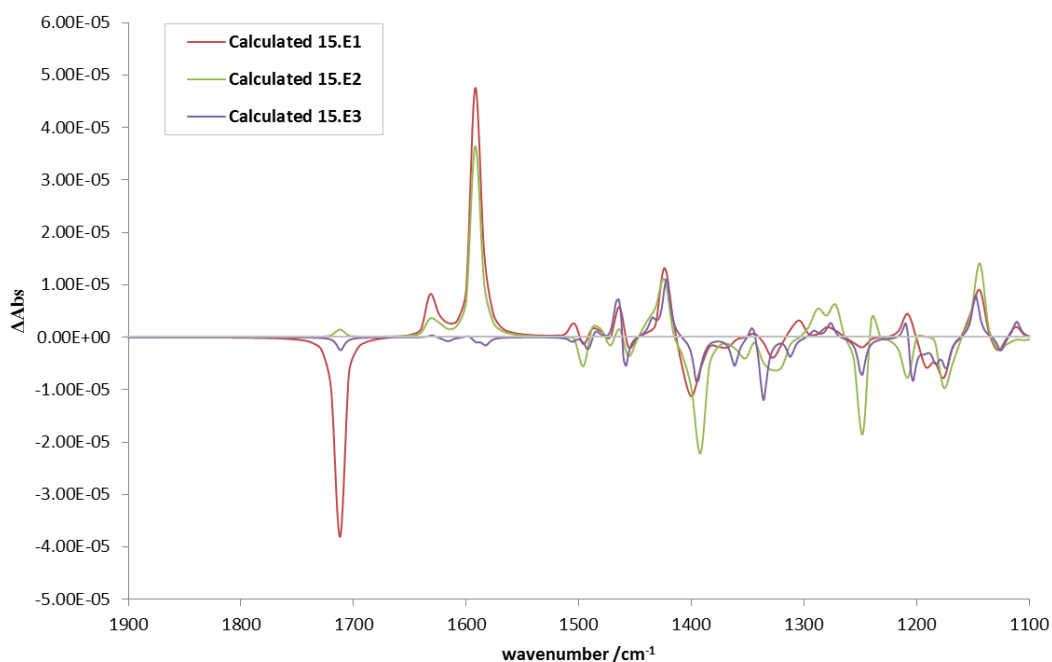


Figure 3.15 Calculated and Experimental VCD Spectra of **115**·PF<sub>6</sub>

The two VCD spectra for **115** displayed a better correlation between calculation and experiment compared to the ROA spectra. Some discrepancies between exact peak locations were present. However, the general shape and pattern of the two spectra correlated significantly better than for any of the ROA spectra. Therefore, VCD was pursued as a method to observe iminium ions. Before obtaining experimental VCD spectra on **15**·PF<sub>6</sub>, calculations were performed on **15.E1**, **15.E2** and **15.E3** to see if the conformers (Figure 3.16) had the potential to be distinguishable by their spectra (Figure 3.17).

Figure 3.16 Low-Energy Conformations of **15**Figure 3.17 Calculated VCD Spectra for **15**

Similarly to the ROA calculations, **15.E3** had a significantly different predicted VCD spectrum between 1750 and 1650  $\text{cm}^{-1}$  compared to **15.E1** and **15.E2**. Again, similarly to the ROA calculations, more subtle differences were present between **15.E1** and **15.E2**. The carbonyl activity at  $\sim 1700 \text{ cm}^{-1}$  was prominent in **15.E1** and not **15.E2**, in addition, between 1300 and 1200  $\text{cm}^{-1}$  **15.E1** displayed little activity compared to **15.E2**. However, despite the similarities, these differences were thought to be enough to distinguish between the three conformers. Therefore a 35  $\text{mg mL}^{-1}$   $d^3$ -acetonitrile solution of **15**·PF<sub>6</sub> was prepared and a VCD spectrum was recorded.

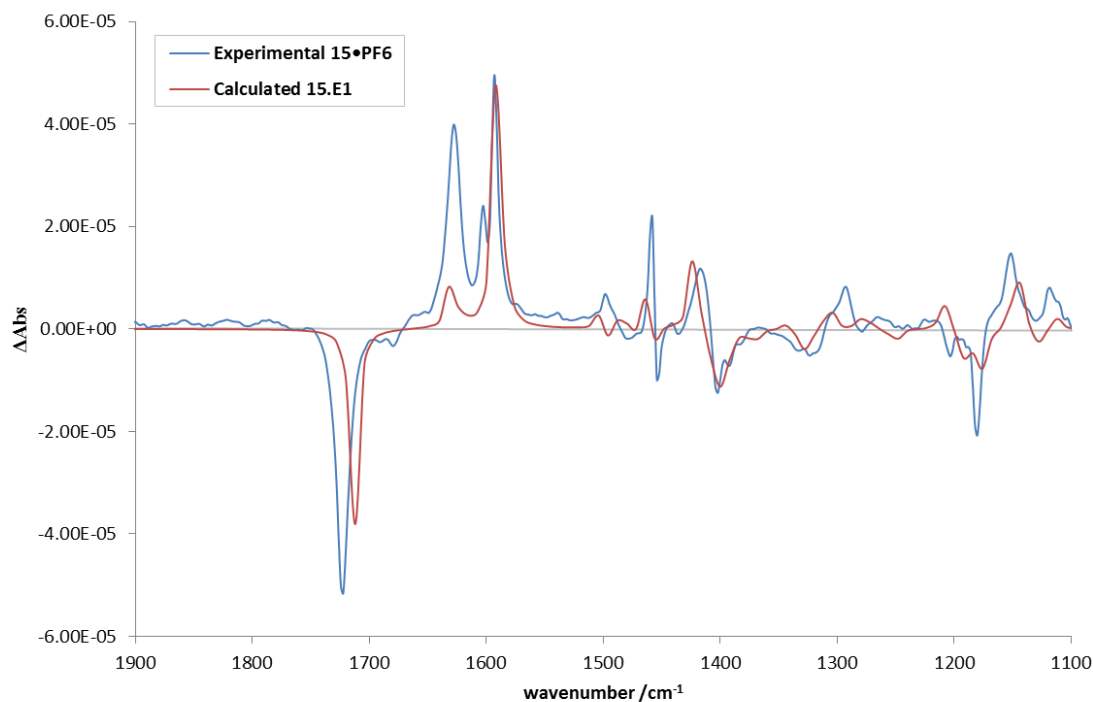


Figure 3.18 Comparison Between Experimental and **15.E1** Calculated VCD Spectra

The acquired VCD spectrum was a good match with the calculated spectrum for **15.E1** (Figure 3.18). Aside from some slight peak location mismatches, only two significant differences between the calculated and experimental VCD spectra were present; the magnitude of the peak at  $1630\text{ cm}^{-1}$  and the absence of the experimentally observed peak at  $1600\text{ cm}^{-1}$  from the calculated spectrum.

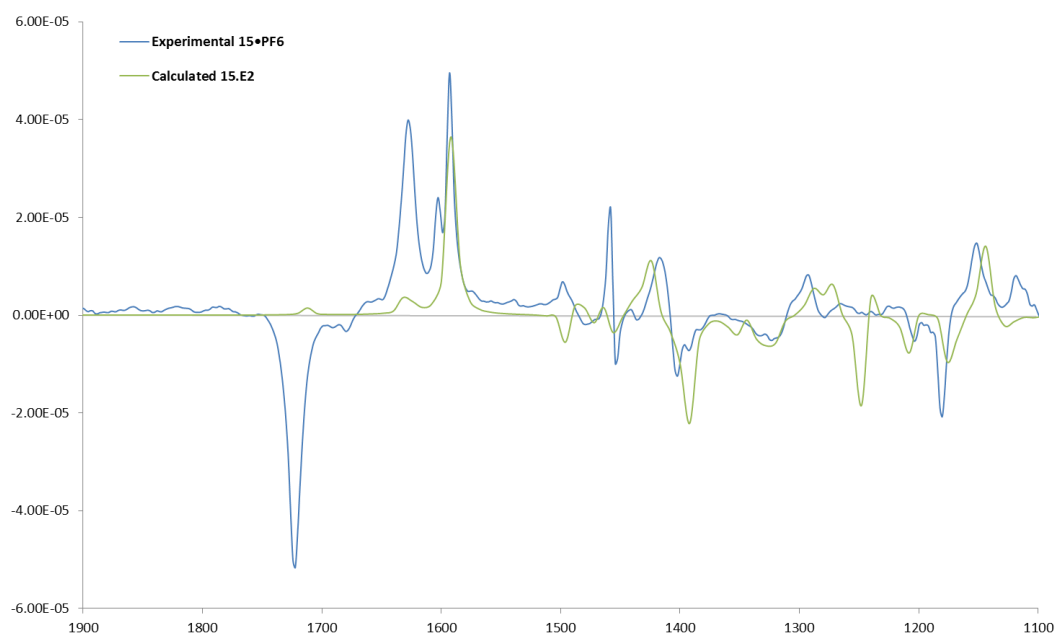


Figure 3.19 Comparison Between Experimental and Calculated Spectra for **15.E2**

Similarities between the experimental and calculated spectra for **15.E2** were significantly less obvious. Alongside similar discrepancies experienced with **15.E1**, further peaks did not match; the peak at  $\sim 1700\text{ cm}^{-1}$  was absent from the calculated spectra for **15.E2**, the peak at  $1500\text{ cm}^{-1}$  was of opposite sign and the large peak at  $1240\text{ cm}^{-1}$  in the calculated spectrum was not observed in the experimental spectrum. This gave good evidence that **15.E2** was not present in large quantity in solution. In addition, the experimental spectrum offered no indication of the presence of **15.E3**. However, like ROA, VCD did not appear to have the capacity to distinguish between conformers enough to quantify the relative populations of **15.E1**, **15.E2** and **15.E3** in solution.

### 3.4 Conclusions

Despite having potential, neither ROA nor VCD were able to quantify the conformations of iminium ion **15•PF<sub>6</sub>** in solution. This was partially due to similarities between the predicted spectra for the two lowest-energy conformations **15.E1** and **15.E2** which led to a lack of spectral regions in which to see unique peaks from each conformer. However, VCD (and somewhat loosely, ROA) indicated that **15.E1** was the majority conformer in solution which agreed with previous findings.

Additionally, using perchlorate and tetrafluoroborate derivatives of **15**, ROA indicated that conformation is independent of the counterion.

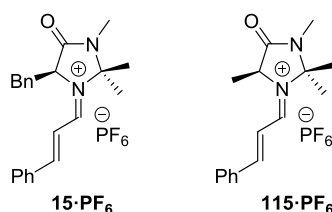


Figure 3.20 Conformationally Flexible (**15·PF<sub>6</sub>**) and Conformationally Rigid (**115·PF<sub>6</sub>**) Iminium Ions studied with ROA and VCD

A conformationally rigid iminium ion (**115·PF<sub>6</sub>**) was prepared and used to probe the correlation between predicted and experimental spectra. The calculated VCD and ROA spectra for **115·PF<sub>6</sub>** were found to have more similarities with the experimental spectra compared with the spectra for the flexible iminium ion (**15·PF<sub>6</sub>**). This suggested that the conformational flexibility of **15·PF<sub>6</sub>** gave rise to poor correlation between calculated and experimental spectra. Overall, VCD was found to have better correlation between theory and experiment compared to ROA.

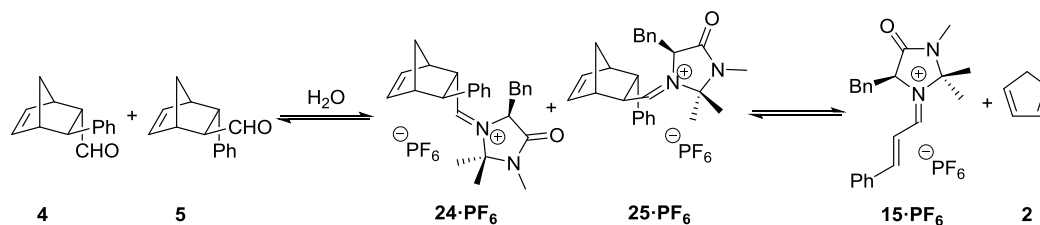
### 3.5 Observing the Catalytic Cycle

Observing intermediates can reinforce proposed catalytic cycles. However, due to the nature of catalytic processes, intermediates are often present in low concentration and combined with short lifetimes and high reactivity, detection can be challenging. The catalytic cycle for the imidazolidinone catalysed Diels-Alder reaction (Figure 3.1) is a prime example whereby one of the proposed intermediates has not been directly observed. The elusive nature of the iminium ions of the products (**24·X** and **25·X**) have rendered the catalytic cycle incomplete.

#### 3.5.1 Isolation of **24** and **25**

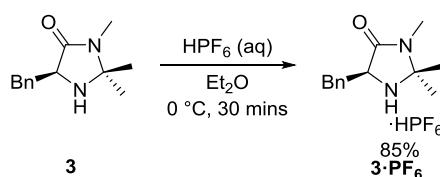
The iminium ions of the products (**24·X** and **25·X**) are thought to be short-lived in the catalytic cycle. This is because they are present in low concentration and undergo rapid hydrolysis or solvolysis to give the product aldehydes (**4** and **5**) and regenerate **3·HX**. In addition, it is known that the reaction between **15·X** and **2** is reversible

suggesting that **24·X** and **25·X** are unstable (Scheme 3.7).<sup>38</sup> Therefore, it seemed somewhat unlikely that **24·X** and/or **25·X** could be isolated. However, due to the ready isolation of **15·PF<sub>6</sub>** it seemed worthwhile to attempt isolation of **24·PF<sub>6</sub>** and **25·PF<sub>6</sub>** using similar methodologies.



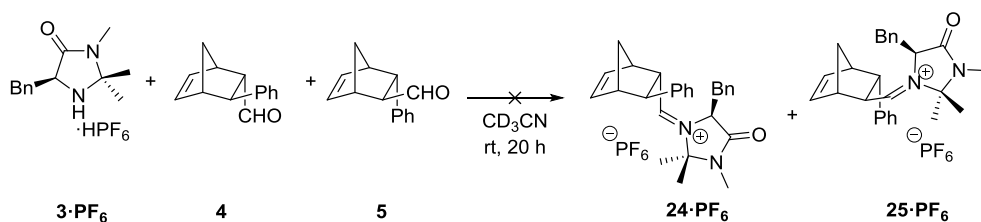
Scheme 3.7 Fate of the Iminium Ions of the Product

To avoid adding water, hexafluorophosphoric acid salt **3·PF<sub>6</sub>** was pre-formed by adding aqueous hexafluorophosphoric acid to an ethereal solution of **3** (Scheme 3.8). **3·PF<sub>6</sub>** precipitated from solution and was dried under reduced pressure (85%).

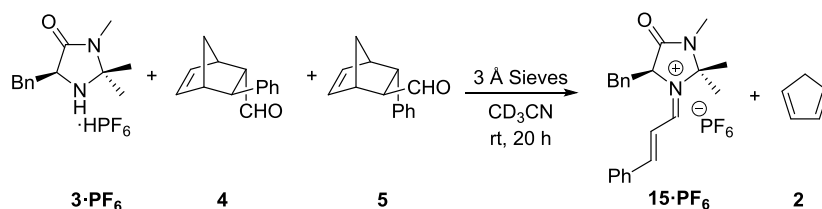


Scheme 3.8 Formation of Hexafluorophosphoric Acid Salt

Stoichiometric **3·PF<sub>6</sub>** was added to a d<sup>3</sup>-acetonitrile solution of **4** and **5** (Scheme 3.9). Unlike during isolation of **15·PF<sub>6</sub>**, methanol was avoided to remove the possibility of **24·PF<sub>6</sub>** and/or **25·PF<sub>6</sub>** being subjected to solvolysis. The mixture was stirred overnight and then analysed by <sup>1</sup>H NMR spectroscopy. No indication of any interaction between **3·PF<sub>6</sub>** and **4** and/or **5** was observed.

Scheme 3.9 Attempted Isolation of  $24 \cdot \text{PF}_6$  and  $25 \cdot \text{PF}_6$ 

Generation of  $24 \cdot \text{PF}_6$  or  $25 \cdot \text{PF}_6$  from **4** or **5** and  $3 \cdot \text{PF}_6$  would result in the formation of water. As  $24 \cdot \text{PF}_6$  and  $25 \cdot \text{PF}_6$  were deemed to be highly susceptible to hydrolysis, the presence of water was thought to hinder the likelihood of successful isolation. To circumvent this problem, freshly activated 3 Å molecular sieves were added to the reaction mixture (Scheme 3.10). Upon opening the vial, the pungent smell of cyclopentadiene was noted which indicated  $24 \cdot \text{PF}_6$  and/or  $25 \cdot \text{PF}_6$  had formed and a retro Diels-Alder reaction had occurred. In addition, the solution had turned pale yellow, characteristic of the presence of iminium ion  $15 \cdot \text{PF}_6$ .  $^1\text{H}$  NMR spectroscopy of the crude reaction mixture showed mainly  $3 \cdot \text{PF}_6$ , **4** and **5** with trace amounts of  $15 \cdot \text{PF}_6$ . No signs of  $24 \cdot \text{PF}_6$  or  $25 \cdot \text{PF}_6$  were present.



Scheme 3.10 Retro Diels-Alder

### 3.5.2 Detection of **24** and **25**

Due to apparent instability and susceptibility to hydrolysis, it became apparent that **24** and **25** would have to be detected rather than isolated. The main intermediates ( $3 \cdot \text{HX}$ ,  $15 \cdot \text{X}$ ,  $24 \cdot \text{X}$  and  $25 \cdot \text{X}$ ) are low molecular weight, moisture sensitive and ionically charged species. Therefore, detection using a chromatographic based technique seemed unlikely to be successful. However, the key intermediates of the catalytic cycle are ionic and this appeared to be a useful handle which could enable detection using mass spectrometry.



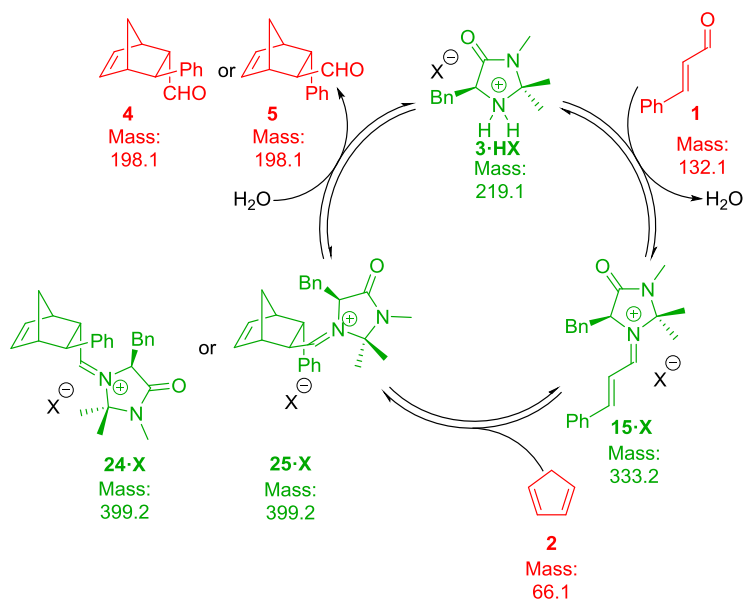
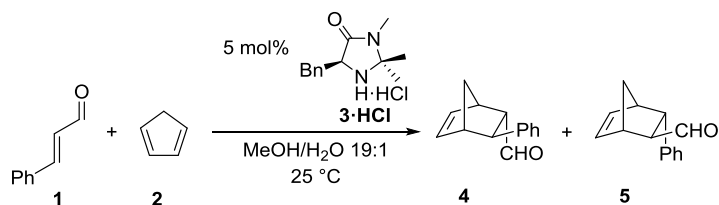


Figure 3.21 Catalytic Cycle Depicting Species Likely to be Observable by ESI Mass Spectrometry (green)

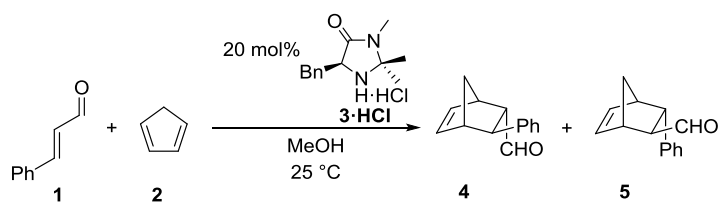
Half of the species in the catalytic cycle would be anticipated to be observable by mass spectrometry using electrospray ionisation. The species not amenable to electrospray ionisation (**1**, **2**, **4** and **5**) are either added to the reaction mixture (**1** and **2**) or readily isolated at the end of the catalytic process (**4** and **5**). Hence, their presence within the reaction mixture is known and detection was not deemed essential.



Scheme 3.12 Literature Reaction Conditions

As with any mechanistic investigation, using conditions relevant to the literature-optimised procedure is desirable. Therefore, a reaction in methanol/water (19:1) with 5 mol% catalyst loading was setup (Scheme 3.12). An aliquot was removed and, after dilution with methanol (approx. 200 fold), was analysed by ESI-MS. **3** was readily detected and some evidence of **15** was also present. However, **24** and/or **25**

were not detected. The reaction was repeated omitting water and was analysed using ESI-MS. Again, **3** and **15** were detected. In addition, a small deviation from the background chromatogram was observed at  $m/z$  of 400 although the concentration of ions was too low to draw any conclusions. Therefore, the catalyst loading was increased to 20 mol% (Scheme 3.13). Post dilution, analysis by ESI-MS showed the presence of **3**, **15** and, at a very low level of ion abundance, a species with  $m/z$  of 399 (Figure 3.22).



Scheme 3.13 Reaction Used for Detecting Intermediates Using ESI-MS

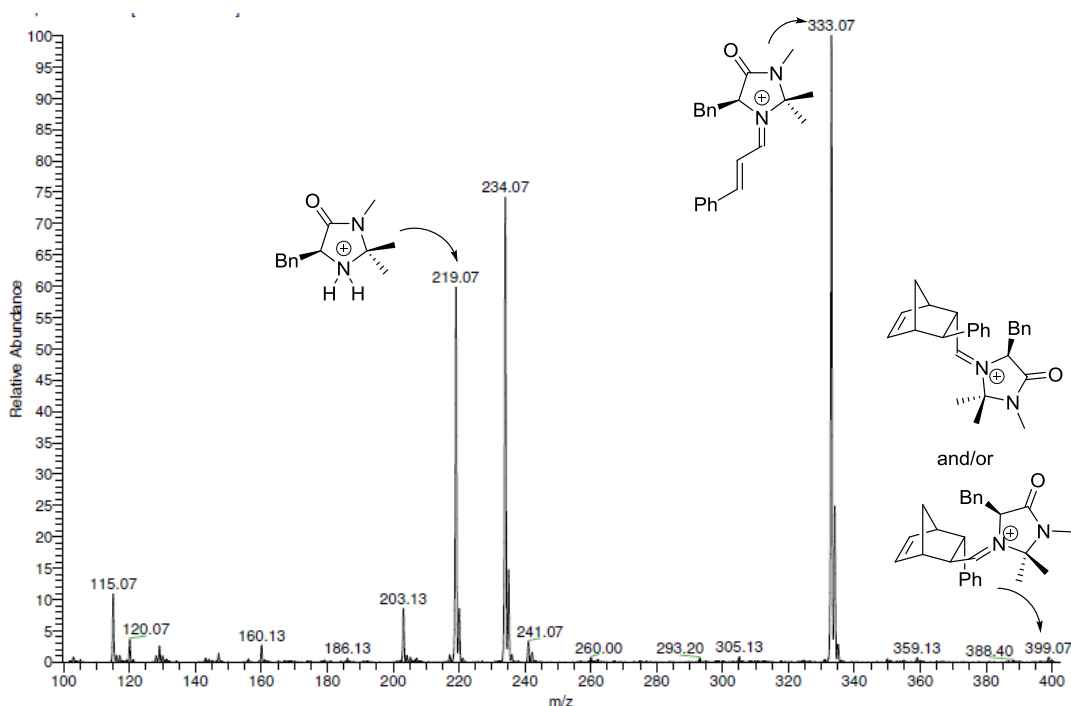


Figure 3.22 Full Ion Chromatogram (+ve)

Although encouraging, the observation of a small ion with the correct mass was by no means conclusive. It could have been an impurity, an ion cluster or coincidence. In addition, it was not possible to account for the ion at  $m/z$  234 which added

additional uncertainty. In an attempt to further inspect the ion at  $m/z$  399, it was isolated using an ion trap. Energised carrier gas was then used to fragment the ion. The ion was found to readily fragment and lose 66 mass units to give  $m/z$  333 (Figure 3.23). This observation was consistent with the ion at  $m/z$  399 being **24** and/or **25** and occurrence of a retro Diels-Alder reaction to give **15** and **2**. This agreed with the previously observed ability of **4** and **5** to undergo a retro Diels-Alder in the presence of **3**·HPF<sub>6</sub> and molecular sieves.

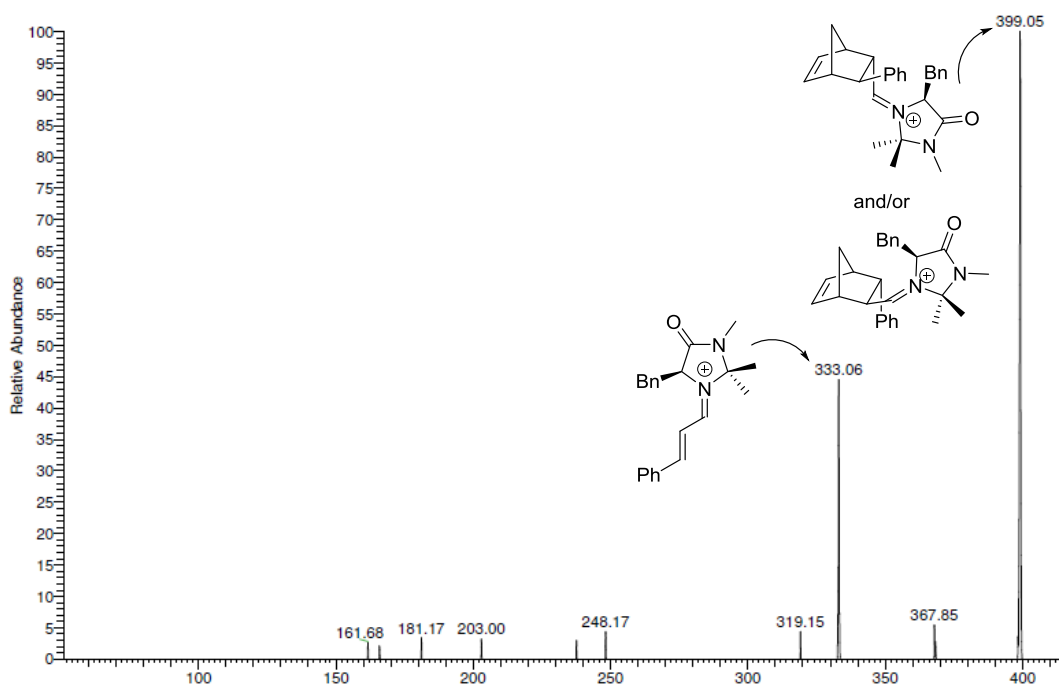


Figure 3.23 Fragmentation of  $m/z$  399

### 3.5.3 Characterisation of Ions

Although the retro Diels-Alder fragmentation of ion  $m/z$  399 was encouraging evidence that the ion was indeed **24** and/or **25**, the result was not conclusive. Therefore, alternative methods for characterising ions by mass spectrometry were sought. Ion mobility spectrometry (IMS) can distinguish between gas-phase ions based upon their ion mobility. It is an electrophoretic technique whereby ions are characterised by mass and charge but also by their size and shape (Collision Cross Section, CCS).<sup>68</sup> The technique is supported by calculation of CCS values which can reinforce experimental observations. Since its renaissance, IMS has been coupled

with both MALDI and ESI ionisation sources to give tandem MS-IMS techniques.<sup>68</sup> MS-IMS has been used in biological applications,<sup>69,70</sup> the pharmaceutical industry,<sup>71</sup> forensics<sup>72</sup> and more recently for probing structure of metal complexes and ligands.<sup>73</sup>

MS-IMS appeared to be a suitable method with which to verify the identity of the detected ions. However, before seeking to obtain experimental data, low-energy conformers of **3·H** and **25** were found (BHandH/6-31+G\*\*, Figure 3.24) to enable calculation of CCS parameters. As the *exo* adduct is the major product isomer, the *endo* isomer was not considered for CCS calculation purposes. The coordinates for the low-energy conformations of **3·H**, **15** and **25** were then used by collaborators in conjunction with Campuzano modified<sup>74</sup> Mobcal software to calculate the CCS of each molecule (Table 3.2). The calculated CCS values showed that, as anticipated, each ion possessed a different CCS and could be distinguished by this parameter.

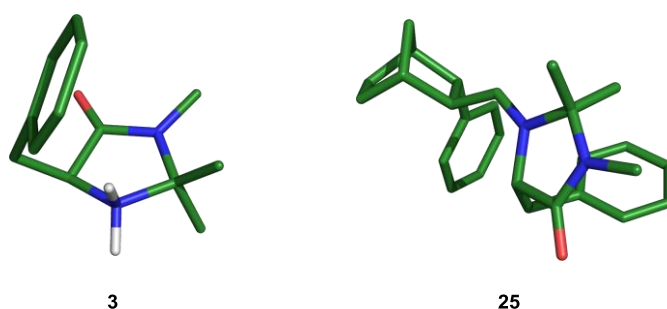
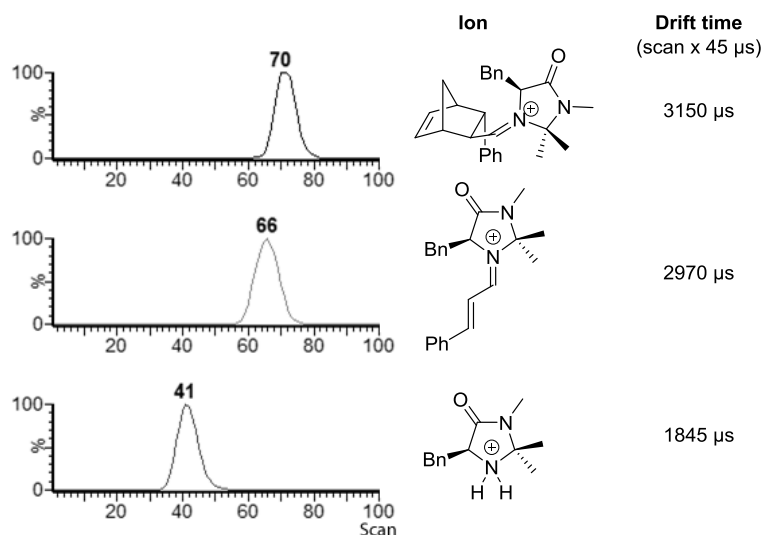


Figure 3.24 Low-Energy Conformers of **3** and **25** (anions omitted)

An experiment similar to that shown in Scheme 3.13 was setup by collaborators and, using an ESI-IMS instrument, ion mobilities and collision cross sections were measured. Ion mobilities were found to correlate, as anticipated, with ion size (Figure 3.25), **25** had the longest drift time (3150  $\mu\text{s}$ ) followed by **15** (2970  $\mu\text{s}$ ) and **3·H** (1845  $\mu\text{s}$ ).

Figure 3.25 Ion Mobility for **25**, **15** and **3·H**

The experimental and calculated CCS values were found to correlate well (Table 3.2) and combined with ion mobility data reinforced that the identity of ions  $m/z$  219, 333, 399 were **3·H**, **15** and **24/25** respectively. Due to **24** and **25** having similar size and shape, they would be anticipated to have similar CCS/ion mobility values. With the current resolution of the two techniques, it was not possible to identify if **24** or **25** was present or a mixture of the two.

Cation	Calculated CCS	Experimental CCS
<b>3</b>	83	83
<b>15</b>	119	118
<b>25</b>	125	129

Table 3.2 CCS Calculated Using the Trajectory Method and Experimentally Determined

### 3.6 Conclusions

For the first time, key intermediates (**3·H**, **15**, **24** and **25**) from the proposed catalytic cycle for the imidazolidinone catalysed Diels-Alder reaction were simultaneously detected.

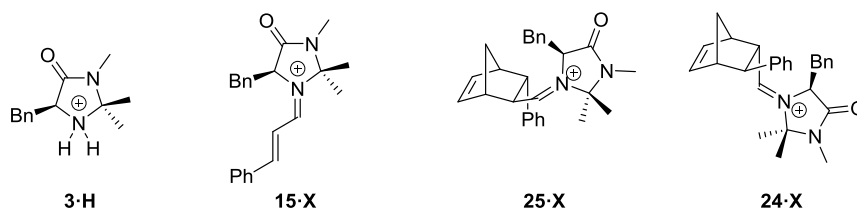
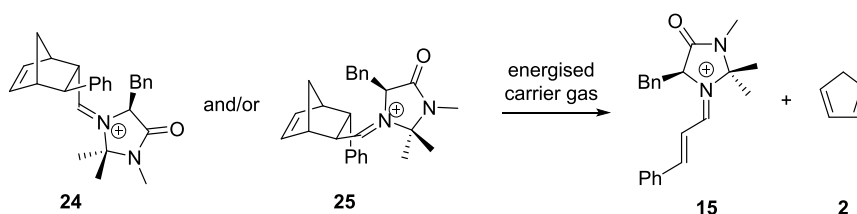


Figure 3.26 Key Components of the Catalytic Cycle Detected Using ESI-MS

The ions generated by ESI-MS were characterised by ion mobility and CCS. The experimentally determined CCS values correlated well with the calculated values derived from computationally determined low-energy conformations of each species. The ion mobility measurements correlated with molecular weight as anticipated. Hence, the combination of ion mobility and CCS measurements gave good evidence towards the identity of each ion.



Scheme 3.14 Retro Diels-Alder Reaction by MS/MS

Of particular note was the direct observation of the elusive iminium ion of the products (**24/25**). This ion ( $m/z$  399) was further characterised by fragmentation using energised carrier gas. Upon fragmentation, a retro Diels-Alder reaction was observed to occur and parent iminium ion **15** was regenerated (Scheme 3.14).

Despite having gained evidence suggesting, unless the reaction is carried out under strictly anhydrous conditions, recombination of **4** and **5** with **3·HX** to form **24·X** and **25·X** is unlikely, no evidence was present to suggest that the observed ion corresponding to **24** and/or **25** was a result of the catalytic cycle operating in the forward direction. Therefore, within this study, strong evidence towards the existence of **24** and/or **25** was obtained but it was not unequivocally determined to be a result of cycloaddition between **15** and **2**.

# **Chapter 4: A Hybrid Imidazolidinone Catalyst**

## 4 A Hybrid Imidazolidinone Catalyst

### 4.1 Introduction

Hayashi and co-workers reported an iminium ion catalysed Diels-Alder reaction which uses diarylprolinol ethers (**9**) rather than imidazolidinones.<sup>45</sup>

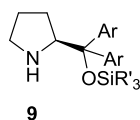
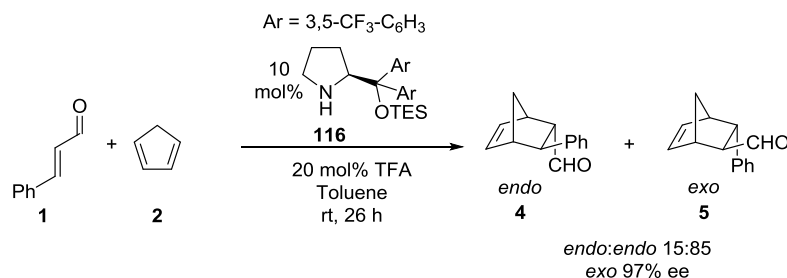


Figure 4.1 Diarylprolinol Ether

The reaction gives products with high enantiomeric excess and isolated yield. In addition, unlike the MacMillan imidazolidinone, the diarylprolinol ether furnishes an improved diastereomeric ratio in favour of the *exo* isomer. The selective formation of this isomer is valuable as the kinetic *endo* isomer usually prevails in Diels-Alder reactions.<sup>75</sup> More recently, the reaction has been made more environmentally benign by substitution of the organic solvent for water using diarylprolinol ether **116**.<sup>76</sup>



Scheme 4.1 Diarylprolinol Ether Catalysed Diels-Alder Reaction

Despite the novel attributes of this reaction, long reaction times of up to 100 h and catalyst loadings of 10–20 mol% render it far from ideal. For example, in the reaction between **1** and **2** catalysed by **116**, a 10 mol% catalyst loading is used and a 26 hour reaction time is required (Scheme 4.1). Imidazolidinones have been shown to offer significantly faster reaction rates compared to diarylprolinol ethers for the Diels-Alder cycloaddition reaction.<sup>22</sup> Therefore, imidazolidinone **117** was envisaged as a viable alternative to diarylprolinol **9** and would be expected to offer improved



catalytic rates. **117** features a similar sterically hindered environment about the nitrogen compared to **9**, hence, in addition to lower catalyst loadings and shorter reaction times, similar levels of enantio and diastereoselectivity would be anticipated.

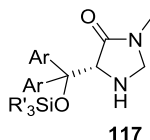


Figure 4.2 Hybrid Imidazolidinone Scaffold

Within this chapter the design rationale of **117** is validated using DFT calculations. Methodology is developed to prepare imidazolidinones unsubstituted at the 1- and 2-positions and **118** is targeted for synthesis.

## 4.2 Results and Discussion

### 4.2.1 Computational Evaluation

The hybrid imidazolidinone **118** was designed to give similar enantio- and diastereoselectivity to the corresponding diarylprolinol ether catalyst **39**. **118** would require a multi-step synthetic route. Therefore, before embarking on a synthetic journey, some validation of the likelihood of **118** being able to replicate the performance of **39** was sought.

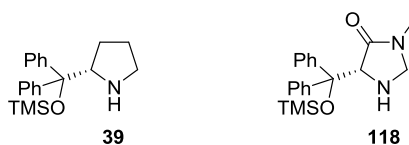


Figure 4.3 Diarylprolinol Ether and Associated Hybrid Imidazolidinone

Cycloaddition occurs after an aldehyde has condensed with the amine to form an iminium ion. Therefore, investigating conformations and the relative energies of iminium ions associated with **39** and **118** was deemed to be a suitable method for probing if **118** would mimic the steric environment, and therefore selectivity, of **39**. Using methodology which had previously been used within the group

(BHandH/6-31+G\*\*),<sup>36</sup> low-energy conformations of iminium ions derived from **39** and acrolein were found. An acrolein derived iminium  $\pi$ -system was used to reduce calculation time.

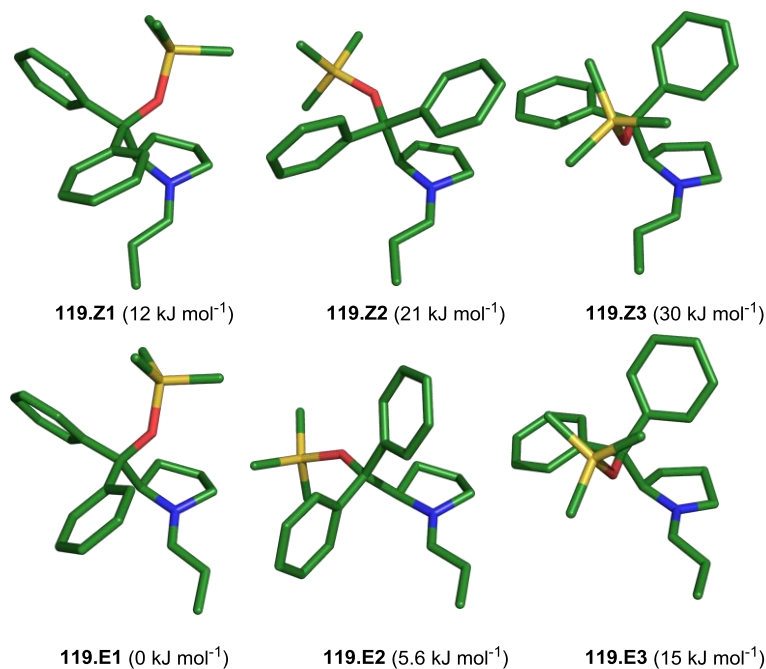


Figure 4.4 Iminium Ions Derived from **39** and Acrolein  
(enantiomer inverted for clarity)

Six low-energy conformations of iminium ions derived from **39** and acrolein were found (Figure 4.4). **119.E1** (0 kJ mol<sup>-1</sup>) was found to be the lowest energy conformer and at 298 K would be expected to occupy 90% of the population distribution. **119.E1** has a distance of 2.85 Å between the iminium nitrogen and the ethereal oxygen atom. The distance is lower than the sum of the Van der Waals radii (3.07 Å) which suggests that this could be a stabilising interaction and give-rise to the low energy of **119.E1**.

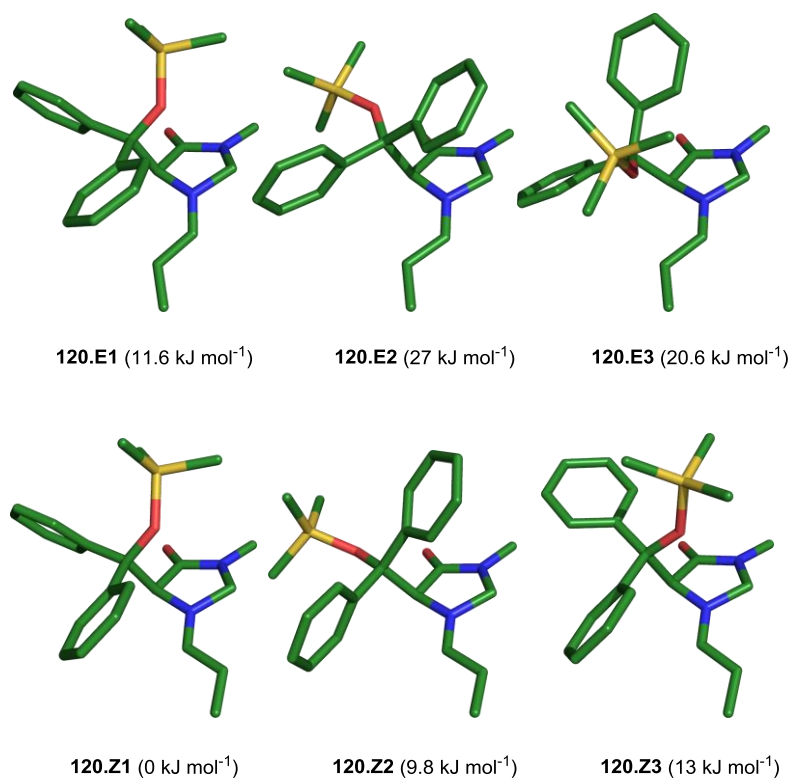


Figure 4.5 Iminium Ions Derived from **118** and Acrolein  
(enantiomer inverted for clarity)

In an analogous fashion, low-energy conformations of iminium ions derived from **118** and acrolein were found. The conformations were very similar to those found for iminium ions derived from **39**. **120.Z1** was found to be the lowest energy conformer which, as isoconformeric to **119.E1**, was a promising result. At 298 K **120.Z1** would be expected to occupy 97% of the population distribution, a similar occupation to **119.E1**. In addition, as seen with **119.E1**, an interaction between the iminium nitrogen and ethereal oxygen was present (2.88 Å) which further enhanced the similarities between the two systems.

The results from computational modelling suggested that, as rationally designed; **118** had the potential to be a substitute for **39**. These promising initial findings rendered **118** to be a worthwhile synthetic target.

### 4.2.2 Synthesis of 1,2-Unsubstituted Imidazolidinones

Although described sparsely within the literature, no preparations of 1,2-unsubstituted imidazolidinones have been reported. This posed a problem for the preparation of **118**. Using a standard disconnection for an imidazolidinone it was thought that **118** could be made by condensation of amino amide **121** and formaldehyde **122**.

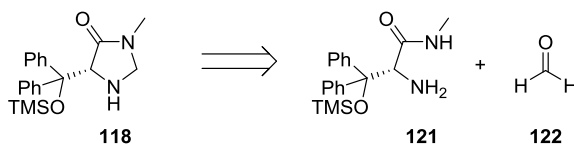
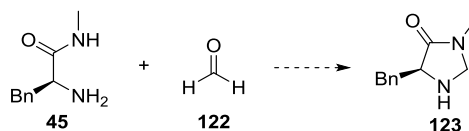


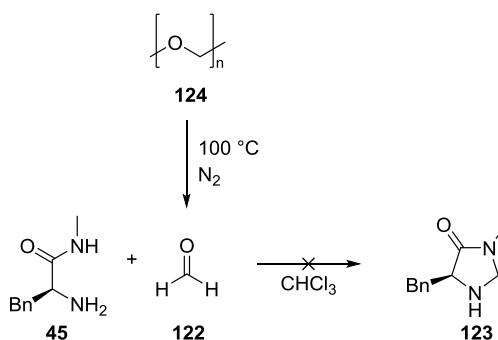
Figure 4.6 Disconnection of **118**

Due to the lack of literature precedent for forming 1,2-unsubstituted imidazolidinones, a screening approach was adopted. Phenylalanine-*N*-methyl amide (**45**) was selected as a model substrate as it can be prepared on a gram scale from the relatively inexpensive ethyl ester and ethanolic methylamine (Scheme 2.1). Using **45** efforts were focused on forming **123**.



Scheme 4.2 Proposed Method for Formation of **123**

Formaldehyde (**122**) has been reported to be readily formed from the thermal decomposition of **124**.<sup>77</sup> This was considered to be a useful method of generating highly reactive **122** which could be used to prepare **123** (Scheme 4.3).

Scheme 4.3 Attempted use of Gaseous **122**

**124** was heated to 100 °C under a slow flow of anhydrous nitrogen. The formation of a white powder on the neck of the flask suggested formaldehyde was being generated and was re-polymerising. A 5 mm bore tube was used to bubble the mixture of **122** and nitrogen through a chloroform solution of **45**. After 4 hours a significant amount of white powder, presumably **124**, had formed. The reaction mixture was analysed by <sup>1</sup>H NMR spectroscopy. Disappointingly **45** was returned with no sign of **123**. The reaction was repeated in the presence of catalytic *p*-TSA but again did not yield the desired products. It seemed likely that any formaldehyde being generated was polymerising before reacting with amine **45**.

Having failed to produce **123** using gaseous **122**, attention was turned to other sources of formaldehyde (Figure 4.7).

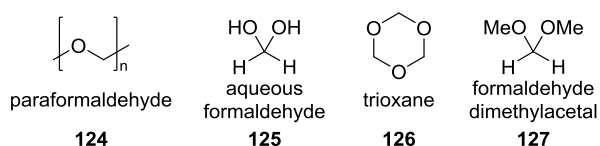
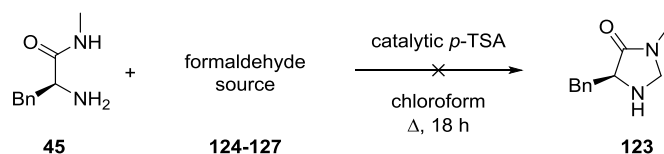


Figure 4.7 Sources of Formaldehyde

To assess the suitability of each formaldehyde source to form **123**, a parallel screening approach was adopted. Four consecutive reactions were run, each containing **45** (1 eq.), catalytic *p*-TSA and a formaldehyde source (3 eq.) in chloroform (Scheme 4.4). After 18 hours at reflux the solutions were analysed by <sup>1</sup>H NMR spectroscopy. Frustratingly, no **123** appeared to have formed. In the reactions

containing **124** a reaction had occurred but resonances characteristic of the desired product **123** were not visible in the  $^1\text{H}$  NMR spectrum.



Scheme 4.4 Attempted Formation of **123** Using a Brønsted Acid

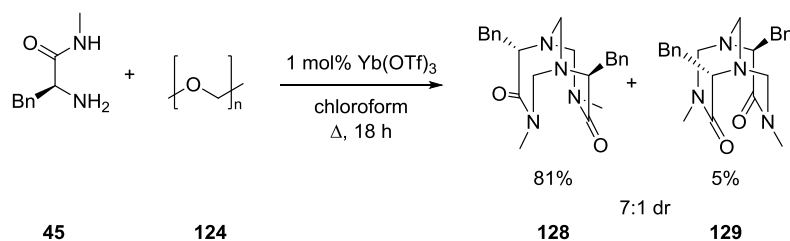
The screening was repeated, substituting the Brønsted acid for a Lewis acid. Ytterbium(III) triflate has previously been used to form imidazolidinones and seemed ideal for this study.<sup>78</sup> Four consecutive reactions were setup with 1 mol% of ytterbium(III) triflate, **45** (1 eq.) and a formaldehyde source in chloroform (Scheme 4.5). After 18 hours under reflux the reaction mixtures were analysed by  $^1\text{H}$  NMR spectroscopy. The reactions using **125**, **126** and **127** all returned starting amide **45**. However, like the Brønsted acid catalysed reaction, **45** was found to react with **124** in the presence of a Lewis acid to give an unexpected product.



Scheme 4.5 Attempted Formation of **123** Using a Lewis Acid

The reaction between **45** and **124** in the presence of ytterbium(III) triflate was very clean and  $^1\text{H}$  NMR spectroscopy of the crude reaction mixture showed complete conversion to two products in a 1:9 ratio. The reaction was repeated on a larger scale to enable isolation of the minor product and after chromatography two compounds (**128** and **129**) were isolated. By  $^1\text{H}$  NMR spectroscopy they clearly contained functionality from **45** and also appeared to contain three methylene groups. Single crystals of each were grown and analysed by X-ray crystallography to confirm their structure (Figure 4.8). It was found that **45** had dimerized with formaldehyde to form the two diastereomeric products **128** and **129** (Scheme 4.6). These novel compounds

were considered to be worthy of further investigation and studies on this architecture can be found in Chapter 7.



Scheme 4.6 Dimerisation of Amino Acid Amides

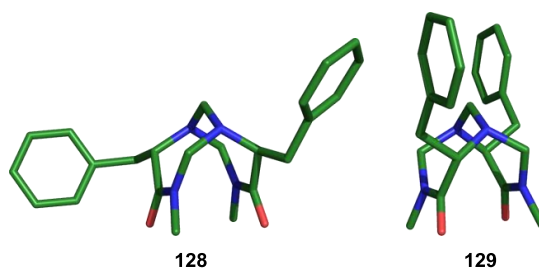
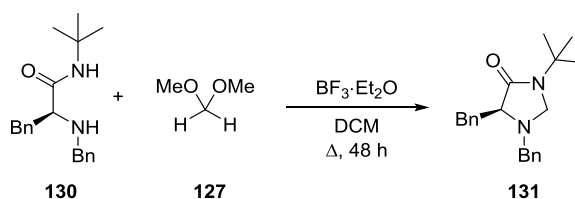


Figure 4.8 Single Crystal X-ray Structures of **128** and **129**

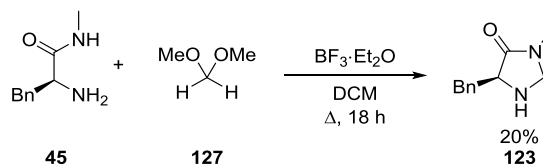
Having had no success forming **123** from **45**, it was beginning to appear that protection of the free amine would be required. A publication by Zheng and co-workers detailed formation of a 1-benzyl imidazolidinone (**131**) using **130**, **127** and  $\text{BF}_3 \cdot \text{Et}_2\text{O}$  (Scheme 4.7).<sup>79</sup>



Scheme 4.7 Zheng Imidazolidinone Synthesis

A model reaction was undertaken reacting amino amide **45** and formaldehyde dimethyl acetal (**127**) in the presence of  $\text{BF}_3 \cdot \text{Et}_2\text{O}$  (Scheme 4.8). Analysis of the crude reaction mixture by  $^1\text{H}$  NMR spectroscopy showed a number of products. However, two doublets (4.22 and 4.04 ppm) were visible in the anticipated region for the methylene group of **123**. Dimers **128** and **129** were not present. The mixture was

chromatographed and pleasingly 5 mg of **123** was isolated. None of the other side-products were recovered, presumably due to their high polarity or instability to chromatographic conditions.



Scheme 4.8 Formation of **123**

The reaction was repeated but only decomposition was observed. The dimethoxymethane was distilled over magnesium sulfate and the reaction was repeated under anhydrous conditions. Again, no **123** was present in the  $^1\text{H}$  NMR spectrum of the crude reaction mixture. To further reduce the likelihood of water entering the system **45** was recrystallized and then dried under reduced pressure over  $\text{P}_2\text{O}_5$  for 24 h. The reaction was repeated using dried **45** and yet again **123** failed to form. With increasing frustration at the non-reproducibility of the process, a new bottle of  $\text{BF}_3 \cdot \text{Et}_2\text{O}$  was purchased and the reaction was repeated. The crude reaction mixture using the newly purchased  $\text{BF}_3 \cdot \text{Et}_2\text{O}$  was quite clean and contained mainly **45** and **123**. This suggested that high quality  $\text{BF}_3 \cdot \text{Et}_2\text{O}$  was crucial for the success of the reaction.

Having established that the reaction was very dependent on the quality of the Lewis acid complex, attempts were made to optimise the reaction conditions. Changing of the number of equivalents of  $\text{BF}_3 \cdot \text{Et}_2\text{O}$  and/or **127** all led to considerable side-product formation with **123** becoming barely visible in the  $^1\text{H}$  NMR spectrum of the crude reaction mixtures. Increasing the scale of the reaction also failed to produce **123**. In addition, changing the Lewis acid or using a Brønsted acid all failed to induce any reaction between **45** and **127** (Scheme 4.4 and 4.5). Due to the lack of success optimising the reaction and in the interests of time, the 20% yield of **123** was accepted and efforts were focused on forming the hybrid imidazolidinone **118**.



### 4.2.3 Synthesis of the Hybrid Imidazolidinone

The hybrid imidazolidinone **118** can be disconnected to the corresponding amino amide **121** and a formaldehyde source (Figure 4.6). **121** can be derived from a literature reported amino acid (**132**) and methylamine (**44**). Conveniently, the reported synthesis of **132** provided the product as a single enantiomer starting from readily available serine methyl ester **133** (Figure 4.9).<sup>80</sup>

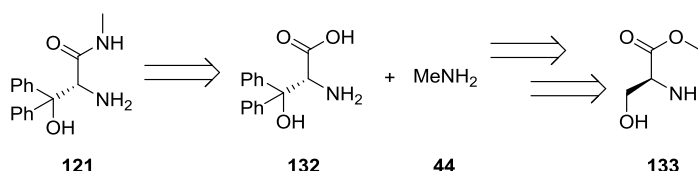
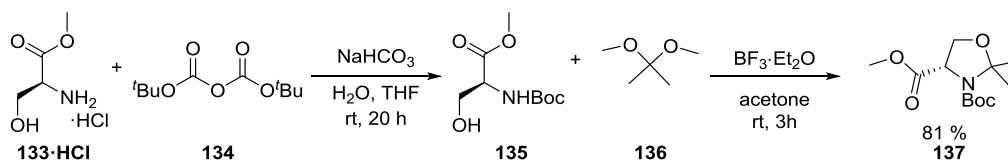


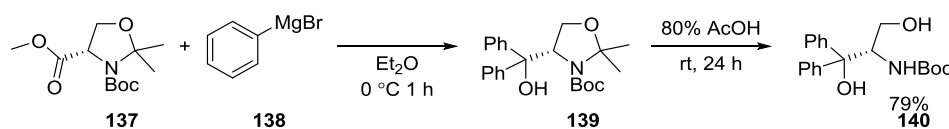
Figure 4.9 Retrosynthesis of **121**

L-Serine methyl ester hydrochloride **133·HCl** was protected using di-*tert*-butyl dicarbonate **134**. The crude protected serine was then cyclised using acetone dimethyl acetal **136** in a Lewis acid catalysed process to give oxazolidine **137** (81%).

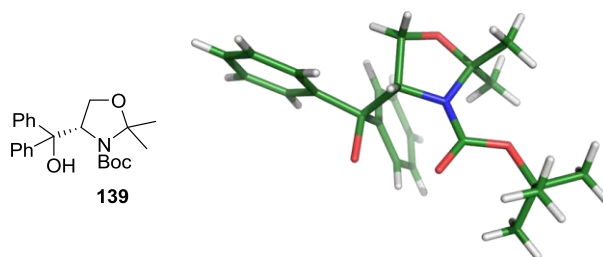


Scheme 4.9 Synthesis of **137**

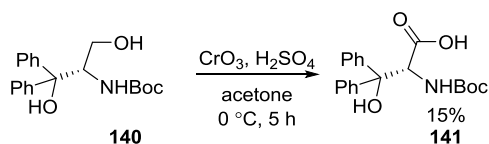
Double Grignard addition into **137** gave intermediate **139**. Although not isolated, amination **139** readily crystallised from the crude reaction mixture and its structure was confirmed by single crystal X-ray crystallography (Figure 4.10). Intermediate **139** was deprotected using aqueous acetic acid to give aminoalcohol **140** (79%, Scheme 4.10).



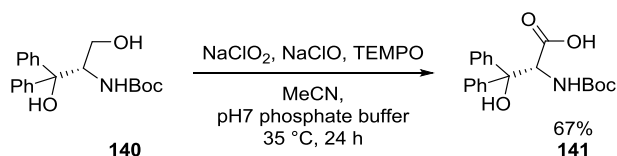
Scheme 4.10 Synthesis of **140**

Figure 4.10 X-ray Structure of **139**

Following a literature procedure, aminoalcohol **140** was oxidised using Jones conditions to the corresponding carboxylic acid (**141**). A poor yield of 15% was obtained, possibly due to the chromium chelating to the many heteroatoms present in **140** and **141**. Hence, an alternative transition-metal-free oxidation was sought.

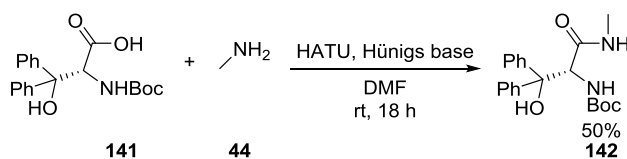
Scheme 4.11 Jones Oxidation of **141**

Oxidation using sodium chlorite, bleach and catalytic TEMPO has been reported to be effective at oxidising primary alcohols to carboxylic acids.<sup>81</sup> The method is heavy-metal-free and is known not to epimerise  $\beta$ -stereogenic centres. Pleasingly, when applied to **140**, carboxylic acid **141** was furnished in good yield (67%, Scheme 4.12).

Scheme 4.12 Metal-Free Oxidation of **140**

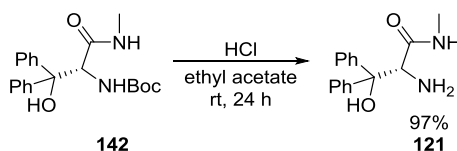
Having accessed the known protected carboxylic acid, peptide coupling was used to form the amide. In the interests of time and reliability, HATU was chosen as the coupling agent of choice despite its cost. Under standard coupling conditions

(DMF/Hünigs base) a reasonable yield of Boc-protected amide **142** was obtained (50%, Scheme 4.13).



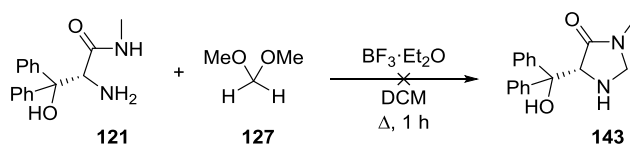
Scheme 4.13 HATU Coupling

The Boc group was observed to be resilient to 50% TFA in DCM and neat TFA. Therefore, 2 M HCl in ethyl acetate was prepared and was found to cleanly remove the Boc protecting group to afford **121** in excellent yield (97%, Scheme 4.14).

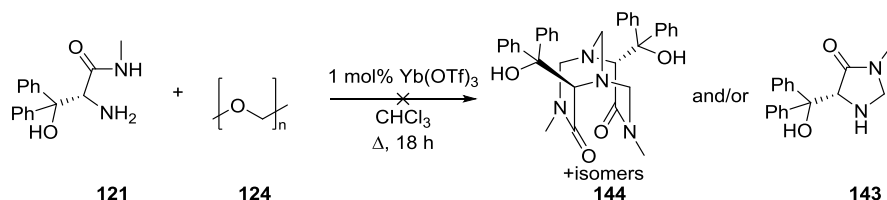


Scheme 4.14 Boc Deprotection

Having accessed amide **121**, the next challenge was to form **143**. This was not considered to be a trivial task as accessing **123** was found to be far from straightforward. Using the methodology previously developed, **121** was reacted with **127** in the presence of  $\text{BF}_3 \cdot \text{Et}_2\text{O}$  (Scheme 4.15). After 1 hour, analysis of the crude reaction mixture by  $^1\text{H}$  NMR spectroscopy indicated that **121** was no longer present. However, signals characteristic of **143** were not present in the  $^1\text{H}$  NMR spectrum either.

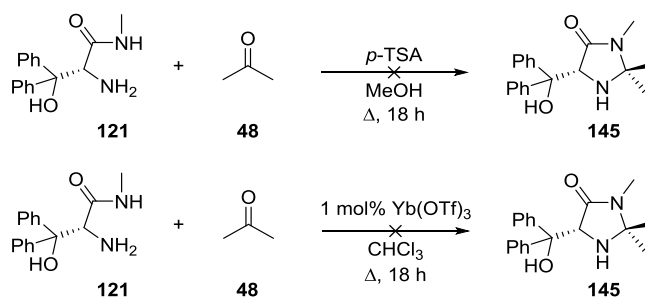
Scheme 4.15 Attempted Formation of **143**

The previously described methodology to form 2-unsubstituted imidazolidinones appeared to be unsuitable for forming **143**. To see if **121** shared any reactivity with **45**, **121** was reacted with **124** in the presence of ytterbium(III) triflate in an attempt to form a dimer (Scheme 4.16). Again, no indications of **121**, **144** or **143** were present in the crude reaction mixture.

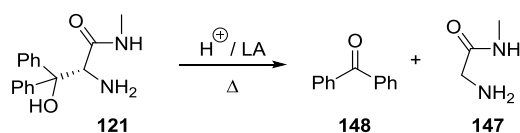


Scheme 4.16 Attempted Dimerisation

With dwindling stocks of **121**, attempts to form a 2,2-dimethyl imidazolidinone (**145**) from **121** and **48** using well known literature procedures were made (Scheme 4.17).<sup>36,78</sup>

Scheme 4.17 Attempted Formation of **145** with a Brønsted and Lewis Acid

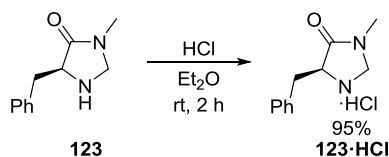
Neither of the two approaches yielded **145**. TLC analysis of the crude reaction mixtures displayed a non-polar, highly UV active spot. The species was isolated by flash chromatography and found to be benzophenone (**148**). <sup>1</sup>H NMR of the crude reaction mixture before aqueous workup (Scheme 4.17) showed the presence of glycine-*N*-methyl amide (**147**). **147** and **148** were both clearly arising from decomposition of **121** (Scheme 4.18).

Scheme 4.18 Acid Catalysed Decomposition of **121**

Due to the apparent instability of **121** it was deemed likely that **118** would have similar stability under acidic conditions. Therefore, despite computational evidence suggesting **118** could be a good alternative catalyst to **39** it was decided that efforts towards its preparation should be terminated.

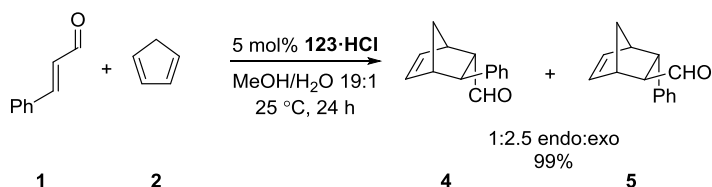
#### 4.2.4 Evaluation of **123** as a Catalyst

Although **123** features within the literature, it has not been used as a secondary amine catalyst. Therefore it was deemed appropriate, having accessed **123**, to evaluate its performance in the benchmark Diels-Alder reaction between **1** and **2**.



Scheme 4.19 Hydrochloride Salt Formation

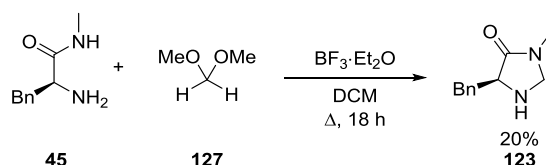
An ethereal solution of **123** was treated with anhydrous hydrogen chloride to form hydrochloride salt **123·HCl** (Scheme 4.19). **123·HCl** was then used at 5 mol% loading as a catalyst in the benchmark Diels-Alder reaction between cinnamaldehyde (**1**) and cyclopentadiene (**2**) (Scheme 4.2).

Scheme 4.20 Evaluation of **123·HCl** in the Benchmark Reaction

Analysis of the crude reaction mixture by  $^1\text{H}$  NMR spectroscopy showed complete conversion of **1** to **4** and **5**. A 2.5:1 *exo:endo* (**5**:**4**) product distribution, after hydrolysis, suggested that catalysis had occurred (normally the *endo* isomer would prevail in the absence of iminium catalysis). However, **123** was not observed in the post hydrolysis  $^1\text{H}$  NMR spectrum of the crude reaction mixture. The  $^1\text{H}$  NMR spectra of the crude reaction mixture before hydrolysis did not show the presence of **123** either. This suggested that **123** may have decomposed. **4** and **5** were derivatized and analysed by HPLC on a chiral stationary phase. **4** and **5** were both found to be racemic. A combination of apparent decomposition and lack of asymmetric induction rendered **123** a poor catalyst unworthy of further investigation.

### 4.3 Conclusions

Due to a lack of literature precedent, using **45** as a model substrate, methodology to prepare 1,2-unsubstituted imidazolidinones was developed. Formaldehyde dimethyl acetal (**127**) in the presence of  $\text{BF}_3 \cdot \text{Et}_2\text{O}$  in DCM were found to be optimal conditions for the preparation of **123** (Scheme 4.21).



Scheme 4.21 Preparation of 1,2-Unsubstituted Imidazolidinone

Computational calculations indicated hybrid imidazolidinone **118** would form iminium ions with a similar steric environment to iminium ions derived from **39**. Therefore, **118** was deemed to be a worthwhile, novel, synthetic target. Problems arose when the precursor amide **121** was observed to decompose, under acidic conditions at elevated temperatures, to give benzophenone **148** and glycine-*N*-methyl amide **147**. All attempts to transform **121** into an imidazolidinone, using novel or known methodology, resulted in decomposition. This suggested that further attempts to prepare **118** from **121** would be futile.

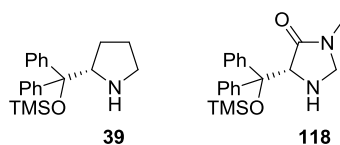
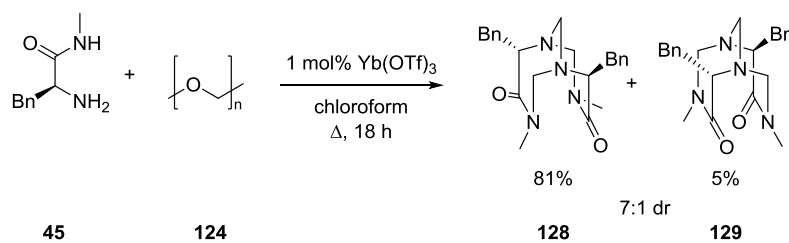


Figure 4.11 Diarylprolinol Ether and Corresponding Imidazolidinone

Novel 1,2-unsubstituted imidazolidinone **123** was evaluated as a catalyst in the benchmark Diels-Alder reaction between cyclopentadiene (**1**) and cinnamaldehyde (**2**). **123** was found to decompose under the reaction conditions and the Diels-Alder adducts (**4** and **5**) were isolated in racemic form. The instability of **123** suggested that even if **118** could be prepared it would likely be unstable under conditions associated with iminium ion activation. Therefore, despite being an attractive idea, a decision was made to abandon efforts towards **118**.



Scheme 4.22 Novel Amino Acid Dimers

Finally, during attempts to prepare **123**, **45** was found to react cleanly with **124** in the presence of ytterbium(III) triflate to give **128** and **129** as a mixture of diastereoisomers (Scheme 4.22). Further investigations into these novel structures can be found in Chapter 7.

# **Chapter 5: EWGs on Imidazolidinones**



## 5 Electron Withdrawing Groups on Imidazolidinones

### 5.1 Introduction

Catalytic rates for secondary amine catalysed Diels-Alder reactions have been shown to be influenced by the substituents on the catalyst. In particular, addition of an electron withdrawing group within the architecture of a secondary amine salt has been seen to increase catalytic rate.<sup>39</sup> Initially found to be applicable to pyrrolidine based catalysts, this has also been shown to be effective on the imidazolidinone scaffold.<sup>40</sup>

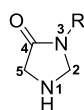


Figure 5.1 Numbered Imidazolidinone

Since MacMillan's introduction of imidazolidinone **3**, many alternatives have appeared in the literature.<sup>1</sup> Each of these have been tailored to the reaction of interest. Modifications to both the 2- and 5-position on the ring are commonplace (Figure 5.1). Due to their intimate proximity to the iminium  $\pi$ -system, these substituents can have a remarked impact on the selectivity and reactivity observed during reactions.

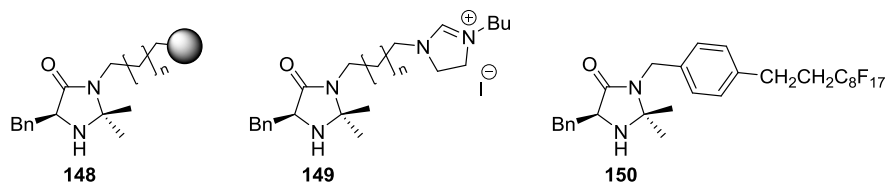


Figure 5.2 Imidazolidinones Modified at the 3-Position

The 3-position of the imidazolidinone is an attractive site for modification due to its distance from the iminium  $\pi$ -system. Within the literature the 3-position has been used as a handle for polymer immobilisation (**148**),<sup>82,83</sup> formation of an ionic liquid support (**149**)<sup>84</sup> and perfluorination (**150**) to render the catalyst susceptible to capture

on FluoroFlash<sup>®</sup> cartridges.<sup>85</sup> All of these modifications have resulted in catalysts which offer high levels of enantioselectivity in Diels-Alder reactions.

Within this chapter modifications of the 3-position on the MacMillan imidazolidinone are made. Both neutral and electron withdrawing groups are installed to probe the effect on enantioselectivity and reactivity in the benchmark Diels-Alder reaction between cinnamaldehyde (**1**) and cyclopentadiene (**2**).

## 5.2 Results and Discussion

### 5.2.1 Non-Electron Withdrawing Substituents

To gain further evidence that substitution at the 3-position has a negligible impact on enantioselectivity, imidazolidinones **151** and **152** were targeted.

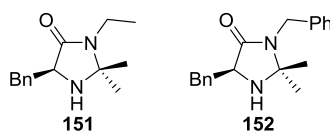
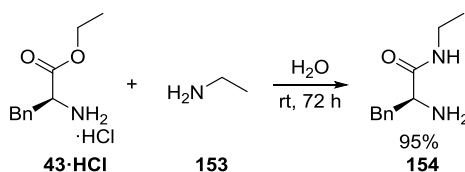


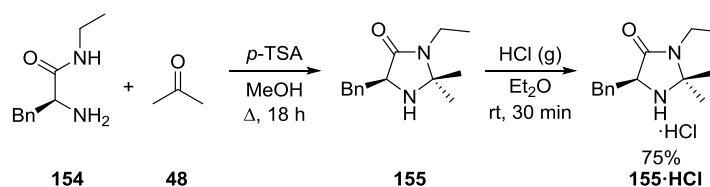
Figure 5.3 Imidazolidinones Modified at the 3-Position

In addition, as the ethyl and benzyl groups are neither strongly electron-withdrawing nor electron-donating it would be anticipated that **151** and **152** would offer similar levels of activity to **3**. Confirmation of this activity profile would further reinforce our perceived understanding of the catalytic cycle.

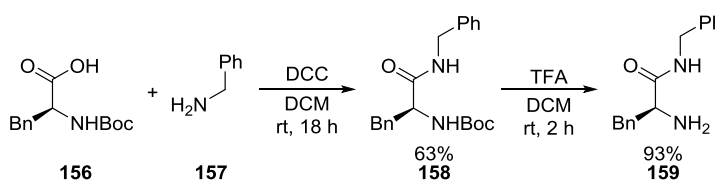


Scheme 5.1 Synthesis of Ethyl Amide **154**

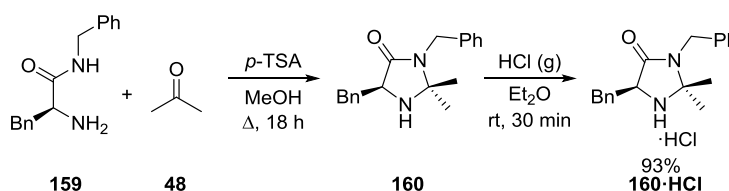
Ethyl amide **154** was prepared in one-step from **43·HCl** and aqueous ethylamine (95%, Scheme 5.1). **154** was then cyclised with **48** in the presence of *p*-TSA. The crude reaction mixture was then treated with dry hydrogen chloride gas to give **155·HCl** in 75% over two steps (Scheme 5.2).

Scheme 5.2 Synthesis of Imidazolidinone **155·HCl**

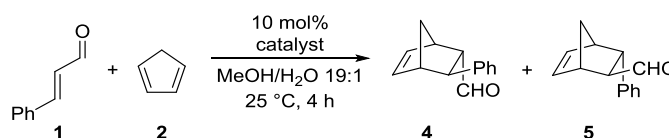
Benzyl amide **159** was prepared in 2-steps from *N*-Boc-L-phenylalanine (**156**). A DCC mediated coupling with **157** was used to obtain **158** (63%) which was deprotected using anhydrous TFA to give **159** (93%, Scheme 5.3).

Scheme 5.3 Synthesis of Benzyl Amide **159**

**159** was then subjected to the standard cyclisation and salt formation conditions as **154** to give **160·HCl** (93%, Scheme 5.4).

Scheme 5.4 Synthesis of Imidazolidinone **160·HCl**

Having accessed **155·HCl** and **160·HCl**, their relative reactivities in the benchmark reaction between cinnamaldehyde **1** and cyclopentadiene **2** were assessed.



Scheme 5.5 Reaction used for Monitoring of Imidazolidinone Reactivity

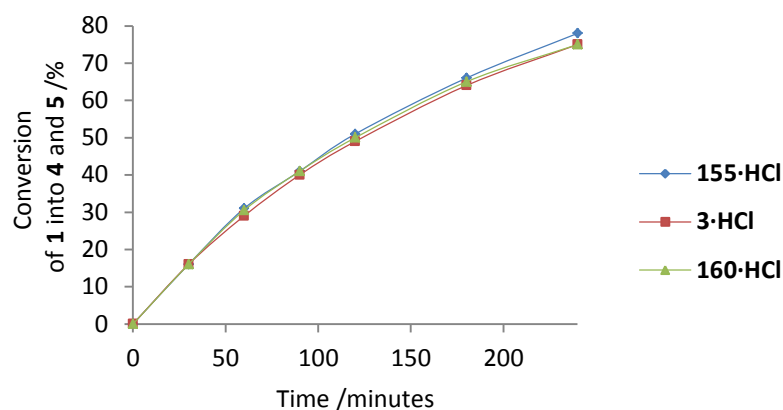


Figure 5.4 Catalytic Rates

As anticipated, methyl (**3·HCl**), ethyl (**155·HCl**) and benzyl (**160·HCl**) amide substituents had little impact on the activity of each amine and roughly equal catalytic activities were observed (Figure 5.4). In addition, each catalyst produced products with near identical enantiomeric excesses for both the *endo* and *exo* product isomers which endorsed the design rationale that altering the 3-position would have little impact on enantioselectivity (Table 5.1).

Amine	4 ee	5 ee	4:5
<b>3·HCl</b>	93	93	1:1.33
<b>155·HCl</b>	94	93	1:1.32
<b>160·HCl</b>	94	92	1:1.32

Table 5.1 Product Enantiomeric Excesses

### 5.2.2 Electron Withdrawing Substituents

Three imidazolidinones with electron-withdrawing groups in the 3-position were envisaged **161–163** (Figure 5.5). As each amine would require a multi-step synthesis, evidence that the EWG could impact the electronics of the nucleophilic nitrogen was sought. Previously linked to catalytic activity, proton affinity was deemed a suitable probe.<sup>22</sup> Proton affinity (B3LYP/6-31+G\*\*) was calculated for imidazolidinones **3**, **155**, **160**, and **161–163** (Table 5.2).

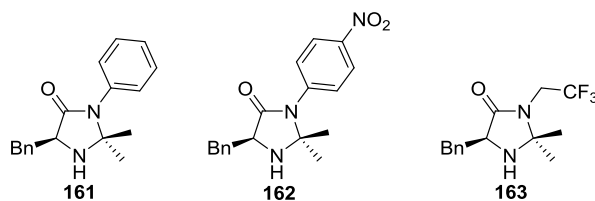
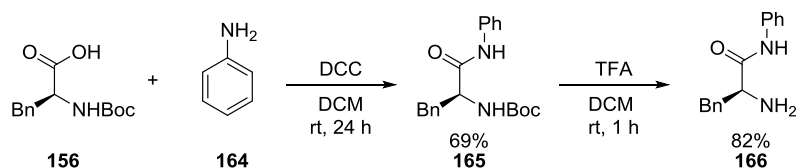


Figure 5.5 Imidazolidinones with EWG's in the 3-Position

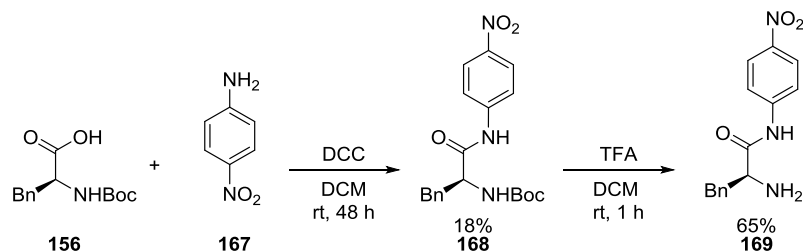
Amine	PA /kJ mol <sup>-1</sup>
<b>3</b>	943
<b>155</b>	954
<b>160</b>	960
<b>161</b>	931
<b>162</b>	903
<b>163</b>	913

Table 5.2 Calculated Proton Affinities

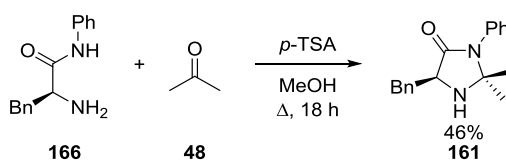
Imidazolidinones **155** and **160** had similar proton affinity values. However, **160** differed from **3** by 17 kJ mol<sup>-1</sup> yet exhibited similar catalytic activity. This suggested that although proton affinity had previously been seen to correlate to catalytic activity, the correlation may not be as robust as previously thought. Despite this, **161**, **162** and **163** displayed lower proton affinity values than **3** suggesting that higher catalytic activity could be anticipated. Therefore, **161**, **162** and **163** were targeted for synthesis.

Scheme 5.6 Synthesis of Amide **166**

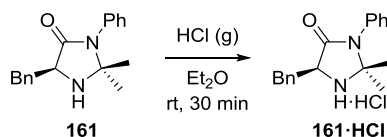
Amide **165** was prepared from **156** and freshly distilled aniline **164** using a DCC coupling (69%). The Boc group on **165** was removed using anhydrous TFA to give **166** (Scheme 5.6). **166** was purified by recrystallization from ethyl acetate and petroleum ether (82%).

Scheme 5.7 Synthesis of Amide **169**

**169** was prepared in an analogous fashion to **166** (Scheme 5.7). Significantly lower yields of the Boc-protected intermediate **168** were obtained (18%), most likely due to the low nucleophilicity of **167**. However, adequate quantities of **169** were accessed and optimisation of the coupling was not deemed appropriate at this time.

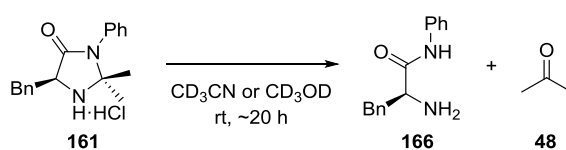
Scheme 5.8 Cyclisation of **166** with **48**

Amide **166** was cyclised with **48** in the presence of *p*-TSA. After flash chromatography **161** was obtained (46%). Unusually for this reaction, a significant amount of **166** was present in the crude reaction mixture which resulted in **161** being isolated in mediocre yield (Scheme 5.8).



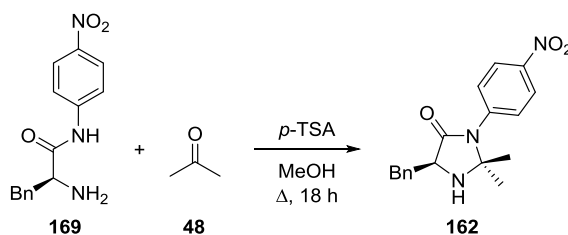
Scheme 5.9 Formation of Hydrochloride Salt

Treatment of an ethereal solution of **161** with anhydrous hydrogen chloride gas resulted in formation of a white precipitate. After recovery on a sinter and washing with diethyl ether and petroleum ether a white powder, presumed to be **161·HCl**, was obtained. Analysis by  $^1\text{H}$  NMR spectroscopy revealed a mixture of compounds. A species resembling **161·HCl** was present along with **166** and/or the corresponding hydrochloride salt. A singlet at  $\sim 2.2$  ppm consistent with the presence of acetone was observed. The relative integral size of the new singlet increased on standing overnight. This suggested that in  $\text{CD}_3\text{CN}$ , **161·HCl** decomposed back to **166** and **48** (Scheme 5.10). Similar decomposition was also observed in  $\text{CD}_3\text{OD}$ .



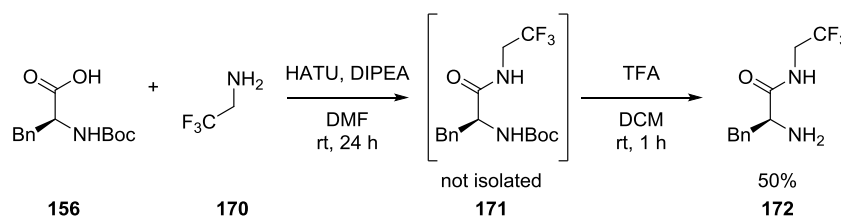
Scheme 5.10 Apparent Decomposition of **161**

Despite the observed instability of **161**, **169** was subjected to the same cyclisation conditions to give **162** (Scheme 5.11). Multiple rounds of flash chromatography gave **162** along with **169** despite their significantly different  $R_f$  values. With little drive to pursue **162** further, the chromatography fractions were left over night. A pale green crystalline solid was observed which TLC analysis suggested was **169**. After confirming the observation by  $^1\text{H}$  NMR spectroscopy, **162** was deemed to be unstable even as the freebase.



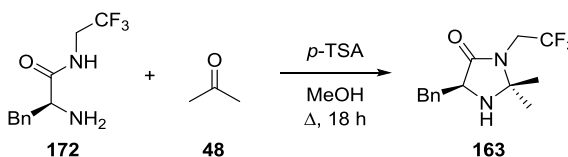
Scheme 5.11 Formation of **162**

At this stage it appeared that an electron-withdrawing group in the 3-position was a flawed design idea leading to unstable imidazolidinones. However, both **161** and **162** incorporated aromatic rings which have significantly greater steric requirements than the aliphatic groups previously examined. Therefore, continuation of the series with the synthesis of **163** was considered to be useful to determine if the instability was linked solely to sterics or if the electron-withdrawing nature of the amide substituent was also contributing.



Scheme 5.12 Preparation of Trifluoroethyl Amide **172**

Despite having had success with DCC couplings, HATU was chosen to prepare **172** from **156** and **170** (Scheme 5.12). Excess HATU and the by-products generated are water soluble and hence **171** was obtained in reasonable purity without chromatographic purification. **171** was then deprotected using anhydrous TFA in DCM to give **172** in 50% yield over two steps.

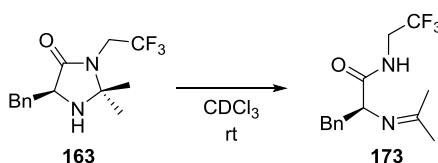


Scheme 5.13 Formation of **163**

**172** was then cyclised with **48** under standard reaction conditions (Scheme 5.13). Pleasingly, analysis of the crude reaction mixture by  $^1\text{H}$  NMR spectroscopy showed clean conversion to **163**. However, upon performing further NMR experiments it became clear that **163** was unstable in  $\text{CDCl}_3$  for periods greater than  $\sim 1$  h. Over time, a species possessing  $^1\text{H}$  NMR resonances consistent with the structure of imine



**173** appeared whilst the integral of resonances associated with **163** decreased. Hence, like **161** and **162**, **163** was not suitably stable for use as a secondary amine catalyst.



Scheme 5.14 Observed Decomposition of **163**

### 5.3 Conclusions

The 3-position on the imidazolidinone was seen as a potential site to install an EWG to influence catalytic rate without affecting enantioselectivity. Modifying the 3-position with electron-neutral substituents gave imidazolidinones **155** and **160** which resulted in levels of asymmetric induction and catalytic efficiency comparable to the MacMillan imidazolidinone (**3**). Installation of an electron-deficient amide substituent resulted in imidazolidinones **161**, **162** and **163** which proved to be insufficiently stable to act as secondary amine catalysts under the conditions examined.

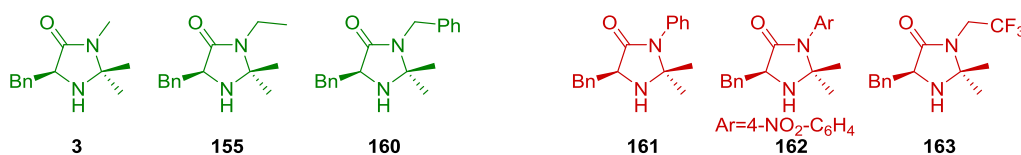


Figure 5.6 Imidazolidinones Suitable for use as Secondary Amine Catalysts (green) and Unsuitable (red)

Despite being unable to assess the catalytic ability of **161**, **162** and **163**, key information was gained about the stability of imidazolidinones. Future rational design of imidazolidinones suitable for use as secondary amine catalysts should not incorporate electron-withdrawing substituents at the 3-position. However, this position has been used to great effect as a useful site of modification and hence should not be entirely disregarded.<sup>82-85</sup>

# **Chapter 6: C<sub>2</sub> Symmetric Catalyst Design**

## 6 $C_2$ Symmetric Catalyst Design

### 6.1 Introduction

$\alpha,\beta$ -Unsaturated aldehydes predominate as dienophile precursors in asymmetric iminium ion catalysed Diels-Alder reactions. Very few examples exist where enones are used as substrates.

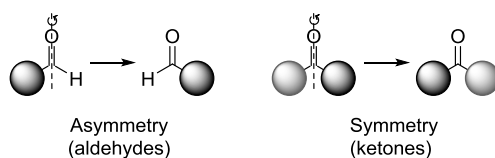
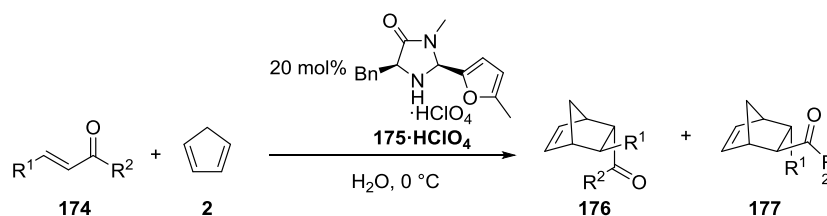


Figure 6.1 Steric Symmetry in Carbonyl Compounds

Enones possess a more sterically symmetrical carbonyl group compared to aldehydes (Figure 6.1). This renders controlled formation of iminium ion isomers challenging as neither orientation is favoured over the other. Hence, it is not a simple task to achieve high levels of asymmetry in subsequent reactions once the iminium ion has formed. This is thought to be somewhat responsible for the absence of examples using enone substrates in the literature.



Scheme 6.1 MacMillan's Asymmetric Enone-Based Diels-Alder Reaction

In a seminal paper, MacMillan described imidazolidinone catalysed asymmetric Diels-Alder cycloaddition reactions using enone substrates and cyclopentadiene (**2**) (Scheme 6.1).<sup>13</sup> Good levels of enantioselectivity were reported. However, only certain enones were tolerated with a specific restriction on  $R^2$  (Table 6.1). For example, where  $R^2$  is an ethyl group high levels of enantiomeric excess (90%) are obtained, however, a less than satisfactory enantiomeric excess of 61% is obtained

when  $R^2$  is a methyl group. Furthermore, a complete lack of asymmetric induction is obtained when  $R^2$  is an *iso*-propyl group.

Entry	$R^1$	$R^2$	ee
1	Me	Me	61
2	Me	Et	90
3	Me	<i>i</i> Pr	0

Table 6.1 Limitations of  $R^2$

To rationalise the observed selectivities and substrate specificities MacMillan performed MM3 calculations. Two isomers of the iminium ion intermediate, formed from imidazolidinone **175** and ethyl vinyl ketone ( $R^2 = \text{Et}$ ), were found (**178-E** and **179-Z**, Figure 6.2). Based upon the observed enantioselectivity MacMillan rationalised the existence of both **178-E** and **179-Z** iminium ion isomers. It was proposed that the benzyl group shields the *Re*-face in **178-E** leaving the *Si*-face available for reaction. In **179-Z**, shielding of both faces is present; the *Si*-face by the benzyl group and/or furan ring and the *Re*-face by the  $\beta$ -methyl group. Therefore, despite possible formation of two isomers only the *Si*-face of **179-E** is open for cycloaddition and hence products are obtained with high levels of asymmetry.

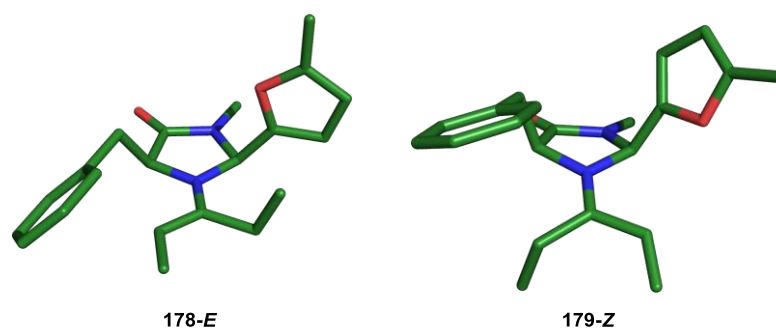
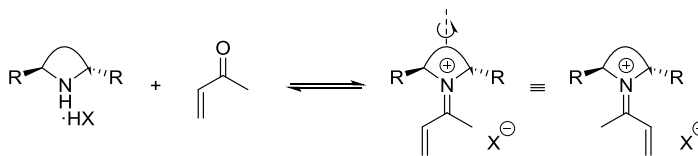


Figure 6.2 Proposed Iminium Ion Intermediates

The transformation was intriguing as high levels of asymmetry were achieved without the need for selective iminium ion formation, something which was previously considered to be essential. MacMillan had used steric hindrance to not only direct but also prevent reaction.

Figure 6.3 Proposed Application of  $C_2$  Symmetric Amine

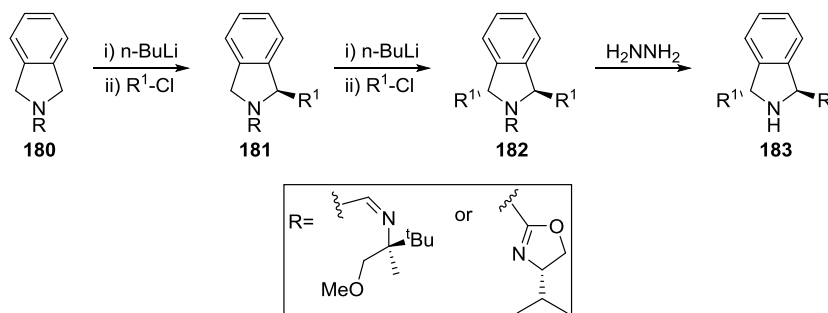
An alternative to rendering one isomer inert would be to use a  $C_2$  symmetric catalyst. An amine with  $C_2$  symmetry about the nitrogen atom can only form one iminium ion isomer (Figure 6.3) and hence the problem of selective isomer formation would no longer exist. In addition, if all iminium ions are available for reaction a faster catalytic turnover could be rationally anticipated.

Within this Chapter  $C_2$  symmetric amine catalysts are targeted. To circumvent multiple complex syntheses DFT calculations were used to predict whether each amine would be anticipated to offer high levels of asymmetry when used with enone substrates.

## 6.2 Results and Discussion

### 6.2.1 $C_2$ Symmetric Amine Modelling

The suitability of isoindolines to act as secondary amine catalysts has previously been investigated within the group.<sup>40</sup> The isoindoline architecture was of interest due to its symmetry. In addition, asymmetric alkylations to give **183** have been described in the literature (Scheme 6.2).<sup>86,87</sup>



Scheme 6.2 Asymmetric Alkylation of Isoindoline

Iminium ion **184**, derived from **183** and methyl vinyl ketone, was found to adopt a low energy conformation whereby both benzyl groups sit over the isoindoline ring (Figure 6.4). It was thought that this would result in no or slow cycloaddition with a lack of asymmetric induction. Addition of methyl or trifluoromethyl groups to the 4- and 7-positions (**184**, Figure 6.4) did little to perturb the low-energy conformation.

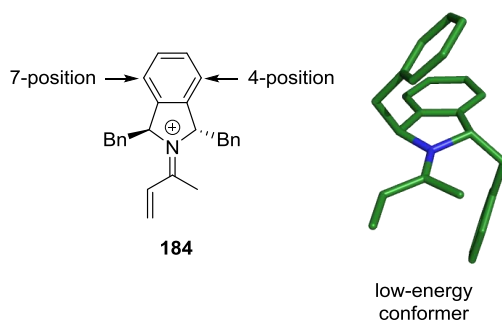


Figure 6.4 Low-Energy Conformation of **184**<sup>40</sup>

To prevent the benzyl groups from sitting over the 5-membered ring, dibenzo-isoindoline **185** and derivatives were investigated (Figure 6.5). The close proximity of the 4- and 11-positions to the 2- and 13-positions (**185**, Figure 6.5) was thought to be a possible handle to influence the conformation of benzyl substituents. Synthesis of an alkylated derivative such as **186** is not present within the literature. However, it was presumed that a similar technique to the alkylation of isoindoline (Scheme 6.2) could be applied to the dibenzo-isoindoline scaffold (**186**).

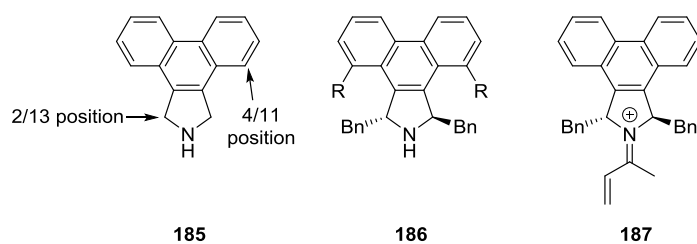


Figure 6.5 Dibenzo-Isoindolines and Iminium Ion

Six low energy conformations of iminium ion **187** were found (Figure 6.6). Not too surprisingly, the lowest energy conformer **187.2** ( $0 \text{ kJ mol}^{-1}$ ) was found to be isoconformer to the low-energy conformation of **184**. This suggested that, in a

similar manner to **184**, cycloaddition would be disfavoured as each benzyl group offers steric hindrance to each face of the  $\pi$ -system (Figure 6.7). The other conformers of higher energy compared to **187.2** (**187.1**, **184.7–184.7**) displayed varying facial discrimination indicating that high levels of enantioselectivity would be unlikely if reaction was to occur.

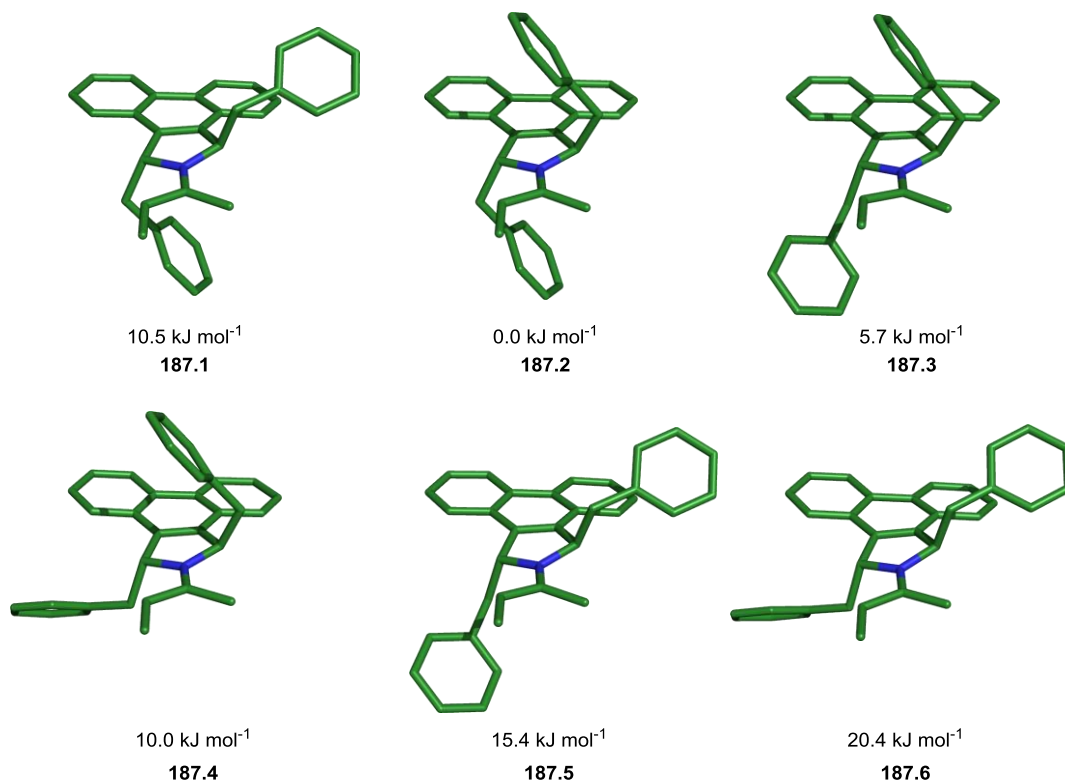


Figure 6.6 Low-Energy Conformations of **187**

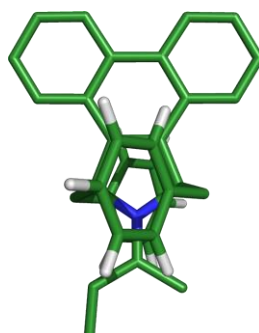


Figure 6.7 View of **187.2** from Above

Derivatives of **187** modified at the 4- and 11-positions were considered. Addition of fluorine was thought to be a possible method to repel the electron-rich benzyl group and encourage it to reside over the  $\pi$ -system and disfavour conformations such as **187.2**. Therefore, the 4-,11-difluorinated iminium ion (**188**) was subjected to the standard modelling regime.

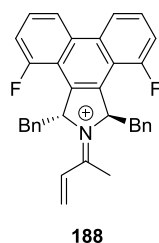


Figure 6.8 Iminium Ion derived from Fluorinated Dibenzo-Isoindoline

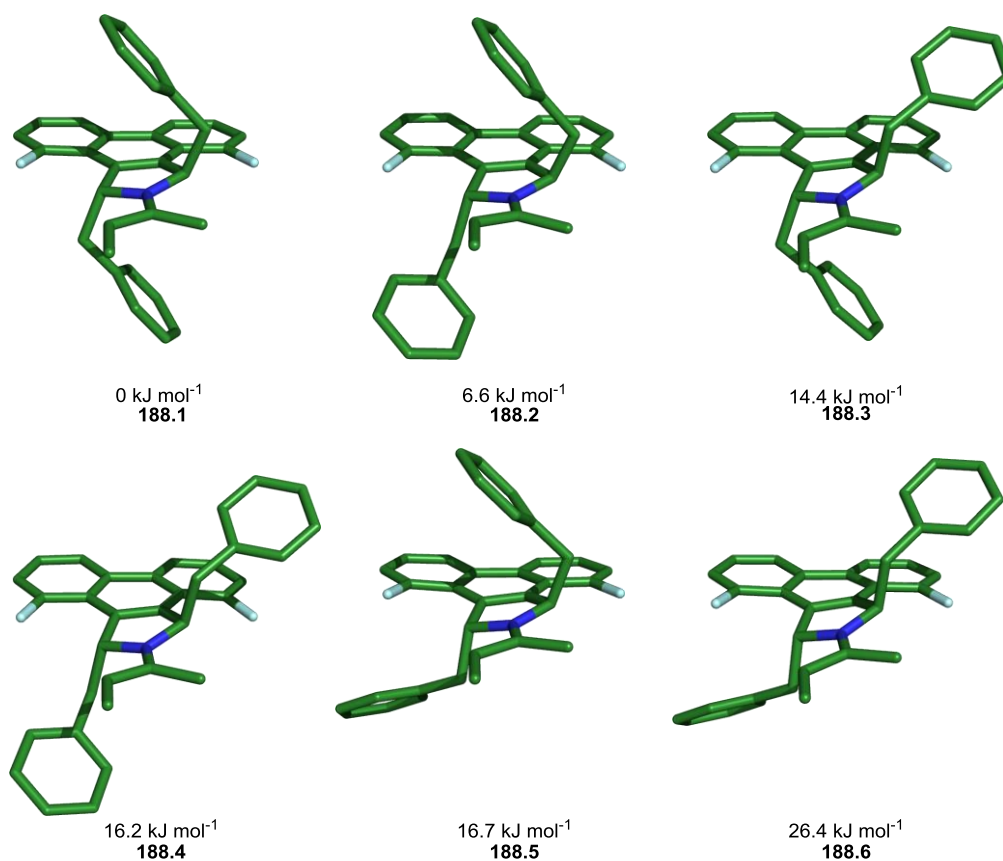


Figure 6.9 Low-Energy Conformations of **188**



A total of six low-energy conformations of **188** were found. Unfortunately, the fluorination did not appear to influence the conformational preference of the benzyl groups and **188.1** ( $0 \text{ kJ mol}^{-1}$ ), isoconformeric to **187.2**, was found to be the lowest energy conformation. All of the other conformers (**188.2–188.6**) were higher in energy and like conformations of **187** offered varying levels of diastereofacial shielding.

Further modifications of the dibenzo-isindoline scaffold were considered. However, designing a catalyst whereby a complex synthesis is required is not rational and can result in expensive and unused methodology. Therefore, a lack of synthetic preparations and commercial availability of dibenzo-isindolines turned our attention to a more accessible amine scaffold.

### 6.2.2 Pseudo $C_2$ Symmetric Amine Modelling

To continue the  $C_2$  symmetric idea, focus was turned to the readily prepared imidazolidinone scaffold. Although imidazolidinones lack  $C_2$  symmetry, a pseudo  $C_2$  symmetric variant (**189**) was envisaged. **189** would be expected to form two iminium ions (**191** and **192**, Figure 6.10). As the substituents at the 2- and 5- positions of the imidazolidinone ring are identical, the iminium  $\pi$ -system would be present in a pseudo  $C_2$  symmetric environment. It was hoped that this would render **191** and **192** somewhat equivalent.

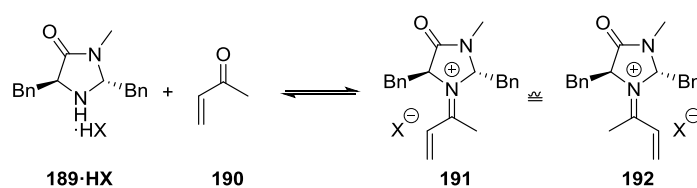


Figure 6.10 Pseudo  $C_2$  Symmetric Imidazolidinone

Each benzyl group on **189** has three possible non-eclipsing positions, therefore, a total of nine possible conformations could exist for each iminium ion isomer. DFT calculations (BHandH/6-31+G\*\*) were performed on **191** and **192** to search for the

eighteen potential conformations. A total of thirteen low-energy conformers were found, six of which had energies lower than  $8.5 \text{ kJ mol}^{-1}$  (Figure 6.11).

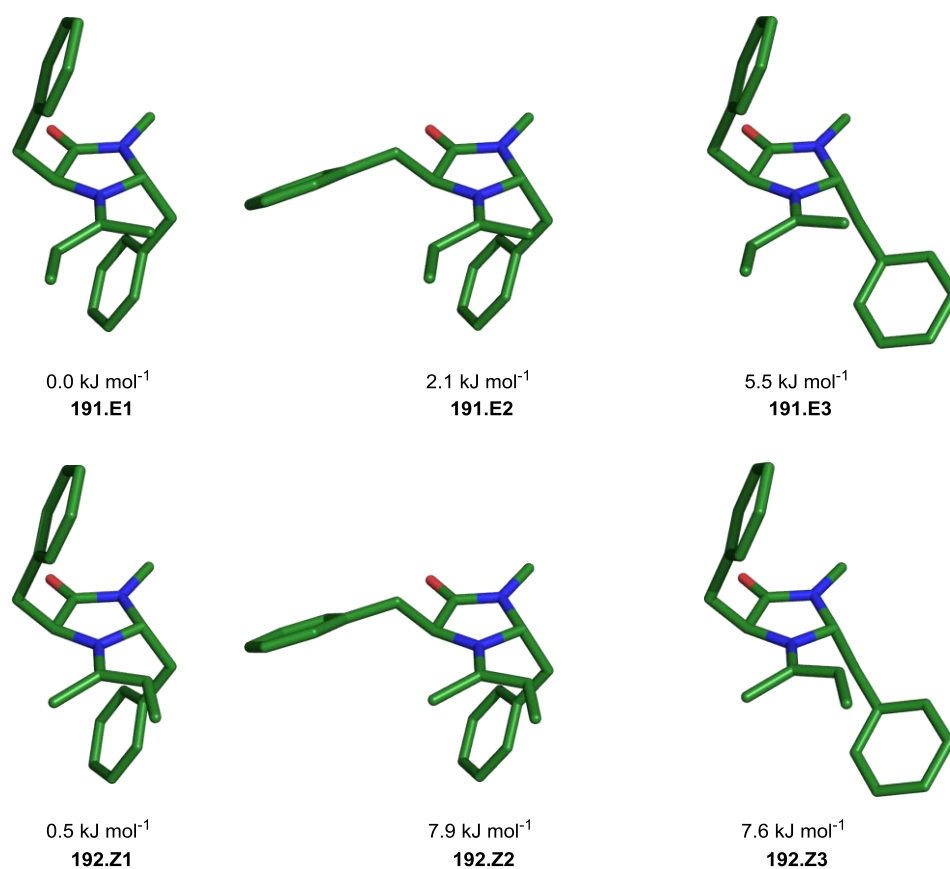


Figure 6.11 Low-Energy Conformations of **191** and **192**

**191.E1** ( $0 \text{ kJ mol}^{-1}$ ) and **192.Z1** ( $0.5 \text{ kJ mol}^{-1}$ ) appeared likely to disfavour cycloaddition as both benzyl groups sterically hinder the  $\alpha$ -carbon of the iminium  $\pi$ -system (c.f. **187.2**). **191.E2** ( $2.1 \text{ kJ mol}^{-1}$ ) has an exposed *Re*-face whereas **191.E3** ( $5.5 \text{ kJ mol}^{-1}$ ) has an exposed *Si*-face rendering the two conformations non-complimentary. **192.Z2** ( $7.9 \text{ kJ mol}^{-1}$ ) would likely react on the *Si*-face and **192.Z3** ( $7.6 \text{ kJ mol}^{-1}$ ) would likely be unreactive on either face. Overall, the modelling results suggest a lack of reactivity and asymmetry would be anticipated.

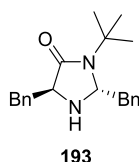


Figure 6.12 Proposed 'Butyl Amide

The apparent preference of the benzyl groups to eclipse the imidazolidinone ring appeared to be stalling the  $C_2$  symmetric design rationale. In an attempt to change the preference of the benzyl arm a 'butyl group was added in the amidic position to give **193**.

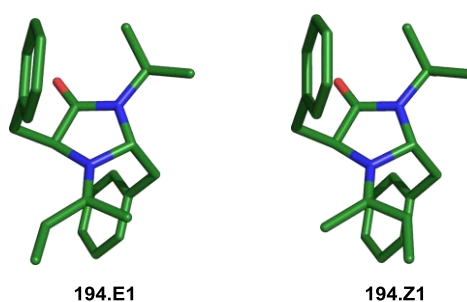
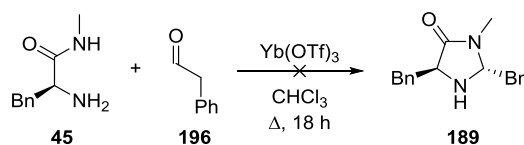


Figure 6.13 Benzyl Groups Eclipsing Imidazolidinone Ring

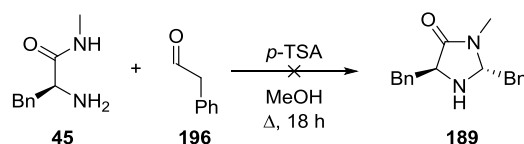
Iminium ions derived from **193** and methyl vinyl ketone were subjected to the modelling regime. Addition of a sterically large substituent in the amidic position did not perturb the undesired conformation of each benzyl group and **194.E1** and **194.Z1** were found as low-energy conformers (both  $<5 \text{ kJ mol}^{-1}$ ). In addition, installation of very sterically demanding amidic groups could potentially destabilise the imidazolidinone ring (see Chapter 5), hence, further modifications of this position were not considered.

### 6.2.3 Pseudo $C_2$ Symmetric Amine Synthesis

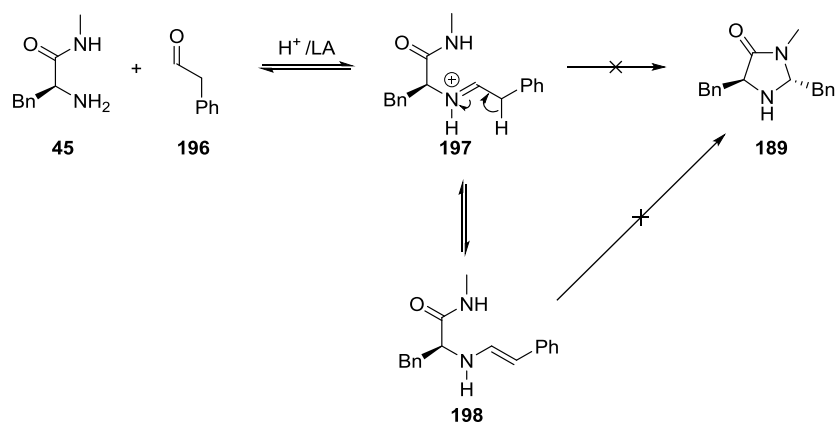
Computational modelling suggested **189** would most likely exhibit poor enantiocontrol. However, verification of theory was important in order to validate our understanding and reinforce our model. Therefore, **189** was targeted for synthesis to confirm if the predicted outcome of poor enantiocontrol would be reflected experimentally.

Scheme 6.3 Attempted Lewis-Acid Catalysed Synthesis of **189**

Using a standard preparation developed within the group, commercially available **196** was added to a chloroform solution of **45** and the mixture was heated in the presence of ytterbium(III) triflate (Scheme 6.3).<sup>78</sup> After workup,  $^1\text{H}$  NMR spectroscopy of the brown residue indicated decomposition had occurred and no **189** was visible. The reaction was repeated using protic acid *p*-TSA in methanol (Scheme 6.4), again, decomposition was apparent.

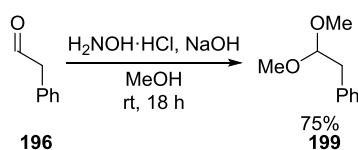
Scheme 6.4 Attempted Brønsted-Acid Mediated Synthesis of **189**

Both preparations were repeated at ambient temperature and analogous results were obtained. This suggested that **196** was very reactive under the acidic reaction conditions. Upon condensation between **45** and **196** the intermediate iminium **197** would be anticipated. **197** is likely to form enamine **198** due to the acidity of the benzylic proton (Scheme 6.5). Once formed, enamine **198** could then react with a multitude of species within the reaction mixture.<sup>88</sup>



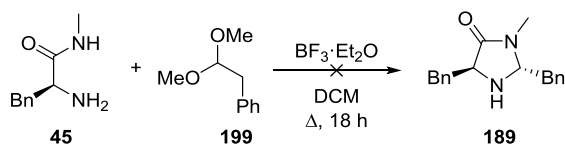
Scheme 6.5 Plausible Decomposition Route

Success with forming imidazolidinones from dimethyl acetals in the presence of borontrifluoride diethyl etherate had previously been achieved (Chapter 4). Due to the anticipated decomposition of **197** it was unlikely that this approach would be successful in forming **189**. However, the simple preparation of **199** (75%) from aldehyde **196** and methanol in the presence of hydroxylamine hydrochloride (Scheme 6.6) rendered the route worthy of attempt.

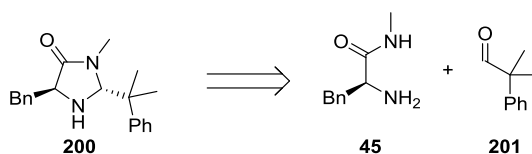


Scheme 6.6 Acetal Formation

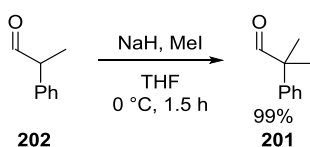
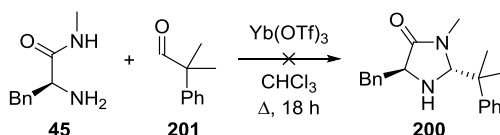
**196** was added to a DCM solution of **45** followed by borontrifluoride diethyl etherate and the mixture was stirred at ambient temperature. Within minutes the solution had turned brown and a white precipitate had formed. TLC analysis indicated many new products were present in the crude reaction mixture.  $^1H$  NMR spectroscopy displayed another undecipherable mixture of reaction products (Scheme 6.7).

Scheme 6.7 Attempted Formation of **189** Using Dimethyl Acetal

A direct synthesis of **189** was looking unlikely. Formation of species analogous to **197** and **198** appeared problematic. Therefore, imidazolidinone **200** was envisaged as a potential alternative to **189**. The addition of two methyl groups would stop formation of an enamine intermediate and hence formation of **198** would be more likely.

Figure 6.14 Retro Synthetic Analysis of **200**

To form aldehyde **201**, commercially available **202** was deprotonated with sodium hydride and alkylated with iodomethane (99%, Scheme 6.8).

Scheme 6.8 Formation of **201**Scheme 6.9 Attempted Lewis Acid Mediated Synthesis of **200**

**201** was added to a chloroform solution of **45** and heated in the presence of ytterbium(III) triflate (Scheme 6.9).  $^1\text{H}$  NMR spectroscopy of the crude reaction mixture indicated many compounds had been formed. Of particular note was the apparent presence of resonances characteristic of *iso*-propyl functionality. The reaction was repeated to ensure nothing untoward had occurred and an identical result was obtained. It was thought that, under the reaction conditions, a methyl or phenyl migration could be occurring to give ketones **203** and/or **204** (Figure 6.15).

This idea was confirmed in a publication by Oshita whereby a similar rearrangement had been observed using Gallium(III) chloride and other Lewis acids.<sup>89</sup>

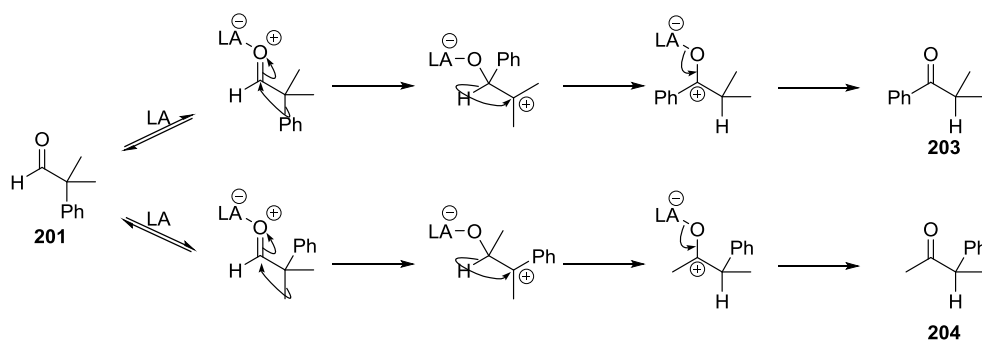
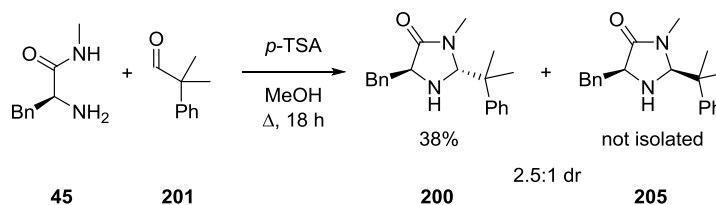


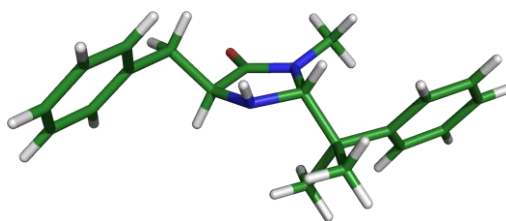
Figure 6.15 Proposed Migratory Routes in the Presence of Lewis Acids

Avoiding Lewis acids, **201** was added to a methanolic solution of **45** and heated in the presence of Brønsted acid *p*-TSA (Scheme 6.10).  $^1\text{H}$  NMR spectroscopy of the crude reaction mixture showed two compounds, **200** and presumably the diastereoisomer **205**, however, only **200** was isolated by flash chromatography in 38% yield.

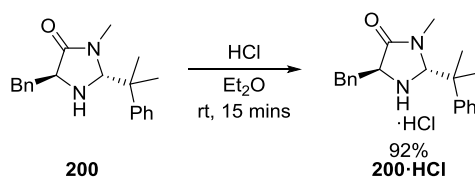


Scheme 6.10 Brønsted Acid Mediated Cyclisation of **45** with **201**

The relative configuration of **200** was confirmed to be correct using NOESY NMR spectroscopy (see Appendix C). In addition, upon trituration, a crystal of **200** was grown which was suitable for X-Ray crystallography. The crystal structure was obtained (Figure 6.16) which gave unequivocal evidence that the compound was the correct diastereoisomer. To check **200** was enantiopure it was subjected to HPLC on a chiral stationary phase and the ee was found to be >98%.

Figure 6.16 Single Crystal X-Ray Structure of **200**

An ethereal solution of **200** was treated with hydrogen chloride gas to give the corresponding hydrochloride salt (**200·HCl**).



Scheme 6.11 Hydrochloride Salt Formation



### 6.2.4 Modelling Pseudo $C_2$ Symmetric Amine **200**

Before evaluating the performance of **200** as an asymmetric catalyst, the corresponding methyl vinyl ketone derived iminium ion was subjected to the modelling regime.

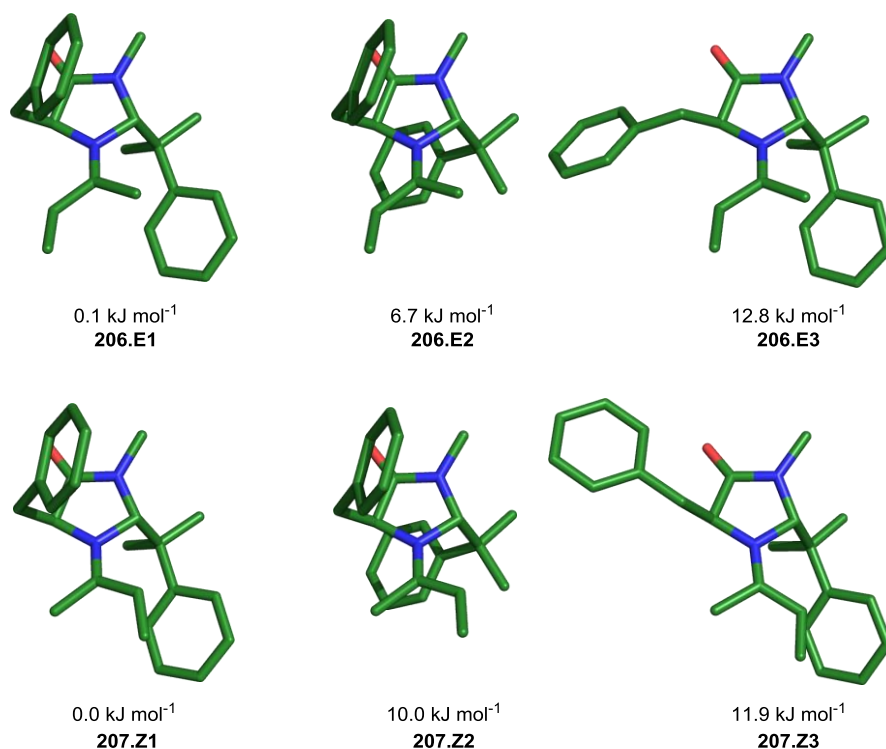


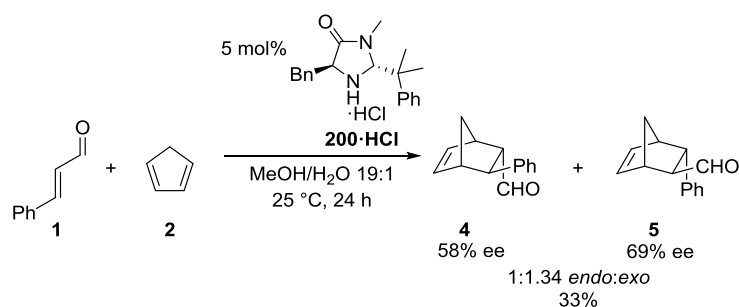
Figure 6.17 Low Energy Conformations of **200** Derived Iminium Ions

A total of ten low energy conformations were found, six of which had energies below 13 kJ mol<sup>-1</sup> (Figure 6.17). The two lowest energy conformers **206.E1** (0.1 kJ mol<sup>-1</sup>) and **207.Z1** (0.0 kJ mol<sup>-1</sup>) displayed potential to be complimentary. Both shield the *Re*-face leaving the *Si*-face open for reaction. **206.E2** (6.7 kJ mol<sup>-1</sup>) and **207.Z2** (10.0 kJ mol<sup>-1</sup>) appeared to offer some shielding to each face. However, unlike previously modelled iminium ions these were not the lowest energy conformers and so would not be anticipated to overly effect reactivity. **207.Z3** (11.9 kJ mol<sup>-1</sup>) had an exposed *Si*-face, which complemented **206.E1** and **206.E2**. Unfortunately **206.E3** had both faces exposed but due to its higher energy (12.8 kJ mol<sup>-1</sup>) was not thought to be too problematic. Overall, the failure to isolate **189** had led to a pseudo  $C_2$

symmetric imidazolidinone (**200**) which appeared to have potential to act as an asymmetric catalyst.

### 6.2.5 Synthetic Evaluation of **200**

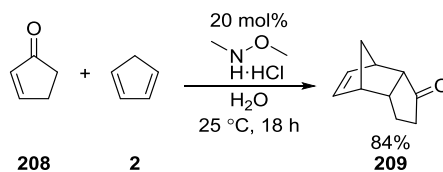
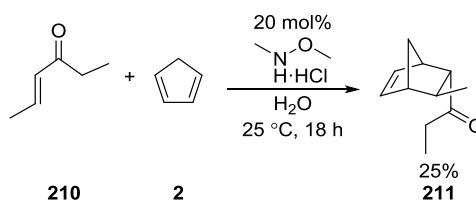
Before evaluating **200**·HCl for use with enone substrates, it was used in the benchmark reaction between cinnamaldehyde (**1**) and cyclopentadiene (**2**).



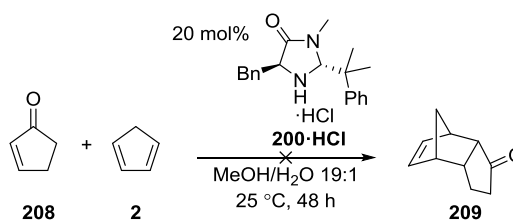
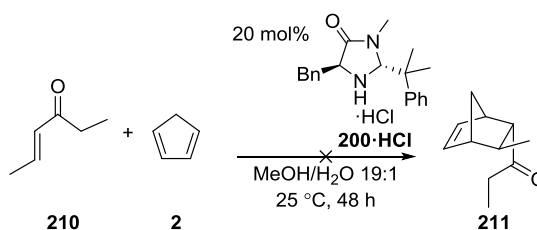
Scheme 6.12 Evaluation of **200**·HCl in the Benchmark Reaction

A poor yield of 33% over 24 h was obtained. This was attributed to the increased sterics around the reactive nitrogen and was somewhat worrying as the reaction rate would likely be lower with enones. Although catalytically slow, **4** and **5** were furnished in a 1:1.34 ratio and in 58% and 69% ee respectively with the major product possessing a higher level of asymmetry.

Before evaluating **200** with enones, authentic samples of the products (**209** and **211**) from the cycloaddition of ketones **208** and **210** with **2** were prepared using 1,2-dimethylhydroylamine hydrochloride as a catalyst (Scheme 6.13 and Scheme 6.14). In each Diels-Alder reaction the *exo* adduct was observed to be formed in trace amount and, after chromatography, only the *endo* adducts were isolated. Modelling had been performed on iminium ions derived from methyl vinyl ketone to reduce calculation time, however, it was not used as a substrate due to its volatility.

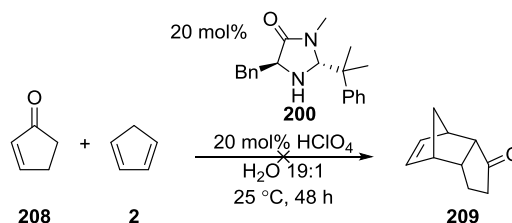
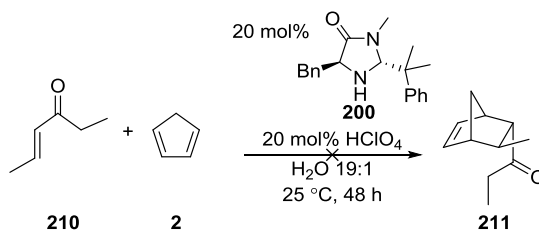
Scheme 6.13 Preparation of Racemic **209**Scheme 6.14 Preparation of Racemic **211**

**209** and **211** were found to visualise on a TLC plate using a 2,4-dinitrophenylhydrazine dip into bright orange and yellow spots respectively which offered a useful handle to detect their presence in reaction mixtures.

Scheme 6.15 Evaluation of **200·HCl**Scheme 6.16 Evaluation of **200·HCl**

In keeping with the reaction conditions used in the benchmark Diels-Alder reaction, each of the ketones **208** and **210** were added to methanol/water (19:1) solutions of **200·HCl** followed by freshly distilled cyclopentadiene (**2**) (Scheme 6.15 and Scheme 6.16). After 48 h only trace **209** and **211** were visible by GC, most likely arising from

a background acid catalysed reaction. Unlike reactions using  $\alpha,\beta$ -unsaturated aldehydes, MacMillan found an aqueous medium combined with perchloric acid as the co-acid to be suitable conditions for enone substrates.<sup>13</sup> Therefore the two reactions were repeated using **200** under these conditions. Again, after 48 h **209** and **211** were not present in significant quantity in either reaction mixture (Scheme 6.17 and Scheme 6.18).

Scheme 6.17 Evaluation of **200** under MacMillan's ConditionsScheme 6.18 Evaluation of **200** under MacMillan's Conditions

GCMS analysis of each reaction revealed many products. Aside from traces of the desired ketone, aldehyde **201** was detected. This indicated that the imidazolidinone was not completely stable under the reaction conditions and rendered a disappointing end to promising modelling results. For completeness, the benchmark reaction was revisited to look for decomposition of the imidazolidinone. A small resonance at 9.52 ppm in the  $^1\text{H}$  NMR spectrum of the crude reaction mixture indicated that **200** had partially decomposed during this cycloaddition. This reinforced that **200** was not suitable to act as a secondary amine catalyst.

### 6.3 Conclusions

A  $C_2$  symmetric amine scaffold was seen as a potential method of circumventing problematic iminium ion selectivity with enone substrates. Computational modelling of iminium ions derived from a  $C_2$  symmetric dibenzo-isoindoline architecture (**186**) indicated that a lack of reactivity would be anticipated and if reaction was to occur no asymmetry would be expected within the products. A complex synthetic pathway turned focus towards the more accessible imidazolidinone scaffold.

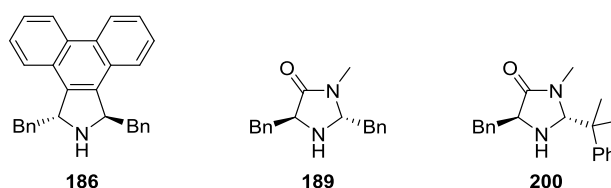


Figure 6.18  $C_2$  Symmetric Catalysts

Pseudo  $C_2$  symmetric **189** was predicted to offer poor selectivity. Synthesis of **189** was attempted but it was not possible to obtain due to side reactions. Dimethyl variant **200** was prepared. Calculations suggested that **200** would offer reasonable levels of asymmetry in closed transition state reactions with enone substrates and reaction at the *Si*-face was predicted to predominate. However, **200** was found to decompose under conditions relevant to iminium catalysis. **200** was also observed to be catalytically inactive with enones. Therefore, it was not possible to evaluate **200** in its intended application.

Development of a  $C_2$  symmetric amine catalyst suitable for use with enones is a significant challenge which has not yet been conquered. Although studies within this Chapter indicate that obtaining selective diastereofacial discrimination even with one iminium ion isomer remains a challenge, it represents an attractive idea. Hence, a  $C_2$  symmetric system is likely to be revisited in the future as a possible solution for tackling enone substrates.

# **Chapter 7: Amino Acid Dimers**

## 7 Chiral at Nitrogen Amino Acid Dimers

### 7.1 Introduction

Tertiary amines, featuring three different substituents about the nitrogen centre are common. However, the pyramidal nitrogen centre can usually invert which renders the amine configurationally unstable (Figure 7.1). Some tertiary amines cannot undergo inversion due to conformational restraint. This fixes the stereochemistry at the nitrogen centre and hence it becomes a useful stereogenic centre. Configurationally stable amines have been exploited as ligands for transition metal catalysis,<sup>90</sup> as additives in asymmetric deprotonation reactions<sup>91</sup> and as phase transfer catalysts.<sup>92</sup> The utility of these amines undoubtedly renders them of significant interest to synthetic chemists.

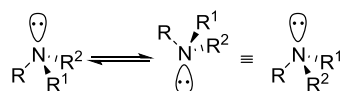


Figure 7.1 Pyramidal Tertiary Amine Inversion

Accessing configurationally stable amines is not always a trivial task. Some can be isolated as natural products, although like many naturally occurring chiral molecules, it is unusual to find an enantiomeric pair existing in nature. The unnatural enantiomer often requires a complex multi-step synthesis which can inhibit the utility of such amines in chemistry. One prime example of this is the enantiomeric pair of Sparteines. (-)-Sparteine (**212**) can be isolated from natural sources whereas to obtain (+)-Sparteine (**213**) a complex 15-step synthesis must be performed.<sup>93</sup> However, this has been somewhat circumvented by O'Brien who has developed a practical and scalable route to **214** which acts as a pseudo-enantiomer of **213**.<sup>91</sup>

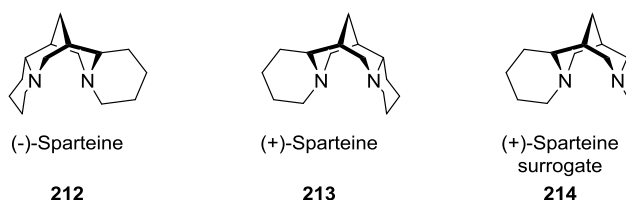


Figure 7.2 Sparteine

Configurationally stable amines **128** and **129** were discovered as unwanted products in Chapter 4. However, the ability to readily prepare enantiomeric pairs using a 2-step synthetic route from commercially available starting materials deemed the molecular motif more than worthy of further investigation.

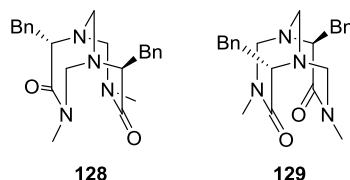


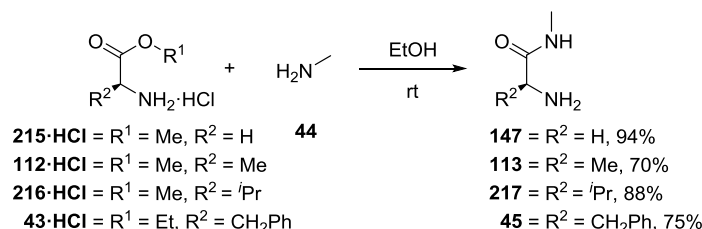
Figure 7.3 Initially Discovered Chiral Amines

Within this chapter, a substrate scope of the amino acid dimer formation is presented along with investigations into their key properties. In addition, DFT calculations are used to probe the conformational flexibility of the dimer structure.

## 7.2 Results and Discussion

### 7.2.1 Amino Acid Substrate Scope

A selection of amino acid amides were prepared from their corresponding ester hydrochloride salts and ethanolic methylamine (Scheme 7.1).



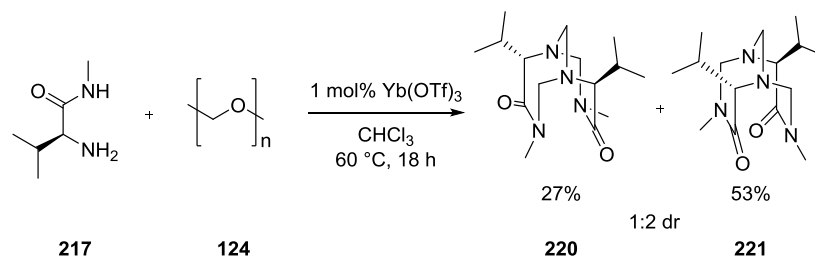
Scheme 7.1 Amino Acid Amide Formation

Amide **147** was reacted with **125** in the presence of ytterbium(III) triflate (Scheme 7.1). Dimer **218** was isolated in high purity by crystallisation (47%). In order to confirm that **218** was configurationally stable at nitrogen it was subjected to HPLC on a chiral stationary phase (ChiralcelOJ, 10% IPA in hexane, 1 mL min<sup>-1</sup>). **218** was found to separate into two peaks ( $t_r = 32.8$  and  $t_r = 42.7$ ) of equal integration which



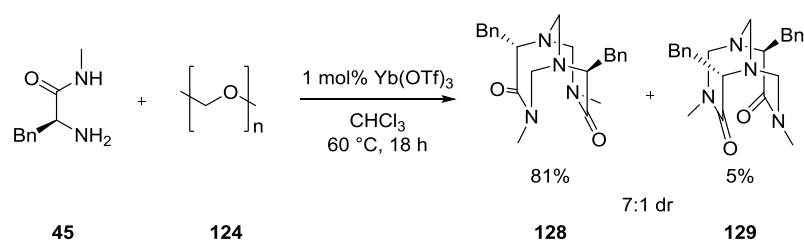


Two valine derived dimers (**220** and **221**) were formed in the reaction between **217** and **124** in a 1:2 ratio (Scheme 7.4). The two diastereoisomers **220** and **221** were isolated by flash chromatography in 27% and 53% yield respectively.



Scheme 7.4 Formation of Valine Dimers

Formation of **128** and **129** was repeated on the same scale used for the other dimers (Scheme 7.5) and the two diastereoisomers were isolated using flash chromatography in 81% and 5% yield respectively. It should be noted that the difference in isolated yield of each diastereomer compared to the diastereomeric ratio can be attributed to problematic isolation of **129** due to its polarity.



Scheme 7.5 Formation of Phenylalanine Dimers

Single crystals were grown of each dimer and X-ray crystallography was used to confirm which diastereoisomers had been made (Figure 7.5). In addition, from knowing the enantiomer of the starting amino amide the absolute configuration at nitrogen was determined. From the product ratio between **128** and **129** and the production of **219** it was assumed that the major diastereoisomer would always have alkyl groups pointing away from the bicyclic core. However, the valine dimers (**220** and **221**) did not obey this trend which removed the ability to predict the major product in each reaction.

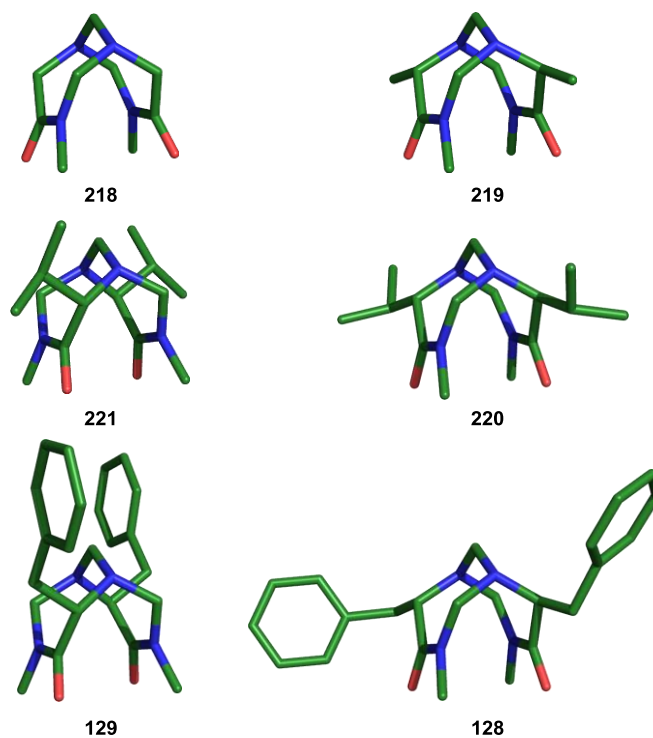
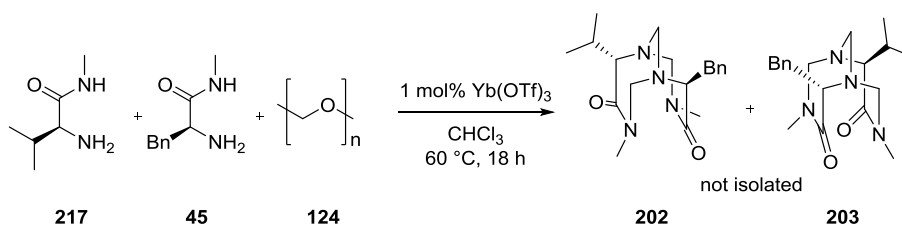


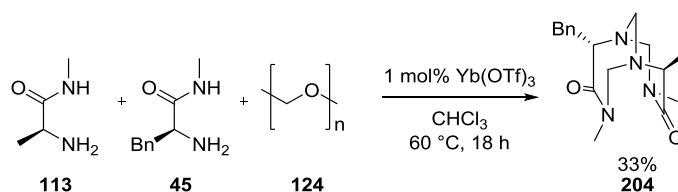
Figure 7.5 Single Crystal X-ray Structures

Thus far, unsubstituted and a variety of alkyl substituted dimers had been isolated. Each was a homo-dimer containing two of the same amino acid residue rendering them  $C_2$  symmetric. Removal of this symmetry was of interest to try and expand the scope of these novel amine structures. Using the normal procedure, **127** and **45** were reacted in a 1:1 ratio with 3 equivalents of **124** (Scheme 7.6). After workup, the crude reaction mixture was analysed by LCMS. Large amounts of homo-dimers **128**, **129**, **220** and **221** were present and only a small trace of a species with a molecular weight corresponding to **202/203** was observed. Despite significant effort, hetero dimers **202** and **203** were not amenable to isolation using flash chromatography.

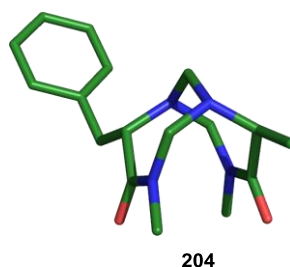


Scheme 7.6 Hetero-Dimer Formation

As phenylalanine and valine are sterically similar it was thought that a hetero-dimer may be disfavoured over the homo-dimers. Therefore a 1:1 mixture of **113** and **45** was condensed with **124** in the hope that using two sterically different residues would lead to formation of significant quantities of hetero-dimer. Analysis of the crude reaction mixture by LCMS showed a large amount of a hetero-coupled species. **204** was isolated by flash chromatography (33%) and to confirm the stereochemistry a single crystal was grown and analysed by X-ray crystallography (Figure 7.6)

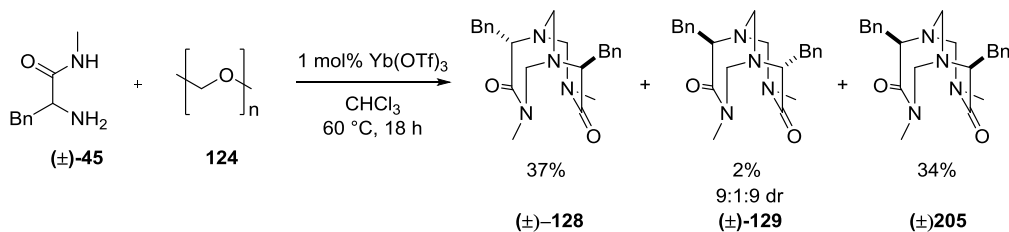


Scheme 7.7 Hetero-Dimer Formation

Figure 7.6 Single Crystal X-ray Structure of **204**

The substituents on each dimer had so far been seen to either point towards the bicyclic core (as observed in **129**) or, more commonly, point away from the bicyclic core (as observed in **128**). With a single enantiomer of starting amide only these two isomers are conceivable. A third isomer was considered to be possible, whereby using a racemic amino amide, one alkyl group could point toward the bicyclic core

and one could point away. As well as being an interesting addition to the dimer series it would also provide a non- $C_2$  symmetric homo-dimer. ( $\pm$ )-**45** was prepared by mixing equal amounts of *R* and *S* **45**. ( $\pm$ )-**45** was then used under the standard reaction conditions (Scheme 7.8).



Scheme 7.8 Formation of 3 Racemic Homo-Dimers

After workup, three spots were visible by TLC. The least polar spot shared the  $R_f$  of **128** whilst the most polar spot shared the  $R_f$  of **129**. The new spot had an  $R_f$  between the two, indicating it was likely to be **205**. Flash chromatography yielded ( $\pm$ )-**128** (37%), ( $\pm$ )-**129** (2%) and pleasingly ( $\pm$ )-**205** (34%). As with the preparation of **129**, isolation was challenging which led to a low isolated yield compared to the diastereomeric ratio observed in the crude reaction mixture by  $^1\text{H}$  NMR spectroscopy. A single crystal of ( $\pm$ )-**205** was grown and analysed by X-ray crystallography to confirm the structural assignment (Figure 7.7).

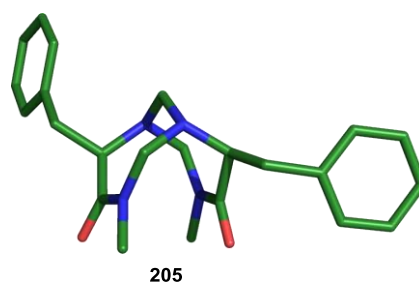
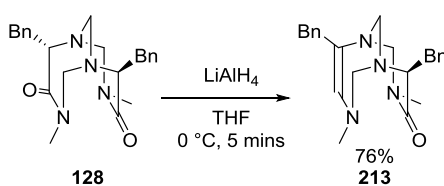


Figure 7.7 Single Crystal X-ray Structure of **205**



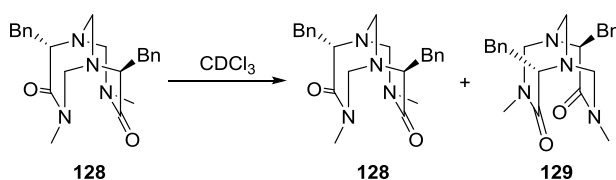


Having failed to produce any identifiable compounds using **210**, attention was turned to reduction of the pre-formed dimer (**128**). Addition of lithium aluminium hydride to a THF solution of **128** at ambient temperature led to an immediate reaction. After 1 hour reaction time, upon workup a brown oil was obtained. Analysis of the crude reaction mixture by  $^1\text{H}$  NMR spectroscopy indicated decomposition had occurred. The reaction was repeated at  $0\text{ }^\circ\text{C}$  and was quenched after 5 minutes. After flash column chromatography, partially reduced and dehydrated **213** was isolated in good yield (76%). Attempts to further reduce **213** all led to decomposition. Therefore, efforts toward **211** were curtailed.

Scheme 7.14 Reduction of **128**

### 7.2.3 Modification of the Methylene Bridge

Upon standing for 24 hours in  $\text{CDCl}_3$ , amino acid dimer **128** was observed to undergo partial isomerisation to give a 10:1 mixture of **128** and **129** (Scheme 7.15). Isomerisation of **220** and **221** was also observed under similar conditions. However, isomerisation was not observed to occur in  $\text{CD}_3\text{CN}$  or  $\text{CD}_3\text{OD}$ . Small quantities of deuterium chloride are often present in  $\text{CDCl}_3$  resulting from decomposition.<sup>94</sup> The acidic nature of bench  $\text{CDCl}_3$  was thought to be responsible for the isomerisation of **128**. Filtration of  $\text{CDCl}_3$  through basic alumina prior to use stopped isomerisation occurring which gave good evidence that the dimer structure was unstable in acidic conditions.

Scheme 7.15 Isomerisation Observed in  $\text{CDCl}_3$



The chiral at nitrogen amine Tröger's base<sup>95,96</sup> (**214**) has also been reported to be unstable under acidic conditions whereby it readily undergoes racemisation.<sup>97</sup> Due to the structural similarity between the dimers and **214** it was assumed that a similar mechanism, involving an iminium intermediate, could be occurring (Figure 7.8).

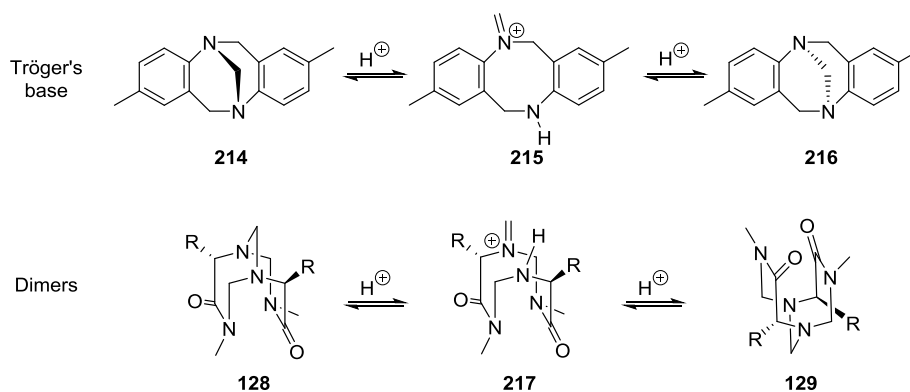


Figure 7.8 Proposed Mechanisms for Racemisation of Tröger's Base and Isomerisation of **128**

Many analogues of **214** have been made. Particular attention has been focused on substitution of the methylene-bridge for an ethylene-bridge. This renders the amine stable under acidic conditions. Unsubstituted ethylene-bridged Tröger's base **218** has been prepared from **214** and dibromoethane **220**, however, resolution is required to obtain **218** as a single enantiomer.<sup>98</sup> More recently, rhodium and copper carbenoid chemistry has been reported to form substituted ethano-bridged Tröger's bases (e.g. **219**) with high enantiomeric and diastereomeric excesses from enantiomerically pure **214**.<sup>99,100</sup>

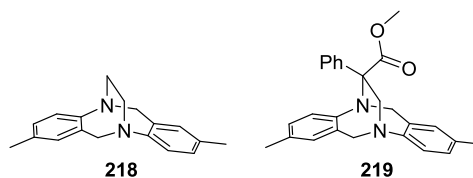
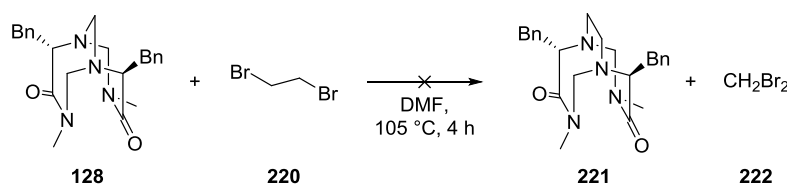
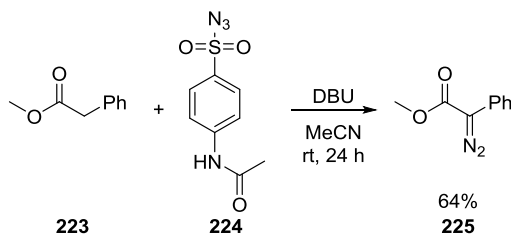


Figure 7.9 Ethano-Bridged Tröger's Bases

Due to the success in forming acid-stable ethano-bridged Tröger's bases, a similar modification of the dimers was envisaged. **128** was heated in the presence of dibromoethane (**220**) (Scheme 7.16). After 4 hours the reaction mixture had turned brown and by  $^1\text{H}$  NMR spectroscopy **128** was present along with some unidentifiable compounds, presumably arising from decomposition. Continued heating of the reaction mixture led to further decomposition. The reaction was repeated at  $50\text{ }^\circ\text{C}$  and after 24 hours only **128** and **220** were visible by  $^1\text{H}$  NMR spectroscopy.

Scheme 7.16 Attempted Formation of **221**

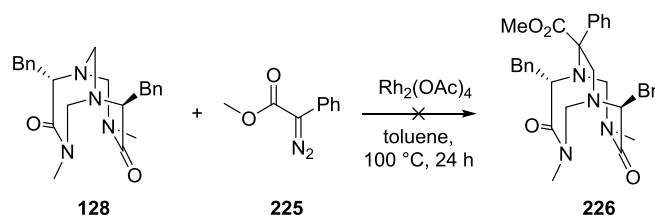
Due to the lack of success forming **221**, carbenoid chemistry was investigated. The highest-yielding diazo compound for forming derivatives of **214** was selected and prepared from **223** and **224** in the presence of DBU (64%, Scheme 7.17).<sup>99</sup>



Scheme 7.17 Formation of Diazo Compound

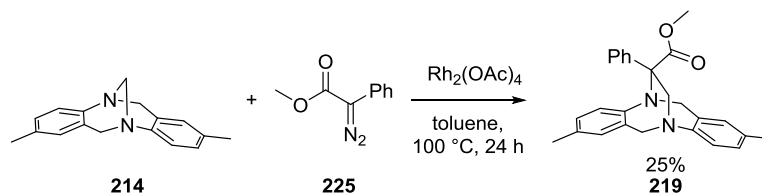
Diazo compound **225** was added to a toluene solution of **128** and rhodium acetate. Upon heating, gas evolution was observed. After 24 h the reaction mixture was analysed by  $^1\text{H}$  NMR spectroscopy. No **226** was visible. However, small amounts of new compounds were present within the mixture along with **128**. Due to its increased sensitivity, LCMS was used to analyse the reaction mixture but disappointingly indicated **226** was not present. The reaction was repeated in the presence of 1 mol% ytterbium(III) triflate in the hope that formation of an open iminium intermediate

similar to **217** would be promoted. However,  $^1\text{H}$  NMR and LCMS analysis of the crude reaction mixture, again, showed no indication of **226** being present.



Scheme 7.18 Attempted Carbenoid Chemistry

Two issues were considered to potentially be responsible for the inability to produce **226**. Failure of the carbenoid chemistry and/or the proposed mechanism of isomerisation was incorrect (Figure 7.8). Using a literature preparation, **219** was prepared from **214** and **225** to check the carbenoid chemistry was operating (Scheme 7.19). A disappointing yield was obtained (25%), however, it confirmed that a carbenoid was being formed under the reaction conditions.



Scheme 7.19 Modification of Tröger's Base

The successful formation of **219** led the dimer structure to be reconsidered. Each dimer possesses three methylene bridges (Figure 7.10) and it had been assumed that the single bridgehead methylene unit (red) was labile and that the other two (blue) were not.

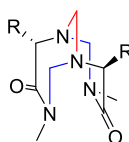
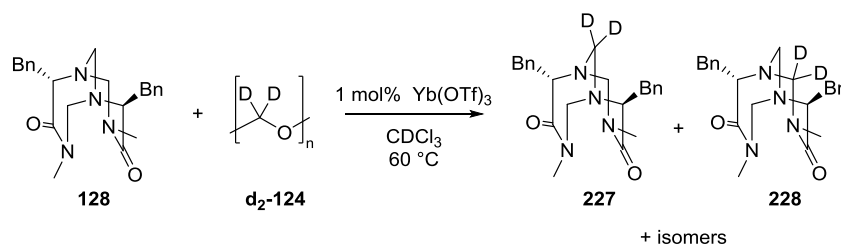


Figure 7.10 Two Methylene Environments (red and blue)

To probe the lability of the methylene groups, a deuteration study was conducted (Scheme 7.20). Due to  $C_2$  symmetry two methylene units are identical (blue) and so any deuterium incorporation at this location was assumed to be equal. Using  $^1\text{H}$  NMR resonances arising from the  $\text{CH}$  and  $\text{CHCHH}$  on **128** as integral references, deuterium incorporation was assessed. Under the reaction conditions, deuteration was observed to occur at a similar rate in each methylene environment suggesting that each unit is equally labile.  $^2\text{H}$  NMR spectroscopy was used to confirm the incorporation of deuterium to give **227**, however, due to the small amounts of **228** formed during the reaction it was not possible to determine incorporation of deuterium in this diastereoisomer. To verify the observed deuteration, **227** and **228** were independently prepared under the standard reaction conditions using **d<sub>2</sub>-124**.



Scheme 7.20 Deuterium Incorporation

The observation that all three of the methylene units in the dimer structure are labile suggested that, for the dimer to be stable under acidic conditions, all three units would need to be targeted for modification. This represented a significant challenge which was well beyond the scope of this work. Hence, efforts to modify **128** were curtailed.

#### 7.2.4 Conformational Rigidity

All of the dimers which had been characterised by X-ray crystallography shared the same core conformation. In addition,  $^1\text{H}$  NMR spectroscopy of each dimer displayed only one species and upon heating no change in chemical shift was observed suggesting that only one conformation was accessible in solution. To further probe this, DFT (B3LYP/6-31+G\*\*) calculations were performed to find rational low-energy conformations of **218**.

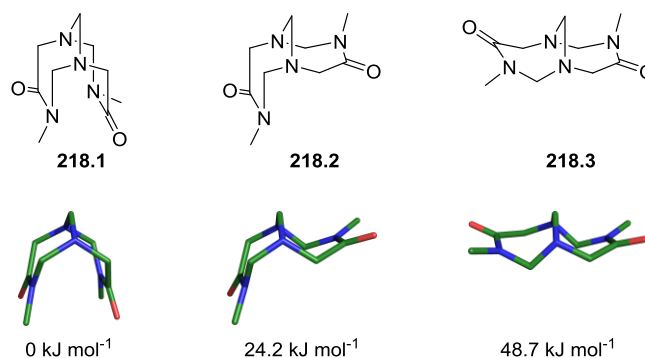


Figure 7.11 Low-Energy Conformations of the Dimer Core

Three conformations were found, **218.1**, **218.2** and **218.3** (Figure 7.11). In agreement with the conformation observed by single crystal X-ray crystallography, **218.1** was found to be the lowest energy conformer. **218.2** and **218.3** were higher in energy by 24.2 kJ mol<sup>-1</sup> and 48.7 kJ mol<sup>-1</sup> respectively. A through-space N...C=O distance of 2.99 Å (greater than the sum of Van der Waals radii) in **218.1** suggested a stabilising interaction was not responsible for the low energy of **218**. Inversion of both sides of the structure (**218.3**) resulted in an energy roughly double that of a single inversion (**218.2**). This suggested that some distinct destabilising interactions are present in the higher energy conformations **218.2** and **218.3**.

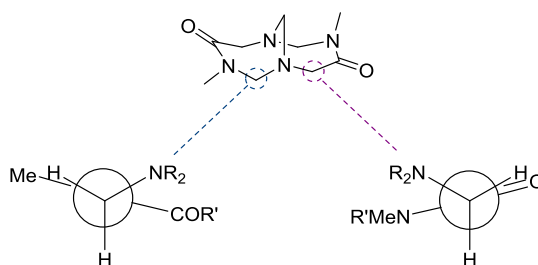


Figure 7.12 Eclipsing Interactions in **218**

Close inspection of **218.3** revealed eclipsing interactions (Figure 7.12). In **218.3** four of these interactions are present whereas in **218.2** only two are present. This nicely accounted for **218.3** being double the energy of **218.2** and provided a rationale for the lowest-energy conformation **218.1**.

### 7.3 Conclusions

Having discovered dimers **128** and **129** as unwanted products (see Chapter 4), investigations were made to further probe the novel molecular motif.

The dimer structure was found to tolerate glycine, alanine, valine and phenylalanine amino acid residues which demonstrated that the preparation and structure has a good substrate tolerance. In general, the use of chiral amino amides furnished two diastereomeric dimers whereas the use of racemic amino amides led to formation of three (Figure 7.13). Using a mixture of two amino amides was found to form hetero-dimers as well as homo-dimers.

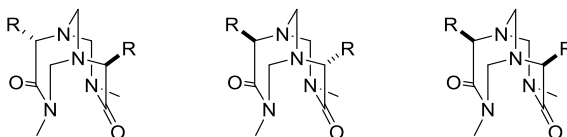


Figure 7.13 Three Observed Dimer Diastereoisomers

Attempts were made to modify the amidic position on the dimer structure. Ethyl amides were found to be tolerable whereas benzyl or carboxamides were found not to be amenable to dimer formation. Diamines were found not to form the dimeric structure and attempts to reduce the amides led to reduction and dehydration of one amide or decomposition.

The dimers were observed to be unstable under acidic conditions. Using methodology developed for modification of Tröger's base, attempts were made to modify the methylene-bridge-head into an ethylene-bridge-head, however, modification was not achieved. A deuteration study indicated that all three methylene-bridges in the dimer structure are labile. Hence, modification to render the dimer motif stable under acidic conditions would represent a significant challenge and this would curtail any subsequent efforts to use these dimers as either catalysts or ligands in transition-metal catalysed processes.

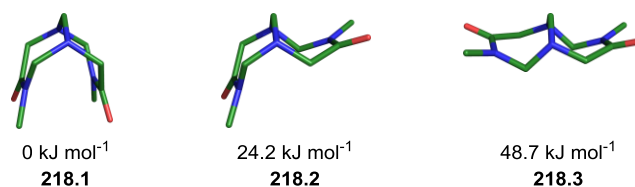


Figure 7.14 Plausible Conformations of the Dimer Structure

DFT calculations confirmed that the conformation of the core structure observed by X-ray crystallography (**218.1**) is the lowest-energy conformation (Figure 7.14). Two other plausible conformations were observed but were found to be significantly higher in energy due to eclipsing interactions (**218.2**, 24.2 kJ mol<sup>-1</sup> and **218.3**, 48.7 kJ mol<sup>-1</sup>). Overall, the dimer structure was determined to be conformationally rigid.

# **Chapter 8: Alkene Dihydroxylation using Malonoyl Peroxides: A Mechanistic Study**



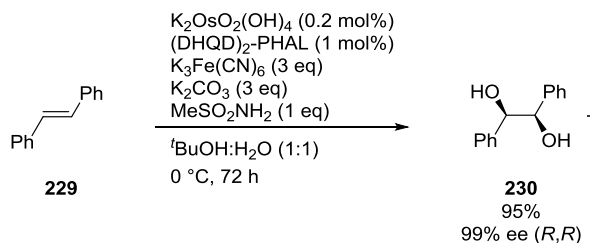
## 8 Alkene Dihydroxylation using Malonoyl Peroxides: A Mechanistic Study

### 8.1 Preface

Alongside projects in iminium catalysis, an opportunity arose to undertake a short investigation in metal-free alkene dihydroxylation. Despite being outside the immediate scope of this thesis; like organocatalysis, metal-free synthesis is a contemporary area of synthetic organic chemistry. Hence this work was deemed worthy of inclusion within this thesis.

### 8.2 Introduction

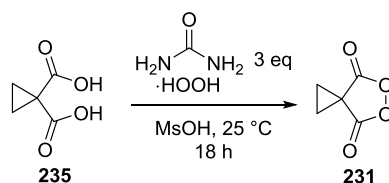
Alkene dihydroxylation is a fundamental transformation in synthetic chemistry. The Sharpless Asymmetric Dihydroxylation (AD) (Scheme 8.1)<sup>101</sup> dominates the area due to the vast substrate scope, outstanding yields and enantioselectivities often observed within the transformation. For example, *trans*-stilbene (**229**) is dihydroxylated in 95% yield and gives a single product diastereoisomer in 99% enantiomeric excess (Scheme 8.1).



Scheme 8.1 The Sharpless AD reaction

The outstanding performance of this reaction has rendered it to be the ‘gold standard’ of alkene dioxygenation.<sup>102</sup> Its popularity is further reflected in the commercial availability of AD-mix- $\alpha$  and AD-mix- $\beta$ , both of which are pre-mixed reagents required for the reaction.





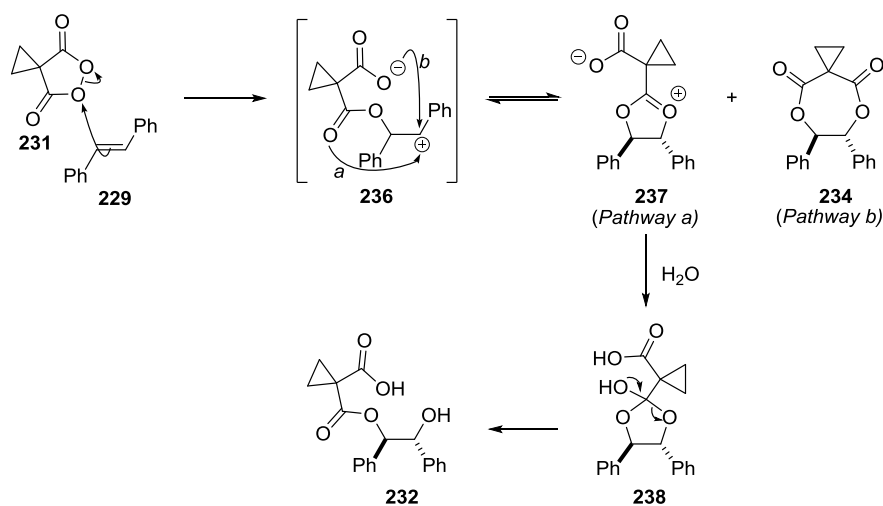
Scheme 8.3 Synthesis of cyclopropyl malonyl peroxide

Although a synthetically useful transformation, limitations prevent malonoyl peroxide mediated dihydroxylation from being competitive with the Sharpless AD reaction. The absence of an asymmetric variant and poor yields obtained with aliphatic substrates are both key problems which need to be addressed. In addition, a catalytic protocol would also assist in making the transformation a worthy replacement for the Sharpless AD.

A thorough mechanistic understanding is key to reaction development. Within this Chapter, DFT calculations and a mechanistic probe are used to study the mechanism of the reaction between peroxide **231** and stilbene (**229**).

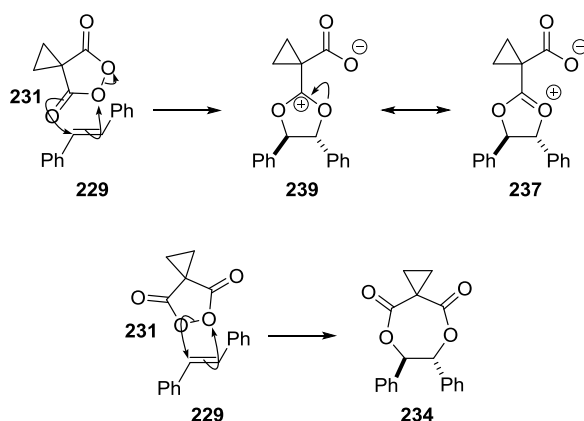
### 8.3 Plausible Mechanistic Pathways

In the initial publication a step-wise ionic interaction between peroxide **231** and alkene **229** was proposed (Scheme 8.4).<sup>104</sup> This proposed mechanism formed two key intermediates; the zwitterion **237** and the 7-membered ring **234**. Upon addition of water to **237**, **232** is formed. Both **232** and **234** are observed experimentally and this proposed mechanism accounted for their formation. However, no robust evidence for this mechanistic pathway was presented.



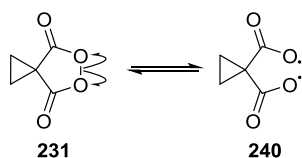
Scheme 8.4 Proposed Step-wise Ionic Mechanism

A number of alternative mechanistic routes to intermediates **232** and **234** could be envisaged. Continuing with an ionic interaction between **231** and **229**, a concerted process to form **237** could operate. **237** could then react directly with water to give intermediate **232**. To form **234**, another concerted interaction between **231** and **229** could be envisaged (Scheme 8.5).

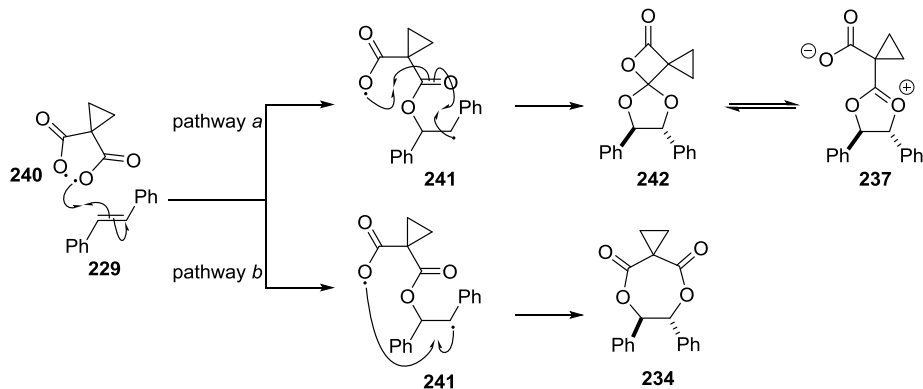


Scheme 8.5 Proposed Concerted Mechanisms

Organic peroxides are known to undergo homolytic fission to give a diradical species. For example, benzoyl peroxide can be used to initiate radical polymerisation of styrenes.<sup>105</sup> Hence, a radical pathway was another mechanistic possibility which had not been previously considered.

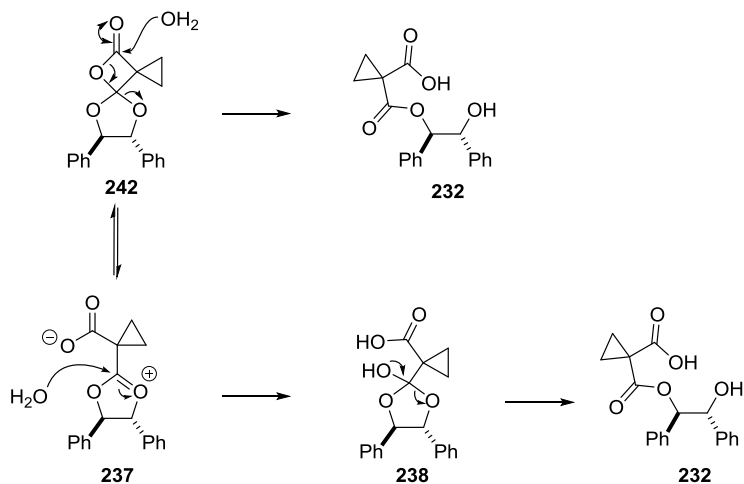


Scheme 8.6 Homolytic Cleavage of the Peroxide Bond



Scheme 8.7 Proposed Radical Mechanism

Homolytic cleavage of the O—O bond of **231** could occur to give diradical species **240** (Scheme 8.7). **240** could then react with alkene **229** and form intermediate **241** (Scheme 8.7). The radicals could then recombine in two possible ways. Pathway *a* could see formation of lactone **242**. Alternatively, the benzylic radical could recombine with the carboxylate radical (pathway *b*) and form intermediate **234**.



Scheme 8.8 Reaction of Intermediates with Water

The  $\beta$ -lactone (**242**) had not been previously considered as a reaction intermediate. It was thought that **242** could either directly react with water to form product **232** or alternatively **242** could be in equilibrium with zwitterion **237** and react with water to give **232** as previously described for the ionic mechanism above (Scheme 8.8). Overall,  $\beta$ -lactone **242** appeared to be a plausible reaction intermediate which could form the observed product **232**.

A single electron transfer (SET) pathway was also thought to be a possibility. If this was to occur it would be likely that the peroxide (**231**) would be reduced and the alkene (**229**) would be oxidised to give **243** and **244**. Recombination of these species could lead to intermediates such as the 7-membered ring **234**, 5-membered oxonium ion **237** and/or the  $\beta$ -lactone **242**.

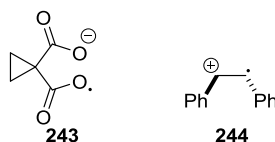


Figure 8.1 Proposed SET Intermediates

#### 8.4 Computational Evidence for Mechanistic Pathways

Having established a number of plausible mechanistic pathways, attention was turned to DFT calculations to gain evidence for or against each proposed mechanism. The functional and basis set can strongly influence the outcome of DFT calculations, hence, they must be carefully chosen. The B3LYP functional has previously been shown to accurately calculate the dissociation energies of O—O and C—O bonds when used with a minimum of a 6-31+G\* basis set.<sup>106</sup> Additionally, Houk, Siegel and co-workers recently used the B3LYP functional to study the mechanism of the phthaloyl peroxide mediated oxidation of arenes.<sup>107</sup> These reports were a good indication that the B3LYP functional and 6-31+G\*\* basis set were suitable for this study. To further replicate the reaction conditions a polarisable continuum model (PCM) was used to represent the chloroform solvent. To increase the speed of calculations, transition states were found at a lower (B3LYP/6-31G) level of theory.

The corresponding energy was then computed at the higher level of theory with solvation.

#### **8.4.1 A Step-Wise Ionic Pathway**

Using the Gaussian09 suite of programmes, attempts at locating transition states for an ionic interaction between peroxide **231** and stilbene **229** were made. Two discrete transition states were found with roughly equal energy **TS1** 123.5 kJ mol<sup>-1</sup> and **TS2** 128.1 kJ mol<sup>-1</sup> (Figure **8.2**). Upon initial inspection **TS1** and **TS2** appeared near-identical with the only difference being the relative orientation of peroxide **231** with respect to stilbene **229**. On following the intrinsic reaction coordinate (IRC) of each transition state, the difference in peroxide orientation had a clear influence on the product formed. In the forward direction **TS1** formed intermediate **237**. This suggested a concerted mechanism could be operating. However, upon animating **TS1** there was only interaction between the alkene and peroxide bond with no simultaneous interaction between the carbonyl and alkene. In addition, closer inspection of the IRC showed the formation of a benzylic carbocation (**236A**) and due to the close proximity of the carbonyl group, subsequent ring closure was occurring to give **237**. Therefore a concerted mechanism was ruled out. **TS2** led to the open-chain zwitterion **236B** as proposed.

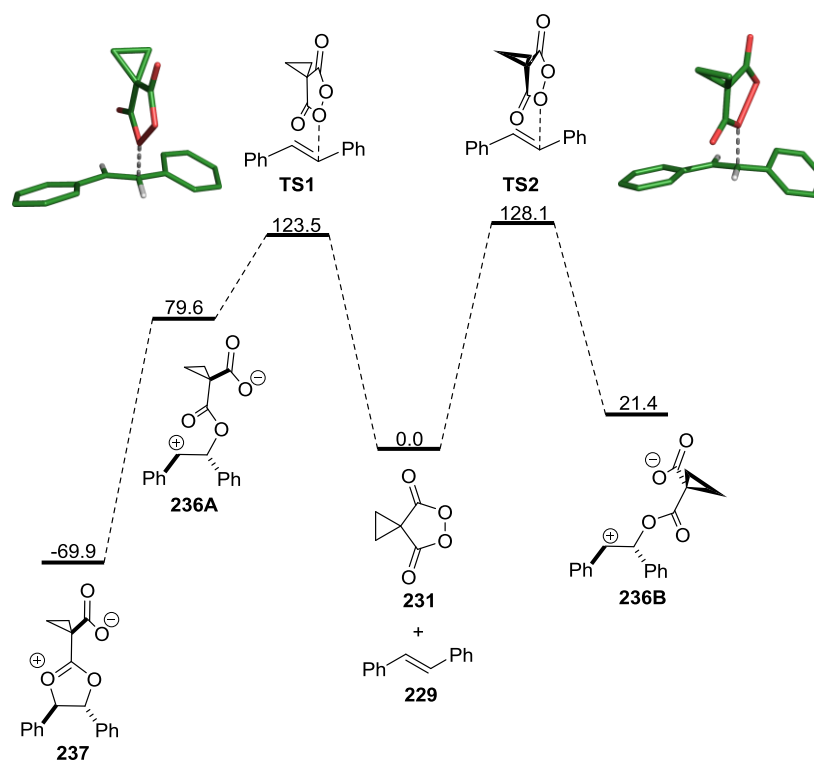


Figure 8.2 Transition States Found for a Concerted Ionic Pathway  
(values in  $\text{kJ mol}^{-1}$ )

The relative energy of **237** to that of **231** and **229** was unexpected. **237** is zwitterionic and hence would be anticipated to lie significantly higher in energy than the neutral reactants. In addition, the energy of zwitterion **236B** appeared to be quite low. The calculations were performed with solvation and it was thought that this could be stabilising the charged intermediates. Hence, solvation was removed and the relative energies of each intermediate and transition state were recalculated (Figure 8.3).



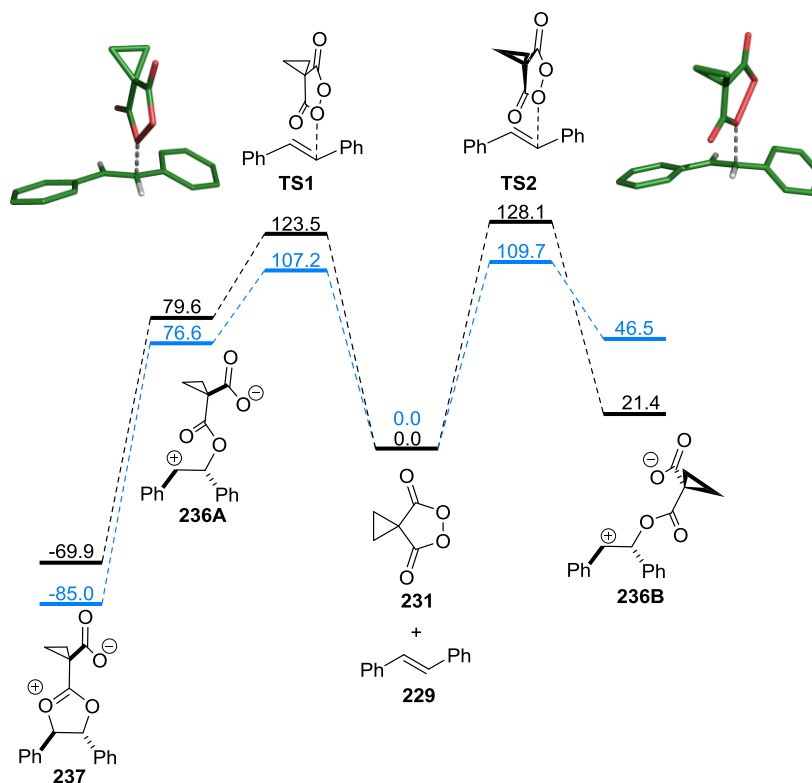


Figure 8.3 Comparison of Gas-Phase (Blue) Energies and Solvated Energies (Black) (values in  $\text{kJ mol}^{-1}$ )

In the absence of solvation, intermediate **236B** significantly increased in energy demonstrating that, as expected, the solvent model was having a significant influence on the stability of this intermediate. **237** decreased in energy by approximately  $15 \text{ kJ mol}^{-1}$  in the absence of solvation. **TS1** and **TS2** also decreased in energy by  $16 \text{ kJ mol}^{-1}$  and  $19 \text{ kJ mol}^{-1}$  respectively. Therefore, the change in energy of **237** was considered negligible. Solvation did not appear to be contributing towards the stability of **237**.

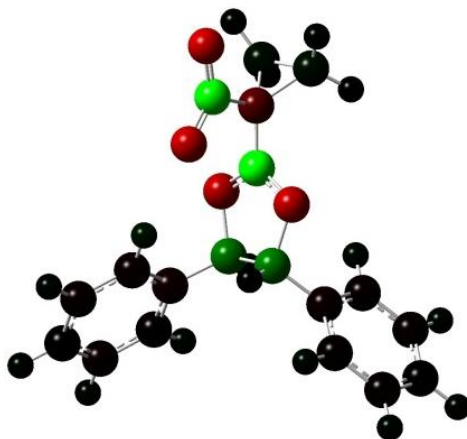


Figure 8.4 Atomic Structure of **237** Displaying APT Charge Localisation  
( $\delta^-$  = red,  $\delta^+$  = green)

To further probe the stability of **237**, the Atomic Polar Tensor (APT) charge distribution was inspected (Figure 8.4). The anion was shown to be fully delocalised across the carboxylate and the cation was shown to be delocalised across the two benzylic carbon atoms and both oxygen atoms in the 5-membered ring. The delocalised charges combined with the close-proximity of the anion and cation were considered to be factors which could contribute to the stability of **237**. Having found some reasons which could contribute to the stability of **237**, the calculated structure and energy was considered to be reasonable.

#### 8.4.2 A $\beta$ -Lactone Intermediate

The evidence obtained thus far suggested that a step-wise ionic mechanism was possible (Scheme 8.4) and no evidence for a concerted process (Scheme 8.5) had been found. Before exploring a radical process (Scheme 8.7) the proposed  $\beta$ -lactone intermediate (**242**), crucial for the proposed radical process, was investigated.

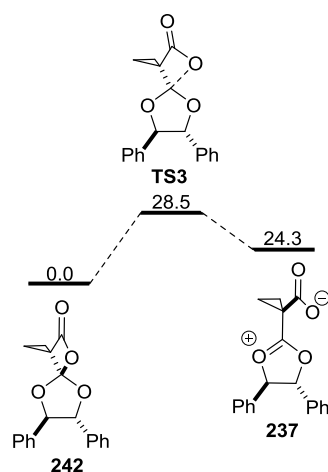


Figure 8.5 Cleavage of  $\beta$ -Lactone into Zwitterion (values in  $\text{kJ mol}^{-1}$ )

$\beta$ -Lactone **242** was found to be  $24.3 \text{ kJ mol}^{-1}$  lower in energy than the zwitterion **237** (Scheme 8.5). A transition state (**TS3**) of  $28.5 \text{ kJ mol}^{-1}$  was found for interconversion between the two. Such low energy barriers indicated that it would be likely that **242** would be in equilibrium with **237** at any one time and that either could be an intermediate in a proposed mechanism. Complimentary to the DFT calculations, **237** and small amounts of **242** have been trapped with methanol indicating that both are plausible intermediates. However, labelling studies have been conducted which show that water preferentially reacts with **237**. This renders **237** of greater relevance than **242** in this mechanistic study.<sup>108</sup>

### 8.4.3 A Radical Pathway

Having found that  $\beta$ -lactone **242** was a plausible intermediate, a radical pathway was considered. For a radical pathway to occur, homolytic cleavage of **231** would be required followed by reaction of the diradical (**240**) with stilbene (**229**).

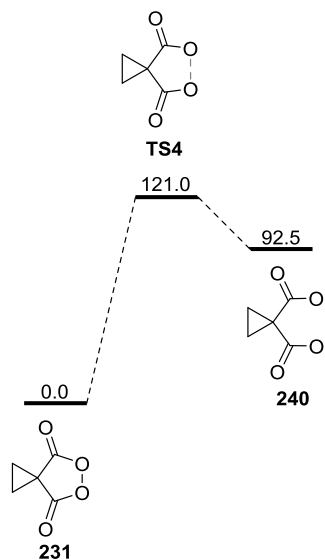


Figure 8.6 Homolytic Cleavage of **231** (values in kJ mol<sup>-1</sup>)

A transition state (**TS4**) for homolytic cleavage of the O—O bond of **231** was found (Figure 8.6). The energy of 121.0 kJ mol<sup>-1</sup> for the cleavage was similar to that of the two transition states found for the ionic reaction between **231** and **229** (**TS1** 123.5 and **TS2** 128.1 kJ mol<sup>-1</sup>). If a lower or equal energy transition state for the diradical **240** reacting with **229** could be found, a radical pathway would have been a plausible option. Unfortunately, despite extensive searching, no interactions between **240** and **229** were found. This suggested that a radical pathway was unlikely.

### 8.4.4 SET Interaction

Due to the difficulty of finding transition states for the movement of a single electron, the proposed SET mechanism was probed by calculating the energies of the radical anion **243** and the radical cation **244**. The combined energies of **243** and **244** were found to be 412 kJ mol<sup>-1</sup> higher in energy than **231** and **229** (Figure 8.7). As this was significantly higher in energy than **TS1** (123.5 kJ mol<sup>-1</sup>) and **TS2**

(128.1 kJ mol<sup>-1</sup>) for the ionic pathway and also **TS4** (121 kJ mol<sup>-1</sup>) for homolytic cleavage of the peroxide bond, a SET mechanism was discounted.

Interestingly, the high combined energy of **243** and **244** was due to the unstable radical cation of stilbene (**244**). Radical anion **243** was found to be 163.3 kJ mol<sup>-1</sup> lower in energy compared to the ground-state peroxide (**231**). Therefore, with the correct substrate, an SET interaction with the peroxide could be a possibility and something to consider in future reaction design.

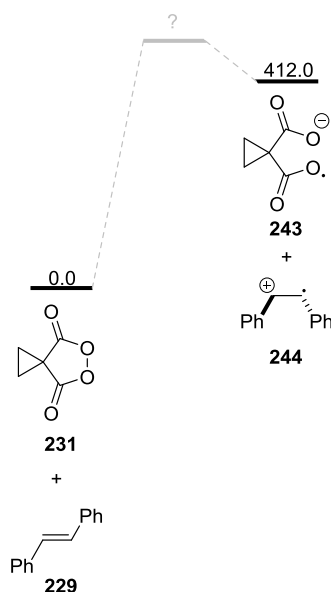


Figure 8.7 Proposed SET Intermediates (values in kJ mol<sup>-1</sup>)

The DFT calculations pointed towards an ionic mechanism operating between **231** and **229**. However, the absence of interaction between **240** and **229** did not allow a radical pathway to be completely discounted. As with any investigation, evidence from a multitude of sources is better than reliance upon a single source. Therefore, to further define the mechanism between **231** and **229**, experimental evidence was sought.

## 8.5 Experimental Evidence for Mechanistic Pathway

### 8.5.1 Radical Clocks

Cyclopropane **245** was designed to distinguish between radical and ionic reaction pathways under picosecond kinetic control.<sup>109</sup> **245** operates by ring-opening the cyclopropane in different places depending on whether the intermediate is cationic or radical. If a radical intermediate (**246**) is present, the cyclopropane opens to give a stabilised benzylic radical (**247**). Alternatively, if a cationic intermediate (**248**) is formed the methoxy group opens the cyclopropane to give an oxonium ion (**249**) (Figure 8.8). Importantly, these two ring-opening pathways result in different connectivity of the carbon framework and hence offer robust evidence towards the nature of the mechanism in operation.

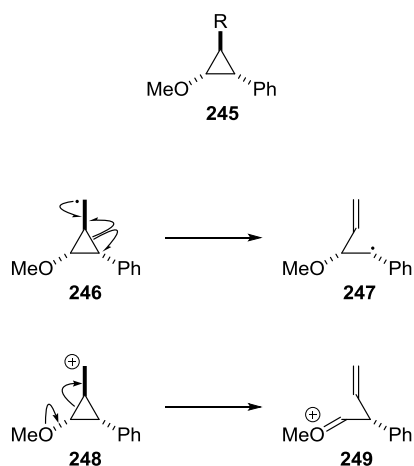


Figure 8.8 Newcomb Radical Clock

Many derivatives of **245** have been made, including an alkene (**250**). **250** has been used to confirm the radical mechanisms of SOMO catalysis<sup>27</sup> and Mn<sup>III</sup> catalysed epoxidation reactions.<sup>110</sup> In addition, it has been used to show that copper catalysed alkene arylation reactions proceed *via* an ionic mechanism.<sup>111</sup> With precedent in the literature showing that **250** is a suitable probe for ionic and radical-based mechanisms it seemed an ideal substrate for reaction with peroxide **231**.

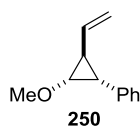
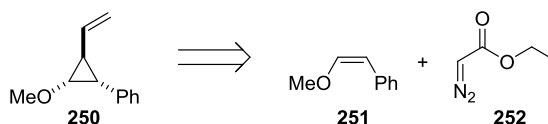
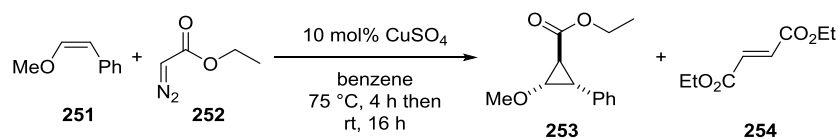


Figure 8.9 Radical Clock Alkene

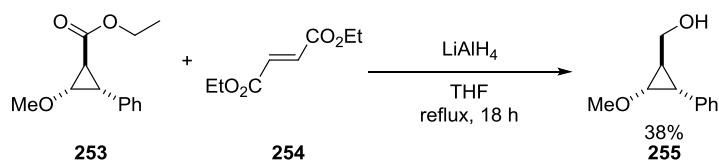
## 8.5.2 Synthesis of Radical Clock Alkene

Scheme 8.9 Retrosynthesis of **250**

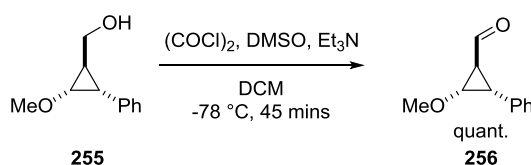
Using carbenoid chemistry, followed by reduction, oxidation and finally olefination **250** can be prepared in 4-steps from  $\beta$ -methoxy styrene **251** and ethyl diazoacetate **252** (Scheme 8.9).<sup>112</sup>

Scheme 8.10 Synthesis of **253**

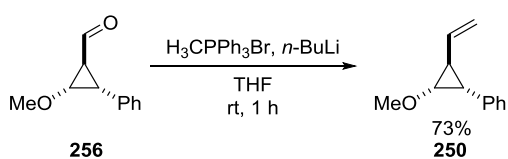
Alkene **251** was cyclopropanated by dropwise addition of diazo compound **252** over 3 hours in the presence of catalytic anhydrous copper sulfate (Scheme 8.10). Flash chromatography yielded an inseparable mixture of cyclopropane **253** and diethyl fumarate **254**. The reaction was also performed using rhodium acetate dimer in place of copper sulfate. However, <sup>1</sup>H NMR spectroscopy and TLC analysis showed significantly more side-products indicating that the copper salt was a more appropriate catalyst for the preparation of **253**.

Scheme 8.11 Reduction of **253** to give **255**

The mixture of ester (**253**) and fumarate (**254**) was treated with lithium aluminium hydride (Scheme 8.11). After workup **255** was obtained as a single product (38%). Conveniently, products arising from reduction of **254** were not observed and were presumably removed upon aqueous workup.

Scheme 8.12 Swern Oxidation of **255**

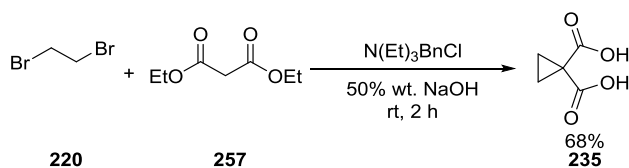
Alcohol **255** was oxidised under Swern conditions to the aldehyde **256** (Scheme 8.12). During workup **256** was washed with 1 M HCl to remove traces of triethylamine. However, complete decomposition of **256** was observed. Subsequently, no acidic wash was performed and residual triethylamine was removed under reduced pressure.



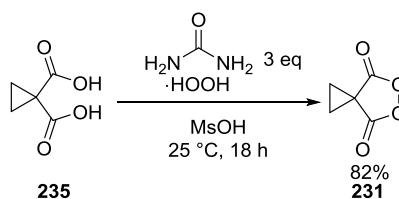
Scheme 8.13 Wittig Reaction

Aldehyde **256** was converted to alkene **250** using Wittig chemistry (Scheme 8.13). Overall, **250** was prepared from **251** in 4-steps on a gram scale with a yield of 28%.

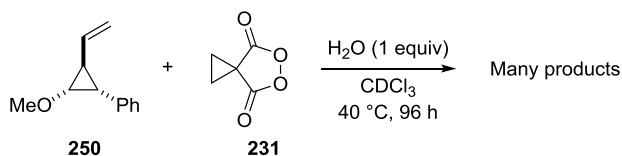


8.5.3 Synthesis of Peroxide **231**Scheme 8.14 Synthesis of Diacid **235**

Despite being commercially available, diacid **235** is relatively expensive and can be readily prepared from diethylmalonate (**257**) and dibromoethane (**220**) in the presence of triethylbenzylammonium chloride. Upon workup **235** was isolated with trace amounts of malonic acid also visible by  $^1\text{H}$  NMR spectroscopy.

Scheme 8.15 Synthesis of Peroxide **231**

Peroxide **231** was prepared from diacid **235** and urea hydrogen peroxide adduct in anhydrous methanesulfonic acid (82%). Aside from aqueous workup, no purification of **231** was required.

8.5.4 Reaction of Radical Clock **250** with Peroxide **231**

Scheme 8.16 Reaction of Radical Clock Alkene with Peroxide

The reaction between 1 equivalent of **231** and 1 equivalent of **250** in  $\text{CDCl}_3$  in the presence of 1 equivalent of water was monitored by TLC and was observed to be

slow (Scheme 8.16). After 4 days both reagents had been fully consumed and by  $^1\text{H}$  NMR spectroscopy many products had been formed. Due to the extensive number of reaction products, attempts at isolation seemed foolish at this stage. The reaction was repeated with the addition of 1,4-dinitrobenzene as an internal standard. Aliquots were periodically removed and the consumption of **231** and **250** was monitored by  $^1\text{H}$  NMR spectroscopy (Figure 8.10).

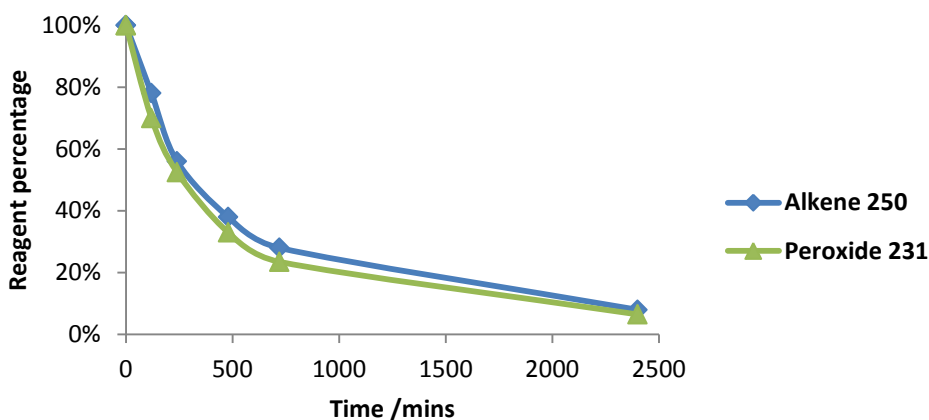


Figure 8.10 Consumption of Alkene **250** and Peroxide **231**

The two reagents (**231** and **250**) were shown to be reacting in a 1:1 stoichiometry. Closer inspection of the  $^1\text{H}$  NMR spectrum of the reaction mixture showed some key chemical functionalities; some aldehydes were present, a multitude of methyl ethers, acetals and/or hemiacetals were also visible and, in addition, a range of alkenes were also observed (a typical  $^1\text{H}$  NMR spectrum of this reaction mixture is shown in Appendix B).

Despite the large number of products, **231** and **250** seemed to be reacting cleanly with no obvious evidence of decomposition. Therefore it appeared sensible to attempt to isolate the intermediates. As the  $^1\text{H}$  NMR spectrum showed the presence of aldehydes, an ethanolic 2,4-dinitrophenylhydrazine and sulphuric acid TLC dip was prepared to try and identify which spots corresponded to these. A fairly non-polar spot with an  $R_f$  of 0.54 (20% ethyl acetate in petroleum ether) reacted with the

hydrazine dip indicating the presence of an aldehyde or ketone. Preparative TLC was used to isolate a sample of the proposed species.

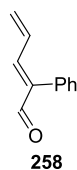
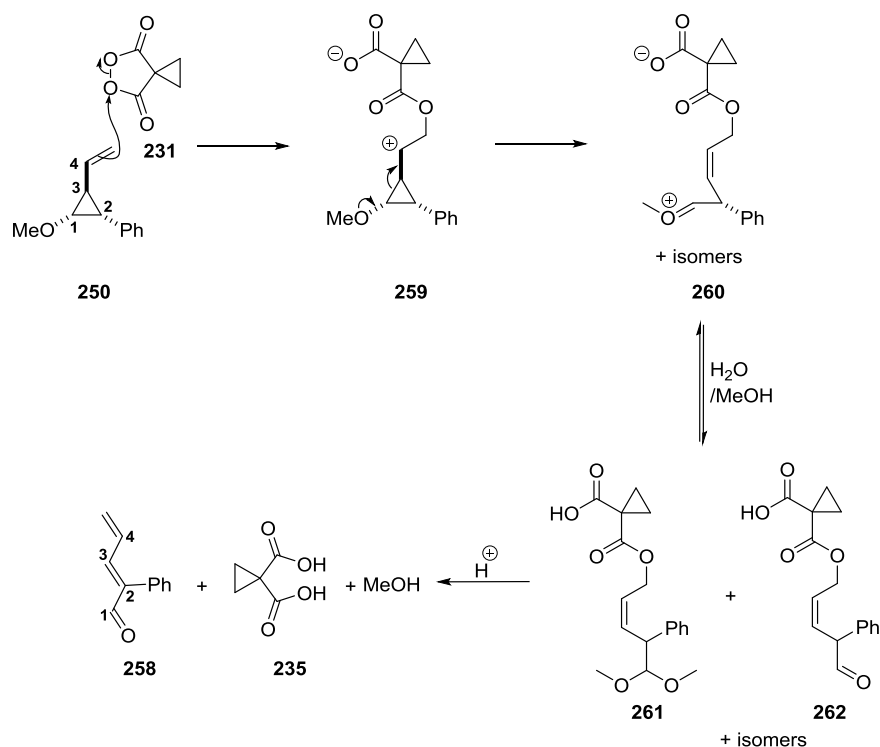


Figure 8.11 Isolated Aldehyde

After full characterisation, the isolated aldehyde was unequivocally assigned to be **258**. This was interesting as **258** was not present in the  $^1\text{H}$  NMR spectrum of the crude reaction mixture and so must have arisen from decomposition on silica. Alkene **250** was stable during chromatography and so **258** was not arising from decomposition of residual **250**. This suggested that some of the reaction intermediates were decomposing under the acidic conditions provided by the silica TLC plate to give **258**.

The reaction of **231** and **250** ( $\text{H}_2\text{O}$ , 1 eq.,  $\text{CDCl}_3$ , 40 °C, 96 h) was repeated and an aliquot was removed and analysed by  $^1\text{H}$  NMR spectroscopy. Full consumption of **231** and **250** was observed. TFA was added to the NMR tube and after 30 minutes at ambient temperature, the majority of the ethers/acetals/hemiacetals had disappeared from the  $^1\text{H}$  NMR spectrum and **258** had begun to form (see Appendix B for spectra). The NMR tube was heated to 40 °C for 18 h and then re-analysed. Virtually all of the intermediates had been consumed and all that remained were **258** and two singlets (~2 ppm and ~4 ppm). The volatiles were removed under reduced pressure and the residue was re-dissolved into  $\text{CDCl}_3$ .  $^1\text{H}$  NMR spectroscopy now showed **258** and one singlet at ~1.8 ppm. The disappearance of the singlet at 4 ppm suggested it was methanol. Its high chemical shift was attributed to the strongly acidic environment that it was present within. The singlet at 1.8 ppm was assigned as cyclopropane-1,1-dicarboxylic acid **235** by comparison to an authentic sample.



The carbon connectivity of **258** was consistent with an ionic interaction between **231** and **250** (Scheme 8.17). A conversion of ~90% could be observed by  $^1\text{H}$  NMR spectroscopy which was thought to be good evidence of an ionic mechanism. However, this result was not as clear cut as first thought. The presence of aldehydes (for example **262**) in the crude reaction mixture indicated that some of the intermediates were forming through an ionic interaction between **231** and **250** but the nature of the other products were uncertain. Despite the cyclopropane being reported to fragment under picosecond kinetics,<sup>112</sup> it was possible that intermediates containing an intact cyclopropane ring were present (Figure 8.12) and ring-opening was occurring after the addition of TFA.

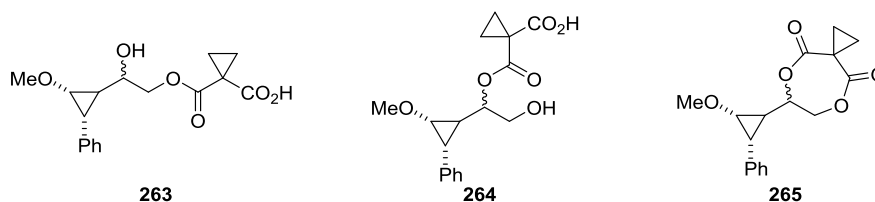


Figure 8.12 Plausible Intermediates with Intact Cyclopropane Ring

Although not entirely conclusive, due to the cleanliness of the transformation from the proposed intermediates (**260-265**) to **258** and the presence of aldehydes (for example **262**) in the crude reaction mixture (which must arise from ionic fragmentation of **250** followed by hydrolysis), the experiment was deemed to give evidence towards an ionic interaction between alkene **250** and malonoyl peroxide **231**.

## **8.6 Conclusions**

A series of mechanistic studies were undertaken to elucidate the mechanism operating during the dihydroxylation of alkenes using malonoyl peroxides.

DFT calculations suggested an ionic pathway between **231** and **229** was viable. Two potential transition states (**TS1** and **TS2**) of near equal energy ( $123.5 \text{ kJ mol}^{-1}$  and  $128.1 \text{ kJ mol}^{-1}$  respectively) were found. In addition, homolytic cleavage of **231** into diradical **240** was found to have a TS barrier (**TS4**,  $121.0 \text{ kJ mol}^{-1}$ ) similar to that of **TS1** and **TS2** suggesting that formation of **240** was plausible. However, no interaction between **240** and **231** could be found which indicated a radical process was unlikely. A SET pathway was discounted due to intermediates **243** and **244** having a combined energy significantly higher ( $412 \text{ kJ mol}^{-1}$ ) than **TS1**, **TS2** and **TS4**.

Experimental evidence was sought to reinforce results gained from DFT calculations. A radical clock alkene (**250**) was reacted with **231** under standard conditions and gave many intermediates. Addition of acid caused the intermediates to decompose giving **235** and **258**. The carbon connectivity of **258** was consistent with an ionic interaction between **231** and **250**. However, due to the number of intermediates, full characterisation could not be carried out. Therefore, despite giving convincing evidence towards an ionic pathway, a full conclusion could not be drawn.

Overall, both DFT and experimental studies were found to provide complimentary evidence towards an ionic mechanism operating in the malonoyl peroxide mediated dihydroxylation of alkenes.

# **Chapter 9: Conclusions and Future Work**

## 9 Conclusions and Future Work

### 9.1 Overview

The goal of work contained within this Thesis was to tackle some of the perceived shortcomings of iminium ion activation, which were deemed to be:

- 1) High catalyst loadings
- 2) Lack of transformations using  $\alpha,\beta$ -unsaturated ketone substrates
- 3) Incomplete understanding of the origins of enantioselectivity

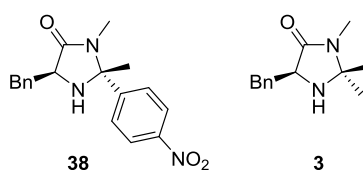


Figure 9.1 Imidazolidinone with  $\alpha$ -EWG and Literature Benchmark

The first goal was achieved through the evaluation of **38**, an imidazolidinone possessing an  $\alpha$ -EWG to increase reactivity and a methyl group *cis*- to the benzyl group to influence asymmetric induction. **38** was found to exhibit high levels of enantioselectivity and superior rates of reaction compared to the literature benchmark (**3**) in Diels-Alder cycloaddition reactions between *para*-substituted cinnamaldehydes and cyclopentadiene.

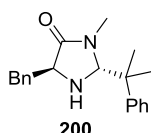


Figure 9.2 Pseudo  $C_2$  Symmetric Imidazolidinone

The second goal was targeted through the use of  $C_2$  and pseudo  $C_2$  symmetric amines (for example **300**) to alleviate the requirement for selective iminium ion formation. DFT calculations were used to assess diastereofacial shielding of iminium  $\pi$ -systems. Despite promising modelling results, pseudo  $C_2$  symmetric amine **200** was found to be catalytically inactive with enone substrates.

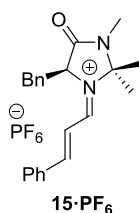


Figure 9.3 Iminium Ion used for Chiral Optical Spectroscopic Measurements

Chiral optical (VCD and ROA) spectroscopy in conjunction with DFT calculations were used to tackle the third goal and probe conformations of iminium ion **15**·PF<sub>6</sub> in solution. The lowest energy conformation **15.E1** was found to be the major conformation in solution with no other conformers evident. This finding agreed with experimental observations whereby only reactions which proceed with closed transition states give products with high levels of enantiomeric excess. In addition, it was in agreement with previously documented observations using variable temperature <sup>1</sup>H NMR spectroscopy.

## 9.2 Imidazolidinone Comparison

Before this work was performed, imidazolidinones possessing an  $\alpha$ -EWG (for example **38**) were known to offer enhanced rates of reaction compared to the MacMillan imidazolidinone (**3**) in the Diels-Alder cycloaddition reaction between cinnamaldehyde and cyclopentadiene. However, the substrate and reaction scope beyond this initial finding was unknown.

**38** was found to offer enhanced levels of reactivity compared to **3** in Diels-Alder cycloaddition reactions with electron-rich and electron-poor cinnamaldehydes and  $\alpha,\beta$ -unsaturated aldehydes possessing a  $\gamma$ -linear alkyl chain. However, **38** was found to offer lower levels of reactivity compared to **3** with  $\gamma$ -disubstituted  $\alpha,\beta$ -unsaturated aldehydes which was believed to be due to dienamine formation.



For other iminium ion activated reactions such as alkylations of pyrrole and indole the MacMillan imidazolidinone (**3**) was found to offer superior reactivity. This was thought to be because these transformations possess a different rate determining step compared to the Diels-Alder cycloaddition reaction. Therefore, for optimal reactivity in these transformations the catalyst scaffold would need to have different properties.

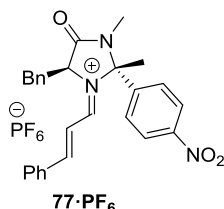


Figure 9.4 Iminium Ion Derived from **38**

Iminium ions derived from **38** and substituted cinnamaldehydes (for example **77·PF<sub>6</sub>**) were found to mimic the conformational behaviour of iminium ions derived from **3** and cinnamaldehyde (for example **15·PF<sub>6</sub>**). This represents a significant milestone as it indicates that catalyst scaffolds can be selectively modified to influence catalytic rate but retain important conformational constraints required for asymmetric induction.

### 9.3 Imidazolidinone Stability

Two different projects highlighted that the imidazolidinone scaffold has the potential to be unstable and, hence, lack the capacity to act as a secondary amine catalyst.

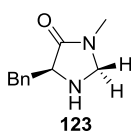


Figure 9.5 Imidazolidinone Unsubstituted at the 2-Position

Firstly, methodology to prepare imidazolidinones unsubstituted at the 2-position was developed in Chapter 4. Imidazolidinone **123** was isolated and found to be stable as the freebase and hydrochloride salt (**123·HCl**). However, when used to catalyse the benchmark Diels-Alder reaction between cinnamaldehyde (**1**) and cyclopentadiene

(**2**), **123** was not recoverable or visible in the  $^1\text{H}$  NMR spectrum of the crude reaction mixture. This suggested that imidazolidinones unsubstituted at the 2-position are unstable under reaction conditions associated with iminium ion activation.

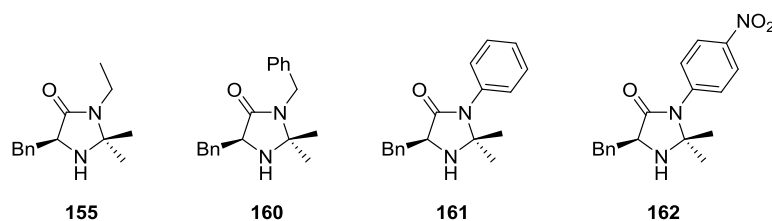


Figure 9.6 Imidazolidinones with Modifications at the 3-Position

Secondly, modifications at the 3-position of the imidazolidinone (to give **155** and **160**) were not observed to influence selectivity in the benchmark reaction between cinnamaldehyde (**1**) and cyclopentadiene (**2**). In an attempt to influence catalytic rate, electron withdrawing groups were installed at the 3-position of the imidazolidinone. However, imidazolidinone **161** was observed to be unstable as the hydrochloride salt (**161·HCl**) and with stronger EWG's the imidazolidinone was observed to be unstable as the freebase, for example **162** was observed to decompose upon standing after chromatography. Therefore, imidazolidinones possessing an EWG in the 3-position were deemed unsuitable for use as catalysts for iminium ion activation.

Overall, in future rational catalyst design, the imidazolidinone should be substituted at the 2-position and possess an alkyl group at the amidic 3-position to render it suitable for use in iminium ion activation.

#### 9.4 The Catalytic Cycle

For the first time, each key intermediate containing the imidazolidinone in the proposed catalytic cycle (**3·HX**, **15·X**, **24·X** and **25·X**) were simultaneously observed (Figure 9.7). This was a significant finding as it gave strong evidence that all of the catalytic species can be present concurrently. However, these species were observed as desolvated ions by ESI-MS in the gas phase. Therefore, the conditions were not directly applicable to reaction conditions used. However, the observation did confirm that **24·X** and/or **25·X** can exist which gave good evidence towards the

proposed catalytic cycle being a true reflection of the imidazolidinone catalysed Diels-Alder cycloaddition reaction between cinnamaldehyde and cyclopentadiene.

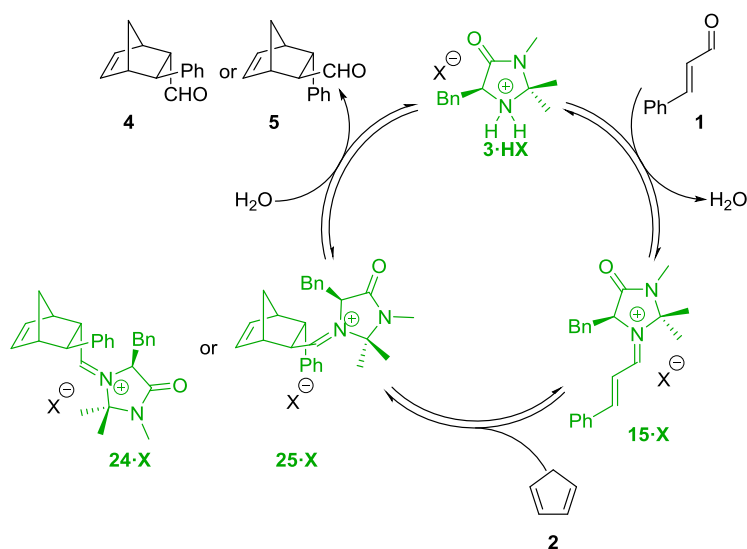
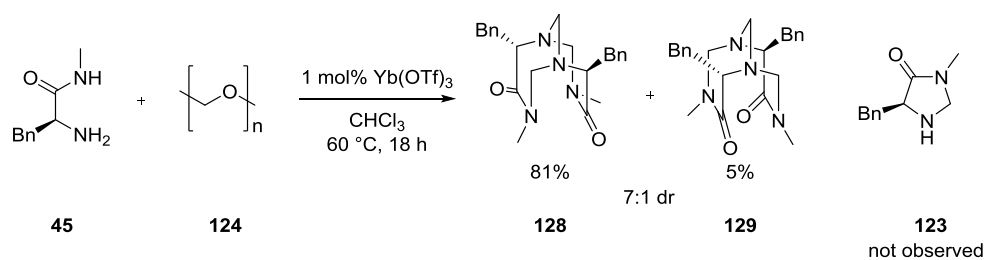


Figure 9.7 Proposed Catalytic Cycle Depicting Observed Intermediates (green)

## 9.5 Amino Acid Amide Dimerisation

Whilst attempting to prepare imidazolidinones unsubstituted at the 2-position (for example **123**) through a condensation reaction between amino amide **45** and paraformaldehyde (**124**) in the presence of ytterbium(III) triflate (Scheme 9.1) two amino amide dimers were formed (**128** and **129**). Imidazolidinone **123** was not observed as a product of the reaction.



Scheme 9.1 Dimerisation of Amino Amide **45**

Due to the novel attributes of the dimer architecture a substrate scope was performed. In addition to phenylalanine; glycine, valine and alanine *N*-methyl amides were found to dimerise to give the corresponding dimers (Figure 9.8). In addition, the use

of mixed amino amides were found to result in dimers containing a mixture of amino acid residues (for example **204**) and the use of racemic amides was found to give a third diastereoisomer (for example **205**).

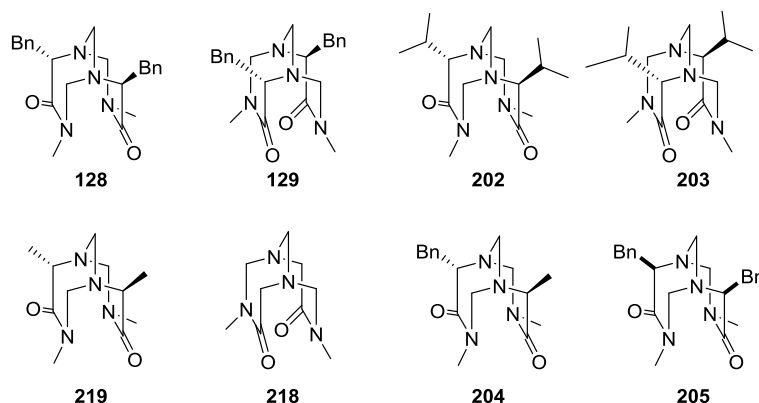
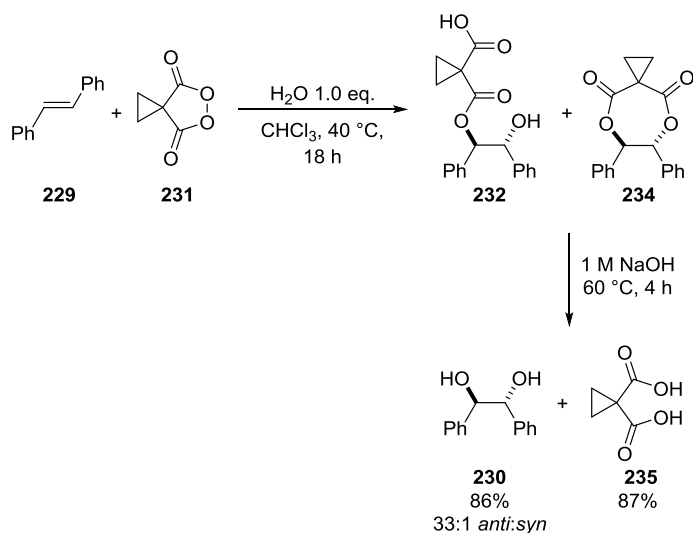


Figure 9.8 Amino Acid Amide Dimers

The dimer structure was found to be unstable under acidic conditions. This instability was thought to be similar to the reported instability of Tröger's base which can be stabilised by modification of the methylene bridge. This led to modifications being attempted on the dimer structure, however, it was not possible to modify the dimer architecture under conditions similar to those reported for Tröger's base. Furthermore, a deuteration study indicated that all three methylene groups of the dimer were labile under acidic conditions. Therefore, modification to render the dimer architecture stable under acidic conditions would represent a significant challenge.

## 9.6 Alkene Dihydroxylation Using Malonoyl Peroxide

Malonoyl peroxide (**231**) has been shown as to be an oxidant suitable for dihydroxylating alkenes. The reaction proceeds in the presence of air and stoichiometric water to give intermediates **232** and **234** which can then be hydrolysed to give diols (**230**) in good yield with good diastereomeric ratio (Scheme 9.2). A study was undertaken which involved DFT calculations and the preparation and reaction of a mechanistic probe to decipher the reaction mechanism between the peroxide (**231**) and alkene (**229**).



Scheme 9.2 Dihydroxylation of alkenes using cyclopropyl malonyl peroxide

DFT calculations indicated that a stepwise ionic interaction between peroxide **231** and stilbene (**229**) was most likely and two transition states of similar energy were found (**TS1** and **TS2**). Importantly, upon following the intrinsic reaction coordinate to the corresponding intermediates, formation of **232** and **234** could be rationalised through ring closure and/or addition of water. A mechanistic probe alkene (**250**) was then used to experimentally probe the reaction mechanism. The reaction of **250** with peroxide **132** followed by acidic fragmentation suggested that an ionic interaction between **132** and **250** was occurring.

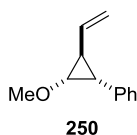


Figure 9.9 Mechanistic Probe Alkene

Overall, DFT calculations and use of a mechanistic probe indicated that an ionic interaction between peroxide (**132**) and alkene was in operation.

## 9.7 Future Work

From the projects contained within this Thesis a number of possible avenues for future investigation emerged.

### 9.7.1 Catalyst Reactivity

From the comparisons between **3** and **38** it emerged that rates of conjugate addition reactions and enamine catalysed reactions are not enhanced by the addition of a *p*-nitrophenyl  $\alpha$ -EWG on the imidazolidinone scaffold. Therefore, a structure activity relationship using a selection of imidazolidinones for these reaction types would make a significant contribution to the area. The preparation and evaluation of  $\alpha$ -substituted imidazolidinones represents an attractive idea to pursue.

### 9.7.2 Chiral Optical Spectroscopy

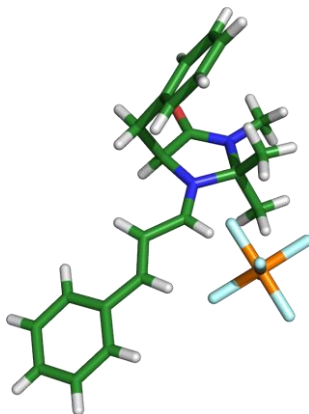
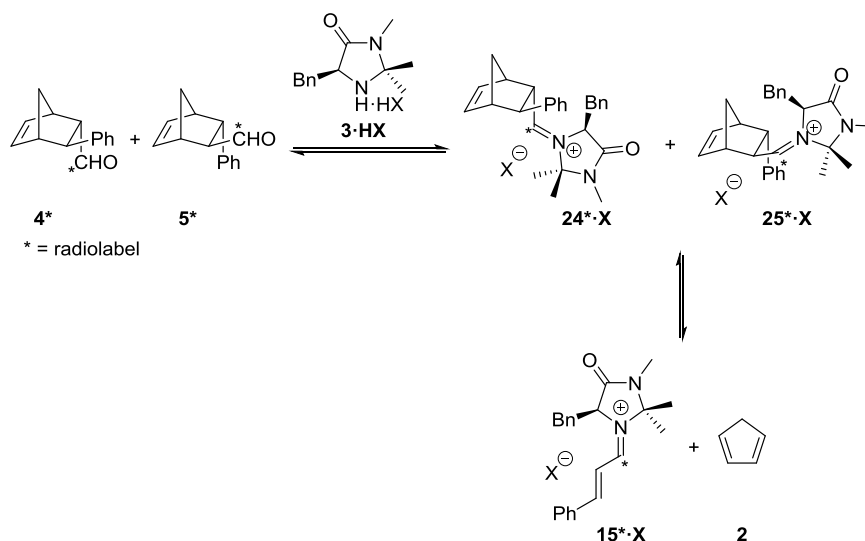


Figure 9.10 Single Crystal X-ray Structure of **15·PF<sub>6</sub>**  
Depicting Low-Energy Conformation **15.E1**

Comparisons between solution phase experimental and computationally determined ROA and VCD spectra of iminium ions were observed to be weak. However, VCD measurements can be performed in the solid-state and the conformation of **15·PF<sub>6</sub>** is known by single crystal X-ray crystallography (Figure 9.10). Therefore, solid state VCD measurements could provide a clean spectrum associated with the lowest energy conformation of the iminium ion which would offer an excellent handle for comparison with the solution-phase spectra. However, obtaining access to a suitably equipped spectrometer may be challenging.

## 9.7.3 Observing the Catalytic Cycle



Scheme 9.3 Radiolabelling Idea to Determine Reversibility of the Catalytic Cycle

Observing the catalytic cycle by ESI-MS eluded to the presence of **24·X** and/or **25·X**. However, it was not certain if this was present due to the catalytic cycle (Figure 9.7) operating in the forward direction. A radiolabelling study could provide insight into this problem. Addition of isotopically labelled **4** (**4\***) and **5** (**5\***) to the reaction mixture containing **3·HX**, cinnamaldehyde (**1**) and cyclopentadiene (**2**) would allow observation of iminium ions resulting from condensation of **3·HX** with **4\*** and/or **5\***. If **24\*·X** and/or **25\*·X** were detected it would indicate that the catalytic cycle can operate in reverse under the conditions used. Additional evidence could be obtained from the detection of **15\*·X** which would indicate that the catalytic cycle can operate in the reverse direction.

## 9.7.4 Amino Acid Dimers

The amino acid dimer architecture has great scope to be expanded. Rendering the structures stable under acidic conditions is key to progress and would provide the opportunity to use the dimers as ligands for transition-metal catalysis. However, all three methylene units in the dimer structure have been observed to be labile which suggests that each would need to be targeted to render the structure stable under acidic conditions. This represents a significant synthetic challenge.

Before embarking on modifications, characterising the nature of the intermediates present under acidic conditions would be of great benefit. Currently it is assumed that they are ionic in nature and that the behaviour of **218** is similar to that of Tröger's base. Obtaining evidence for the nature of these intermediates is essential to employ the correct chemistry to intercept these intermediates and modify the structure. A large amount of work exists on the isomerisation of Tröger's base and due to similarities in structure, applying some of this work to the dimer structure would be a rational starting point.

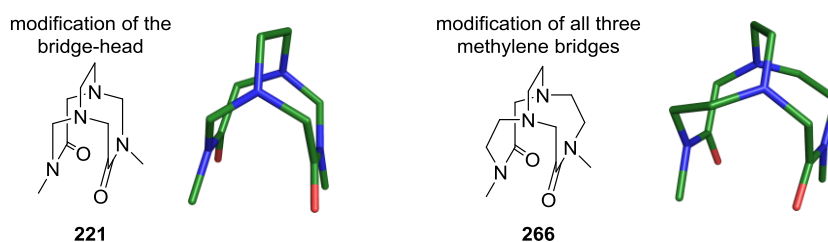


Figure 9.11 Conformational Changes Upon Modification of the Dimer Structure

It should be noted that, upon modification, the shape and conformational preference for the dimer structure may change. Initial DFT calculations (B3LYP/6-31G) indicate that modification of one methylene bridge would lead to the structure retaining the majority of its shape (see **221**). However, modification of all three methylene bridges to ethylene bridges significantly distorts the core conformation (see **266**) and due to the expanded ring-sizes would likely give-rise to a higher number of possible conformations. Therefore, before embarking on a synthetic approach, DFT calculations should be used to fully appreciate the structural changes which modification would bring.

### 9.7.5 Alkene Dihydroxylation

The discovery that cyclopropyl malonyl peroxide (**231**) reacts with alkenes *via* an ionic mechanism provides the possibility for a wide array of chemistry using this reagent. The ionic intermediates (**236** and **237**) could be exploited and a variety of nucleophiles could be used to intercept them. This could provide access to a range of metal-free alkene modification protocols such as oxyamination and



*anti*-dihydroxylation (Figure 9.12). However attractive these ideas first appear, the nucleophilic reagents would need to be chosen carefully so they only react with the ionic intermediates and not the electrophilic peroxide. Work towards an *anti*-dihydroxylation reaction using acetic acid as the nucleophile has already commenced in the group.

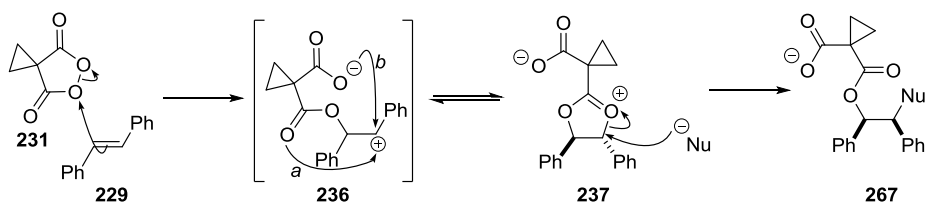


Figure 9.12 Nucleophilic Attack on Ionic Intermediates

In addition to exploiting the ionic nature of the reaction between peroxide **231** and alkenes, DFT calculations showed that the radical anion of cyclopropyl malonyl peroxide is an energetically stable species. Therefore, with careful substrate selection **231** could potentially react *via* a single electron transfer process which could increase the reaction scope of this reagent. Related phthaloyl peroxide **269** has been suggested to react with carbon nanotubes *via* a SET mechanism (Figure 9.13) which gives further backing towards the likelihood of **231** also being able to react through this mechanistic pathway.<sup>113</sup>

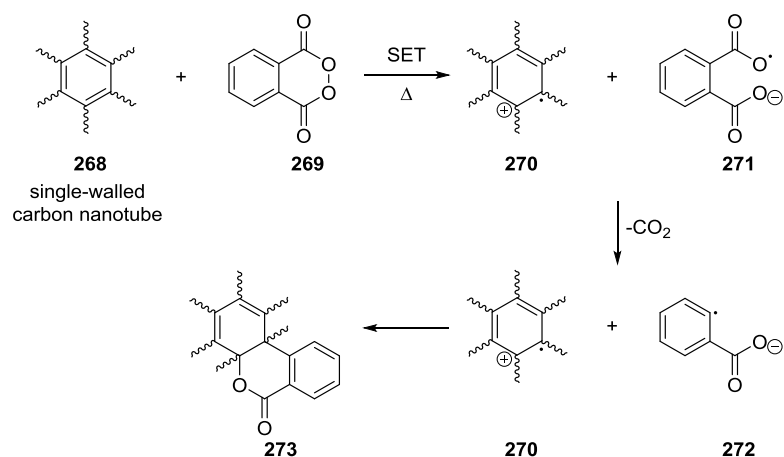


Figure 9.13 Reported SET Interaction Between Phthaloyl Peroxide (**269**) and Single-Walled Carbon Nanotubes (**268**)

# **Experimental**

## 10 Experimental

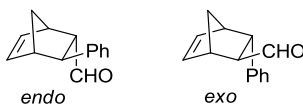
### 10.1 Generic Methods

All reagents and solvents were purchased from Sigma Aldrich, Alfa Aesar, Fisher Scientific or Fluorochem and were used as received. Flash chromatography was performed using Merck Kieselgel 60 H silica. Analytical thin layer chromatography was carried out using aluminium-backed plates coated with Merck Kieselgel 60 GF254. Depending on compound functionality, TLC plates were visualized using either UV light (254 nm), a basic  $\text{KMnO}_4$  dip or an acidic ethanolic 2,4-dinitrophenylhydrazine dip. Nuclear magnetic resonance (NMR) spectra were recorded at 300 K on a Bruker Avance III 400 MHz, Bruker Avance DRX 500 MHz or Bruker Avance II 600 MHz. All spectra were referenced internally to residual solvent signals.  $J$  values were reported in hertz and multiplicities were expressed using usual conventions. Low-resolution mass spectra (MS) were determined on an Agilent 6130 single quadrupole with an APCI/electrospray dual source or ThermoQuest Finnigan LCQ DUO electrospray. High-resolution mass spectra were obtained courtesy of the EPSRC National Mass Spectrometry Facility at Swansea University, Swansea, UK. Infra-red spectra were recorded in the range 4000–600  $\text{cm}^{-1}$  on a Shimadzu IRAffinity-1 equipped with an ATR accessory. Melting points were determined on a Stuart SMP11 and were measured to the nearest 1 °C. Optical rotations were recorded on a PerkinElmer 341 polarimeter. GCMS analysis was performed using an Agilent 7890A GC system, equipped with a 30 m DB5MS column connected to a 5975C inert XL CI MSD with Triple-Axis Detector or Thermo Finnigan Polaris Q equipped with an Agilent DB-5MS UI column connected to an EI MSD. HPLC was performed on an Agilent 1200 series system equipped with an auto mixer, auto sampler, column oven and variable wavelength detector. ROA spectra were recorded on a BioTools ChiralRAMAN II instrument using a 532 nm laser. VCD spectra were recorded on a BioTools ChiralIR II instrument. Single crystal diffraction data were recorded on a diffractometer equipped with a cryostat using graphite monochromated  $\text{Mo K}\alpha$  radiation ( $\lambda(\text{Mo-K}\alpha) = 0.71073 \text{ \AA}$ ) radiation or on a diffractometer using  $\text{Cu}$  ( $\lambda = 1.5418 \text{ \AA}$ ) radiation. All structures were processed and refined using SHELX-97.<sup>114</sup> Selected crystallographic and refinement parameters are given in Appendix A.

## 10.2 Reaction Monitoring and General Procedures

### 10.2.1 Reaction Monitoring

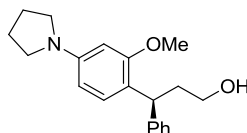
#### *endo*-3-Phenylbicyclo[2.2.1]hept-5-ene-2-carbaldehyde **4** and *exo*-3-Phenylbicyclo[2.2.1]hept-5-ene-2-carbaldehyde **5**



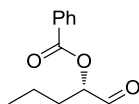
Secondary amine salt (0.25 mmol, 5 mol%) was dissolved in methanol (4.75 mL) and water (0.25 mL). The mixture was stirred at 25 °C. After 5 minutes, cinnamaldehyde (630  $\mu$ L, 5 mmol) was added. After another 10 minutes, freshly distilled cyclopentadiene (1020  $\mu$ L, 12.5 mmol) was added and the reaction timer started. 100  $\mu$ L aliquots were periodically removed and concentrated under reduced pressure (25 °C, 15 torr, 10 minutes). Water (5 mL) was added and extracted with diethyl ether (3  $\times$  5 mL). The combined organics were concentrated under reduced pressure. Chloroform (2 mL) was added followed by a mixture of TFA/water 1:1 (2 mL). The biphasic mixture was vigorously stirred for 2 h. The reaction was quenched with saturated sodium carbonate solution (5 mL) and extracted with diethyl ether (3  $\times$  5 mL). The combined organics were dried over magnesium sulfate and the solvent was removed under reduced pressure to give a yellow oil.  $^1\text{H}$  NMR ( $\text{CDCl}_3$ ) was used to assess reaction conversion from the *CHO* resonances: *exo* 9.93 ppm (1H, d,  $J$  = 2.0 Hz, *CHO*), cinnamaldehyde 9.71 ppm (1H, d,  $J$  = 7.7 Hz, *CHO*) and *endo* 9.60 ppm (1H, d,  $J$  = 2.2 Hz, *CHO*). The Diels-Alder adducts can be isolated by flash chromatography (20% ethyl acetate in petroleum ether) to give a pale yellow viscous oil. *endo/exo* mixture  $\nu_{\text{max}}$  (film)/ $\text{cm}^{-1}$  3414, 2972, 1717; *exo*  $^1\text{H}$  NMR (500 MHz,  $\text{CDCl}_3$ )  $\delta$  9.93 (1H, d,  $J$  = 2.0 Hz, *CHO*), 7.41–7.12 (5H, m, *CH*), 6.35 (1H, dd,  $J$  = 5.5, 3.5 Hz, *HCCH*), 6.09 (1H, dd,  $J$  = 5.5, 2.9 Hz, *HCCH*), 3.77–3.72 (1H, m, *CHPh*), 3.26–3.21 (2H, m,  $\text{CH}_2\text{CH}$ ), 2.62–2.58 (1H, m, *CHCHO*), 1.66–1.55 (2H, m,  $\text{CH}_2$ ); *endo*  $^1\text{H}$  NMR (500 MHz,  $\text{CDCl}_3$ )  $\delta$  9.61 (1H, d,  $J$  = 2.2 Hz, *CHO*), 7.38–7.11 (5H, m, *CH*), 6.43 (1H, dd,  $J$  = 5.6, 3.2 Hz, *HCCH*), 6.19 (1H, dd,  $J$  = 5.6, 2.8 Hz, *HCCH*), 3.35 (1H, br. s, *CHPh*), 3.16–3.09 (1H, m,  $\text{CHCH}_2$ ), 3.03–2.96 (1H, m, *CHCHO*), 1.60–1.55 (2H, m,  $\text{CH}_2$ ); *endo/exo* mixture  $^{13}\text{C}$  NMR (126 MHz,  $\text{CDCl}_3$ )  $\delta$  203.4, 202.8, 143.6, 142.7, 139.3, 136.6, 136.4, 133.9, 128.7, 128.2, 127.9, 127.4,

126.4, 126.3, 60.9, 59.5, 48.5, 48.4, 47.6, 47.2, 45.8, 45.5, 45.5, 45.2;  $m/z$  (EI): 198.1 ( $M^+$ ). Analytical data were in accordance with literature values.<sup>1</sup>

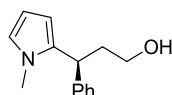
**(S)-3-(2-Methoxy-4-(pyrrolidin-1-yl)phenyl)-3-phenylpropan-1-ol 97**



Secondary amine salt (10 mol%, 0.16 mmol) was added to dichloromethane (2 mL). 1-(3-Methoxyphenyl)pyrrolidine (560 mg, 3.16 mmol) was added and the mixture was stirred for 5 minutes at 25 °C. Cinnamaldehyde (200  $\mu$ L, 1.60 mmol) was added in one portion. Periodically, aliquots (100  $\mu$ L) were removed and added to a mixture of ethanol (0.5 mL) and sodium borohydride (6 mg). After 5 minutes the reduction was quenched with saturated sodium carbonate solution (5 mL) and extracted with dichloromethane (2  $\times$  5 mL). The organics were dried over sodium sulfate. The solvent was removed under reduced pressure and the residue analysed by  $^1\text{H}$  NMR. Using two integrals  $^1\text{H}$  NMR (400 MHz,  $\text{CDCl}_3$ ) 4.53 (1H, dd, product PhCH) and 4.33 (2H, dd, cinnamyl alcohol HOCH<sub>2</sub>) reaction conversion was calculated. The product was isolated using flash chromatography (50% diethyl ether in petroleum ether) to give a colourless oil.  $\nu_{\text{max}}$  (film)/ $\text{cm}^{-1}$  3357, 3056, 3026, 2935, 2879;  $^1\text{H}$  NMR (400 MHz,  $\text{CDCl}_3$ )  $\delta$  7.34–7.25 (4H, m, CH), 7.20–7.14 (1H, m, CH), 6.98 (1H, d,  $J = 8.3$  Hz, CHCH), 6.17 (1H, dd,  $J = 8.3, 2.3$  Hz, CHCH), 6.12 (1H, d,  $J = 2.3$  Hz, CH), 4.53 (1H, dd,  $J = 9.3, 6.7$  Hz, PhCH), 3.86 (3H, s, CH<sub>3</sub>), 3.72–3.52 (2H, m, CH<sub>2</sub>OH), 3.34–3.27 (4H, m, NCH<sub>2</sub>), 2.41–2.12 (2H, m, CH<sub>2</sub>CH<sub>2</sub>OH), 2.05–1.98 (4H, m, NCH<sub>2</sub>CH<sub>2</sub>) 1.89 (1H, s, OH);  $^{13}\text{C}$  NMR (126 MHz,  $\text{CDCl}_3$ )  $\delta$  158.0, 147.8, 145.8, 128.9, 128.2, 128.1, 125.7, 119.9, 104.4, 95.4, 61.5, 55.7, 47.8, 38.6, 38.0, 25.6;  $m/z$  (EI): 311.2 ( $M^+$ ); HRMS (EI): Calculated  $m/z$  for  $\text{C}_{20}\text{H}_{25}\text{NO}_2$ : 311.1880, found  $m/z$ : 311.1876 ( $M^+$ ). Analytical data were consistent with literature values.<sup>49</sup>

**(S)-1-Oxopentan-2-yl benzoate 104**

Secondary amine (20 mol%, 0.23 mmol) and 4-nitrobenzoic acid (38 mg, 0.23 mmol) were dissolved in THF (2 mL). Valeraldehyde (125  $\mu$ L, 1.18 mmol) was added and the reaction was stirred at 25  $^{\circ}$ C. Wet benzoyl peroxide (70%, 402 mg, 1.16 mmol) was added and stirring was maintained at 25  $^{\circ}$ C. 50  $\mu$ L aliquots were periodically taken and diluted into  $\text{CDCl}_3$  (0.55 mL).  $^1\text{H}$  NMR spectroscopy was used to assess reaction conversion.  $^1\text{H}$  NMR (400 MHz,  $\text{CDCl}_3$ ) 9.72 (1H, t, valeraldehyde *CHO*), 9.64 (1H, d, product *CHO*). The product was isolated using flash chromatography (10% ethyl acetate in petroleum ether) to give a colourless oil.  $\nu_{\text{max}}$  (ATR)/ $\text{cm}^{-1}$  2961, 2936, 2874, 2812, 1717;  $^1\text{H}$  NMR (400 MHz,  $\text{CDCl}_3$ )  $\delta$  9.64 (1H, d,  $J = 0.8$  Hz, *CHO*), 8.13–8.08 (2H, m, *CH*), 7.63–7.58 (1H, m, *CH*), 7.51–7.45 (2H, m, *CH*), 5.26–5.21 (1H, m, *OCH*), 1.95–1.87 (2H, m,  $\text{CH}_2$ ), 1.61–1.50 (2H, m,  $\text{CH}_2\text{CH}_3$ ), 1.00 (3H, t,  $J = 7.4$  Hz,  $\text{CH}_3$ );  $^{13}\text{C}$  NMR (101 MHz,  $\text{CDCl}_3$ )  $\delta$  198.7, 166.3, 133.7, 130.0, 129.3, 128.7, 78.7, 31.0, 18.5, 13.9;  $m/z$  (ES): 207.1 ( $\text{M}+\text{H}^+$ ). Analytical data were in accordance with literature values.<sup>50</sup>

**(S)-3-(1-Methyl-1*H*-pyrrol-2-yl)-3-phenylpropan-1-ol 111**

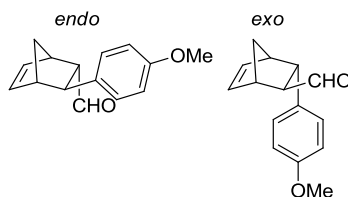
Secondary amine salt (10 mol%, 0.21 mmol) was dissolved in THF (4 mL) and water (0.6 mL). The mixture was stirred at 25  $^{\circ}$ C and after 5 minutes cinnamaldehyde (250  $\mu$ L, 2 mmol) was added. Stirring was continued for 10 minutes before *N*-methyl pyrrole (530  $\mu$ L, 5.97 mmol) was added in one portion. Aliquats (100  $\mu$ L) were periodically taken and added to a mixture of sodium borohydride (5 mg, 0.13 mmol) in ethanol (1 mL). After 15 minutes the reduction was quenched with saturated sodium bicarbonate solution (5 mL) and extracted with dichloromethane ( $2 \times 10$  mL). The organics were dried over sodium sulfate and the solvent removed under reduced pressure. The residue was analysed by  $^1\text{H}$  NMR to determine reaction conversion using resonances: 4.33 ppm (2H, dd,  $\text{CH}_2\text{OH}$ ) from cinnamyl alcohol and 4.15 (1H, t, *PhCH*) from the product. The product was isolated using flash

chromatography (16% ethyl acetate in petroleum ether) as a colourless oil.  $\nu_{\max}$  (ATR)/ $\text{cm}^{-1}$  3246, 2965, 2930, 2864;  $^1\text{H}$  NMR (500 MHz,  $\text{CDCl}_3$ )  $\delta$  7.34–7.28 (2H, m, CH), 7.24–7.17 (3H, m, CH), 6.58–6.54 (1H, m, CH), 6.20–6.14 (2H, m, CH), 4.15 (1H, app. t,  $J = 7.6$  Hz, PhCH), 3.74–3.57 (2H, m,  $\text{CH}_2\text{OH}$ ), 3.32 (3H, s,  $\text{NCH}_3$ ), 2.42–2.31 (1H, m, CHH), 2.17–2.07 (1H, m, CHH), 1.78 (1H, s, OH);  $^{13}\text{C}$  NMR (126 MHz,  $\text{CDCl}_3$ )  $\delta$  143.6, 135.0, 128.6, 128.0, 126.4, 121.9, 106.4, 105.8, 60.6, 39.5, 39.0, 33.9;  $m/z$  (ES): 216.0 ( $\text{M}+\text{H}^+$ ). Analytical data were in accordance with literature values.<sup>15</sup>

### 10.2.2 General Procedure for Cinnamaldehyde Screening

Imidazolidinone hydrochloride salt (0.1 mmol, 5 mol%) was dissolved in a 19:1 methanol/water mixture (2 mL). The flask was placed into a 25 °C oil bath. The appropriate cinnamaldehyde (2.0 mmol) was added and the mixture was stirred for 10 minutes before freshly distilled cyclopentadiene (420  $\mu\text{L}$ , 5.0 mmol) was added in one portion. The reaction mixture was stirred until the cinnamaldehyde had been consumed (monitored by TLC) and then the volatiles were removed under reduced pressure. The residue was taken up into chloroform (10 mL) and water (10 mL) and the aqueous layer was extracted with chloroform ( $2 \times 10$  mL). The combined organics were dried over sodium sulfate and the solvent was removed under reduced pressure. Chloroform (2 mL), water (1 mL) and TFA (1 mL) were added and the biphasic mixture was vigorously stirred for 2 hours. Potassium carbonate (20 mL) was added and the mixture was extracted with chloroform ( $3 \times 10$  mL). The combined organics were dried over sodium sulfate and the solvent was removed under reduced pressure. The products were isolated using flash chromatography (10% ethyl acetate in petroleum ether) as oils.

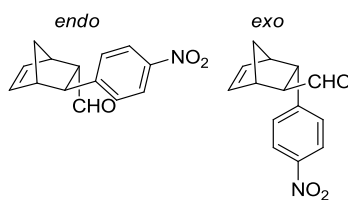
***endo*-3-(4-Methoxyphenyl)bicyclo[2.2.1]hept-5-ene-2-carbaldehyde 67 and *exo*-3-(4-Methoxyphenyl)bicyclo[2.2.1]hept-5-ene-2-carbaldehyde 68**



Prepared using the general procedure.

*endo/exo* mixture  $\nu_{\max}$  (film)/ $\text{cm}^{-1}$ : 2965, 2934, 2907, 2833, 1712; *exo*  $^1\text{H}$  NMR (500 MHz,  $\text{CDCl}_3$ )  $\delta$  9.92 (1H, d,  $J = 2.1$  Hz, CHO), 7.10–7.06 (2H, m, CHCHCOMe), 6.83–6.79 (2H, m, CHCOMe), 6.35 (1H, dd,  $J = 5.6, 3.2$  Hz, HCCH), 6.08 (1H, dd,  $J = 5.6, 2.9$  Hz, HCCH), 3.78 (3H, s,  $\text{CH}_3$ ), 3.67 (1H, dd,  $J = 5.1, 3.7$  Hz, CH), 3.22 (1H, s, CH), 3.18 (1H, s, CH), 2.56–2.53 (1H, m, CH), 1.64–1.60 (1H, m, CHH), 1.58–1.54 (1H, m, CHH); *endo*  $^1\text{H}$  NMR (500 MHz,  $\text{CDCl}_3$ )  $\delta$  9.59 (1H, d,  $J = 2.3$  Hz, CHO), 7.22–7.18 (2H, m, CHCHCOMe), 6.88–6.84 (2H, m, CHCOMe), 6.42 (1H, dd,  $J = 5.6, 3.2$  Hz, HCCH), 6.17 (1H, dd,  $J = 5.6, 2.8$  Hz, HCCH), 3.80 (3H, s,  $\text{CH}_3$ ), 3.33 (1H, s, CH), 3.08 (1H, s, CH), 3.04 (1H, d,  $J = 4.5$  Hz, CH), 2.96–2.93 (1H, m, CH), 1.80 (1H, app. d,  $J = 8.7$  Hz, CHH), 1.64–1.60 (1H, m, CHH); *endo/exo* mixture  $^{13}\text{C}$  NMR (126 MHz,  $\text{CDCl}_3$ )  $\delta$  203.8, 203.0, 158.3, 158.1, 139.4, 136.7, 136.4, 135.7, 134.8, 133.8, 128.9, 128.4, 114.1, 113.7, 61.0, 59.8, 55.4, 55.4, 48.8, 48.7, 47.7, 47.2, 45.6, 45.2, 45.2, 44.9;  $m/z$  of corresponding alcohol (CD): 231.1 ( $\text{M}+\text{H}^+$ ). Analytical data were in accordance with literature values.<sup>115</sup>

***endo*-3-(4-Nitrophenyl)bicyclo[2.2.1]hept-5-ene-2-carbaldehyde 69 and *exo*-3-(4-Nitrophenyl)bicyclo[2.2.1]hept-5-ene-2-carbaldehyde 70**



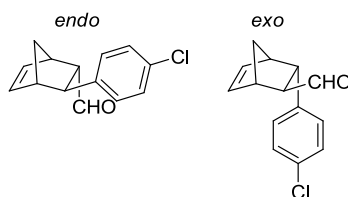
Prepared using the general procedure.

*endo/exo* mixture  $\nu_{\max}$  (film)/ $\text{cm}^{-1}$ : 3063, 2972, 2943, 2872, 2818, 2717, 1713, 1514, 1342; *exo*:  $^1\text{H}$  NMR (500 MHz,  $\text{CDCl}_3$ )  $\delta$  9.90 (1H, d,  $J = 1.4$  Hz, CHO), 8.07 (2H, d,  $J = 8.7$  Hz, CHCNO<sub>2</sub>), 7.28 (2H, d,  $J = 8.7$  Hz, CHCHCNO<sub>2</sub>), 6.39 (1H, dd,  $J =$



5.6, 3.2 Hz, *HCCH*), 6.03 (1H, dd,  $J = 5.6, 2.8$  Hz, *HCCH*), 3.88–3.84 (1H, m, *PhCH*), 3.28 (1H, s, *CH*), 3.24 (1H, s, *CH*), 2.61 (1H, app. d,  $J = 5.1$  Hz, *CHCHO*), 1.59 (2H, br. s, *CH*<sub>2</sub>); *endo*: <sup>1</sup>H NMR (500 MHz, CDCl<sub>3</sub>) δ 9.62 (1H, d,  $J = 1.4$  Hz, *CHO*), 8.13 (2H, d,  $J = 8.6$  Hz, *CHCNO*<sub>2</sub>), 7.41 (2H, d,  $J = 8.6$  Hz, *CHCHCNO*<sub>2</sub>), 6.42 (1H, dd,  $J = 5.6, 3.3$  Hz, *HCCH*), 6.18 (1H, dd,  $J = 5.6, 3.0$  Hz, *HCCH*), 3.41 (1H, s, *PhCH*), 3.19 (1H, d,  $J = 4.9$  Hz, *CH*), 3.17 (1H, s, *CH*), 2.96–2.93 (1H, m, *CH*), 1.77–1.66 (2H, m, *CH*<sub>2</sub>); *endo/exo* mixture: <sup>13</sup>C NMR (126 MHz, CDCl<sub>3</sub>) δ 202.2, 201.6, 151.7, 150.7, 146.6, 146.5, 139.1, 137.1, 136.1, 134.1, 128.8, 128.3, 123.9, 123.4, 61.2, 59.6, 48.5, 48.0, 47.7, 47.2, 45.7, 45.6, 45.2, 45.1; *m/z* of corresponding alcohol (CI): 246.1 (M+H<sup>+</sup>). Analytical data were consistent with literature values.<sup>116</sup>

***endo*-3-(4-Chloro)bicyclo[2.2.1]hept-5-ene-2-carbaldehyde 71 and *exo*-3-(4-Chloro)bicyclo[2.2.1]hept-5-ene-2-carbaldehyde 72**

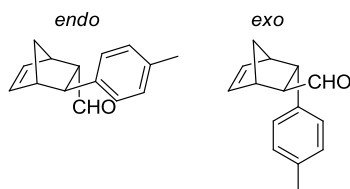


Prepared using the general procedure.

*endo/exo* mixture  $\nu_{\max}$  (film)/cm<sup>-1</sup>: 3061, 2970, 2872, 2810, 2712, 1715; *exo*: <sup>1</sup>H NMR (500 MHz, CDCl<sub>3</sub>) δ 9.91 (1H, d,  $J = 1.8$  Hz, *CHO*), 7.24–7.20 (2H, m, *CH*), 7.10–7.06 (2H, m, *CH*), 6.36 (1H, dd,  $J = 5.6, 3.2$  Hz, *HCCH*), 6.06 (1H, dd,  $J = 5.6, 2.9$  Hz, *HCCH*), 3.71 (1H, dd,  $J = 5.1, 3.6$  Hz, *PhCH*), 3.26–3.22 (1H, m, *CH*), 3.19 (1H, br. s, *CH*), 2.52–2.55 (1H, m, *CHCHO*), 1.62–1.56 (2H, m, *CH*<sub>2</sub>); *endo*: <sup>1</sup>H NMR (500 MHz, CDCl<sub>3</sub>) δ 9.60 (1H, d,  $J = 2.1$  Hz, *CHO*), 7.30–7.26 (2H, m, *CH*), 7.22–7.19 (2H, m, *CH*), 6.42 (1H, dd,  $J = 5.7, 3.2$  Hz, *HCCH*), 6.18 (1H, dd,  $J = 5.7, 2.8$  Hz, *HCCH*), 3.36 (1H, s, *PhCH*), 3.12–3.08 (1H, m, *CH*), 3.07 (1H, d,  $J = 4.1$  Hz, *CH*), 2.95–2.90 (1H, m, *CHCHO*), 1.77 (1H, app. d,  $J = 8.7$  Hz, *CHH*), 1.67–1.63 (1H, m, *CHH*); *endo/exo* mixture: <sup>13</sup>C NMR (126 MHz, CDCl<sub>3</sub>) δ 203.1, 202.4, 142.2, 141.2, 139.3, 136.6, 136.4, 133.9, 132.2, 132.1, 129.3, 128.8, 128.8, 128.3, 61.1, 59.7, 48.5, 48.4, 47.7, 47.2, 45.6, 45.2, 45.2, 44.9; *m/z* (EI): 232.0 (M<sup>+</sup>); HRMS

(EI) calculated for  $C_{14}H_{13}OCl^{35}$  232.0649 ( $M^+$ ), found 232.0652. Analytical data were consistent with literature values.<sup>116</sup>

***endo*-3-(4-Methyl)bicyclo[2.2.1]hept-5-ene-2-carbaldehyde 72 and *exo*-3-(4-Methyl)bicyclo[2.2.1]hept-5-ene-2-carbaldehyde 73**

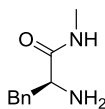


Prepared using the general procedure.

*endo/exo* mixture  $\nu_{\max}$  (film)/ $cm^{-1}$ : 2968, 2941, 2918, 2874, 2912, 2710, 1715; *exo*:  $^1H$  NMR (500 MHz,  $CDCl_3$ )  $\delta$  9.92 (1H, d,  $J = 2.1$  Hz, CHO), 7.09–7.03 (4H, m, CH), 6.34 (1H, dd,  $J = 5.7, 3.2$  Hz, HCCH), 6.08 (1H, dd,  $J = 5.7, 2.9$  Hz, HCCH), 3.69 (1H, dd,  $J = 5.2, 3.2$  Hz, PhCH), 3.24–3.19 (2H, m, CH), 2.57 (1H, app. dt,  $J = 5.2, 1.8$  Hz, CHCHO), 2.31 (3H, s,  $CH_3$ ), 1.64–1.53 (2H, m,  $CH_2$ ); *endo*:  $^1H$  NMR (500 MHz,  $CDCl_3$ )  $\delta$  9.60 (1H, d,  $J = 2.3$  Hz, CHO), 7.20–7.11 (4H, m, CH), 6.42 (1H, dd,  $J = 5.6, 3.2$  Hz, HCCH), 6.17 (1H, dd,  $J = 5.6, 2.8$  Hz, HCCH), 3.33 (1H, s, PhCH), 3.10 (1H, s, CH), 3.05 (1H, d,  $J = 4.6$  Hz, CH), 2.98–2.95 (1H, m, CHCHO), 2.33 (3H, s,  $CH_3$ ), 1.81 (1H, app. d,  $J = 8.7$  Hz, CHH), 1.64–1.53 (1H, m, CHH); *endo/exo* mixture:  $^{13}C$  NMR (126 MHz,  $CDCl_3$ )  $\delta$  203.7, 203.0, 140.6, 139.7, 139.3, 136.7, 136.4, 136.0, 135.9, 133.9, 129.4, 129.0, 127.9, 127.4, 60.9, 59.6, 48.7, 48.5, 47.7, 47.2, 45.6, 45.5, 45.2, 21.0;  $m/z$  of corresponding alcohol (CI): 215.1 ( $M+H^+$ ).

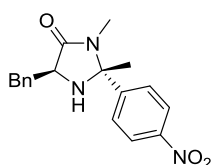
### 10.3 Compounds

#### L-Phenylalanine *N*-methyl amide **45**<sup>78</sup>



L-Phenylalanine ethyl ester hydrochloride (30.0 g, 131 mmol) was stirred in an ethanolic solution of methylamine 33 wt.% (150 mL, 1.2 mol) for 72 hours at ambient temperature. The solvent was removed under reduced pressure. The resultant slurry was taken up in saturated sodium carbonate (50 mL) and extracted with chloroform (3 × 50 mL). The combined organic extracts were dried over anhydrous potassium carbonate and the solvent removed under reduced pressure to give a white solid. The residue was recrystallized from ethyl acetate and petroleum ether to give the product as white needles (17.6 g, 75%). mp: 67–69 °C [lit.<sup>78</sup> 58–60 °C];  $[\alpha]_D^{20} = -89.6$  (c=1, CHCl<sub>3</sub>);  $\nu_{\max}$  (film)/cm<sup>-1</sup> 3371, 3345, 3290, 2939, 2875, 1644; <sup>1</sup>H NMR (400 MHz, CDCl<sub>3</sub>)  $\delta$  7.47–7.12 (6H, m, 5 × CH, NH), 3.54 (1H, dd, *J* = 9.5, 3.9 Hz, CH), 3.22 (1H, dd, *J* = 13.7, 3.9 Hz, CHH), 2.83 (3H, d, *J* = 5.0 Hz, NCH<sub>3</sub>), 2.60 (1H, dd, *J* = 13.7, 9.5 Hz, CHH), 1.38 (2H, s, NH<sub>2</sub>); <sup>13</sup>C NMR (101 MHz, CDCl<sub>3</sub>)  $\delta$  174.8, 138.0, 129.3, 128.7, 126.8, 56.5, 41.0, 25.8; *m/z* (ES): 179.1 (M+H<sup>+</sup>). Analytical data were in accordance with literature values.<sup>78</sup>

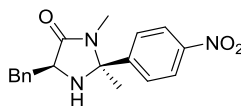
#### (2*R*,5*S*)-5-Benzyl-2,3-dimethyl-2-(4-nitrophenyl)imidazolidin-4-one **38**<sup>40</sup>



L-Phenylalanine-*N*-methyl amide (3.86 g, 21.7 mmol) was dissolved in DMF (20 mL). 4-Nitroacetophenone (3.96 g, 24 mmol) was added followed by methanesulfonic acid (0.3 mL, 4.63 mmol, 20 mol%). The mixture was separated into two microwave vials and subjected to microwave irradiation at 150 °C for 30 minutes. The contents of the two vials were combined and concentrated under reduced pressure. Chloroform (40 mL) and saturated sodium carbonate solution (40 mL) were added. The aqueous layer was extracted with chloroform (2 × 40 mL) and dried over anhydrous potassium carbonate. The solvent was removed under reduced

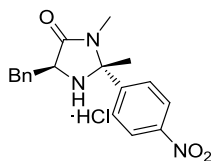
pressure and the residue purified by flash chromatography (20% ethyl acetate in petroleum ether) to give the title compound as an orange oil (500 mg, 7%).  $[\alpha]_{\text{D}}^{20} = +24.2$  ( $c=2.0$ , MeOH);  $\nu_{\text{max}}$  (ATR)/ $\text{cm}^{-1}$  3350, 3028, 2924, 2855, 1688;  $^1\text{H}$  NMR (400 MHz,  $\text{CDCl}_3$ )  $\delta$  8.26–8.16 (2H, m, CH), 7.51–7.44 (2H, m, CH), 7.36–7.22 (5H, m, CH), 3.83 (1H, app. t,  $J = 5.3$  Hz, CH), 3.18 (1H, dd,  $J = 14.1, 4.6$  Hz, CHH), 3.11 (1H, dd,  $J = 14.1, 6.5$  Hz, CHH), 2.80 (3H, s,  $\text{NCH}_3$ ), 2.04 (1H, s, NH), 1.57 (3H, s,  $\text{CH}_3$ );  $^{13}\text{C}$  NMR (101 MHz,  $\text{CDCl}_3$ )  $\delta$  173.7, 150.0, 147.8, 136.9, 129.8, 128.8, 127.1, 126.5, 124.2, 78.2, 59.1, 37.7, 26.4, 26.1;  $m/z$  (ES/APCI): 326.2 ( $\text{M}+\text{H}^+$ ).

**(2*S*,5*S*)-5-Benzyl-2,3-dimethyl-2-(4-nitrophenyl)imidazolidin-4-one 47<sup>40</sup>**



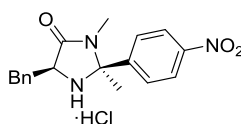
L-Phenylalanine-*N*-methyl amide (3.86 g, 21.7 mmol) was dissolved in DMF (20 mL). 4-Nitroacetophenone (3.96 g, 24.0 mmol) was added followed by methanesulfonic acid (0.3 mL, 4.6 mmol, 20 mol%). The mixture was separated into two microwave vials and subjected to microwave irradiation at 150 °C for 30 minutes. The contents of the two vials were combined and concentrated under reduced pressure. Chloroform (40 mL) and saturated sodium carbonate solution (40 mL) were added. The aqueous layer was extracted with chloroform (2 × 40 mL) and dried over anhydrous potassium carbonate. The solvent was removed under reduced pressure and the residue was purified using flash chromatography (20% ethyl acetate in petroleum ether) to give the title compound as an orange oil (796 mg, 11%).  $[\alpha]_{\text{D}}^{20} = -97.5$  ( $c=1.2$ ,  $\text{CHCl}_3$ );  $\nu_{\text{max}}$  (ATR)/ $\text{cm}^{-1}$  3320, 3026, 2976, 2924, 2857, 1688;  $^1\text{H}$  NMR (400 MHz,  $\text{CDCl}_3$ )  $\delta$  8.06–8.01 (2H, m, CH), 7.33–7.27 (3H, m, CH), 7.21–7.16 (2H, m, CH), 7.06–7.01 (2H, m, CH), 3.97 (1H, app. t,  $J = 4.9$  Hz, CH), 3.25 (1H, dd,  $J = 13.9, 5.5$  Hz, CHH), 3.05 (1H, dd,  $J = 13.9, 4.7$  Hz, CHH), 2.54 (3H, s,  $\text{NCH}_3$ ), 1.99 (1H, s, NH), 1.75 (3H, s,  $\text{CH}_3$ );  $^{13}\text{C}$  NMR (101 MHz,  $\text{CDCl}_3$ )  $\delta$  173.4, 149.34, 147.9, 136.8, 130.1, 129.0, 127.4, 127.2, 123.9, 78.3, 59.4, 36.8, 26.2, 23.3;  $m/z$  (ES/APCI): 326.2 ( $\text{M}+\text{H}^+$ ).

**(2*R*,5*S*)-5-Benzyl-2,3-dimethyl-2-(4-nitrophenyl)imidazolidin-4-one hydrochloride 38·HCl**



(2*R*,5*S*)-5-Benzyl-2,3-dimethyl-2-(4-nitrophenyl)imidazolidin-4-one (500 mg, 1.54 mmol) was dissolved in diethyl ether (50 mL). Hydrogen chloride gas was bubbled through the mixture for 30 minutes. The precipitated product was recovered on a sinter, washed with diethyl ether (20 mL) and dried under reduced pressure to give a cream solid (448 mg, 81%). mp: 153–155 °C;  $[\alpha]_{\text{D}}^{20} = +36.4$  (c=2.0, MeOH);  $\nu_{\text{max}}$  (ATR)/ $\text{cm}^{-1}$  1732;  $^1\text{H}$  NMR (400 MHz,  $\text{CDCl}_3$ )  $\delta$  8.26 (2H, d,  $J = 8.8$  Hz, CH), 7.58 (2H, d,  $J = 8.8$  Hz, CH), 7.44–7.27 (5H, m, CH), 4.28 (1H, app. t,  $J = 5.7$  Hz, CH), 3.43 (1H, dd,  $J = 15.1, 5.7$  Hz, CHH), 3.31 (1H, dd,  $J = 15.1, 5.7$  Hz, CHH), 2.80 (3H, s,  $\text{NCH}_3$ ), 1.82 (3H, s,  $\text{CH}_3$ );  $^{13}\text{C}$  NMR (101 MHz,  $\text{CDCl}_3$ )  $\delta$  167.5, 149.3, 140.9, 134.3, 130.1, 129.1, 128.3, 128.1, 124.6, 79.3, 58.0, 34.6, 26.6, 23.3;  $m/z$  (ES/APCI): 326.1 (M-Cl<sup>-</sup>). HRMS (ES) calculated for  $\text{C}_{18}\text{H}_{20}\text{O}_3\text{N}_3$  326.1499 (M+H<sup>+</sup>), found 326.1498.

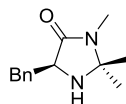
**(2*S*,5*S*)-5-Benzyl-2,3-dimethyl-2-(4-nitrophenyl)imidazolidin-4-one hydrochloride 47·HCl**



(2*S*,5*S*)-5-Benzyl-2,3-dimethyl-2-(4-nitrophenyl)imidazolidin-4-one (796 mg, 2.45 mmol) was dissolved in diethyl ether (60 mL). Hydrogen chloride gas was bubbled through the mixture for 30 minutes. The precipitated product was recovered on a sinter, washed with diethyl ether (20 mL) and dried under reduced pressure to give a cream solid (638 mg, 72%). mp: 139–141 °C;  $[\alpha]_{\text{D}}^{20} = -118.2$  (c=1.1, MeOH);  $\nu_{\text{max}}$  (ATR)/ $\text{cm}^{-1}$  2913, 2887, 1730;  $^1\text{H}$  NMR (400 MHz, MeOD)  $\delta$  8.38–8.27 (2H, m, CH), 7.73–7.63 (2H, m, CH), 7.42–7.22 (5H, m, CH), 4.72 (1H, dd,  $J = 8.7, 4.2$  Hz, CH), 3.45 (1H, dd,  $J = 15.2, 4.2$  Hz, CHH), 3.17 (dd,  $J = 15.2, 8.7$  Hz, CHH), 2.81 (3H, s,  $\text{NCH}_3$ ), 2.15 (3H, s,  $\text{CH}_3$ );  $^{13}\text{C}$  NMR (101 MHz, MeOD)  $\delta$  169.9, 150.4,

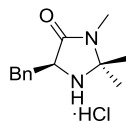
143.2, 136.4, 130.4, 130.0, 130.0, 128.6, 125.4, 81.0, 60.1, 35.7, 27.5, 21.3;  $m/z$  (ES/APCI): 326.1 (M-Cl<sup>-</sup>). 128.3, 128.1, 124.6, 79.3, 58.0, 34.6, 26.6, 23.3;  $m/z$  (ES/APCI): 326.1 (M-Cl<sup>-</sup>). HRMS (ES) calculated for C<sub>18</sub>H<sub>20</sub>O<sub>3</sub>N<sub>3</sub> 326.1499 (M+H<sup>+</sup>), found 326.1490.

**(S)-5-Benzyl-2,2,3-trimethylimidazolidin-4-one 3<sup>36</sup>**



L-Phenylalanine-*N*-methyl amide (2.00 g, 11.2 mmol) was dissolved in acetone (10 mL) and methanol (30 mL). A small crystal of *p*-toluenesulfonic acid (<1 mg) was added and the mixture was heated under reflux for 18 h. The solvent was removed under reduced pressure and the residue taken up in chloroform (30 mL) and saturated sodium carbonate solution (30 mL). The aqueous layer was extracted with chloroform (2 × 30 mL) and the combined organics were dried over potassium carbonate. The solvent was removed under reduced pressure to give the target compound as a pale yellow oil (2.40 g, quant.).  $[\alpha]_D^{20} = -33.5$  (c=1.3, MeOH);  $\nu_{\max}$  (film)/cm<sup>-1</sup> 3473, 3329, 3060, 3030, 2975, 2929, 1685; <sup>1</sup>H NMR (400 MHz, CDCl<sub>3</sub>)  $\delta$  7.38–7.14 (5H, m, CH), 3.82 (1H, dd,  $J = 6.5, 4.5$  Hz, CH), 3.17 (1H, dd,  $J = 14.2, 4.5$  Hz, CHH), 3.03 (1H, dd,  $J = 14.2, 6.5$  Hz, CHH), 2.77 (3H, s, NCH<sub>3</sub>), 1.28 (3H, s, CCH<sub>3</sub>), 1.18 (3H, s, CCH<sub>3</sub>); <sup>13</sup>C NMR (126 MHz, CDCl<sub>3</sub>)  $\delta$  173.7, 137.6, 129.9, 129.0, 127.2, 75.9, 59.7, 37.7, 27.6, 25.7, 25.6;  $m/z$  (APCI): 219.2 (M+H<sup>+</sup>). Analytical data were in accordance with literature values.<sup>78</sup>

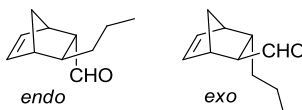
**(S)-5-Benzyl-2,2,3-trimethylimidazolidin-4-one hydrochloride 3·HCl**



(S)-5-Benzyl-2,2,3-trimethylimidazolidin-4-one (2.40 g, 11.0 mmol) was dissolved in diethyl ether (150 mL). Hydrogen chloride gas was bubbled through the solution for 30 minutes. The precipitate was recovered on a sinter and washed with diethyl ether (50 mL). The white powder was dried under reduced pressure (2.02 g, 72%). mp: 104–106 °C  $[\alpha]_D^{20} = -71.5$  (c=1.3, MeOH);  $\nu_{\max}$  (ATR)/cm<sup>-1</sup> 3416, 3380, 1710;

$^1\text{H}$  NMR (400 MHz, MeOD)  $\delta$  7.49–7.27 (5H, m, CH), 4.67 (1H, dd,  $J = 10.7, 3.5$  Hz, CH), 3.53 (1H, dd,  $J = 15.2, 3.5$  Hz, CHH), 3.09 (1H, dd,  $J = 15.2, 10.7$  Hz, CHH), 2.92 (3H, s,  $\text{NCH}_3$ ), 1.75 (3H, s,  $\text{CH}_3$ ), 1.60 (3H, s,  $\text{CH}_3$ );  $^{13}\text{C}$  NMR (101 MHz, MeOD)  $\delta$  170.4, 139.2, 132.9, 132.7, 131.3, 81.7, 62.3, 37.5, 28.3, 26.9, 24.9;  $m/z$  (ES): 219.0 (M-Cl). Analytical data were in accordance with literature values.<sup>1</sup>

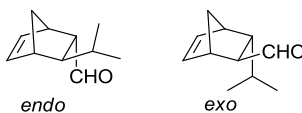
***endo*-3-Propylbicyclo[2.2.1]hept-5-ene-2-carbaldehyde 51 and *exo*-3-Propylbicyclo[2.2.1]hept-5-ene-2-carbaldehyde 52**



Secondary amine salt (0.1 mmol, 1 mol%) was dissolved in methanol (9.5 mL) and water (0.5 mL). The mixture was stirred at 25 °C. *trans*-2-Hexenal (1.16 mL, 10 mmol) was added and the mixture stirred for 10 minutes before freshly distilled cyclopentadiene (2.00 mL, 25 mmol) was added. After 18 h the solvent was removed under reduced pressure (100 mbar, 25 °C). Water (20 mL) and diethyl ether (20 mL) were added to the residue and the aqueous layer extracted with diethyl ether ( $2 \times 20$  mL). The organics were dried over sodium sulfate and the solvent removed under reduced pressure (100 mbar, 25 °C). Chloroform (4 mL) was added to the residue followed by a 1:1 water and TFA mixture (4 mL). The biphasic mixture was vigorously stirred for 2 hours. The reaction was then quenched with saturated sodium carbonate solution and the aqueous layer extracted with diethyl ether ( $3 \times 20$  mL). The combined organics were dried over sodium sulfate and the solvent removed under reduced pressure (100 mbar, 25 °C). The product was isolated by flash chromatography (5% diethyl ether in petroleum ether) to give a colourless oil.  $\nu_{\text{max}}$  (ATR)/ $\text{cm}^{-1}$ : 2957, 2918, 2870, 1717; *exo*  $^1\text{H}$  NMR (400 MHz,  $\text{CDCl}_3$ )  $\delta$  9.77 (1H, d,  $J = 2.7$  Hz, CHO), 6.20 (1H, dd,  $J = 5.6, 3.1$  Hz, HCCH), 6.13 (1H, dd,  $J = 5.6, 2.9$  Hz, HCCH), 3.01 (1H, s,  $J = 1.3$  Hz, CHCH<sub>2</sub>), 2.87 (1H, s, CHCH<sub>2</sub>), 2.32–2.24 (1H, m, CHCH<sub>2</sub>CH<sub>2</sub>), 1.77–1.73 (1H, m, CHCHO), 1.55–1.04 (6H, m, CHCH<sub>2</sub>CH, CH<sub>2</sub>CH<sub>2</sub>), 0.90 (3H, t,  $J = 7.1$  Hz, CH<sub>3</sub>); *endo*  $^1\text{H}$  NMR (400 MHz,  $\text{CDCl}_3$ )  $\delta$  9.36 (1H, d,  $J = 3.4$  Hz, CHO), 6.27 (1H, dd,  $J = 5.7, 3.2$  Hz, HCCH), 6.05 (1H, dd,  $J = 5.7, 2.8$  Hz, HCCH), 3.11 (1H, s, CHCH<sub>2</sub>), 2.66 (1H, d,  $J = 1.5$  Hz, CHCH<sub>2</sub>), 2.37 (1H, dd,  $J = 7.8, 3.4$  Hz, CHCHO), 1.71–1.65 (1H, m, CHCH<sub>2</sub>CH<sub>2</sub>), 1.56–1.03 (6H,

m, CHCH<sub>2</sub>CH, CH<sub>2</sub>CH<sub>2</sub>), 0.90 (3H, t,  $J = 7.1$  Hz, CH<sub>3</sub>). *endo* and *exo* mixture: <sup>13</sup>C NMR (101 MHz, CDCl<sub>3</sub>) δ 205.1, 204.0, 138.8, 136.1, 135.9, 132.8, 60.0, 58.8, 47.2, 47.0, 46.5, 45.7, 45.1, 44.8, 41.9, 41.6, 38.0, 36.4, 21.6, 21.5, 14.1;  $m/z$  (CI): 181 (M<sup>+</sup>CH<sub>5</sub>), 163 (M-H<sup>-</sup>). Analytical data were in accordance with literature values.<sup>1</sup>

***endo*-3-Isopropylbicyclo[2.2.1]hept-5-ene-2-carbaldehyde 53 and *exo*-3-Isopropylbicyclo[2.2.1]hept-5-ene-2-carbaldehyde 54**

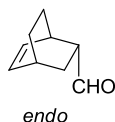


Secondary amine salt (0.1 mmol, 1 mol%) was dissolved in methanol (9.5 mL) and water (0.5 mL). The mixture was stirred at 25 °C. *trans*-4-Methyl-2-hexenal (1.16 mL, 10 mmol) was added and the mixture stirred for 10 minutes before freshly distilled cyclopentadiene (2.00 mL, 25 mmol) was added. After 18 h the solvent was removed under reduced pressure (100 mbar, 25 °C). Water (20 mL) and diethyl ether (20 mL) were added to the residue and the aqueous layer extracted with diethyl ether (2 × 20 mL). The organics were dried over sodium sulfate and the solvent removed under reduced pressure (100 mbar, 25 °C). Chloroform (4 mL) was added to the residue followed by a 1:1 water and TFA mixture (4 mL). The biphasic mixture was vigorously stirred for 2 hours. The reaction was then quenched with saturated sodium carbonate solution and the aqueous layer extracted with diethyl ether (3 × 20 mL). The combined organics were dried over sodium sulfate and the solvent removed under reduced pressure (100 mbar, 25 °C). The product was isolated by flash chromatography (5% diethyl ether in petroleum ether) to give a colourless oil.  $\nu_{\max}$  (ATR)/cm<sup>-1</sup>: 2957, 2911, 2895, 2870, 1701; *exo* <sup>1</sup>H NMR (400 MHz, CDCl<sub>3</sub>) δ 9.78 (1H, d,  $J = 2.6$  Hz, CHO), 6.19 (1H, dd,  $J = 5.6, 3.1$  Hz, HCCH), 6.15 (1H, dd,  $J = 5.6, 2.8$  Hz, HCCH), 3.04–3.00 (1H, m, CH), 2.96 (1H, s, CH), 1.92–1.84 (2H, m, CHCHO, CHH), 1.51–1.40 (2H, m, CHH, CH), 1.08–0.97 (1H, m, CH(CH<sub>3</sub>)<sub>2</sub>), 0.94 (3H, d,  $J = 6.2$  Hz, CH<sub>3</sub>), 0.84 (3H, d,  $J = 6.4$  Hz, CH<sub>3</sub>); *endo* <sup>1</sup>H NMR (400 MHz, CDCl<sub>3</sub>) δ 9.36 (1H, d,  $J = 3.4$  Hz, CHO), 6.26 (1H, dd,  $J = 5.7, 3.3$  Hz, HCCH), 6.06 (1H, dd,  $J = 5.7, 2.8$  Hz, HCCH), 3.11 (1H, s, CH), 2.87–2.83 (1H, m, CH), 2.51–2.47 (1H, m, CHCHO), 1.51–1.39 (1H, m, CHCH), 1.34–1.29 (1H, m, CH(CH<sub>3</sub>)<sub>2</sub>), 1.01 (1H, d,  $J = 6.5$  Hz, CH<sub>3</sub>), 0.91 (1H, d,  $J = 6.6$  Hz, CH<sub>3</sub>); *endo/exo* mixture <sup>13</sup>C



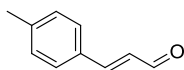
NMR (101 MHz,  $\text{CDCl}_3$ )  $\delta$  205.4, 204.3, 139.1, 136.4, 135.9, 133.2, 58.8, 58.1, 50.4, 50.2, 47.0, 46.6, 45.3, 45.3, 45.1, 45.1, 32.9, 32.6, 22.1, 22.1, 21.9, 21.6;  $m/z$  (CI): 181 ( $\text{M}^+\text{CH}_5$ ), 163 ( $\text{M}-\text{H}^-$ ). Analytical data were in accordance with literature values.<sup>1</sup>

***endo*-Bicyclo[2.2.2]oct-5-ene-2-carbaldehyde 58**

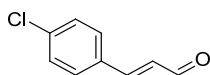


Secondary amine salt (1 mol%, 0.05 mmol) was dissolved in acetonitrile (4.75 mL) and water (0.25 mL). 90% Acrolein (370  $\mu\text{L}$ , 5.00 mmol) was added and the mixture was stirred at 25 °C for 10 minutes. Cyclohexadiene (1.2 mL, 12.5 mmol) was added and the mixture stirred for 18 h. The solvent was removed under reduced pressure (100 mbar, 25 °C) and the residue was taken up in water (10 mL) and diethyl ether (10 mL). The aqueous layer was extracted with diethyl ether ( $2 \times 10$  mL) and the combined organics dried over magnesium sulfate. The solvent was removed under reduced pressure and the residue was purified by flash chromatography (5% diethyl ether in petroleum ether) to give a colourless oil.  $\nu_{\text{max}}$  (ATR)/ $\text{cm}^{-1}$ : 3046, 2938, 2866, 2805, 2704, 1721; *endo*- $^1\text{H}$  NMR (500 MHz,  $\text{CDCl}_3$ )  $\delta$  9.45 (1H, d,  $J = 1.6$  Hz, CHO), 6.34 (1H, app. t,  $J = 7.5$  Hz, HCCH), 6.12 (1H, app. t,  $J = 7.3$  Hz, HCCH), 2.98–2.93 (1H, m, HCCHCH), 2.68–2.63 (1H, m, HCCHCH), 2.60–2.53 (1H, m, CHCHO), 1.77–1.61 (3H, m,  $\text{CH}_2$  and CHH), 1.59–1.52 (1H, m, CHH), 1.40–1.24 (2H, m, CHH and CHH);  $^{13}\text{C}$  NMR (126 MHz,  $\text{CDCl}_3$ )  $\delta$  204.4, 136.4, 131.0, 51.3, 31.1, 29.5, 27.1, 25.5, 25.1;  $m/z$  (CI): 137 ( $\text{M}+\text{H}^+$ ).

To determine *endo/exo* ratio; integrals of the two CHO peaks were used. *exo*- $^1\text{H}$  NMR (500 MHz,  $\text{CDCl}_3$ )  $\delta$  9.77 (1H, br s, CHO).<sup>117</sup>

**4-Methylcinnamaldehyde 60**<sup>44</sup>

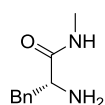
4-Iodotoluene (1.83 g, 8.39 mmol) was dissolved in anhydrous DMF (30 mL). In the following order, tetrabutylammonium acetate (5.06 g, 16.8 mmol), potassium chloride (0.63 g, 8.39 mmol), potassium carbonate (1.74 g, 12.6 mmol), acrolein diethyl acetal (3.84 mL, 25.2 mmol) and palladium acetate (56 mg, 0.25 mmol, 3 mol%) were added. The flask was sealed and the mixture heated to 90 °C for 2 hours. The reaction mixture was cooled and 2.4 M hydrochloric acid (30 mL) added. After stirring for 10 minutes the reaction mixture was poured onto water (200 mL) and extracted with diethyl ether (1 × 200 mL, 1 × 100 mL). The combined organics were dried over magnesium sulfate and the solvent was removed under reduced pressure. The product was isolated using flash chromatography (10% ethyl acetate in petroleum ether) as a white crystalline solid (1.05 g, 86%). mp: 37–38 °C [lit.<sup>44</sup> 42–43];  $\nu_{\max}$  (ATR)/ $\text{cm}^{-1}$  3050, 3040, 2988, 2913, 2824, 2745, 1678;  $^1\text{H}$  NMR (500 MHz,  $\text{CDCl}_3$ )  $\delta$  9.68 (1H, d,  $J = 7.7$  Hz, CHO), 7.46 (2H, d,  $J = 8.0$  Hz, CH), 7.45 (1H, d,  $J = 15.8$  Hz, CHCH), 7.24 (2H, d,  $J = 8.0$  Hz, CH), 6.68 (1H, dd,  $J = 15.8, 7.7$  Hz, CHCHO), 2.40 (3H, s,  $\text{CH}_3$ );  $^{13}\text{C}$  NMR (126 MHz,  $\text{CDCl}_3$ )  $\delta$  193.9, 153.0, 142.1, 131.5, 130.0, 128.7, 127.9, 21.7;  $m/z$  (ES): 147.0 ( $\text{M}+\text{H}^+$ ). Analytical data were in accordance with literature values.<sup>44</sup>

**4-Chlorocinnamaldehyde 62**<sup>44</sup>

4-Chloriodobenzene (2.00 g, 8.39 mmol) was dissolved in anhydrous DMF (30 mL). In the following order, tetrabutylammonium acetate (5.06 g, 16.8 mmol), potassium chloride (0.63 g, 8.39 mmol), potassium carbonate (1.74 g, 12.6 mmol), acrolein diethyl acetal (3.84 mL, 25.2 mmol) and palladium acetate (56 mg, 0.25 mmol, 3 mol%) were added. The flask was sealed and the mixture heated to 90 °C for 2 hours. The reaction mixture was cooled and 2.4 M hydrochloric acid (30 mL) added. After stirring for 10 minutes the reaction mixture was poured onto water (200 mL) and extracted with diethyl ether (1 × 200 mL, 1 × 100 mL). The combined organics were dried over magnesium sulfate and the solvent was removed under

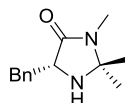
reduced pressure. The product was isolated using flash chromatography (10% ethyl acetate in petroleum ether) as a white crystalline solid (1.19 g, 85%). mp: 57–58 °C [lit.<sup>44</sup> 62–63 °C];  $\nu_{\max}$  (ATR)/ $\text{cm}^{-1}$  3057, 2995, 2853, 2762, 1694, 1670;  $^1\text{H}$  NMR (500 MHz,  $\text{CDCl}_3$ )  $\delta$  9.68 (1H, d,  $J = 7.6$  Hz, CHO), 7.50–7.46 (2H, m, CH), 7.41 (1H, d,  $J = 16.0$  Hz, CHCH), 7.39–7.36 (2H, m, CH), 6.66 (1H, dd,  $J = 16.0, 7.6$  Hz, CHOCH);  $^{13}\text{C}$  NMR (126 MHz,  $\text{CDCl}_3$ )  $\delta$  193.4, 151.1, 137.3, 132.6, 129.7, 129.5, 129.0;  $m/z$  (ES): 166.9 ( $\text{M}^{(35}\text{Cl})+\text{H}^+$ ). Analytical data were in accordance with literature values.<sup>44</sup>

**(R)-2-Amino-N-methyl-3-phenylpropanamide D-45**



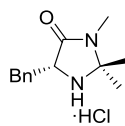
Exhibited identical physical and spectral data to the (*S*)-enantiomer.  $[\alpha]_{\text{D}}^{20} = -26.0$  ( $c=1.5$ , MeOH).

**(R)-5-Benzyl-2,2,3-trimethylimidazolidin-4-one 75**



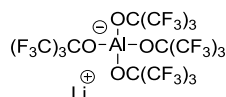
Exhibited identical physical and spectral data to the (*S*)-enantiomer.  $[\alpha]_{\text{D}}^{20} = +59.2$  ( $c=1.2$ , MeOH).

**(R)-5-Benzyl-2,2,3-trimethylimidazolidin-4-one hydrochloride 75·HCl**



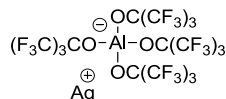
Exhibited identical physical and spectral data to the (*S*)-enantiomer.  $[\alpha]_{\text{D}}^{20} = +85.8$  ( $c=0.6$ , MeOH).

**Lithium tetrakis((1,1,1,3,3,3-hexafluoro-2-(trifluoromethyl)propan-2-yl)oxy)aluminate 81**<sup>118</sup>



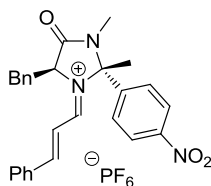
Lithium aluminium hydride (260 mg, 6.8 mmol) was added to anhydrous toluene (25 mL). The solution was cooled to 0 °C and perfluoro-*tert*-butanol (3.9 mL, 28.0 mmol) was added drop wise over 1 h. After complete addition the mixture was stirred at ambient temperature for 5 h before being heated under reflux for 17 h. The mixture was decanted (leaving behind a grey solid) whilst hot and cooled to -24 °C for 1.5 h. The supernatant was removed and the white solid was washed with cold toluene (20 mL). The residue was dried under reduced pressure to give a white powder (2.67 g, 40%). mp: >300 °C;  $\nu_{\text{max}}$  (ATR)/ $\text{cm}^{-1}$  1354, 1296, 1271, 1244, 1163, 966, 833, 725;  $^7\text{Li}$  NMR (155 MHz, DMSO)  $\delta$  -1.04 (s);  $^{19}\text{F}$  NMR (376 MHz, DMSO)  $\delta$  -75.13 (s);  $^{27}\text{Al}$  NMR (104 MHz, DMSO)  $\delta$  34.69 (s);  $m/z$  (ES): 966.9 (M-Li<sup>+</sup>).

**Silver(I) tetrakis((1,1,1,3,3,3-hexafluoro-2-(trifluoromethyl)propan-2-yl)oxy)aluminate 82**<sup>118</sup>



Lithium tetrakis((1,1,1,3,3,3-hexafluoro-2-(trifluoromethyl)propan-2-yl)oxy)aluminate (2.0 g, 2.0 mmol) was suspended in anhydrous DCM (15 mL). Silver(I) fluoride (460 mg, 3.6 mmol) was added and the mixture was heated under reflux with sonication for 12 h. The solution was filtered through Celite and the filter pad was washed with dichloromethane (15 mL). The organics were combined and the solvent was removed under reduced pressure to give a cream solid (1.68 g, 76%). mp (decomp.): 80 °C;  $\nu_{\text{max}}$  (ATR)/ $\text{cm}^{-1}$  1352, 1296, 1265, 1242, 1203, 1169, 964, 833, 723;  $^{19}\text{F}$  NMR (376 MHz, DMSO)  $\delta$  -75.17 (s);  $^{27}\text{Al}$  NMR (104 MHz, DMSO)  $\delta$  34.67 (s);  $m/z$  (ES/APCI): 966.8 (M-Ag<sup>+</sup>).

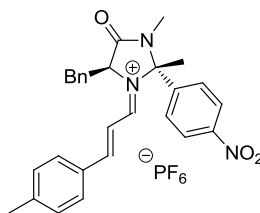
**(2*S*,5*S*,*E*)-5-Benzyl-2,3-dimethyl-2-(4-nitrophenyl)-4-oxo-1-((*E*)-3-phenylallylidene)imidazolidin-1-ium hexafluorophosphate 77·PF<sub>6</sub>**



65% Hexafluorophosphoric acid solution (1.00 mL, 7.35 mmol) was added to ethanol (10 mL). Activated 3 Å molecular sieves (1 g) were added and the mixture left overnight to give a ~0.7 M solution of HPF<sub>6</sub> in ethanol (after 3 days the solution degrades and should be disposed of).

(2*R*,5*S*)-5-Benzyl-2,3-dimethyl-2-(4-nitrophenyl)imidazolidin-4-one (230 mg, 0.71 mmol) was dissolved in anhydrous ethanol (5 mL). Cinnamaldehyde (80 µL, 0.64 mmol) was added followed by 0.7 M ethanolic hexafluorophosphoric acid (1 mL, 0.7 mmol). The reaction mixture was stirred for 1 h and a yellow precipitate formed. The supernatant was removed using a syringe. The precipitate was washed with anhydrous ethanol (2 × 10 mL), diethyl ether (10 mL) and then dried under reduced pressure to give a yellow powder (255 mg, 68%). mp (decomp.): 108–110 °C;  $\nu_{\max}$  (ATR)/cm<sup>-1</sup> 1717, 1614, 1603, 1684; <sup>1</sup>H NMR (400 MHz, CD<sub>3</sub>CN)  $\delta$  8.31–8.26 (2H, m, NO<sub>2</sub>CCH), 8.22 (1H, dd, *J* = 10.8, 1.8 Hz, N=CH), 7.99 (1H, d, *J* = 14.9 Hz, PhCH), 7.85–7.81 (2H, m, CH), 7.74–7.68 (3H, m, CH, NO<sub>2</sub>CCHCH), 7.58 (2H, app. t, *J* = 7.7 Hz, CH), 7.41–7.31 (3H, m, CH), 7.25–7.16 (3H, m, CH, N=CHCH), 5.46 (1H, app. t, *J* = 4.1 Hz, CH), 3.71 (1H, dd, *J* = 14.7, 5.7 Hz, CHH), 3.59 (1H, dd, *J* = 14.7, 4.1 Hz, CHH), 2.57 (3H, s, NCH<sub>3</sub>), 1.37 (3H, s, CH<sub>3</sub>); <sup>13</sup>C NMR (101 MHz, CD<sub>3</sub>CN)  $\delta$  170.3, 168.8, 165.9, 150.5, 144.1, 136.8, 134.9, 134.3, 132.9, 131.3, 130.8, 130.3, 130.2, 129.5, 125.6, 118.2, 87.7, 65.2, 37.6, 26.6, 22.6; <sup>19</sup>F NMR (376 MHz, CD<sub>3</sub>CN)  $\delta$  -72.9 (d, *J* = 706 Hz, PF<sub>6</sub>); <sup>31</sup>P NMR (162 MHz, CD<sub>3</sub>CN)  $\delta$  -144.6 (hept, *J* = 706 Hz, PF<sub>6</sub>); *m/z* (ES): 440.1 (M<sup>+</sup>PF<sub>6</sub>); HRMS (ES) calculated for C<sub>27</sub>H<sub>26</sub>O<sub>3</sub>N<sub>3</sub> 440.1969 (M<sup>+</sup>PF<sub>6</sub>), found 440.1963.

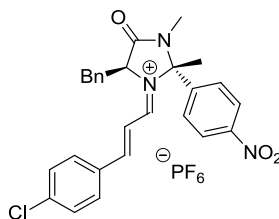
**(2*S*,5*S*,*E*)-5-Benzyl-2,3-dimethyl-2-(4-nitrophenyl)-4-oxo-1-((*E*)-3-(*p*-tolyl)allylidene)imidazolidin-1-ium hexafluorophosphate 83·PF<sub>6</sub>**



65% Hexafluorophosphoric acid solution (1.00 mL, 7.35 mmol) was added to ethanol (20 mL). Activated 3 Å molecular sieves (1 g) were added and the mixture left for 36 h to give a ~0.34 M solution of HPF<sub>6</sub> in ethanol (after 3 days the solution degrades and should be disposed of).

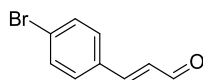
(2*R*,5*S*)-5-Benzyl-2,3-dimethyl-2-(4-nitrophenyl)imidazolidin-4-one (358 mg, 1.1 mmol) was dissolved in anhydrous ethanol (6 mL). *p*-Methylcinnamaldehyde (144 mg, 0.98 mmol) was added followed by 0.34 M ethanolic hexafluorophosphoric acid (3.2 mL, 1.1 mmol). The reaction mixture was stirred for 30 minutes to give a yellow suspension. The supernatant was removed using a syringe. The residue was washed with anhydrous ethanol (2 × 10 mL), diethyl ether (10 mL) and then dried under reduced pressure to give a yellow powder (241 mg, 41%). mp (decomp.): 119–120 °C;  $\nu_{\text{max}}$  (ATR)/cm<sup>-1</sup> 1719, 1618, 1578, 1522; <sup>1</sup>H NMR (500 MHz, CD<sub>3</sub>CN)  $\delta$  8.31–8.27 (2H, m, NO<sub>2</sub>CCH), 8.22–8.17 (1H, m, N=CH), 7.98 (1H, d, *J* = 14.8 Hz, PhCH), 7.75 (2H, d, *J* = 8.2 Hz, MeCCHCH), 7.74–7.70 (2H, m, NO<sub>2</sub>CCHCH), 7.42 (2H, d, *J* = 8.2 Hz, MeCH), 7.41–7.15 (6H, m, CH, N=CHCH), 5.45 (1H, app. t, *J* = 3.9 Hz, CH), 3.71 (1H, dd, *J* = 14.7, 5.7 Hz, CHH), 3.59 (1H, dd, *J* = 14.7, 3.9 Hz, CHH), 2.57 (3H, s, CH<sub>3</sub>), 2.46 (3H, s, NCH<sub>3</sub>), 1.34 (3H, s, CH<sub>3</sub>); <sup>13</sup>C NMR (126 MHz, CD<sub>3</sub>CN)  $\delta$  169.7, 169.0, 166.0, 150.4, 149.4, 144.3, 135.0, 133.2, 131.5, 131.3, 130.3, 130.1, 129.4, 125.5, 124.9, 117.1, 87.5, 65.0, 37.4, 26.6, 22.5, 22.3; <sup>19</sup>F NMR (376 MHz, CD<sub>3</sub>CN)  $\delta$  -72.6 (d, *J* = 707 Hz, PF<sub>6</sub>); <sup>31</sup>P NMR (162 MHz, CD<sub>3</sub>CN)  $\delta$  -144.6 (hept, *J* = 707 Hz, PF<sub>6</sub>); *m/z* (ES): 454.1 (M<sup>-</sup>PF<sub>6</sub>); HRMS (ES) calculated for C<sub>28</sub>H<sub>28</sub>O<sub>3</sub>N<sub>3</sub> 454.2122 (M<sup>-</sup>PF<sub>6</sub>), found 454.2125.

**(2*S*,5*S*,*E*)-5-Benzyl-1-((*E*)-3-(4-chlorophenyl)allylidene)-2,3-dimethyl-2-(4-nitrophenyl)-4-oxoimidazolidin-1-ium hexafluorophosphate 84·PF<sub>6</sub>**

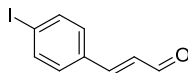


65% Hexafluorophosphoric acid solution (1.00 mL, 7.35 mmol) was added to ethanol (20 mL). Activated 3 Å molecular sieves (1 g) were added and the mixture left for 36 h to give a ~0.34 M solution of HPF<sub>6</sub> in ethanol (after 3 days the solution degrades and should be disposed of).

(2*R*,5*S*)-5-Benzyl-2,3-dimethyl-2-(4-nitrophenyl)imidazolidin-4-one (313 mg, 0.96 mmol) was dissolved in anhydrous ethanol (5 mL). 4-Chlorocinnamaldehyde (144 mg, 0.87 mmol) was added followed by 0.34 M ethanolic hexafluorophosphoric acid (2.8 mL, 0.95 mmol). The reaction mixture was stirred for 30 minutes to give a pale yellow suspension. The supernatant was removed using a syringe. The residue was washed with anhydrous ethanol (2 × 10 mL), diethyl ether (10 mL) and then dried under reduced pressure to give a fine yellow powder (135 mg, 25%). mp: 155–157 °C, decomp. 165 °C;  $\nu_{\max}$  (ATR)/cm<sup>-1</sup> 1724, 1618, 1599, 1578; <sup>1</sup>H NMR (500 MHz, CD<sub>3</sub>CN)  $\delta$  8.30–8.26 (2H, m, NO<sub>2</sub>CCH), 8.23 (1H, dd,  $J$  = 10.7, 1.7 Hz, N=CH), 7.94 (1H, d,  $J$  = 14.9 Hz, PhCH), 7.78 (2H, d,  $J$  = 8.6 Hz, ClCCHCH), 7.73–7.69 (2H, m, NO<sub>2</sub>CCHCH), 7.60–7.56 (2H, m, ClCCH), 7.40–7.30 (3H, m, CH), 7.22–7.18 (2H, m, CH), 7.15 (1H, dd,  $J$  = 14.9, 10.7 Hz, N=CHCH), 5.45 (1H, app. t,  $J$  = 4.1 Hz, NCH), 3.70 (1H, dd,  $J$  = 14.8, 5.6 Hz, CHH), 3.58 (1H, dd,  $J$  = 14.8, 4.1 Hz, CHH), 2.57 (3H, s, NCH<sub>3</sub>), 1.38 (3H, s, CH<sub>3</sub>); <sup>13</sup>C NMR (126 MHz, CD<sub>3</sub>CN)  $\delta$  170.4, 166.9, 165.8, 150.5, 144.0, 142.4, 134.9, 134.2, 132.9, 131.3, 130.9, 130.4, 130.2, 129.5, 125.5, 118.7, 87.9, 65.3, 37.7, 26.6, 22.6; <sup>19</sup>F NMR (376 MHz, CD<sub>3</sub>CN)  $\delta$  -72.5 (d,  $J$  = 707 Hz, PF<sub>6</sub>); <sup>31</sup>P NMR (162 MHz, CD<sub>3</sub>CN)  $\delta$  -144.6 (hept,  $J$  = 707 Hz, PF<sub>6</sub>);  $m/z$  (ES): 474.0 (M(<sup>35</sup>Cl)-PF<sub>6</sub>); HRMS (ES) calculated for C<sub>27</sub>H<sub>25</sub>O<sub>3</sub>N<sub>3</sub><sup>35</sup>Cl 474.1579 (M-PF<sub>6</sub>), found 474.1573.

**4-Bromocinnamaldehyde 85**<sup>48</sup>

4-Bromobenzaldehyde (925 mg, 5.00 mmol) was dissolved in dry toluene (50 mL). (Triphenylphosphoranylidene)acetaldehyde (1.52 g, 5.00 mmol) was added and the mixture was heated to 80 °C for 15 h. Once cooled the mixture was poured onto water (50 mL) and extracted with chloroform (3 × 50 mL). The combined organics were dried over magnesium sulfate and the solvent removed under reduced pressure. The dark brown residue was purified by flash chromatography (20% ethyl acetate in petroleum ether). The product was further purified by trituration from diethyl ether and hexanes to give a yellow solid (480 mg, 46%). mp: 75–78 °C [lit. 81–82 °C]<sup>119</sup>;  $\nu_{\max}$  (ATR)/cm<sup>-1</sup> 3055, 2992, 2851, 1670; <sup>1</sup>H NMR (500 MHz, CDCl<sub>3</sub>)  $\delta$  9.71 (1H, d,  $J$  = 7.6 Hz, CHO), 7.60–7.55 (2H, m, CH), 7.45–7.40 (3H, m, CH, PhCH), 6.70 (1H, dd,  $J$  = 16.0, 7.6 Hz, CHOCH); <sup>13</sup>C NMR (126 MHz, CDCl<sub>3</sub>)  $\delta$  193.5, 151.2, 133.1, 132.6, 129.9, 129.2, 125.9;  $m/z$  (ES): 210.9 (M(<sup>79</sup>Br)+H<sup>+</sup>). Analytical data were in accordance with literature values.<sup>119</sup>

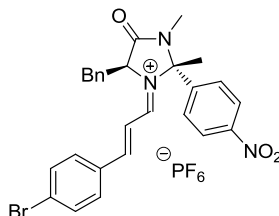
**4-Iodocinnamaldehyde 86**<sup>48</sup>

4-Iodobenzaldehyde (1.16 g, 5.00 mmol) was dissolved in dry toluene (50 mL). (Triphenylphosphoranylidene)acetaldehyde (1.52 g, 5.00 mmol) was added and the mixture was heated to 80 °C for 15 h. Once cooled the mixture was poured onto water (50 mL) and extracted with chloroform (3 × 50 mL). The combined organics were dried over magnesium sulfate and the solvent removed under reduced pressure. The dark brown residue was purified by flash chromatography (20% ethyl acetate in petroleum ether). The product was further purified by trituration from diethyl ether and hexanes to give a yellow solid (440 mg, 34%). mp: 82–84 °C [lit.<sup>48</sup> 86–88 °C];  $\nu_{\max}$  (ATR)/cm<sup>-1</sup> 2814, 2735, 1659; <sup>1</sup>H NMR (500 MHz, CDCl<sub>3</sub>)  $\delta$  9.70 (1H, d,  $J$  = 7.6 Hz, CHO), 7.78 (2H, d,  $J$  = 8.3 Hz, CH), 7.39 (1H, d,  $J$  = 16.0 Hz, PhCH), 7.28 (2H, d,  $J$  = 8.3 Hz, CH), 6.71 (1H, dd,  $J$  = 16.0, 7.6 Hz, CHCHO); <sup>13</sup>C NMR (126



MHz, CDCl<sub>3</sub>)  $\delta$  193.5, 151.4, 138.5, 133.6, 129.9, 129.2, 98.0;  $m/z$  (ES): 259.0 (M+H<sup>+</sup>). Analytical data were in accordance with literature values.<sup>48</sup>

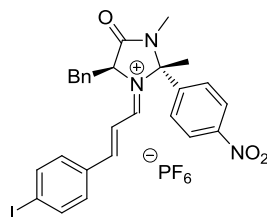
**(2*S*,5*S*,*E*)-5-Benzyl-1-((*E*)-3-(4-bromophenyl)allylidene)-2,3-dimethyl-2-(4-nitrophenyl)-4-oxoimidazolidin-1-ium hexafluorophosphate 90·PF<sub>6</sub>**



65% Hexafluorophosphoric acid solution (1.00 mL, 7.35 mmol) was added to ethanol (10 mL). Activated 3 Å molecular sieves (1 g) were added and the mixture left overnight to give a ~0.7 M solution of HPF<sub>6</sub> in ethanol (after 3 days the solution degrades and should be disposed of).

(2*R*,5*S*)-5-Benzyl-2,3-dimethyl-2-(4-nitrophenyl)imidazolidin-4-one (210 mg, 0.64 mmol) was dissolved in anhydrous ethanol (4 mL). 4-Bromocinnamaldehyde (129 mg, 0.61 mmol) was added followed by 0.7M ethanolic hexafluorophosphoric acid (0.95 mL, 0.66 mmol). The reaction mixture was stirred for 30 minutes to give a yellow precipitate. The supernatant was removed with a syringe. The residue was washed with anhydrous ethanol (2 × 5 mL), diethyl ether (5 mL) and then dried under reduced pressure to give a yellow powder (122 mg, 30%). mp (decomp.): 153–155 °C;  $\nu_{\max}$  (ATR)/cm<sup>-1</sup> 3028, 1722, 1616, 1597, 1571, 1526; <sup>1</sup>H NMR (500 MHz, CD<sub>3</sub>CN)  $\delta$  8.30–8.26 (2H, m, NO<sub>2</sub>CCH), 8.21 (1H, dd,  $J$  = 10.8, 1.8 Hz, N=CH), 7.89 (1H, d,  $J$  = 14.9 Hz, PhCH), 7.78–7.74 (2H, m, BrCCHCH), 7.72–7.67 (4H, m, NO<sub>2</sub>CCHCH, BrCCH), 7.40–7.30 (3H, m, CH), 7.21–7.18 (2H, m, CH), 7.15 (1H, dd,  $J$  = 14.9, 10.8 Hz, N=CHCH), 5.42 (1H, app. t,  $J$  = 4.2 Hz, CH), 3.69 (1H, dd,  $J$  = 14.8, 5.6 Hz, CHH), 3.58 (1H, dd,  $J$  = 14.8, 4.2 Hz, CHH), 2.57 (3H, s, NCH<sub>3</sub>), 1.37 (3H, s, CH<sub>3</sub>); <sup>13</sup>C NMR (126 MHz, CD<sub>3</sub>CN)  $\delta$  170.4, 166.9, 165.8, 150.5, 144.0, 134.9, 134.1, 134.0, 133.2, 131.3, 130.4, 130.2, 129.5, 125.5, 118.7, 87.9, 65.3, 37.7, 26.6, 22.6; <sup>19</sup>F NMR (376 MHz, CD<sub>3</sub>CN)  $\delta$  -72.9 (d,  $J$  = 706 Hz, PF<sub>6</sub>); <sup>31</sup>P NMR (162 MHz, CD<sub>3</sub>CN)  $\delta$  -144.6 (hept,  $J$  = 706 Hz, PF<sub>6</sub>);  $m/z$  (ES): 518.0 (M(<sup>79</sup>Br)<sup>-</sup>PF<sub>6</sub>); HRMS (ES) calculated for C<sub>27</sub>H<sub>25</sub>O<sub>3</sub>N<sub>3</sub><sup>79</sup>Br 518.1074 (M-PF<sub>6</sub>), found 518.1065.

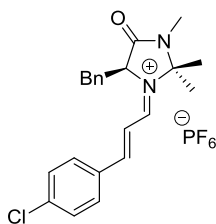
**(2*S*,5*S*,*E*)-5-Benzyl-1-((*E*)-3-(4-iodophenyl)allylidene)-2,3-dimethyl-2-(4-nitrophenyl)-4-oxoimidazolidin-1-ium hexafluorophosphate 91·PF<sub>6</sub>**



65% Hexafluorophosphoric acid solution (1.00 mL, 7.35 mmol) was added to ethanol (10 mL). Activated 3 Å molecular sieves (1 g) were added and the mixture left overnight to give a ~7.0 M solution of HPF<sub>6</sub> in ethanol (after 3 days the solution degrades and should be disposed of).

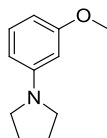
(2*R*,5*S*)-5-Benzyl-2,3-dimethyl-2-(4-nitrophenyl)imidazolidin-4-one (190 mg, 0.58 mmol) was dissolved in anhydrous ethanol (2 mL). 4-Iodocinnamaldehyde (143 mg, 0.55 mmol) was added followed by 0.7M ethanolic hexafluorophosphoric acid (0.85 mL, 0.59 mmol). The mixture was stirred for 1 h. to give a yellow gum. The supernatant was removed with a syringe. The residue was washed with anhydrous ethanol (2 × 5 mL), diethyl ether (5 mL) and then dried under reduced pressure to give a yellow powder (200 mg, 51%). mp (decomp.): 148–151 °C;  $\nu_{\max}$  (ATR)/cm<sup>-1</sup> 3082, 1721, 1614, 1595, 1568, 1524; <sup>1</sup>H NMR (500 MHz, CD<sub>3</sub>CN)  $\delta$  8.31–8.27 (2H, m, NO<sub>2</sub>CCH), 8.20 (1H, dd, *J* = 10.8, 1.8 Hz, N=CH), 7.98 (2H, d, *J* = 8.5 Hz, ICCHCH), 7.87 (1H, d, *J* = 14.8 Hz, PhCH), 7.72–7.67 (2H, m, NO<sub>2</sub>CCHCH), 7.52 (2H, d, *J* = 8.5 Hz, ICCH), 7.40–7.27 (3H, m, CH), 7.21–7.12 (3H, m, CH, N=CHCH), 5.42 (1H, app. t, *J* = 4.1 Hz, CH), 3.69 (1H, dd, *J* = 14.8, 5.7 Hz, CHH), 3.57 (1H, dd, *J* = 14.8, 4.2 Hz, CHH), 2.56 (3H, s, NCH<sub>3</sub>), 1.36 (3H, s, CH<sub>3</sub>); <sup>13</sup>C NMR (126 MHz, CD<sub>3</sub>CN)  $\delta$  170.3, 167.2, 165.8, 150.5, 144.0, 140.1, 134.9, 133.7, 131.3, 130.4, 130.2, 129.5, 125.5, 118.7, 104.8, 87.9, 65.3, 37.7, 26.6, 22.6; <sup>19</sup>F NMR (376 MHz, CD<sub>3</sub>CN)  $\delta$  -72.9 (d, *J* = 706 Hz, PF<sub>6</sub>); <sup>31</sup>P NMR (162 MHz, CD<sub>3</sub>CN)  $\delta$  -144.6 (hept, *J* = 706 Hz, PF<sub>6</sub>); *m/z* (ES): 566.0 (M<sup>-</sup>PF<sub>6</sub>); HRMS (ES) calculated for C<sub>27</sub>H<sub>25</sub>O<sub>3</sub>N<sub>3</sub>I 566.0935 (M<sup>-</sup>PF<sub>6</sub>), found 566.0930.

**(*S,E*)-5-Benzyl-1-((*E*)-3-(4-chlorophenyl)allylidene)-2,2,3-trimethyl-4-oxoimidazolidin-1-ium hexafluorophosphate 92·PF<sub>6</sub>**

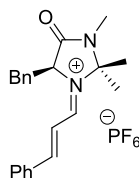


65% Hexafluorophosphoric acid solution (1.00 mL, 7.35 mmol) was added to ethanol (10 mL). Activated 3 Å molecular sieves (1 g) were added and the mixture left overnight to give a ~0.7 M solution of HPF<sub>6</sub> in ethanol (after 3 days the solution degrades and should be disposed of).

(*S*)-5-Benzyl-2,2,3-trimethylimidazolidin-4-one (200 mg, 0.92 mmol) was dissolved in anhydrous ethanol (8 mL). 4-Chlorocinnamaldehyde (145 mg, 0.87 mmol) was added followed by 0.7M ethanolic hexafluorophosphoric acid (1.34 mL, 0.94 mmol). The reaction mixture was stirred for 1 h to give a pale yellow precipitate. The supernatant was removed with a syringe. The residue was washed with anhydrous ethanol (2 x 5 mL), diethyl ether (5 mL) and then dried under reduced pressure to give a yellow powder (106 mg, 24%). mp: 110–113 °C;  $\nu_{\max}$  (ATR)/cm<sup>-1</sup> 2988, 2976, 1697, 1626, 1601, 1582; <sup>1</sup>H NMR (400 MHz, CD<sub>3</sub>CN)  $\delta$  8.72 (1H, dd,  $J$  = 10.6, 2.0 Hz, N=CH), 8.12 (1H, d,  $J$  = 15.1 Hz, PhCH), 7.94–7.89 (2H, m, ClCCHCH), 7.69–7.63 (2H, m, ClCCH), 7.41–7.23 (4H, m, CH, N=CHCH), 7.14–7.10 (2H, m, CH), 5.21 (1H, s, CH), 3.59 (1H, dd,  $J$  = 14.7, 5.7 Hz, CHH), 3.49 (1H, dd,  $J$  = 14.7, 3.8 Hz, CHH), 2.81 (3H, s, NCH<sub>3</sub>), 1.72 (3H, s, CH<sub>3</sub>), 0.83 (3H, s, CH<sub>3</sub>); <sup>13</sup>C NMR (101 MHz, CD<sub>3</sub>CN)  $\delta$  168.1, 165.2, 164.7, 141.7, 134.7, 133.8, 133.1, 131.2, 130.9, 130.1, 129.2, 118.9, 86.7, 65.3, 37.3, 27.5, 26.1, 24.8; <sup>19</sup>F NMR (376 MHz, CD<sub>3</sub>CN)  $\delta$  -72.7 (d,  $J$  = 707 Hz, PF<sub>6</sub>); <sup>31</sup>P NMR (162 MHz, CD<sub>3</sub>CN)  $\delta$  -144.6 (hept,  $J$  = 707 Hz, PF<sub>6</sub>);  $m/z$  (ES): 367.4 (M(<sup>35</sup>Cl)-PF<sub>6</sub>); HRMS (ES): calculated  $m/z$  for C<sub>22</sub>H<sub>24</sub>N<sub>2</sub>OCl<sup>+</sup>: 367.1572, found  $m/z$ : 367.1567 (M(<sup>35</sup>Cl)-PF<sub>6</sub>).

**1-(3-Methoxyphenyl)pyrrolidine 95**

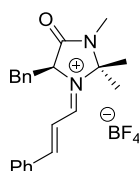
*m*-Anisidine (2.10 mL, 18.7 mmol) and 1,4-dibromobutane (1.10 mL, 9.35 mmol) were added to a solution of Hünigs base (4.07 mL 23.4 mmol) in toluene (50 mL). The mixture was heated under reflux for 18 h. Once cooled the mixture was filtered. The filtrate was concentrated under reduced pressure. Flash chromatography (5% ethyl acetate in petroleum ether) afforded the title compound as a pale beige oil (1.64 g, 99%).  $\nu_{\max}$  (film)/ $\text{cm}^{-1}$  2964, 2896, 2871, 2833, 1608, 1573;  $^1\text{H}$  NMR (500 MHz,  $\text{CDCl}_3$ )  $\delta$  7.14 (1H, t,  $J = 8.1$  Hz, CH), 6.29–6.22 (2H, m, CH), 6.12 (1H, t,  $J = 2.3$  Hz, CH), 3.81 (3H, s,  $\text{OCH}_3$ ), 3.31–3.34 (4H, m,  $\text{NCH}_2$ ), 2.02–1.96 (4H, m,  $\text{CH}_2$ );  $^{13}\text{C}$  NMR (126 MHz,  $\text{CDCl}_3$ )  $\delta$  160.8, 149.3, 129.8, 105.0, 100.7, 98.1, 55.1, 47.7, 25.5;  $m/z$  (EI): 176.1 (M-H<sup>+</sup>); HRMS (EI) calculated for  $\text{C}_{11}\text{H}_{14}\text{ON}$  176.1070 (M-H<sup>+</sup>), found 176.1071.

**(*S,E*)-5-Benzyl-2,2,3-trimethyl-4-oxo-1-((*E*)-3-phenylallylidene)imidazolidin-1-ium hexafluorophosphate 15·PF<sub>6</sub><sup>36</sup>**

(*S*)-5-Benzyl-2,2,3-trimethylimidazolidin-4-one (2.1 g, 9.6 mmol) was dissolved in anhydrous methanol. *trans*-Cinnamaldehyde (1.2 mL, 9.5 mmol) was added followed by dropwise addition of 65% wt. hexafluorophosphoric acid solution (1.3 mL, 9.6 mmol). The reaction mixture was stirred for 1 hour and the precipitate was recovered on a sinter, washed with methanol (20 mL) and diethyl ether (20 mL). The yellow powder was recrystallized from *iso*-propanol and acetonitrile to give yellow cubic crystals (2.2 g, 48%). mp 195–196 °C [lit.<sup>36</sup> 162–165 °C];  $\nu_{\max}$  (ATR)/ $\text{cm}^{-1}$  3078, 3057, 3032, 2986, 2942, 1718, 1630, 1603, 1592;  $^1\text{H}$  NMR (500 MHz,  $\text{CD}_3\text{CN}$ )  $\delta$  8.69 (1H, dd,  $J = 10.7, 1.7$  Hz, N=CH), 8.16 (1H, d,  $J = 15.0$  Hz, PhCH), 7.93–7.90 (2H, m, CH), 7.72 (1H, t,  $J = 7.4$  Hz, CH), 7.62 (2H, t,  $J = 7.7$  Hz, CH), 7.33–7.25

(4H, m, CH, N=CHCH), 7.10 (2H, d,  $J = 7.0$  Hz, CH), 5.19 (1H, br. s, CH), 3.57 (1H, dd,  $J = 14.7, 5.7$  Hz, CHH), 3.47 (1H, dd,  $J = 14.7, 3.6$  Hz, CHH), 2.79 (3H, s, NCH<sub>3</sub>), 1.70 (3H, s, CH<sub>3</sub>), 0.82 (3H, s, CH<sub>3</sub>); <sup>13</sup>C NMR (126 MHz, CD<sub>3</sub>CN)  $\delta$  168.2, 166.8, 165.3, 136.2, 134.9, 134.5, 132.6, 131.2, 130.8, 130.1, 129.3, 118.5, 86.6, 65.2, 37.4, 27.6, 26.2, 24.9; <sup>19</sup>F NMR (376 MHz, CD<sub>3</sub>CN)  $\delta$  -72.6 (d,  $J = 707$  Hz, PF<sub>6</sub>); <sup>31</sup>P NMR (162 MHz, CD<sub>3</sub>CN)  $\delta$  -144.5 (hept,  $J = 707$  Hz, PF<sub>6</sub>);  $m/z$  (ES): 333.2 (M<sup>-</sup>PF<sub>6</sub>); HRMS (ES): calculated  $m/z$  for C<sub>22</sub>H<sub>25</sub>N<sub>2</sub>O<sup>+</sup>: 333.1961, found  $m/z$ : 333.1965 (M<sup>-</sup>PF<sub>6</sub>). Analytical data were in accordance with literature values.<sup>36</sup>

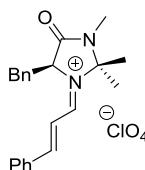
**(*S,E*)-5-Benzyl-2,2,3-trimethyl-4-oxo-1-((*E*)-3-phenylallylidene)imidazolidin-1-ium tetrafluoroborate 15·BF<sub>4</sub>**



Prepared using 48% wt. tetrafluoroboric acid solution (1.2 mL, 9.2 mmol) and (*S*)-5-benzyl-2,2,3-trimethylimidazolidin-4-one (2.1 g, 9.6 mmol) in an analogous fashion to the hexafluorophosphate salt.

Yellow crystals (1.30 g, 32%). mp 202–204 °C;  $\nu_{\max}$  (ATR)/cm<sup>-1</sup> 3075, 1715, 1626, 1591, 1574; <sup>1</sup>H NMR (400 MHz, CD<sub>3</sub>CN)  $\delta$  8.75 (1H, dd,  $J = 10.7, 1.9$  Hz, N=CH), 8.20 (1H, d,  $J = 15.0$  Hz, PhCH), 7.94–7.91 (2H, m, CH), 7.74–7.69 (1H, m, CH), 7.65–7.59 (2H, m, CH), 7.35–7.24 (4H, m, CH, N=CHCH), 7.12–7.08 (2H, m, CH), 5.20 (1H, br. s, CH), 3.58 (1H, dd,  $J = 14.7, 5.7$  Hz, CHH), 3.47 (1H, dd,  $J = 14.7, 3.7$  Hz, CHH), 2.79 (3H, s, NCH<sub>3</sub>), 1.71 (3H, s, CH<sub>3</sub>), 0.82 (3H, s, CH<sub>3</sub>); <sup>11</sup>B NMR (128 MHz, CD<sub>3</sub>CN)  $\delta$  -1.10 (s, BF<sub>4</sub>); <sup>13</sup>C NMR (101 MHz, CD<sub>3</sub>CN)  $\delta$  168.3, 166.8, 165.3, 136.1, 134.8, 134.5, 132.5, 131.2, 130.7, 130.1, 129.2, 118.5, 86.6, 65.2, 37.3, 27.5, 26.1, 24.8; <sup>19</sup>F NMR (376 MHz, CD<sub>3</sub>CN)  $\delta$  -151.25 (s, <sup>10</sup>BF<sub>4</sub>), -151.31 (s, <sup>11</sup>BF<sub>4</sub>);  $m/z$  (ES): 333.2 (M<sup>-</sup>BF<sub>4</sub>). Analytical data were in accordance with literature values.<sup>36</sup>

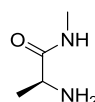
**(*S,E*)-5-Benzyl-2,2,3-trimethyl-4-oxo-1-((*E*)-3-phenylallylidene)imidazolidin-1-ium perchlorate 15·ClO<sub>4</sub>**



Prepared using 70% perchloric acid solution (0.8 mL, 9.2 mmol) and (*S*)-5-benzyl-2,2,3-trimethylimidazolidin-4-one (2.1 g, 9.6 mmol) in an analogous fashion to the hexafluorophosphate salt.

Pale yellow crystals (1.54 g, 37%). mp (decomp.) 208–209 °C [lit.<sup>120</sup> 190–192 °C];  $\nu_{\max}$  (ATR)/cm<sup>-1</sup> 3069, 1715, 1626, 1601, 1591; <sup>1</sup>H NMR (400 MHz, CD<sub>3</sub>CN)  $\delta$  8.77 (1H, dd, *J* = 10.7, 1.9 Hz, N=CH), 8.23 (1H, d, *J* = 15.0 Hz, PhCH), 7.94–7.90 (2H, m, CH), 7.75–7.69 (1H, m, CH), 7.65–7.59 (2H, m, CH), 7.35–7.23 (4H, m, CH, N=CHCH), 7.12–7.08 (2H, m, CH), 5.22 (1H, br. s, CH), 3.58 (1H, dd, *J* = 14.7, 5.7 Hz, CHH), 3.47 (1H, dd, *J* = 14.7, 3.7 Hz, CHH), 2.79 (3H, s, NCH<sub>3</sub>), 1.71 (3H, s, CH<sub>3</sub>), 0.82 (3H, s, CH<sub>3</sub>); <sup>13</sup>C NMR (101 MHz, CD<sub>3</sub>CN)  $\delta$  168.3, 166.8, 165.3, 136.1, 134.8, 134.5, 132.5, 131.2, 130.7, 130.1, 129.2, 118.5, 86.6, 65.2, 37.3, 27.6, 26.1, 24.8; *m/z* (ES): 333.1 (M<sup>-</sup>ClO<sub>4</sub>). Analytical data were in accordance with literature values.<sup>120</sup>

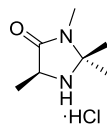
**L-Alanine *N*-methyl amide 113**



L-Alanine methyl ester hydrochloride (10.0 g, 71.7 mmol) was stirred in an ethanolic solution of methylamine 33 wt.% (60.0 mL, 483 mmol) for 72 h at ambient temperature. The mixture was concentrated under reduced pressure. The resulting slurry was taken up into saturated sodium carbonate (50 mL) and extracted with chloroform (4 × 50 mL). The combined organics were dried over anhydrous potassium carbonate and the solvent removed under reduced pressure to give the product as a pale yellow oil (5.1 g, 70%).  $[\alpha]_{\text{D}}^{20} = +4.1$  (c=2.0, MeOH);  $\nu_{\max}$  (ATR)/cm<sup>-1</sup> 3298, 2968, 2934, 1651; <sup>1</sup>H NMR (400 MHz, CDCl<sub>3</sub>)  $\delta$  7.31 (1H, br. s, NH), 3.40 (1H, q, *J* = 7.0 Hz, CH), 2.72 (3H, d, *J* = 5.0 Hz, NCH<sub>3</sub>), 1.40 (2H, s, NH<sub>2</sub>),

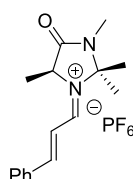
1.24 (3H, d,  $J = 7.0$  Hz,  $\text{CH}_3$ );  $^{13}\text{C}$  NMR (101 MHz,  $\text{CDCl}_3$ )  $\delta$  176.4, 50.7, 25.8, 21.7;  $m/z$  (ES): 102.9 ( $\text{M}+\text{H}^+$ ). Analytical data were in accordance with literature values.<sup>78</sup>

**(*S*)-2,2,3,5-Tetramethylimidazolidin-4-one hydrochloride 114·HCl**<sup>36</sup>



L-Alanine *N*-methyl amide (3.10 g, 30.4 mmol) was dissolved in methanol (80 mL). Acetone (40 mL) and one small crystal of *p*-toluenesulfonic acid (<1 mg) were added and the reaction mixture was heated under reflux for 18 h. The mixture was then cooled to ambient temperature and concentrated under reduced pressure to give a white solid. The residue was taken up in dioxane (150 mL) and dry hydrogen chloride was bubbled through for 20 minutes. The resultant precipitate was recovered on a sinter, washed with dioxane (20 mL) and diethyl ether (20 mL) to give the title compound as a white powder (4.40 g, 81%). mp: 191–193 °C [lit.<sup>36</sup> 141–144 °C];  $[\alpha]_{\text{D}}^{20} = -6.1$  ( $c=1.0$ , MeOH);  $\nu_{\text{max}}$  (ATR)/ $\text{cm}^{-1}$  2984, 2916, 1717;  $^1\text{H}$  NMR (500 MHz, MeOD)  $\delta$  4.35 (1H, q,  $J = 7.1$  Hz, CH), 2.89 (3H, s,  $\text{NCH}_3$ ), 1.78 (3H, s,  $\text{CH}_3$ ), 1.67 (3H, s,  $\text{CH}_3$ ), 1.57 (3H, d,  $J = 7.1$  Hz,  $\text{CHCH}_3$ );  $^{13}\text{C}$  NMR (101 MHz, MeOD)  $\delta$  168.8, 78.7, 53.9, 25.6, 24.7, 22.7, 13.9;  $m/z$  (ES): 143.0 ( $\text{M}-\text{Cl}$ ). Analytical data were in accordance with literature values.<sup>36</sup>

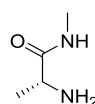
**(*S,E*)-2,2,3,5-Tetramethyl-4-oxo-1-((*E*)-3-phenylallylidene)imidazolidin-1-ium hexafluorophosphate 115·PF<sub>6</sub>**



65% Hexafluorophosphoric acid solution (1.00 mL, 7.35 mmol) was added to ethanol (10 mL). Activated 3 Å molecular sieves (1 g) were added and the mixture left overnight to give a ~0.7 M solution of HPF<sub>6</sub> in ethanol (after 3 days the solution degrades and should be disposed of).

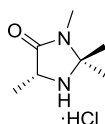
(*S*)-2,2,3,5-Tetramethylimidazolidin-4-one hydrochloride (900 mg, 5.00 mmol) was added to saturated sodium carbonate solution (25 mL) and extracted with chloroform (3 × 25 mL). The combined organics were dried over sodium sulfate and the solvent removed under reduced pressure to give a white solid. Anhydrous ethanol (15 mL) was added followed by cinnamaldehyde (600 μL, 4.77 mmol). 0.7 M Ethanolic hexafluorophosphoric acid (7.4 mL, 5.2 mmol) was added dropwise and the mixture was stirred for 20 minutes. After 20 minutes further cinnamaldehyde (400 μL, 3.18 mmol) was added to the suspension and stirring was continued for 20 minutes. The precipitated product was recovered on a sinter, washed with anhydrous ethanol (20 mL) and diethyl ether (20 mL) and then dried under reduced pressure to give a pale yellow powder (1.20 g, 60%). mp: 162–164 °C;  $\nu_{\max}$  (ATR)/cm<sup>-1</sup> 1724, 1711, 1626, 1605, 1589, 1572; <sup>1</sup>H NMR (400 MHz, CD<sub>3</sub>CN)  $\delta$  8.76 (1H, dd, *J* = 10.6, 1.6 Hz, N=CH), 8.16 (1H, d, *J* = 15.1 Hz, PhCH), 7.92 (2H, d, *J* = 7.5 Hz, CH), 7.69 (1H, t, *J* = 7.5 Hz, CH), 7.60 (2H, app. t, *J* = 7.5 Hz, CH), 7.29 (1H, dd, *J* = 15.1, 10.6 Hz, PhCHCH), 4.88 (1H, q, *J* = 7.1 Hz, CH), 2.92 (3H, s, CH<sub>3</sub>), 1.83 (3H, s, CH<sub>3</sub>), 1.81 (3H, s, CH<sub>3</sub>), 1.70 (3H, d, *J* = 7.1 Hz, CHCH<sub>3</sub>); <sup>13</sup>C NMR (126 MHz, CD<sub>3</sub>CN)  $\delta$  167.3, 166.6, 166.0, 135.9, 134.5, 132.2, 130.7, 118.2, 86.4, 59.5, 27.8, 26.3, 26.2, 18.9; <sup>19</sup>F NMR (376 MHz, CD<sub>3</sub>CN)  $\delta$  -72.8 (d, *J* = 706 Hz, PF<sub>6</sub>); <sup>31</sup>P NMR (162 MHz, CD<sub>3</sub>CN)  $\delta$  -144.6 (hept, *J* = 706 Hz, PF<sub>6</sub>); *m/z* (ES): 257.0 (M<sup>-</sup>PF<sub>6</sub>); HRMS (ES) calculated for C<sub>16</sub>H<sub>21</sub>N<sub>2</sub>O 257.1648 (M<sup>-</sup>PF<sub>6</sub>), found 257.1641.

#### **D-Alanine *N*-methyl amide D-113**

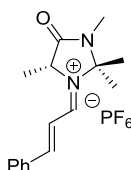


Exhibited identical physical and spectral data to the (*S*)-enantiomer.  $[\alpha]_{\text{D}}^{20} = -4.2$  (c=1.3, MeOH).

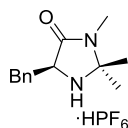


**(R)-2,2,3,5-Tetramethylimidazolidin-4-one hydrochloride D-114**

Exhibited identical physical and spectral data to the (*S*)-enantiomer.  $[\alpha]_{\text{D}}^{20} = +5.3$  ( $c=1.4$ , MeOH).

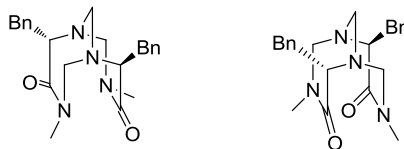
**(R,E)-2,2,3,5-Tetramethyl-4-oxo-1-((E)-3-phenylallylidene)imidazolidin-1-ium hexafluorophosphate D-115**

Exhibited identical physical and spectral data to the (*S*)-enantiomer.

**(S)-5-Benzyl-2,2,3-trimethylimidazolidin-4-one hexafluorophosphate 3·HPF<sub>6</sub><sup>36</sup>**

(*S*)-5-Benzyl-2,2,3-trimethylimidazolidin-4-one (1.04 g, 4.50 mmol) was dissolved in diethyl ether (80 mL) and cooled to 0 °C. 60% wt. Hexafluorophosphoric acid solution (0.4 mL, 4.52 mmol) was added dropwise. The solution was stirred for 30 minutes and the precipitate was recovered on a sinter and washed with diethyl ether (20 mL) to give a white powder (1.40 g, 85%). mp 144–145 °C [lit.<sup>36</sup> 126–128 °C];  $[\alpha]_{\text{D}}^{20} = -42.0$  ( $c=1.0$ , MeOH);  $\nu_{\text{max}}$  (film)/ $\text{cm}^{-1}$  3197, 3158, 2895, 1700, 1596; <sup>1</sup>H NMR (400 MHz, MeOD)  $\delta$  7.44–7.30 (5H, m, CH), 4.63 (1H, dd,  $J = 10.7, 3.5$  Hz, CH), 3.55 (1H, dd,  $J = 15.3, 3.5$  Hz, CHH), 2.97 (1H, dd,  $J = 15.3, 10.7$  Hz, CHH), 2.92 (3H, s, NCH<sub>3</sub>), 1.72 (3H, s, CH<sub>3</sub>), 1.59 (3H, s, CH<sub>3</sub>); <sup>13</sup>C NMR (101 MHz, MeOD)  $\delta$  167.6, 136.3, 130.2, 130.1, 128.8, 79.1, 59.6, 35.1, 25.7, 24.2, 22.0; <sup>19</sup>F NMR (376 MHz, MeOD)  $\delta$  -74.2 (d,  $J = 708$  Hz, PF<sub>6</sub>); <sup>31</sup>P NMR (162 MHz, MeOD)  $\delta$  -144.5 (hept,  $J = 708$  Hz, PF<sub>6</sub>);  $m/z$  (ES): 219.2 (M-PF<sub>6</sub>). Analytical data were in accordance with literature values.<sup>36</sup>

**(5*S*,10*S*)-5,10-Dibenzyl-3,8-dimethyl-1,3,6,8-tetraaza-bicyclo[4.4.1]undecane-4,9-dione 128 and 129**



L-Phenylalanine *N*-methyl amide (890 mg, 5.00 mmol) was dissolved in chloroform (20 mL). Paraformaldehyde (450 mg, 15.0 mmol, 3 eq) and ytterbium (III) trifluoromethanesulfonate hydrate (31 mg, 0.05 mmol, 1 mol%) were added. The mixture was stirred at 60 °C for 18 h. Once cooled to ambient temperature the mixture was diluted with dichloromethane (30 mL), washed with saturated sodium hydrogen carbonate (3 × 20 mL), brine (30 mL) and then dried over anhydrous sodium sulfate. The solvent was removed under reduced pressure and the two diastereomers were separated by flash chromatography (gradient elution from 80% ethyl acetate in petroleum ether to 100% ethyl acetate) to give first **128** (791 mg, 81%) and second **129** (50 mg, 5%) as white crystalline solids.

**(-)-(1*S*,5*S*,6*S*,10*S*)-5,10-Dibenzyl-3,8-dimethyl-1,3,6,8-tetraaza-bicyclo[4.4.1]undecane-4,9-dione 128**

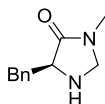
mp: 128–130 °C; ;  $[\alpha]_{\text{D}}^{20} = -128.9$  (c=0.85, MeOH);  $\nu_{\text{max}}$  (ATR)/cm<sup>-1</sup> 2926, 2907, 1626, 1639; <sup>1</sup>H NMR (400 MHz, CDCl<sub>3</sub>)  $\delta$  7.34–7.20 (10H, m, CH), 4.69 (2H, d, *J* = 15.3 Hz, MeNCHH), 4.40 (2H, d, *J* = 15.3 Hz, MeNCHH), 4.11 (2H, s, NCH<sub>2</sub>N), 3.83 (2H, dd, *J* = 9.0, 5.5 Hz, COCH), 3.41 (2H, dd, *J* = 14.7, 5.5 Hz, CHCHH), 2.97 (6H, s, NCH<sub>3</sub>), 2.95 (2H, dd, *J* = 14.7, 9.0 Hz, CHCHH); <sup>13</sup>C NMR (101 MHz, CDCl<sub>3</sub>)  $\delta$  174.6, 139.6, 129.2, 128.3, 126.3, 82.6, 65.2, 64.4, 37.2, 34.7; *m/z* (ES): 415.1 (M+Na<sup>+</sup>); HRMS (ES) calculated for C<sub>23</sub>H<sub>29</sub>O<sub>2</sub>N<sub>4</sub> 393.2285 (M+H<sup>+</sup>), found 393.2297.

**(+)-(1*R*,5*S*,6*R*,10*S*)-5,10-Dibenzyl-3,8-dimethyl-1,3,6,8-tetraaza-bicyclo[4.4.1]undecane-4,9-dione 129**

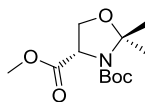
mp: 215–218 °C;  $[\alpha]_{\text{D}}^{20} = +78.7$  (c=0.75, MeOH);  $\nu_{\text{max}}$  (ATR)/cm<sup>-1</sup> 2953, 2922, 2804, 1680, 1618; <sup>1</sup>H NMR (500 MHz, CDCl<sub>3</sub>)  $\delta$  7.38–7.16 (10H, m, CH), 4.92 (2H, d, *J* = 14.9 Hz, MeNCHH), 4.24 (2H, s, NCH<sub>2</sub>N), 4.06 (2H, d, *J* = 14.9 Hz, MeNCHH),

3.93 (2H, dd,  $J = 10.3, 6.2$  Hz, COCH), 3.16–3.09 (4H, m, PhCH<sub>2</sub>), 2.93 (6H, s, NCH<sub>3</sub>); <sup>13</sup>C NMR (126 MHz, CDCl<sub>3</sub>)  $\delta$  176.5, 137.6, 128.8, 128.7, 126.9, 72.4, 70.8, 62.6, 36.9, 34.6;  $m/z$  (ES): 415.2 (M+Na<sup>+</sup>); HRMS (ES) calculated for C<sub>23</sub>H<sub>29</sub>O<sub>2</sub>N<sub>4</sub> 393.2285 (M+H<sup>+</sup>), found 393.2282.

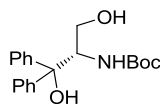
**(S)-5-Benzyl-3-methylimidazolidin-4-one 123**



*S*-Phenylalanine-*N*-methyl amide (100 mg, 0.56 mmol) was dissolved in DCM (11.2 mL). Dimethoxymethane (100  $\mu$ L, 1.12 mmol) was added followed by boron trifluoride diethyl etherate (140  $\mu$ L, 1.12 mmol). 6 Reactions were prepared in parallel and stirred at 40 °C for 18 h. The reactions were combined by pouring onto water (10 mL) and saturated sodium bicarbonate (10 mL). The layers were separated and the aqueous layer extracted with DCM (2  $\times$  20 mL). The organics were combined, washed with brine (20 mL) and dried over anhydrous potassium carbonate. The solvent was removed under reduced pressure and the residue purified by flash chromatography (5% methanol in DCM) to give the title compound as a slowly crystallising white solid (131 mg, 20%). mp: 63–65 °C;  $[\alpha]_D^{20} = -118$  (c=0.1, MeOH);  $\nu_{\max}$  (film)/cm<sup>-1</sup> 3318, 3089, 3059, 3029, 2923, 2860, 1686. <sup>1</sup>H NMR (400 MHz, CDCl<sub>3</sub>)  $\delta$  7.34–7.22 (5H, m, CH), 4.22 (1H, dd,  $J = 7.1, 0.5$  Hz, NCHH), 4.04 (1H, dd,  $J = 7.1, 0.7$  Hz, NCHH), 3.75 (1H, dd,  $J = 7.0, 4.3$  Hz, CH), 3.14 (1H, dd,  $J = 14.1, 4.3$  Hz, CHH), 2.97 (1H, dd,  $J = 14.1, 7.0$  Hz, CHH), 2.81 (3H, s, CH<sub>3</sub>), 2.02 (1H, br. s, NH); <sup>13</sup>C NMR (101 MHz, CDCl<sub>3</sub>)  $\delta$  173.8, 136.8, 129.0, 128.1, 126.3, 64.5, 60.0, 36.7, 27.3. HRMS (ES): Calculated  $m/z$  for C<sub>11</sub>H<sub>15</sub>N<sub>2</sub>O: 191.1184, found  $m/z$ : 191.1179 (M+H<sup>+</sup>).

**(S)-3-tert-Butyl 4-methyl 2,2-dimethyloxazolidine-3,4-dicarboxylate 137**<sup>121</sup>

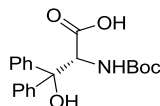
L-Serine methyl ester hydrochloride (5.00 g, 32.2 mmol) was added to a mixture of saturated sodium carbonate (40 mL) and THF (10 mL). Di-*tert*-butyl dicarbonate (8.77 g, 40.2 mmol) was added in one portion and the mixture stirred at room temperature for 18 h. The reaction mixture was poured onto water (100 mL) and extracted with ethyl acetate (3 × 100 mL). The organics were washed with 0.2 M HCl (100 mL) and brine (50 mL) before being dried over anhydrous potassium carbonate. The solvent was removed under reduced pressure. Acetone (120 mL), 2,2-dimethoxypropane (40.0 mL, 325 mmol) and boron trifluoride diethyl etherate (0.26 mL, 2.1 mmol) were added and the mixture stirred for 3 h at room temperature. The solvent was removed under reduced pressure and the residue was dissolved in DCM (100 mL), washed with a mixture of saturated sodium bicarbonate (40 mL) and water (40 mL), brine (80 mL) and dried over anhydrous potassium carbonate. The solvent was removed under reduced pressure and the residue was purified by column chromatography (20% ethyl acetate in petroleum ether) to give the target as a pale yellow oil (6.79 g, 81%).  $[\alpha]_D^{20} = -33.5$  ( $c=1.05$ , MeOH);  $\nu_{\max}$  (film)/ $\text{cm}^{-1}$  2979, 2955, 2936, 2884, 1760, 1741, 1708,  $^1\text{H NMR}$  (301 MHz, DMSO)  $\delta$  4.41 (1H, dd,  $J = 7.1$ , 3.0 Hz, CH), 4.17 (1H, dd,  $J = 9.2$ , 7.1 Hz, CHH), 3.94 (1H, dd,  $J = 9.2$ , 3.0 Hz, CHH), 3.70 (3H, s, OCH<sub>3</sub>), 1.57 (3H, s, CH<sub>3</sub>), 1.46 (3H, s, CH<sub>3</sub>), 1.40 (9H, s, C(CH<sub>3</sub>)<sub>3</sub>),  $^{13}\text{C NMR}$  (76 MHz, DMSO)  $\delta$  171.7, 151.4, 94.5, 80.2, 66.2, 59.4, 52.4, 28.5, 25.5, 24.9, HRMS (ES): Calculated  $m/z$  for C<sub>12</sub>H<sub>22</sub>NO<sub>5</sub>: 260.1498, found  $m/z$ : 260.1495 (M+H<sup>+</sup>). Analytical data were in accordance with literature values.<sup>122</sup>

**(S)-tert-Butyl (1,3-dihydroxy-1,1-diphenylpropan-2-yl)carbamate 140**

(S)-3-*tert*-Butyl 4-methyl 2,2-dimethyloxazolidine-3,4-dicarboxylate (5.0 g, 19.3 mmol) was dissolved in dry diethyl ether (100 mL) and cooled to 0 °C. 3M phenylmagnesium bromide in diethyl ether (26 mL, 78 mmol) was added dropwise

and the mixture was stirred for 1 h. The reaction was poured onto saturated ammonium chloride solution (50 mL) and extracted with ethyl acetate (3 × 100 mL). The combined organics were washed with brine (80 mL) and dried with anhydrous sodium sulfate. The solvent was removed under reduced pressure to give a pale yellow solid (7.13 g). 80% Acetic acid in water (95 mL) was added and the mixture was stirred for 24 h at room temperature. The solvent was removed under reduced pressure and the residue was purified using flash chromatography (40% ethyl acetate in petroleum ether) to give the target as a slowly crystallising pale yellow solid (4.60 g, 79%). mp: 117–118 °C [lit.<sup>123</sup> 123 °C],  $[\alpha]_{\text{D}}^{20} = -61.3$  (c=0.91, MeOH);  $\nu_{\text{max}}$  (film)/cm<sup>-1</sup> 3412, 3063, 2979, 2936, 1678, <sup>1</sup>H NMR (500 MHz, CDCl<sub>3</sub>)  $\delta$  7.44–7.40 (4H, m, CH), 7.27–7.18 (4H, m, CH), 7.15–7.07 (2H, m, CH), 5.37 (1H, d, *J* = 8.1 Hz, NH), 4.60 (1H, br. d, *J* = 7.4 Hz, NCH), 4.56 (1H, s, (Ph)<sub>2</sub>COH), 3.77 (1H, br. d, *J* = 10.1 Hz, CHH), 3.65 (1H, dd, *J* = 11.2, 2.3 Hz, CHH), 2.24 (1H, br. s, OH), 1.28 (9H, s, C(CH<sub>3</sub>)<sub>3</sub>), <sup>13</sup>C NMR (126 MHz, CDCl<sub>3</sub>)  $\delta$  156.0, 145.4, 144.6, 128.5, 128.2, 127.0, 126.9, 125.5, 125.1, 81.6, 79.8, 64.0, 55.5, 28.3, *m/z* (ES) 342.1 (M-H<sup>+</sup>), HRMS (ES): Calculated *m/z* for C<sub>20</sub>H<sub>24</sub>NO<sub>4</sub>: 342.1711, found *m/z*: 342.1704 (M-H<sup>+</sup>). Analytical data were in accordance with literature values.<sup>123</sup>

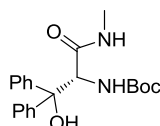
**(*R*)-2-((*tert*-Butoxycarbonyl)amino)-3-hydroxy-3,3-diphenylpropanoic acid 141**



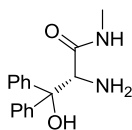
(*S*)-*tert*-Butyl (1,3-dihydroxy-1,1-diphenylpropan-2-yl)carbamate (1.00 g, 2.91 mmol) and TEMPO (45 mg, 0.29 mmol) were dissolved in acetonitrile (20 mL) and pH 6.7 phosphate buffer (12 mL). 2M sodium chlorite solution (2.91 mL, 5.82 mmol) and 0.04M bleach solution (1.45 mL, 0.058 mmol) were simultaneously added drop wise over 2 h (Note: pre mixing of sodium chlorite and bleach generates chlorine gas and should be avoided). The mixture was heated to 35 °C for 24 h. The acetonitrile was removed under reduced pressure and the residue dissolved in water (80 mL). The aqueous layer was adjusted to pH 12 with 0.5M sodium hydroxide solution and extracted with ethyl acetate (80 mL). The pH of the aqueous layer was then adjusted to pH 3 with 1M phosphoric acid and the white precipitate was extracted using ethyl acetate (3 × 80 mL) the organics were combined, dried with

anhydrous sodium sulfate and the solvent removed under reduced pressure to give a white solid (700 mg, 67%). mp: 179–181 °C;  $[\alpha]_D^{20} = -37.9$  (c=0.93, MeOH);  $\nu_{\max}$  (film)/cm<sup>-1</sup> 3397, 2978, 1720, 1686, 1641; <sup>1</sup>H NMR (500 MHz, Acetone)  $\delta$  7.52–7.42 (4H, m, CH), 7.19–7.02 (6H, m, CH), 5.96 (1H, d,  $J = 9.6$  Hz, NH), 5.30 (1H, d,  $J = 9.6$  Hz, CH), 1.16 (9H, s, C(CH<sub>3</sub>)<sub>3</sub>); <sup>13</sup>C NMR (126 MHz, Acetone)  $\delta$  173.5, 156.1, 146.0, 145.1, 128.9, 128.7, 127.9, 127.7, 126.8, 126.6, 80.2, 79.8, 59.7, 28.4;  $m/z$  (ES): 356.1 (M-H<sup>+</sup>); HRMS (ES): Calculated  $m/z$  for C<sub>20</sub>H<sub>22</sub>NO<sub>5</sub>: 356.1498, found  $m/z$ : 356.1503 (M-H<sup>+</sup>).

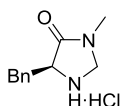
**(R)-tert-Butyl(1-hydroxy-3-(methylamino)-3-oxo-1,1-diphenylpropan-2-yl)carbamate 142**



(R)-2-((tert-Butoxycarbonyl)amino)-3-hydroxy-3,3-diphenylpropanoic acid (200 mg, 0.56 mmol) was dissolved in DMF (6 mL) and diisopropylethylamine (100  $\mu$ L) added. HATU (220 mg, 0.58 mmol) was added and the solution was stirred for 5 minutes. To the dark orange solution, 2M methylamine in THF (600  $\mu$ L, 1.2 mmol) was added and the solution was stirred for 18 h. at ambient temperature. The majority of the solvent was removed under reduced pressure and the residue taken up in water (15 mL) and chloroform (15 mL). The aqueous layer was further extracted with chloroform (2  $\times$  15 mL) and the combined organics were dried over sodium sulfate. The solvent was removed under reduced pressure and the residue purified using flash chromatography (1% methanol in DCM) to give a white crystalline solid (103 mg, 50%). mp: 156–157 °C;  $[\alpha]_D^{20} = -16$  (c=1.0, MeOH);  $\nu_{\max}$  (film)/cm<sup>-1</sup> 3433, 3343, 3093, 3058, 2978, 2935, 1685, 1654; <sup>1</sup>H NMR (400 MHz, CDCl<sub>3</sub>)  $\delta$  7.45–7.36 (4H, m, CH), 7.24–7.09 (6H, m, CH), 6.35 (1H, br. d,  $J = 3.6$  Hz, MeNH), 6.08 (1H, s, OH), 5.56 (1H, d,  $J = 8.7$  Hz, CHNH), 4.97 (1H, d,  $J = 8.7$  Hz, CH), 2.57 (3H, d,  $J = 4.9$  Hz, NCH<sub>3</sub>), 1.26 (9H, s, C(CH<sub>3</sub>)<sub>3</sub>); <sup>13</sup>C NMR (126 MHz, CDCl<sub>3</sub>)  $\delta$  172.8, 156.3, 145.1, 143.2, 128.4, 128.2, 127.1, 127.0, 125.3, 124.9, 80.4, 79.1, 57.6, 28.2, 26.0; HRMS (ES): Calculated  $m/z$  for C<sub>21</sub>H<sub>27</sub>N<sub>2</sub>O<sub>4</sub>: 371.1971, found  $m/z$ : 371.1969 (M+H<sup>+</sup>).

**(R)-2-Amino-3-hydroxy-N-methyl-3,3-diphenylpropanamide 121**

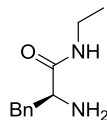
(*R*)-*tert*-Butyl(1-hydroxy-3-(methylamino)-3-oxo-1,1-diphenylpropan-2-yl)carbamate (110 mg, 0.29 mmol) was added to a solution of 2M dry HCl in ethyl acetate (10 mL) and stirred at room temperature for 24 h. The solvent was removed under reduced pressure and the residue dissolved in chloroform (10 mL) and saturated sodium bicarbonate (10 mL). The aqueous layer was further extracted with chloroform ( $2 \times 10$  mL) and the combined organics were dried over sodium sulfate. The solvent was removed under reduced pressure to give the title compound as a white crystalline solid (76 mg, 97%). mp: 45–47 °C;  $[\alpha]_{\text{D}}^{20} = -2.8$  ( $c=1.0$ , MeOH);  $\nu_{\text{max}}$  (film)/ $\text{cm}^{-1}$  3306, 2957, 2920, 1646;  $^1\text{H}$  NMR (500 MHz,  $\text{CDCl}_3$ )  $\delta$  7.44–7.33 (4H, m, CH), 7.28–7.11 (6H, m, CH), 6.94 (1H, s, OH), 4.07 (1H, br. s, CH), 2.57 (3H, d,  $J = 4.9$  Hz,  $\text{CH}_3$ ), 1.77 (2H, br. s,  $\text{NH}_2$ );  $^{13}\text{C}$  NMR (126 MHz,  $\text{CDCl}_3$ )  $\delta$  174.5, 144.9, 143.6, 128.3, 128.3, 127.3, 127.3, 126.5, 126.3, 80.1, 61.3, 25.9; HRMS (ES): Calculated  $m/z$  for  $\text{C}_{16}\text{H}_{19}\text{N}_2\text{O}_2$ : 271.1447, found  $m/z$ : 271.1444 ( $\text{M}+\text{H}^+$ ).

**(S)-5-Benzyl-3-methylimidazolidin-4-one hydrochloride 123·HCl**

(*S*)-5-Benzyl-3-methylimidazolidin-4-one (118 mg, 0.62 mmol) was dissolved in warm diethyl ether (80 mL). The solution was then cooled to ambient temperature. Dry hydrogen chloride was bubbled through the solution for 40 minutes. The title compound precipitated from solution, was recovered on a sinter and dried under reduced pressure to give cream powder (129 mg, 92%). mp (decomp.): 180 °C;  $[\alpha]_{\text{D}}^{20} = -68.0$  ( $c=0.2$ , MeOH)  $\nu_{\text{max}}$  (film)/ $\text{cm}^{-1}$  1711;  $^1\text{H}$  NMR (400 MHz, MeOD)  $\delta$  7.49–7.29 (5H, m, CH), 4.62 (1H, d,  $J = 7.5$  Hz, NCHH), 4.60 (1H, d,  $J = 7.5$  Hz, NCHH), 4.42 (1H, dd,  $J = 10.4, 3.8$  Hz, CH), 3.50 (1H, dd,  $J = 15.1, 3.8$  Hz, CHH), 3.06 (1H, dd,  $J = 15.1, 10.4$  Hz, CHH), 2.97 (3H, s,  $\text{NCH}_3$ );  $^{13}\text{C}$  NMR (101 MHz, MeOD)  $\delta$

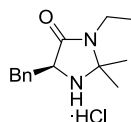
166.5, 134.2, 128.4, 128.2, 127.0, 59.1, 58.8, 33.4, 26.4. HRMS Calculated  $m/z$  for  $C_{11}H_{15}N_2O$ : 191.1184, found  $m/z$  (ES): 191.1175 (M-Cl<sup>-</sup>).

**(S)-2-Amino-N-ethyl-3-phenylpropanamide 154**



L-Phenylalanine ethyl ester hydrochloride (5.00 g, 21.8 mmol) was dissolved in 70% ethylamine in water (50 mL, 900 mmol). The reaction mixture was stirred for 72 h and then poured onto saturated sodium carbonate solution (30 mL). The mixture was extracted with chloroform (2 × 50 mL) and the combined organics were dried over anhydrous sodium carbonate. The solvent was removed under reduced pressure to give a colourless oil (3.98 g, 95%).  $[\alpha]_D^{20} = +30.6$  (c=2.2, MeOH);  $\nu_{\max}$  (ATR)/ $\text{cm}^{-1}$  3302, 3084, 3063, 3026, 2972, 2932, 2872, 1645;  $^1\text{H}$  NMR (400 MHz,  $\text{CDCl}_3$ )  $\delta$  7.56–7.02 (6H, m, CH and NH), 3.60 (1H, dd,  $J = 9.3, 4.1$  Hz, CH), 3.44–3.16 (3H, m, PhCHH and  $\text{CH}_2$ ), 2.71 (1H, dd,  $J = 13.7, 9.3$  Hz, PhCHH), 1.35 (2H, br. s,  $\text{NH}_2$ ), 1.14 (3H, t,  $J = 7.3$  Hz,  $\text{CH}_3$ );  $^{13}\text{C}$  NMR (101 MHz,  $\text{CDCl}_3$ )  $\delta$  174.1, 138.2, 129.5, 128.8, 126.9, 56.6, 41.2, 34.0, 14.9;  $m/z$  (ES/APCI): 193.1 (M+H<sup>+</sup>).

**(S)-5-Benzyl-3-ethyl-2,2-dimethylimidazolidin-4-one hydrochloride 155·HCl**

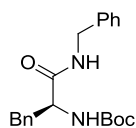


(S)-2-Amino-N-ethyl-3-phenylpropanamide (800 mg, 4.17 mmol) was dissolved in methanol (20 mL) and acetone (10 mL). A small crystal of *p*-toluenesulfonic acid (<1 mg) was added and the mixture was heated under reflux for 18 h. The solvent was removed under reduced pressure and the residue taken up in chloroform (50 mL) and washed with saturated sodium carbonate solution (2 × 30 mL). The organic layer was dried over anhydrous sodium carbonate and concentrated under reduced pressure. The residue was taken up in diethyl ether (100 mL) and hydrogen chloride gas was bubbled through for 30 minutes. The resultant precipitate was recovered on a sinter, washed with diethyl ether (30 mL) and dried under reduced pressure to give a white powder (840 mg, 75%). mp: 77–78 °C  $[\alpha]_D^{20} = -68.2$  (c=1.0, MeOH);  $\nu_{\max}$

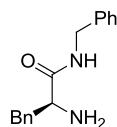


(ATR)/cm<sup>-1</sup> 2978, 2936, 1707; <sup>1</sup>H NMR (400 MHz, MeOD) δ 7.57–7.20 (5H, m, CH), 4.67 (1H, dd, *J* = 10.6, 3.5 Hz, CH), 3.52 (1H, dd, *J* = 15.3, 3.5 Hz, CHCHH), 3.52–3.44 (1H, m, CHH), 3.39–3.30 (1H, m, CHH), 3.13 (1H, dd, *J* = 15.3, 10.6 Hz, CHCHH), 1.78 (3H, s, CH<sub>3</sub>), 1.62 (3H, s, CH<sub>3</sub>), 1.25 (3H, t, *J* = 7.2 Hz, CH<sub>2</sub>CH<sub>3</sub>); <sup>13</sup>C NMR (101 MHz, MeOD) δ 167.9, 136.5, 130.3, 130.2, 128.7, 79.3, 59.4, 36.4, 34.9, 24.9, 23.7, 14.7; *m/z* (ES): 233.1 (M-Cl<sup>-</sup>); HRMS (ES) calculated for C<sub>14</sub>H<sub>21</sub>N<sub>2</sub>O 233.1648 (M-Cl<sup>-</sup>), found 233.1648.

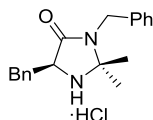
**(*S*)-tert-Butyl (1-(benzylamino)-1-oxo-3-phenylpropan-2-yl)carbamate 158**<sup>124</sup>



*N*-Boc-L-Phenylalanine (1.00 g, 3.8 mmol) was dissolved in dry dichloromethane (30 mL). The reaction mixture was cooled to 0 °C before *N,N'*-dicyclohexylcarbodiimide (0.86 g, 4.20 mmol) was added followed by dropwise addition of benzylamine (0.58 mL, 5.3 mmol). The reaction mixture was allowed to reach ambient temperature and was stirred for 18 h. The mixture was filtered through a pad of celite and the filter cake was washed with dichloromethane (20 mL). The solvent was removed under reduced pressure and the residue purified using flash chromatography (20% ethyl acetate in petroleum ether) to give a white solid (850 mg, 63%). mp: 129–131 °C [lit.<sup>125</sup> 120 °C]; [α]<sub>D</sub><sup>20</sup> = -8.0 (c=0.2, MeOH); ν<sub>max</sub> (ATR)/cm<sup>-1</sup> 3336, 3295, 3068, 3027, 2984, 2934, 2872, 1677, 1658; <sup>1</sup>H NMR (400 MHz, CDCl<sub>3</sub>) δ 7.33–7.09 (10H, m, CH), 6.12 (1H, s, NH), 5.08 (1H, s, NH), 4.44–4.32 (3H, m, NCH<sub>2</sub>Ph and CH), 3.18–3.03 (2H, m, CHCH<sub>2</sub>), 1.41 (9H, s, C(CH<sub>3</sub>)<sub>3</sub>); <sup>13</sup>C NMR (101 MHz, CDCl<sub>3</sub>) δ 170.5, 154.9, 137.2, 136.2, 128.8, 128.2, 128.1, 127.2, 126.9, 126.4, 79.8, 55.6, 42.9, 38.1, 27.8; *m/z* (ES): 377.0 (M+Na<sup>+</sup>). Analytical data were in accordance with literature values.<sup>125</sup>

**(S)-2-Amino-N-benzyl-3-phenylpropanamide 159**

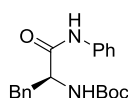
(*S*)-*tert*-Butyl (1-(benzylamino)-1-oxo-3-phenylpropan-2-yl)carbamate (700 mg, 2.00 mmol) was dissolved in dichloromethane (40 mL). Trifluoroacetic acid (10 mL) was added dropwise and the reaction mixture was rapidly stirred for 2 h. The mixture was carefully poured onto saturated sodium carbonate solution (50 mL) and extracted with dichloromethane (2 × 30 mL). The combined organics were dried over anhydrous sodium carbonate and the solvent was removed under reduced pressure to give a white solid (470 mg, 93%). mp: 62–64 °C [lit.<sup>126</sup> 59–61 °C];  $[\alpha]_{\text{D}}^{20} = -42.0$  (c=0.1, MeOH);  $\nu_{\text{max}}$  (ATR)/ $\text{cm}^{-1}$  3364, 3302, 3085, 3060, 3029, 2928, 2856, 1654;  $^1\text{H}$  NMR (400 MHz,  $\text{CDCl}_3$ )  $\delta$  7.70 (1H, br. s, NH), 7.45–7.13 (10H, m, CH), 4.55–4.35 (2H, m,  $\text{NCH}_2$ ), 3.63 (1H, dd,  $J = 8.9, 4.3$  Hz, CH), 3.26 (1H, dd,  $J = 13.7, 4.3$  Hz, CHH), 2.78 (1H, dd,  $J = 13.7, 8.9$  Hz, CHH), 1.31 (2H, br. s,  $\text{NH}_2$ );  $^{13}\text{C}$  NMR (101 MHz,  $\text{CDCl}_3$ )  $\delta$  174.1, 138.3, 137.7, 129.2, 128.5, 128.5, 127.5, 127.2, 126.6, 56.3, 42.9, 40.9;  $m/z$  (ES): 255.0 ( $\text{M}+\text{H}^+$ ). Analytical data were in accordance with literature values.<sup>127</sup>

**(S)-3,5-Dibenzyl-2,2-dimethylimidazolidin-4-one hydrochloride 160·HCl**

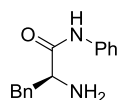
(*S*)-2-Amino-*N*-benzyl-3-phenylpropanamide (470 mg, 1.85 mmol) was dissolved in methanol (40 mL) and acetone (20 mL). A small crystal of *p*-toluenesulfonic acid (<1 mg) was added and the mixture was heated under reflux for 18 h. The solvent was removed under reduced pressure and the residue was taken up in chloroform (50 mL) and washed with saturated sodium carbonate solution (2 × 30 mL). The organic layer was dried over anhydrous sodium carbonate and concentrated under reduced pressure. The residue was taken up in diethyl ether (100 mL) and hydrogen chloride gas was bubbled through for 30 minutes. The resultant precipitate was recovered on a sinter, washed with diethyl ether (30 mL) and dried under reduced pressure to give a

white powder (570 mg, 93%). mp: 112–114 °C  $[\alpha]_{\text{D}}^{20} = -42.4$  (c=1.0, MeOH);  $\nu_{\text{max}}$  (ATR)/ $\text{cm}^{-1}$  1735;  $^1\text{H}$  NMR (400 MHz, MeOD)  $\delta$  7.60–7.20 (10H, m, CH), 4.78 (1H, dd,  $J = 10.6, 3.6$  Hz, CH), 4.67 (1H, d,  $J = 15.7$  Hz, PhCHH), 4.59 (1H, d,  $J = 15.7$  Hz, PhCHH), 3.61 (1H, dd,  $J = 15.2, 3.6$  Hz, CHCHH), 3.16 (1H, dd,  $J = 15.2, 10.6$  Hz, CHCHH), 1.65 (3H, s,  $\text{CH}_3$ ), 1.49 (3H, s,  $\text{CH}_3$ );  $^{13}\text{C}$  NMR (101 MHz, MeOD)  $\delta$  168.5, 138.0, 136.5, 130.3, 130.2, 129.9, 129.1, 129.0, 128.8, 79.5, 59.5, 44.4, 35.0, 25.1, 23.6;  $m/z$  (ES/APCI): 295.2 (M-Cl<sup>-</sup>); HRMS (ES) calculated for  $\text{C}_{19}\text{H}_{23}\text{N}_2\text{O}$  295.1805 (M-Cl<sup>-</sup>), found 295.1807.

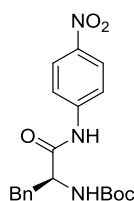
**(S)-tert-Butyl (1-oxo-3-phenyl-1-(phenylamino)propan-2-yl)carbamate 165**<sup>128</sup>



(S)-2-((tert-Butoxycarbonyl)amino)-3-phenylpropanoic acid (1.00 g, 3.77 mmol) was dissolved in dry DCM (20 mL) and cooled to 0 °C. *N,N*-Dicyclohexylcarbodiimide (860 mg, 4.15 mmol) was dissolved in dry DCM (10 mL) and added drop wise over 5 minutes whilst rapidly stirring. Distilled aniline (0.48 mL, 5.3 mmol) was added and the mixture allowed to reach ambient temperature. After stirring for 24 h the mixture was filtered through celite and concentrated under reduced pressure. The residue was purified using flash chromatography (20% ethyl acetate in petroleum ether) to give the title compound as a white solid (880 mg, 69%). mp: 125–127 °C [lit.<sup>129</sup> 123 °C];  $[\alpha]_{\text{D}}^{20} = +34$  (c=0.4, MeOH);  $\nu_{\text{max}}$  (film)/ $\text{cm}^{-1}$  3344, 3312, 2969, 1686;  $^1\text{H}$  NMR (400 MHz,  $\text{CDCl}_3$ )  $\delta$  7.99 (1H, s, NH), 7.41–7.24 (9H, m, CH), 7.10 (1H, app. t,  $J = 7.4$  Hz, CH), 5.30 (1H, s, NH), 4.54 (1H, br. s, CH), 3.27–3.05 (2H, m,  $\text{CH}_2$ ), 1.44 (9H, s,  $\text{C}(\text{CH}_3)_3$ );  $^{13}\text{C}$  NMR (101 MHz,  $\text{CDCl}_3$ )  $\delta$  169.2, 155.3, 136.8, 136.2, 128.8, 128.4, 128.3, 126.5, 124.0, 119.6, 80.1, 56.3, 38.0, 27.8; HRMS Calculated  $m/z$  for  $\text{C}_{20}\text{H}_{24}\text{N}_2\text{O}_3\text{Na}$ : 363.1679, found  $m/z$  (ES): 363.1673 (M+Na<sup>+</sup>). Analytical data were in accordance with literature values.<sup>129</sup>

**(S)-2-Amino-N,3-diphenylpropanamide 166**<sup>128</sup>

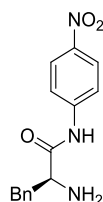
(*S*)-*tert*-Butyl (1-oxo-3-phenyl-1-(phenylamino)propan-2-yl)carbamate (760 mg 2.24 mmol) was dissolved in DCM (50 mL) and TFA (10 mL). The mixture was stirred at ambient temperature for 30 minutes. The solvent was removed under reduced pressure and the residue was dissolved in minimal ethyl acetate (~3 mL). Diethyl ether (~180 mL) was added and the TFA salt was allowed to precipitate. The solid was recovered on a sinter, dissolved in chloroform (30 mL) and washed with saturated sodium carbonate (15 mL). The organics were dried over anhydrous potassium carbonate and the solvent was removed under reduced pressure. The residue was recrystallized from petroleum ether and ethyl acetate to give the title compound as white flakes (443 mg, 82%). mp: 71–72 °C [lit.<sup>130</sup> 59–61 °C];  $[\alpha]_D^{20} = +62$  (c=0.1, MeOH);  $\nu_{\max}$  (film)/cm<sup>-1</sup> 3384, 3263, 3083, 3057, 3027, 2938, 1664; <sup>1</sup>H NMR (400 MHz, CDCl<sub>3</sub>)  $\delta$  9.43 (1H, s, NH), 7.65–7.60 (2H, m, CH), 7.40–7.26 (7H, m, CH), 7.16–7.11 (1H, m, CH), 3.76 (1H, dd, *J* = 9.5, 4.0 Hz, CH), 3.41 (1H, dd, *J* = 13.8, 4.0 Hz, CHH), 2.82 (1H, dd, *J* = 13.8, 9.5 Hz, CHH), 1.50 (2H, s, NH<sub>2</sub>); <sup>13</sup>C NMR (101 MHz, CDCl<sub>3</sub>)  $\delta$  171.9, 137.2 (2C), 128.8, 128.5, 128.3, 126.5, 123.6, 119.0, 56.3, 40.2; HRMS calculated *m/z* for C<sub>15</sub>H<sub>17</sub>N<sub>2</sub>O: 241.1335, found *m/z*: 241.1333 (M+H<sup>+</sup>). Analytical data were in accordance with literature values.<sup>130</sup>

**(S)-2-((*tert*-Butoxycarbonyl)amino)-1-oxo-3-phenylpropanoic acid 168**

(*S*)-2-((*tert*-Butoxycarbonyl)amino)-3-phenylpropanoic acid (1.00 g, 3.77 mmol) was dissolved in dry DCM (30 mL) and cooled to 0 °C. *N,N'*-Dicyclohexylcarbodiimide (0.86 g, 4.15 mmol) was added over 5 minutes followed by 4-nitroaniline (0.73 g, 5.3 mmol). The reaction was sealed and stirred for 48 h. The mixture was filtered through celite and the solvent was removed under reduced pressure. The residue was

purified using flash chromatography (20% ethyl acetate in petroleum ether) to give the compound as an off white crispy solid (373 mg, 18%). mp: 160–162 °C [lit.<sup>131</sup> 158–160 °C];  $[\alpha]_{\text{D}}^{20} = +76$  (c=0.5, MeOH);  $\nu_{\text{max}}$  (film)/ $\text{cm}^{-1}$ : 3411, 3334, 3280, 3252, 3541, 3094, 3055, 2986, 2932, 1688, 1660;  $^1\text{H}$  NMR (400 MHz,  $\text{CDCl}_3$ )  $\delta$  8.81 (1H, br. s, NH), 8.14 (2H, d,  $J = 9.0$  Hz,  $\text{NO}_2\text{CCH}$ ), 7.58–7.53 (2H, m, HNCCH), 7.38–7.19 (5H, m, CH), 5.20 (1H, d,  $J = 7.6$  Hz, CHNH), 4.56 (1H, br. d,  $J = 6.0$  Hz, CH), 3.21 (1H, dd,  $J = 13.9, 6.8$  Hz, CHH), 3.12 (1H, dd,  $J = 13.9, 7.7$  Hz, CHH), 1.44 (9H, s,  $\text{C}(\text{CH}_3)_3$ );  $^{13}\text{C}$  NMR (101 MHz,  $\text{CDCl}_3$ )  $\delta$  170.5, 156.4, 143.7, 143.4, 136.2, 129.3, 129.1, 127.4, 125.1, 119.3, 81.4, 57.0, 37.9, 28.4; HRMS calculated  $m/z$  for  $\text{C}_{20}\text{H}_{22}\text{N}_3\text{O}_5$ : 384.1565, found  $m/z$ : 384.1567 ( $\text{M}-\text{H}^+$ ). Analytical data were in accordance with literature values.<sup>131</sup>

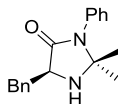
### (*S*)-2-Amino-*N*-(4-nitrophenyl)-3-phenylpropanamide 169



(*S*)-*tert*-Butyl(1-((4-nitrophenyl)amino)-1-oxo-3-phenylpropan-2-yl)carbamate (329 mg, 0.85 mmol) was dissolved in dry DCM (25 mL). Trifluoroacetic acid (5 mL) was added and the reaction mixture was stirred at ambient temperature. The reaction was monitored by TLC (20% ethyl acetate in petroleum ether) and once observed to be complete was quenched with saturated sodium bicarbonate (~60 mL). The organic layer was separated, washed with brine (20 mL) and dried over anhydrous sodium sulfate. The solvent was removed under reduced pressure and the residue was recrystallized from ethyl acetate and petroleum ether to give the product as pale green crystals (157 mg, 65%). mp: 144–145 °C [lit.<sup>130</sup> 155–156 °C];  $[\alpha]_{\text{D}}^{20} = +81$  (c=1.0, MeOH);  $\nu_{\text{max}}$  (film)/ $\text{cm}^{-1}$  3400, 3340, 3228, 1684;  $^1\text{H}$  NMR (500 MHz,  $\text{CDCl}_3$ )  $\delta$  9.91 (1H, s, OCNH), 8.26–8.21 (2H, m,  $\text{NO}_2\text{CCH}$ ), 7.81–7.76 (2H, m, NCCH), 7.38–7.24 (5H, m, CH), 3.79 (1H, dd,  $J = 9.4, 4.0$  Hz, CH), 3.38 (1H, dd,  $J = 13.9, 4.0$  Hz, CHH), 2.84 (1H, dd,  $J = 13.9, 9.4$  Hz, CHH), 1.56 (2H, s,  $\text{NH}_2$ );  $^{13}\text{C}$  NMR (126 MHz,  $\text{CDCl}_3$ )  $\delta$  173.1, 143.7, 143.6, 137.3, 129.4, 129.1, 127.4, 125.3,

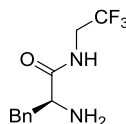
119.0, 56.9, 40.6; HRMS calculated  $m/z$  for  $C_{15}H_{16}N_3O_3$ : 286.1186, found  $m/z$ : 286.1183 ( $M+H^+$ ). Analytical data were in accordance with literature values.<sup>130</sup>

### (*S*)-5-Benzyl-2,2-dimethyl-3-phenylimidazolidin-4-one 161



(*S*)-2-Amino-*N*,3-diphenylpropanamide (200 mg, 0.83 mmol) was dissolved in methanol (15 mL) and acetone (5 mL). One small crystal of *p*-toluenesulfonic acid (<1 mg) was added and the mixture was heated to reflux for 18 h. The solvent was removed under reduced pressure and the residue was purified using flash chromatography (50% ethyl acetate in petroleum ether) to give the target compound as a colourless oil (130 mg, 46%).  $[\alpha]_D^{20} = -129$  ( $c=2.0$ , MeOH);  $\nu_{\max}$  (film)/ $\text{cm}^{-1}$  3331, 3062, 3029, 2978, 2928, 2871, 1694;  $^1\text{H NMR}$  (400 MHz,  $\text{CDCl}_3$ )  $\delta$  7.50–7.24 (8H, m, CH), 7.16–7.02 (2H, m, CH), 4.03 (1H, dd,  $J = 5.8, 4.9$  Hz, CH), 3.26 (1H, dd,  $J = 14.2, 5.8$  Hz, CHH), 3.20 (1H, dd,  $J = 14.2, 4.9$  Hz, CHH), 1.39 (3H, s,  $\text{CH}_3$ ), 1.14 (3H, s,  $\text{CH}_3$ );  $^{13}\text{C NMR}$  (101 MHz,  $\text{CDCl}_3$ )  $\delta$  174.3, 136.9, 136.1, 129.9, 129.4, 128.9, 128.7, 128.2, 127.1, 78.0, 59.3, 36.9, 28.5, 27.4;  $m/z$  (ES): 281.1 ( $M+H$ ). HRMS HRMS calculated  $m/z$  for  $C_{18}H_{21}N_2O$ : 281.1648, found  $m/z$ : 281.1645 ( $M+H^+$ ).

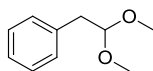
### (*S*)-2-Amino-3-phenyl-*N*-(2,2,2-trifluoroethyl)propanamide 172



(*S*)-2-((*tert*-Butoxycarbonyl)amino)-3-phenylpropanoic acid (2.00 g, 7.55 mmol) was dissolved in DMF (24 mL). HATU (2.88 g, 7.58 mmol) was added in portions. The mixture was stirred and Hünigs base (2.6 mL, 15 mmol) was added dropwise. After stirring for 15 minutes the mixture was cooled to 0 °C. Trifluoroethylamine (660  $\mu\text{L}$ , 8.41 mmol) was added dropwise and the mixture allowed to reach ambient temperature. After 18 hours the DMF was removed under reduced pressure. Dichloromethane (100 mL) was added to the resultant oil and the organic layer was washed with saturated sodium bicarbonate solution ( $2 \times 50$  mL), 5% lithium chloride

solution (2 × 50 mL) and water (50 mL). The organics were then dried over sodium sulfate and the solvent was removed under reduced pressure. Dichloromethane (40 mL) was added followed by TFA (10 mL) and the mixture was stirred for 15 minutes. The reaction was quenched with saturated sodium bicarbonate solution and extracted with dichloromethane (2 × 50 mL). The organics were combined and then dried over potassium carbonate. The solvent was removed under reduced pressure. The resultant solid was recrystallized from ethyl acetate and petroleum ether to give a white crystalline solid (927 mg, 50%). mp: 97–98 °C;  $[\alpha]_D^{20} = +14$  (c=1.0, MeOH);  $\nu_{\max}$  (ATR)/ $\text{cm}^{-1}$  3387, 3308, 3069, 3036, 3001, 2959, 2922, 2857, 1667;  $^1\text{H}$  NMR (500 MHz,  $\text{CDCl}_3$ )  $\delta$  7.82 (1H, br. s, NH), 7.36–7.20 (5H, m, CH), 4.00–3.84 (2H, m,  $\text{CF}_3\text{CH}_2$ ), 3.69 (1H, dd,  $J = 9.1, 3.8$  Hz, CH), 3.29 (1H, dd,  $J = 13.8, 3.8$  Hz, CHH), 2.75 (1H, dd,  $J = 13.8, 9.1$  Hz, CHH), 1.43 (2H, s,  $\text{NH}_2$ );  $^{13}\text{C}$  NMR (126 MHz,  $\text{CDCl}_3$ )  $\delta$  174.9, 137.5, 129.4, 129.0, 127.1, 124.1 (1C,  $J = 278$  Hz,  $\text{CF}_3$ ), 56.3, 40.8, 40.2 (1C, q,  $J = 35$  Hz,  $\text{CH}_2\text{CF}_3$ );  $^{19}\text{F}$  NMR (376 MHz,  $\text{CDCl}_3$ )  $\delta$  -72.48 (t,  $J = 9.1$  Hz,  $\text{CF}_3$ );  $m/z$  (ES): 247.0 ( $\text{M}+\text{H}^+$ ); HRMS calculated  $m/z$  for  $\text{C}_{11}\text{H}_{14}\text{N}_2\text{O}_1\text{F}_3$ : 247.1053, found  $m/z$ : 247.1056 ( $\text{M}+\text{H}^+$ ).

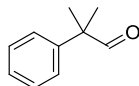
### Phenylacetaldehyde dimethyl acetal **199**<sup>132</sup>



Phenylacetaldehyde (1.17 g, 7.07 mmol) was dissolved in methanol (33 mL). Hydroxylamine hydrochloride was added (70 mg, 0.73 mmol) followed by powdered sodium hydroxide (40 mg, 1 mmol). The mixture was stirred for 18 h and then poured onto a mixture of saturated ammonium chloride (10 mL) and water (10 mL) and then extracted with diethyl ether (3 × 20 mL). The organics were combined, washed with brine (20 mL) and dried over magnesium sulfate. The solvent was removed under reduced pressure and the residue was purified by flash chromatography (20% ethyl acetate in petroleum ether) to give a colourless oil (1.24 g, 75%).  $\nu_{\max}$  (ATR)/ $\text{cm}^{-1}$  2932, 2899, 2830;  $^1\text{H}$  NMR (500 MHz,  $\text{CDCl}_3$ )  $\delta$  7.36–7.17 (5H, m, CH), 4.56 (1H, t,  $J = 5.6$  Hz, CH), 3.36 (6H, s,  $\text{OCH}_3$ ), 2.93 (2H, d,  $J = 5.6$  Hz,  $\text{CH}_2$ );  $^{13}\text{C}$  NMR (126 MHz,  $\text{CDCl}_3$ )  $\delta$  137.2, 129.6, 128.5, 126.5, 105.5, 53.5,

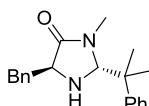
39.8;  $m/z$  (CI): 135.0 ( $M^-OCH_3$ ). Analytical data were in accordance with literature values.<sup>133</sup>

### 2-Methyl-2-phenylpropanal 201<sup>134</sup>



60% Sodium hydride in mineral oil (1.05 g, 26.4 mmol) was added to anhydrous THF (10 mL). 2-Phenylpropanal (3.20 mL, 24.0 mmol) was added drop wise over 1 h. The mixture was stirred for 30 minutes and then cooled to 0 °C. Iodomethane (3.00 mL, 48.0 mmol) was added dropwise and the mixture was allowed to warm to ambient temperature. The white suspension was poured onto saturated sodium bicarbonate solution (25 mL) and extracted with diethyl ether (3 × 50 mL). The combined organics were dried over magnesium sulfate and the solvent removed under reduced pressure to give a colourless oil (3.50 g, 99%).  $\nu_{\max}$  (ATR)/ $\text{cm}^{-1}$  2970, 2926, 2803, 2704, 1721;  $^1\text{H}$  NMR (500 MHz,  $\text{CDCl}_3$ )  $\delta$  9.52 (1H, s, CHO), 7.43–7.36 (2H, m, CH), 7.32–7.27 (3H, m, CH), 1.48 (6H, s,  $\text{CH}_3$ );  $^{13}\text{C}$  NMR (126 MHz,  $\text{CDCl}_3$ )  $\delta$  202.3, 141.4, 129.0, 127.4, 126.8, 50.6, 22.6;  $m/z$  (CI): 149.0 ( $M+H^+$ ). Analytical data were in accordance with literature values.<sup>135</sup>

### (2*R*,5*S*)-5-Benzyl-3-methyl-2-(2-phenylpropan-2-yl)imidazolidin-4-one 200

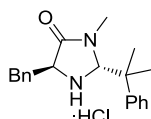


*S*-Phenylalanine-*N*-methyl amide (2.00 g, 11.2 mmol) was dissolved in methanol (150 mL). 2-Methyl-2-phenylpropanal (1.60 mL, 10.7 mmol) was added followed by a small crystal of *p*-toluenesulfonic acid (<1 mg). The mixture was heated under reflux for 18 h. and then cooled to ambient temperature. The solvent was removed under reduced pressure and the residue was purified by flash chromatography (60% ethyl acetate in petroleum ether). The chromatographed product was further purified by recrystallization from ethyl acetate and petroleum ether to give colourless needles (1.30 g, 38%). mp: 114–116 °C;  $[\alpha]_D^{25} = -20.0$  ( $c=0.7$ , MeOH);  $\nu_{\max}$  (ATR)/ $\text{cm}^{-1}$  3057, 3026, 2969, 2920, 1688;  $^1\text{H}$  NMR (400 MHz,  $\text{CDCl}_3$ )  $\delta$  7.38–7.17 (10H, m, CH), 4.37 (1H, d,  $J = 1.8$  Hz, NCHN), 3.70–3.62 (1H, m, CH), 3.09 (1H, dd,  $J =$



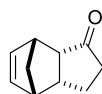
14.1, 4.3 Hz, *CHH*), 2.89 (1H, dd,  $J = 14.1, 7.0$  Hz, *CHH*), 2.34 (3H, s, *NCH*<sub>3</sub>), 1.94 (1H, br. s, *NH*), 1.32 (3H, s, *PhCH*<sub>3</sub>), 1.32 (3H, s, *PhCH*<sub>3</sub>); <sup>13</sup>C NMR (101 MHz, CDCl<sub>3</sub>)  $\delta$  175.1, 146.0, 137.5, 129.6, 128.7, 128.5, 126.8, 126.7, 126.5, 83.2, 59.4, 44.3, 38.6, 30.5, 26.7, 21.0;  $m/z$  (ES/APCI): 309.1 ( $M+H^+$ ); HRMS (ES) calculated for C<sub>20</sub>H<sub>25</sub>N<sub>2</sub>O 309.1961 ( $M+H^+$ ), found 309.1962.

**(2*R*,5*S*)-5-Benzyl-3-methyl-2-(2-phenylpropan-2-yl)imidazolidin-4-one hydrochloride 200·HCl**



(2*R*,5*S*)-5-Benzyl-3-methyl-2-(2-phenylpropan-2-yl)imidazolidin-4-one (370 mg, 1.20 mmol) was dissolved in diethyl ether (80 mL). Hydrogen chloride gas was bubbled through the solution for 15 minutes. The white precipitate was recovered on a sinter, washed with diethyl ether (20 mL) and dried under reduced pressure to give a white powder (380 mg, 92%). mp: 198–200 °C;  $[\alpha]_D^{25} = -62.7$  ( $c=1.0$ , MeOH);  $\nu_{\max}$  (ATR)/cm<sup>-1</sup> 1722; <sup>1</sup>H NMR (400 MHz, DMSO)  $\delta$  7.49–7.21 (10H, m, *CH*), 5.13 (1H, br. s, *NCHN*), 3.87 (1H, br. s, *CH*), 3.15 (2H, app. d,  $J = 5.9$  Hz, *CH*<sub>2</sub>), 2.38 (3H, s, *NCH*<sub>3</sub>), 1.45 (3H, s, *CH*<sub>3</sub>), 1.44 (3H, s, *CH*<sub>3</sub>); <sup>13</sup>C NMR (101 MHz, DMSO)  $\delta$  168.8, 143.4, 136.1, 129.3, 128.5, 128.3, 127.2, 126.8, 126.5, 79.5, 57.7, 42.2, 34.7, 30.6, 25.1, 21.2;  $m/z$  (ES/APCI): 309.3 ( $M-Cl$ ); HRMS (ES) calculated for C<sub>20</sub>H<sub>25</sub>N<sub>2</sub>O 309.1961 ( $M-Cl$ ), found 309.1963.

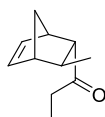
***endo*-Tricyclo[5.2.1.0(2,6)]dec-8-en-3-one 209**



Cyclopentenone (500  $\mu$ L, 5.98 mmol) was added to a solution of *N,O*-dimethylhydroxylamine hydrochloride (116 mg, 1.19 mmol, 20 mol%) in water (1.5 mL). Freshly distilled cyclopentadiene (750  $\mu$ L, 8.93 mmol) was added and the mixture was rapidly stirred for 20 h. at ambient temperature. The reaction mixture was subjected to flash chromatography (10% diethyl ether in petroleum ether) to give the product as a white volatile solid (740 mg, 84%). mp: 73–74 °C;  $\nu_{\max}$  (ATR)/cm<sup>-1</sup>

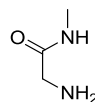
2961, 2938, 2864, 1724;  $^1\text{H}$  NMR (400 MHz,  $\text{CDCl}_3$ )  $\delta$  6.20 (1H, dd,  $J = 5.7, 2.9$  Hz), 6.09 (1H, dd,  $J = 5.7, 2.9$  Hz), 3.21–3.14 (1H, m), 3.02–2.92 (2H, m), 2.83 (1H, ddd,  $J = 8.9, 4.6, 1.4$  Hz), 2.18–2.07 (1H, m), 2.05–1.91 (2H, m), 1.57–1.44 (2H, m), 1.44–1.37 (1H, m);  $^{13}\text{C}$  NMR (101 MHz,  $\text{CDCl}_3$ )  $\delta$  222.4, 136.3, 134.9, 54.4, 52.4, 47.6, 47.1, 41.4, 40.7, 22.8;  $m/z$  (CI): 148.9 ( $\text{M}+\text{H}^+$ ). Analytical data were consistent with literature values.<sup>13</sup>

### ***endo*--Methylbicyclo[2.2.1]hept-5-en-2-yl)propan-1-one 211**



4-Hexen-3-one (680  $\mu\text{L}$ , 5.95 mmol) was added to a solution of *N,O*-dimethylhydroxylamine hydrochloride (116 mg, 1.19 mmol, 20 mol%) in water (1.5 mL). Freshly distilled cyclopentadiene (750  $\mu\text{L}$ , 8.93 mmol) was added and the mixture was rapidly stirred for 20 h. at ambient temperature. The reaction mixture was subjected to flash chromatography (10% diethyl ether in petroleum ether) to give the product as a colourless oil (240 mg, 24%).  $\nu_{\text{max}}$  (ATR)/ $\text{cm}^{-1}$  2959, 2870, 1705;  $^1\text{H}$  NMR (400 MHz,  $\text{CDCl}_3$ )  $\delta$  6.22 (1H, dd,  $J = 5.7, 3.1$  Hz, *CHCH*), 5.90 (1H, dd,  $J = 5.7, 2.8$  Hz, *CHCH*), 3.14 (1H, br. s), 2.49–2.37 (4H, m), 1.93–1.85 (1H, m), 1.60–1.56 (1H, m), 1.46–1.40 (1H, m), 1.15 (3H, d,  $J = 7.0$  Hz,  $\text{CH}_3$ ), 1.02 (3H, t,  $J = 7.3$  Hz,  $\text{CH}_2\text{CH}_3$ );  $^{13}\text{C}$  NMR (101 MHz,  $\text{CDCl}_3$ )  $\delta$  211.7, 138.6, 132.7, 60.8, 49.2, 46.4, 35.9, 34.9, 21.2, 7.9;  $m/z$  (CI): 165.0 ( $\text{M}+\text{H}^+$ ). Analytical data were consistent with literature values.<sup>136</sup>

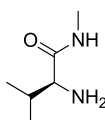
### **Glycine *N*-methyl amide 215<sup>78</sup>**



Glycine methyl ester hydrochloride (10.0 g, 79.7 mmol) was stirred in an ethanolic solution of methylamine 33 wt.% (50 mL, 402 mmol) for 78 h at ambient temperature. Sodium hydroxide (3.5 g, 88 mmol, 1.1 eq) was added and stirring continued for 30 minutes. The solvent was removed under reduced pressure and the residue extracted into ethyl acetate (3  $\times$  40 mL). The combined extractions were

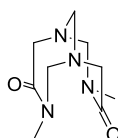
filtered through a sinter and the solvent was removed under reduced pressure to give the product as a yellow oil (6.57 g, 94%).  $\nu_{\max}$  (ATR)/  $\text{cm}^{-1}$  3340, 3078, 2941, 2899, 1643, 1537;  $^1\text{H}$  NMR (400 MHz,  $\text{CDCl}_3$ )  $\delta$  7.35 (1H, br. s, NH), 3.10 (2H, s,  $\text{CH}_2$ ), 2.60 (3H, d,  $J = 4.9$  Hz,  $\text{NCH}_3$ ), 1.37 (2H, br. s,  $\text{NH}_2$ );  $^{13}\text{C}$  NMR (101 MHz,  $\text{CDCl}_3$ )  $\delta$  173.4, 44.4, 25.3;  $m/z$  (ES): 88.9 ( $\text{M}+\text{H}^+$ ). Analytical data were in accordance with literature values.<sup>78</sup>

### L-Valine N-methyl amide 217



L-Valine methyl ester hydrochloride (5.0 g, 30 mmol) was stirred in an ethanolic solution of methylamine 33 wt.% (30 mL, 240 mmol) for 72 h at ambient temperature. The mixture was concentrated under reduced pressure. The resulting slurry was taken up in saturated sodium carbonate (15 mL) and extracted with chloroform ( $3 \times 30$  mL). The combined organic extracts were dried over anhydrous potassium carbonate and the solvent was removed under reduced pressure to give the product as a colourless oil (3.43 g, 88%).  $[\alpha]_{\text{D}}^{20} = +17.3$  ( $c=2.4$ , MeOH);  $\nu_{\max}$  (ATR)/  $\text{cm}^{-1}$  3293, 2959, 2934, 2907, 1645, 1530;  $^1\text{H}$  NMR (400 MHz,  $\text{CDCl}_3$ )  $\delta$  7.25 (1H, br. s, NH), 3.20 (1H, d,  $J = 3.9$  Hz,  $\text{NH}_2\text{CH}$ ), 2.80 (3H, d,  $J = 5.0$  Hz,  $\text{NCH}_3$ ), 2.27 (1H, heptd,  $J = 6.9, 3.9$  Hz,  $(\text{CH}_3)_2\text{CH}$ ), 1.25 (2H, s,  $\text{NH}_2$ ), 0.96 (3H, d,  $J = 6.9$  Hz,  $\text{CH}_3$ ), 0.80 (3H, d,  $J = 6.9$  Hz,  $\text{CH}_3$ );  $^{13}\text{C}$  NMR (101 MHz,  $\text{CDCl}_3$ )  $\delta$  175.1, 60.3, 30.9, 25.7, 19.8, 16.1;  $m/z$  (ES): 130.9 ( $\text{M}+\text{H}^+$ ). Analytical data were in accordance with literature values.<sup>137</sup>

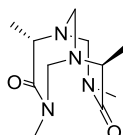
### 3,8-Dimethyl-1,3,6,8-tetraaza-bicyclo[4.4.1]undecane-4,9-dione 218



Glycine N-methyl amide (440 mg, 5.00 mmol) was dissolved in chloroform (20 mL). Paraformaldehyde (450 mg, 15.0 mmol, 3 eq.) and ytterbium (III) trifluoromethanesulfonate hydrate (31 mg, 0.05 mmol, 1 mol%) were added. The

mixture was stirred at 60 °C for 18 h. Once cooled to ambient temperature the mixture was filtered through a 1 cm plug of Celite and the filter cake was washed with 100 mL dichloromethane. The solvent was removed under reduced pressure and the residue dissolved in hot ethyl acetate (~20 mL). The solution was allowed to cool and left at ambient temperature for 24 h. The precipitate was filtered, washed with diethyl ether (10 mL) and discarded. The filtrate was concentrated under reduced pressure and dissolved in hot ethyl acetate (15 mL), the solution was cooled to -24 °C and allowed to crystallise for 48 h. The white crystals were recovered on a sinter, washed with diethyl ether (20 mL) and dried under reduced pressure (247 mg, 47%). mp: 176–179 °C;  $\nu_{\max}$  (ATR)/ $\text{cm}^{-1}$  2967, 2936, 2907, 1618;  $^1\text{H}$  NMR (500 MHz,  $\text{CDCl}_3$ )  $\delta$  4.81 (2H, dd,  $J = 14.7, 1.3$  Hz, MeNCHH), 4.19 (2H, d,  $J = 14.7$  Hz, MeNCHH), 4.11 (2H, s,  $\text{NCH}_2$ ), 3.88 (2H, d,  $J = 16.2$  Hz, OCCHH), 3.63 (2H, d,  $J = 16.2$  Hz, OCCHH), 2.88 (6H, s,  $\text{NCH}_3$ );  $^{13}\text{C}$  NMR (126 MHz,  $\text{CDCl}_3$ )  $\delta$  175.1, 78.3, 70.6, 59.0, 36.1;  $m/z$  (ES/APCI): 213.1 ( $\text{M}+\text{H}^+$ ); HRMS (ES) calculated for  $\text{C}_9\text{H}_{16}\text{O}_2\text{N}_4$  213.1346 ( $\text{M}+\text{H}^+$ ), found 213.1348.

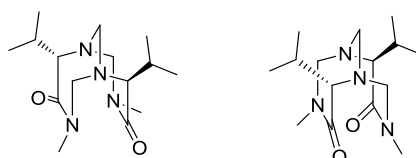
**(-)-(1*S*,5*S*,6*S*,10*S*)-3,5,8,10-Tetramethyl-1,3,6,8-tetraaza-bicyclo[4.4.1]undecane-4,9-dione 219**



L-Alanine *N*-methyl amide (510 mg, 5.00 mmol) was dissolved in chloroform (20 mL). Paraformaldehyde (450 mg, 15.0 mmol, 3 eq.) and ytterbium (III) trifluoromethanesulfonate hydrate (31 mg, 0.05 mmol, 1 mol%) were added. The mixture was stirred at 60 °C for 18 h. Once cooled to ambient temperature the mixture was diluted with dichloromethane (30 mL), washed with saturated sodium hydrogen carbonate (3  $\times$  20 mL), brine (30 mL) and then dried over anhydrous sodium sulfate. The solvent was removed under reduced pressure and the residue crystallised from dichloromethane and petroleum ether to give the product as white crystals (280 mg, 47%). mp: 206–208 °C;  $[\alpha]_{\text{D}}^{20} = -82.8$  ( $c=1.0$ , MeOH);  $\nu_{\max}$  (ATR)/ $\text{cm}^{-1}$  2995, 2980, 2931, 2955, 1632;  $^1\text{H}$  NMR (400 MHz,  $\text{CDCl}_3$ )  $\delta$  4.59 (2H, d,  $J = 15.2$  Hz, MeNCHH), 4.27 (2H, d,  $J = 15.2$  Hz, MeNCHH), 4.23 (2H, s,

$\text{NCH}_2\text{N}$ ), 3.67 (2H, q,  $J = 7.0$  Hz,  $\text{CH}$ ), 2.79 (6H, s,  $\text{NCH}_3$ ), 1.32 (6H, d,  $J = 7.0$  Hz,  $\text{CH}_3$ );  $^{13}\text{C}$  NMR (101 MHz,  $\text{CDCl}_3$ )  $\delta$  174.7, 81.2, 64.2, 57.4, 36.2, 14.9;  $m/z$  (ES/APCI): 241.1 ( $\text{M}+\text{H}^+$ ); HRMS (ES) calculated for  $\text{C}_{11}\text{H}_{21}\text{O}_2\text{N}_4$  241.1659 ( $\text{M}+\text{H}^+$ ), found 241.1659.

**(5*S*,10*S*)-5,10-Diisopropyl-3,8-dimethyl-1,3,6,8-tetraaza-bicyclo[4.4.1]undecane-4,9-dione **200** and **201****



L-Valine *N*-methyl amide (650 mg, 5.00 mmol) was dissolved in chloroform (20 mL). Paraformaldehyde (450 mg, 15.0 mmol, 3 eq.) and ytterbium (III) trifluoromethanesulfonate hydrate (31 mg, 0.05 mmol, 1 mol%) were added. The mixture was stirred at 60 °C for 18 h. Once cooled to ambient temperature the mixture was diluted with dichloromethane (30 mL), washed with saturated sodium hydrogen carbonate (3 × 20 mL), brine (30 mL) and then dried over anhydrous sodium sulfate. The solvent was removed under reduced pressure and the two diastereomers were separated by flash chromatography (gradient elution from 50% ethyl acetate in petroleum ether to 100% ethyl acetate) to give first **200** (198 mg, 27%) and second **201** (390 mg, 53%) as white crystalline solids.

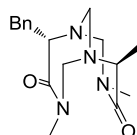
**(-)-(1*S*,5*S*,6*S*,10*S*)-5,10-Diisopropyl-3,8-dimethyl-1,3,6,8-tetraaza-bicyclo[4.4.1]undecane-4,9-dione **200****

mp: 125–127 °C;  $[\alpha]_{\text{D}}^{20} = -12.9$  ( $c=0.82$ , MeOH);  $\nu_{\text{max}}$  (ATR)/ $\text{cm}^{-1}$  2967, 2955, 2926, 2876, 2862, 1640;  $^1\text{H}$  NMR (400 MHz,  $\text{CD}_3\text{CN}$ )  $\delta$  4.73 (2H, d,  $J = 15.3$  Hz,  $\text{MeNCHH}$ ), 4.21 (2H, s,  $\text{NCH}_2\text{N}$ ), 4.04 (2H, d,  $J = 15.3$  Hz,  $\text{MeNCHH}$ ), 3.07 (2H, d,  $J = 10.3$  Hz,  $\text{COCH}$ ), 2.70 (6H, s,  $\text{NCH}_3$ ), 2.30–2.17 (2H, m,  $(\text{CH}_3)_2\text{CH}$ ), 0.95 (6H, d,  $J = 6.3$  Hz,  $\text{CH}_3$ ), 0.89 (6H, d,  $J = 6.8$  Hz,  $\text{CH}_3$ );  $^{13}\text{C}$  NMR (101 MHz,  $\text{CD}_3\text{CN}$ )  $\delta$  174.8, 83.2, 69.0, 66.0, 37.2, 27.1, 22.4, 20.2;  $m/z$  (ES): 319.1 ( $\text{M}+\text{Na}^+$ ); HRMS (ES) calculated for  $\text{C}_{15}\text{H}_{29}\text{O}_2\text{N}_4$  297.2285 ( $\text{M}+\text{H}^+$ ), found 297.2281.

**(+)-(1*R*,5*S*,6*R*,10*S*)-5,10-Diisopropyl-3,8-dimethyl-1,3,6,8-tetraaza-bicyclo[4.4.1]undecane-4,9-dione 201**

mp: 144–155 °C;  $[\alpha]_D^{20} = +21.9$  ( $c=0.75$ , MeOH);  $\nu_{\max}$  (ATR)/ $\text{cm}^{-1}$  2965, 2924, 2868, 1626;  $^1\text{H}$  NMR (400 MHz,  $\text{CD}_3\text{CN}$ )  $\delta$  4.90 (2H, d,  $J = 14.8$  Hz, MeNCHH), 4.07 (2H, s, NCH<sub>2</sub>N), 4.03 (2H, d,  $J = 14.9$  Hz, MeNCHH), 2.96 (2H, d,  $J = 11.4$  Hz, COCH), 2.75 (6H, s, NCH<sub>3</sub>), 2.34–2.23 (2H, m, (CH<sub>3</sub>)<sub>2</sub>CH), 0.95 (6H, d,  $J = 6.4$  Hz, CH<sub>3</sub>), 0.91 (6H, d,  $J = 6.6$  Hz, CH<sub>3</sub>);  $^{13}\text{C}$  NMR (101 MHz,  $\text{CD}_3\text{CN}$ )  $\delta$  176.6, 77.0, 72.3, 63.5, 36.7, 26.2, 20.8, 20.2;  $m/z$  (ES) 319.1 ( $\text{M}+\text{Na}^+$ ); HRMS (ES) calculated for  $\text{C}_{15}\text{H}_{29}\text{O}_2\text{N}_4$  297.2285 ( $\text{M}+\text{H}^+$ ), found 297.2290.

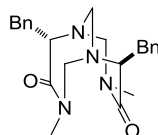
**(-)-(1*S*,5*S*,6*S*,10*S*)-5-Benzyl-3,8,10-trimethyl-1,3,6,8-tetraazabicyclo[4.4.1]undecane-4,9-dione 204**



L-Phenylalanine *N*-methyl amide (445 mg, 2.50 mmol) and L-alanine *N*-methyl amide (255 mg, 2.50 mmol) were dissolved in chloroform (20 mL). Paraformaldehyde (450 mg, 15.0 mmol, 3 eq) and ytterbium (III) trifluoromethanesulfonate hydrate (31 mg, 0.05 mmol, 1 mol%) were added. The mixture was stirred at 60 °C for 18 h. Once cooled to ambient temperature the mixture was diluted with dichloromethane (30 mL), washed with saturated sodium hydrogen carbonate (3 × 20 mL), brine (30 mL) and then dried over anhydrous sodium sulfate. The solvent was removed under reduced pressure and product isolated by flash chromatography (gradient elution from 50% ethyl acetate in petroleum ether to 100% ethyl acetate) to give a white crystalline solid (260 mg, 33%). mp: 216–218 °C;  $[\alpha]_D^{20} = -106.8$  ( $c=1.0$ , MeOH);  $\nu_{\max}$  (ATR)/ $\text{cm}^{-1}$  2982, 2953, 2922, 2862, 1626;  $^1\text{H}$  NMR (400 MHz,  $\text{CDCl}_3$ )  $\delta$  7.33–7.16 (5H, m, CH), 4.67 (1H, d,  $J = 15.2$  Hz, MeNCHH), 4.66 (1H, d,  $J = 15.2$  Hz, MeNCHH), 4.39 (1H, d,  $J = 15.3$  Hz, MeNCHH), 4.32 (1H, d,  $J = 15.3$  Hz, MeNCHH), 4.23 (1H, d,  $J = 14.2$  Hz, NCHHN), 4.14 (1H, d,  $J = 14.2$  Hz, NCHHN), 3.83 (1H, dd,  $J = 9.3, 5.2$  Hz, CHCH<sub>2</sub>), 3.70 (1H, q,  $J = 7.0$  Hz, CHCH<sub>3</sub>), 3.37 (1H, dd,  $J = 14.8, 5.2$  Hz, CHCHH), 2.94 (1H, dd,  $J = 14.8, 9.3$  Hz, CHCHH), 2.94 (3H, s, NCH<sub>3</sub>), 2.87 (3H, s, NCH<sub>3</sub>), 1.39 (3H, d,  $J = 7.0$  Hz, CHCH<sub>3</sub>);  $^{13}\text{C}$  NMR (101

MHz, CDCl<sub>3</sub>)  $\delta$  175.3, 174.7, 139.7, 129.2, 128.3, 126.3, 82.2, 65.1, 64.8, 64.3, 58.2, 37.0, 36.9, 34.6, 15.5;  $m/z$  (ES/APCI):317.3 (M+H<sup>+</sup>); HRMS (ES) calculated for C<sub>17</sub>H<sub>25</sub>O<sub>2</sub>N<sub>4</sub> 317.1972 (M+H<sup>+</sup>), found 317.1978.

**(±)-5,10-Dibenzyl-3,8-dimethyl-1,3,6,8-tetraaza-bicyclo[4.4.1]undecane-4,9-dione 205**



DL-Phenylalanine *N*-methyl amide (890 mg, 5.00 mmol) was dissolved in chloroform (20 mL). Paraformaldehyde (450 mg, 15.0 mmol, 3 eq) and ytterbium (III) trifluoromethanesulfonate hydrate (31 mg, 0.05 mmol, 1 mol%) were added. The mixture was stirred at 60 °C for 18 h. Once cooled to ambient temperature the mixture was diluted with dichloromethane (30 mL), washed with saturated sodium hydrogen carbonate (3 × 20 mL), brine (30 mL) and then dried over anhydrous sodium sulfate. The solvent was removed under reduced pressure and the three diastereomers were separated by flash chromatography (gradient elution from 80% ethyl acetate in petroleum ether to 100% ethyl acetate) to give first (±)-**128** (366 mg, 37%), second (±)-**129** (337 mg, 34%) and third **205** (18 mg, 2%) as white crystalline solids.

**(±)-5,10-Dibenzyl-3,8-dimethyl-1,3,6,8-tetraaza-bicyclo[4.4.1]undecane-4,9-dione (±)-128 and (±)-129**

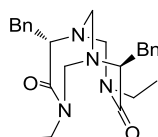
Exhibited identical spectral data to the enantiopure compounds

**(±)-5,10-Dibenzyl-3,8-dimethyl-1,3,6,8-tetraaza-bicyclo[4.4.1]undecane-4,9-dione 205**

mp: 185–187 °C;  $\nu_{\max}$  (ATR)/cm<sup>-1</sup> 2924, 1651, 1614; <sup>1</sup>H NMR (400 MHz, CDCl<sub>3</sub>)  $\delta$  7.35-7.17 (10H, m, CH), 4.83 (1H, d,  $J$  = 14.8 Hz, MeNCHH), 4.77 (1H, d,  $J$  = 15.1 Hz, MeNCHH), 4.53 (1H, d,  $J$  = 14.9 Hz, NCHHN), 4.38 (1H, d,  $J$  = 15.1 Hz, MeNCHH), 4.09 (1H, d,  $J$  = 14.8 Hz, MeNCHH), 3.94 (1H, dd,  $J$  = 10.9, 5.5 Hz, CH), 3.86 (1H, dd,  $J$  = 5.4, 9.2 Hz, CH), 3.84 (1H, d,  $J$  = 14.9 Hz, NCHHN), 3.36 (1H, dd,  $J$  = 14.8, 5.4 Hz, CHCHH), 3.17 (1H, dd,  $J$  = 14.5, 5.5 Hz, CHCHH), 3.11

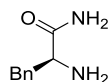
(1H, dd,  $J = 14.5, 10.9$  Hz, CHCHH), 2.98 (1H, dd,  $J = 9.2, 14.8$  Hz, CHCHH), 2.96 (3H, s, NCH<sub>3</sub>), 2.96 (3H, s, NCH<sub>3</sub>); <sup>13</sup>C NMR (101 MHz, CDCl<sub>3</sub>)  $\delta$  176.7, 174.4, 139.5, 137.7, 129.2, 128.9, 128.6, 128.4, 126.9, 126.4, 72.3, 72.3, 70.5, 65.0, 64.0, 37.1, 36.8, 35.0, 34.6;  $m/z$  (ES): 415.2 (M+Na<sup>+</sup>); HRMS (ES) calculated for C<sub>23</sub>H<sub>29</sub>O<sub>2</sub>N<sub>4</sub> 393.2285 (M+H<sup>+</sup>), found 393.2289.

**(-)-(1S,5S,6S,10S)-5,10-Dibenzyl-3,8-diethyl-1,3,6,8-tetraaza-bicyclo[4.4.1]undecane-4,9-dione 206**

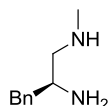


(*S*)-2-Amino-*N*-ethyl-3-phenylpropanamide (960 mg, 5 mmol) was dissolved in chloroform (20 mL). Paraformaldehyde (450 mg, 15 mmol, 3 eq) and ytterbium (III) trifluoromethanesulfonate hydrate (31 mg, 0.05 mmol, 1 mol%) were added. The mixture was stirred at 60 °C for 18 h. Once cooled to ambient temperature the mixture was diluted with dichloromethane (30 mL), washed with saturated sodium hydrogen carbonate (3 × 20 mL), brine (30 mL) and then dried over anhydrous sodium sulfate. The solvent was removed under reduced pressure and the residue was purified using flash chromatography (60% ethyl acetate in petroleum ether) to give a white solid (670 mg, 64%).  $[\alpha]_D^{20} = -164.8$  ( $c=0.75$ , MeOH); mp: 159–161 °C;  $\nu_{\max}$  (ATR)/cm<sup>-1</sup> 3083, 3062, 3027, 2960, 2928, 2867, 1641, 1625; <sup>1</sup>H NMR (400 MHz, CDCl<sub>3</sub>)  $\delta$  7.33–7.18 (10H, m, CH), 4.64 (2H, d,  $J = 15.2$  Hz, CH<sub>3</sub>CH<sub>2</sub>NCHH), 4.42 (2H, d,  $J = 15.2$  Hz, CH<sub>3</sub>CH<sub>2</sub>NCHH), 4.07 (2H, s, NCH<sub>2</sub>N), 4.06–3.98 (2H, m, CH<sub>3</sub>CHH), 3.80 (2H, dd,  $J = 9.4, 5.0$  Hz, CH), 3.39 (2H, dd,  $J = 14.9, 5.0$  Hz, PhCHH), 2.91 (2H, dd,  $J = 14.9, 9.4$  Hz, PhCHH), 2.79–2.66 (2H, m, CH<sub>3</sub>CHH), 1.07 (6H, t,  $J = 7.2$  Hz, CH<sub>3</sub>); <sup>13</sup>C NMR (101 MHz, CDCl<sub>3</sub>)  $\delta$  174.1, 139.9, 129.2, 128.4, 126.3, 82.9, 64.7, 63.5, 45.0, 34.6, 14.3; HRMS (ES) calculated for C<sub>25</sub>H<sub>33</sub>N<sub>4</sub>O<sub>2</sub> 421.2598 (M+H<sup>+</sup>), found 421.2601.



**(S)-2-Amino-3-phenylpropanamide 204**

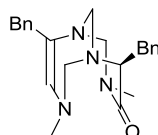
L-Phenylalanine ethyl ester hydrochloride (5.00 g, 2.18 mmol) was added to concentrated ammonium hydroxide solution (85 mL). The mixture was stirred for 48 hours and then concentrated under reduced pressure. Saturated sodium carbonate solution (20 mL) was added and the organics were extracted into chloroform (3 × 15 mL). The combined organics were dried over anhydrous potassium carbonate and the solvent was removed under reduced pressure to give a white solid. The solid was recrystallized from ethyl acetate and petroleum ether to give the product as a white crystalline solid (1.48 g, 41%).  $[\alpha]_{\text{D}}^{20} = +17$  (c=1.0, MeOH); mp: 78–80 °C;  $\nu_{\text{max}}$  (ATR)/ $\text{cm}^{-1}$  3348, 3027, 1662, 1603;  $^1\text{H}$  NMR (400 MHz,  $\text{CDCl}_3$ )  $\delta$  7.39–7.23 (5H, m, CH), 7.14 (1H, br. s, NHH), 5.91 (1H, br. s, NHH), 3.63 (1H, dd,  $J = 9.5, 4.0$  Hz, CH), 3.29 (1H, dd,  $J = 13.7, 4.0$  Hz, CHH), 2.73 (1H, dd,  $J = 13.7, 9.5$  Hz, CHH), 1.54 (2H, br. s,  $\text{NH}_2$ );  $^{13}\text{C}$  NMR (101 MHz,  $\text{CDCl}_3$ )  $\delta$  177.6, 137.9, 129.4, 128.9, 127.0, 56.6, 41.1; HRMS (ES) calculated for  $\text{C}_9\text{H}_{13}\text{N}_2\text{O}$  165.1022 ( $\text{M}+\text{H}^+$ ), found 165.1019.

**(S)-N<sup>1</sup>-methyl-3-phenylpropane-1,2-diamine 210**

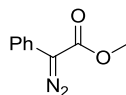
L-Phenylalanine-*N*-methyl amide (1.00 g, 5.61 mmol), was dissolved in anhydrous THF (30 mL). Lithium aluminium hydride (427 mg, 11.2 mmol) was added. The mixture was heated under reflux for 18 h. The mixture was cooled to 0 °C and the reaction was quenched with minimal iced water (~2 mL). The mixture was filtered through a 1 cm plug of celite and the filter cake was washed with dichloromethane (100 mL). The solvent was removed under reduced pressure and the product was isolated by Kugelrohr distillation (1.1 mbar, 131 °C) to give the product as a colourless oil (800 mg, 92%).  $[\alpha]_{\text{D}}^{20} = -2.4$  (c=1.0, MeOH);  $\nu_{\text{max}}$  (ATR)/ $\text{cm}^{-1}$  3289, 2930, 2911, 2889, 2841, 2785;  $^1\text{H}$  NMR (400 MHz,  $\text{CDCl}_3$ )  $\delta$  7.34–7.19 (5H, m, CH), 3.12 (1H, app. tdd,  $J = 8.6, 4.9, 4.1$  Hz, CH), 2.80 (1H, dd,  $J = 13.4, 4.9$  Hz, PhCHH), 2.67 (1H, dd,  $J = 11.7, 4.1$  Hz, NCHH), 2.52 (1H, dd,  $J = 13.4, 8.6$  Hz,

PhCHH), 2.46 (1H, dd,  $J = 11.7, 8.3$  Hz, NHCHH), 2.45 (3H, s, NCH<sub>3</sub>), 1.24 (3H, s, NH and NH<sub>2</sub>); <sup>13</sup>C NMR (126 MHz, CDCl<sub>3</sub>)  $\delta$  139.4, 129.4, 128.6, 126.4, 58.6, 52.5, 43.0, 36.8;  $m/z$  (APCI/ES): 165.6 (M+H<sup>+</sup>). Analytical data were in accordance with literature values.<sup>138</sup>

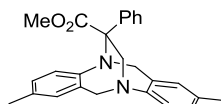
**(-)-(1*S*,5*S*,6*S*)-5,10-Dibenzyl-3,8-dimethyl-1,3,6,8-tetraazabicyclo[4.4.1]undec-9-en-4-one 213**



(1*S*,5*S*,6*S*,10*S*)-5,10-Dibenzyl-3,8-dimethyl-1,3,6,8-tetraazabicyclo[4.4.1]undec-9-en-4-one (200 mg, 0.5 mmol) was dissolved in anhydrous THF (20 mL) and cooled to 0 °C. Lithium aluminium hydride powder (41 mg, 1 mmol) was added and the mixture stirred for 5 minutes. The reaction was quenched by careful drop-wise addition of saturated sodium bicarbonate (0.5 mL) and then diluted with saturated ammonium chloride (10 mL). The mixture was extracted with chloroform (3 × 15 mL) and the combined extracts dried over anhydrous potassium carbonate. The solvent was removed under reduced pressure and the product was purified by flash chromatography (1% triethylamine, 59% ethyl acetate and 40% petroleum ether) to give a colourless oil (145 mg, 76%).  $[\alpha]_D^{20} = -29.5$  ( $c=2.25$ , MeOH);  $\nu_{\max}$  (ATR)/cm<sup>-1</sup> 3061, 3026, 2924, 1643; <sup>1</sup>H NMR (400 MHz, CDCl<sub>3</sub>)  $\delta$  7.33-7.16 (10H, m, CH), 5.71 (1H, s, C=CH), 4.64 (1H, d,  $J = 14.9$  Hz, OCNCHH), 4.16 (1H, d,  $J = 14.9$  Hz, OCNCHH), 4.04 (1H, d,  $J = 12.8$  Hz, MeNCHH), 4.02 (1H, d,  $J = 13.8$  Hz, NCHHN), 3.84 (1H, dd,  $J = 8.4, 5.8$  Hz, CH), 3.60 (1H, d,  $J = 12.8$  Hz, MeNCHH), 3.57 (1H, d,  $J = 13.8$  Hz, NCHHN), 3.38 (1H, d,  $J = 14.9$  Hz, CCHH), 3.35 (1H, dd,  $J = 14.5, 5.8$  Hz, CHCHH), 3.28 (1H, d,  $J = 14.9$  Hz, CCHH), 2.95 (1H, dd,  $J = 14.5, 8.4$  Hz, CHCHH), 2.94 (3H, s, CONCH<sub>3</sub>), 2.64 (3H, s, NCH<sub>3</sub>); <sup>13</sup>C NMR (101 MHz, CDCl<sub>3</sub>)  $\delta$  175.7, 141.1, 140.4, 136.5, 129.4, 128.8, 128.4, 128.2, 126.3, 126.0, 124.6, 76.2, 68.1, 66.8, 62.8, 43.0, 39.9, 37.2, 35.2;  $m/z$  (ES): 377.1 (M+H<sup>+</sup>); HRMS (ES) calculated for C<sub>23</sub>H<sub>29</sub>O<sub>1</sub>N<sub>4</sub> 377.2336 (M+H<sup>+</sup>), found 377.2335.

**Methyl 2-diazo-2-phenylacetate 225**<sup>139</sup>

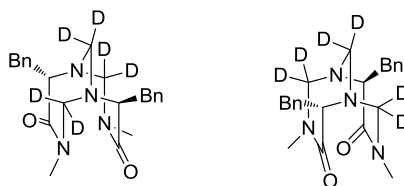
Methyl phenylacetate (0.94 mL, 6.68 mmol) was dissolved in acetonitrile (20 mL). 4-Acetamidobenzenesulfonyl azide (1.92 g, 8.00 mmol) was added to the solution followed by DBU (1.4 mL, 9.37 mmol). The mixture stirred for 20 h at ambient temperature. Water (20 mL) was added and the reaction mixture was extracted with diethyl ether (3 × 20 mL). The combined organics were washed with brine (20 mL) and dried over sodium sulfate. The solvent was removed under reduced pressure and the orange residue was purified using flash chromatography (10% diethyl ether in petroleum ether) to afford the product as an orange oil (755 mg, 64%).  $\nu_{\max}$  (ATR)/ $\text{cm}^{-1}$  3059, 3024, 2999, 2953, 2081, 1697;  $^1\text{H}$  NMR (400 MHz,  $\text{CDCl}_3$ )  $\delta$  7.51–7.47 (2H, m, *o*-CH), 7.42–7.35 (2H, m, *m*-CH), 7.22–7.15 (1H, m, *p*-CH), 3.87 (3H, s,  $\text{OCH}_3$ );  $^{13}\text{C}$  NMR (101 MHz,  $\text{CDCl}_3$ )  $\delta$  165.7, 129.1, 126.0, 125.6, 124.1, 52.1 (C=N<sub>2</sub> absent);  $m/z$  (ES): 161.8 ( $-\text{CH}_3, +\text{H}^+$ ), 148.9 ( $-\text{N}_2, +\text{H}$ ), 118 ( $-\text{N}_2\text{OCH}_3, +\text{H}^+$ ). Analytical data were in accordance with literature values.<sup>140</sup>

**Methyl-3,9-dimethyl-14-phenyl-5,11-dihydro-6,12-ethanodibenzo[b,f][1,5]diazocine-14-carboxylate 219**<sup>99</sup>

Trögers base (100 mg, 0.40 mmol) was added to anhydrous toluene (1 mL) followed by rhodium acetate dimer (1.76 mg, 0.004 mmol). Methyl 2-diazo-2-phenylacetate (70.4 mg, 0.4 mmol) was added and the mixture was heated to 100 °C. After 1 h a further portion of methyl 2-diazo-2-phenylacetate (70.4 mg, 0.4 mmol) was added and the reaction was stirred at 100 °C for 23 h. The solvent was removed under reduced pressure and the residue was purified by flash chromatography to give a white solid (40 mg, 25%). mp: 192–194 °C;  $\nu_{\max}$  (ATR)/ $\text{cm}^{-1}$  2916, 2876, 1717;  $^1\text{H}$  NMR (400 MHz,  $\text{CDCl}_3$ )  $\delta$  7.77–7.73 (2H, m, CH), 7.40 (2H, t,  $J = 7.6$  Hz, CH), 7.33–7.28 (2H, m, CH), 7.04 (1H, d,  $J = 8.0$  Hz, CH), 6.96 (1H, dd,  $J = 8.0, 1.7$  Hz, CH), 6.87 (1H, dd,  $J = 8.0, 1.7$  Hz, CH), 6.69–6.61 (2H, m, CH), 5.24 (1H, d,  $J = 14.7$  Hz, PhCCHH), 4.83 (1H, d,  $J = 17.4$  Hz, CHH), 4.58 (1H, d,  $J = 17.7$  Hz,

*CHH*), 4.38 (1H, d,  $J = 17.4$  Hz, *CHH*), 4.35 (1H, d,  $J = 17.7$  Hz, *CHH*), 3.83 (1H, d,  $J = 14.7$  Hz, *PhCCHH*), 3.22 (3H, s, *OCH*<sub>3</sub>), 2.21 (3H, s, *CH*<sub>3</sub>), 2.16 (3H, s, *CH*<sub>3</sub>); <sup>13</sup>C NMR (101 MHz, CDCl<sub>3</sub>)  $\delta$  173.4, 147.4, 145.3, 142.7, 136.6, 136.3, 134.8, 134.3, 130.2, 128.8, 128.6, 128.5, 128.2, 127.9, 127.8, 127.6, 127.0, 75.8, 62.2, 59.1, 56.0, 52.3, 21.0, 20.9;  $m/z$  (ES): 399.1 (M+H<sup>+</sup>). All data were consistent with literature values.<sup>99</sup>

**D<sub>6</sub>-(5*S*,10*S*)-5,10-Dibenzyl-3,8-dimethyl-1,3,6,8-tetraaza-bicyclo[4.4.1]undecane-4,9-dione **227** and **228****



L-Phenylalanine *N*-methyl amide (181.6 mg, 1.02 mmol) was dissolved in chloroform (4 mL). Deuterated paraformaldehyde (97.9 mg, 3.05 mmol, 3 eq) and ytterbium (III) trifluoromethanesulfonate hydrate (6.4 mg, 0.01 mmol, 1 mol%) were added. The mixture was stirred at 60 °C for 18 h. Once cooled to ambient temperature the mixture was diluted with dichloromethane (5 mL), washed with saturated sodium hydrogen carbonate (3 × 5 mL), brine (10 mL) and then dried over anhydrous sodium sulfate. The solvent was removed under reduced pressure and the two diastereomers were separated by flash chromatography (gradient elution from 80% ethyl acetate in petroleum ether to 100% ethyl acetate) to give first **227** (148 mg, 73%) and second **228** (22 mg, 11%) as white crystalline solids.

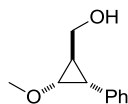
**D<sub>6</sub>-(-)-(1*S*,5*S*,6*S*,10*S*)-5,10-Dibenzyl-3,8-dimethyl-1,3,6,8-tetraaza-bicyclo[4.4.1]undecane-4,9-dione **227****

mp: 129–131 °C;  $\nu_{\max}$  (ATR)/cm<sup>-1</sup> 3001, 2938, 2914, 2882, 1638; <sup>1</sup>H NMR (400 MHz, CDCl<sub>3</sub>)  $\delta$  7.35–7.15 (10H, m, *CH*), 3.80 (2H, dd,  $J = 9.0, 5.4$  Hz, *COCH*), 3.40 (2H, dd,  $J = 14.8, 5.4$  Hz, *CHH*), 2.95 (6H, s, *NCH*<sub>3</sub>), 2.93 (2H, dd,  $J = 14.8, 9.0$  Hz, *CHH*); <sup>2</sup>H NMR (61 MHz, CHCl<sub>3</sub>)  $\delta$  4.65 (2D, s, *CD*<sub>2</sub>), 4.35 (2D, s, *CD*<sub>2</sub>), 4.06 (2D, s, *CD*<sub>2</sub>); <sup>13</sup>C {<sup>1</sup>H, <sup>2</sup>H} NMR (151 MHz, CDCl<sub>3</sub>)  $\delta$  174.6, 139.6, 129.2, 128.3, 126.2, 81.7, 64.5, 64.3, 37.1, 34.7  $m/z$  (ES): 421.2 (M+Na<sup>+</sup>); HRMS (ES) calculated for C<sub>23</sub>H<sub>23</sub>D<sub>6</sub>O<sub>2</sub>N<sub>4</sub> 399.2667 (M+H<sup>+</sup>), found 399.2666.

**D<sub>6</sub>-(+)-(1*R*,5*S*,6*R*,10*S*)-5,10-Dibenzyl-3,8-dimethyl-1,3,6,8-tetraaza-bicyclo[4.4.1]undecane-4,9-dione 228**

mp: 220–222 °C;  $\nu_{\max}$  (ATR)/ $\text{cm}^{-1}$  3021, 3922, 2905, 2853, 1697;  $^1\text{H}$  NMR (400 MHz,  $\text{CDCl}_3$ )  $\delta$  7.39–7.20 (10H, m, CH), 3.93 (2H, dd,  $J = 10.2, 6.3$  Hz, COCH), 3.22–3.05 (4H, m,  $\text{CH}_2$ ), 2.93 (6H, s,  $\text{NCH}_3$ );  $^2\text{H}$  NMR (77 MHz,  $\text{CHCl}_3$ )  $\delta$  4.90 (2D, s,  $\text{CD}_2$ ), 4.23 (2D, s,  $\text{CD}_2$ ), 4.05 (2D, s,  $\text{CD}_2$ );  $^{13}\text{C}$  { $^1\text{H}$ ,  $^2\text{H}$ } NMR (151 MHz,  $\text{CDCl}_3$ )  $\delta$  176.5, 137.6, 128.8, 128.7, 126.9, 71.7, 70.7, 61.9, 36.8, 34.5;  $m/z$  (ES): 421.2 ( $\text{M}+\text{Na}^+$ ); HRMS (ES) calculated for  $\text{C}_{23}\text{H}_{23}\text{D}_6\text{O}_2\text{N}_4$  399.2667 ( $\text{M}+\text{H}^+$ ), found 399.2665.

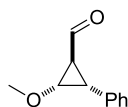
**(*trans,trans*-2-Methoxy-3-phenylcyclopropyl)methanol 255<sup>112</sup>**



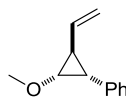
*cis*- $\beta$ -Methoxystyrene (3.4 mL, 25.6 mmol) was added to a suspension of anhydrous copper sulfate (420 mg, 2.6 mmol) in anhydrous benzene (10 mL). The mixture was heated to 75 °C and whilst being rapidly stirred a solution of ethyl diazoacetate (87%, 6.21 mL, 51.2 mmol) in anhydrous benzene (20 mL) was added drop wise over 3 h. Stirring was continued for 1 h at 75 °C before being cooled to ambient temperature and stirred for a further 16 h. The contents of the reaction flask were poured onto water (50 mL) and the aqueous layer was extracted with diethyl ether (2  $\times$  50 mL). The combined organics were washed with water (3  $\times$  50 mL) and brine (2  $\times$  50 mL) and then dried over magnesium sulfate. The solvent was removed under reduced pressure to give a brown oil. The oil was subjected to flash chromatography (10% ethyl acetate in petroleum ether) to yield a colourless oil (2.8 g, a mixture of ethyl *trans,trans*-2-methoxy-3-phenylcyclopropanecarboxylate and diethyl fumarate). The oil was dissolved in anhydrous diethyl ether (100 mL) and cooled to 0 °C. Lithium aluminium hydride (950 mg, 25.0 mmol) was added in portions and the mixture was heated under reflux for 18 h. The reaction was cooled to 0 °C and quenched with ice (2 g) and 0.5 M sodium hydroxide solution (8 mL). After stirring for 15 minutes the contents of the flask were filtered through celite. The filter and flask were washed with diethyl ether (60 mL) and the combined organics were washed with water (50 mL) and brine (50 mL) and then dried over magnesium

sulfate. The solvent was removed under reduced pressure to give the target as a colourless oil (1.71 g, 38%).  $\nu_{\max}$  (ATR)/ $\text{cm}^{-1}$  3379, 3061, 3024, 2990, 2934, 2874, 2826;  $^1\text{H}$  NMR (400 MHz,  $\text{CDCl}_3$ )  $\delta$  7.33–7.19 (5H, m, CH), 3.75–3.60 (2H, m,  $\text{CH}_2\text{OH}$ ), 3.40 (1H, dd,  $J = 6.6, 3.2$  Hz,  $\text{CHOMe}$ ), 3.18 (3H, s,  $\text{OCH}_3$ ), 1.99 (1H, app. t,  $J = 6.6$  Hz,  $\text{PhCH}$ ), 1.84–1.77 (1H, m,  $\text{CHCH}_2$ ), 1.61 (1H, br. s, OH);  $^{13}\text{C}$  NMR (101 MHz,  $\text{CDCl}_3$ )  $\delta$  137.0, 128.1, 128.1, 125.9, 64.2, 64.0, 58.3, 28.8, 27.9;  $m/z$  (CI): 161.0 ( $\text{M}-\text{H}_2\text{O}+\text{H}^+$ ); HRMS (APCI) calculated for  $\text{C}_{11}\text{H}_{13}\text{O}$  161.0961 ( $\text{M}-\text{H}_2\text{O}+\text{H}^+$ ), found 161.0959. Analytical data were in agreement with literature values.<sup>112</sup>

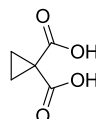
***trans,trans*-2-Methoxy-3-phenylcyclopropanecarbaldehyde 256**<sup>112</sup>



Oxalyl chloride (610  $\mu\text{L}$ , 7.23 mmol) was added to anhydrous dichloromethane (20 mL). The mixture was cooled to  $-78$   $^{\circ}\text{C}$  and dimethyl sulfoxide (1.10 mL, 15.8 mmol) was added drop wise. The mixture was stirred for 10 minutes and a solution of triethylamine (4.60 mL, 32.8 mmol) and (*trans,trans*-2-methoxy-3-phenylcyclopropyl)methanol (1.17 g, 6.57 mmol) in dichloromethane (15 mL) was added drop wise over 15 minutes. The reaction was monitored by TLC and upon complete consumption of starting alcohol (approx. 30 minutes) the reaction was allowed to warm to ambient temperature. Water (15 mL) and diethyl ether (20 mL) were added and the mixture was poured into a separatory funnel. The layers were separated and the aqueous layer was extracted with diethyl ether ( $2 \times 20$  mL). The combined organics were washed with water (20 mL) and brine (20 mL) and then dried over sodium sulfate. The solvent was removed under reduced pressure to give a light brown oil (1.16 g, quant.).  $\nu_{\max}$  (ATR)/ $\text{cm}^{-1}$  3059, 3028, 2990, 2936, 2830, 1701;  $^1\text{H}$  NMR (400 MHz,  $\text{CDCl}_3$ )  $\delta$  9.81 (1H, d,  $J = 2.7$  Hz, CHO), 7.37–7.25 (5H, m, CH), 3.95 (1H, dd,  $J = 7.1, 2.6$  Hz,  $\text{CHOMe}$ ), 3.37 (3H, s,  $\text{OCH}_3$ ), 2.99–2.94 (1H, m,  $\text{CHPh}$ ), 2.62–2.58 (1H, m,  $\text{CHCHO}$ );  $^{13}\text{C}$  NMR (101 MHz,  $\text{CDCl}_3$ )  $\delta$  198.6, 134.5, 128.5, 128.4, 127.1, 68.5, 59.1, 38.0, 34.4;  $m/z$  (CI): 177.0 ( $\text{M}+\text{H}^+$ ); HRMS (APCI) calculated for  $\text{C}_{11}\text{H}_{13}\text{O}_2$  177.0910 ( $\text{M}+\text{H}^+$ ), found 177.0909. Analytical data were in agreement with literature values.<sup>112</sup>

**(*trans,trans*-2-Methoxy-3-phenylcyclopropyl)ethylene 250**<sup>112</sup>

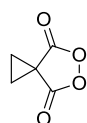
Methyltriphenylphosphonium bromide (3.93 g, 11.0 mmol) was added to anhydrous THF (26 mL). The suspension was cooled to 0 °C and 1.7 M n-butyllithium in hexane (4.40 mL) was added. The mixture was stirred for 15 minutes, over which time a pale yellow colour developed. A solution of *trans,trans*-2-methoxy-3-phenylcyclopropanecarbaldehyde (1.14 g, 6.48 mmol) in anhydrous THF (8 mL) was added drop wise and the mixture was stirred at ambient temperature. The reaction was monitored by TLC and upon complete consumption of starting aldehyde (approx. 1 h) the reaction mixture was poured into a separatory funnel containing a mixture of ammonium chloride (20 mL) and diethyl ether (20 mL). The layers were separated and the aqueous layer was further extracted with diethyl ether (2 × 20 mL). The combined organics were washed with brine (30 mL) and dried over sodium sulfate. The solvent was removed under reduced pressure and the residue purified by flash chromatography (3% ethyl acetate in petroleum ether) to give the target compound as a colourless oil (835 mg, 73%).  $\nu_{\max}$  (ATR)/ $\text{cm}^{-1}$  3084, 3061, 3026, 2982, 2934, 2826;  $^1\text{H}$  NMR (400 MHz,  $\text{CDCl}_3$ )  $\delta$  7.30–7.15 (5H, m, CH), 5.66 (1H, ddd,  $J = 17.2, 10.4, 7.7$  Hz,  $\text{CH}_2\text{CH}$ ), 5.13–5.07 (1H, m, CHCHH), 5.00–4.96 (1H, m, CHCHH), 3.43 (1H, dd,  $J = 6.6, 3.3$  Hz,  $\text{CHOCH}_3$ ), 3.20 (3H, s,  $\text{OCH}_3$ ), 2.10 (1H, app t,  $J = 6.6$  Hz, PhCH), 2.06–2.00 (1H, m, CHCHCH<sub>2</sub>);  $^{13}\text{C}$  NMR (101 MHz,  $\text{CDCl}_3$ )  $\delta$  137.7, 137.1, 128.1, 128.1, 126.0, 113.8, 66.9, 58.4, 31.9, 30.4;  $m/z$  (CI): 175.0 ( $\text{M}+\text{H}^+$ ); HRMS (APCI) calculated for  $\text{C}_{12}\text{H}_{15}\text{O}$  175.1117 ( $\text{M}+\text{H}^+$ ), found 175.1116. Analytical data were in agreement with literature values.<sup>112</sup>

**Cyclopropane-1,1-dicarboxylic acid 235**<sup>141</sup>

Benzyltriethylammonium chloride (28.2 g, 124 mmol) was added to a vigorously stirred solution of 50% wt. sodium hydroxide (125 mL). Diethyl malonate (18.8 mL, 124 mmol) and 1,2-dibromoethane (16.0 mL, 185 mmol) were mixed and then poured into the reaction mixture. Vigorous stirring was maintained for 2 h. 37%

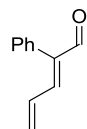
Hydrochloric acid (~250 mL) was added until pH 1 was obtained. The solution was poured into a separatory funnel and extracted with diethyl ether (3 × 200 mL). The organics were combined and washed with brine (250 mL) and then dried over magnesium sulfate. The solvent was removed under reduced pressure to give a fluffy white solid (11.0 g, 68%). mp: 136–137 °C [lit.<sup>142</sup> 139–141 °C];  $\nu_{\max}$  (ATR)/ $\text{cm}^{-1}$  2835, 1709;  $^1\text{H}$  NMR (400 MHz,  $\text{CD}_3\text{CN}$ )  $\delta$  10.76 (2H, s, OH), 1.73 (4H, s,  $\text{CH}_2$ );  $^{13}\text{C}$  NMR (101 MHz,  $\text{CD}_3\text{CN}$ )  $\delta$  175.3, 25.4, 22.5;  $m/z$  (ES): 130.8 ( $\text{M}+\text{H}^+$ ).

### Cyclopropyl malonyl peroxide 231<sup>143</sup>



Cyclopropane-1,1-dicarboxylic acid (2.00 g, 15.4 mmol) was added to methanesulfonic acid (15 mL). Urea hydrogen peroxide (4.34 g, 46.1 mmol) was added in portions and the mixture stirred for 24 h. Iced water (30 mL) was added and the mixture was extracted with ethyl acetate (3 × 30 mL). The combined organics were washed with saturated sodium bicarbonate solution (2 × 30 mL) and brine (30 mL) and then dried over magnesium sulfate. The solvent was removed under reduced pressure to give a white crystalline solid (1.61 g, 82%). mp: 88–90 °C [lit.<sup>104</sup> 90 °C];  $\nu_{\max}$  (ATR)/ $\text{cm}^{-1}$  3121, 1829, 1788, 1746;  $^1\text{H}$  NMR (400 MHz,  $\text{CDCl}_3$ )  $\delta$  2.10 (4H, s,  $\text{CH}_2$ );  $^{13}\text{C}$  NMR (101 MHz,  $\text{CDCl}_3$ )  $\delta$  172.3, 23.7, 19.9. Mass spectrometric analysis is not possible for malonyl peroxides. Analytical data were in agreement with literature values.<sup>104</sup>

### 2-Phenylpenta-2,4-dienal 258



(*trans,trans*-2-Methoxy-3-phenylcyclopropyl)ethylene (49 mg, 0.28 mmol) was dissolved in deuterated chloroform (0.5 mL). Deuterium oxide (5  $\mu\text{L}$ , 0.28 mmol) was added followed by cyclopropyl malonyl peroxide (36 mg, 0.28 mmol). The reaction mixture was heated to 40 °C for 96 h. 40  $\mu\text{L}$  of reaction mixture was added to 0.5 mL  $\text{CDCl}_3$  and analysed by  $^1\text{H}$  NMR. Complete consumption of starting



materials was observed. To the NMR tube trifluoroacetic acid (40  $\mu\text{L}$ , 0.52 mmol) was added. The tube was shaken and heated to 40  $^{\circ}\text{C}$  for 18 h over which time all of the intermediates cleanly converted to 2-phenylpenta-2,4-dienal, cyclopropane-1,1-dicarboxylic acid and methanol. The reaction intermediates also decompose on silica. A sample of 2-phenylpenta-2,4-dienal for analysis was isolated from the crude reaction mixture using preparative TLC (20% ethyl acetate in petroleum ether,  $R_f = 0.54$ ).  $\nu_{\text{max}}$  (ATR)/ $\text{cm}^{-1}$  2957, 2924, 2853, 1686;  $^1\text{H}$  NMR (400 MHz,  $\text{CDCl}_3$ )  $\delta$  9.69 (1H, s, CHO), 7.45–7.34 (3H, m, CH), 7.24–7.20 (2H, m, CH), 7.07 (1H, d,  $J = 11.2$  Hz, PhCCH), 6.72 (1H, ddd,  $J = 16.9, 11.2, 10.0$  Hz,  $\text{CH}_2\text{CH}$ ), 5.86–5.80 (1H, m, CHH), 5.63–5.59 (1H, m, CHH);  $^{13}\text{C}$  NMR (101 MHz,  $\text{CDCl}_3$ )  $\delta$  193.6, 149.5, 142.2, 133.1, 132.4, 129.9, 128.4, 128.4, 128.0;  $m/z$  (CI): 158.9 ( $\text{M}+\text{H}^+$ ); HRMS (APCI) calculated for  $\text{C}_{11}\text{H}_{11}\text{O}$  159.0804 ( $\text{M}+\text{H}^+$ ), found 159.0801. Analytical data were consistent with literature values.<sup>144</sup>

#### 10.4 General Method for Detecting Intermediates by ESI-MS

Cinnamaldehyde (12  $\mu\text{L}$ , 0.095 mmol) was added to a mixture of methanol (0.4 mL) and (*S*)-5-Benzyl-2,2,3-trimethylimidazolidin-4-one hydrochloride (5 mg, 0.02 mmol). The mixture was stirred at 25  $^{\circ}\text{C}$  for 5 minutes before freshly distilled cyclopentadiene (21  $\mu\text{L}$ , 0.25 mmol) was added. The mixture was stirred for a further 5 minutes before an aliquot (5  $\mu\text{L}$ ) was removed and diluted with methanol (1 mL). The dilution was then analysed using direct infusion ESI-MS.

#### 10.5 HPLC

##### 10.5.1 Preparation of Racemates for Separation

All racemic imidazolidinones were prepared from racemic starting materials in an analogous fashion to the enantiopure derivatives. Where required, racemic Diels-Alder adducts were prepared using racemic **3**·HCl. The *endo* and *exo* Diels-Alder adducts were observed to have slightly different  $R_f$  values. Therefore, to obtain a product ratio whereby the *endo* and *exo* isomers could be easily identified flash chromatography was used.

### 10.5.2 Derivatisations

#### General Method for Hydrazone Formation

2,4-Dinitrophenylhydrazine (100 mg, 0.5 mmol, 2 eq.) was added to aldehyde (0.25 mmol, 1 eq.). A mixture of ethanol (2 mL) and 2.4 M hydrochloric acid (0.2 mL) was then added. The orange suspension was then vigorously stirred until all aldehyde had been consumed by TLC (~4–10 h). The solvent was removed under reduced pressure and the residue was subjected to flash chromatography (20% ethyl acetate in petroleum ether) and the hydrazones were obtained as yellow/orange solids. It should be noted that, due to streaking, chromatography of these species was not quantitative. In addition, diastereomeric ratios were observed to change from the chromatographic process; hence, diastereomeric ratios were determined from the aldehyde precursors.

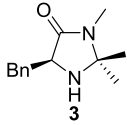
#### General Method for Reduction of Aldehydes with NaBH<sub>4</sub> for HPLC

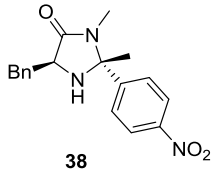
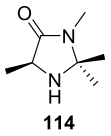
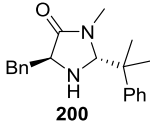
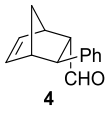
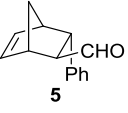
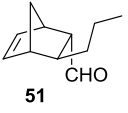
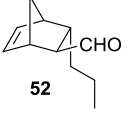
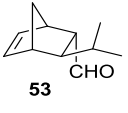
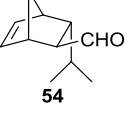
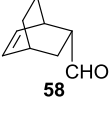
Aldehyde (0.24 mmol, 1 eq.) was dissolved in ethanol (1 mL). Sodium borohydride (10 mg, 0.26 mmol, 1.1 eq.) was added. The mixture was stirred until complete consumption of the aldehyde was observed by TLC (~1 h). The flask contents were then poured into a separatory funnel containing saturated ammonium chloride (5 mL) and water (5 mL). The organics were extracted into chloroform (3 × 5 mL) and dried over sodium sulfate. The solvent was removed under reduced pressure. The residue was subjected to flash chromatography (25% ethyl acetate in petroleum ether) and the alcohols were obtained as colourless oils.

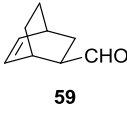
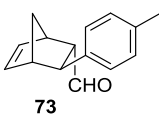
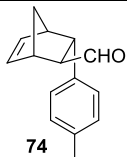
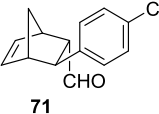
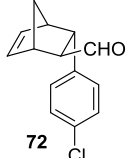
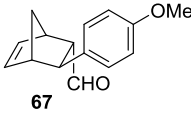
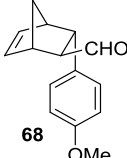
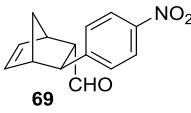
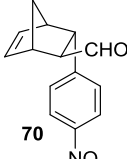
### 10.5.3 HPLC Separation Conditions

All chromatographic separations were performed using 250 mm x 4.6 mm analytical columns, manufactured by Chiral Technologies Europe (Diacel).

2,4-DNP = Dinitrophenylhydrazone of the corresponding aldehyde

Compound	Derivatised to	HPLC Conditions	Retention Times (min)
	N/A	Chiralpak IC, 30 °C, 1 mL min <sup>-1</sup> , 10% IPA in Hexanes	t <sub>r</sub> (S) = 21.8 t <sub>r</sub> (R) = 27.4

 38	N/A	Chiralcel OJ, 25 °C, 1.5 mL min <sup>-1</sup> , 10% IPA in Hexanes	$t_r(2S,5R) = 40.0$ $t_r(2R,5S) = 47.9$
 114	N/A	Chiralpak IC, 20 °C, 1 mL min <sup>-1</sup> , 10% IPA in Hexanes	$t_r(S) = 36.9$ $t_r(R) = 42.2$
 200	N/A	Chiralpak IC, 20 °C, 1 mL min <sup>-1</sup> , 20% IPA in Hexanes	$t_r(2R,5S) = 11.9$ $t_r(2S,5R) = 15.9$
 4	2,4-DNP	Chiralcel OD-R, 25 °C 0.85 mL min <sup>-1</sup> , 75% MeCN in H <sub>2</sub> O	$t_r(1R,2S,3S,4S) = 22.8$ $t_r(1S,2R,3R,4R) = 28.9$
 5	2,4-DNP	Chiralcel OD-R, 25 °C 0.85 mL min <sup>-1</sup> , 75% MeCN in H <sub>2</sub> O	$t_r(1S,2S,3S,4R) = 32.6$ $t_r(1R,2R,3R,4S) = 44.1$
 51	2,4-DNP	Chiralpak IB, 20 °C, 1 mL min <sup>-1</sup> , 10% IPA in Hexanes	$t_r(1R,2S,3S,4S) = 9.7$ $t_r(1S,2R,3R,4R) = 10.5$
 52	2,4-DNP	Chiralpak IA, 20 °C, 0.5 mL min <sup>-1</sup> , 2.5% IPA in Hexanes	$t_r(1R,2R,3R,4S) = 32.2$ $t_r(1S,2S,3S,4R) = 35.9$
 53	2,4-DNP	Chiralpak IB, 20 °C, 0.75 mL min <sup>-1</sup> , 10% IPA in Hexanes	$t_r(1R,2S,3S,4S) = 13.0$ $t_r(1S,2R,3R,4R) = 13.9$
 54	2,4-DNP	Chiralpak IB, 20 °C, 0.75 mL min <sup>-1</sup> , 10% IPA in Hexanes	$t_r(1R,2R,3R,4S) = 18.3$ $t_r(1S,2S,3S,4R) = 19.4$
 58	2,4-DNP	Chiralpak IB, 20 °C, 0.5 mL min <sup>-1</sup> , 10% IPA in Hexanes	$t_r(1R,2R,4R) = 26.2$ $t_r(1S,2S,4S) = 31.0$

 <b>59</b>	2,4-DNP	Chiralpak IB, 20 °C, 0.5 mL min <sup>-1</sup> , 10% IPA in Hexanes	$t_r(1S,2R,4S) = 29.8$ $t_r(1R,2S,4R) = 34.9$
 <b>73</b>	Alcohol	Chiralpak IC, 20 °C, 1 mL min <sup>-1</sup> , 5% IPA in Hexanes	$t_r(1S,2R,3R,4R) = 10.2$ $t_r(1R,2S,3S,4S) = 8.2$
 <b>74</b>	Alcohol	Chiralpak IC, 20 °C, 1 mL min <sup>-1</sup> , 5% IPA in Hexanes	$t_r(1R,2R,3R,4S) = 7.6$ $t_r(1S,2S,3S,4R) = 9.5$
 <b>71</b>	Alcohol	Chiralpak IB, 20 °C, 1 mL min <sup>-1</sup> , 2.5% IPA in Hexanes	$t_r(1S,2R,3R,4R) = 13.3$ $t_r(1R,2S,3S,4S) = 18.6$
 <b>72</b>	Alcohol	Chiralpak IB, 20 °C, 1 mL min <sup>-1</sup> , 2.5% IPA in Hexanes	$t_r(1R,2R,3R,4S) = 14.2$ $t_r(1S,2S,3S,4R) = 21.4$
 <b>67</b>	Alcohol	Chiralpak IB, 20 °C, 0.75 mL min <sup>-1</sup> , 10% IPA in Hexanes	$t_r(1S,2R,3R,4R) = 9.6$ $t_r(1R,2S,3S,4S) = 11.0$
 <b>68</b>	Alcohol	Chiralpak IB, 20 °C, 0.75 mL min <sup>-1</sup> , 10% IPA in Hexanes	$t_r(1R,2R,3R,4S) = 9.2$ $t_r(1S,2S,3S,4R) = 12.3$
 <b>69</b>	Alcohol	Chiralpak IA, 27.5 °C, 0.75 mL min <sup>-1</sup> , 10% IPA in Hexanes	$t_r(1R,2S,3S,4S) = 48.0$ $t_r(1S,2R,3R,4R) = 51.2$
 <b>70</b>	Alcohol	Chiralpak IA, 27.5 °C, 0.75 mL min <sup>-1</sup> , 10% IPA in Hexanes	$t_r(1R,2R,3R,4S) = 43.1$ $t_r(1S,2S,3S,4R) = 45.0$

## **10.6 DFT Calculations**

DFT calculations were performed using the Gaussian09 suite of programmes.<sup>145</sup> Structures were optimised and then characterised using frequency calculations. A classical approach was used when analysing frequency data whereby fully converged local minima (reactants and intermediates) contain no imaginary frequencies and first order saddle points (transition states, TS's) possess one imaginary frequency (which when animated moves in the anticipated direction). Solvation was used where specified and all functionals and basis sets mentioned were used as present within Gaussian09.

# **Appendices**

## **11 Appendices**

### **11.1 Appendix A: X-Ray Crystallography Parameters**

Within this appendix selected X-ray crystallography parameters are given. For structures deposited with the Cambridge Crystallographic Data Centre (CCDC) a summary table is given and the relevant CCDC depository number. For structures not deposited in the CCDC full crystallographic tables are provided.

**(2*S*,5*S*,*E*)-5-Benzyl-1-((*E*)-3-(4-chlorophenyl)allylidene)-2,3-dimethyl-2-(4-nitrophenyl)-4-oxoimidazolidin-1-ium hexafluorophosphate 84·PF<sub>6</sub>**

Table 11.1. Crystal data and structure refinement for tompjr2013smart.

Identification code	tompjr2013smart	
Empirical formula	C <sub>27</sub> H <sub>25</sub> Cl F <sub>6</sub> N <sub>3</sub> O <sub>3</sub> P	
Formula weight	619.92	
Temperature	123(2) K	
Wavelength	1.54180 Å	
Crystal system	Triclinic	
Space group	P-1	
Unit cell dimensions	a = 10.5241(13) Å      α = 68.067(11)° b = 15.9076(19) Å      β = 75.254(10)° c = 19.455(2) Å      γ = 75.501(11)°	
Volume	2877.7(6) Å <sup>3</sup>	
Z	4	
Density (calculated)	1.431 Mg/m <sup>3</sup>	
Absorption coefficient	2.361 mm <sup>-1</sup>	
F(000)	1272	
Crystal size	0.30 x 0.20 x 0.04 mm <sup>3</sup>	
Theta range for data collection	6.38 to 70.00°.	
Index ranges	-12 ≤ h ≤ 12, -19 ≤ k ≤ 16, -23 ≤ l ≤ 23	
Reflections collected	22456	
Independent reflections	10847 [R(int) = 0.0556]	
Completeness to theta = 70.00°	99.5%	
Absorption correction	Semi-empirical from equivalents	
Max. and min. transmission	1.00000 and 0.48049	
Refinement method	Full-matrix least-squares on F <sup>2</sup>	
Data / restraints / parameters	10847 / 259 / 765	
Goodness-of-fit on F <sup>2</sup>	0.940	
Final R indices [I > 2σ(I)]	R1 = 0.0787, wR2 = 0.2015	
R indices (all data)	R1 = 0.1175, wR2 = 0.2326	
Largest diff. peak and hole	0.659 and -0.548 e.Å <sup>-3</sup>	



Table 11.2. Atomic coordinates ( $\times 10^4$ ) and equivalent isotropic displacement parameters ( $\text{\AA}^2 \times 10^3$ ) for *tompjr2013smart*.  $U(\text{eq})$  is defined as one third of the trace of the orthogonalized  $U^{ij}$  tensor.

	x	y	z	U(eq)
Cl(1)	23996(1)	-12774(1)	-6750(1)	69(1)
Cl(2)	35837(1)	-10691(1)	-7016(1)	71(1)
O(1)	30448(3)	-17721(2)	-2231(2)	51(1)
O(2)	22213(16)	-17688(9)	-446(5)	67(2)
O(3)	22088(7)	-17060(5)	412(4)	78(2)
O(4)	28018(3)	-8606(2)	-2069(2)	49(1)
O(5)	36047(3)	-11009(2)	-600(2)	55(1)
O(6)	35376(3)	-9546(3)	-845(2)	60(1)
N(1)	27807(3)	-15855(3)	-2453(2)	44(1)
N(2)	28820(3)	-16968(3)	-1537(2)	47(1)
N(3)	22623(8)	-17249(9)	-160(6)	64(2)
N(4)	30803(3)	-10225(2)	-2443(2)	39(1)
N(5)	29343(3)	-9898(3)	-1449(2)	43(1)
N(6)	35218(3)	-10315(3)	-772(2)	47(1)
C(1)	29523(4)	-17110(3)	-2180(2)	42(1)
C(2)	28962(4)	-16364(3)	-2830(3)	47(1)
C(3)	27759(4)	-16157(3)	-1619(3)	47(1)
C(4)	28066(5)	-15434(4)	-1399(3)	54(1)
C(5)	29151(5)	-17537(4)	-802(3)	57(1)
C(6)	26848(4)	-15276(3)	-2772(3)	45(1)
C(7)	26721(4)	-14996(3)	-3526(3)	48(1)
C(8)	25567(4)	-14457(3)	-3732(3)	50(1)
C(9)	25210(4)	-14095(3)	-4470(3)	49(1)
C(10)	23909(5)	-13629(4)	-4544(3)	58(1)
C(11)	23520(5)	-13234(4)	-5241(3)	57(1)
C(12)	24450(5)	-13299(4)	-5866(3)	55(1)
C(13)	25737(5)	-13773(4)	-5815(3)	57(1)
C(14)	26120(4)	-14165(4)	-5120(3)	53(1)
C(15)	30035(4)	-15792(3)	-3369(2)	49(1)
C(16)	30663(4)	-15355(4)	-2999(3)	50(1)
C(17)	30248(5)	-14434(4)	-3068(3)	58(1)

---

C(18)	30830(6)	-14031(4)	-2739(4)	71(2)
C(19)	31815(6)	-14540(5)	-2317(3)	73(2)
C(20)	32228(5)	-15465(4)	-2239(3)	66(1)
C(21)	31664(4)	-15876(4)	-2579(3)	54(1)
C(22)	26398(4)	-16454(3)	-1214(2)	43(1)
C(23)	25562(5)	-16089(4)	-680(3)	58(1)
C(24)	24320(5)	-16357(4)	-338(3)	64(1)
C(25)	23961(4)	-16975(3)	-557(3)	55(1)
C(26)	24781(4)	-17380(3)	-1062(3)	52(1)
C(27)	26023(4)	-17110(3)	-1385(3)	47(1)
C(28)	28959(4)	-9226(3)	-2061(2)	42(1)
C(29)	29892(4)	-9368(3)	-2764(2)	40(1)
C(30)	30489(4)	-10590(3)	-1584(2)	40(1)
C(31)	30138(4)	-11534(3)	-1321(3)	49(1)
C(32)	28651(4)	-9971(4)	-688(2)	49(1)
C(33)	31820(4)	-10642(3)	-2811(2)	41(1)
C(34)	32276(4)	-10377(3)	-3591(2)	43(1)
C(35)	33280(4)	-10952(3)	-3859(2)	44(1)
C(36)	33879(4)	-10859(3)	-4635(3)	46(1)
C(37)	33446(4)	-10119(4)	-5244(3)	51(1)
C(38)	34054(4)	-10075(4)	-5972(3)	56(1)
C(39)	35077(4)	-10765(4)	-6095(3)	55(1)
C(40)	35531(5)	-11492(4)	-5515(3)	58(1)
C(41)	34934(4)	-11540(4)	-4777(3)	53(1)
C(42)	29112(4)	-9396(3)	-3324(2)	47(1)
C(43)	28649(4)	-10293(3)	-3118(3)	47(1)
C(44)	27652(4)	-10580(3)	-2488(2)	48(1)
C(45)	27246(5)	-11405(4)	-2305(3)	61(1)
C(46)	27799(6)	-11967(4)	-2735(4)	71(2)
C(47)	28775(5)	-11685(4)	-3374(4)	65(1)
C(48)	29200(4)	-10862(4)	-3550(3)	54(1)
C(49)	31692(4)	-10541(3)	-1294(2)	39(1)
C(50)	31909(4)	-9683(3)	-1363(2)	42(1)
C(51)	33043(4)	-9601(3)	-1171(2)	43(1)
C(52)	33957(3)	-10396(3)	-924(2)	40(1)
C(53)	33755(4)	-11244(3)	-843(2)	46(1)

C(54)	32597(4)	-11325(3)	-1026(2)	44(1)
P(1)	30686(1)	-7159(1)	-4855(1)	53(1)
P(2)	24441(1)	-13238(1)	-1938(1)	63(1)
F(1)	29701(3)	-7277(3)	-5291(2)	80(1)
F(2)	29598(3)	-7375(2)	-4099(2)	64(1)
F(3)	31295(3)	-8234(2)	-4660(2)	69(1)
F(4)	31777(3)	-6949(2)	-5601(2)	77(1)
F(5)	31680(3)	-7059(3)	-4407(2)	83(1)
F(6)	30073(4)	-6100(2)	-5032(2)	83(1)
F(7)	24528(3)	-12185(2)	-2129(2)	79(1)
F(8)	24347(3)	-14274(2)	-1770(2)	71(1)
F(9)	25113(6)	-13101(4)	-2778(4)	91(1)
F(10)	23805(7)	-13338(4)	-1068(3)	89(1)
F(11)	23007(5)	-12863(4)	-2139(4)	79(1)
F(12)	25871(6)	-13539(4)	-1698(4)	101(2)
F(9A)	25966(13)	-13518(8)	-2311(8)	91(1)
F(10A)	22885(14)	-13070(9)	-1644(8)	89(1)
F(11A)	24012(11)	-13119(7)	-2736(7)	79(1)
F(12A)	24822(14)	-13414(9)	-1205(9)	101(2)
N(3A)	22585(13)	-17170(19)	-360(13)	64(2)
O(3A)	21760(15)	-16822(12)	71(9)	78(2)
O(2A)	22270(40)	-17620(20)	-658(13)	67(2)

Table 11.3. Bond lengths [ $\text{\AA}$ ] and angles [ $^\circ$ ] for tompjr2013smart.

Cl(1)-C(12)	1.740(5)
Cl(2)-C(39)	1.740(5)
O(1)-C(1)	1.204(5)
O(2)-N(3)	1.245(11)
O(3)-N(3)	1.221(11)
O(4)-C(28)	1.209(5)
O(5)-N(6)	1.218(5)
O(6)-N(6)	1.225(5)
N(1)-C(6)	1.295(6)
N(1)-C(2)	1.472(5)
N(1)-C(3)	1.501(6)

---

N(2)-C(1)	1.350(6)
N(2)-C(5)	1.454(6)
N(2)-C(3)	1.467(6)
N(3)-C(25)	1.506(9)
N(4)-C(33)	1.307(5)
N(4)-C(29)	1.477(5)
N(4)-C(30)	1.526(5)
N(5)-C(28)	1.343(6)
N(5)-C(32)	1.449(5)
N(5)-C(30)	1.458(5)
N(6)-C(52)	1.477(5)
C(1)-C(2)	1.505(6)
C(2)-C(15)	1.550(6)
C(2)-H(2)	1.0000
C(3)-C(4)	1.495(6)
C(3)-C(22)	1.543(6)
C(4)-H(4A)	0.9800
C(4)-H(4B)	0.9800
C(4)-H(4C)	0.9800
C(5)-H(5A)	0.9800
C(5)-H(5B)	0.9800
C(5)-H(5C)	0.9800
C(6)-C(7)	1.397(6)
C(6)-H(6)	0.9500
C(7)-C(8)	1.356(6)
C(7)-H(7)	0.9500
C(8)-C(9)	1.443(6)
C(8)-H(8)	0.9500
C(9)-C(10)	1.399(6)
C(9)-C(14)	1.401(6)
C(10)-C(11)	1.385(7)
C(10)-H(10)	0.9500
C(11)-C(12)	1.373(7)
C(11)-H(11)	0.9500
C(12)-C(13)	1.384(7)
C(13)-C(14)	1.378(6)

---

C(13)-H(13)	0.9500
C(14)-H(14)	0.9500
C(15)-C(16)	1.511(6)
C(15)-H(15A)	0.9900
C(15)-H(15B)	0.9900
C(16)-C(17)	1.385(7)
C(16)-C(21)	1.399(6)
C(17)-C(18)	1.378(8)
C(17)-H(17)	0.9500
C(18)-C(19)	1.386(9)
C(18)-H(18)	0.9500
C(19)-C(20)	1.386(9)
C(19)-H(19)	0.9500
C(20)-C(21)	1.391(7)
C(20)-H(20)	0.9500
C(21)-H(21)	0.9500
C(22)-C(27)	1.374(6)
C(22)-C(23)	1.386(7)
C(23)-C(24)	1.399(7)
C(23)-H(23)	0.9500
C(24)-C(25)	1.368(8)
C(24)-H(24)	0.9500
C(25)-C(26)	1.374(7)
C(25)-N(3A)	1.481(10)
C(26)-C(27)	1.396(6)
C(26)-H(26)	0.9500
C(27)-H(27)	0.9500
C(28)-C(29)	1.523(6)
C(29)-C(42)	1.540(5)
C(29)-H(29)	1.0000
C(30)-C(31)	1.503(6)
C(30)-C(49)	1.540(5)
C(31)-H(31A)	0.9800
C(31)-H(31B)	0.9800
C(31)-H(31C)	0.9800
C(32)-H(32A)	0.9800

---

C(32)-H(32B)	0.9800
C(32)-H(32C)	0.9800
C(33)-C(34)	1.401(6)
C(33)-H(33)	0.9500
C(34)-C(35)	1.348(6)
C(34)-H(34)	0.9500
C(35)-C(36)	1.448(6)
C(35)-H(35)	0.9500
C(36)-C(41)	1.396(7)
C(36)-C(37)	1.400(7)
C(37)-C(38)	1.382(6)
C(37)-H(37)	0.9500
C(38)-C(39)	1.377(7)
C(38)-H(38)	0.9500
C(39)-C(40)	1.365(8)
C(40)-C(41)	1.394(7)
C(40)-H(40)	0.9500
C(41)-H(41)	0.9500
C(42)-C(43)	1.501(7)
C(42)-H(42A)	0.9900
C(42)-H(42B)	0.9900
C(43)-C(48)	1.386(7)
C(43)-C(44)	1.407(6)
C(44)-C(45)	1.373(7)
C(44)-H(44)	0.9500
C(45)-C(46)	1.374(8)
C(45)-H(45)	0.9500
C(46)-C(47)	1.402(8)
C(46)-H(46)	0.9500
C(47)-C(48)	1.383(7)
C(47)-H(47)	0.9500
C(48)-H(48)	0.9500
C(49)-C(54)	1.381(6)
C(49)-C(50)	1.391(6)
C(50)-C(51)	1.387(5)
C(50)-H(50)	0.9500

C(51)-C(52)	1.388(6)
C(51)-H(51)	0.9500
C(52)-C(53)	1.362(6)
C(53)-C(54)	1.400(5)
C(53)-H(53)	0.9500
C(54)-H(54)	0.9500
P(1)-F(1)	1.580(3)
P(1)-F(6)	1.583(3)
P(1)-F(4)	1.588(3)
P(1)-F(5)	1.590(3)
P(1)-F(2)	1.598(3)
P(1)-F(3)	1.603(3)
P(2)-F(12A)	1.486(14)
P(2)-F(9)	1.562(6)
P(2)-F(11)	1.569(5)
P(2)-F(8)	1.580(3)
P(2)-F(10A)	1.581(14)
P(2)-F(12)	1.595(5)
P(2)-F(7)	1.596(4)
P(2)-F(9A)	1.609(12)
P(2)-F(10)	1.616(6)
P(2)-F(11A)	1.656(11)
N(3A)-O(2A)	1.221(10)
N(3A)-O(3A)	1.225(10)
C(6)-N(1)-C(2)	125.3(4)
C(6)-N(1)-C(3)	121.8(4)
C(2)-N(1)-C(3)	112.5(3)
C(1)-N(2)-C(5)	122.4(4)
C(1)-N(2)-C(3)	116.4(4)
C(5)-N(2)-C(3)	121.0(4)
O(3)-N(3)-O(2)	127.0(9)
O(3)-N(3)-C(25)	118.3(9)
O(2)-N(3)-C(25)	114.5(10)
C(33)-N(4)-C(29)	127.1(4)
C(33)-N(4)-C(30)	120.3(4)

---

C(29)-N(4)-C(30)	112.5(3)
C(28)-N(5)-C(32)	123.2(4)
C(28)-N(5)-C(30)	116.4(3)
C(32)-N(5)-C(30)	120.4(3)
O(5)-N(6)-O(6)	124.2(3)
O(5)-N(6)-C(52)	118.1(4)
O(6)-N(6)-C(52)	117.7(4)
O(1)-C(1)-N(2)	126.4(4)
O(1)-C(1)-C(2)	125.5(4)
N(2)-C(1)-C(2)	108.1(4)
N(1)-C(2)-C(1)	102.9(3)
N(1)-C(2)-C(15)	115.6(4)
C(1)-C(2)-C(15)	111.1(3)
N(1)-C(2)-H(2)	109.0
C(1)-C(2)-H(2)	109.0
C(15)-C(2)-H(2)	109.0
N(2)-C(3)-C(4)	112.4(4)
N(2)-C(3)-N(1)	99.3(3)
C(4)-C(3)-N(1)	111.4(4)
N(2)-C(3)-C(22)	110.1(4)
C(4)-C(3)-C(22)	114.2(4)
N(1)-C(3)-C(22)	108.3(3)
C(3)-C(4)-H(4A)	109.5
C(3)-C(4)-H(4B)	109.5
H(4A)-C(4)-H(4B)	109.5
C(3)-C(4)-H(4C)	109.5
H(4A)-C(4)-H(4C)	109.5
H(4B)-C(4)-H(4C)	109.5
N(2)-C(5)-H(5A)	109.5
N(2)-C(5)-H(5B)	109.5
H(5A)-C(5)-H(5B)	109.5
N(2)-C(5)-H(5C)	109.5
H(5A)-C(5)-H(5C)	109.5
H(5B)-C(5)-H(5C)	109.5
N(1)-C(6)-C(7)	127.5(4)
N(1)-C(6)-H(6)	116.3



---

C(7)-C(6)-H(6)	116.3
C(8)-C(7)-C(6)	118.4(4)
C(8)-C(7)-H(7)	120.8
C(6)-C(7)-H(7)	120.8
C(7)-C(8)-C(9)	128.0(4)
C(7)-C(8)-H(8)	116.0
C(9)-C(8)-H(8)	116.0
C(10)-C(9)-C(14)	118.5(4)
C(10)-C(9)-C(8)	118.6(4)
C(14)-C(9)-C(8)	122.9(4)
C(11)-C(10)-C(9)	121.3(5)
C(11)-C(10)-H(10)	119.4
C(9)-C(10)-H(10)	119.4
C(12)-C(11)-C(10)	118.4(4)
C(12)-C(11)-H(11)	120.8
C(10)-C(11)-H(11)	120.8
C(11)-C(12)-C(13)	122.0(4)
C(11)-C(12)-Cl(1)	119.1(4)
C(13)-C(12)-Cl(1)	118.9(4)
C(14)-C(13)-C(12)	119.4(5)
C(14)-C(13)-H(13)	120.3
C(12)-C(13)-H(13)	120.3
C(13)-C(14)-C(9)	120.4(4)
C(13)-C(14)-H(14)	119.8
C(9)-C(14)-H(14)	119.8
C(16)-C(15)-C(2)	114.6(4)
C(16)-C(15)-H(15A)	108.6
C(2)-C(15)-H(15A)	108.6
C(16)-C(15)-H(15B)	108.6
C(2)-C(15)-H(15B)	108.6
H(15A)-C(15)-H(15B)	107.6
C(17)-C(16)-C(21)	119.2(5)
C(17)-C(16)-C(15)	120.3(4)
C(21)-C(16)-C(15)	120.6(5)
C(18)-C(17)-C(16)	120.4(5)
C(18)-C(17)-H(17)	119.8

C(16)-C(17)-H(17)	119.8
C(17)-C(18)-C(19)	121.0(6)
C(17)-C(18)-H(18)	119.5
C(19)-C(18)-H(18)	119.5
C(18)-C(19)-C(20)	119.0(5)
C(18)-C(19)-H(19)	120.5
C(20)-C(19)-H(19)	120.5
C(19)-C(20)-C(21)	120.6(5)
C(19)-C(20)-H(20)	119.7
C(21)-C(20)-H(20)	119.7
C(20)-C(21)-C(16)	119.9(5)
C(20)-C(21)-H(21)	120.1
C(16)-C(21)-H(21)	120.1
C(27)-C(22)-C(23)	119.5(4)
C(27)-C(22)-C(3)	118.4(4)
C(23)-C(22)-C(3)	122.0(4)
C(22)-C(23)-C(24)	120.4(5)
C(22)-C(23)-H(23)	119.8
C(24)-C(23)-H(23)	119.8
C(25)-C(24)-C(23)	117.8(5)
C(25)-C(24)-H(24)	121.1
C(23)-C(24)-H(24)	121.1
C(24)-C(25)-C(26)	123.5(4)
C(24)-C(25)-N(3A)	123.0(9)
C(26)-C(25)-N(3A)	112.9(9)
C(24)-C(25)-N(3)	115.4(6)
C(26)-C(25)-N(3)	121.0(6)
N(3A)-C(25)-N(3)	14.3(12)
C(25)-C(26)-C(27)	117.3(5)
C(25)-C(26)-H(26)	121.3
C(27)-C(26)-H(26)	121.3
C(22)-C(27)-C(26)	121.2(4)
C(22)-C(27)-H(27)	119.4
C(26)-C(27)-H(27)	119.4
O(4)-C(28)-N(5)	126.5(4)
O(4)-C(28)-C(29)	124.3(4)

---

N(5)-C(28)-C(29)	109.3(3)
N(4)-C(29)-C(28)	102.1(3)
N(4)-C(29)-C(42)	115.7(3)
C(28)-C(29)-C(42)	111.5(3)
N(4)-C(29)-H(29)	109.1
C(28)-C(29)-H(29)	109.1
C(42)-C(29)-H(29)	109.1
N(5)-C(30)-C(31)	112.5(3)
N(5)-C(30)-N(4)	99.7(3)
C(31)-C(30)-N(4)	109.8(3)
N(5)-C(30)-C(49)	111.3(3)
C(31)-C(30)-C(49)	114.8(4)
N(4)-C(30)-C(49)	107.4(3)
C(30)-C(31)-H(31A)	109.5
C(30)-C(31)-H(31B)	109.5
H(31A)-C(31)-H(31B)	109.5
C(30)-C(31)-H(31C)	109.5
H(31A)-C(31)-H(31C)	109.5
H(31B)-C(31)-H(31C)	109.5
N(5)-C(32)-H(32A)	109.5
N(5)-C(32)-H(32B)	109.5
H(32A)-C(32)-H(32B)	109.5
N(5)-C(32)-H(32C)	109.5
H(32A)-C(32)-H(32C)	109.5
H(32B)-C(32)-H(32C)	109.5
N(4)-C(33)-C(34)	127.6(4)
N(4)-C(33)-H(33)	116.2
C(34)-C(33)-H(33)	116.2
C(35)-C(34)-C(33)	117.8(4)
C(35)-C(34)-H(34)	121.1
C(33)-C(34)-H(34)	121.1
C(34)-C(35)-C(36)	128.3(4)
C(34)-C(35)-H(35)	115.8
C(36)-C(35)-H(35)	115.8
C(41)-C(36)-C(37)	119.1(4)
C(41)-C(36)-C(35)	118.0(4)

C(37)-C(36)-C(35)	122.9(4)
C(38)-C(37)-C(36)	120.0(5)
C(38)-C(37)-H(37)	120.0
C(36)-C(37)-H(37)	120.0
C(39)-C(38)-C(37)	119.7(5)
C(39)-C(38)-H(38)	120.2
C(37)-C(38)-H(38)	120.2
C(40)-C(39)-C(38)	121.9(4)
C(40)-C(39)-Cl(2)	119.2(4)
C(38)-C(39)-Cl(2)	118.9(4)
C(39)-C(40)-C(41)	119.0(5)
C(39)-C(40)-H(40)	120.5
C(41)-C(40)-H(40)	120.5
C(40)-C(41)-C(36)	120.4(5)
C(40)-C(41)-H(41)	119.8
C(36)-C(41)-H(41)	119.8
C(43)-C(42)-C(29)	114.3(4)
C(43)-C(42)-H(42A)	108.7
C(29)-C(42)-H(42A)	108.7
C(43)-C(42)-H(42B)	108.7
C(29)-C(42)-H(42B)	108.7
H(42A)-C(42)-H(42B)	107.6
C(48)-C(43)-C(44)	118.2(5)
C(48)-C(43)-C(42)	120.3(4)
C(44)-C(43)-C(42)	121.5(4)
C(45)-C(44)-C(43)	120.7(4)
C(45)-C(44)-H(44)	119.6
C(43)-C(44)-H(44)	119.6
C(44)-C(45)-C(46)	120.8(5)
C(44)-C(45)-H(45)	119.6
C(46)-C(45)-H(45)	119.6
C(45)-C(46)-C(47)	119.4(5)
C(45)-C(46)-H(46)	120.3
C(47)-C(46)-H(46)	120.3
C(48)-C(47)-C(46)	119.7(5)
C(48)-C(47)-H(47)	120.1

C(46)-C(47)-H(47)	120.1
C(47)-C(48)-C(43)	121.1(5)
C(47)-C(48)-H(48)	119.4
C(43)-C(48)-H(48)	119.4
C(54)-C(49)-C(50)	120.4(4)
C(54)-C(49)-C(30)	120.6(4)
C(50)-C(49)-C(30)	118.8(4)
C(51)-C(50)-C(49)	120.6(4)
C(51)-C(50)-H(50)	119.7
C(49)-C(50)-H(50)	119.7
C(50)-C(51)-C(52)	117.8(4)
C(50)-C(51)-H(51)	121.1
C(52)-C(51)-H(51)	121.1
C(53)-C(52)-C(51)	122.5(4)
C(53)-C(52)-N(6)	118.8(4)
C(51)-C(52)-N(6)	118.6(4)
C(52)-C(53)-C(54)	119.4(4)
C(52)-C(53)-H(53)	120.3
C(54)-C(53)-H(53)	120.3
C(49)-C(54)-C(53)	119.2(4)
C(49)-C(54)-H(54)	120.4
C(53)-C(54)-H(54)	120.4
F(1)-P(1)-F(6)	91.0(2)
F(1)-P(1)-F(4)	90.66(19)
F(6)-P(1)-F(4)	91.5(2)
F(1)-P(1)-F(5)	179.0(2)
F(6)-P(1)-F(5)	90.0(2)
F(4)-P(1)-F(5)	89.7(2)
F(1)-P(1)-F(2)	89.76(18)
F(6)-P(1)-F(2)	88.84(19)
F(4)-P(1)-F(2)	179.5(2)
F(5)-P(1)-F(2)	89.88(19)
F(1)-P(1)-F(3)	89.4(2)
F(6)-P(1)-F(3)	179.0(2)
F(4)-P(1)-F(3)	89.38(19)
F(5)-P(1)-F(3)	89.6(2)

F(2)-P(1)-F(3)	90.27(17)
F(12A)-P(2)-F(9)	139.2(7)
F(12A)-P(2)-F(11)	126.7(7)
F(9)-P(2)-F(11)	92.7(4)
F(12A)-P(2)-F(8)	94.5(5)
F(9)-P(2)-F(8)	93.0(3)
F(11)-P(2)-F(8)	93.6(2)
F(12A)-P(2)-F(10A)	95.6(8)
F(9)-P(2)-F(10A)	124.8(6)
F(11)-P(2)-F(10A)	32.5(5)
F(8)-P(2)-F(10A)	87.5(5)
F(12A)-P(2)-F(12)	49.4(6)
F(9)-P(2)-F(12)	90.4(4)
F(11)-P(2)-F(12)	174.2(4)
F(8)-P(2)-F(12)	91.1(3)
F(10A)-P(2)-F(12)	144.8(6)
F(12A)-P(2)-F(7)	86.9(5)
F(9)-P(2)-F(7)	85.9(3)
F(11)-P(2)-F(7)	85.6(2)
F(8)-P(2)-F(7)	178.6(2)
F(10A)-P(2)-F(7)	92.5(5)
F(12)-P(2)-F(7)	89.7(3)
F(12A)-P(2)-F(9A)	91.8(8)
F(9)-P(2)-F(9A)	49.1(6)
F(11)-P(2)-F(9A)	141.4(6)
F(8)-P(2)-F(9A)	84.8(4)
F(10A)-P(2)-F(9A)	169.7(7)
F(12)-P(2)-F(9A)	42.5(5)
F(7)-P(2)-F(9A)	95.1(5)
F(12A)-P(2)-F(10)	38.2(6)
F(9)-P(2)-F(10)	176.4(3)
F(11)-P(2)-F(10)	89.3(4)
F(8)-P(2)-F(10)	89.9(3)
F(10A)-P(2)-F(10)	57.5(6)
F(12)-P(2)-F(10)	87.3(4)
F(7)-P(2)-F(10)	91.2(3)

F(9A)-P(2)-F(10)	129.2(6)
F(12A)-P(2)-F(11A)	176.0(6)
F(9)-P(2)-F(11A)	41.7(4)
F(11)-P(2)-F(11A)	53.9(4)
F(8)-P(2)-F(11A)	81.5(4)
F(10A)-P(2)-F(11A)	84.3(6)
F(12)-P(2)-F(11A)	130.3(5)
F(7)-P(2)-F(11A)	97.1(4)
F(9A)-P(2)-F(11A)	87.8(7)
F(10)-P(2)-F(11A)	141.2(5)
O(2A)-N(3A)-O(3A)	121(2)
O(2A)-N(3A)-C(25)	120(2)
O(3A)-N(3A)-C(25)	118.3(15)

Table 11.4. Anisotropic displacement parameters ( $\text{\AA}^2 \times 10^3$ ) for tompjr2013smart. The anisotropic displacement factor exponent takes the form:  $-2\pi^2 [ h^2 a^{*2} U^{11} + \dots + 2 h k a^* b^* U^{12} ]$

	$U^{11}$	$U^{22}$	$U^{33}$	$U^{23}$	$U^{13}$	$U^{12}$
Cl(1)	68(1)	83(1)	58(1)	-13(1)	-30(1)	-12(1)
Cl(2)	56(1)	114(1)	57(1)	-48(1)	7(1)	-29(1)
O(1)	33(1)	53(2)	63(2)	-16(2)	-7(1)	-4(1)
O(2)	40(2)	89(3)	57(6)	4(4)	-16(5)	-21(2)
O(3)	48(3)	82(4)	84(5)	-21(4)	13(3)	-10(3)
O(4)	36(2)	60(2)	55(2)	-26(2)	-11(1)	-1(1)
O(5)	32(2)	68(2)	67(2)	-22(2)	-17(1)	-3(1)
O(6)	42(2)	71(2)	76(2)	-24(2)	-21(2)	-14(2)
N(1)	36(2)	51(2)	46(2)	-17(2)	-8(2)	-8(2)
N(2)	32(2)	56(2)	50(2)	-14(2)	-11(2)	-5(2)
N(3)	37(2)	64(3)	70(5)	-6(4)	-3(3)	-4(2)
N(4)	26(1)	58(2)	38(2)	-20(2)	-5(1)	-8(1)
N(5)	27(2)	66(2)	39(2)	-23(2)	-6(1)	-6(2)
N(6)	28(2)	65(2)	51(2)	-22(2)	-10(2)	-9(2)
C(1)	30(2)	51(2)	48(2)	-17(2)	-9(2)	-9(2)
C(2)	39(2)	58(3)	47(2)	-21(2)	-9(2)	-8(2)
C(3)	37(2)	56(3)	47(2)	-16(2)	-11(2)	-5(2)

---

C(4)	43(2)	73(3)	48(2)	-22(2)	-7(2)	-13(2)
C(5)	40(2)	75(3)	48(3)	-13(2)	-14(2)	-2(2)
C(6)	34(2)	54(2)	52(2)	-22(2)	-10(2)	-7(2)
C(7)	39(2)	59(3)	46(2)	-19(2)	-9(2)	-4(2)
C(8)	36(2)	66(3)	50(2)	-23(2)	-5(2)	-9(2)
C(9)	40(2)	60(3)	49(2)	-19(2)	-12(2)	-7(2)
C(10)	39(2)	72(3)	63(3)	-25(3)	-15(2)	2(2)
C(11)	42(2)	73(3)	57(3)	-22(2)	-19(2)	0(2)
C(12)	45(2)	68(3)	53(3)	-17(2)	-17(2)	-9(2)
C(13)	47(2)	74(3)	52(3)	-22(2)	-14(2)	-10(2)
C(14)	36(2)	74(3)	49(2)	-17(2)	-12(2)	-10(2)
C(15)	37(2)	62(3)	43(2)	-15(2)	-5(2)	-6(2)
C(16)	36(2)	70(3)	44(2)	-17(2)	-8(2)	-8(2)
C(17)	48(2)	66(3)	54(3)	-13(2)	-12(2)	-8(2)
C(18)	71(3)	61(3)	77(4)	-17(3)	-7(3)	-21(3)
C(19)	73(4)	90(4)	67(4)	-28(3)	-10(3)	-34(3)
C(20)	50(3)	92(4)	56(3)	-12(3)	-17(2)	-21(3)
C(21)	35(2)	63(3)	54(3)	-10(2)	-5(2)	-7(2)
C(22)	30(2)	55(2)	41(2)	-14(2)	-10(2)	-1(2)
C(23)	48(2)	66(3)	63(3)	-29(3)	-4(2)	-10(2)
C(24)	46(2)	71(3)	65(3)	-25(3)	10(2)	-7(2)
C(25)	32(2)	55(3)	62(3)	-9(2)	-4(2)	-3(2)
C(26)	40(2)	55(3)	58(3)	-12(2)	-15(2)	-4(2)
C(27)	33(2)	60(3)	48(2)	-21(2)	-10(2)	0(2)
C(28)	30(2)	58(3)	45(2)	-24(2)	-7(2)	-9(2)
C(29)	29(2)	51(2)	41(2)	-15(2)	-9(2)	-7(2)
C(30)	33(2)	55(2)	34(2)	-14(2)	-5(2)	-13(2)
C(31)	36(2)	65(3)	46(2)	-13(2)	-9(2)	-15(2)
C(32)	31(2)	81(3)	43(2)	-30(2)	-4(2)	-10(2)
C(33)	31(2)	51(2)	44(2)	-19(2)	-10(2)	-6(2)
C(34)	31(2)	61(3)	40(2)	-22(2)	-7(2)	-6(2)
C(35)	32(2)	57(3)	44(2)	-20(2)	-7(2)	-6(2)
C(36)	32(2)	65(3)	46(2)	-25(2)	-4(2)	-10(2)
C(37)	35(2)	76(3)	48(2)	-25(2)	-6(2)	-10(2)
C(38)	36(2)	85(4)	50(3)	-26(2)	-6(2)	-15(2)
C(39)	40(2)	88(4)	47(2)	-35(3)	5(2)	-23(2)



---

C(40)	40(2)	78(3)	65(3)	-41(3)	4(2)	-13(2)
C(41)	38(2)	67(3)	57(3)	-26(2)	-5(2)	-8(2)
C(42)	36(2)	64(3)	45(2)	-21(2)	-15(2)	-4(2)
C(43)	31(2)	65(3)	51(2)	-24(2)	-17(2)	-1(2)
C(44)	42(2)	72(3)	41(2)	-26(2)	-9(2)	-15(2)
C(45)	55(3)	83(4)	54(3)	-20(3)	-13(2)	-27(3)
C(46)	68(3)	66(3)	90(4)	-24(3)	-27(3)	-19(3)
C(47)	55(3)	70(3)	84(4)	-38(3)	-18(3)	-8(2)
C(48)	36(2)	77(3)	60(3)	-33(2)	-10(2)	-12(2)
C(49)	28(2)	53(2)	37(2)	-19(2)	-4(2)	-5(2)
C(50)	28(2)	57(2)	41(2)	-19(2)	-6(2)	-2(2)
C(51)	34(2)	55(2)	43(2)	-19(2)	-4(2)	-11(2)
C(52)	23(2)	62(3)	40(2)	-22(2)	-5(1)	-7(2)
C(53)	31(2)	55(3)	48(2)	-15(2)	-10(2)	-1(2)
C(54)	32(2)	52(2)	48(2)	-14(2)	-10(2)	-9(2)
P(1)	46(1)	59(1)	51(1)	-18(1)	-5(1)	-7(1)
P(2)	45(1)	65(1)	84(1)	-33(1)	-18(1)	1(1)
F(1)	56(2)	119(3)	78(2)	-53(2)	-14(2)	-4(2)
F(2)	56(2)	73(2)	56(2)	-23(1)	4(1)	-12(1)
F(3)	62(2)	64(2)	74(2)	-25(2)	0(2)	-5(1)
F(4)	62(2)	87(2)	68(2)	-21(2)	13(2)	-22(2)
F(5)	54(2)	109(3)	108(3)	-67(2)	-20(2)	-1(2)
F(6)	91(2)	60(2)	76(2)	-13(2)	-9(2)	4(2)
F(7)	59(2)	66(2)	114(3)	-38(2)	-12(2)	-4(1)
F(8)	62(2)	63(2)	90(2)	-34(2)	-16(2)	3(1)
F(9)	94(3)	77(3)	99(3)	-44(3)	10(2)	-13(2)
F(10)	97(3)	76(3)	91(3)	-36(2)	-11(3)	-4(2)
F(11)	67(2)	64(2)	106(3)	-14(2)	-38(2)	-10(2)
F(12)	76(3)	95(3)	135(4)	-29(3)	-50(3)	-4(3)
F(9A)	94(3)	77(3)	99(3)	-44(3)	10(2)	-13(2)
F(10A)	97(3)	76(3)	91(3)	-36(2)	-11(3)	-4(2)
F(11A)	67(2)	64(2)	106(3)	-14(2)	-38(2)	-10(2)
F(12A)	76(3)	95(3)	135(4)	-29(3)	-50(3)	-4(3)
N(3A)	37(2)	64(3)	70(5)	-6(4)	-3(3)	-4(2)
O(3A)	48(3)	82(4)	84(5)	-21(4)	13(3)	-10(3)
O(2A)	40(2)	89(3)	57(6)	4(4)	-16(5)	-21(2)

Table 11.5. Hydrogen coordinates ( $\times 10^4$ ) and isotropic displacement parameters ( $\text{\AA}^2 \times 10^3$ ) for tompjr2013smart.

	x	y	z	U(eq)
H(2)	28638	-16652	-3116	56
H(4A)	28066	-15662	-857	81
H(4B)	27387	-14879	-1523	81
H(4C)	28945	-15287	-1675	81
H(5A)	29955	-17992	-864	85
H(5B)	28408	-17855	-492	85
H(5C)	29314	-17149	-554	85
H(6)	26150	-15012	-2455	54
H(7)	27425	-15178	-3886	57
H(8)	24913	-14298	-3343	60
H(10)	23280	-13581	-4107	70
H(11)	22631	-12927	-5285	69
H(13)	26351	-13829	-6254	68
H(14)	27005	-14484	-5082	63
H(15A)	30747	-16197	-3599	59
H(15B)	29622	-15300	-3780	59
H(17)	29557	-14078	-3344	69
H(18)	30551	-13395	-2802	85
H(19)	32202	-14260	-2085	87
H(20)	32903	-15821	-1951	80
H(21)	31958	-16509	-2527	65
H(23)	25833	-15653	-546	70
H(24)	23745	-16118	34	77
H(26)	24513	-17825	-1186	63
H(27)	26620	-17386	-1729	56
H(29)	30410	-8851	-3015	48
H(31A)	29927	-11762	-770	74
H(31B)	30896	-11952	-1497	74
H(31C)	29361	-11503	-1527	74

---

H(32A)	27902	-9458	-703	74
H(32B)	29269	-9949	-396	74
H(32C)	28315	-10554	-452	74
H(33)	32306	-11188	-2515	49
H(34)	31890	-9812	-3919	51
H(35)	33641	-11487	-3491	53
H(37)	32734	-9647	-5156	62
H(38)	33767	-9570	-6386	67
H(40)	36243	-11959	-5612	69
H(41)	35246	-12040	-4368	64
H(42A)	28325	-8898	-3360	56
H(42B)	29687	-9272	-3828	56
H(44)	27256	-10200	-2185	58
H(45)	26573	-11589	-1877	73
H(46)	27523	-12541	-2600	86
H(47)	29144	-12059	-3685	78
H(48)	29880	-10683	-3975	65
H(50)	31276	-9149	-1544	51
H(51)	33190	-9020	-1206	52
H(53)	34394	-11775	-665	55
H(54)	32436	-11912	-966	52

**(2*S*,5*S*,*E*)-5-Benzyl-1-((*E*)-3-(4-iodophenyl)allylidene)-2,3-dimethyl-2-(4-nitrophenyl)-4-oxoimidazolidin-1-ium hexafluorophosphate 91·PF<sub>6</sub>**

Table 11.6. Crystal data and structure refinement for temp\_jhr592.

Identification code	temp_jhr592		
Empirical formula	C <sub>29</sub> H <sub>30</sub> F <sub>6</sub> I N <sub>3</sub> O <sub>3.50</sub> P		
Formula weight	748.43		
Temperature	123(2) K		
Wavelength	1.54180 Å		
Crystal system	Triclinic		
Space group	P-1		
Unit cell dimensions	a = 10.4383(4) Å b = 16.5706(7) Å c = 18.8976(9) Å		α = 86.399(4)° β = 86.024(4)° γ = 73.657(4)°
Volume	3125.9(2) Å <sup>3</sup>		
Z	4		
Density (calculated)	1.590 Mg/m <sup>3</sup>		
Absorption coefficient	9.185 mm <sup>-1</sup>		
F(000)	1500		
Crystal size	0.40 x 0.18 x 0.06 mm <sup>3</sup>		
Theta range for data collection	4.42 to 73.56°		
Index ranges	-12 ≤ h ≤ 12, -20 ≤ k ≤ 20, -23 ≤ l ≤ 23		
Reflections collected	25306		
Independent reflections	25307 [R(int) = 0.0000]		
Completeness to theta = 70.00°	99.6%		
Absorption correction	Analytical		
Max. and min. transmission	0.613 and 0.182		
Refinement method	Full-matrix least-squares on F <sup>2</sup>		
Data / restraints / parameters	25307 / 0 / 791		
Goodness-of-fit on F <sup>2</sup>	1.053		
Final R indices [I > 2σ(I)]	R1 = 0.0564, wR2 = 0.1354		
R indices (all data)	R1 = 0.0735, wR2 = 0.1501		
Largest diff. peak and hole	1.985 and -0.891 e.Å <sup>-3</sup>		

Table 11.7. Atomic coordinates ( $\times 10^4$ ) and equivalent isotropic displacement parameters ( $\text{\AA}^2 \times 10^3$ ) for *tomp\_jhr592*.  $U(\text{eq})$  is defined as one third of the trace of the orthogonalized  $U^{\text{ij}}$  tensor.

	x	y	z	$U(\text{eq})$
I(1)	15576(1)	3648(1)	-2087(1)	45(1)
I(2)	4043(1)	11605(1)	-1922(1)	54(1)
P(1)	15142(1)	2580(1)	2652(1)	34(1)
P(2)	10375(1)	7729(1)	201(1)	42(1)
F(1)	14908(2)	1666(1)	2780(1)	43(1)
F(2)	16701(2)	2149(2)	2519(2)	59(1)
F(3)	15364(2)	3495(2)	2523(2)	47(1)
F(4)	13582(2)	3012(2)	2785(2)	48(1)
F(5)	15346(3)	2603(2)	3478(2)	59(1)
F(6)	14923(3)	2555(2)	1828(1)	55(1)
F(7)	9773(4)	7716(2)	997(2)	82(1)
F(8)	9539(3)	8689(2)	119(2)	65(1)
F(9)	9201(3)	7438(2)	-77(2)	94(1)
F(10)	11573(3)	8029(2)	468(2)	75(1)
F(11)	11014(3)	7748(2)	-580(2)	69(1)
F(12)	11226(4)	6771(2)	297(2)	73(1)
O(1)	8610(3)	7136(2)	2992(2)	39(1)
O(2)	17111(3)	5088(2)	4428(2)	54(1)
O(3)	16245(3)	6426(2)	4405(2)	69(1)
O(4)	11067(3)	7913(2)	2962(2)	42(1)
O(5)	3214(3)	8521(2)	4452(3)	75(1)
O(6)	2439(3)	9843(2)	4607(2)	53(1)
O(7)	10431(3)	2609(2)	4371(2)	41(1)
N(1)	11403(3)	5473(2)	2513(2)	26(1)
N(2)	10178(3)	6034(2)	3499(2)	33(1)
N(3)	16181(3)	5717(2)	4320(2)	42(1)
N(4)	8379(3)	9647(2)	2505(2)	28(1)
N(5)	9444(3)	8973(2)	3484(2)	34(1)
N(6)	3331(3)	9228(3)	4417(2)	44(1)
C(1)	11316(3)	5328(2)	3314(2)	26(1)
C(2)	9606(4)	6540(2)	2954(2)	31(1)

---

C(3)	10353(3)	6226(2)	2268(2)	30(1)
C(4)	11022(4)	4490(2)	3508(2)	32(1)
C(5)	9675(4)	6163(3)	4236(2)	41(1)
C(6)	12598(4)	5414(2)	3617(2)	29(1)
C(7)	12734(4)	6211(2)	3711(2)	32(1)
C(8)	13880(4)	6321(3)	3949(2)	36(1)
C(9)	14928(4)	5606(3)	4086(2)	33(1)
C(10)	14833(4)	4802(3)	4010(2)	34(1)
C(11)	13646(4)	4710(2)	3775(2)	30(1)
C(12)	9427(4)	6054(2)	1726(2)	33(1)
C(13)	9034(4)	5253(2)	1881(2)	32(1)
C(14)	9563(4)	4577(3)	1454(2)	37(1)
C(15)	9220(4)	3827(3)	1580(3)	48(1)
C(16)	8337(5)	3747(3)	2141(3)	51(1)
C(17)	7805(5)	4416(3)	2571(2)	49(1)
C(18)	8142(4)	5165(3)	2444(2)	37(1)
C(19)	12345(3)	4994(2)	2126(2)	28(1)
C(20)	12580(4)	5051(2)	1379(2)	28(1)
C(21)	13550(4)	4418(2)	1094(2)	33(1)
C(22)	13978(4)	4278(2)	348(2)	33(1)
C(23)	15046(4)	3575(3)	196(2)	39(1)
C(24)	15495(4)	3391(3)	-497(2)	41(1)
C(25)	14876(4)	3919(3)	-1042(2)	36(1)
C(26)	13821(4)	4629(3)	-903(2)	38(1)
C(27)	13373(4)	4809(3)	-212(2)	34(1)
C(28)	8352(4)	9706(2)	3307(2)	29(1)
C(29)	10112(4)	8532(2)	2931(2)	34(1)
C(30)	9489(4)	8946(2)	2251(2)	33(1)
C(31)	8644(4)	10516(2)	3490(2)	34(1)
C(32)	9816(4)	8754(3)	4216(2)	41(1)
C(33)	7013(4)	9597(2)	3628(2)	29(1)
C(34)	6806(4)	8805(2)	3640(2)	32(1)
C(35)	5591(4)	8686(3)	3904(2)	36(1)
C(36)	4620(4)	9359(3)	4144(2)	36(1)
C(37)	4792(4)	10153(2)	4141(2)	33(1)
C(38)	5999(4)	10270(2)	3884(2)	33(1)

C(39)	10532(4)	9189(3)	1736(2)	35(1)
C(40)	11041(4)	9889(2)	1972(2)	32(1)
C(41)	10589(4)	10693(3)	1672(2)	42(1)
C(42)	11096(5)	11337(3)	1849(3)	55(1)
C(43)	12077(5)	11187(3)	2326(3)	53(1)
C(44)	12545(5)	10381(4)	2638(2)	51(1)
C(45)	12032(4)	9743(3)	2458(2)	42(1)
C(46)	7474(4)	10152(2)	2139(2)	34(1)
C(47)	7302(4)	10161(2)	1401(2)	34(1)
C(48)	6223(4)	10737(2)	1148(2)	36(1)
C(49)	5761(4)	10891(3)	429(2)	37(1)
C(50)	6469(4)	10464(3)	-150(2)	39(1)
C(51)	5964(4)	10660(3)	-817(2)	42(1)
C(52)	4762(4)	11277(3)	-905(2)	40(1)
C(53)	4034(5)	11684(3)	-335(3)	47(1)
C(54)	4531(4)	11493(3)	333(2)	43(1)
C(55)	12741(5)	2400(3)	4530(3)	49(1)
C(56)	11731(4)	2225(3)	4082(3)	45(1)
C(57)	9431(5)	2486(3)	3970(3)	56(1)
C(58)	8085(5)	2872(4)	4326(3)	66(2)

Table 11.8. Bond lengths [ $\text{\AA}$ ] and angles [ $^\circ$ ] for tomp\_jhr592.

I(1)-C(25)	2.088(4)
I(2)-C(52)	2.096(4)
P(1)-F(2)	1.592(2)
P(1)-F(4)	1.593(2)
P(1)-F(5)	1.594(3)
P(1)-F(6)	1.596(3)
P(1)-F(3)	1.598(3)
P(1)-F(1)	1.602(3)
P(2)-F(9)	1.570(3)
P(2)-F(11)	1.580(3)
P(2)-F(8)	1.588(3)
P(2)-F(7)	1.591(3)
P(2)-F(10)	1.592(3)

---

P(2)-F(12)	1.594(3)
O(1)-C(2)	1.216(4)
O(2)-N(3)	1.226(5)
O(3)-N(3)	1.216(5)
O(4)-C(29)	1.214(5)
O(5)-N(6)	1.209(5)
O(6)-N(6)	1.225(5)
O(7)-C(57)	1.398(5)
O(7)-C(56)	1.414(5)
N(1)-C(19)	1.291(5)
N(1)-C(3)	1.484(4)
N(1)-C(1)	1.517(4)
N(2)-C(2)	1.347(5)
N(2)-C(1)	1.454(4)
N(2)-C(5)	1.461(5)
N(3)-C(9)	1.471(5)
N(4)-C(46)	1.283(5)
N(4)-C(30)	1.469(5)
N(4)-C(28)	1.523(5)
N(5)-C(29)	1.348(5)
N(5)-C(28)	1.452(4)
N(5)-C(32)	1.460(5)
N(6)-C(36)	1.477(5)
C(1)-C(4)	1.522(5)
C(1)-C(6)	1.537(5)
C(2)-C(3)	1.509(5)
C(3)-C(12)	1.546(5)
C(3)-H(3)	1.0000
C(4)-H(4A)	0.9800
C(4)-H(4B)	0.9800
C(4)-H(4C)	0.9800
C(5)-H(5A)	0.9800
C(5)-H(5B)	0.9800
C(5)-H(5C)	0.9800
C(6)-C(11)	1.389(5)
C(6)-C(7)	1.391(5)



---

C(7)-C(8)	1.369(5)
C(7)-H(7)	0.9500
C(8)-C(9)	1.392(5)
C(8)-H(8)	0.9500
C(9)-C(10)	1.381(6)
C(10)-C(11)	1.395(5)
C(10)-H(10)	0.9500
C(11)-H(11)	0.9500
C(12)-C(13)	1.502(6)
C(12)-H(12A)	0.9900
C(12)-H(12B)	0.9900
C(13)-C(14)	1.383(6)
C(13)-C(18)	1.394(6)
C(14)-C(15)	1.390(6)
C(14)-H(14)	0.9500
C(15)-C(16)	1.381(7)
C(15)-H(15)	0.9500
C(16)-C(17)	1.378(7)
C(16)-H(16)	0.9500
C(17)-C(18)	1.386(6)
C(17)-H(17)	0.9500
C(18)-H(18)	0.9500
C(19)-C(20)	1.418(5)
C(19)-H(19)	0.9500
C(20)-C(21)	1.347(5)
C(20)-H(20)	0.9500
C(21)-C(22)	1.461(5)
C(21)-H(21)	0.9500
C(22)-C(23)	1.396(6)
C(22)-C(27)	1.398(6)
C(23)-C(24)	1.383(6)
C(23)-H(23)	0.9500
C(24)-C(25)	1.380(6)
C(24)-H(24)	0.9500
C(25)-C(26)	1.391(6)
C(26)-C(27)	1.379(6)

---

C(26)-H(26)	0.9500
C(27)-H(27)	0.9500
C(28)-C(31)	1.522(5)
C(28)-C(33)	1.538(5)
C(29)-C(30)	1.517(5)
C(30)-C(39)	1.532(5)
C(30)-H(30)	1.0000
C(31)-H(31A)	0.9800
C(31)-H(31B)	0.9800
C(31)-H(31C)	0.9800
C(32)-H(32A)	0.9800
C(32)-H(32B)	0.9800
C(32)-H(32C)	0.9800
C(33)-C(34)	1.387(5)
C(33)-C(38)	1.389(5)
C(34)-C(35)	1.392(5)
C(34)-H(34)	0.9500
C(35)-C(36)	1.357(6)
C(35)-H(35)	0.9500
C(36)-C(37)	1.375(6)
C(37)-C(38)	1.380(6)
C(37)-H(37)	0.9500
C(38)-H(38)	0.9500
C(39)-C(40)	1.507(6)
C(39)-H(39A)	0.9900
C(39)-H(39B)	0.9900
C(40)-C(41)	1.380(6)
C(40)-C(45)	1.391(6)
C(41)-C(42)	1.386(6)
C(41)-H(41)	0.9500
C(42)-C(43)	1.371(7)
C(42)-H(42)	0.9500
C(43)-C(44)	1.394(7)
C(43)-H(43)	0.9500
C(44)-C(45)	1.380(7)
C(44)-H(44)	0.9500

C(45)-H(45)	0.9500
C(46)-C(47)	1.415(6)
C(46)-H(46)	0.9500
C(47)-C(48)	1.349(5)
C(47)-H(47)	0.9500
C(48)-C(49)	1.457(6)
C(48)-H(48)	0.9500
C(49)-C(50)	1.391(6)
C(49)-C(54)	1.401(6)
C(50)-C(51)	1.385(6)
C(50)-H(50)	0.9500
C(51)-C(52)	1.390(6)
C(51)-H(51)	0.9500
C(52)-C(53)	1.371(6)
C(53)-C(54)	1.382(6)
C(53)-H(53)	0.9500
C(54)-H(54)	0.9500
C(55)-C(56)	1.496(6)
C(55)-H(55A)	0.9800
C(55)-H(55B)	0.9800
C(55)-H(55C)	0.9800
C(56)-H(56A)	0.9900
C(56)-H(56B)	0.9900
C(57)-C(58)	1.501(7)
C(57)-H(57A)	0.9900
C(57)-H(57B)	0.9900
C(58)-H(58A)	0.9800
C(58)-H(58B)	0.9800
C(58)-H(58C)	0.9800
F(2)-P(1)-F(4)	179.9(2)
F(2)-P(1)-F(5)	90.00(17)
F(4)-P(1)-F(5)	90.08(16)
F(2)-P(1)-F(6)	90.51(17)
F(4)-P(1)-F(6)	89.41(15)
F(5)-P(1)-F(6)	179.38(19)

F(2)-P(1)-F(3)	90.93(15)
F(4)-P(1)-F(3)	89.05(14)
F(5)-P(1)-F(3)	90.27(16)
F(6)-P(1)-F(3)	90.07(15)
F(2)-P(1)-F(1)	89.47(14)
F(4)-P(1)-F(1)	90.55(14)
F(5)-P(1)-F(1)	89.97(15)
F(6)-P(1)-F(1)	89.68(15)
F(3)-P(1)-F(1)	179.53(15)
F(9)-P(2)-F(11)	90.3(2)
F(9)-P(2)-F(8)	91.18(19)
F(11)-P(2)-F(8)	91.79(17)
F(9)-P(2)-F(7)	91.5(2)
F(11)-P(2)-F(7)	178.1(2)
F(8)-P(2)-F(7)	88.47(18)
F(9)-P(2)-F(10)	178.9(2)
F(11)-P(2)-F(10)	88.7(2)
F(8)-P(2)-F(10)	88.68(18)
F(7)-P(2)-F(10)	89.5(2)
F(9)-P(2)-F(12)	89.8(2)
F(11)-P(2)-F(12)	88.82(17)
F(8)-P(2)-F(12)	178.9(2)
F(7)-P(2)-F(12)	90.89(18)
F(10)-P(2)-F(12)	90.38(19)
C(57)-O(7)-C(56)	112.6(4)
C(19)-N(1)-C(3)	126.9(3)
C(19)-N(1)-C(1)	121.0(3)
C(3)-N(1)-C(1)	112.1(3)
C(2)-N(2)-C(1)	116.3(3)
C(2)-N(2)-C(5)	122.7(3)
C(1)-N(2)-C(5)	121.0(3)
O(3)-N(3)-O(2)	122.9(4)
O(3)-N(3)-C(9)	118.7(4)
O(2)-N(3)-C(9)	118.4(4)
C(46)-N(4)-C(30)	127.6(3)
C(46)-N(4)-C(28)	120.7(3)

---

C(30)-N(4)-C(28)	111.6(3)
C(29)-N(5)-C(28)	116.1(3)
C(29)-N(5)-C(32)	122.6(3)
C(28)-N(5)-C(32)	121.3(3)
O(5)-N(6)-O(6)	123.4(4)
O(5)-N(6)-C(36)	118.6(4)
O(6)-N(6)-C(36)	118.0(4)
N(2)-C(1)-N(1)	100.0(3)
N(2)-C(1)-C(4)	111.5(3)
N(1)-C(1)-C(4)	110.3(3)
N(2)-C(1)-C(6)	110.9(3)
N(1)-C(1)-C(6)	109.0(3)
C(4)-C(1)-C(6)	114.2(3)
O(1)-C(2)-N(2)	126.5(4)
O(1)-C(2)-C(3)	124.3(4)
N(2)-C(2)-C(3)	109.2(3)
N(1)-C(3)-C(2)	102.4(3)
N(1)-C(3)-C(12)	114.9(3)
C(2)-C(3)-C(12)	112.4(3)
N(1)-C(3)-H(3)	109.0
C(2)-C(3)-H(3)	109.0
C(12)-C(3)-H(3)	109.0
C(1)-C(4)-H(4A)	109.5
C(1)-C(4)-H(4B)	109.5
H(4A)-C(4)-H(4B)	109.5
C(1)-C(4)-H(4C)	109.5
H(4A)-C(4)-H(4C)	109.5
H(4B)-C(4)-H(4C)	109.5
N(2)-C(5)-H(5A)	109.5
N(2)-C(5)-H(5B)	109.5
H(5A)-C(5)-H(5B)	109.5
N(2)-C(5)-H(5C)	109.5
H(5A)-C(5)-H(5C)	109.5
H(5B)-C(5)-H(5C)	109.5
C(11)-C(6)-C(7)	119.3(3)
C(11)-C(6)-C(1)	121.2(3)

C(7)-C(6)-C(1)	119.5(3)
C(8)-C(7)-C(6)	121.7(4)
C(8)-C(7)-H(7)	119.2
C(6)-C(7)-H(7)	119.2
C(7)-C(8)-C(9)	117.9(4)
C(7)-C(8)-H(8)	121.0
C(9)-C(8)-H(8)	121.0
C(10)-C(9)-C(8)	122.5(4)
C(10)-C(9)-N(3)	119.1(3)
C(8)-C(9)-N(3)	118.5(4)
C(9)-C(10)-C(11)	118.3(3)
C(9)-C(10)-H(10)	120.9
C(11)-C(10)-H(10)	120.9
C(6)-C(11)-C(10)	120.4(4)
C(6)-C(11)-H(11)	119.8
C(10)-C(11)-H(11)	119.8
C(13)-C(12)-C(3)	114.4(3)
C(13)-C(12)-H(12A)	108.7
C(3)-C(12)-H(12A)	108.7
C(13)-C(12)-H(12B)	108.7
C(3)-C(12)-H(12B)	108.7
H(12A)-C(12)-H(12B)	107.6
C(14)-C(13)-C(18)	118.2(4)
C(14)-C(13)-C(12)	119.7(4)
C(18)-C(13)-C(12)	122.0(4)
C(13)-C(14)-C(15)	121.4(4)
C(13)-C(14)-H(14)	119.3
C(15)-C(14)-H(14)	119.3
C(16)-C(15)-C(14)	119.8(4)
C(16)-C(15)-H(15)	120.1
C(14)-C(15)-H(15)	120.1
C(17)-C(16)-C(15)	119.5(5)
C(17)-C(16)-H(16)	120.3
C(15)-C(16)-H(16)	120.3
C(16)-C(17)-C(18)	120.7(4)
C(16)-C(17)-H(17)	119.6

---

C(18)-C(17)-H(17)	119.6
C(17)-C(18)-C(13)	120.4(4)
C(17)-C(18)-H(18)	119.8
C(13)-C(18)-H(18)	119.8
N(1)-C(19)-C(20)	128.0(3)
N(1)-C(19)-H(19)	116.0
C(20)-C(19)-H(19)	116.0
C(21)-C(20)-C(19)	116.3(3)
C(21)-C(20)-H(20)	121.9
C(19)-C(20)-H(20)	121.9
C(20)-C(21)-C(22)	129.1(4)
C(20)-C(21)-H(21)	115.4
C(22)-C(21)-H(21)	115.4
C(23)-C(22)-C(27)	119.0(4)
C(23)-C(22)-C(21)	117.6(4)
C(27)-C(22)-C(21)	123.4(4)
C(24)-C(23)-C(22)	121.1(4)
C(24)-C(23)-H(23)	119.5
C(22)-C(23)-H(23)	119.5
C(25)-C(24)-C(23)	118.9(4)
C(25)-C(24)-H(24)	120.5
C(23)-C(24)-H(24)	120.5
C(24)-C(25)-C(26)	121.1(4)
C(24)-C(25)-I(1)	118.8(3)
C(26)-C(25)-I(1)	120.2(3)
C(27)-C(26)-C(25)	119.8(4)
C(27)-C(26)-H(26)	120.1
C(25)-C(26)-H(26)	120.1
C(26)-C(27)-C(22)	120.1(4)
C(26)-C(27)-H(27)	120.0
C(22)-C(27)-H(27)	120.0
N(5)-C(28)-C(31)	111.4(3)
N(5)-C(28)-N(4)	100.4(3)
C(31)-C(28)-N(4)	110.3(3)
N(5)-C(28)-C(33)	110.7(3)
C(31)-C(28)-C(33)	114.6(3)

---

N(4)-C(28)-C(33)	108.4(3)
O(4)-C(29)-N(5)	126.4(4)
O(4)-C(29)-C(30)	124.9(4)
N(5)-C(29)-C(30)	108.7(3)
N(4)-C(30)-C(29)	103.1(3)
N(4)-C(30)-C(39)	115.8(3)
C(29)-C(30)-C(39)	110.9(3)
N(4)-C(30)-H(30)	108.9
C(29)-C(30)-H(30)	108.9
C(39)-C(30)-H(30)	108.9
C(28)-C(31)-H(31A)	109.5
C(28)-C(31)-H(31B)	109.5
H(31A)-C(31)-H(31B)	109.5
C(28)-C(31)-H(31C)	109.5
H(31A)-C(31)-H(31C)	109.5
H(31B)-C(31)-H(31C)	109.5
N(5)-C(32)-H(32A)	109.5
N(5)-C(32)-H(32B)	109.5
H(32A)-C(32)-H(32B)	109.5
N(5)-C(32)-H(32C)	109.5
H(32A)-C(32)-H(32C)	109.5
H(32B)-C(32)-H(32C)	109.5
C(34)-C(33)-C(38)	119.5(4)
C(34)-C(33)-C(28)	118.5(3)
C(38)-C(33)-C(28)	122.0(4)
C(33)-C(34)-C(35)	120.3(4)
C(33)-C(34)-H(34)	119.9
C(35)-C(34)-H(34)	119.9
C(36)-C(35)-C(34)	118.6(4)
C(36)-C(35)-H(35)	120.7
C(34)-C(35)-H(35)	120.7
C(35)-C(36)-C(37)	122.7(4)
C(35)-C(36)-N(6)	118.2(4)
C(37)-C(36)-N(6)	119.1(4)
C(36)-C(37)-C(38)	118.8(4)
C(36)-C(37)-H(37)	120.6



C(38)-C(37)-H(37)	120.6
C(37)-C(38)-C(33)	120.2(4)
C(37)-C(38)-H(38)	119.9
C(33)-C(38)-H(38)	119.9
C(40)-C(39)-C(30)	114.7(3)
C(40)-C(39)-H(39A)	108.6
C(30)-C(39)-H(39A)	108.6
C(40)-C(39)-H(39B)	108.6
C(30)-C(39)-H(39B)	108.6
H(39A)-C(39)-H(39B)	107.6
C(41)-C(40)-C(45)	117.8(4)
C(41)-C(40)-C(39)	120.2(4)
C(45)-C(40)-C(39)	121.9(4)
C(40)-C(41)-C(42)	121.4(4)
C(40)-C(41)-H(41)	119.3
C(42)-C(41)-H(41)	119.3
C(43)-C(42)-C(41)	120.4(5)
C(43)-C(42)-H(42)	119.8
C(41)-C(42)-H(42)	119.8
C(42)-C(43)-C(44)	119.2(5)
C(42)-C(43)-H(43)	120.4
C(44)-C(43)-H(43)	120.4
C(45)-C(44)-C(43)	120.0(4)
C(45)-C(44)-H(44)	120.0
C(43)-C(44)-H(44)	120.0
C(44)-C(45)-C(40)	121.2(4)
C(44)-C(45)-H(45)	119.4
C(40)-C(45)-H(45)	119.4
N(4)-C(46)-C(47)	128.4(4)
N(4)-C(46)-H(46)	115.8
C(47)-C(46)-H(46)	115.8
C(48)-C(47)-C(46)	116.8(4)
C(48)-C(47)-H(47)	121.6
C(46)-C(47)-H(47)	121.6
C(47)-C(48)-C(49)	129.9(4)
C(47)-C(48)-H(48)	115.0

C(49)-C(48)-H(48)	115.0
C(50)-C(49)-C(54)	119.7(4)
C(50)-C(49)-C(48)	123.1(4)
C(54)-C(49)-C(48)	117.2(4)
C(51)-C(50)-C(49)	119.3(4)
C(51)-C(50)-H(50)	120.4
C(49)-C(50)-H(50)	120.4
C(50)-C(51)-C(52)	120.2(4)
C(50)-C(51)-H(51)	119.9
C(52)-C(51)-H(51)	119.9
C(53)-C(52)-C(51)	121.1(4)
C(53)-C(52)-I(2)	118.9(3)
C(51)-C(52)-I(2)	120.0(3)
C(52)-C(53)-C(54)	119.1(4)
C(52)-C(53)-H(53)	120.5
C(54)-C(53)-H(53)	120.5
C(53)-C(54)-C(49)	120.6(4)
C(53)-C(54)-H(54)	119.7
C(49)-C(54)-H(54)	119.7
C(56)-C(55)-H(55A)	109.5
C(56)-C(55)-H(55B)	109.5
H(55A)-C(55)-H(55B)	109.5
C(56)-C(55)-H(55C)	109.5
H(55A)-C(55)-H(55C)	109.5
H(55B)-C(55)-H(55C)	109.5
O(7)-C(56)-C(55)	109.4(4)
O(7)-C(56)-H(56A)	109.8
C(55)-C(56)-H(56A)	109.8
O(7)-C(56)-H(56B)	109.8
C(55)-C(56)-H(56B)	109.8
H(56A)-C(56)-H(56B)	108.2
O(7)-C(57)-C(58)	109.6(4)
O(7)-C(57)-H(57A)	109.7
C(58)-C(57)-H(57A)	109.7
O(7)-C(57)-H(57B)	109.7
C(58)-C(57)-H(57B)	109.7

H(57A)-C(57)-H(57B)	108.2
C(57)-C(58)-H(58A)	109.5
C(57)-C(58)-H(58B)	109.5
H(58A)-C(58)-H(58B)	109.5
C(57)-C(58)-H(58C)	109.5
H(58A)-C(58)-H(58C)	109.5
H(58B)-C(58)-H(58C)	109.5

Table 11.9. Anisotropic displacement parameters ( $\text{\AA}^2 \times 10^3$ ) for *tomp\_jhr592*. The anisotropic displacement factor exponent takes the form:  $-2\pi^2 [ h^2 a^{*2} U^{11} + \dots + 2 h k a^* b^* U^{12} ]$

	$U^{11}$	$U^{22}$	$U^{33}$	$U^{23}$	$U^{13}$	$U^{12}$
I(1)	48(1)	54(1)	38(1)	-15(1)	9(1)	-24(1)
I(2)	63(1)	63(1)	49(1)	18(1)	-27(1)	-35(1)
P(1)	28(1)	27(1)	42(1)	0(1)	-4(1)	2(1)
P(2)	44(1)	35(1)	38(1)	-4(1)	-3(1)	2(1)
F(1)	40(1)	28(1)	56(2)	2(1)	-3(1)	-3(1)
F(2)	30(1)	40(2)	96(2)	9(2)	3(1)	4(1)
F(3)	39(1)	32(1)	69(2)	-1(1)	-6(1)	-5(1)
F(4)	28(1)	37(1)	72(2)	-6(1)	-4(1)	2(1)
F(5)	68(2)	59(2)	48(2)	-2(1)	-18(1)	-10(1)
F(6)	79(2)	35(1)	42(1)	-2(1)	-7(1)	2(1)
F(7)	134(3)	51(2)	57(2)	-10(2)	37(2)	-27(2)
F(8)	70(2)	44(2)	67(2)	-6(1)	-10(2)	12(1)
F(9)	50(2)	102(3)	135(3)	-71(3)	9(2)	-21(2)
F(10)	53(2)	75(2)	91(2)	-38(2)	-11(2)	0(2)
F(11)	94(2)	52(2)	52(2)	-7(1)	9(2)	-9(2)
F(12)	97(2)	40(2)	61(2)	-1(1)	5(2)	13(2)
O(1)	29(1)	29(2)	53(2)	-11(1)	-7(1)	6(1)
O(2)	29(2)	56(2)	74(2)	-7(2)	-18(2)	-3(2)
O(3)	47(2)	53(2)	115(3)	-23(2)	-23(2)	-15(2)
O(4)	30(2)	32(2)	56(2)	6(1)	-2(1)	1(1)
O(5)	42(2)	50(2)	131(4)	3(2)	15(2)	-14(2)
O(6)	28(2)	62(2)	62(2)	-8(2)	7(1)	-4(2)
O(7)	41(2)	37(2)	44(2)	-4(1)	-9(1)	-4(1)

N(1)	21(1)	23(2)	32(2)	0(1)	-3(1)	-2(1)
N(2)	23(2)	31(2)	40(2)	-8(1)	-1(1)	1(1)
N(3)	31(2)	53(2)	43(2)	-7(2)	-3(2)	-13(2)
N(4)	25(2)	23(2)	34(2)	-1(1)	-3(1)	-2(1)
N(5)	26(2)	30(2)	40(2)	5(1)	-6(1)	0(1)
N(6)	29(2)	53(2)	48(2)	3(2)	-2(2)	-10(2)
C(1)	23(2)	23(2)	29(2)	-4(1)	-1(1)	0(1)
C(2)	24(2)	26(2)	43(2)	-4(2)	-4(2)	-4(2)
C(3)	21(2)	24(2)	42(2)	-2(2)	-8(2)	1(1)
C(4)	26(2)	29(2)	40(2)	0(2)	-2(2)	-7(2)
C(5)	32(2)	44(2)	44(2)	-13(2)	4(2)	-2(2)
C(6)	28(2)	30(2)	29(2)	-4(2)	-2(2)	-6(2)
C(7)	27(2)	28(2)	37(2)	0(2)	-3(2)	-1(2)
C(8)	31(2)	33(2)	43(2)	-5(2)	-4(2)	-7(2)
C(9)	24(2)	39(2)	34(2)	-6(2)	-4(2)	-6(2)
C(10)	27(2)	34(2)	36(2)	-3(2)	-1(2)	-1(2)
C(11)	25(2)	29(2)	35(2)	-2(2)	-2(2)	-4(2)
C(12)	26(2)	30(2)	41(2)	-1(2)	-7(2)	-2(2)
C(13)	21(2)	34(2)	37(2)	-3(2)	-8(2)	0(2)
C(14)	26(2)	39(2)	44(2)	-6(2)	-3(2)	-4(2)
C(15)	39(2)	37(2)	65(3)	-8(2)	-16(2)	-4(2)
C(16)	43(3)	44(3)	71(3)	5(2)	-19(2)	-21(2)
C(17)	43(3)	70(3)	39(2)	6(2)	-10(2)	-27(2)
C(18)	29(2)	46(2)	38(2)	-8(2)	-6(2)	-11(2)
C(19)	19(2)	25(2)	32(2)	-3(2)	-2(1)	6(1)
C(20)	26(2)	25(2)	31(2)	-1(2)	-4(2)	-2(1)
C(21)	28(2)	30(2)	38(2)	-1(2)	-5(2)	-4(2)
C(22)	27(2)	30(2)	39(2)	-4(2)	-2(2)	-3(2)
C(23)	35(2)	37(2)	40(2)	1(2)	-1(2)	-4(2)
C(24)	38(2)	34(2)	46(2)	-8(2)	6(2)	-3(2)
C(25)	38(2)	49(2)	29(2)	-16(2)	6(2)	-22(2)
C(26)	31(2)	42(2)	39(2)	-1(2)	-5(2)	-9(2)
C(27)	25(2)	39(2)	37(2)	-5(2)	-3(2)	-5(2)
C(28)	25(2)	28(2)	32(2)	-1(2)	-3(2)	-2(2)
C(29)	21(2)	27(2)	51(2)	2(2)	-2(2)	-2(2)
C(30)	26(2)	27(2)	40(2)	-5(2)	-1(2)	0(2)

C(31)	33(2)	29(2)	39(2)	-3(2)	-5(2)	-6(2)
C(32)	35(2)	45(3)	40(2)	7(2)	-10(2)	-4(2)
C(33)	24(2)	29(2)	29(2)	2(2)	-7(2)	1(2)
C(34)	29(2)	28(2)	35(2)	-1(2)	-8(2)	0(2)
C(35)	38(2)	36(2)	36(2)	1(2)	-4(2)	-14(2)
C(36)	26(2)	44(2)	36(2)	5(2)	-9(2)	-4(2)
C(37)	29(2)	32(2)	30(2)	-4(2)	-2(2)	5(2)
C(38)	30(2)	27(2)	38(2)	0(2)	-7(2)	-2(2)
C(39)	28(2)	35(2)	40(2)	-3(2)	-4(2)	-2(2)
C(40)	25(2)	35(2)	34(2)	-1(2)	-2(2)	-3(2)
C(41)	41(2)	41(2)	43(2)	6(2)	-11(2)	-11(2)
C(42)	61(3)	42(3)	62(3)	9(2)	-11(3)	-18(2)
C(43)	62(3)	58(3)	48(3)	-9(2)	-4(2)	-30(3)
C(44)	43(3)	80(4)	37(2)	0(2)	-11(2)	-26(2)
C(45)	39(2)	48(3)	38(2)	9(2)	-4(2)	-11(2)
C(46)	29(2)	25(2)	42(2)	-5(2)	-3(2)	0(2)
C(47)	28(2)	29(2)	39(2)	1(2)	-1(2)	-3(2)
C(48)	37(2)	28(2)	40(2)	-4(2)	-5(2)	-6(2)
C(49)	32(2)	34(2)	43(2)	-4(2)	-8(2)	-7(2)
C(50)	28(2)	41(2)	44(2)	4(2)	-6(2)	-5(2)
C(51)	36(2)	52(3)	41(2)	-3(2)	-5(2)	-16(2)
C(52)	43(2)	46(2)	36(2)	10(2)	-16(2)	-21(2)
C(53)	41(2)	45(3)	49(3)	2(2)	-15(2)	-2(2)
C(54)	42(2)	35(2)	46(2)	-5(2)	-8(2)	1(2)
C(55)	43(3)	47(3)	52(3)	1(2)	1(2)	-3(2)
C(56)	49(3)	33(2)	48(3)	-5(2)	0(2)	-5(2)
C(57)	55(3)	51(3)	66(3)	-9(2)	-19(3)	-15(2)
C(58)	51(3)	59(3)	87(4)	4(3)	-28(3)	-10(3)

Table 11.10. Hydrogen coordinates ( $\times 10^4$ ) and isotropic displacement parameters ( $\text{\AA}^2 \times 10^3$ ) for temp\_jhr592.

	x	y	z	U(eq)
H(3)	10789	6656	2054	36

---

H(4A)	10154	4502	3334	48
H(4B)	11001	4394	4025	48
H(4C)	11722	4035	3289	48
H(5A)	9274	5713	4404	62
H(5B)	8999	6708	4266	62
H(5C)	10415	6153	4531	62
H(7)	12012	6692	3608	38
H(8)	13958	6868	4019	43
H(10)	15556	4324	4116	41
H(11)	13554	4163	3723	36
H(12A)	8605	6532	1716	40
H(12B)	9884	6033	1248	40
H(14)	10173	4627	1068	45
H(15)	9592	3370	1280	57
H(16)	8099	3236	2231	61
H(17)	7200	4362	2959	58
H(18)	7762	5622	2743	44
H(19)	12957	4548	2372	33
H(20)	12081	5511	1096	34
H(21)	14022	4003	1424	39
H(23)	15471	3217	574	47
H(24)	16218	2909	-597	49
H(26)	13411	4990	-1284	45
H(27)	12653	5293	-116	41
H(30)	9115	8541	2020	39
H(31A)	9524	10527	3280	51
H(31B)	8636	10542	4007	51
H(31C)	7958	11000	3300	51
H(32A)	10230	9167	4378	62
H(32B)	10452	8192	4242	62
H(32C)	9015	8755	4520	62
H(34)	7497	8342	3468	38
H(35)	5445	8145	3915	43
H(37)	4091	10611	4312	40
H(38)	6138	10813	3883	39
H(39A)	11301	8685	1666	42

---

H(39B)	10135	9362	1270	42
H(41)	9915	10806	1337	50
H(42)	10763	11886	1639	65
H(43)	12434	11626	2443	64
H(44)	13217	10270	2973	61
H(45)	12362	9195	2671	51
H(46)	6836	10574	2395	40
H(47)	7917	9781	1099	40
H(48)	5683	11097	1491	43
H(50)	7291	10043	-89	47
H(51)	6440	10372	-1216	50
H(53)	3200	12091	-399	56
H(54)	4035	11773	730	52
H(55A)	12662	2152	5010	74
H(55B)	12581	3010	4553	74
H(55C)	13641	2153	4320	74
H(56A)	11836	2451	3590	54
H(56B)	11872	1610	4068	54
H(57A)	9561	1876	3924	67
H(57B)	9484	2748	3487	67
H(58A)	7974	3472	4385	99
H(58B)	8018	2589	4793	99
H(58C)	7384	2808	4033	99

**(*S,E*)-5-Benzyl-1-((*E*)-3-(4-chlorophenyl)allylidene)-2,2,3-trimethyl-4-oxoimidazolidin-1-ium hexafluorophosphate 92·PF<sub>6</sub>**

Table 11.11. Crystal data and structure refinement for jr583smart.

Identification code	jr583smart	
Empirical formula	C <sub>24</sub> H <sub>27</sub> Cl F <sub>6</sub> N <sub>3</sub> O <sub>3</sub> P	
Formula weight	553.91	
Temperature	123(2) K	
Wavelength	0.71073 Å	
Crystal system	Triclinic	
Space group	P1	
Unit cell dimensions	a = 9.1358(3) Å	α = 68.439(3)°.
	b = 11.4186(4) Å	β = 84.941(3)°.
	c = 13.3963(5) Å	γ = 85.534(3)°.
Volume	1293.07(8) Å <sup>3</sup>	
Z	2	
Density (calculated)	1.423 Mg/m <sup>3</sup>	
Absorption coefficient	0.275 mm <sup>-1</sup>	
F(000)	572	
Crystal size	0.4 x 0.3 x 0.25 mm <sup>3</sup>	
Theta range for data collection	3.02 to 30.47°.	
Index ranges	-12 ≤ h ≤ 12, -15 ≤ k ≤ 15, -18 ≤ l ≤ 19	
Reflections collected	19974	
Independent reflections	13213 [R(int) = 0.0203]	
Completeness to theta = 27.00°	99.8%	
Absorption correction	Semi-empirical from equivalents	
Max. and min. transmission	1.00000 and 0.96718	
Refinement method	Full-matrix least-squares on F <sup>2</sup>	
Data / restraints / parameters	13213 / 3 / 658	
Goodness-of-fit on F <sup>2</sup>	1.025	
Final R indices [I > 2σ(I)]	R1 = 0.0406, wR2 = 0.0829	
R indices (all data)	R1 = 0.0519, wR2 = 0.0895	
Absolute structure parameter	0.02(4)	
Largest diff. peak and hole	0.284 and -0.289 e.Å <sup>-3</sup>	

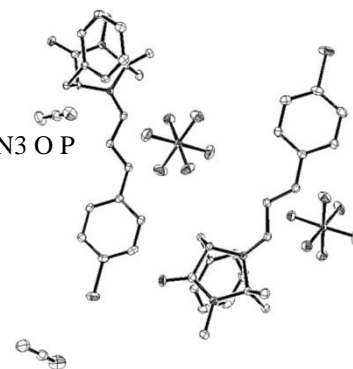




Table 11.12. Atomic coordinates ( $\times 10^4$ ) and equivalent isotropic displacement parameters ( $\text{\AA}^2 \times 10^3$ ) for jr583smart.  $U(\text{eq})$  is defined as one third of the trace of the orthogonalized  $U^{\text{ij}}$  tensor.

	x	y	z	U(eq)
Cl(1)	10908(1)	-3532(1)	10706(1)	51(1)
Cl(2)	17403(1)	8711(1)	9173(1)	45(1)
P(1)	14335(1)	2612(1)	8255(1)	27(1)
P(2)	13942(1)	-306(1)	14470(1)	27(1)
F(1)	14612(2)	3886(2)	8414(2)	56(1)
F(2)	15960(2)	2093(2)	8614(1)	48(1)
F(3)	13735(2)	2030(2)	9483(1)	50(1)
F(4)	12724(2)	3131(2)	7895(1)	42(1)
F(5)	14976(2)	3180(2)	7029(1)	50(1)
F(6)	14063(2)	1324(2)	8110(1)	53(1)
F(7)	14582(2)	-1575(2)	15338(1)	54(1)
F(8)	14111(2)	440(1)	15259(1)	40(1)
F(9)	15551(1)	57(1)	13938(1)	38(1)
F(10)	13755(2)	-1055(2)	13691(1)	46(1)
F(11)	12311(2)	-659(2)	15013(1)	46(1)
F(12)	13253(2)	946(1)	13604(1)	36(1)
O(2)	8368(2)	7733(2)	3887(1)	30(1)
O(1)	19848(2)	3966(2)	9566(1)	30(1)
N(1)	18398(2)	1174(2)	11420(1)	20(1)
N(4)	7800(2)	6184(2)	5510(1)	22(1)
N(2)	20337(2)	2403(2)	11178(1)	23(1)
N(3)	9807(2)	6155(2)	6410(1)	20(1)
N(6)	19874(3)	10680(3)	9225(3)	66(1)
N(5)	8587(3)	9177(3)	6205(2)	61(1)
C(1)	19776(2)	1221(2)	11948(2)	21(1)
C(2)	19551(2)	2985(2)	10317(2)	23(1)
C(3)	18167(2)	2280(2)	10430(2)	21(1)
C(4)	20813(2)	109(2)	11966(2)	30(1)
C(5)	19396(2)	1270(2)	13061(2)	24(1)
C(6)	21724(2)	2869(2)	11310(2)	32(1)
C(7)	16785(2)	3110(2)	10496(2)	22(1)

---

C(8)	16654(2)	3518(2)	11449(2)	21(1)
C(9)	15645(2)	2964(2)	12303(2)	30(1)
C(10)	15521(3)	3287(3)	13202(2)	43(1)
C(11)	16414(3)	4199(3)	13256(2)	48(1)
C(12)	17407(3)	4770(2)	12409(2)	37(1)
C(13)	17546(2)	4434(2)	11511(2)	26(1)
C(14)	17608(2)	191(2)	11801(2)	21(1)
C(15)	16398(2)	-68(2)	11328(2)	23(1)
C(16)	15779(2)	-1180(2)	11863(2)	23(1)
C(17)	14591(2)	-1720(2)	11551(2)	21(1)
C(18)	13835(2)	-1084(2)	10629(2)	26(1)
C(19)	12701(2)	-1639(2)	10371(2)	31(1)
C(20)	12335(2)	-2840(2)	11033(2)	31(1)
C(21)	13083(3)	-3506(2)	11947(2)	34(1)
C(22)	14187(3)	-2934(2)	12207(2)	28(1)
C(23)	8374(2)	5528(2)	6574(2)	21(1)
C(24)	8640(2)	7064(2)	4811(2)	22(1)
C(25)	10061(2)	7090(2)	5310(2)	22(1)
C(26)	7407(3)	5816(2)	7444(2)	30(1)
C(27)	8661(2)	4116(2)	6821(2)	26(1)
C(28)	6342(2)	5946(2)	5291(2)	32(1)
C(29)	11414(2)	6760(2)	4687(2)	22(1)
C(30)	11460(2)	5444(2)	4668(2)	20(1)
C(31)	10556(2)	5124(2)	4026(2)	24(1)
C(32)	10603(2)	3909(2)	4035(2)	28(1)
C(33)	11555(3)	2989(2)	4670(2)	31(1)
C(34)	12460(2)	3297(2)	5303(2)	30(1)
C(35)	12409(2)	4518(2)	5305(2)	24(1)
C(36)	10634(2)	5923(2)	7212(2)	22(1)
C(37)	11863(2)	6597(2)	7222(2)	24(1)
C(38)	12554(2)	6212(2)	8148(2)	24(1)
C(39)	13738(2)	6839(2)	8381(2)	22(1)
C(40)	14510(2)	6214(2)	9301(2)	26(1)
C(41)	15643(2)	6781(2)	9542(2)	30(1)
C(42)	15991(2)	7987(2)	8870(2)	29(1)
C(43)	15224(2)	8641(2)	7969(2)	29(1)

---

C(44)	14106(2)	8061(2)	7724(2)	25(1)
C(48)	21007(4)	10556(4)	7446(3)	63(1)
C(47)	20361(3)	10640(3)	8431(2)	41(1)
C(46)	7270(4)	11364(3)	5802(3)	64(1)
C(45)	8010(3)	10134(3)	6020(2)	41(1)

Table 11.13. Bond lengths [Å] and angles [°] for jr583smart.

Cl(1)-C(20)	1.741(2)
Cl(2)-C(42)	1.737(2)
P(1)-F(1)	1.5866(16)
P(1)-F(4)	1.5901(15)
P(1)-F(6)	1.5929(16)
P(1)-F(3)	1.5951(16)
P(1)-F(2)	1.6019(15)
P(1)-F(5)	1.6025(16)
P(2)-F(9)	1.5914(15)
P(2)-F(7)	1.5951(16)
P(2)-F(12)	1.5981(14)
P(2)-F(10)	1.5998(15)
P(2)-F(8)	1.6056(15)
P(2)-F(11)	1.6129(15)
O(2)-C(24)	1.228(2)
O(1)-C(2)	1.229(2)
N(1)-C(14)	1.296(3)
N(1)-C(3)	1.475(2)
N(1)-C(1)	1.511(2)
N(4)-C(24)	1.334(3)
N(4)-C(28)	1.456(3)
N(4)-C(23)	1.467(3)
N(2)-C(2)	1.340(3)
N(2)-C(6)	1.461(3)
N(2)-C(1)	1.462(3)
N(3)-C(36)	1.303(3)
N(3)-C(25)	1.479(2)
N(3)-C(23)	1.501(2)
N(6)-C(47)	1.132(4)

---

N(5)-C(45)	1.126(4)
C(1)-C(4)	1.518(3)
C(1)-C(5)	1.522(3)
C(2)-C(3)	1.518(3)
C(3)-C(7)	1.535(3)
C(3)-H(3)	1.0000
C(4)-H(4A)	0.9800
C(4)-H(4B)	0.9800
C(4)-H(4C)	0.9800
C(5)-H(5A)	0.9800
C(5)-H(5B)	0.9800
C(5)-H(5C)	0.9800
C(6)-H(6A)	0.9800
C(6)-H(6B)	0.9800
C(6)-H(6C)	0.9800
C(7)-C(8)	1.504(3)
C(7)-H(7A)	0.9900
C(7)-H(7B)	0.9900
C(8)-C(9)	1.390(3)
C(8)-C(13)	1.405(3)
C(9)-C(10)	1.378(4)
C(9)-H(9)	0.9500
C(10)-C(11)	1.397(4)
C(10)-H(10)	0.9500
C(11)-C(12)	1.379(4)
C(11)-H(11)	0.9500
C(12)-C(13)	1.384(3)
C(12)-H(12)	0.9500
C(13)-H(13)	0.9500
C(14)-C(15)	1.423(3)
C(14)-H(14)	0.9500
C(15)-C(16)	1.348(3)
C(15)-H(15)	0.9500
C(16)-C(17)	1.451(3)
C(16)-H(16)	0.9500
C(17)-C(18)	1.394(3)

---

C(17)-C(22)	1.399(3)
C(18)-C(19)	1.386(3)
C(18)-H(18)	0.9500
C(19)-C(20)	1.380(3)
C(19)-H(19)	0.9500
C(20)-C(21)	1.388(4)
C(21)-C(22)	1.377(3)
C(21)-H(21)	0.9500
C(22)-H(22)	0.9500
C(23)-C(26)	1.518(3)
C(23)-C(27)	1.529(3)
C(24)-C(25)	1.519(3)
C(25)-C(29)	1.531(3)
C(25)-H(25)	1.0000
C(26)-H(26A)	0.9800
C(26)-H(26B)	0.9800
C(26)-H(26C)	0.9800
C(27)-H(27A)	0.9800
C(27)-H(27B)	0.9800
C(27)-H(27C)	0.9800
C(28)-H(28A)	0.9800
C(28)-H(28B)	0.9800
C(28)-H(28C)	0.9800
C(29)-C(30)	1.510(3)
C(29)-H(29A)	0.9900
C(29)-H(29B)	0.9900
C(30)-C(35)	1.386(3)
C(30)-C(31)	1.400(3)
C(31)-C(32)	1.380(3)
C(31)-H(31)	0.9500
C(32)-C(33)	1.384(3)
C(32)-H(32)	0.9500
C(33)-C(34)	1.383(3)
C(33)-H(33)	0.9500
C(34)-C(35)	1.393(3)
C(34)-H(34)	0.9500

C(35)-H(35)	0.9500
C(36)-C(37)	1.415(3)
C(36)-H(36)	0.9500
C(37)-C(38)	1.351(3)
C(37)-H(37)	0.9500
C(38)-C(39)	1.457(3)
C(38)-H(38)	0.9500
C(39)-C(44)	1.398(3)
C(39)-C(40)	1.398(3)
C(40)-C(41)	1.383(3)
C(40)-H(40)	0.9500
C(41)-C(42)	1.384(3)
C(41)-H(41)	0.9500
C(42)-C(43)	1.383(3)
C(43)-C(44)	1.383(3)
C(43)-H(43)	0.9500
C(44)-H(44)	0.9500
C(48)-C(47)	1.431(5)
C(48)-H(48A)	0.9800
C(48)-H(48B)	0.9800
C(48)-H(48C)	0.9800
C(46)-C(45)	1.450(5)
C(46)-H(46A)	0.9800
C(46)-H(46B)	0.9800
C(46)-H(46C)	0.9800
F(1)-P(1)-F(4)	90.42(9)
F(1)-P(1)-F(6)	179.30(10)
F(4)-P(1)-F(6)	90.01(9)
F(1)-P(1)-F(3)	89.49(10)
F(4)-P(1)-F(3)	90.99(9)
F(6)-P(1)-F(3)	89.94(9)
F(1)-P(1)-F(2)	89.52(9)
F(4)-P(1)-F(2)	179.83(12)
F(6)-P(1)-F(2)	90.05(9)
F(3)-P(1)-F(2)	89.17(9)

F(1)-P(1)-F(5)	90.71(10)
F(4)-P(1)-F(5)	90.38(8)
F(6)-P(1)-F(5)	89.84(10)
F(3)-P(1)-F(5)	178.61(10)
F(2)-P(1)-F(5)	89.46(9)
F(9)-P(2)-F(7)	91.03(9)
F(9)-P(2)-F(12)	90.60(8)
F(7)-P(2)-F(12)	178.19(10)
F(9)-P(2)-F(10)	90.56(8)
F(7)-P(2)-F(10)	89.42(9)
F(12)-P(2)-F(10)	89.78(9)
F(9)-P(2)-F(8)	90.15(8)
F(7)-P(2)-F(8)	90.51(9)
F(12)-P(2)-F(8)	90.27(8)
F(10)-P(2)-F(8)	179.29(9)
F(9)-P(2)-F(11)	179.32(10)
F(7)-P(2)-F(11)	89.23(9)
F(12)-P(2)-F(11)	89.15(8)
F(10)-P(2)-F(11)	90.08(8)
F(8)-P(2)-F(11)	89.21(9)
C(14)-N(1)-C(3)	126.43(17)
C(14)-N(1)-C(1)	120.39(16)
C(3)-N(1)-C(1)	112.99(15)
C(24)-N(4)-C(28)	123.25(17)
C(24)-N(4)-C(23)	115.82(16)
C(28)-N(4)-C(23)	120.71(17)
C(2)-N(2)-C(6)	122.26(18)
C(2)-N(2)-C(1)	116.02(17)
C(6)-N(2)-C(1)	121.59(16)
C(36)-N(3)-C(25)	126.43(17)
C(36)-N(3)-C(23)	120.42(17)
C(25)-N(3)-C(23)	112.96(15)
N(2)-C(1)-N(1)	99.66(14)
N(2)-C(1)-C(4)	111.02(17)
N(1)-C(1)-C(4)	109.22(17)
N(2)-C(1)-C(5)	112.67(17)

---

N(1)-C(1)-C(5)	110.68(16)
C(4)-C(1)-C(5)	112.80(17)
O(1)-C(2)-N(2)	126.4(2)
O(1)-C(2)-C(3)	124.22(18)
N(2)-C(2)-C(3)	109.32(17)
N(1)-C(3)-C(2)	101.74(15)
N(1)-C(3)-C(7)	114.25(16)
C(2)-C(3)-C(7)	110.93(17)
N(1)-C(3)-H(3)	109.9
C(2)-C(3)-H(3)	109.9
C(7)-C(3)-H(3)	109.9
C(1)-C(4)-H(4A)	109.5
C(1)-C(4)-H(4B)	109.5
H(4A)-C(4)-H(4B)	109.5
C(1)-C(4)-H(4C)	109.5
H(4A)-C(4)-H(4C)	109.5
H(4B)-C(4)-H(4C)	109.5
C(1)-C(5)-H(5A)	109.5
C(1)-C(5)-H(5B)	109.5
H(5A)-C(5)-H(5B)	109.5
C(1)-C(5)-H(5C)	109.5
H(5A)-C(5)-H(5C)	109.5
H(5B)-C(5)-H(5C)	109.5
N(2)-C(6)-H(6A)	109.5
N(2)-C(6)-H(6B)	109.5
H(6A)-C(6)-H(6B)	109.5
N(2)-C(6)-H(6C)	109.5
H(6A)-C(6)-H(6C)	109.5
H(6B)-C(6)-H(6C)	109.5
C(8)-C(7)-C(3)	114.76(16)
C(8)-C(7)-H(7A)	108.6
C(3)-C(7)-H(7A)	108.6
C(8)-C(7)-H(7B)	108.6
C(3)-C(7)-H(7B)	108.6
H(7A)-C(7)-H(7B)	107.6
C(9)-C(8)-C(13)	118.6(2)



---

C(9)-C(8)-C(7)	119.55(19)
C(13)-C(8)-C(7)	121.79(18)
C(10)-C(9)-C(8)	121.3(2)
C(10)-C(9)-H(9)	119.4
C(8)-C(9)-H(9)	119.4
C(9)-C(10)-C(11)	119.6(2)
C(9)-C(10)-H(10)	120.2
C(11)-C(10)-H(10)	120.2
C(12)-C(11)-C(10)	119.9(2)
C(12)-C(11)-H(11)	120.1
C(10)-C(11)-H(11)	120.1
C(11)-C(12)-C(13)	120.6(2)
C(11)-C(12)-H(12)	119.7
C(13)-C(12)-H(12)	119.7
C(12)-C(13)-C(8)	120.0(2)
C(12)-C(13)-H(13)	120.0
C(8)-C(13)-H(13)	120.0
N(1)-C(14)-C(15)	127.26(19)
N(1)-C(14)-H(14)	116.4
C(15)-C(14)-H(14)	116.4
C(16)-C(15)-C(14)	116.28(19)
C(16)-C(15)-H(15)	121.9
C(14)-C(15)-H(15)	121.9
C(15)-C(16)-C(17)	128.5(2)
C(15)-C(16)-H(16)	115.8
C(17)-C(16)-H(16)	115.8
C(18)-C(17)-C(22)	118.6(2)
C(18)-C(17)-C(16)	122.98(19)
C(22)-C(17)-C(16)	118.44(19)
C(19)-C(18)-C(17)	120.7(2)
C(19)-C(18)-H(18)	119.7
C(17)-C(18)-H(18)	119.7
C(20)-C(19)-C(18)	119.2(2)
C(20)-C(19)-H(19)	120.4
C(18)-C(19)-H(19)	120.4
C(19)-C(20)-C(21)	121.4(2)

---

C(19)-C(20)-Cl(1)	118.98(19)
C(21)-C(20)-Cl(1)	119.6(2)
C(22)-C(21)-C(20)	118.8(2)
C(22)-C(21)-H(21)	120.6
C(20)-C(21)-H(21)	120.6
C(21)-C(22)-C(17)	121.2(2)
C(21)-C(22)-H(22)	119.4
C(17)-C(22)-H(22)	119.4
N(4)-C(23)-N(3)	99.92(15)
N(4)-C(23)-C(26)	111.37(17)
N(3)-C(23)-C(26)	109.53(17)
N(4)-C(23)-C(27)	112.19(18)
N(3)-C(23)-C(27)	109.97(16)
C(26)-C(23)-C(27)	113.07(17)
O(2)-C(24)-N(4)	126.8(2)
O(2)-C(24)-C(25)	123.66(19)
N(4)-C(24)-C(25)	109.53(16)
N(3)-C(25)-C(24)	101.63(15)
N(3)-C(25)-C(29)	113.66(17)
C(24)-C(25)-C(29)	112.14(17)
N(3)-C(25)-H(25)	109.7
C(24)-C(25)-H(25)	109.7
C(29)-C(25)-H(25)	109.7
C(23)-C(26)-H(26A)	109.5
C(23)-C(26)-H(26B)	109.5
H(26A)-C(26)-H(26B)	109.5
C(23)-C(26)-H(26C)	109.5
H(26A)-C(26)-H(26C)	109.5
H(26B)-C(26)-H(26C)	109.5
C(23)-C(27)-H(27A)	109.5
C(23)-C(27)-H(27B)	109.5
H(27A)-C(27)-H(27B)	109.5
C(23)-C(27)-H(27C)	109.5
H(27A)-C(27)-H(27C)	109.5
H(27B)-C(27)-H(27C)	109.5
N(4)-C(28)-H(28A)	109.5

N(4)-C(28)-H(28B)	109.5
H(28A)-C(28)-H(28B)	109.5
N(4)-C(28)-H(28C)	109.5
H(28A)-C(28)-H(28C)	109.5
H(28B)-C(28)-H(28C)	109.5
C(30)-C(29)-C(25)	114.35(16)
C(30)-C(29)-H(29A)	108.7
C(25)-C(29)-H(29A)	108.7
C(30)-C(29)-H(29B)	108.7
C(25)-C(29)-H(29B)	108.7
H(29A)-C(29)-H(29B)	107.6
C(35)-C(30)-C(31)	118.62(19)
C(35)-C(30)-C(29)	119.73(18)
C(31)-C(30)-C(29)	121.65(19)
C(32)-C(31)-C(30)	120.6(2)
C(32)-C(31)-H(31)	119.7
C(30)-C(31)-H(31)	119.7
C(31)-C(32)-C(33)	120.6(2)
C(31)-C(32)-H(32)	119.7
C(33)-C(32)-H(32)	119.7
C(34)-C(33)-C(32)	119.3(2)
C(34)-C(33)-H(33)	120.3
C(32)-C(33)-H(33)	120.3
C(33)-C(34)-C(35)	120.4(2)
C(33)-C(34)-H(34)	119.8
C(35)-C(34)-H(34)	119.8
C(30)-C(35)-C(34)	120.52(19)
C(30)-C(35)-H(35)	119.7
C(34)-C(35)-H(35)	119.7
N(3)-C(36)-C(37)	126.31(19)
N(3)-C(36)-H(36)	116.8
C(37)-C(36)-H(36)	116.8
C(38)-C(37)-C(36)	116.73(19)
C(38)-C(37)-H(37)	121.6
C(36)-C(37)-H(37)	121.6
C(37)-C(38)-C(39)	126.2(2)

---

C(37)-C(38)-H(38)	116.9
C(39)-C(38)-H(38)	116.9
C(44)-C(39)-C(40)	118.7(2)
C(44)-C(39)-C(38)	122.05(19)
C(40)-C(39)-C(38)	119.2(2)
C(41)-C(40)-C(39)	120.7(2)
C(41)-C(40)-H(40)	119.6
C(39)-C(40)-H(40)	119.6
C(40)-C(41)-C(42)	119.2(2)
C(40)-C(41)-H(41)	120.4
C(42)-C(41)-H(41)	120.4
C(43)-C(42)-C(41)	121.5(2)
C(43)-C(42)-Cl(2)	118.96(19)
C(41)-C(42)-Cl(2)	119.50(18)
C(42)-C(43)-C(44)	119.0(2)
C(42)-C(43)-H(43)	120.5
C(44)-C(43)-H(43)	120.5
C(43)-C(44)-C(39)	120.9(2)
C(43)-C(44)-H(44)	119.5
C(39)-C(44)-H(44)	119.5
C(47)-C(48)-H(48A)	109.5
C(47)-C(48)-H(48B)	109.5
H(48A)-C(48)-H(48B)	109.5
C(47)-C(48)-H(48C)	109.5
H(48A)-C(48)-H(48C)	109.5
H(48B)-C(48)-H(48C)	109.5
N(6)-C(47)-C(48)	178.2(3)
C(45)-C(46)-H(46A)	109.5
C(45)-C(46)-H(46B)	109.5
H(46A)-C(46)-H(46B)	109.5
C(45)-C(46)-H(46C)	109.5
H(46A)-C(46)-H(46C)	109.5
H(46B)-C(46)-H(46C)	109.5
N(5)-C(45)-C(46)	178.9(3)

Table 11.14. Anisotropic displacement parameters ( $\text{\AA}^2 \times 10^3$ ) for jr583smart. The anisotropic

displacement factor exponent takes the form:  $-2\pi^2[ h^2a^2U^{11} + \dots + 2 h k a^* b^* U^{12} ]$

	U <sup>11</sup>	U <sup>22</sup>	U <sup>33</sup>	U <sup>23</sup>	U <sup>13</sup>	U <sup>12</sup>
Cl(1)	33(1)	74(1)	62(1)	-39(1)	3(1)	-24(1)
Cl(2)	31(1)	69(1)	48(1)	-35(1)	-1(1)	-14(1)
P(1)	34(1)	21(1)	26(1)	-6(1)	-10(1)	-3(1)
P(2)	36(1)	22(1)	22(1)	-7(1)	3(1)	-5(1)
F(1)	64(1)	30(1)	82(1)	-24(1)	-27(1)	-3(1)
F(2)	45(1)	54(1)	46(1)	-17(1)	-25(1)	16(1)
F(3)	68(1)	48(1)	26(1)	-5(1)	0(1)	0(1)
F(4)	29(1)	49(1)	44(1)	-10(1)	-7(1)	-4(1)
F(5)	34(1)	71(1)	31(1)	0(1)	-5(1)	-7(1)
F(6)	72(1)	36(1)	63(1)	-29(1)	-12(1)	-7(1)
F(7)	87(1)	29(1)	34(1)	-3(1)	4(1)	16(1)
F(8)	56(1)	35(1)	37(1)	-20(1)	-9(1)	2(1)
F(9)	29(1)	41(1)	42(1)	-13(1)	-1(1)	-3(1)
F(10)	59(1)	49(1)	42(1)	-30(1)	15(1)	-22(1)
F(11)	50(1)	41(1)	47(1)	-17(1)	24(1)	-20(1)
F(12)	32(1)	36(1)	31(1)	-1(1)	-5(1)	-5(1)
O(2)	34(1)	27(1)	22(1)	-2(1)	-6(1)	2(1)
O(1)	30(1)	28(1)	23(1)	2(1)	3(1)	-5(1)
N(1)	22(1)	20(1)	16(1)	-6(1)	-3(1)	0(1)
N(4)	23(1)	22(1)	22(1)	-7(1)	-4(1)	-2(1)
N(2)	19(1)	24(1)	21(1)	-3(1)	0(1)	-5(1)
N(3)	23(1)	18(1)	18(1)	-5(1)	1(1)	-2(1)
N(6)	49(2)	80(2)	83(2)	-50(2)	-2(2)	14(1)
N(5)	56(2)	65(2)	74(2)	-43(2)	14(1)	-2(1)
C(1)	23(1)	20(1)	18(1)	-5(1)	-4(1)	-2(1)
C(2)	20(1)	28(1)	20(1)	-8(1)	2(1)	0(1)
C(3)	26(1)	21(1)	16(1)	-4(1)	-4(1)	-1(1)
C(4)	28(1)	28(1)	33(1)	-11(1)	-6(1)	3(1)
C(5)	31(1)	25(1)	18(1)	-7(1)	-4(1)	-3(1)
C(6)	25(1)	38(1)	30(1)	-5(1)	-3(1)	-11(1)
C(7)	21(1)	20(1)	21(1)	-3(1)	-5(1)	-3(1)
C(8)	19(1)	19(1)	21(1)	-3(1)	-7(1)	3(1)

C(9)	26(1)	29(1)	30(1)	-7(1)	0(1)	-2(1)
C(10)	47(2)	43(2)	32(1)	-10(1)	9(1)	4(1)
C(11)	63(2)	50(2)	34(1)	-24(1)	-11(1)	24(2)
C(12)	42(1)	30(1)	46(2)	-21(1)	-20(1)	8(1)
C(13)	23(1)	22(1)	32(1)	-8(1)	-8(1)	2(1)
C(14)	27(1)	17(1)	19(1)	-6(1)	-2(1)	1(1)
C(15)	27(1)	18(1)	21(1)	-7(1)	-3(1)	-1(1)
C(16)	26(1)	23(1)	20(1)	-8(1)	-1(1)	-1(1)
C(17)	21(1)	22(1)	23(1)	-11(1)	1(1)	-2(1)
C(18)	29(1)	19(1)	29(1)	-8(1)	-2(1)	3(1)
C(19)	24(1)	36(1)	35(1)	-18(1)	-5(1)	5(1)
C(20)	22(1)	44(1)	38(1)	-27(1)	7(1)	-8(1)
C(21)	39(1)	35(1)	29(1)	-14(1)	11(1)	-17(1)
C(22)	33(1)	30(1)	21(1)	-8(1)	2(1)	-8(1)
C(23)	20(1)	21(1)	19(1)	-5(1)	0(1)	-3(1)
C(24)	27(1)	18(1)	22(1)	-7(1)	-4(1)	4(1)
C(25)	27(1)	17(1)	18(1)	-4(1)	1(1)	-4(1)
C(26)	30(1)	31(1)	27(1)	-10(1)	7(1)	-4(1)
C(27)	28(1)	20(1)	29(1)	-6(1)	1(1)	-4(1)
C(28)	28(1)	30(1)	38(1)	-12(1)	-8(1)	-2(1)
C(29)	23(1)	24(1)	17(1)	-5(1)	0(1)	-6(1)
C(30)	20(1)	22(1)	16(1)	-7(1)	4(1)	-5(1)
C(31)	23(1)	29(1)	21(1)	-11(1)	-1(1)	0(1)
C(32)	28(1)	32(1)	30(1)	-20(1)	-3(1)	-2(1)
C(33)	33(1)	28(1)	37(1)	-19(1)	0(1)	3(1)
C(34)	30(1)	30(1)	31(1)	-12(1)	-5(1)	8(1)
C(35)	21(1)	30(1)	21(1)	-12(1)	-2(1)	-1(1)
C(36)	28(1)	21(1)	16(1)	-7(1)	0(1)	0(1)
C(37)	28(1)	24(1)	19(1)	-7(1)	-1(1)	-6(1)
C(38)	27(1)	23(1)	19(1)	-7(1)	0(1)	-1(1)
C(39)	22(1)	25(1)	19(1)	-11(1)	-1(1)	1(1)
C(40)	31(1)	23(1)	23(1)	-8(1)	-2(1)	2(1)
C(41)	28(1)	40(1)	26(1)	-17(1)	-10(1)	10(1)
C(42)	22(1)	40(1)	32(1)	-22(1)	1(1)	-3(1)
C(43)	30(1)	29(1)	27(1)	-12(1)	4(1)	-5(1)
C(44)	30(1)	28(1)	18(1)	-7(1)	-3(1)	0(1)

C(48)	52(2)	90(3)	47(2)	-21(2)	-3(2)	-19(2)
C(47)	31(1)	36(2)	56(2)	-14(1)	-11(1)	2(1)
C(46)	53(2)	40(2)	90(3)	-11(2)	-4(2)	-5(2)
C(45)	39(1)	46(2)	41(2)	-19(1)	6(1)	-10(1)

Table 11.15. Hydrogen coordinates ( $\times 10^4$ ) and isotropic displacement parameters ( $\text{\AA}^2 \times 10^3$ ) for jr583smart.

	x	y	z	U(eq)
H(3)	18140	2002	9806	26
H(4A)	20971	91	11239	45
H(4B)	20381	-675	12449	45
H(4C)	21756	193	12223	45
H(5A)	20300	1327	13380	37
H(5B)	18905	504	13518	37
H(5C)	18740	2010	13002	37
H(6A)	21900	3678	10725	48
H(6B)	22530	2258	11290	48
H(6C)	21671	2985	12002	48
H(7A)	16778	3872	9832	26
H(7B)	15908	2640	10520	26
H(9)	15028	2350	12265	36
H(10)	14833	2893	13783	51
H(11)	16337	4425	13875	57
H(12)	18002	5399	12443	44
H(13)	18244	4822	10937	31
H(14)	17866	-425	12470	25
H(15)	16047	509	10671	27
H(16)	16171	-1675	12531	27
H(18)	14099	-261	10172	31
H(19)	12183	-1199	9746	37
H(21)	12838	-4340	12385	41
H(22)	14684	-3373	12843	34
H(25)	10151	7943	5343	26

H(26A)	7276	6732	7250	45
H(26B)	7875	5445	8130	45
H(26C)	6446	5458	7515	45
H(27A)	7722	3717	6910	40
H(27B)	9177	3738	7485	40
H(27C)	9268	3986	6226	40
H(28A)	5596	6259	5716	47
H(28B)	6258	5037	5484	47
H(28C)	6192	6381	4524	47
H(29A)	11440	7372	3937	26
H(29B)	12308	6856	5012	26
H(31)	9905	5748	3580	29
H(32)	9975	3702	3601	33
H(33)	11586	2155	4672	37
H(34)	13120	2671	5738	36
H(35)	13030	4719	5746	28
H(36)	10386	5233	7852	27
H(37)	12188	7287	6608	28
H(38)	12238	5460	8701	28
H(40)	14254	5392	9765	31
H(41)	16176	6347	10162	36
H(43)	15461	9476	7525	34
H(44)	13582	8500	7102	30
H(48A)	22081	10538	7446	95
H(48B)	20669	11289	6839	95
H(48C)	20713	9783	7377	95
H(46A)	6352	11401	5461	97
H(46B)	7909	12016	5319	97
H(46C)	7047	11508	6478	97



**(*S,E*)-5-Benzyl-2,2,3-trimethyl-4-oxo-1-((*E*)-3-phenylallylidene)imidazolidin-1-ium hexafluorophosphate 15·PF<sub>6</sub>**

Table 11.16. Crystal data and structure refinement for nct1011.

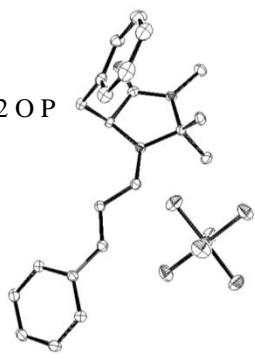
Identification code	nct1011		
Empirical formula	C <sub>22</sub> H <sub>25</sub> F <sub>6</sub> N <sub>2</sub> O P		
Formula weight	478.41		
Temperature	150(2) K		
Wavelength	0.71073 Å		
Crystal system	Orthorhombic		
Space group	P212121		
Unit cell dimensions	a = 9.7053(3) Å		α = 90°.
	b = 13.2565(4) Å		β = 90°.
	c = 17.3967(3) Å		γ = 90°.
Volume	2238.23(10) Å <sup>3</sup>		
Z	4		
Density (calculated)	1.420 Mg/m <sup>3</sup>		
Absorption coefficient	0.189 mm <sup>-1</sup>		
F(000)	992		
Crystal size	0.35 x 0.35 x 0.35 mm <sup>3</sup>		
Theta range for data collection	2.85 to 27.48°.		
Index ranges	-12 ≤ h ≤ 12, -17 ≤ k ≤ 17, -22 ≤ l ≤ 22		
Reflections collected	5010		
Independent reflections	5010 [R(int) = 0.0300]		
Completeness to theta = 27.48°	98.7%		
Absorption correction	Empirical		
Max. and min. transmission	0.9367 and 0.9367		
Refinement method	Full-matrix least-squares on F <sup>2</sup>		
Data / restraints / parameters	5010 / 0 / 292		
Goodness-of-fit on F <sup>2</sup>	1.076		
Final R indices [I > 2σ(I)]	R1 = 0.0434, wR2 = 0.0999		
R indices (all data)	R1 = 0.0501, wR2 = 0.1053		
Absolute structure parameter	0.02(10)		
Largest diff. peak and hole	0.208 and -0.300 e.Å <sup>-3</sup>		

Table 11.17. Atomic coordinates ( $\times 10^4$ ) and equivalent isotropic displacement parameters ( $\text{\AA}^2 \times 10^3$ ) for nct1011.  $U(\text{eq})$  is defined as one third of the trace of the orthogonalized  $U^{ij}$  tensor.

	x	y	z	$U(\text{eq})$
C(1)	5305(2)	1812(2)	4335(1)	22(1)
C(2)	6792(2)	1827(2)	4596(1)	23(1)
C(3)	6890(2)	1222(2)	3309(1)	22(1)
C(4)	4434(2)	1069(2)	4811(1)	26(1)
C(5)	4921(2)	-10(2)	4788(1)	27(1)
C(6)	4220(3)	-726(2)	4353(1)	38(1)
C(7)	4697(3)	-1712(2)	4305(2)	46(1)
C(8)	5883(4)	-2003(2)	4692(2)	47(1)
C(9)	6566(3)	-1308(2)	5136(2)	42(1)
C(10)	6102(3)	-313(2)	5188(1)	32(1)
C(11)	9074(2)	1318(2)	4119(1)	33(1)
C(12)	7425(2)	1877(2)	2652(1)	30(1)
C(13)	6970(2)	101(2)	3116(1)	28(1)
C(14)	4511(2)	1653(2)	2993(1)	23(1)
C(15)	3210(2)	2126(2)	3094(1)	24(1)
C(16)	2456(2)	2289(2)	2453(1)	25(1)
C(17)	1231(2)	2918(2)	2381(1)	23(1)
C(18)	595(2)	2988(2)	1657(1)	29(1)
C(19)	-501(2)	3651(2)	1546(1)	33(1)
C(20)	-963(2)	4235(2)	2153(1)	33(1)
C(21)	-349(2)	4165(2)	2874(1)	31(1)
C(22)	739(2)	3507(2)	2988(1)	26(1)
N(1)	5444(2)	1533(1)	3517(1)	21(1)
N(2)	7596(2)	1469(1)	4027(1)	23(1)
O(1)	7170(2)	2091(1)	5236(1)	28(1)
F(1)	3207(2)	-1121(1)	993(1)	45(1)
F(2)	4002(2)	-281(1)	2032(1)	41(1)
F(3)	4988(2)	889(1)	1267(1)	38(1)
F(4)	4174(2)	60(1)	219(1)	49(1)
F(5)	5480(2)	-767(1)	1097(1)	44(1)
F(6)	2708(2)	535(1)	1155(1)	40(1)
P(1)	4094(1)	-119(1)	1122(1)	27(1)

Table 11.18. Bond lengths [ $\text{\AA}$ ] and angles [ $^\circ$ ] for nct1011.

---

C(1)-N(1)	1.476(2)
C(1)-C(2)	1.513(3)
C(1)-C(4)	1.539(3)
C(1)-H(1)	1.0000
C(2)-O(1)	1.224(2)
C(2)-N(2)	1.346(3)
C(3)-N(2)	1.462(3)
C(3)-N(1)	1.506(3)
C(3)-C(13)	1.526(3)
C(3)-C(12)	1.526(3)
C(4)-C(5)	1.507(3)
C(4)-H(4A)	0.9900
C(4)-H(4B)	0.9900
C(5)-C(6)	1.391(3)
C(5)-C(10)	1.399(3)
C(6)-C(7)	1.390(4)
C(6)-H(6)	0.9500
C(7)-C(8)	1.388(4)
C(7)-H(7)	0.9500
C(8)-C(9)	1.373(4)
C(8)-H(8)	0.9500
C(9)-C(10)	1.396(3)
C(9)-H(9)	0.9500
C(10)-H(10)	0.9500
C(11)-N(2)	1.457(3)
C(11)-H(11A)	0.9800
C(11)-H(11B)	0.9800
C(11)-H(11C)	0.9800
C(12)-H(12A)	0.9800
C(12)-H(12B)	0.9800
C(12)-H(12C)	0.9800
C(13)-H(13A)	0.9800
C(13)-H(13B)	0.9800
C(13)-H(13C)	0.9800
C(14)-N(1)	1.295(3)

---

C(14)-C(15)	1.422(3)
C(14)-H(14)	0.9500
C(15)-C(16)	1.351(3)
C(15)-H(15)	0.9500
C(16)-C(17)	1.457(3)
C(16)-H(16)	0.9500
C(17)-C(22)	1.397(3)
C(17)-C(18)	1.407(3)
C(18)-C(19)	1.393(3)
C(18)-H(18)	0.9500
C(19)-C(20)	1.382(3)
C(19)-H(19)	0.9500
C(20)-C(21)	1.393(3)
C(20)-H(20)	0.9500
C(21)-C(22)	1.384(3)
C(21)-H(21)	0.9500
C(22)-H(22)	0.9500
F(1)-P(1)	1.5986(15)
F(2)-P(1)	1.6006(14)
F(3)-P(1)	1.6122(14)
F(4)-P(1)	1.5896(14)
F(5)-P(1)	1.5963(15)
F(6)-P(1)	1.6010(15)
N(1)-C(1)-C(2)	101.81(16)
N(1)-C(1)-C(4)	114.09(17)
C(2)-C(1)-C(4)	111.80(16)
N(1)-C(1)-H(1)	109.6
C(2)-C(1)-H(1)	109.6
C(4)-C(1)-H(1)	109.6
O(1)-C(2)-N(2)	126.6(2)
O(1)-C(2)-C(1)	124.23(19)
N(2)-C(2)-C(1)	109.15(16)
N(2)-C(3)-N(1)	99.78(14)
N(2)-C(3)-C(13)	112.45(17)
N(1)-C(3)-C(13)	111.53(16)
N(2)-C(3)-C(12)	110.67(17)
N(1)-C(3)-C(12)	109.96(17)

---

C(13)-C(3)-C(12)	111.85(17)
C(5)-C(4)-C(1)	114.89(17)
C(5)-C(4)-H(4A)	108.5
C(1)-C(4)-H(4A)	108.5
C(5)-C(4)-H(4B)	108.5
C(1)-C(4)-H(4B)	108.5
H(4A)-C(4)-H(4B)	107.5
C(6)-C(5)-C(10)	118.4(2)
C(6)-C(5)-C(4)	120.5(2)
C(10)-C(5)-C(4)	121.1(2)
C(7)-C(6)-C(5)	120.8(3)
C(7)-C(6)-H(6)	119.6
C(5)-C(6)-H(6)	119.6
C(8)-C(7)-C(6)	120.5(2)
C(8)-C(7)-H(7)	119.7
C(6)-C(7)-H(7)	119.7
C(9)-C(8)-C(7)	119.1(2)
C(9)-C(8)-H(8)	120.4
C(7)-C(8)-H(8)	120.4
C(8)-C(9)-C(10)	121.0(3)
C(8)-C(9)-H(9)	119.5
C(10)-C(9)-H(9)	119.5
C(9)-C(10)-C(5)	120.2(2)
C(9)-C(10)-H(10)	119.9
C(5)-C(10)-H(10)	119.9
N(2)-C(11)-H(11A)	109.5
N(2)-C(11)-H(11B)	109.5
H(11A)-C(11)-H(11B)	109.5
N(2)-C(11)-H(11C)	109.5
H(11A)-C(11)-H(11C)	109.5
H(11B)-C(11)-H(11C)	109.5
C(3)-C(12)-H(12A)	109.5
C(3)-C(12)-H(12B)	109.5
H(12A)-C(12)-H(12B)	109.5
C(3)-C(12)-H(12C)	109.5
H(12A)-C(12)-H(12C)	109.5
H(12B)-C(12)-H(12C)	109.5
C(3)-C(13)-H(13A)	109.5

---

C(3)-C(13)-H(13B)	109.5
H(13A)-C(13)-H(13B)	109.5
C(3)-C(13)-H(13C)	109.5
H(13A)-C(13)-H(13C)	109.5
H(13B)-C(13)-H(13C)	109.5
N(1)-C(14)-C(15)	126.04(18)
N(1)-C(14)-H(14)	117.0
C(15)-C(14)-H(14)	117.0
C(16)-C(15)-C(14)	116.74(18)
C(16)-C(15)-H(15)	121.6
C(14)-C(15)-H(15)	121.6
C(15)-C(16)-C(17)	127.18(19)
C(15)-C(16)-H(16)	116.4
C(17)-C(16)-H(16)	116.4
C(22)-C(17)-C(18)	119.29(19)
C(22)-C(17)-C(16)	122.25(19)
C(18)-C(17)-C(16)	118.27(19)
C(19)-C(18)-C(17)	120.1(2)
C(19)-C(18)-H(18)	120.0
C(17)-C(18)-H(18)	120.0
C(20)-C(19)-C(18)	119.7(2)
C(20)-C(19)-H(19)	120.2
C(18)-C(19)-H(19)	120.2
C(19)-C(20)-C(21)	120.8(2)
C(19)-C(20)-H(20)	119.6
C(21)-C(20)-H(20)	119.6
C(22)-C(21)-C(20)	119.8(2)
C(22)-C(21)-H(21)	120.1
C(20)-C(21)-H(21)	120.1
C(21)-C(22)-C(17)	120.39(19)
C(21)-C(22)-H(22)	119.8
C(17)-C(22)-H(22)	119.8
C(14)-N(1)-C(1)	125.74(18)
C(14)-N(1)-C(3)	121.01(16)
C(1)-N(1)-C(3)	112.70(15)
C(2)-N(2)-C(11)	122.54(18)
C(2)-N(2)-C(3)	115.77(17)
C(11)-N(2)-C(3)	121.68(17)

F(4)-P(1)-F(5)	90.70(9)
F(4)-P(1)-F(1)	90.67(9)
F(5)-P(1)-F(1)	90.18(8)
F(4)-P(1)-F(2)	179.07(9)
F(5)-P(1)-F(2)	90.09(9)
F(1)-P(1)-F(2)	89.82(8)
F(4)-P(1)-F(6)	89.83(9)
F(5)-P(1)-F(6)	179.38(9)
F(1)-P(1)-F(6)	90.13(8)
F(2)-P(1)-F(6)	89.38(9)
F(4)-P(1)-F(3)	90.34(8)
F(5)-P(1)-F(3)	89.82(8)
F(1)-P(1)-F(3)	178.99(9)
F(2)-P(1)-F(3)	89.17(7)
F(6)-P(1)-F(3)	89.86(8)

Table 11.19. Anisotropic displacement parameters ( $\text{\AA}^2 \times 10^3$ ) for nct1011. The anisotropic displacement factor exponent takes the form:  $-2\pi^2 [ h^2 a^{*2} U^{11} + \dots + 2 h k a^* b^* U^{12} ]$

	$U^{11}$	$U^{22}$	$U^{33}$	$U^{23}$	$U^{13}$	$U^{12}$
C(1)	25(1)	23(1)	18(1)	-3(1)	0(1)	2(1)
C(2)	28(1)	18(1)	22(1)	1(1)	-2(1)	-2(1)
C(3)	19(1)	26(1)	21(1)	-3(1)	-1(1)	1(1)
C(4)	27(1)	30(1)	22(1)	1(1)	4(1)	2(1)
C(5)	30(1)	26(1)	24(1)	3(1)	4(1)	-3(1)
C(6)	37(1)	35(1)	41(1)	-1(1)	0(1)	-9(1)
C(7)	63(2)	29(1)	47(2)	-9(1)	9(1)	-14(1)
C(8)	73(2)	23(1)	45(1)	2(1)	11(2)	4(1)
C(9)	60(2)	30(1)	37(1)	5(1)	-3(1)	10(1)
C(10)	42(1)	25(1)	29(1)	1(1)	-2(1)	2(1)
C(11)	22(1)	42(1)	35(1)	-2(1)	-6(1)	3(1)
C(12)	27(1)	39(1)	26(1)	5(1)	2(1)	-3(1)
C(13)	24(1)	29(1)	30(1)	-7(1)	-1(1)	4(1)
C(14)	24(1)	24(1)	21(1)	-3(1)	-1(1)	2(1)
C(15)	24(1)	25(1)	24(1)	-2(1)	-1(1)	3(1)
C(16)	25(1)	25(1)	26(1)	-4(1)	0(1)	1(1)
C(17)	21(1)	24(1)	26(1)	2(1)	0(1)	0(1)
C(18)	27(1)	33(1)	26(1)	0(1)	-2(1)	2(1)
C(19)	27(1)	41(1)	31(1)	7(1)	-6(1)	1(1)
C(20)	22(1)	36(1)	39(1)	7(1)	1(1)	4(1)
C(21)	27(1)	31(1)	35(1)	1(1)	6(1)	3(1)
C(22)	24(1)	29(1)	25(1)	1(1)	1(1)	1(1)
N(1)	21(1)	20(1)	21(1)	-4(1)	-1(1)	2(1)
N(2)	23(1)	26(1)	22(1)	-2(1)	-5(1)	2(1)
O(1)	34(1)	29(1)	22(1)	-5(1)	-6(1)	0(1)
F(1)	44(1)	31(1)	61(1)	-14(1)	-12(1)	-4(1)
F(2)	49(1)	46(1)	28(1)	3(1)	1(1)	-13(1)
F(3)	44(1)	31(1)	38(1)	-3(1)	7(1)	-11(1)
F(4)	63(1)	59(1)	25(1)	-7(1)	-1(1)	14(1)
F(5)	36(1)	40(1)	56(1)	-7(1)	-5(1)	12(1)
F(6)	34(1)	35(1)	51(1)	-9(1)	1(1)	9(1)
P(1)	31(1)	25(1)	26(1)	-6(1)	-1(1)	1(1)



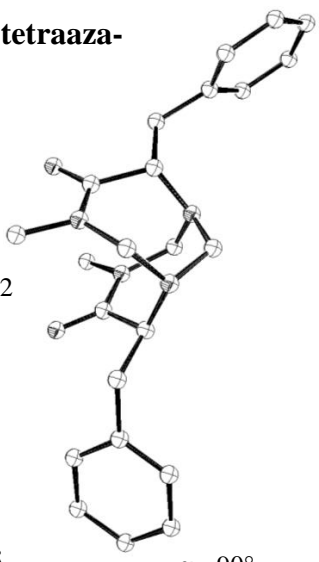
Table 11.20. Hydrogen coordinates ( $\times 10^4$ ) and isotropic displacement parameters ( $\text{\AA}^2 \times 10^3$ ) for nct1011.

	x	y	z	U(eq)
H(1)	4906	2506	4377	26
H(4A)	4428	1299	5352	31
H(4B)	3472	1094	4622	31
H(6)	3405	-538	4087	45
H(7)	4208	-2191	4004	56
H(8)	6217	-2674	4651	56
H(9)	7366	-1506	5411	50
H(10)	6590	160	5495	38
H(11A)	9573	1835	3828	50
H(11B)	9327	648	3927	50
H(11C)	9316	1369	4665	50
H(12A)	7252	2588	2769	46
H(12B)	6948	1694	2175	46
H(12C)	8417	1767	2590	46
H(13A)	7918	-74	2976	41
H(13B)	6355	-48	2684	41
H(13C)	6688	-296	3565	41
H(14)	4716	1400	2495	28
H(15)	2886	2319	3588	29
H(16)	2757	1956	2000	30
H(18)	913	2584	1242	34
H(19)	-930	3702	1057	40
H(20)	-1707	4689	2076	39
H(21)	-676	4568	3288	37
H(22)	1155	3457	3481	31

**(-)-(1*S*,5*S*,6*S*,10*S*)-5,10-Dibenzyl-3,8-dimethyl-1,3,6,8-tetraaza-bicyclo[4.4.1]undecane-4,9-dione 128**

Available from the CCDC as deposition number 909951

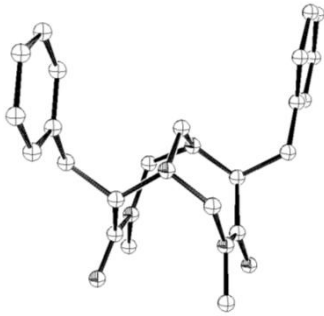
Crystal data and structure refinement for nct0909b.

Identification code	nct0909b		
Empirical formula	C <sub>23</sub> H <sub>28</sub> N <sub>4</sub> O <sub>2</sub>		
Formula weight	392.49		
Temperature	150(2) K		
Wavelength	0.71073 Å		
Crystal system	Tetragonal		
Space group	P43212		
Unit cell dimensions	a = 8.6628(4) Å		$\alpha = 90^\circ$ .
	b = 8.6628(4) Å		$\beta = 90^\circ$ .
	c = 55.161(2) Å		$\gamma = 90^\circ$ .
Volume	4139.5(3) Å <sup>3</sup>		
Z	8		
Density (calculated)	1.260 Mg/m <sup>3</sup>		
Absorption coefficient	0.082 mm <sup>-1</sup>		
F(000)	1680		
Crystal size	0.15 x 0.10 x 0.10 mm <sup>3</sup>		
Theta range for data collection	2.60 to 27.49°.		
Index ranges	-11 ≤ h ≤ 9, -10 ≤ k ≤ 11, -71 ≤ l ≤ 50		
Reflections collected	12695		
Independent reflections	4561 [R(int) = 0.0798]		
Completeness to theta = 27.49°	96.3%		
Absorption correction	Empirical		
Max. and min. transmission	0.9918 and 0.9878		
Refinement method	Full-matrix least-squares on F <sup>2</sup>		
Data / restraints / parameters	4561 / 0 / 265		
Goodness-of-fit on F <sup>2</sup>	1.066		
Final R indices [I > 2σ(I)]	R1 = 0.0413, wR2 = 0.0966		
R indices (all data)	R1 = 0.0495, wR2 = 0.1014		
Absolute structure parameter	0.4(12)		
Extinction coefficient	0.011(3)		
Largest diff. peak and hole	0.144 and -0.139 e.Å <sup>-3</sup>		

**(+)-(1*R*,5*S*,6*R*,10*S*)-5,10-Dibenzyl-3,8-dimethyl-1,3,6,8-tetraaza-bicyclo[4.4.1]undecane-4,9-dione 129**

Available from the CCDC as deposition number 909952

Crystal data and structure refinement for nct1006.

Identification code	nct1006	
Empirical formula	C <sub>23</sub> H <sub>28</sub> N <sub>4</sub> O <sub>2</sub>	
Formula weight	392.49	
Temperature	293(2) K	
Wavelength	0.71073 Å	
Crystal system	Monoclinic	
Space group	C2	
Unit cell dimensions	a = 12.9249(4) Å	α = 90°.
	b = 20.3503(5) Å	β = 124.7300(10)°.
	c = 9.3869(4) Å	γ = 90°.
Volume	2029.13(12) Å <sup>3</sup>	
Z	4	
Density (calculated)	1.285 Mg/m <sup>3</sup>	
Absorption coefficient	0.084 mm <sup>-1</sup>	
F(000)	840	
Crystal size	0.20 x 0.15 x 0.12 mm <sup>3</sup>	
Theta range for data collection	3.19 to 27.49°.	
Index ranges	-16 ≤ h ≤ 16, -26 ≤ k ≤ 23, -12 ≤ l ≤ 12	
Reflections collected	3962	
Independent reflections	3962 [R(int) = 0.0500]	
Completeness to theta = 27.49°	99.0%	
Absorption correction	Empirical	
Max. and min. transmission	0.9900 and 0.9834	
Refinement method	Full-matrix least-squares on F <sup>2</sup>	
Data / restraints / parameters	3962 / 1 / 266	
Goodness-of-fit on F <sup>2</sup>	1.059	
Final R indices [I > 2σ(I)]	R1 = 0.0509, wR2 = 0.1056	
R indices (all data)	R1 = 0.0644, wR2 = 0.1156	
Absolute structure parameter	1.9(15)	
Extinction coefficient	0.035(2)	
Largest diff. peak and hole	0.262 and -0.215 e.Å <sup>-3</sup>	

***tert*-Butyl (*S*)-4-(hydroxydiphenylmethyl)-2,2-dimethyloxazolidine-3-carboxylate 140**

Table 11.21. Crystal data and structure refinement for nct1102.

Identification code	nct1102	
Empirical formula	C <sub>23</sub> H <sub>29</sub> N O <sub>4</sub>	
Formula weight	383.47	
Temperature	150(2) K	
Wavelength	0.71073 Å	
Crystal system	Orthorhombic	
Space group	P212121	
Unit cell dimensions	a = 9.0642(3) Å	α = 90°.
	b = 14.2803(5) Å	β = 90°.
	c = 16.6484(3) Å	γ = 90°.
Volume	2154.96(11) Å <sup>3</sup>	
Z	4	
Density (calculated)	1.182 Mg/m <sup>3</sup>	
Absorption coefficient	0.080 mm <sup>-1</sup>	
F(000)	824	
Crystal size	0.40 x 0.25 x 0.25 mm <sup>3</sup>	
Theta range for data collection	2.93 to 27.66°.	
Index ranges	-9 ≤ h ≤ 11, -17 ≤ k ≤ 18, -21 ≤ l ≤ 16	
Reflections collected	11752	
Independent reflections	4902 [R(int) = 0.0426]	
Completeness to theta = 27.66°	98.6%	
Absorption correction	Empirical	
Max. and min. transmission	0.9802 and 0.9686	
Refinement method	Full-matrix least-squares on F <sup>2</sup>	
Data / restraints / parameters	4902 / 0 / 260	
Goodness-of-fit on F <sup>2</sup>	1.070	
Final R indices [I > 2σ(I)]	R1 = 0.0490, wR2 = 0.1038	
R indices (all data)	R1 = 0.0646, wR2 = 0.1135	
Absolute structure parameter	1.1(11)	
Extinction coefficient	0.090(4)	
Largest diff. peak and hole	0.166 and -0.210 e.Å <sup>-3</sup>	

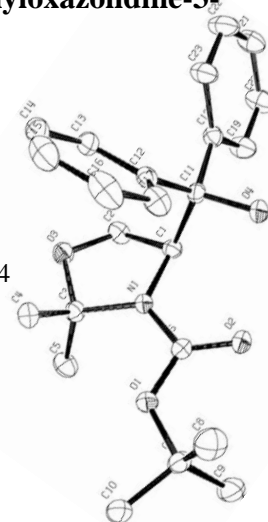


Table 11.22. Atomic coordinates ( $\times 10^4$ ) and equivalent isotropic displacement parameters ( $\text{\AA}^2 \times 10^3$ ) for nct1102.  $U(\text{eq})$  is defined as one third of the trace of the orthogonalized  $U^{ij}$  tensor.

	x	y	z	$U(\text{eq})$
C(1)	4688(2)	6595(1)	414(1)	30(1)
C(2)	3601(2)	7372(1)	199(1)	37(1)
C(3)	3627(2)	6436(1)	-939(1)	32(1)
C(4)	2660(2)	5663(1)	-1266(1)	39(1)
C(5)	4296(3)	7025(2)	-1605(1)	45(1)
C(6)	5908(2)	5528(1)	-537(1)	35(1)
C(7)	7008(2)	4595(1)	-1624(1)	39(1)
C(8)	6968(3)	3670(2)	-1185(2)	65(1)
C(9)	8506(2)	5065(2)	-1584(2)	60(1)
C(10)	6497(3)	4490(2)	-2487(1)	50(1)
C(11)	4251(2)	5963(1)	1146(1)	30(1)
C(12)	2992(2)	5307(1)	918(1)	32(1)
C(13)	1537(2)	5615(2)	850(1)	40(1)
C(14)	424(3)	5018(2)	607(1)	56(1)
C(15)	737(3)	4097(2)	422(2)	66(1)
C(16)	2164(4)	3781(2)	476(2)	65(1)
C(17)	3284(3)	4377(1)	726(1)	46(1)
C(18)	3947(2)	6577(1)	1884(1)	32(1)
C(19)	4857(3)	7329(2)	2057(1)	49(1)
C(20)	4682(3)	7861(2)	2745(1)	56(1)
C(21)	3603(3)	7635(2)	3289(1)	57(1)
C(22)	2713(3)	6873(2)	3138(1)	63(1)
C(23)	2883(3)	6349(2)	2447(1)	49(1)
N(1)	4757(2)	6092(1)	-358(1)	30(1)
O(1)	5861(2)	5226(1)	-1294(1)	40(1)
O(2)	6866(2)	5313(1)	-47(1)	47(1)
O(3)	2715(2)	7005(1)	-436(1)	37(1)
O(4)	5519(2)	5428(1)	1380(1)	40(1)

Table 11.23. Bond lengths [Å] and angles [°] for nct1102.

---

C(1)-N(1)	1.473(2)
C(1)-C(2)	1.526(3)
C(1)-C(11)	1.568(2)
C(1)-H(1)	1.0000
C(2)-O(3)	1.427(2)
C(2)-H(2A)	0.9900
C(2)-H(2B)	0.9900
C(3)-O(3)	1.430(2)
C(3)-N(1)	1.493(2)
C(3)-C(4)	1.511(3)
C(3)-C(5)	1.517(3)
C(4)-H(4A)	0.9800
C(4)-H(4B)	0.9800
C(4)-H(4C)	0.9800
C(5)-H(5A)	0.9800
C(5)-H(5B)	0.9800
C(5)-H(5C)	0.9800
C(6)-O(2)	1.230(2)
C(6)-O(1)	1.333(2)
C(6)-N(1)	1.352(2)
C(7)-O(1)	1.481(2)
C(7)-C(8)	1.510(3)
C(7)-C(9)	1.517(3)
C(7)-C(10)	1.517(3)
C(8)-H(8A)	0.9800
C(8)-H(8B)	0.9800
C(8)-H(8C)	0.9800
C(9)-H(9A)	0.9800
C(9)-H(9B)	0.9800
C(9)-H(9C)	0.9800
C(10)-H(10A)	0.9800
C(10)-H(10B)	0.9800
C(10)-H(10C)	0.9800
C(11)-O(4)	1.434(2)

---

C(11)-C(12)	1.525(3)
C(11)-C(18)	1.533(3)
C(12)-C(17)	1.391(3)
C(12)-C(13)	1.394(3)
C(13)-C(14)	1.381(3)
C(13)-H(13)	0.9500
C(14)-C(15)	1.381(4)
C(14)-H(14)	0.9500
C(15)-C(16)	1.373(4)
C(15)-H(15)	0.9500
C(16)-C(17)	1.389(3)
C(16)-H(16)	0.9500
C(17)-H(17)	0.9500
C(18)-C(23)	1.384(3)
C(18)-C(19)	1.385(3)
C(19)-C(20)	1.384(3)
C(19)-H(19)	0.9500
C(20)-C(21)	1.371(3)
C(20)-H(20)	0.9500
C(21)-C(22)	1.377(3)
C(21)-H(21)	0.9500
C(22)-C(23)	1.382(3)
C(22)-H(22)	0.9500
C(23)-H(23)	0.9500
O(4)-H(4)	0.8400
N(1)-C(1)-C(2)	100.22(14)
N(1)-C(1)-C(11)	114.08(14)
C(2)-C(1)-C(11)	115.94(16)
N(1)-C(1)-H(1)	108.7
C(2)-C(1)-H(1)	108.7
C(11)-C(1)-H(1)	108.7
O(3)-C(2)-C(1)	105.65(14)
O(3)-C(2)-H(2A)	110.6
C(1)-C(2)-H(2A)	110.6
O(3)-C(2)-H(2B)	110.6

---

C(1)-C(2)-H(2B)	110.6
H(2A)-C(2)-H(2B)	108.7
O(3)-C(3)-N(1)	101.74(14)
O(3)-C(3)-C(4)	106.92(16)
N(1)-C(3)-C(4)	113.02(15)
O(3)-C(3)-C(5)	110.08(15)
N(1)-C(3)-C(5)	112.43(16)
C(4)-C(3)-C(5)	111.99(16)
C(3)-C(4)-H(4A)	109.5
C(3)-C(4)-H(4B)	109.5
H(4A)-C(4)-H(4B)	109.5
C(3)-C(4)-H(4C)	109.5
H(4A)-C(4)-H(4C)	109.5
H(4B)-C(4)-H(4C)	109.5
C(3)-C(5)-H(5A)	109.5
C(3)-C(5)-H(5B)	109.5
H(5A)-C(5)-H(5B)	109.5
C(3)-C(5)-H(5C)	109.5
H(5A)-C(5)-H(5C)	109.5
H(5B)-C(5)-H(5C)	109.5
O(2)-C(6)-O(1)	124.72(18)
O(2)-C(6)-N(1)	123.15(17)
O(1)-C(6)-N(1)	112.12(16)
O(1)-C(7)-C(8)	109.60(17)
O(1)-C(7)-C(9)	110.04(17)
C(8)-C(7)-C(9)	112.8(2)
O(1)-C(7)-C(10)	101.43(16)
C(8)-C(7)-C(10)	111.35(19)
C(9)-C(7)-C(10)	111.03(18)
C(7)-C(8)-H(8A)	109.5
C(7)-C(8)-H(8B)	109.5
H(8A)-C(8)-H(8B)	109.5
C(7)-C(8)-H(8C)	109.5
H(8A)-C(8)-H(8C)	109.5
H(8B)-C(8)-H(8C)	109.5
C(7)-C(9)-H(9A)	109.5



---

C(7)-C(9)-H(9B)	109.5
H(9A)-C(9)-H(9B)	109.5
C(7)-C(9)-H(9C)	109.5
H(9A)-C(9)-H(9C)	109.5
H(9B)-C(9)-H(9C)	109.5
C(7)-C(10)-H(10A)	109.5
C(7)-C(10)-H(10B)	109.5
H(10A)-C(10)-H(10B)	109.5
C(7)-C(10)-H(10C)	109.5
H(10A)-C(10)-H(10C)	109.5
H(10B)-C(10)-H(10C)	109.5
O(4)-C(11)-C(12)	109.85(14)
O(4)-C(11)-C(18)	103.40(14)
C(12)-C(11)-C(18)	114.61(15)
O(4)-C(11)-C(1)	108.37(15)
C(12)-C(11)-C(1)	110.41(14)
C(18)-C(11)-C(1)	109.84(14)
C(17)-C(12)-C(13)	117.6(2)
C(17)-C(12)-C(11)	120.08(19)
C(13)-C(12)-C(11)	122.26(17)
C(14)-C(13)-C(12)	121.3(2)
C(14)-C(13)-H(13)	119.3
C(12)-C(13)-H(13)	119.3
C(15)-C(14)-C(13)	120.2(2)
C(15)-C(14)-H(14)	119.9
C(13)-C(14)-H(14)	119.9
C(16)-C(15)-C(14)	119.5(2)
C(16)-C(15)-H(15)	120.2
C(14)-C(15)-H(15)	120.2
C(15)-C(16)-C(17)	120.4(2)
C(15)-C(16)-H(16)	119.8
C(17)-C(16)-H(16)	119.8
C(16)-C(17)-C(12)	121.0(2)
C(16)-C(17)-H(17)	119.5
C(12)-C(17)-H(17)	119.5
C(23)-C(18)-C(19)	117.11(18)

C(23)-C(18)-C(11)	122.24(17)
C(19)-C(18)-C(11)	120.24(17)
C(20)-C(19)-C(18)	122.1(2)
C(20)-C(19)-H(19)	119.0
C(18)-C(19)-H(19)	119.0
C(21)-C(20)-C(19)	119.9(2)
C(21)-C(20)-H(20)	120.1
C(19)-C(20)-H(20)	120.1
C(20)-C(21)-C(22)	119.0(2)
C(20)-C(21)-H(21)	120.5
C(22)-C(21)-H(21)	120.5
C(21)-C(22)-C(23)	120.9(2)
C(21)-C(22)-H(22)	119.6
C(23)-C(22)-H(22)	119.6
C(22)-C(23)-C(18)	121.0(2)
C(22)-C(23)-H(23)	119.5
C(18)-C(23)-H(23)	119.5
C(6)-N(1)-C(1)	121.06(15)
C(6)-N(1)-C(3)	125.65(15)
C(1)-N(1)-C(3)	112.09(14)
C(6)-O(1)-C(7)	121.69(15)
C(2)-O(3)-C(3)	108.51(14)
C(11)-O(4)-H(4)	109.5

Table 11.24. Anisotropic displacement parameters ( $\text{\AA}^2 \times 10^3$ ) for nct1102. The anisotropic displacement factor exponent takes the form:  $-2\pi^2 [ h^2 a^{*2} U^{11} + \dots + 2 h k a^* b^* U^{12} ]$

	$U^{11}$	$U^{22}$	$U^{33}$	$U^{23}$	$U^{13}$	$U^{12}$
C(1)	30(1)	31(1)	29(1)	-1(1)	1(1)	-4(1)
C(2)	49(1)	29(1)	33(1)	1(1)	-2(1)	0(1)
C(3)	34(1)	29(1)	33(1)	2(1)	-3(1)	5(1)
C(4)	37(1)	40(1)	39(1)	0(1)	-7(1)	-1(1)
C(5)	56(1)	42(1)	38(1)	9(1)	-3(1)	-5(1)
C(6)	28(1)	42(1)	33(1)	-2(1)	1(1)	2(1)
C(7)	31(1)	46(1)	41(1)	-9(1)	4(1)	5(1)

---

C(8)	71(2)	51(1)	72(2)	2(1)	4(1)	12(1)
C(9)	37(1)	91(2)	53(1)	-20(1)	6(1)	-9(1)
C(10)	40(1)	64(2)	44(1)	-16(1)	2(1)	2(1)
C(11)	26(1)	32(1)	31(1)	4(1)	-2(1)	2(1)
C(12)	35(1)	33(1)	28(1)	6(1)	-2(1)	-5(1)
C(13)	33(1)	49(1)	37(1)	4(1)	-2(1)	-6(1)
C(14)	42(1)	84(2)	42(1)	11(1)	-6(1)	-23(1)
C(15)	76(2)	68(2)	53(1)	11(1)	-16(1)	-44(2)
C(16)	106(2)	35(1)	53(1)	5(1)	-17(2)	-24(1)
C(17)	63(2)	32(1)	44(1)	5(1)	-7(1)	-4(1)
C(18)	33(1)	33(1)	31(1)	3(1)	-2(1)	-2(1)
C(19)	56(1)	52(1)	39(1)	-5(1)	5(1)	-19(1)
C(20)	79(2)	49(1)	41(1)	-7(1)	6(1)	-23(1)
C(21)	74(2)	62(1)	35(1)	-9(1)	4(1)	-5(1)
C(22)	66(2)	86(2)	38(1)	-13(1)	16(1)	-21(2)
C(23)	54(1)	58(1)	34(1)	-5(1)	7(1)	-17(1)
N(1)	27(1)	34(1)	27(1)	0(1)	-2(1)	3(1)
O(1)	37(1)	51(1)	32(1)	-7(1)	-1(1)	11(1)
O(2)	31(1)	70(1)	38(1)	-5(1)	-5(1)	15(1)
O(3)	39(1)	37(1)	37(1)	-2(1)	-3(1)	11(1)
O(4)	33(1)	51(1)	35(1)	4(1)	-5(1)	11(1)

---

Table 11.25. Hydrogen coordinates ( $\times 10^4$ ) and isotropic displacement parameters ( $\text{\AA}^2 \times 10^3$ ) for nct1102.

	x	y	z	U(eq)
H(1)	5674	6883	523	36
H(2A)	2982	7535	668	45
H(2B)	4133	7940	19	45
H(4A)	2297	5277	-821	58
H(4B)	3235	5272	-1635	58
H(4C)	1822	5937	-1554	58
H(5A)	3507	7285	-1939	68
H(5B)	4944	6634	-1935	68
H(5C)	4870	7538	-1368	68
H(8A)	7290	3762	-629	97
H(8B)	7628	3225	-1452	97
H(8C)	5959	3423	-1189	97
H(9A)	8442	5692	-1821	90
H(9B)	9227	4691	-1883	90
H(9C)	8818	5117	-1022	90
H(10A)	5506	4215	-2496	74
H(10B)	7181	4079	-2777	74
H(10C)	6475	5106	-2746	74
H(13)	1307	6248	972	47
H(14)	-561	5242	568	67
H(15)	-30	3685	258	79
H(16)	2386	3150	341	77
H(17)	4264	4146	766	56
H(19)	5625	7485	1693	59
H(20)	5308	8383	2841	67
H(21)	3471	7997	3761	68
H(22)	1972	6705	3516	76
H(23)	2259	5825	2356	58
H(4)	6065	5343	979	59

**(2*R*,5*S*)-5-Benzyl-3-methyl-2-(2-phenylpropan-2-yl)imidazolidin-4-one 200**

Table 11.26. Crystal data and structure refinement for tomp\_jhr631.

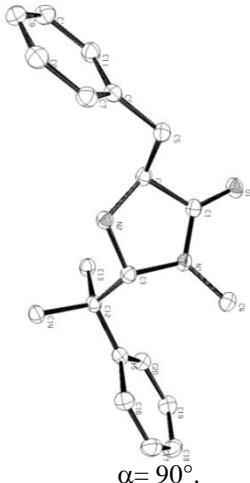
Identification code	tomp_jhr631		
Empirical formula	C <sub>20</sub> H <sub>24</sub> N <sub>2</sub> O		
Formula weight	308.41		
Temperature	123(2) K		
Wavelength	1.54180 Å		
Crystal system	Monoclinic		
Space group	P2 <sub>1</sub>		
Unit cell dimensions	a = 6.0870(3) Å b = 13.3602(6) Å c = 10.3790(5) Å		α = 90°. β = 90.361(4)°. γ = 90°.
Volume	844.04(7) Å <sup>3</sup>		
Z	2		
Density (calculated)	1.214 Mg/m <sup>3</sup>		
Absorption coefficient	0.584 mm <sup>-1</sup>		
F(000)	332		
Crystal size	0.35 x 0.10 x 0.05 mm <sup>3</sup>		
Theta range for data collection	4.26 to 73.46°.		
Index ranges	-7 ≤ h ≤ 7, -16 ≤ k ≤ 16, -12 ≤ l ≤ 12		
Reflections collected	6677		
Independent reflections	2857 [R(int) = 0.0399]		
Completeness to theta = 70.00°	100.0%		
Absorption correction	Semi-empirical from equivalents		
Max. and min. transmission	1.00000 and 0.77032		
Refinement method	Full-matrix least-squares on F <sup>2</sup>		
Data / restraints / parameters	2857 / 1 / 215		
Goodness-of-fit on F <sup>2</sup>	1.073		
Final R indices [I > 2σ(I)]	R1 = 0.0441, wR2 = 0.1070		
R indices (all data)	R1 = 0.0487, wR2 = 0.1105		
Absolute structure parameter	-0.3(4)		
Largest diff. peak and hole	0.209 and -0.206 e.Å <sup>-3</sup>		

Table 11.27. Atomic coordinates ( $\times 10^4$ ) and equivalent isotropic displacement parameters ( $\text{\AA}^2 \times 10^3$ ) for *tomp\_jhr631*.  $U(\text{eq})$  is defined as one third of the trace of the orthogonalized  $U^{\text{ij}}$  tensor.

	x	y	z	$U(\text{eq})$
O(1)	-1581(2)	7100(1)	7770(2)	37(1)
N(1)	1307(3)	7391(1)	6414(2)	28(1)
N(2)	3887(3)	6283(2)	7228(2)	29(1)
C(1)	287(3)	6927(2)	7390(2)	29(1)
C(2)	1868(4)	6173(2)	7976(2)	29(1)
C(3)	3512(3)	6990(2)	6177(2)	28(1)
C(4)	420(4)	8295(2)	5831(2)	35(1)
C(5)	2130(4)	6397(2)	9414(2)	33(1)
C(6)	3608(4)	5677(2)	10126(2)	30(1)
C(7)	5702(4)	5967(2)	10542(2)	35(1)
C(8)	7047(4)	5301(2)	11196(2)	39(1)
C(9)	6347(4)	4340(2)	11441(2)	40(1)
C(10)	4266(5)	4043(2)	11037(3)	41(1)
C(11)	2928(4)	4707(2)	10385(2)	36(1)
C(12)	3753(3)	6475(2)	4832(2)	28(1)
C(13)	2253(4)	5555(2)	4758(2)	33(1)
C(14)	6138(4)	6102(2)	4750(2)	32(1)
C(15)	3275(4)	7237(2)	3770(2)	29(1)
C(16)	4662(4)	8062(2)	3596(2)	36(1)
C(17)	4197(5)	8792(2)	2702(3)	43(1)
C(18)	2332(5)	8731(2)	1935(3)	42(1)
C(19)	950(4)	7926(2)	2079(2)	40(1)
C(20)	1426(4)	7178(2)	2973(2)	34(1)

Table 11.28. Bond lengths [ $\text{\AA}$ ] and angles [ $^\circ$ ] for *tomp\_jhr631*.

O(1)-C(1)	1.228(3)
N(1)-C(1)	1.343(3)
N(1)-C(4)	1.454(3)
N(1)-C(3)	1.467(3)
N(2)-C(3)	1.459(3)

---

N(2)-C(2)	1.466(3)
N(2)-H(1N)	0.85(3)
C(1)-C(2)	1.517(3)
C(2)-C(5)	1.530(3)
C(2)-H(2)	1.0000
C(3)-C(12)	1.564(3)
C(3)-H(3)	1.0000
C(4)-H(4A)	0.9800
C(4)-H(4B)	0.9800
C(4)-H(4C)	0.9800
C(5)-C(6)	1.508(3)
C(5)-H(5A)	0.9900
C(5)-H(5B)	0.9900
C(6)-C(11)	1.387(4)
C(6)-C(7)	1.398(3)
C(7)-C(8)	1.385(4)
C(7)-H(7)	0.9500
C(8)-C(9)	1.376(4)
C(8)-H(8)	0.9500
C(9)-C(10)	1.390(4)
C(9)-H(9)	0.9500
C(10)-C(11)	1.379(4)
C(10)-H(10)	0.9500
C(11)-H(11)	0.9500
C(12)-C(15)	1.528(3)
C(12)-C(13)	1.533(3)
C(12)-C(14)	1.538(3)
C(13)-H(13A)	0.9800
C(13)-H(13B)	0.9800
C(13)-H(13C)	0.9800
C(14)-H(14A)	0.9800
C(14)-H(14B)	0.9800
C(14)-H(14C)	0.9800
C(15)-C(20)	1.395(3)
C(15)-C(16)	1.401(3)
C(16)-C(17)	1.374(4)

---

C(16)-H(16)	0.9500
C(17)-C(18)	1.385(4)
C(17)-H(17)	0.9500
C(18)-C(19)	1.374(4)
C(18)-H(18)	0.9500
C(19)-C(20)	1.393(4)
C(19)-H(19)	0.9500
C(20)-H(20)	0.9500
C(1)-N(1)-C(4)	121.65(19)
C(1)-N(1)-C(3)	112.70(18)
C(4)-N(1)-C(3)	124.9(2)
C(3)-N(2)-C(2)	109.49(17)
C(3)-N(2)-H(1N)	111(2)
C(2)-N(2)-H(1N)	112(2)
O(1)-C(1)-N(1)	126.0(2)
O(1)-C(1)-C(2)	125.7(2)
N(1)-C(1)-C(2)	108.27(18)
N(2)-C(2)-C(1)	104.63(19)
N(2)-C(2)-C(5)	114.49(18)
C(1)-C(2)-C(5)	108.85(19)
N(2)-C(2)-H(2)	109.6
C(1)-C(2)-H(2)	109.6
C(5)-C(2)-H(2)	109.6
N(2)-C(3)-N(1)	104.45(17)
N(2)-C(3)-C(12)	111.54(19)
N(1)-C(3)-C(12)	113.63(18)
N(2)-C(3)-H(3)	109.0
N(1)-C(3)-H(3)	109.0
C(12)-C(3)-H(3)	109.0
N(1)-C(4)-H(4A)	109.5
N(1)-C(4)-H(4B)	109.5
H(4A)-C(4)-H(4B)	109.5
N(1)-C(4)-H(4C)	109.5
H(4A)-C(4)-H(4C)	109.5
H(4B)-C(4)-H(4C)	109.5



C(6)-C(5)-C(2)	114.3(2)
C(6)-C(5)-H(5A)	108.7
C(2)-C(5)-H(5A)	108.7
C(6)-C(5)-H(5B)	108.7
C(2)-C(5)-H(5B)	108.7
H(5A)-C(5)-H(5B)	107.6
C(11)-C(6)-C(7)	118.2(2)
C(11)-C(6)-C(5)	120.9(2)
C(7)-C(6)-C(5)	120.9(2)
C(8)-C(7)-C(6)	120.5(2)
C(8)-C(7)-H(7)	119.7
C(6)-C(7)-H(7)	119.7
C(9)-C(8)-C(7)	120.5(2)
C(9)-C(8)-H(8)	119.7
C(7)-C(8)-H(8)	119.7
C(8)-C(9)-C(10)	119.5(2)
C(8)-C(9)-H(9)	120.2
C(10)-C(9)-H(9)	120.2
C(11)-C(10)-C(9)	119.9(3)
C(11)-C(10)-H(10)	120.0
C(9)-C(10)-H(10)	120.0
C(10)-C(11)-C(6)	121.3(2)
C(10)-C(11)-H(11)	119.3
C(6)-C(11)-H(11)	119.3
C(15)-C(12)-C(13)	112.81(18)
C(15)-C(12)-C(14)	110.57(18)
C(13)-C(12)-C(14)	107.43(19)
C(15)-C(12)-C(3)	109.40(19)
C(13)-C(12)-C(3)	109.82(18)
C(14)-C(12)-C(3)	106.62(18)
C(12)-C(13)-H(13A)	109.5
C(12)-C(13)-H(13B)	109.5
H(13A)-C(13)-H(13B)	109.5
C(12)-C(13)-H(13C)	109.5
H(13A)-C(13)-H(13C)	109.5
H(13B)-C(13)-H(13C)	109.5

C(12)-C(14)-H(14A)	109.5
C(12)-C(14)-H(14B)	109.5
H(14A)-C(14)-H(14B)	109.5
C(12)-C(14)-H(14C)	109.5
H(14A)-C(14)-H(14C)	109.5
H(14B)-C(14)-H(14C)	109.5
C(20)-C(15)-C(16)	116.9(2)
C(20)-C(15)-C(12)	122.6(2)
C(16)-C(15)-C(12)	120.4(2)
C(17)-C(16)-C(15)	121.6(2)
C(17)-C(16)-H(16)	119.2
C(15)-C(16)-H(16)	119.2
C(16)-C(17)-C(18)	120.8(3)
C(16)-C(17)-H(17)	119.6
C(18)-C(17)-H(17)	119.6
C(19)-C(18)-C(17)	118.9(3)
C(19)-C(18)-H(18)	120.6
C(17)-C(18)-H(18)	120.6
C(18)-C(19)-C(20)	120.6(2)
C(18)-C(19)-H(19)	119.7
C(20)-C(19)-H(19)	119.7
C(19)-C(20)-C(15)	121.2(2)
C(19)-C(20)-H(20)	119.4
C(15)-C(20)-H(20)	119.4

Table 11.29. Anisotropic displacement parameters ( $\text{\AA}^2 \times 10^3$ ) for *tomp\_jhr631*. The anisotropic displacement factor exponent takes the form:  $-2\pi^2 [ h^2 a^{*2} U^{11} + \dots + 2 h k a^* b^* U^{12} ]$

	$U^{11}$	$U^{22}$	$U^{33}$	$U^{23}$	$U^{13}$	$U^{12}$
O(1)	23(1)	43(1)	45(1)	-1(1)	4(1)	3(1)
N(1)	24(1)	25(1)	36(1)	0(1)	-2(1)	3(1)
N(2)	22(1)	32(1)	33(1)	0(1)	0(1)	1(1)
C(1)	24(1)	28(1)	35(1)	-4(1)	-3(1)	0(1)
C(2)	24(1)	26(1)	39(1)	0(1)	0(1)	0(1)
C(3)	23(1)	28(1)	34(1)	1(1)	-2(1)	0(1)

---

C(4)	35(1)	32(1)	38(1)	1(1)	-4(1)	6(1)
C(5)	34(1)	29(1)	36(1)	-1(1)	4(1)	4(1)
C(6)	31(1)	31(1)	29(1)	0(1)	4(1)	1(1)
C(7)	37(1)	34(2)	35(1)	0(1)	3(1)	-4(1)
C(8)	36(1)	48(2)	34(1)	-3(1)	-3(1)	-1(1)
C(9)	44(1)	45(2)	31(1)	7(1)	-1(1)	11(1)
C(10)	47(2)	34(1)	43(1)	6(1)	7(1)	1(1)
C(11)	31(1)	35(1)	41(1)	0(1)	4(1)	-1(1)
C(12)	22(1)	27(1)	34(1)	-1(1)	2(1)	-1(1)
C(13)	31(1)	27(1)	42(1)	-3(1)	1(1)	-1(1)
C(14)	27(1)	35(1)	36(1)	-2(1)	4(1)	2(1)
C(15)	27(1)	32(1)	30(1)	-4(1)	2(1)	-2(1)
C(16)	33(1)	37(1)	39(1)	-1(1)	-3(1)	-5(1)
C(17)	48(2)	37(2)	43(1)	3(1)	4(1)	-9(1)
C(18)	54(2)	39(2)	34(1)	6(1)	-1(1)	7(1)
C(19)	39(1)	46(2)	33(1)	-5(1)	-6(1)	2(1)
C(20)	34(1)	35(1)	33(1)	-3(1)	-1(1)	-3(1)

---

Table 11.30. Hydrogen coordinates ( $\times 10^4$ ) and isotropic displacement parameters ( $\text{\AA}^2 \times 10^3$ ) for temp\_jhr631.

	x	y	z	U(eq)
H(2)	1269	5482	7859	35
H(3)	4606	7546	6247	34
H(4A)	-769	8556	6368	52
H(4B)	-154	8140	4970	52
H(4C)	1584	8799	5764	52
H(5A)	2728	7082	9515	40
H(5B)	661	6385	9818	40
H(7)	6206	6627	10375	42
H(8)	8463	5508	11478	47
H(9)	7280	3883	11883	48
H(10)	3766	3383	11209	49
H(11)	1511	4496	10107	43
H(13A)	2408	5236	3913	50
H(13B)	724	5762	4878	50
H(13C)	2669	5079	5434	50
H(14A)	7145	6670	4841	49
H(14B)	6370	5778	3914	49
H(14C)	6420	5619	5442	49
H(16)	5955	8118	4108	43
H(17)	5166	9344	2609	51
H(18)	2013	9238	1320	51
H(19)	-342	7880	1564	47
H(20)	474	6617	3041	41
H(1N)	4960(50)	6470(30)	7690(30)	50(9)

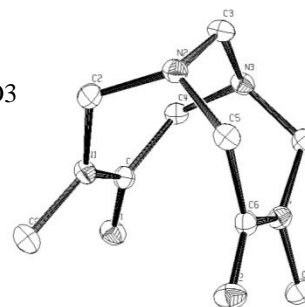
**3,8-Dimethyl-1,3,6,8-tetraaza-bicyclo[4.4.1]undecane-4,9-dione 218**

Available from the CCDC as deposition number 909956



Crystal data and structure refinement for nct0907.

Identification code	nct0907	
Empirical formula	C <sub>9</sub> H <sub>18</sub> N <sub>4</sub> O <sub>3</sub>	
Formula weight	230.27	
Temperature	150(2) K	
Wavelength	0.71073 Å	
Crystal system	Monoclinic	
Space group	P21/n	
Unit cell dimensions	a = 6.6979(2) Å	α = 90°.
	b = 12.3452(5) Å	β = 103.061(2)°.
	c = 13.8609(4) Å	γ = 90°.
Volume	1116.46(6) Å <sup>3</sup>	
Z	4	
Density (calculated)	1.370 Mg/m <sup>3</sup>	
Absorption coefficient	0.104 mm <sup>-1</sup>	
F(000)	496	
Crystal size	0.30 x 0.10 x 0.04 mm <sup>3</sup>	
Theta range for data collection	3.53 to 27.52°.	
Index ranges	-8 ≤ h ≤ 8, -16 ≤ k ≤ 15, -18 ≤ l ≤ 17	
Reflections collected	4759	
Independent reflections	2553 [R(int) = 0.0532]	
Completeness to theta = 27.52°	99.3%	
Absorption correction	Empirical	
Max. and min. transmission	0.9958 and 0.9694	
Refinement method	Full-matrix least-squares on F <sup>2</sup>	
Data / restraints / parameters	2553 / 0 / 156	
Goodness-of-fit on F <sup>2</sup>	1.048	
Final R indices [I > 2σ(I)]	R1 = 0.0540, wR2 = 0.1145	
R indices (all data)	R1 = 0.0896, wR2 = 0.1291	
Extinction coefficient	0.064(6)	
Largest diff. peak and hole	0.206 and -0.208 e.Å <sup>-3</sup>	

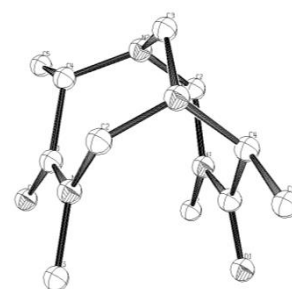


**(-)-(1*S*,5*S*,6*S*,10*S*)-3,5,8,10-Tetramethyl-1,3,6,8-tetraaza-bicyclo[4.4.1]undecane-4,9-dione 219**

Available from the CCDC as deposition number 909953

Crystal data and structure refinement for nct0910.

Identification code	nct0910	
Empirical formula	C <sub>11</sub> H <sub>20</sub> N <sub>4</sub> O <sub>2</sub>	
Formula weight	240.31	
Temperature	150(2) K	
Wavelength	0.71073 Å	
Crystal system	Tetragonal	
Space group	P43212	
Unit cell dimensions	a = 7.9849(3) Å	α = 90°.
	b = 7.9849(3) Å	β = 90°.
	c = 19.6071(8) Å	γ = 90°.
Volume	1250.12(8) Å <sup>3</sup>	
Z	4	
Density (calculated)	1.277 Mg/m <sup>3</sup>	
Absorption coefficient	0.090 mm <sup>-1</sup>	
F(000)	520	
Crystal size	0.40 x 0.20 x 0.05 mm <sup>3</sup>	
Theta range for data collection	3.76 to 27.55°.	
Index ranges	-10 ≤ h ≤ 10, -7 ≤ k ≤ 7, -17 ≤ l ≤ 25	
Reflections collected	2349	
Independent reflections	1446 [R(int) = 0.0256]	
Completeness to theta = 27.55°	99.6%	
Absorption correction	Empirical	
Max. and min. transmission	0.9955 and 0.9648	
Refinement method	Full-matrix least-squares on F <sup>2</sup>	
Data / restraints / parameters	1446 / 0 / 85	
Goodness-of-fit on F <sup>2</sup>	1.020	
Final R indices [I > 2σ(I)]	R1 = 0.0414, wR2 = 0.1043	
R indices (all data)	R1 = 0.0507, wR2 = 0.1118	
Absolute structure parameter	0(2)	
Extinction coefficient	0.112(13)	
Largest diff. peak and hole	0.184 and -0.170 e.Å <sup>-3</sup>	

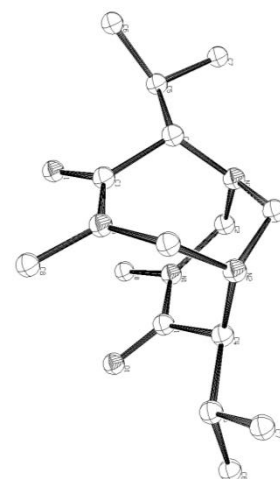


**(-)-(1*S*,5*S*,6*S*,10*S*)-5,10-Diisopropyl-3,8-dimethyl-1,3,6,8-tetraaza-bicyclo[4.4.1]undecane-4,9-dione 200**

Available from the CCDC as deposition number 909954.

Crystal data and structure refinement for nct0908.

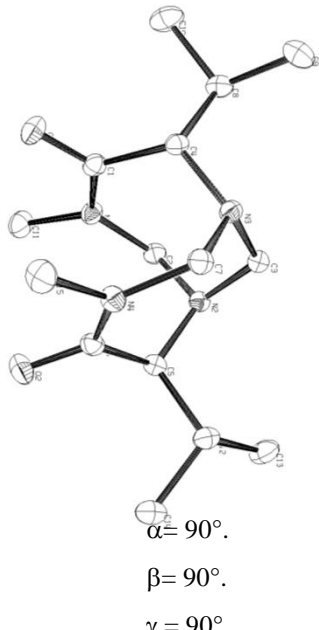
Identification code	nct0908	
Empirical formula	C <sub>15</sub> H <sub>28</sub> N <sub>4</sub> O <sub>2</sub>	
Formula weight	296.41	
Temperature	150(2) K	
Wavelength	0.71073 Å	
Crystal system	Orthorhombic	
Space group	C2221	
Unit cell dimensions	a = 8.1565(8) Å	α = 90°.
	b = 12.7760(15) Å	β = 90°.
	c = 15.5401(17) Å	γ = 90°.
Volume	1619.4(3) Å <sup>3</sup>	
Z	4	
Density (calculated)	1.216 Mg/m <sup>3</sup>	
Absorption coefficient	0.082 mm <sup>-1</sup>	
F(000)	648	
Crystal size	0.30 x 0.08 x 0.05 mm <sup>3</sup>	
Theta range for data collection	3.96 to 24.75°.	
Index ranges	-9 ≤ h ≤ 9, -14 ≤ k ≤ 14, -18 ≤ l ≤ 18	
Reflections collected	1325	
Independent reflections	1325 [R(int) = 0.0000]	
Completeness to theta = 24.75°	96.8%	
Absorption correction	Empirical	
Max. and min. transmission	0.9959 and 0.9757	
Refinement method	Full-matrix least-squares on F <sup>2</sup>	
Data / restraints / parameters	1325 / 1 / 102	
Goodness-of-fit on F <sup>2</sup>	1.068	
Final R indices [I > 2σ(I)]	R1 = 0.0775, wR2 = 0.1471	
R indices (all data)	R1 = 0.1156, wR2 = 0.1639	
Absolute structure parameter	5(4)	
Largest diff. peak and hole	0.183 and -0.212 e.Å <sup>-3</sup>	



**(+)-(1*R*,5*S*,6*R*,10*S*)-5,10-Diisopropyl-3,8-dimethyl-1,3,6,8-tetraaza-bicyclo[4.4.1]undecane-4,9-dione 201**

Available from the CCDC as deposition number 909955.

Crystal data and structure refinement for nct0906.

Identification code	nct0906	
Empirical formula	C <sub>15</sub> H <sub>28</sub> N <sub>4</sub> O <sub>2</sub>	
Formula weight	296.41	
Temperature	150(2) K	
Wavelength	0.71073 Å	
Crystal system	Orthorhombic	
Space group	P212121	
Unit cell dimensions	a = 14.0399(3) Å b = 8.1422(2) Å c = 14.4418(3) Å	
Volume	1650.92(6) Å <sup>3</sup>	
Z	4	
Density (calculated)	1.193 Mg/m <sup>3</sup>	
Absorption coefficient	0.081 mm <sup>-1</sup>	
F(000)	648	
Crystal size	0.35 x 0.30 x 0.08 mm <sup>3</sup>	
Theta range for data collection	3.17 to 27.48°.	
Index ranges	-18 ≤ h ≤ 18, -10 ≤ k ≤ 10, -18 ≤ l ≤ 18	
Reflections collected	3767	
Independent reflections	3767 [R(int) = 0.0300]	
Completeness to theta = 27.48°	99.6%	
Absorption correction	Empirical	
Max. and min. transmission	0.9936 and 0.9723	
Refinement method	Full-matrix least-squares on F <sup>2</sup>	
Data / restraints / parameters	3767 / 0 / 197	
Goodness-of-fit on F <sup>2</sup>	1.036	
Final R indices [I > 2σ(I)]	R1 = 0.0450, wR2 = 0.0982	
R indices (all data)	R1 = 0.0570, wR2 = 0.1057	
Absolute structure parameter	-1.5(14)	
Extinction coefficient	0.104(5)	
Largest diff. peak and hole	0.166 and -0.153 e.Å <sup>-3</sup>	

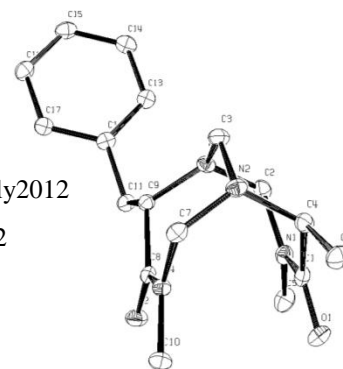


**(-)-(1*S*,5*S*,6*S*,10*S*)-5-Benzyl-3,8,10-trimethyl-1,3,6,8-tetraazabicyclo[4.4.1]undecane-4,9-dione 204**

Available from the CCDC as deposition number 908491.

Crystal data and structure refinement for tompkin\_jul\_july2012.

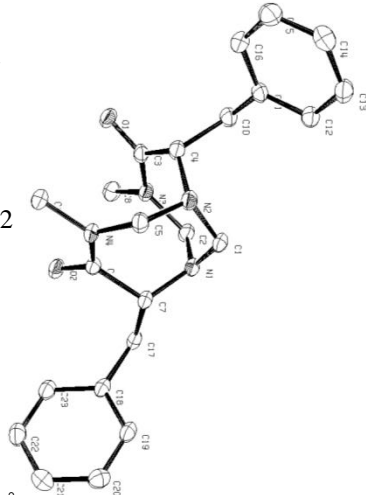
Identification code	tompkin_jul_july2012	
Empirical formula	C <sub>17</sub> H <sub>24</sub> N <sub>4</sub> O <sub>2</sub>	
Formula weight	316.40	
Temperature	123(2) K	
Wavelength	1.54180 Å	
Crystal system	Orthorhombic	
Space group	P2 <sub>1</sub> 2 <sub>1</sub> 2 <sub>1</sub>	
Unit cell dimensions	a = 8.5300(3) Å	α = 90°.
	b = 12.4076(4) Å	β = 90°.
	c = 15.1863(7) Å	γ = 90°.
Volume	1607.27(11) Å <sup>3</sup>	
Z	4	
Density (calculated)	1.308 Mg/m <sup>3</sup>	
Absorption coefficient	0.708 mm <sup>-1</sup>	
F(000)	680	
Crystal size	0.35 x 0.25 x 0.15 mm <sup>3</sup>	
Theta range for data collection	4.60 to 73.43°.	
Index ranges	-8 ≤ h ≤ 10, -15 ≤ k ≤ 15, -18 ≤ l ≤ 18	
Reflections collected	7943	
Independent reflections	3080 [R(int) = 0.0204]	
Completeness to theta = 70.00°	96.9%	
Absorption correction	Semi-empirical from equivalents	
Max. and min. transmission	1.00000 and 0.85183	
Refinement method	Full-matrix least-squares on F <sup>2</sup>	
Data / restraints / parameters	3080 / 0 / 211	
Goodness-of-fit on F <sup>2</sup>	1.154	
Final R indices [I > 2σ(I)]	R1 = 0.0387, wR2 = 0.1035	
R indices (all data)	R1 = 0.0444, wR2 = 0.1165	
Absolute structure parameter	-0.1(3)	
Largest diff. peak and hole	0.204 and -0.274 e.Å <sup>-3</sup>	

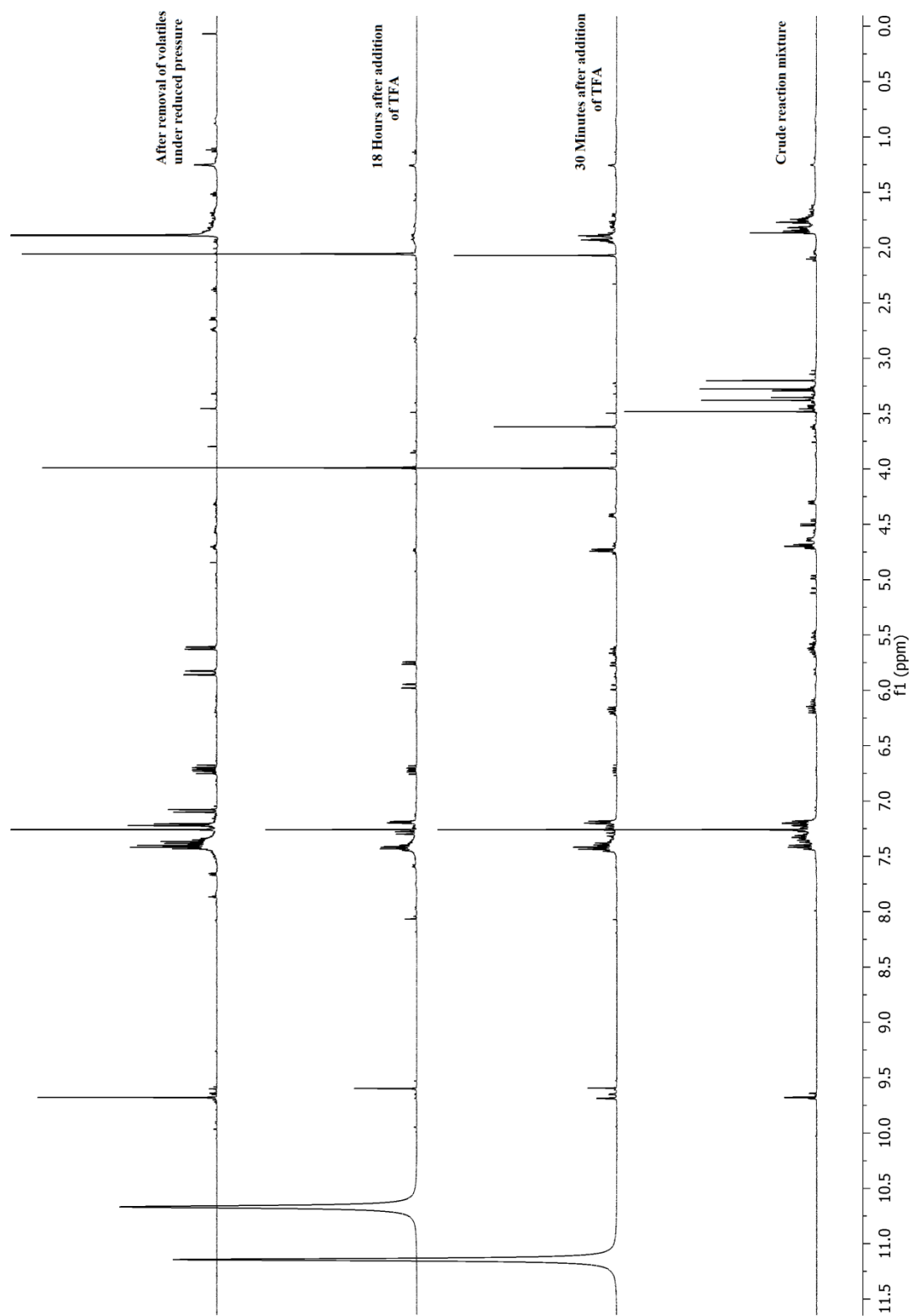


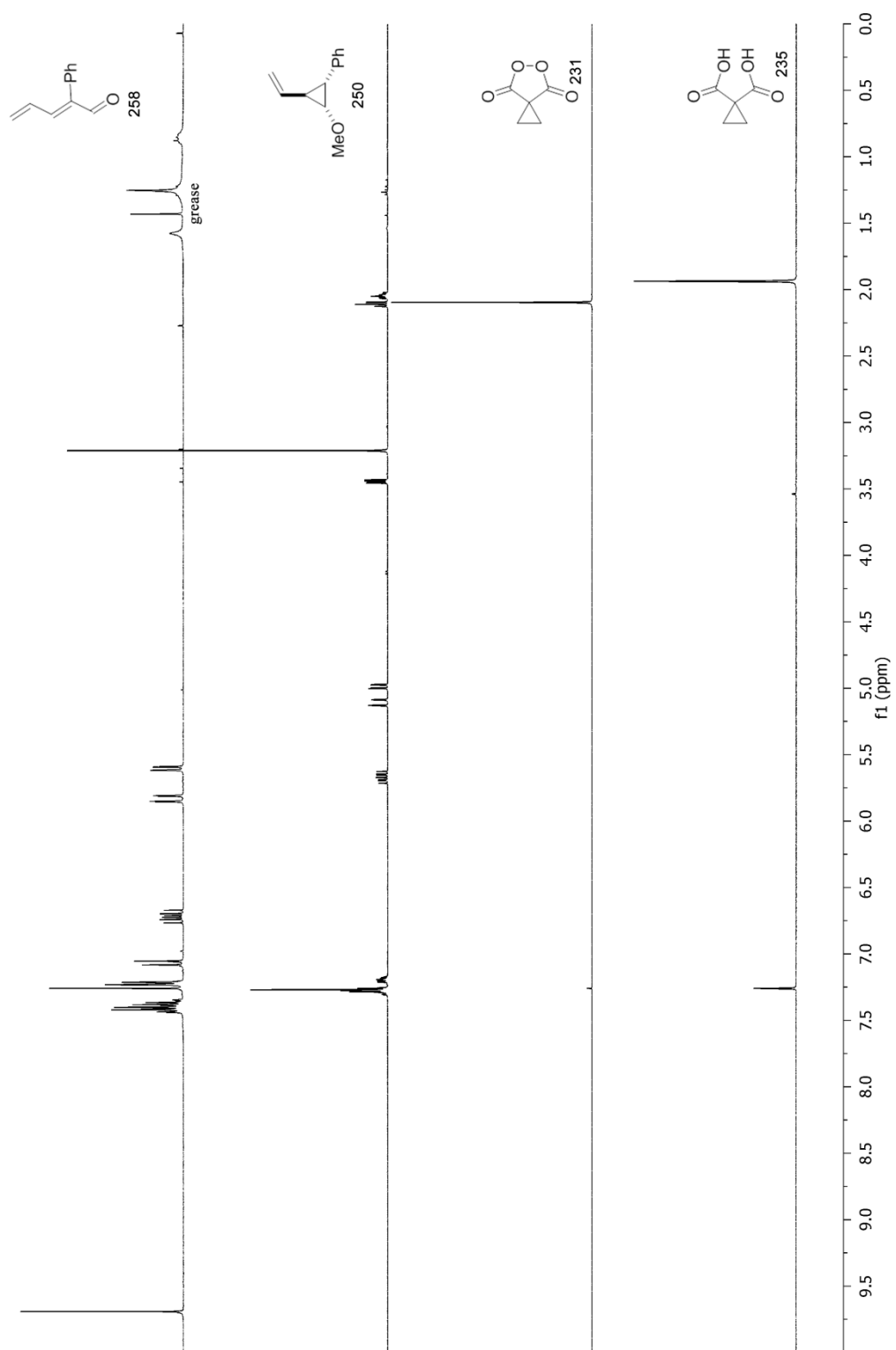
**(±)-5,10-Dibenzyl-3,8-dimethyl-1,3,6,8-tetraaza-bicyclo[4.4.1]undecane-4,9-dione 205**

Available from the CCDC as deposition number 908492.

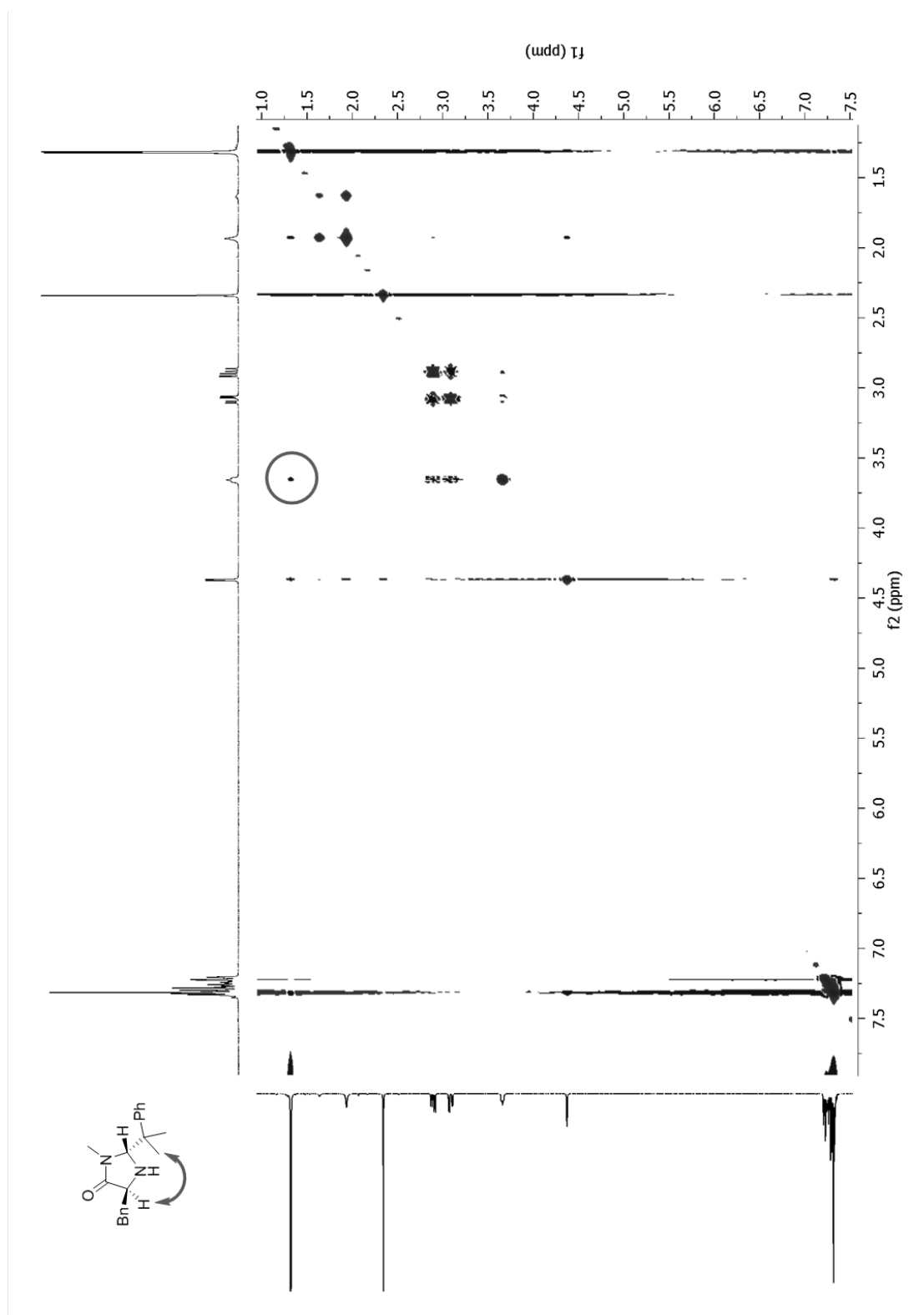
Crystal data and structure refinement for tompkin2012.

Identification code	tompkin2012		
Empirical formula	C <sub>23</sub> H <sub>28</sub> N <sub>4</sub> O <sub>2</sub>		
Formula weight	392.49		
Temperature	123(2) K		
Wavelength	1.54180 Å		
Crystal system	Monoclinic		
Space group	P2 <sub>1</sub> /c		
Unit cell dimensions	a = 15.0424(7) Å		$\alpha = 90^\circ$ .
	b = 11.6660(4) Å		$\beta = 111.569(5)^\circ$ .
	c = 12.3412(5) Å		$\gamma = 90^\circ$ .
Volume	2014.04(14) Å <sup>3</sup>		
Z	4		
Density (calculated)	1.294 Mg/m <sup>3</sup>		
Absorption coefficient	0.672 mm <sup>-1</sup>		
F(000)	840		
Crystal size	0.28 x 0.18 x 0.05 mm <sup>3</sup>		
Theta range for data collection	7.38 to 69.98°.		
Index ranges	-14 ≤ h ≤ 18, -13 ≤ k ≤ 14, -15 ≤ l ≤ 13		
Reflections collected	8335		
Independent reflections	3785 [R(int) = 0.0799]		
Completeness to theta = 69.98°	99.1%		
Absorption correction	Semi-empirical from equivalents		
Max. and min. transmission	1.00000 and 0.83381		
Refinement method	Full-matrix least-squares on F <sup>2</sup>		
Data / restraints / parameters	3785 / 0 / 264		
Goodness-of-fit on F <sup>2</sup>	1.097		
Final R indices [I > 2σ(I)]	R1 = 0.0809, wR2 = 0.2029		
R indices (all data)	R1 = 0.1001, wR2 = 0.2153		
Largest diff. peak and hole	0.438 and -0.254 e.Å <sup>-3</sup>		

11.2 Appendix B:  $^1\text{H}$  NMR Spectra for Radical Clock Reaction

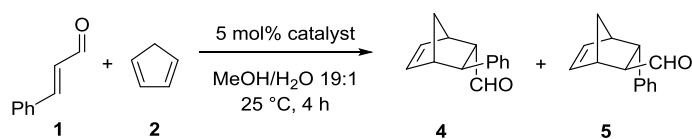


## 11.3 Appendix C: NOESY NMR Spectrum for 200

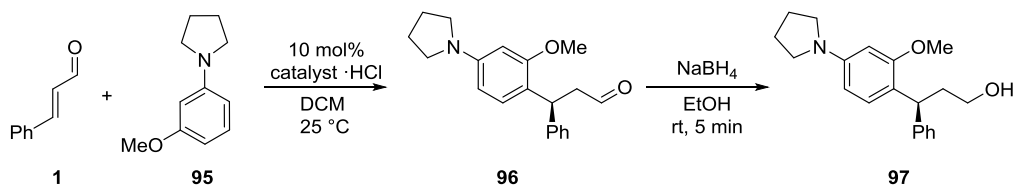


## 11.4 Appendix D: Crude Data from Reaction Monitoring

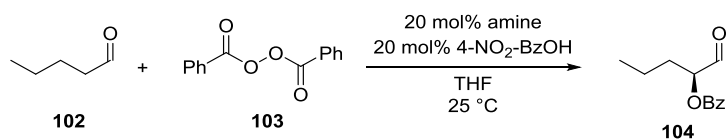
## 11.4.1 Data from Chapter 2



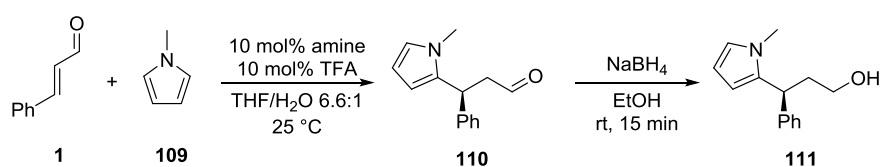
Time /Minutes	Reaction Conversion/%					
	3·HCl	3·HCl	Average	38·HCl	38·HCl	Average
0	0	0	0	0	0	0
15	4.5	4.7	4.6	33	33	33
30	9	9	9	58	56	57
45	14	12	13	75	72	73.5
60	17	17	17	85	83	84
90	24	24	24	93	91	92
120	33	31	32	97	96	96.5
150	37	38	37.5	98	97	97.5
180	45	44	44.5	98.5	98	98.25
210	48	47	47.5	98.7	99	98.85
240	53	52	52.5	99	100	99.5



Time /Minutes	Reaction Conversion/%	
	3·HCl	38·HCl
0	0	0
15	3	1.5
30	6.5	4
60	13	7.5
90	19	11
120	26.5	13.5
150	33.5	17
180	39.5	20
240	50	25.5
300	59.5	30.5
360	67	34.5
420	74	39

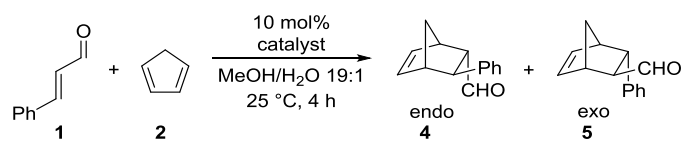


Time /Minutes	Reaction Conversion/%		
	<b>3</b>	<b>38</b>	<b>47</b>
0	0	0	0
60	13.5	0.8	0.5
120	26	1.6	1
240	46	5.5	5.5
360	59	11.5	9.5
480	68	18	16.5



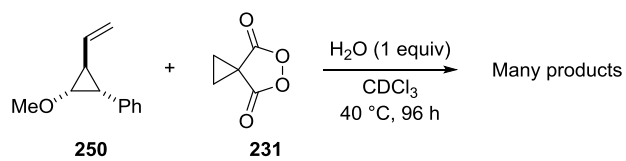
Time /Minutes	Reaction Conversion/%	
	<b>3·TFA</b>	<b>38·TFA</b>
0	0	0
15	21	18.5
30	36	35
60	58	55.5
90	72	67.5
120	81	78
180	91	88
240	96	93
300	98	94.5
360	99	95

## 11.4.2 Data from Chapter 5



Time /Minutes	Reaction Conversion/%		
	155·HCl	3·HCl	160·HCl
0	0	0	0
30	16	16	16
60	31	29	30.5
90	41	40	41
120	51	49	50
180	66	64	65
240	78	75	75

## 11.4.3 Data from Chapter 8



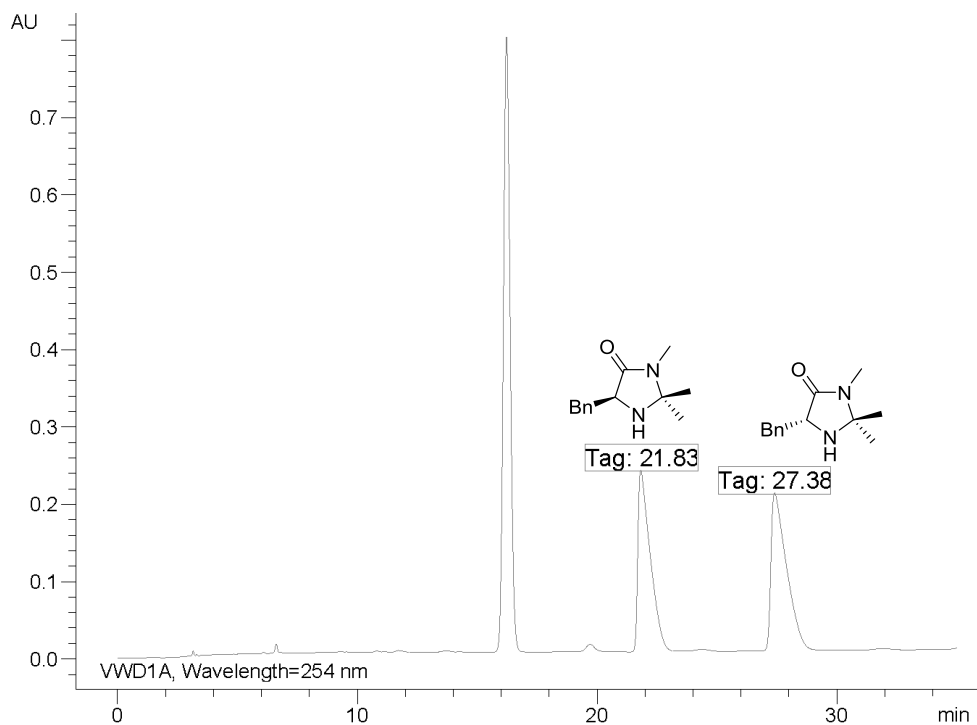
Time /mins	Alkene %	Peroxide %
0	100	100
1	100	100
120	78	70
240	56	52.5
480	38	33
720	28	23.5
2400	8	6.5



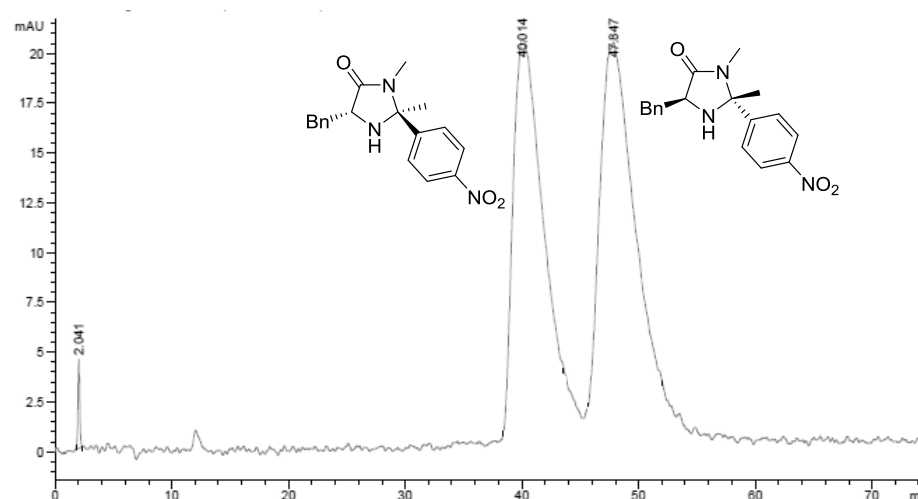
## 11.5 Appendix E: Example HPLC Traces

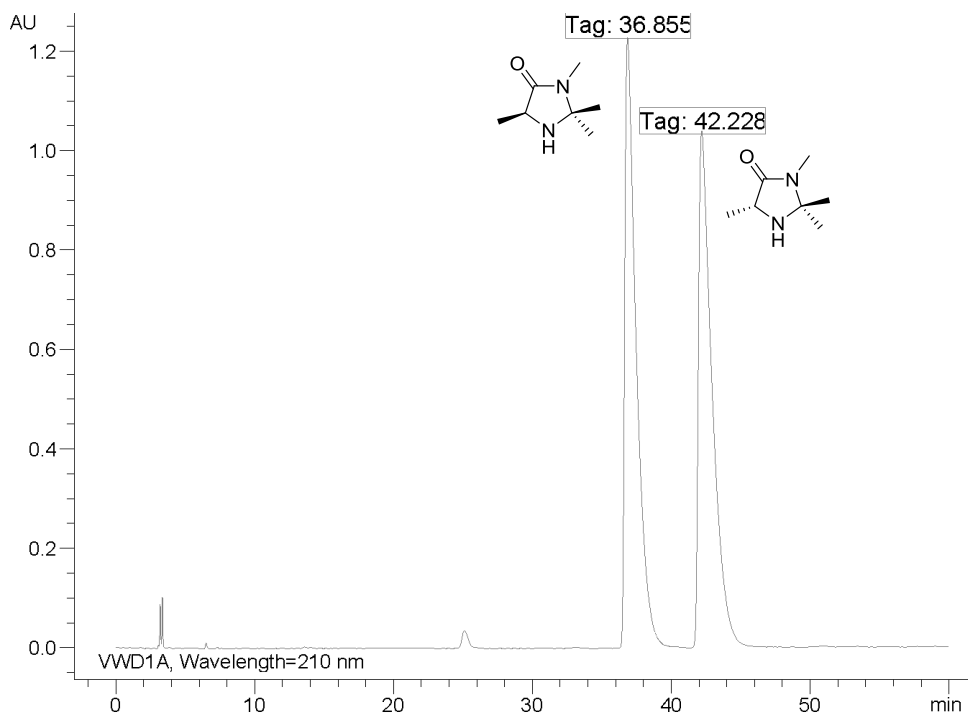
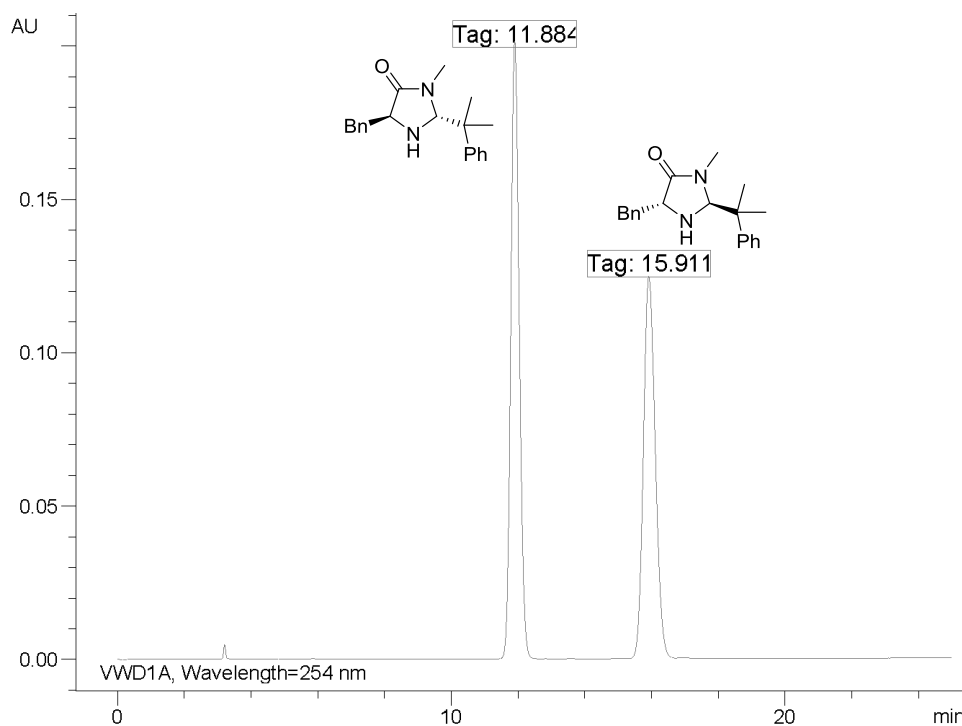
Full details for each separation can be found in Chapter 10

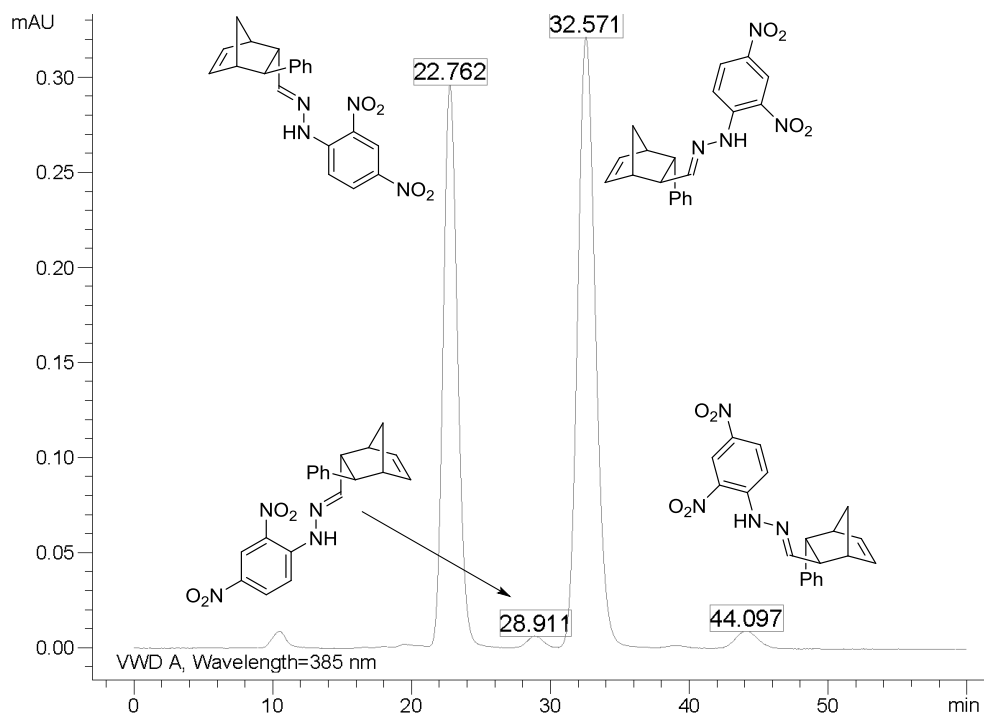
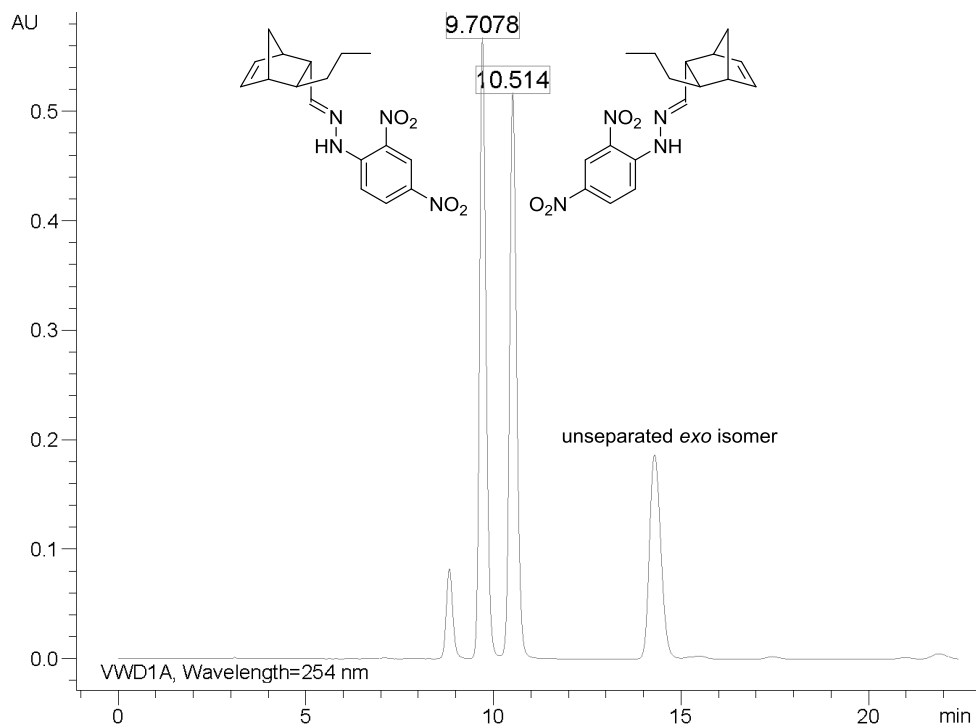
### Enantiomeric Separation of **3**



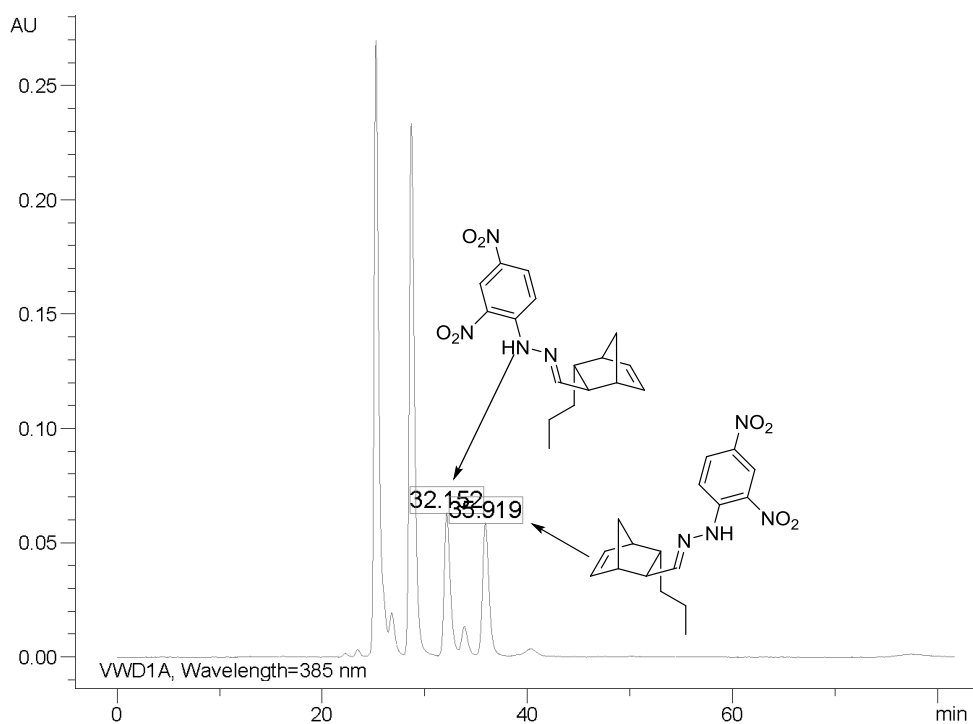
### Enantiomeric Separation of **38**



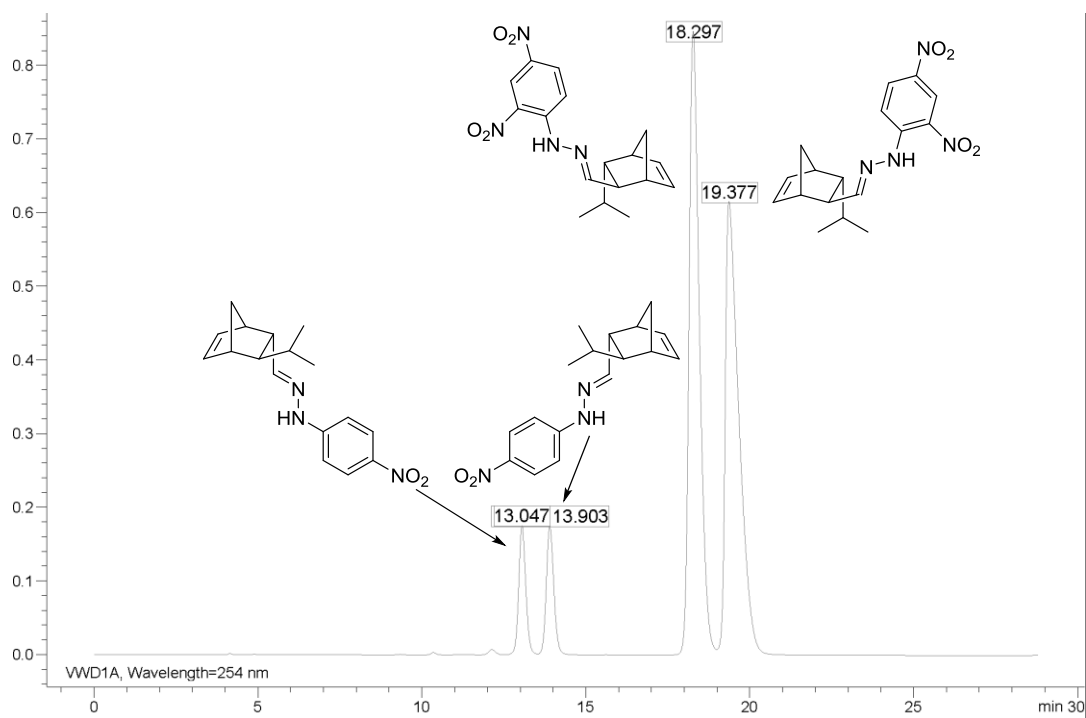
Enantiomeric Separation of **114**Enantiomeric Separation of **200**

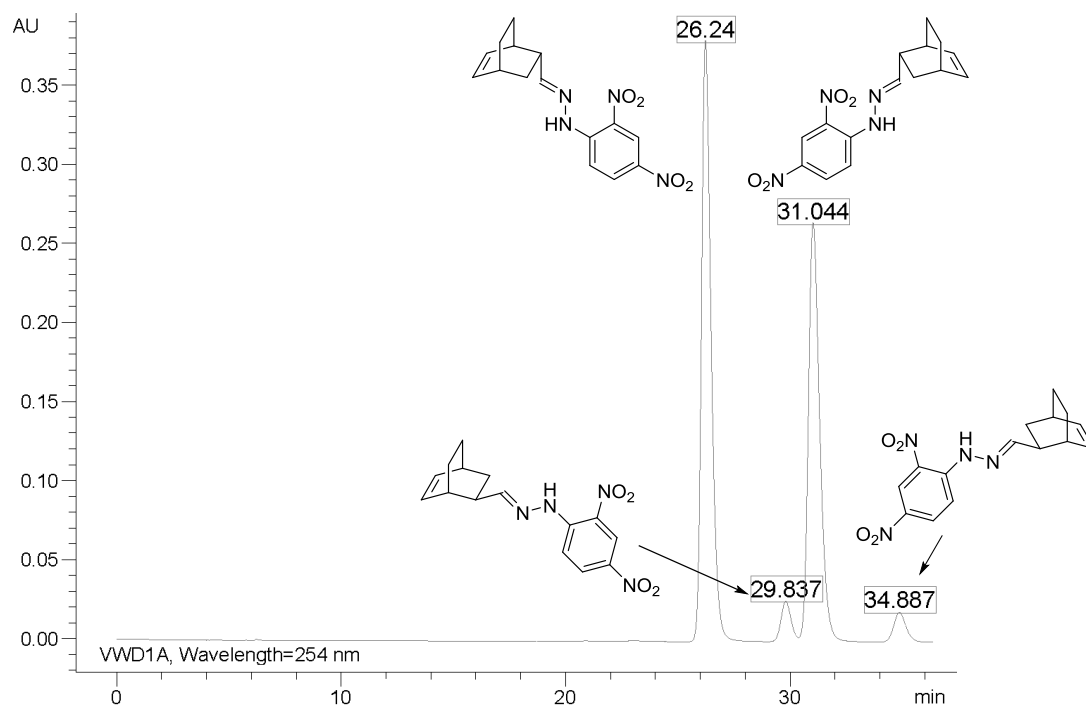
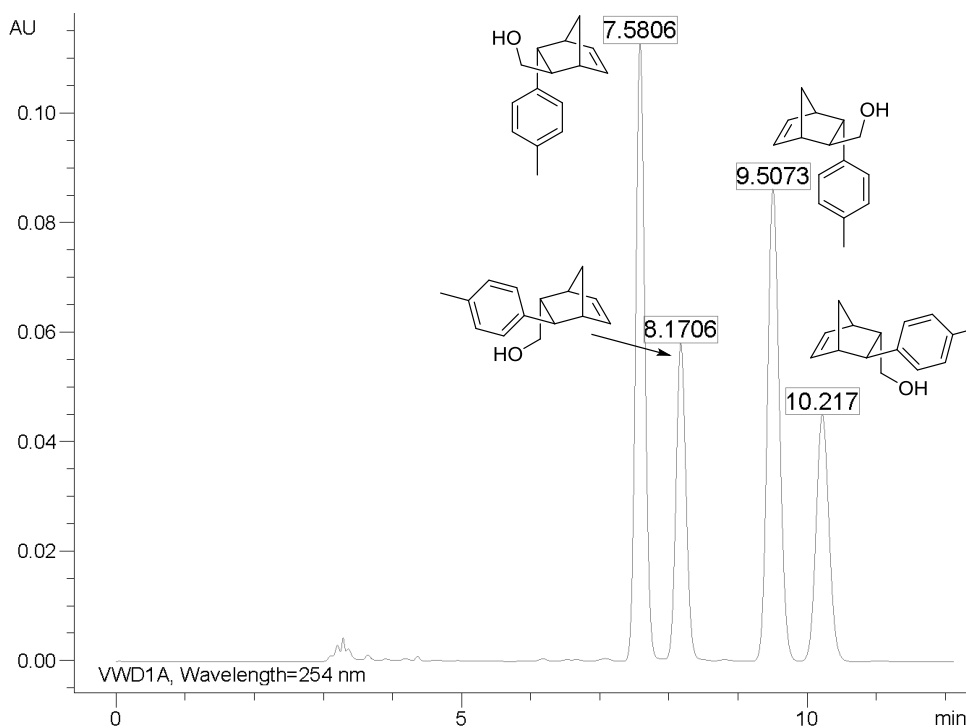
Enantiomeric Separation of 2,4-DNP Hydrazones of **4** and **5**Enantiomeric Separation of 2,4-DNP Hydrazones of **51**

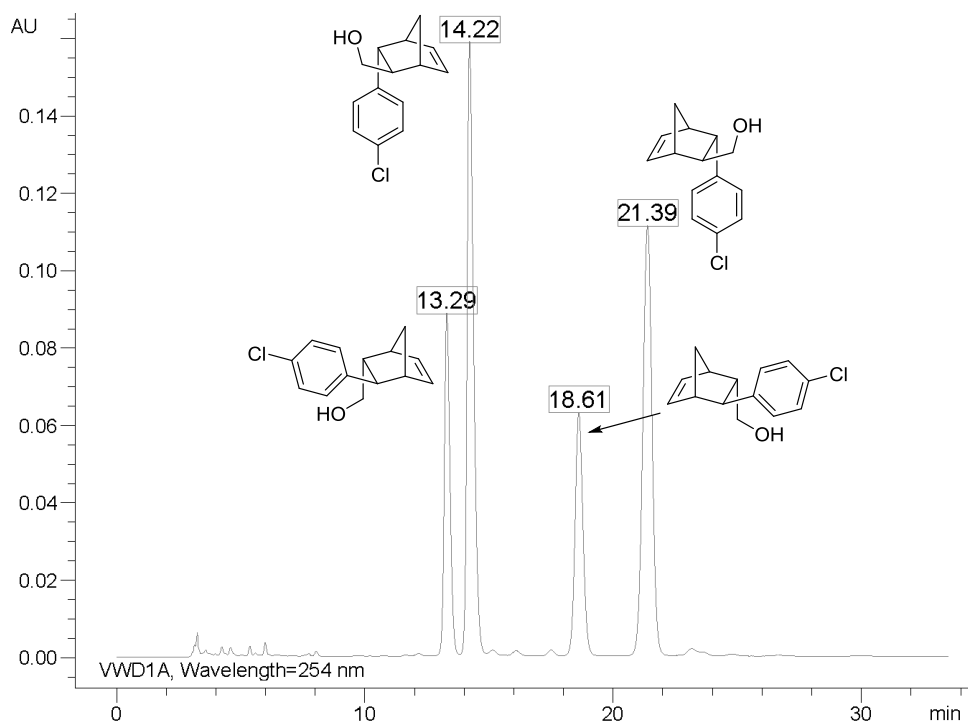
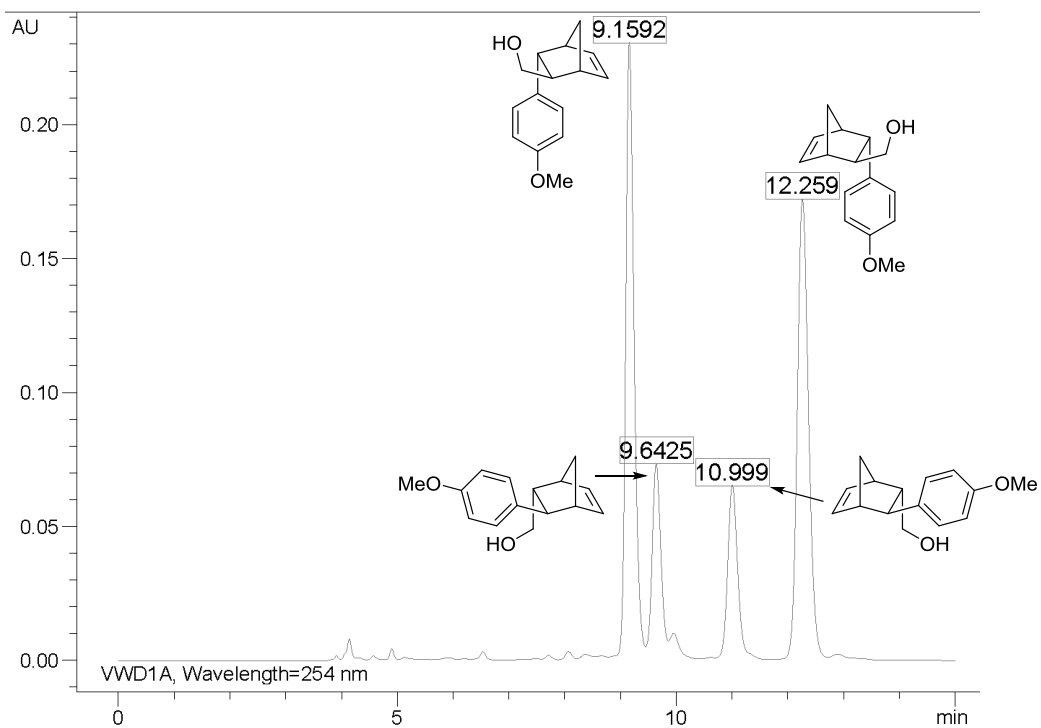
Enantiomeric Separation of 2,4-DNP Hydrazones of **52**

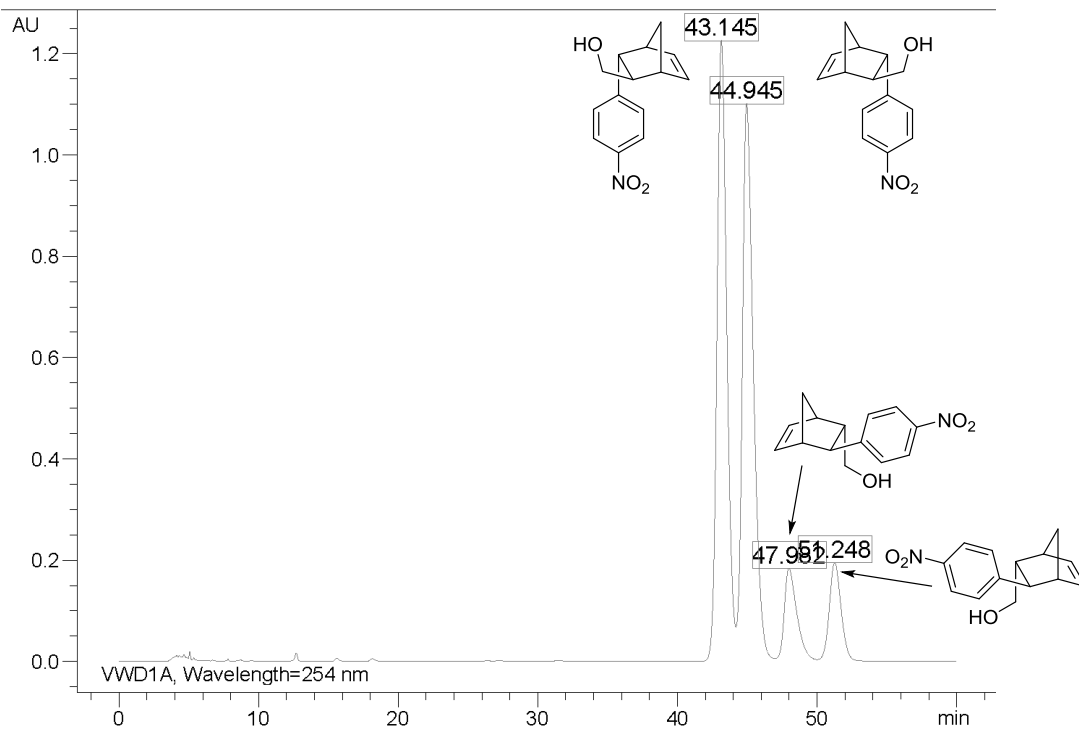


Enantiomeric Separation of 2,4-DNP Hydrazones of **53** and **54**



Enantiomeric Separation of 2,4-DNP Hydrazones of **58** and **59**Enantiomeric Separation of Reduced **73** and **74** as Alcohols

Enantiomeric Separation of Reduced **71** and **72** as AlcoholsEnantiomeric Separation of Reduced **67** and **68** as Alcohols

Enantiomeric Separation of Reduced **69** and **70** as Alcohols

---

## 11.6 Appendix F: Publications from Work Contained within this Thesis To Date

Mechanistic insights into the malonyl peroxide *syn*-dihydroxylation of alkenes”. Michael J. Rawling, Julian H. Rowley, Matthew Campbell, Alan R. Kennedy, John A. Parkinson and Nicholas C. O. Tomkinson, *Chem. Sci.*, 2014, 5, 1777–1785.

“Readily accessible chiral at nitrogen cage structures”. Julian H. Rowley, Sze Chak Yau, Benson M. Kariuki, Alan R. Kennedy and Nicholas C. O. Tomkinson. *Org. Biomol. Chem.*, 2013, 11, 2198–2205.

“Organocatalysed transformations of  $\alpha,\beta$ -unsaturated carbonyl compounds through iminium ion intermediates” Julian H. Rowley and Nicholas C. O. Tomkinson. In: *Asymmetric Synthesis II: More Methods and Applications*, 2012, 29–34.



# References

## 12 References

1. K. A. Ahrendt, C. J. Borths and D. W. C. MacMillan, *J. Am. Chem. Soc.*, **2000**, 122, 4243-4244.
2. E. Knoevenagel, *Ber. Dtsch. Chem. Ges.*, **1898**, 31, 2596-2619.
3. A. Erkkilä, I. Majander and P. M. Pihko, *Chem. Rev.*, **2007**, 107, 5416-5470.
4. D. Seebach, *Angew. Chem. Int. Ed.*, **1990**, 29, 1320-1367.
5. M. Aitken, IMS Health, **2011**.
6. J. H. Clark, *Green Chemistry*, **1999**, 1, 1-8.
7. D. W. C. MacMillan, *Nature*, **2008**, 455, 304-308.
8. M. S. Taylor and E. N. Jacobsen, *Angew. Chem. Int. Ed.*, **2006**, 45, 1520-1543.
9. M. Mahlau and B. List, *Angew. Chem. Int. Ed.*, **2013**, 52, 518-533.
10. S. Mukherjee, J. W. Yang, S. Hoffmann and B. List, *Chem. Rev.*, **2007**, 107, 5471-5569.
11. S. Bertelsen, M. Marigo, S. Brandes, P. Dinér and K. A. Jørgensen, *J. Am. Chem. Soc.*, **2006**, 128, 12973-12980.
12. H.-Y. Jang, J.-B. Hong and D. W. C. MacMillan, *J. Am. Chem. Soc.*, **2007**, 129, 7004-7005.
13. A. B. Northrup and D. W. C. MacMillan, *J. Am. Chem. Soc.*, **2002**, 124, 2458-2460.
14. W. S. Jen, J. J. M. Wiener and D. W. C. MacMillan, *J. Am. Chem. Soc.*, **2000**, 122, 9874-9875.
15. N. A. Paras and D. W. C. MacMillan, *J. Am. Chem. Soc.*, **2001**, 123, 4370-4371.
16. Y. K. Chen, M. Yoshida and D. W. C. MacMillan, *J. Am. Chem. Soc.*, **2006**, 128, 9328-9329.
17. J. F. Austin and D. W. C. MacMillan, *J. Am. Chem. Soc.*, **2002**, 124, 1172-1173.
18. S. G. Ouellet, J. B. Tuttle and D. W. C. MacMillan, *J. Am. Chem. Soc.*, **2004**, 127, 32-33.

19. R. K. Kunz and D. W. C. MacMillan, *J. Am. Chem. Soc.*, **2005**, 127, 3240-3241.
20. K. L. Jensen, G. Dickmeiss, H. Jiang, Ł. Albrecht and K. A. Jørgensen, *Acc. Chem. Res.*, **2011**, 45, 248-264.
21. S. Lakhdar, B. Maji and H. Mayr, *Angew. Chem. Int. Ed.*, **2012**, 51, 5739-5742.
22. J. B. Brazier, G. P. Hopkins, M. Jirari, S. Mutter, R. Pommereuil, L. Samulis, J. A. Platts and N. C. O. Tomkinson, *Tetrahedron Lett.*, **2011**, 52, 2783-2785.
23. T. D. Beeson and D. W. C. MacMillan, *J. Am. Chem. Soc.*, **2005**, 127, 8826-8828.
24. M. P. Brochu, S. P. Brown and D. W. C. MacMillan, *J. Am. Chem. Soc.*, **2004**, 126, 4108-4109.
25. H. Kim and D. W. C. MacMillan, *J. Am. Chem. Soc.*, **2008**, 130, 398-399.
26. T. H. Graham, C. M. Jones, N. T. Jui and D. W. C. MacMillan, *J. Am. Chem. Soc.*, **2008**, 130, 16494-16495.
27. T. D. Beeson, A. Mastracchio, J.-B. Hong, K. Ashton and D. W. C. MacMillan, *Science*, **2007**, 316, 582-585.
28. A. Mastracchio, A. A. Warkentin, A. M. Walji and D. W. C. MacMillan, *PNAS*, **2010**, 107, 20648-20651.
29. A. E. Allen and D. W. C. MacMillan, *J. Am. Chem. Soc.*, **2011**, 133, 4260-4263.
30. E. Skucas and D. W. C. MacMillan, *J. Am. Chem. Soc.*, **2012**, 134, 9090-9093.
31. J. Brazier and N. O. Tomkinson, in *Asymmetric Organocatalysis*, ed. B. List, Springer Berlin Heidelberg, 2009, vol. 291, ch. 28, pp. 281-347.
32. G. Lelais and D. W. MacMillan, *Aldrichimica Acta*, **2006**, 39, 79-87.
33. Q. Ren and J. Wang, *Asian Journal of Organic Chemistry*, **2013**, 2, 542-557.
34. H.-H. Lu, F. Tan and W.-J. Xiao, *Curr. Org. Chem.*, **2011**, 15, 4022-4045.
35. R. Gordillo, J. Carter and K. N. Houk, *Adv. Synth. Catal.*, **2004**, 346, 1175-1185.
36. J. B. Brazier, G. Evans, T. J. K. Gibbs, S. J. Coles, M. B. Hursthouse, J. A. Platts and N. C. O. Tomkinson, *Org. Lett.*, **2009**, 11, 133-136.

37. D. Seebach, R. Gilmour, U. Grošelj, G. Deniau, C. Sparr, M.-O. Ebert, A. K. Beck, L. B. McCusker, D. Šišak and T. Uchimaru, *Helv. Chim. Acta*, **2010**, 93, 603-634.
38. J. B. Brazier, K. M. Jones, J. A. Platts and N. C. O. Tomkinson, *Angew. Chem. Int. Ed.*, **2011**, 50, 1613-1616.
39. G. Evans, T. J. K. Gibbs, R. L. Jenkins, S. J. Coles, M. B. Hursthouse, J. A. Platts and N. C. O. Tomkinson, *Angew. Chem. Int. Ed.*, **2008**, 47, 2820-2823.
40. L. Samulis, Cardiff University, **2011**.
41. T. J. K. Gibbs, Cardiff University, **2008**.
42. J. S. Rao and G. N. Sastry, *Int. J. Quantum Chem*, **2006**, 106, 1217-1224.
43. A. Hall, L. D. Harris, C. L. Jones, R. L. Jenkins and N. C. O. Tomkinson, *Tetrahedron Lett.*, **2003**, 44, 111-114.
44. L. Tichotová, E. Matoušová, M. Špulák, J. Kuneš, I. Votruba, V. Buchta and M. Pour, *Bioorg. Med. Chem. Lett.*, **2011**, 21, 6062-6066.
45. H. Gotoh and Y. Hayashi, *Org. Lett.*, **2007**, 9, 2859-2862.
46. S. El-Fayyoumy, M. H. Todd and C. J. Richards, *Beilstein J. Org. Chem.*, **2009**, 5, 67.
47. U. Grošelj, D. Seebach, D. M. Badine, W. B. Schweizer, A. K. Beck, I. Krossing, P. Klose, Y. Hayashi and T. Uchimaru, *Helv. Chim. Acta*, **2009**, 92, 1225-1259.
48. J. Kulhánek, F. Bureš, O. Pytela, T. Mikysek and J. Ludvík, *Chemistry – An Asian Journal*, **2011**, 6, 1604-1612.
49. N. A. Paras and D. W. C. MacMillan, *J. Am. Chem. Soc.*, **2002**, 124, 7894-7895.
50. M. J. P. Vaismaa, S. C. Yau and N. C. O. Tomkinson, *Tetrahedron Lett.*, **2009**, 50, 3625-3627.
51. S. Lakhdar and H. Mayr, *Chem. Commun.*, **2011**, 47, 1866-1868.
52. G. J. S. Evans, K. White, J. A. Platts and N. C. O. Tomkinson, *Org. Biomol. Chem.*, **2006**, 4, 2616-2627.
53. D. Seebach, U. Grošelj, D. M. Badine, W. B. Schweizer and A. K. Beck, *Helv. Chim. Acta*, **2008**, 91, 1999-2034.

54. U. Grošelj, W. B. Schweizer, M.-O. Ebert and D. Seebach, *Helv. Chim. Acta*, **2009**, 92, 1-13.
55. A. Casoni, E. Borsini, A. Contini, A. Ruffoni, S. Pellegrino and F. Clerici, *Curr. Org. Chem.*, **2011**, 15, 3514-3522.
56. S. M. Kelly and N. C. Price, *Curr. Protein Pept. Sci.*, **2000**, 1, 349-384.
57. K. W. Busch and M. A. Busch, *Chiral Analysis*, Elsevier Science, 2011.
58. T. A. Keiderling, *Curr. Opin. Chem. Biol.*, **2002**, 6, 682-688.
59. D. Clarke, in *Protein Folding, Misfolding, and Disease*, eds. A. F. Hill, K. J. Barnham, S. P. Bottomley and R. Cappai, Humana Press, 2011, vol. 752, ch. 5, pp. 59-72.
60. L. D. Barron and A. D. Buckingham, *Chem. Phys. Lett.*, **2010**, 492, 199-213.
61. P. Bouř, *Chirality*, **2012**, 24, 1096-1096.
62. L. A. Nafie, G.-S. Yu, X. Qu and T. B. Freedman, *Faraday Discuss.*, **1994**, 99, 13-34.
63. C. Johannessen, E. W. Blanch, C. Villani, S. Abbate, G. Longhi, N. R. Agarwal, M. Tommasini and D. A. Lightner, *J. Phys. Chem. B*, **2013**, 117, 2221-2230.
64. F. J. Devlin, P. J. Stephens, C. Österle, K. B. Wiberg, J. R. Cheeseman and M. J. Frisch, *J. Org. Chem.*, **2002**, 67, 8090-8096.
65. T. B. Freedman, X. Cao, R. V. Oliveira, Q. B. Cass and L. A. Nafie, *Chirality*, **2003**, 15, 196-200.
66. M. Pecul, C. Deillon, A. J. Thorvaldsen and K. Ruud, *Journal of Raman Spectroscopy*, **2010**, 41, 1200-1210.
67. P. Zhu, G. Yang, M. R. Poopari, Z. Bie and Y. Xu, *ChemPhysChem*, **2012**, 13, 1272-1281.
68. C. S. Creaser, J. R. Griffiths, C. J. Bramwell, S. Noreen, C. A. Hill and C. L. P. Thomas, *Analyst*, **2004**, 129, 984-994.
69. E. Jurneczko and P. E. Barran, *Analyst*, **2011**, 136, 20-28.
70. C. Uetrecht, R. J. Rose, E. van Duijn, K. Lorenzen and A. J. R. Heck, *Chem. Soc. Rev.*, **2010**, 39, 1633-1655.
71. C. Laphorn, F. Pullen and B. Z. Chowdhry, *Mass Spectrom. Rev.*, **2013**, 32, 43-71.

72. T. Keller, A. Keller, E. Tutsch-Bauer and F. Monticelli, *Forensic Science International*, **2006**, 161, 130-140.
73. V. Wright, F. Castro-Gómez, E. Jurneczko, J. Reynolds, A. Poulton, S. R. Christie, P. Barran, C. Bo and C. Creaser, *Int. J. Ion Mobil. Spec.*, **2013**, 16, 61-67.
74. I. Campuzano, M. F. Bush, C. V. Robinson, C. Beaumont, K. Richardson, H. Kim and H. I. Kim, *Anal. Chem.*, **2011**, 84, 1026-1033.
75. H. Pellissier, *Tetrahedron*, **2012**, 68, 2197-2232.
76. Y. Hayashi, S. Samanta, H. Gotoh and H. Ishikawa, *Angew. Chem.*, **2008**, 120, 6736-6739.
77. C. J. M. Fletcher, *Proc. R. Soc. London, Ser. A*, **1934**, 146, 357-362.
78. L. Samulis and N. C. O. Tomkinson, *Tetrahedron*, **2011**, 67, 4263-4267.
79. J.-F. Zheng, J.-N. Guo, S.-Y. Huang, B. Teng and L.-R. Jin, *Acta Crystallogr. Sect. E.*, **2008**, E64, o1330.
80. A. M. P. Koskinen, H. Hassilla, V. T. Myllymäki and K. Rissanen, *Tetrahedron Lett.*, **1995**, 36, 5619-5622.
81. Matthew M. Zhao, Jing Li, Eiichi Mano, Zhiguo J. Song and D. M. Tschaen, *Org. Synth.*, **2005**, 81, 195-203.
82. S. A. Selkälä, J. Tois, P. M. Pihko and A. M. P. Koskinen, *Adv. Synth. Catal.*, **2002**, 344, 941-945.
83. T. E. Kristensen, K. Vestli, M. G. Jakobsen, F. K. Hansen and T. Hansen, *J. Org. Chem.*, **2010**, 75, 1620-1629.
84. Z.-L. Shen, H.-L. Cheong, Y.-C. Lai, W.-Y. Loo and T.-P. Loh, *Green Chemistry*, **2012**, 14, 2626-2630.
85. Q. Chu, W. Zhang and D. P. Curran, *Tetrahedron Lett.*, **2006**, 47, 9287-9290.
86. A. I. Meyers and B. Santiago, *Tetrahedron Lett.*, **1995**, 36, 5877-5880.
87. R. E. Gawley, S. R. Chemburkar, A. L. Smith and T. V. Anklekar, *J. Org. Chem.*, **1988**, 53, 5381-5383.
88. A. Córdova, W. Zou, P. Dziejczak, I. Ibrahim, E. Reyes and Y. Xu, *Chemistry – A European Journal*, **2006**, 12, 5383-5397.
89. M. Oshita, T. Okazaki, K. Ohe and N. Chatani, *Org. Lett.*, **2004**, 7, 331-334.
90. J.-C. Kizirian, *Chem. Rev.*, **2007**, 108, 140-205.

91. M. J. Dearden, C. R. Firkin, J.-P. R. Hermet and P. O'Brien, *J. Am. Chem. Soc.*, **2002**, 124, 11870-11871.
92. S.-s. Jew and H.-g. Park, *Chem. Commun.*, **2009**, 7090-7103.
93. B. T. Smith, J. A. Wendt and J. Aubé, *Org. Lett.*, **2002**, 4, 2577-2579.
94. G. P. Semeluk and R. B. Bernstein, *J. Am. Chem. Soc.*, **1954**, 76, 3793-3796.
95. V. Prelog and P. Wieland, *Helv. Chim. Acta*, **1944**, 27, 1127-1134.
96. J. Tröger, *J. Prakt. Chem.*, **1887**, 36, 225-245.
97. S. Sergeev, *Helv. Chim. Acta*, **2009**, 92, 415-444.
98. Y. Hamada and S. Mukai, *Tetrahedron: Asymm.*, **1996**, 7, 2671-2674.
99. A. Sharma, L. Guénée, J.-V. Naubron and J. Lacour, *Angew. Chem. Int. Ed.*, **2011**, 50, 3677-3680.
100. A. Sharma, C. Besnard, L. Guenee and J. Lacour, *Org. Biomol. Chem.*, **2012**, 10, 966-969.
101. H. C. Kolb, M. S. VanNieuwenhze and K. B. Sharpless, *Chem. Rev.*, **1994**, 94, 2483-2547.
102. M. J. Rawling and N. C. O. Tomkinson, *Org. Biomol. Chem.*, **2013**, 11, 1434-1440.
103. C. J. R. Bataille and T. J. Donohoe, *Chem. Soc. Rev.*, **2011**, 40, 114-128.
104. J. C. Griffith, K. M. Jones, S. Picon, M. J. Rawling, B. M. Kariuki, M. Campbell and N. C. O. Tomkinson, *J. Am. Chem. Soc.*, **2010**, 132, 14409-14411.
105. R. N. Haward and W. Simpson, *Transactions of the Faraday Society*, **1951**, 47, 212-225.
106. B. S. Jursic and R. M. Martin, *Int. J. Quantum Chem*, **1996**, 59, 495-501.
107. C. Yuan, Y. Liang, T. Hernandez, A. Berriochoa, K. N. Houk and D. Siegel, *Nature*, **2013**, 499, 192-196.
108. M. J. Rawling, J. H. Rowley, M. Campbell, A. R. Kennedy, J. A. Parkinson and N. C. O. Tomkinson, *Chem. Sci.*, **2014**, 5, 1777-1785.
109. M. Newcomb and D. L. Chestney, *J. Am. Chem. Soc.*, **1994**, 116, 9753-9754.
110. W. Adam, K. J. Roschmann, C. R. Saha-Möller and D. Seebach, *J. Am. Chem. Soc.*, **2002**, 124, 5068-5073.

111. R. J. Phipps, L. McMurray, S. Ritter, H. A. Duong and M. J. Gaunt, *J. Am. Chem. Soc.*, **2012**, 134, 10773-10776.
112. M.-H. Le Tadic-Biadatti and M. Newcomb, *J. Chem. Soc., Perk. Trans. 2*, **1996**, 1467-1473.
113. P. S. Engel, W. E. Billups, D. W. Abmayr, K. Tsvaygboym and R. Wang, *The Journal of Physical Chemistry C*, **2008**, 112, 695-700.
114. G. Sheldrick, *Acta Crystallographica Section A*, **2008**, 64, 112-122.
115. H. He, B.-J. Pei, H.-H. Chou, T. Tian, W.-H. Chan and A. W. M. Lee, *Org. Lett.*, **2008**, 10, 2421-2424.
116. M. Lemay and W. W. Ogilvie, *Org. Lett.*, **2005**, 7, 4141-4144.
117. K. Ishihara, H. Kurihara, M. Matsumoto and H. Yamamoto, *J. Am. Chem. Soc.*, **1998**, 120, 6920-6930.
118. I. Krossing, *Chemistry – A European Journal*, **2001**, 7, 490-502.
119. A. Nordqvist, C. Björkelid, M. Andaloussi, A. M. Jansson, S. L. Mowbray, A. Karlén and M. Larhed, *J. Org. Chem.*, **2011**, 76, 8986-8998.
120. M. C. Holland, S. Paul, W. B. Schweizer, K. Bergander, C. Mück-Lichtenfeld, S. Lakhdar, H. Mayr and R. Gilmour, *Angew. Chem. Int. Ed.*, **2013**, 52, 7967-7971.
121. N. Micale, A. P. Kozikowski, R. Ettari, S. Grasso, M. Zappalà, J.-J. Jeong, A. Kumar, M. Hanspal and A. H. Chishti, *J. Med. Chem.*, **2006**, 49, 3064-3067.
122. J. Linder, T. P. Garner, H. E. L. Williams, M. S. Searle and C. J. Moody, *J. Am. Chem. Soc.*, **2010**, 133, 1044-1051.
123. R. Dave and N. A. Sasaki, *Tetrahedron: Asymm.*, **2006**, 17, 388-401.
124. P. Strazzolini, N. Misuri and P. Polese, *Tetrahedron Lett.*, **2005**, 46, 2075-2078.
125. K. C. Nadimpally, K. Thalluri, N. B. Palakurthy, A. Saha and B. Mandal, *Tetrahedron Lett.*, **2011**, 52, 2579-2582.
126. J.-Z. Liu, B.-A. Song, H.-T. Fan, P. S. Bhadury, W.-T. Wan, S. Yang, W. Xu, J. Wu, L.-H. Jin, X. Wei, D.-Y. Hu and S. Zeng, *European Journal of Medicinal Chemistry*, **2010**, 45, 5108-5112.
127. J. Escorihuela, B. Altava, M. I. Burguete and S. V. Luis, *Tetrahedron*, **2013**, 69, 551-558.



128. P. Pelagatti, M. Carcelli, F. Calbiani, C. Cassi, L. Elviri, C. Pelizzi, U. Rizzotti and D. Rogolino, *Organometallics*, **2005**, 24, 5836-5844.
129. F. Fécourt, B. Delpech, O. Melnyk and D. Crich, *Org. Lett.*, **2013**, 15, 3758-3761.
130. J. Dong, Y. Wang, Q. Xiang, X. Lv, W. Weng and Q. Zeng, *Adv. Synth. Catal.*, **2013**, 355, 692-696.
131. A. Beauchard, V. A. Phillips, M. D. Lloyd and M. D. Threadgill, *Tetrahedron*, **2009**, 65, 8176-8184.
132. K. J. Mickelsen, C. M. Tajc, K. R. Greenwood and C. C. Browder, *Synth. Commun.*, **2011**, 42, 186-194.
133. A. Dutta Chowdhury and G. Kumar Lahiri, *Chem. Commun.*, **2012**, 48, 3448-3450.
134. A. S. Dudnik, T. Schwier and V. Gevorgyan, *Org. Lett.*, **2008**, 10, 1465-1468.
135. M. Yamashita, Y. Ono and H. Tawada, *Tetrahedron*, **2004**, 60, 2843-2849.
136. S. Barroso, G. Blay, L. Al-Midfa, M. C. Muñoz and J. R. Pedro, *J. Org. Chem.*, **2008**, 73, 6389-6392.
137. Z. Liu, J. Hu, J. Sun, G. He, Y. Li and G. Zhang, *J. Polym. Sci., Part A: Polym. Chem.*, **2010**, 48, 3573-3586.
138. J. Li, S. Luo and J.-P. Cheng, *J. Org. Chem.*, **2009**, 74, 1747-1750.
139. W.-W. Chan, S.-H. Yeung, Z. Zhou, A. S. C. Chan and W.-Y. Yu, *Org. Lett.*, **2009**, 12, 604-607.
140. J. M. Fraile, K. Le Jeune, J. A. Mayoral, N. Ravasio and F. Zaccheria, *Org. Biomol. Chem.*, **2013**, 11, 4327-4332.
141. R. K. Singh, S. Danishefsky, M. R. Czarny, M. F. Semmelhack, S. Tumidajski and R. L. Danheiser, *Org. Synth.*, **1981**, 70, 66-71.
142. J. L. Mokrosz and M. H. Paluchowska, *J. Chem. Soc., Perk. Trans. 2*, **1986**, 1391-1396.
143. S. Picon, M. Rawling, M. Campbell and N. C. O. Tomkinson, *Org. Lett.*, **2012**, 14, 6250-6253.
144. S. E. Gottschling, T. N. Grant, K. K. Milnes, M. C. Jennings and K. M. Baines, *J. Org. Chem.*, **2005**, 70, 2686-2695.

- 
145. M. J. Frisch, G. W. Trucks, H. B. Schlegel, G. E. Scuseria, M. A. Robb, J. R. Cheeseman, G. Scalmani, V. Barone, B. Mennucci, G. A. Petersson, H. Nakatsuji, M. Caricato, X. Li, H. P. Hratchian, A. F. Izmaylov, J. Bloino, G. Zheng, J. L. Sonnenberg, M. Hada, M. Ehara, K. Toyota, R. Fukuda, J. Hasegawa, M. Ishida, T. Nakajima, Y. Honda, O. Kitao, H. Nakai, T. Vreven, J. A. Montgomery, J. E. Peralta, F. Ogliaro, M. Bearpark, J. J. Heyd, E. Brothers, K. N. Kudin, V. N. Staroverov, R. Kobayashi, J. Normand, K. Raghavachari, A. Rendell, J. C. Burant, S. S. Iyengar, J. Tomasi, M. Cossi, N. Rega, J. M. Millam, M. Klene, J. E. Knox, J. B. Cross, V. Bakken, C. Adamo, J. Jaramillo, R. Gomperts, R. E. Stratmann, O. Yazyev, A. J. Austin, R. Cammi, C. Pomelli, J. W. Ochterski, R. L. Martin, K. Morokuma, V. G. Zakrzewski, G. A. Voth, P. Salvador, J. J. Dannenberg, S. Dapprich, A. D. Daniels, Farkas, J. B. Foresman, J. V. Ortiz, J. Cioslowski and D. J. Fox, Wallingford CT, 2009.